

THE UNIVERSITY OF MICHIGAN

A THEORETICAL METHOD FOR THE CALCULATION OF THE RADAR
CROSS SECTIONS OF AIRCRAFT AND MISSILES

by

J. W. Crispin, Jr., R. F. Goodrich, and K. M. Siegel

July 1959

2591-1-H = RL-2059

Report No. 2591-1-H

on

Contract AF 19(604)-1949

Prepared for

AIR FORCE CAMBRIDGE RESEARCH CENTER
AIR RESEARCH AND DEVELOPMENT COMMAND
BEDFORD, MASSACHUSETTS

TABLE OF CONTENTS

<u>Section</u>	<u>Title</u>	<u>Page</u>
1	Introduction	1
2	Sphere	8
3	Physical Optics Approximation	13
4	Monostatic Cross Section of Simple Shapes	28
4.1	Introduction	28
4.2	The Ellipsoid	28
4.3	The Truncated Elliptic Cone	35
4.4	The Cylinder and the Thin Wire	39
4.5	The Torus and the Wire Loop	55
4.6	The Ogive	62
4.6.1	The Complete Ogive	62
4.6.2	The Truncated Ogive	68
4.7	The Flat Plate	73
4.7.1	The Rectangular Flat Plate	73
4.7.2	The Circular Flat Plate	75
4.7.3	The General Flat Plate	75
4.8	The Tapered Wedge	76
4.9	Corner Reflectors and Multiple Reflectors	77
4.10	The Paraboloid	79
4.11	Summary	80
5	Bistatic Radar Cross Sections	88
5.1	Bistatic Cross Sections for Angles of Separation less than 180°	88
5.2	Bistatic Cross Sections for An Angle of Separation of 180° -Forward Scattering	93
5.3	Bistatic Cross Section - Illustrative Examples	96
6	The Combination of Component Cross Sections	107

<u>Section</u>	<u>Title</u>	<u>Page</u>
7	Illustrative Examples	117
7.1	Radar Cross Section of a Missile	117
7.2	Radar Cross Section of an Aircraft	128
8	Conclusions	138
	References	146

Appendices

Appendix

A	Complete Scattering Matrices and Circular Polarization Cross Sections	148
1	Scattering Matrices	148
1.1	Scattered Field in S-Matrix Notation	150
1.2	S-Matrix in Terms of Fixed but Arbitrary Basis	153
2	Approach to the Multiple-Component Body Problem	159
3	Independent Cross Sections Appropriate to Multiple-Component Bodies	163
4	Polarization Effects and the Physical Optics Approximation	168
5	Cross-Polarization Cross Sections of Wedges	172
5.1	General Theory	172
5.2	Remark on the Use of Asymptotic Expansions of Hankel Functions in the Integral Representation of the Scattered Field for a Wedge	177
5.3	Electric Fields for Linear Polarizations	181
5.4	Electric Fields for Arbitrary Polarizations	181
5.5	Cross Sections for Linear Polarizations	182
5.6	Cross Sections for Circular Polarizations	183
5.7	Summary of Formulas	185
5.8	Coordinate Systems	185
5.9	Wedge S-Matrices in the Airplane Coordinate System	189

<u>Appendix</u>	<u>Title</u>	<u>Page</u>
6	Cross-Polarization Cross Sections of Wire Loops	191
6.1	General Theory	191
6.2	Cross Section Formulas	194
7	Dihedral Scattering	196
7.1	Wing-Body Dihedral Scattering in the Dihedral Coordinate System	196
7.2	Transformation to the Aircraft Coordinate System	200
8	Cross-Polarization Cross Sections for Cylinders	203
	References	216
B	Far Field Scattering from Bodies of Revolution	218
1	Summary	218
2	Introduction	219
3	Rayleigh Cross Section of Bodies of Revolution	220
4	The Optics Region	233
5	The Resonance Region	263
	References	274
C	Cross Sections of Corner Reflectors and Other Multiple Scatterers at Microwave Frequencies	276
1	Introduction and Summary	276
2	The Corner Reflector	278
2.1	Analytical Method for Determining the Radar Cross Section of the Corner Reflector	278
2.2	An Optical Model for Corner Reflectors	280
2.3	Monostatic Cross Sections of Square and Triangular Corner Reflectors	283
2.4	Bistatic Cross Section of a Square Corner Reflector for the Symmetric Case	284
2.5	Effect of Constructional Errors, Compensation and Truncation	297

<u>Appendix</u>	<u>Title</u>	<u>Page</u>
3	Other Multiple Scatterers	299
3.1	Formulas for Scattering from Curved Surfaces: Fock's Method	299
3.2	Scattering from Two Spheres	301
3.3	Formulas for Scattering from Curved Surfaces: The Method of Stationary Phase	308
3.4	The Biconical Reflector	313
4	Experimental Data on Multiple Scatterers	320
	References	329
D	Monostatic Radar Cross Section of the Elliptical Corner Reflector	330
1	Introduction	330
2	Projection of the Equivalent Aperture	331
3	The Intersections, Semi-Axes, and Orientations of the Curves	334
4	Discussion of Results	341
E	Bistatic Radars and Forward Scattering	362
1	Summary	362
2	Introduction	362
3	Forward Scattering and Radar Cross Sections of Arbitrary Convex Shapes	365
4	Illustration of Results for an Arbitrary Shape by Scalar Theory	372
5	Conclusions	378
	References	379
F	Power Spectra for Experimental Data	380
1	Introduction	380
2	The Definitions of the Autocorrelation Function, $R(\tau)$, and the Power Spectrum, $S(\omega)$, Used in the Computations	382

	References	389
G	Determination of Power Spectra from Theoretical Estimates of the Radar Cross Section	390
1	Introduction	390
2	Spectrum of the Cross Section	391
3	Spectrum of the Square Root of the Cross Section	398
3.1	Maximum Value of $\sqrt{2} C_n / C_o $ as a Function of the Maximum Change in σ	398
3.2	Maximum Value of $\sqrt{2} C_n / C_o $ as a Function of the Change in Phase Angle	400
H	Radiation Laboratory Reports	403
1	Studies in Radar Cross Sections	403
2	Miscellaneous Reports	407

INTRODUCTION

The problem of characterizing the radar properties of complex targets is such as to forbid a precise delineation of the methods. That this obtains will be made clear below as we point out the methods by means of examples. We will find that, although the formal solutions are known, the application of them to a given radar target usually leads to such complicated and involved treatments as to render these formal solutions practically useless. What is necessary is to first approximate the complex target by a collection of simple shapes, to next find appropriate methods of characterizing the radar properties of the simple shapes, and finally to recombine the simple shapes along with their radar characteristics to give a useful radar description of the original complex target.

We start with an outline and review of the pertinent electromagnetic formalism. This is a necessary starting point in defining the quantities which are used to characterize radar targets and in developing the approximate methods used in finding these quantities. The basis of the development is Maxwell's equations which can be found in any standard text in electromagnetic theory (Ref. 1).

In rationalized MKS units Maxwell's equations are

$$\begin{aligned} \nabla \times \vec{E} &= -\frac{\partial \vec{B}}{\partial t}, & \nabla \cdot \vec{D} &= \rho \\ \nabla \times \vec{H} &= \frac{\partial \vec{D}}{\partial t} + \vec{J}, & \nabla \cdot \vec{B} &= 0 \end{aligned} \tag{1.1}$$

where \vec{E} = electric field intensity, \vec{H} = magnetic field intensity, \vec{D} = electric displacement, \vec{B} = magnetic induction, \vec{J} = current density, and ρ = charge density.

If now we assume an harmonic time dependence of the electromagnetic quantities of the form $e^{-i\omega t}$ these become

$$\begin{cases} \nabla \times \vec{E} = i\omega \vec{B} , & \nabla \cdot \vec{D} = \rho \\ \nabla \times \vec{H} = -i\omega \vec{D} + \vec{J} , & \nabla \cdot \vec{B} = 0 . \end{cases} \quad (1.2)$$

Now in an homogeneous, isotropic, and source-free region we have

$$\begin{aligned} \vec{B} &= \mu \vec{H} \\ \vec{D} &= \epsilon \vec{E} \\ \vec{J} &= 0 \end{aligned} \quad (1.3)$$

where μ and ϵ are the magnetic permeability and the dielectric constant of the medium respectively.

Substituting in equation (1.2) and separately eliminating \vec{E} and \vec{H} we have that both \vec{E} and \vec{H} satisfy

$$\nabla \times (\nabla \times \vec{\psi}) = k^2 \vec{\psi} \quad (1.4)$$

where $k^2 = \omega^2 \mu \epsilon$. Since both field quantities \vec{E} and \vec{H} are solenoidal in a source-free region equation (1.4) becomes

$$(\nabla^2 + k^2) \vec{\psi} = 0 . \quad (1.5)$$

The conditions imposed on the electromagnetic fields at the interface of two perfect dielectrics with unit normal \hat{n} are

$$\begin{aligned}\hat{n} \times (\vec{E}_1 - \vec{E}_2) &= 0, & \hat{n} \cdot (\vec{D}_1 - \vec{D}_2) &= 0 \\ \hat{n} \times (\vec{H}_1 - \vec{H}_2) &= 0, & \hat{n} \cdot (\vec{B}_1 - \vec{B}_2) &= 0\end{aligned}\tag{1.6}$$

where the subscripts 1 and 2 refer to the two sides of the interface. In the case of a perfectly conducting surface the conditions are

$$\begin{cases} \hat{n} \times \vec{E} = 0 \\ \hat{n} \cdot \vec{B} = 0 \end{cases}.\tag{1.7}$$

In our determination of the radar characteristics of the various targets we take them to be illuminated by a plane wave. This is no essential restriction on the source of illumination since an arbitrary source can be expressed in every case as some combination of plane waves. Assuming an incident plane wave we have that the field quantities are of the form

$$\vec{\psi} = \vec{\psi}_o + \vec{\psi}_s\tag{1.8}$$

where $\vec{\psi}$ is one of the vector fields satisfying Maxwell's equations and the boundary conditions, $\vec{\psi}_o$ is the incident plane wave, and $\vec{\psi}_s$ is the scattered field.

The problem is now specified except for the behavior of the fields at infinity, the radiation condition. This condition is equivalent to the physical requirement that the scattered field behave as outgoing or diverging waves at large distances from the scattering surface. Moreover, it is a mathematical requirement that the solution be specified uniquely. We state it in the form

(Ref. 2)

$$\lim_{r \rightarrow \infty} \int_{S_r} \left| \hat{r} \times (\nabla \times \vec{\psi}_s) - ik \vec{\psi}_s \right|^2 dS = 0\tag{1.9}$$

where r is the distance from the origin of the fixed reference frame to an enveloping sphere S_r of radius r .

The above formulation of the problem, in terms of a differential equation and boundary condition, leads to an integral equation formulation making use of a Green's function. To show this we consider first a scalar problem. Let ψ satisfy

$$(\nabla^2 + k^2) \psi = 0 \quad (1.10)$$

and the boundary conditions

$$\begin{cases} \psi = f \\ \frac{\partial \psi}{\partial n} = g \end{cases} \quad (1.11)$$

on a finite closed surface S . Let the source of radiation be surrounded by a small sphere S_0 and let the entire region be bounded by a large sphere S_∞ .

Then, in general

$$\psi(\vec{r}) = - \int \left(\psi(\vec{r}') \frac{\partial G(\vec{r}, \vec{r}')}{\partial n} - G(\vec{r}, \vec{r}') \frac{\partial \psi(\vec{r}')}{\partial n} \right) dS \quad , \quad (1.12)$$

where G is the free space Green's function

$$G(\vec{r}, \vec{r}') = \frac{1}{4\pi} \frac{e^{ik|\vec{r} - \vec{r}'|}}{|\vec{r} - \vec{r}'|} \quad , \quad (1.13)$$

$\frac{\partial}{\partial n}$ is the outward normal derivative and the integration is over the bounding surfaces, S , S_0 , and S_∞ . The integration over S_∞ vanishes by virtue of the requirement that ψ satisfy the radiation condition and the integration over S_0 gives the incident wave. Therefore

$$\psi(\vec{r}) = \psi_0(\vec{r}) + \int_S \left(f \frac{\partial G}{\partial n} - g G \right) dS \quad . \quad (1.14)$$

In the case of the vector electromagnetic fields we get the similar expressions

$$\vec{E} = \int_S \left[\nabla G \times (\vec{E} \times \hat{n}) \right] dS - \frac{1}{ik} \nabla \times \int_S \left[\nabla G \times (\vec{H} \times \hat{n}) \right] dS \quad (1.15)$$

$$\vec{H} = \int_S \left[\nabla G \times (\vec{H} \times \hat{n}) \right] dS + \frac{1}{ik} \nabla \times \int_S \left[\nabla G \times (\vec{E} \times \hat{n}) \right] dS .$$

If the scattering surface is perfectly conducting the boundary conditions require

$$\hat{n} \times \vec{E} = 0 \quad \text{on } S . \quad (1.16)$$

In addition we can recognize the surface current density as

$$\vec{K} = \hat{n} \times \vec{H} \quad \text{on } S . \quad (1.17)$$

These reduce the equations (1.15)

$$\begin{aligned} \vec{E} &= \vec{E}_0 + \frac{1}{ik} \nabla \times \int_S \nabla G \times \vec{K} dS \\ \vec{H} &= \vec{H}_0 - \int_S \nabla G \times \vec{K} dS \end{aligned} \quad (1.18)$$

To put the second of equations (1.18) in the form usually considered we

note that for r very large,

$$\nabla G \cong \frac{e^{ikr}}{4\pi r} ik \hat{r} e^{-i\vec{k}_f \cdot \vec{r}'} , \quad (1.19)$$

where $\vec{k}_f = k\hat{r}$; hence,

$$\vec{H} = \vec{H}_0 - \frac{e^{ikr}}{4\pi r} ik \hat{r} \times \int_S e^{-i\vec{k}_f \cdot \vec{r}'} (\hat{n} \times \vec{H}) dS . \quad (1.20)$$

The scattered field is

$$\vec{H}_s = - \frac{e^{ikr}}{4\pi r} ik \hat{r} \times \int_S e^{-i\vec{k}_f \cdot \vec{r}'} (\hat{n} \times \vec{H}) dS . \quad (1.21)$$

The electromagnetic fields are not physically measurable quantities as such. A physical measurement can be made of such things as distances, times, and energies. Hence, we are led to characterize the properties of a radar target in terms of the radar cross section which is a measure of the energy scattered from the target. Precisely, the radar cross section is defined as

$$\sigma(\theta, \phi) = \lim_{r \rightarrow \infty} 4\pi r^2 \left| \frac{H_s(\theta, \phi)}{H_o} \right|^2$$

or

$$\sigma(\theta, \phi) = \lim_{r \rightarrow \infty} 4\pi r^2 \left| \frac{E_s(\theta, \phi)}{E_o} \right|^2 \quad (1.22)$$

where H_s or E_s are the scattered fields propagating in the direction given by the angles (θ, ϕ) and E_o or H_o are the strengths of the incident fields.

There is a class of problems which are soluble by means of separation of variable. These are those for which the operator in equation (1.5), $\nabla^2 + k^2$, is separable in some coordinate system such that the scattering surface is a coordinate surface. We refer to these as separable problems. The solutions then appear as a series of the special functions of mathematical physics. The usefulness of this approach is restricted by two considerations: First the special functions are not sufficiently tabulated in all cases and second the series solution may be too slowly convergent. In fact, only in the case of the sphere has this approach received much attention.

Although we will make little use of these separable solutions in characterizing the radar properties of complex targets we will briefly consider one such solution, the sphere. We will use this solution as a starting point for considering the various approximation methods which will be used for more general shapes.

To motivate this consideration of the sphere solution we repeat the point made above: After the resolution of a complex radar target into a number of simple shapes we need a way of deciding what approximate methods are appropriate to finding the radar properties of the simple shapes. For a given orientation of the simple target and polarization of the radiation this decision, in most cases, is made after comparing certain "characteristic dimensions" of the target with the wavelength of the radiation. Since the behavior of the sphere as a radar target is invariant under rotations and since it has a single dimension, the radius, we first consider this simplest case.

THE SPHERE

We take the harmonic series solution for the scattering of a plane electromagnetic wave by a perfectly conducting sphere. This solution, first given by Mie (Ref. 3), is expressed in spherical coordinates. We take the incident plane wave directed along the axis $\theta = 0$, the z-axis, and polarized with the electric vector along $\phi = 0$, the x-axis. With a perfectly conducting sphere of radius a at the origin the scattered field at any point (r, θ, ϕ) in space is given by

$$E_{\theta}^S = -E_0 \cos\phi \sum_1^{\infty} (i)^n \frac{2n+1}{n(n+1)} \left[\frac{j_n(ka)}{h_n^{(1)}(ka)} h_n^{(1)}(kr) \frac{P_n^{(1)}(\cos\theta)}{\sin\theta} - i \frac{[ka j_n(ka)]'}{[ka h_n^{(1)}(ka)]'} \frac{[kr h_n^{(1)}(kr)]'}{kr} \frac{d}{d\theta} P_n^{(1)}(\cos\theta) \right] \quad (2.1)$$

$$E_{\phi}^S = E_0 \sin\phi \sum_1^{\infty} (i)^n \frac{2n+1}{n(n+1)} \left[\frac{j_n(ka)}{h_n^{(1)}(ka)} h_n^{(1)}(kr) \frac{d}{d\theta} P_n^{(1)}(\cos\theta) - i \frac{[ka j_n(ka)]'}{[ka h_n^{(1)}(ka)]'} \frac{[kr h_n^{(1)}(kr)]'}{kr} \frac{P_n^{(1)}(\cos\theta)}{\sin\theta} \right]$$

where E_0 is the amplitude of the incident field, j_n and $h_n^{(1)}$ are the spherical Bessel and Hankel functions respectively, and $P_n^{(1)}$ is an associated Legendre function. The primes denote differentiation with respect to the argument of the functions. The far field form of this solution is found by using the asymptotic form

$$h_n^{(1)}(kr) = (-i)^{n+1} \frac{e^{ikr}}{kr}$$

in equations (2.1), retaining terms of order $\frac{1}{r}$,

$$E_\theta^s = i E_0 \cos\phi \sum_1^\infty \frac{2n+1}{n(n+1)} \left\{ \frac{j_n(ka)}{h_n^{(1)}(ka)} \frac{P_n^{(1)}(\cos\theta)}{\sin\theta} - \frac{[ka j_n'(ka)]'}{[ka h_n^{(1)'}(ka)]'} \frac{d}{d\theta} P_n^{(1)}(\cos\theta) \right\} \quad (2.2)$$

$$E_\phi^s = -E_0 \sin\phi \frac{e^{ikr}}{kr} \sum_1^\infty \frac{2n+1}{n(n+1)} \left\{ \frac{j_n(ka)}{h_n^{(1)}(ka)} \frac{d}{d\theta} P_n^{(1)}(\cos\theta) - \frac{[ka j_n'(ka)]'}{[ka h_n^{(1)'}(ka)]'} \frac{P_n^{(1)}(\cos\theta)}{\sin\theta} \right\}.$$

The limitation on this representation of the sphere solution is the rate of convergence of the series as a function of the parameter ka . This parameter, in the case of the sphere, gives the comparison of the characteristic dimension of the sphere, the radius a , with the wavelength $\lambda = \frac{2\pi}{k}$. Hence, a study of

various approximations to the solution and the validity of these approximations as a function of ka will serve as an introduction to the consideration of more complicated shapes and the approximation of their behavior as radar targets.

First we make the restriction $ka \ll 1$; i. e., we consider spheres which are very small compared with the wavelength. On examining the terms in the series of equation (2.2) we see that since

$$\begin{cases} j_n(ka) = 2^n \frac{n!}{(2n+1)!} (ka)^n + O\left[(ka)^{n+2}\right] \\ h_n^{(1)}(ka) = -\frac{i}{2^n} \frac{(2n)!}{n!} (ka)^{-n-1} + O\left[(ka)^{-n-3}\right] \end{cases} \quad (2.3)$$

only the first order terms need be considered for ka sufficiently small. In this approximation the fields (2.2) become

$$E_{\theta}^s = \frac{e^{ikr}}{r} E_0 \cos\phi k^2 a^3 \left(\cot\theta - \frac{1}{2}\right) \quad (2.4)$$

$$E_{\phi}^s = -\frac{e^{ikr}}{r} E_0 \sin\phi k^2 a^3 \left(1 - \frac{\cos\theta}{2}\right)$$

and the radar cross section is

$$\sigma = 4\pi (k^2 a^3)^2 \left[\left(\cos\theta - \frac{1}{2}\right)^2 \cos^2\phi + \left(1 - \frac{1}{2} \cos\theta\right) \sin^2\phi \right]. \quad (2.5)$$

On examining the way the parameters enter the expression for the cross section we see that we can rewrite equation (2.5) as

$$\sigma = \frac{3^2 V_k^2 k^4}{4\pi} \left[\left(\frac{1}{2} - \cos\theta\right)^2 \cos^2\phi + \left(1 - \frac{1}{2} \cos\theta\right) \sin^2\phi \right] \quad (2.6)$$

where V is the volume of the scatterer. This is characteristic of the large wavelength or Rayleigh approximation: The cross section is proportional to the volume squared and inversely proportional to the fourth power of the wavelength.

The physical content of this result is essentially that our probe, the electromagnetic radiation of large wavelength, is not fine enough to sense more than the over-all size of the target, the volume. This result also obtains for other shaped targets so long as they are sufficiently small (Ref. 4). Quite generally we have in the Rayleigh region for backscattering

$$\sigma = \frac{4}{\pi} k^4 V^2 f(a, b, \dots) \quad (2.7)$$

where f is a correction factor taking into account a more detailed description of the target, a, b, \dots , being the parameters describing the shape of the target.

We can continue this process, computing the higher magnetic and electric multipole moments. The resulting series of multipole moments would be precisely the series of equation (2.1). This important observation leads us to point out that generally the radiation from the excitation of any target can be considered as arising from a collection of electric and magnetic multipoles. As in the case of the sphere, as the wavelength of the radiation becomes smaller with respect to certain characteristic dimensions of the target, the more multipoles are necessary to characterize the target.

In the high frequency region for the sphere, $ka \gg 1$, the rate of convergence of the series (2.1) is so slow as to make this representation of

the solution inappropriate. There is an alternative formulation making use of the Watson transform (Ref. 5), however, we will approach the problem in a more generally applicable, although approximate, way.

PHYSICAL OPTICS APPROXIMATION

Substituting (1.13) and (1.17) into (1.18) the following expression for the scattered field is obtained

$$\vec{H}_s = \frac{1}{4\pi} \int_S (\hat{n} \times \vec{H}) \times \nabla \frac{e^{ikR}}{R} dS . \quad (3.1)$$

If the field induced on the directly illuminated portion of the surface by the incident radiation is taken to be approximately the geometrical optics field the scattered field can be approximated. By this we mean that, at a given point on the geometrically illuminated part of the sphere, the field is approximately that which would be induced in the limit $ka \rightarrow \infty$. This is also the field which would be induced on an infinite plane tangent to the sphere at the point in question which, after an elementary consideration, is found to be twice the tangential component of the incident magnetic field on the geometrically illuminated side of the sphere and zero in the shadow.

Equation (3.1) is then rewritten

$$\vec{H}_s \cong \frac{1}{4\pi} \int_{\substack{\text{illuminated} \\ \text{side}}} (\hat{n} \times \vec{H}_{GO}) \times \nabla \frac{e^{ikR}}{R} dS, \quad (3.2)$$

where $\vec{H}_{GO} = 2 \vec{H}_i$ with \vec{H}_i the tangential component of the incident field.

The cross section in this approximation is

$$\frac{\sigma(\theta)}{\pi a^2} = (2ka)^2 \left| \int_0^{\pi/2} \sin \beta \cos \beta J_0(ka \sin \theta \sin \beta) e^{ika(1+\cos \theta) \cos \beta} d\beta \right|^2, \quad (3.3)$$

where θ is the angular separation of the incident and emergent direction. For backscattering this reduces to the simpler expression

$$\frac{\sigma(0)}{\pi a^2} = 1 - \frac{\sin 2ka}{ka} + \frac{1 - \cos 2ka}{(ka)^2}, \quad (3.4)$$

where we note that the leading term is just the geometrical optics result.

In the above we have made no special use of the fact that the physical optics method was applied to a sphere. The only requirement was that the surface be able to be locally approximated by a plane for the purpose of finding the field on the surface. Hence, we suggest that the method of physical optics is more generally applicable. The important reservation in its application can be seen from a comparison of the results of summing the series (2.1) computing the cross section for backscattering and comparing it with the result (3.4). As ka increases both the exact solution and the physical optics solution oscillate about the geometrical optics value but the oscillations are not the same. From this we conclude that physical optics can be used to approximate the magnitude, although no better than geometrical optics, but can give no information about the oscillations about the geometrical optics value.

We start with equation (3.2) and consider the physical optics approximation to the field scattered by a perfectly conducting surface S . Let the incident field be given by

$$\vec{H}_i = H_0 \hat{a} e^{i\hat{k} \cdot \vec{r}} \quad (3.5)$$

We now divide the surface S into the geometrically illuminated side S_1 , and the shadowed side, S_2 (Figure 3-1) by means of the shadow curve $\hat{k} \cdot \hat{n} = 0$ where \hat{k} is the unit vector in the direction of propagation of the incident wave and \hat{n} is the normal to S .

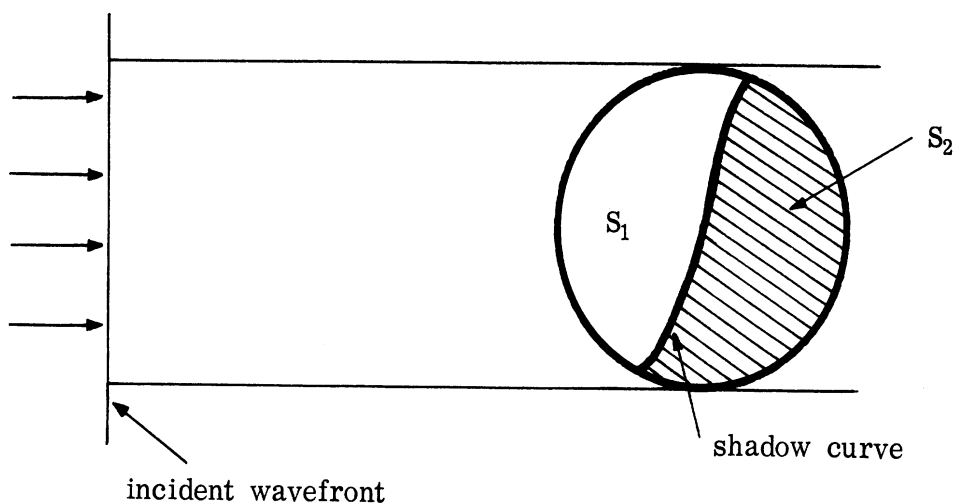


FIG. 3-1

The geometric optics current is given by

$$\vec{K}_{GO} = \begin{cases} 2\hat{n} \times \vec{H}_i, & \text{on } S_1 \\ 0, & \text{on } S_2 \end{cases} \quad (3.6)$$

If \vec{r} is the position vector of the field point and \vec{r}' the position vector of a surface element of S , the gradient of the Green's function in the far field

approximation can be written as

$$\nabla \frac{e^{ikR}}{4\pi R} \sim \frac{e^{ikr}}{4\pi r} e^{-i\vec{k}_f \cdot \vec{r}'} e^{i\vec{k}_f \cdot \vec{r}}, \quad (3.7)$$

where $R = |\vec{r} - \vec{r}'|$ and $\vec{k}_f = k\hat{r}$. Substituting in (3.5)

$$\vec{H}_s = \frac{ik}{2\pi} \frac{e^{ikr}}{r} \int_{S'} (\hat{n} \times \vec{H}_i) \times \hat{r} e^{-i\vec{k}_f \cdot \vec{r}'} dS = \frac{e^{ikr}}{r} \vec{F}(\beta), \quad (3.8)^*$$

where

$$\vec{F}(\beta) = \frac{-ikH_0}{2\pi} \left[(\hat{r} \cdot \hat{a}) \vec{f} - (\hat{r} \cdot \vec{f}) \hat{a} \right], \quad (3.9)$$

and

$$\vec{f} = \int_{S'} \hat{n} e^{ik\vec{r}' \cdot (\hat{k} - \hat{r})} dS. \quad (3.10)$$

Hence, the radar cross section is given by

$$\sigma(\beta) = 4\pi \left| \vec{F} \right|^2. \quad (3.11)$$

If we take into account the polarization of the receiver, we can define an effective cross section,

$$\sigma_e(\beta) = 4\pi \left| \vec{F} \cdot \hat{d} \right|^2, \quad (3.12)$$

where \hat{d} is a unit vector in the direction of the receiver polarization.

* where S' refers to the illuminated portion of the surface.

In the simpler case of backscattering we have $\hat{\mathbf{r}} = -\hat{\mathbf{k}}$ and

$$\sigma = \frac{4\pi}{\lambda^2} \left| \mathbf{g} \right|^2, \quad (3.13)$$

where

$$\mathbf{g} = \hat{\mathbf{k}} \cdot \int \hat{\mathbf{n}} e^{2i\hat{\mathbf{k}} \cdot \vec{\mathbf{r}}'} d\mathbf{S}. \quad (3.14)$$

To simplify the discussion we orient the coordinate system such that $\hat{\mathbf{k}} = \hat{\mathbf{z}}$,

then

$$g = \int n_z e^{2ikz'} d\mathbf{S}. \quad (3.15)$$

But we note that $n_z d\mathbf{S}$ is just the projection of the elementary area $d\mathbf{S}$ on a plane perpendicular to the direction of incidence and we write

$$n_z d\mathbf{S} = \frac{\partial \mathbf{S}}{\partial z'} dz'$$

Finally

$$g = \int e^{2ikz'} \frac{\partial \mathbf{S}}{\partial z'} dz', \quad (3.16)$$

or more generally

$$g = \int e^{2ik\rho} \frac{\partial A}{\partial \rho} d\rho, \quad (3.17)$$

where ρ is the distance measured in the direction of incidence and A is the area of the projection of the part of the scatterer to one side of a plane of constant ρ (the side indicated by arrows in Figure 3-2), the projection being

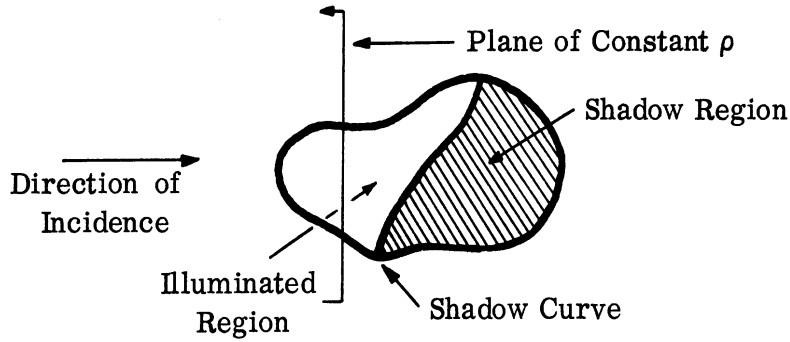


FIG. 3-2: THE SHADOW CURVE (GENERAL)

made onto the plane of constant ρ . From equation (3.17) we see that physical optics predicts no dependence of monostatic cross section on polarization (at least the form of physical optics which we are using here). Equation (3.17) may be interpreted as saying that each element of area makes a contribution to g , but with a phase factor $e^{2ik\rho}$ so that two contributions may either add or cancel depending on their relative phases.

As an example of physical optics we will again consider the cross section of a sphere. For the sphere in Figure 3-3 the area function is

$$A = \begin{cases} 0 & (\rho \leq -a) \\ \pi(a^2 - \rho^2) & (-a \leq \rho \leq 0) \\ \pi a^2 & (0 \leq \rho) \end{cases} \quad (3.18)$$

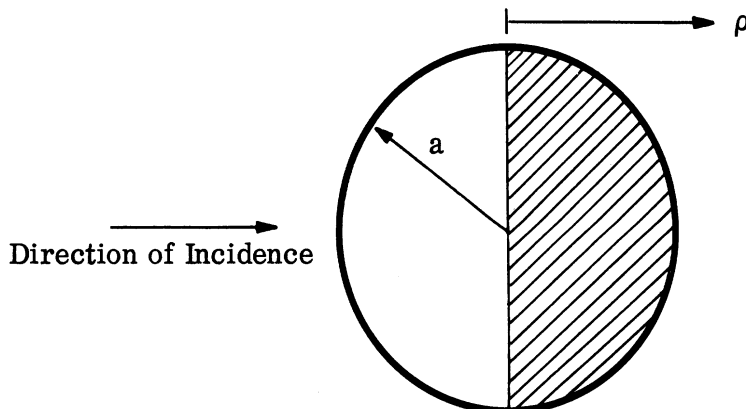


FIG. 3-3: SHADOW CURVE (SPHERE)

From equation (3.18) we find:

$$\frac{dA}{d\rho} = \begin{cases} 0 & (\rho \leq -a) \\ -2\pi\rho & (-a \leq \rho \leq 0) \\ 0 & (0 \leq \rho) \end{cases} \quad (3.19)$$

The variation of A and $dA/d\rho$ with ρ is shown in Figure 3-4. For short wavelengths, k is large and $e^{2ik\rho}$ oscillates very rapidly (that is its real and imaginary parts oscillate very rapidly). As a result, whenever $dA/d\rho$

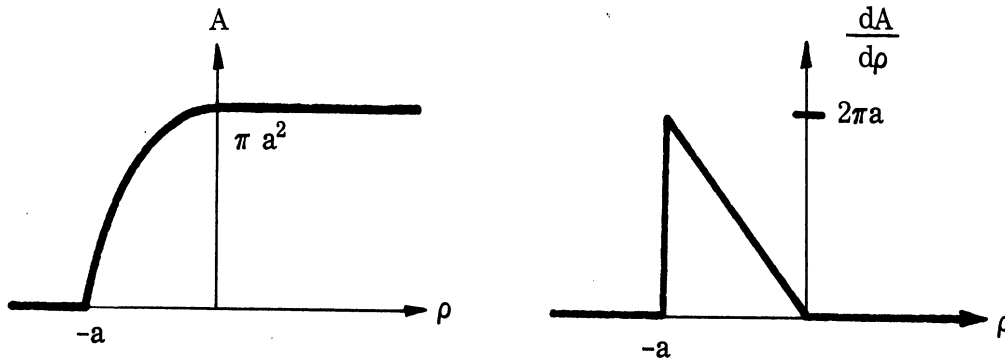


FIG. 3-4: A AND $dA/d\rho$ - I

varies slowly the contributions for values of ρ differing by $\lambda/4$ will nearly cancel. Only the regions where $dA/d\rho$ changes rapidly will contribute appreciably to the integral. From Fig. 3-4 it is clear that the main contribution comes from $\rho = -a$. For this particular problem the integral can be evaluated exactly; so, let us see whether the above ideas agree with the exact solution. We have

$$g = \int_{-a}^0 e^{2ik\rho} (-2\pi\rho) d\rho = \frac{\pi ia}{k} e^{-2ika} + \frac{\pi}{2k^2} (e^{-2ika} - 1). \quad (3.20)$$

The terms having an e^{-2ika} factor can be interpreted as the contribution from $\rho = 0$. With this interpretation we see that the contributions from the intermediate region have cancelled each other. For large k the term, $\frac{\pi ia}{k} e^{-2ika}$ dominates the others. This term is due to the jump in $dA/d\rho$ at $\rho = -a$. The other two terms are due to the discontinuity in $\frac{d^2 A}{d\rho^2}$ at $\rho = -a$ and at $\rho = 0$. According to the interpretation used here we should find that another area function for which $dA/d\rho$ has a jump of $2\pi a$ at $\rho = -a$ but is otherwise continuous (varying but little in a distance of a wavelength) should give the same result (for large k). For example, suppose that as in (Fig. 3-5)

$$A = \begin{cases} 0 & (\rho < -a) \\ \frac{2\pi a}{\beta} \left[1 - e^{-\beta(\rho+a)} \right] & (\rho \geq -a) \end{cases} \quad \text{and} \quad \frac{dA}{d\rho} = \begin{cases} 0 & (\rho < -a) \\ 2\pi a e^{-\beta(\rho+a)} & (\rho \geq -a) \end{cases}, \quad (3.21)$$

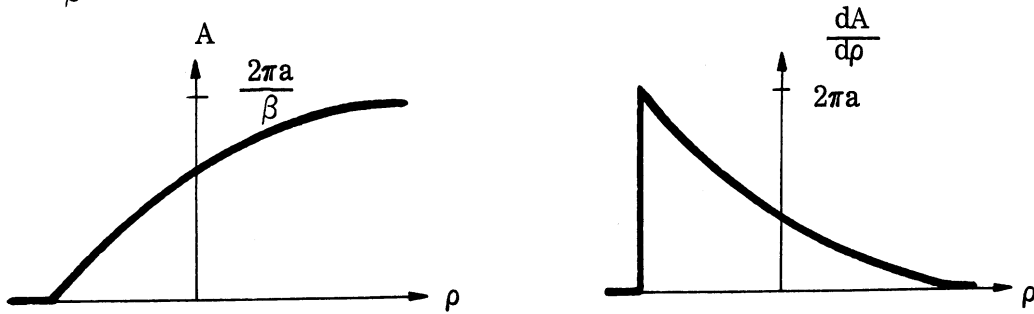


FIG. 3-5: A AND $dA/d\rho$ - II

then we can again evaluate g exactly with the result

$$g = \int_{-a}^{\infty} e^{2ik\rho} 2\pi a e^{-\beta(\rho+a)} d\rho = \frac{\pi ia}{k + \frac{\beta i}{2}} e^{-2ika} \quad (3.22)$$

For large k , equations (3.20) and (3.22) are in agreement so that the interpretation which we have been using seems to be accurate.

There is another way of looking at the physical optics integral which can be very illuminating. If, for the sphere problem, we let

$$f(\rho) = \int_{-a}^{\rho} e^{2ikz} (-2\pi z) dz, \quad \text{then } g = f(0).$$

Now $f(\rho)$ is a complex number and as ρ varies from $-a$, to 0 , $f(\rho)$ traces out a curve in the complex plane. This curve is called a vibration curve. The vibration curve is the limiting form of a vibration polygon obtained by replacing the integral in equation (3.17) by an approximating sum

$$\sum_n e^{2ikz_n} \left(\frac{dA}{dz} \right)_n \Delta z_n.$$

The individual terms in this series can be looked on as little vectors in the complex plane which add up as shown in Figure 3-6. The magnitude of each vector is $\left(\frac{dA}{dz} \right)_n \Delta z_n$, and the vector points in a direction making an angle $2kz_n$ with the real axis. If we take a constant value of Δz_n then the angle which the resultant vectors make with the real axis will increase steadily. If $\frac{dA}{dz}$ is constant then the vectors will go around a circle of radius $\frac{1}{2k} \left| \frac{dA}{dz} \right|$. If $\frac{dA}{dz}$ varies slowly then the vibration curve will

spiral about a relatively fixed point with a slowly changing radius. However each time $\frac{dA}{dz}$ has a discontinuity the point about which the vibration curve is spiraling will jump proportionately. For the sphere, the vibration curve will appear roughly as in Figure 3-7. It can be seen that the spiral ends at approximately the original center of curvature which is $\frac{\pi ia}{k} e^{-2ika}$. As a second example of a vibration curve, let us take an area function for which $\frac{dA}{d\rho}$ has two jump discontinuities as shown in Figure 3-8. In this case the vibration curve will take the form shown in Figure 3-9.

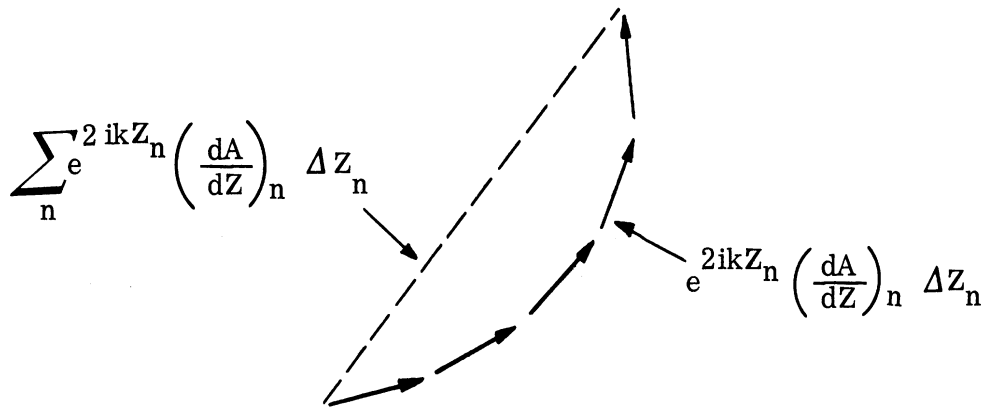


FIG. 3-6: VIBRATION CURVE - I

This can be analyzed as follows: at $\rho = 0$ the center of the vibration spiral is shifted to the point A (Fig. 3-10) and the spiral follows the large circle. The radius of the circle slowly decreases until the spiral is following the small circle. At the second discontinuity the center is again shifted, this time, to the point B. The center of the spiral ends at the same place as the spiral itself. Thus by tracing the motion of the center of the spiral we can find the value of the integral. In more complicated cases this can be quite a useful aid to our thinking.

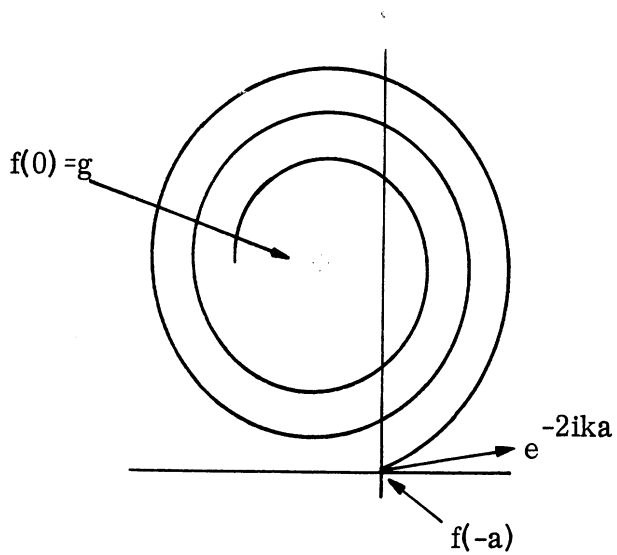


FIG. 3-7: VIBRATION CURVE - II

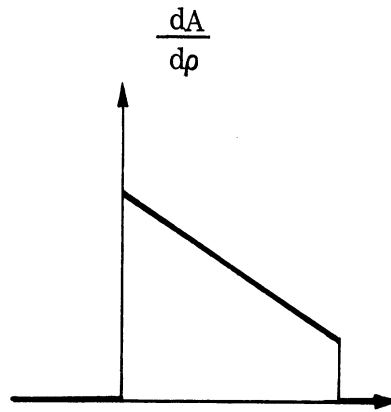


FIG. 3-8: $\frac{dA}{dp}$ HAVING TWO JUMP DISCONTINUITIES

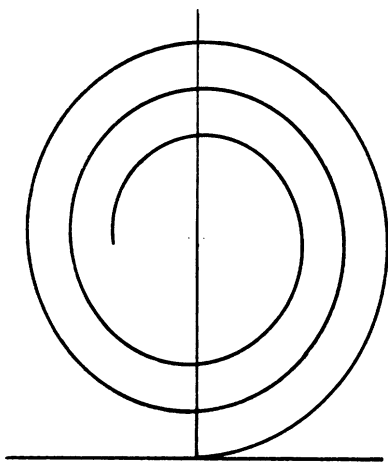


FIG. 3-9: VIBRATION CURVE - III

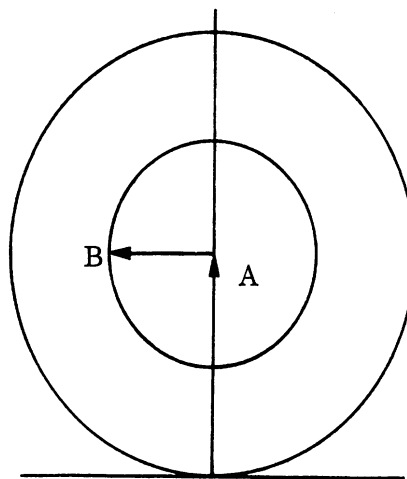


FIG. 3-10: SHIFT IN CENTER OF VIBRATION SPIRAL

If $\frac{dA}{d\rho}$ behaves in the same manner for two bodies then the physical optics cross section for the two bodies will be nearly equal. We have seen that bodies like the sphere which have finite radii of curvature will have a $\frac{dA}{d\rho}$ which has a jump where the incident field first hits the body and then goes smoothly to zero. At the point at which the incident wave first hits such a smooth body we can approximate the body by a paraboloid having the same principle radii of curvature. Once we have found the cross section for such a paraboloid we will have an approximate cross section for all such smooth bodies. We take the equation of the paraboloid (Fig. 3-11) to be

$$\rho = \frac{x^2}{2R_1} + \frac{y^2}{2R_2} \quad (3.23)$$

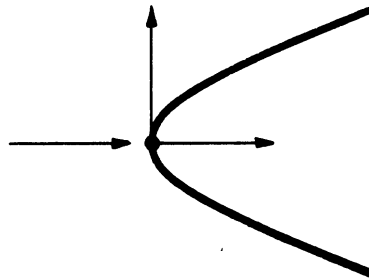


FIG. 3-11: THE PARABOLOID

where R_1 and R_2 are principle radii of curvature at the point $(0, 0, 0)$ where the incident wave first hits the paraboloid. The area function is

$$A = 2\pi\rho \sqrt{R_1 R_2} \quad (\rho \geq 0).$$

Thus

$$\frac{dA}{d\rho} = 2\pi \sqrt{R_1 R_2} \quad (\rho \geq 0).$$

This does not go to zero for large ρ but we can modify the body very slightly so that

$$\frac{dA}{d\rho} = 2\pi \sqrt{R_1 R_2} e^{-\beta\rho} \quad (\rho \geq 0)$$

where β is very small. We then have

$$g = \int_0^{\infty} e^{2ik\rho} 2\pi \sqrt{R_1 R_2} e^{-\beta\rho} d\rho \xrightarrow{\beta \rightarrow 0} \frac{\pi i \sqrt{R_1 R_2}}{k} \quad (3.24)$$

Substitution of equation (3.24) into equation (3.17) shows that the approximate cross section of a smooth body is

$$\sigma = \pi R_1 R_2 \quad (3.25)$$

where R_1 and R_2 are the principle radii of curvature at the specular reflection point. This formula was obtained by assuming k large so that the return was essentially from the specular reflection point. Hence the same result could be obtained alternatively by using geometric optics. As a result this formula for σ is often called the geometric optics formula for σ .

Equation (3.25) is one of the most useful cross section formulas due to its extreme simplicity. It is convenient for applications to have a few formulas giving R_1 and R_2 .

If the equation of the surface is given in the form $z = f(x, y)$ then

$$R_1 R_2 = \frac{(1 + f_x^2 + f_y^2)^2}{f_{xx} f_{yy} - f_{xy}^2} \quad (3.26)$$

If the equation of the surface is given in the form $F(x, y, z) = 0$, then

$$R_1 R_2 = \frac{(F_x^2 + F_y^2 + F_z^2)^2}{\Delta} \quad (3.27)$$

$$\Delta = \begin{vmatrix} F_{xx} & F_{xy} & F_{xz} & F_x \\ F_{xy} & F_{yy} & F_{yz} & F_y \\ F_{xz} & F_{yz} & F_{zz} & F_z \\ F_x & F_y & F_z & 0 \end{vmatrix}$$

If the equation of the surface is given parametrically as $x = x(u, v)$,
 $y = y(u, v)$, $z = z(u, v)$ then

$$R_1 R_2 = \frac{(EG - F^2)^2}{LN - M^2} \quad (3.28)$$

$$E = x_u^2 + y_u^2 + z_u^2, \quad F = x_u x_v + y_u y_v + z_u z_v, \quad G = x_v^2 + y_v^2 + z_v^2,$$

$$L = \begin{vmatrix} x_{uu} & x_u & x_v \\ y_{uu} & y_u & y_v \\ z_{uu} & z_u & z_v \end{vmatrix} \quad M = \begin{vmatrix} x_{uv} & x_u & x_v \\ y_{uv} & y_u & y_v \\ z_{uv} & z_u & z_v \end{vmatrix} \quad N = \begin{vmatrix} x_{vv} & x_u & x_v \\ y_{vv} & y_u & y_v \\ z_{vv} & z_u & z_v \end{vmatrix}$$

For a body of revolution given by the equation $\rho = \rho(z)$ (Fig. 3-12) we have

$$R_1 R_2 = \left| \frac{\rho}{\rho'' \sin^4 a} \right| \quad (3.29)$$

where α is the angle between the direction of incidence and the axis of the body. ρ and ρ'' must, of course, be evaluated at the specular reflection point.

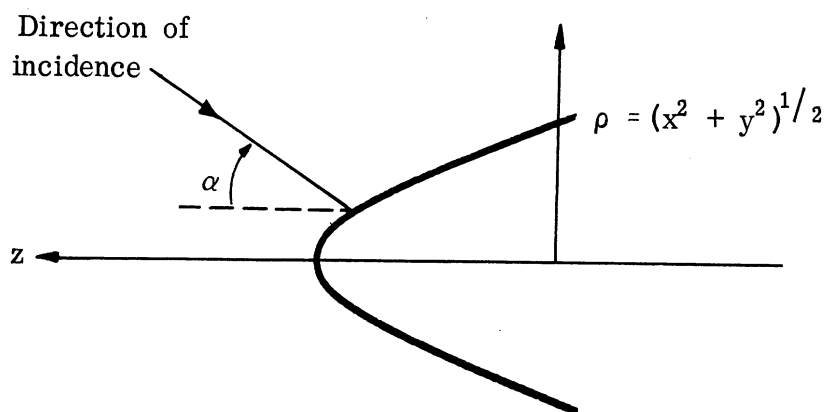


FIG. 3-12: A BODY OF REVOLUTION

In many cases in determining the cross section of a simple shape we find that there is one expression for "normal" incidence and a second expression for the cross section at "non-normal" incidence. In these cases the cross section (for short wavelengths) is much larger at normal incidence than at non-normal aspects. When the actual value of the cross section at the non-normal aspects can be neglected, we might use, instead of the non-normal incidence formulas, an expression giving the width of the peak. To obtain such peak width formulas we require that the sum of the non-normal cross section contributions be equal to the desired fraction of the normal incidence value; such expressions are presented in Section 4.11.

MONOSTATIC CROSS SECTION OF SIMPLE SHAPES

4.1 Introduction

In the preceding section we have presented in some detail the methods to be employed in obtaining expressions for the radar cross sections of simple shapes. Here in Section 4 we shall concentrate on the simple shape configurations; i. e., ellipsoids, elliptic cones, cylinders, and thin wires, tori and wire loops, the ogive, flat plates, the tapered wedge, corner reflectors (and multiple scattering in general), and the paraboloid. These discussions will be devoted primarily to the optics region.

4.2 The Ellipsoid

The ellipsoid has been found to be extremely useful in modeling parts of aircraft and missiles. Ellipsoids of various dimensions model quite well such components as the fuselage, the engine nacelles, the wing tanks, and the wing tips. In most instances it is portions of prolate spheroids which are of the greatest use and thus we shall concentrate on the prolate spheroid.

The equation of the ellipsoid can be taken to be

$$\left(\frac{x}{a}\right)^2 + \left(\frac{y}{b}\right)^2 + \left(\frac{z}{c}\right)^2 = 1 \quad (4.2.1)$$

and the coordinate system employed is shown in Figure 4.2-1.

In the case of vanishingly small wavelengths we obtain, through the use of equations (3.25) and (3.27), the following expressions for the monostatic cross section:

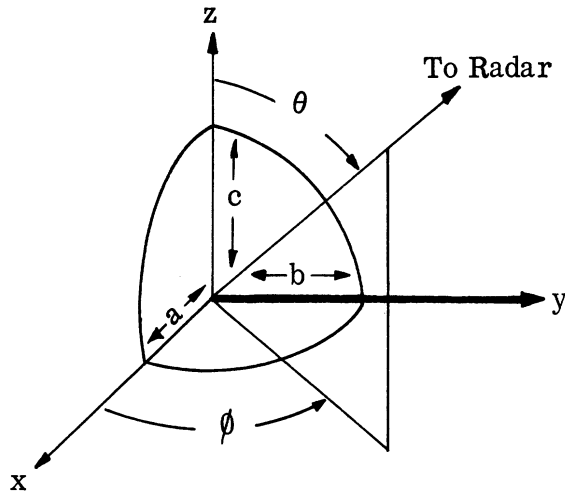


FIG. 4.2-1: THE COORDINATE SYSTEM USED IN THE ELLIPSOID ANALYSIS

For the general ellipsoid

$$\sigma = \frac{\pi a^2 b^2 c^2}{(a^2 \sin^2 \theta \cos^2 \phi + b^2 \sin^2 \theta \sin^2 \phi + c^2 \cos^2 \theta)^2} . \quad (4.2.2)$$

For the prolate spheroid ($a = b$)

$$\sigma = \frac{\pi b^4 c^2}{(b^2 \sin^2 \theta + c^2 \cos^2 \theta)^2} . \quad (4.2.3)$$

For the sphere ($a = b = c$)

$$\sigma = \pi a^2 . \quad (4.2.4)$$

For larger wavelengths, still in the optics region, the application of equation (3.17) to the prolate spheroid problem for the case of $\theta = 0^\circ$ yields

$$\sigma(0^\circ) = \pi \left(\frac{b^4}{c^2} \right) \left(1 - \frac{\sin(2kc)}{kc} + \frac{1 - \cos(2kc)}{2(kc)^2} \right) . \quad (4.2.5)$$

In the Rayleigh region we can employ the methods presented in Appendix B for incidence along the major axis.

In the resonance region the methods of Appendix B are applicable, but we should call attention to the work which has been done on the sphere and the prolate spheroid whose ratio of major to minor axis is 10:1. A summary of the work performed on the sphere is presented in Reference 6 and the efforts expended on the 10:1 prolate spheroid are documented in References 7 and 8. The radar cross section patterns for the sphere and the 10:1 prolate spheroid in the resonance region (for incidence along the axis of revolution) are presented in Figure 4.2-2.

The above enables us to obtain good estimates of the radar cross section contributions from ellipsoids used in modeling portions of aircraft and missiles over almost the entire range of wavelength-to-body dimension ratios.

As an aid in the application of equation (4.2.3) we present in Figures 4.2-3 and 4.2-4 graphical presentations of the cross section of a prolate spheroid for various values of the length-to-width ratio, $\frac{b}{c}$. Figure 4.2-3 shows the way in which the cross section at $\theta = 0^\circ$ varies with the ratio $\frac{c}{b}$ ($1 \leq \frac{c}{b} \leq 15$) for a fixed value of the semi-minor axis, b . Figure 4.2-4 gives the ratio of $\sigma(\theta)$ to $\sigma(0^\circ)$ as a function of θ for various values of $\frac{b}{c}$. The "upper bound" to this ratio (obtained by setting $\frac{b}{c} = 0$) is extremely useful in deciding whether or not an aircraft component so modeled will contribute significantly.

It is of interest to compare the results obtained through the application of equation (4.2.2) with some recent experimental data on oblate spheroids

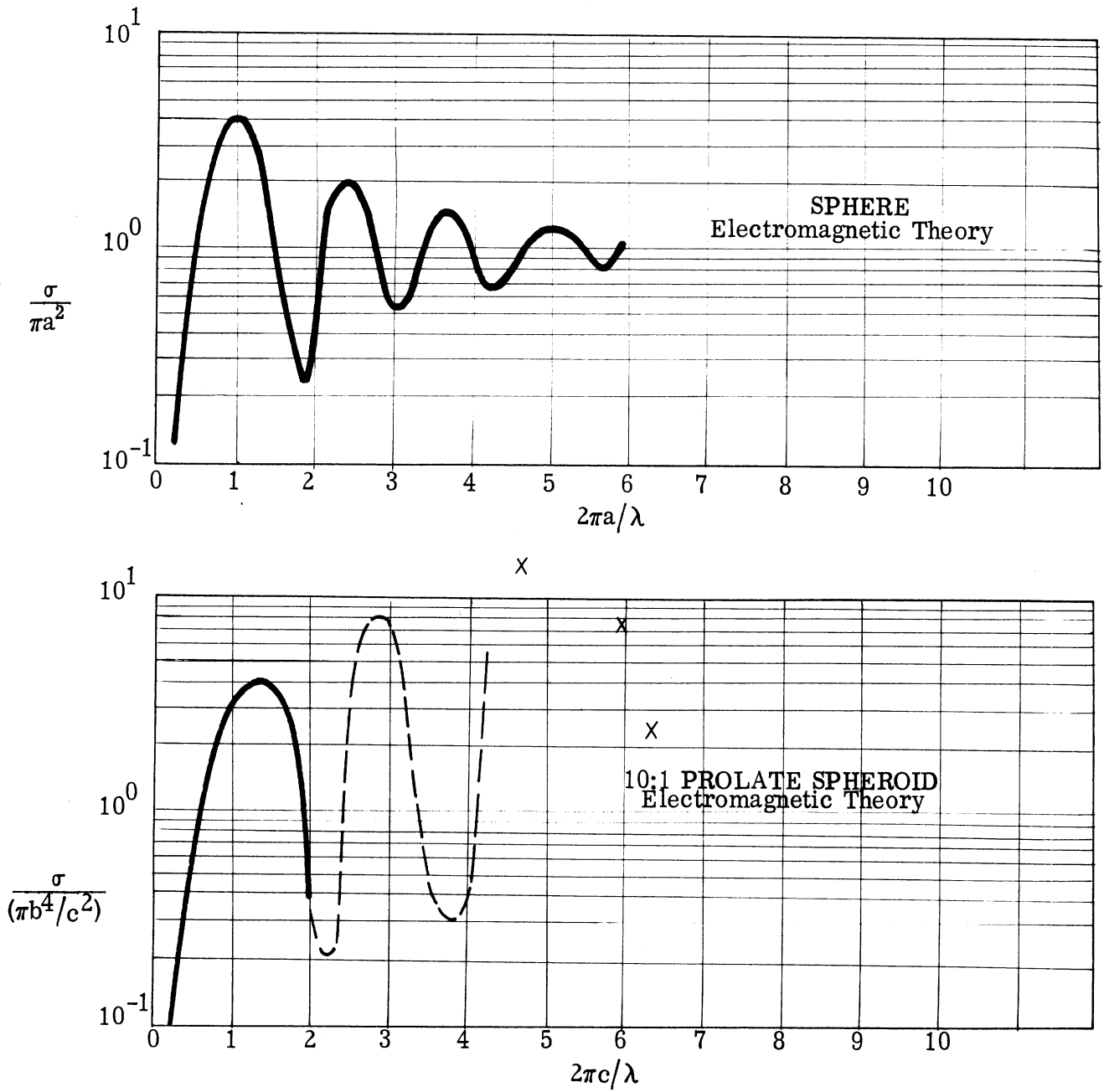


FIG. 4.2-2: CROSS SECTIONS OF THE SPHERE AND THE 10:1 PROLATE SPHEROID IN THE RESONANCE REGION

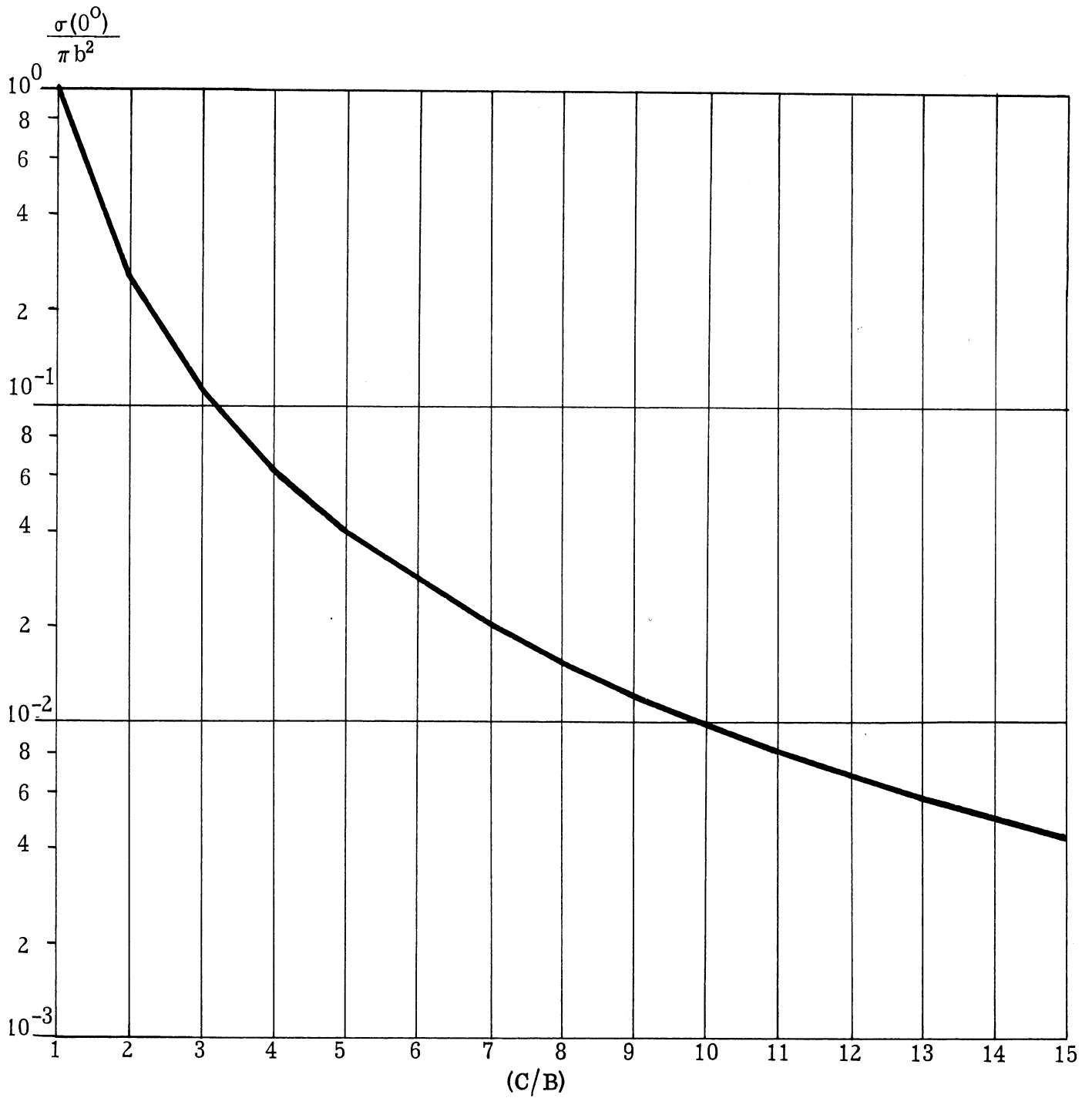


FIG. 4.2-3: RADAR CROSS SECTION OF A PROLATE SPHEROID (OPTICS) - THE NOSE-ON CROSS SECTION AS A FUNCTION OF THE LENGTH-TO-WIDTH RATIO (see equation (4.2.3))

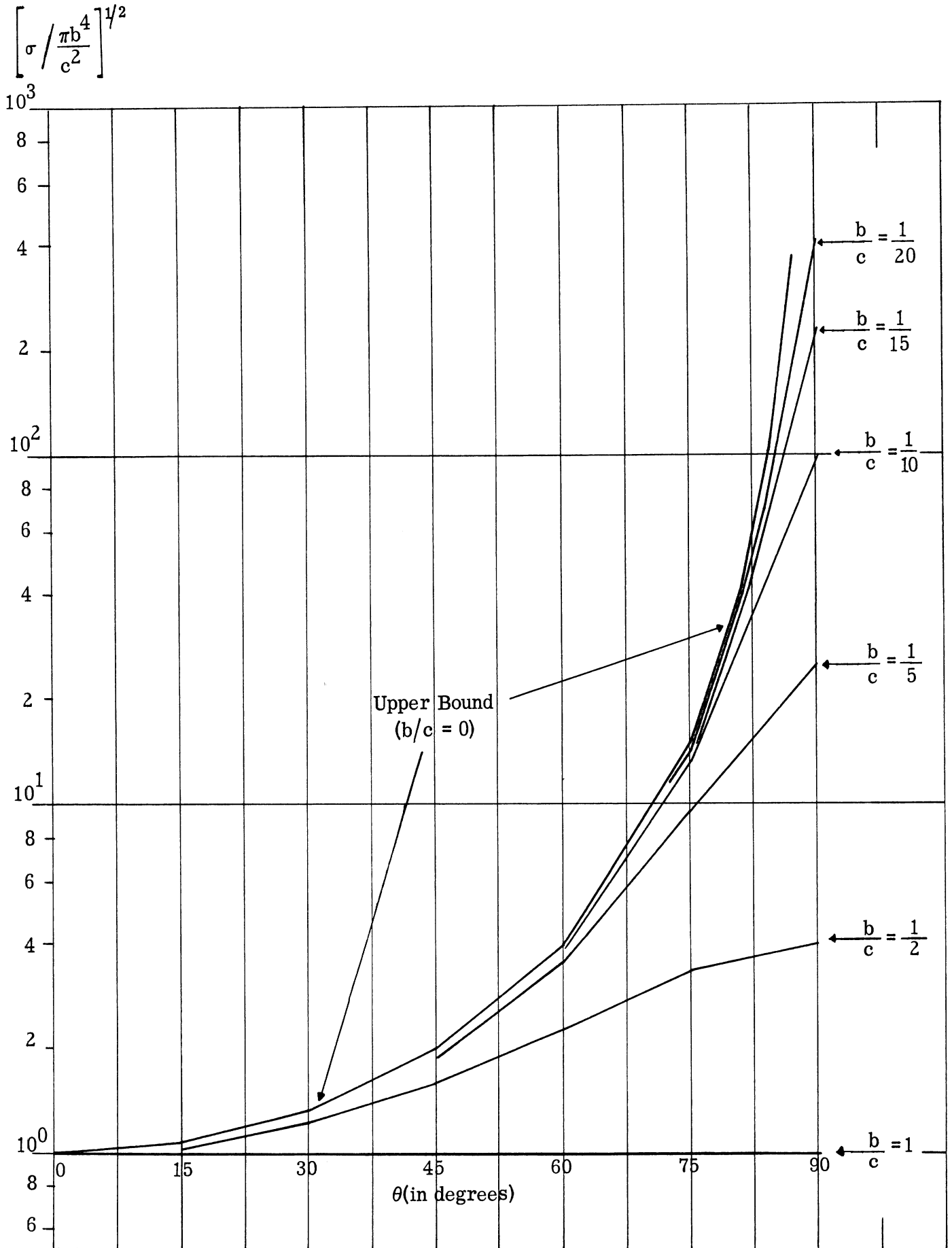


FIG. 4.2-4: RADAR CROSS SECTION OF A PROLATE SPHEROID (OPTICS) - $\sigma(\theta)/\sigma(0^\circ)$ AS A FUNCTION OF θ AND THE LENGTH-TO-WIDTH RATIO (see equation (4.2.3))

obtained at the University of California (Elect. Res. Lab., Quarterly Progress Report, 1 April - 30 June 1958; Series No. 60, Issue No. 21; 15 July 1958). In terms of the notation of equation (4.2.2), the experimental parameters were $a = b = 2\lambda$, $c/\lambda = 1.5, 1.0, 0.75, 0.50$, and 0.25 . The aspect can be defined by taking $\theta = 90^\circ$ and $\phi = 0^\circ$. In the experiment, which was conducted at 9340 Mc, the incident electric field was polarized along the minor axis and a three-inch diameter sphere was used as a standard. The results of the experiment and the theoretical value of cross section (compared to the return from the sphere) are shown in the following table:

RADAR CROSS SECTION OF OBLATE SPHEROIDS - THEORY AND EXPERIMENT
(in db above the return from a 3" diameter sphere)

a, b	c	Cross Section		
		Experimental		Theoretical
		Measured	Ave.	
2λ	1.5 λ	3.7	3.2	1
		4.2		
		2.7		
		3.3		
2λ	1.0 λ	-0.2	0	-.8
		0		
		0.2		
2λ	0.75λ	-3.4	-4.2	-4.0
		-4.3		
		-4.0		
		-4.2		
2λ	0.50λ	-9.6	-10.2	-7.5
		-10.0		
		-10.6		
		-10.6		
2λ	0.25λ	-15.0	-14.5	-13.6
		-14.2		
		-14.7		
		-14.4		

4.3 The Truncated Elliptic Cone*

The truncated elliptic cone has proved to be very useful in modeling wing surfaces and portions of fuselage surfaces. The truncated cone is placed in the coordinate system shown in Figure 4.3-1; the cone is assumed to be truncated by the planes $z = L_1$ and $z = L_2$ with $L_2 > L_1$. The half-angle of the cone in the xz -plane is taken to be α (i. e. $\tan \alpha = \frac{a}{L_2}$). The ratio of a to b is given by η and the direction to the transmitter-receiver is specified as shown in Figure 4.2-1. The equation of the cone is taken as

$$x^2 + \eta^2 y^2 = z^2 \tan^2 \alpha \quad (4.3.1)$$

with $\eta = \frac{a}{b}$.

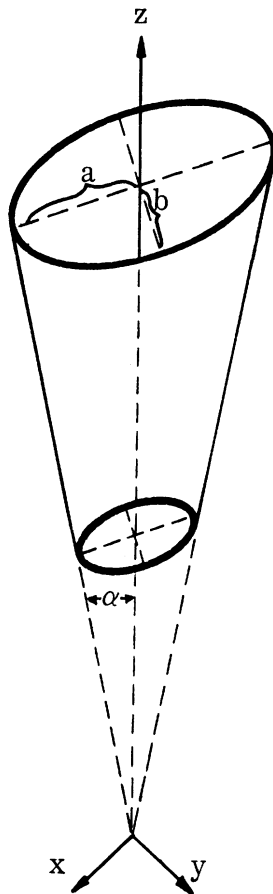


FIG. 4.3-1: THE TRUNCATED ELLIPTIC CONE

* See Appendix B for a discussion of the finite cone at the nose-on aspect.

This can be written in the parametric form

$$\begin{aligned}
 x' &= z' \tan \alpha \cos \phi' \\
 y' &= \left(\frac{z'}{\eta} \right) \tan \alpha \sin \phi' \\
 z' &= z'.
 \end{aligned} \tag{4.3.2}$$

A small displacement on the surface can be written as

$$\begin{aligned}
 \vec{ds} &= dx' \hat{i}_x + dy' \hat{i}_y + dz' \hat{i}_z = \\
 &(\tan \alpha \cos \phi' \hat{i}_x + \frac{1}{\eta} \tan \alpha \sin \phi' \hat{i}_y + \hat{i}_z) dz' + \\
 &(-\sin \phi' \hat{i}_x + \frac{1}{\eta} \cos \phi' \hat{i}_y) z' \tan \alpha d\phi'.
 \end{aligned} \tag{4.3.3}$$

The surface area element is (from equation 4.3.3)

$$\begin{aligned}
 d\vec{S} &= \left[(-\sin \phi' \hat{i}_x + \frac{1}{\eta} \cos \phi' \hat{i}_y) z' \tan \alpha d\phi' \right] \times \\
 &\left[(\tan \alpha \cos \phi' \hat{i}_x + \frac{1}{\eta} \tan \alpha \sin \phi' \hat{i}_y + \hat{i}_z) dz' \right] \\
 &= z' \tan \alpha \left(\frac{\cos \phi'}{\eta} \hat{i}_x + \sin \phi' \hat{i}_y - \frac{\tan \alpha}{\eta} \hat{i}_z \right) d\phi' dz'.
 \end{aligned} \tag{4.3.4}$$

The projection of this on the direction of incidence is

$$\begin{aligned}
 dA &= z' \tan \alpha d\phi' dz' \left(\frac{\cos \phi'}{\eta} \hat{i}_x + \sin \phi' \hat{i}_y - \frac{\tan \alpha}{\eta} \hat{i}_z \right) \cdot \\
 &(\sin \theta \cos \phi' \hat{i}_x + \sin \theta \sin \phi' \hat{i}_y + \cos \theta \hat{i}_z) \\
 &= z' \tan \alpha d\phi' dz' \left(\frac{1}{\eta} \sin \theta \cos \phi' \cos \phi' + \sin \theta \sin \phi' \sin \phi' - \frac{1}{\eta} \cos \theta \tan \alpha \right)
 \end{aligned} \tag{4.3.5}$$

where the polar angles θ and ϕ are shown in Figure 4.2-1. The phase factor

on the surface is

$$\begin{aligned}
 e^{2ik\rho} &= \exp. \left[-2ik(\sin \theta \cos \phi' \hat{i}_x + \sin \theta \sin \phi' \hat{i}_y + \cos \theta \hat{i}_z) \cdot (x' \hat{i}_x + y' \hat{i}_y + z' \hat{i}_z) \right] \\
 &= \exp. \left[-2ikz'(\sin \theta \cos \phi' \tan \alpha \cos \phi' + \frac{1}{\eta} \sin \theta \sin \phi' \tan \alpha \sin \phi' + \cos \theta) \right].
 \end{aligned} \tag{4.3.6}$$

The physical optics integral is $g = \int e^{2ik\rho} dA$. There is a stationary phase point at (the other stationary phase point is not on the illuminated side of the cone)

$$\begin{aligned} \frac{\partial}{\partial \phi'} (\sin\theta \cos\phi \tan\alpha \cos\phi' + \frac{1}{\eta} \sin\theta \sin\phi \tan\alpha \sin\phi' + \cos\theta) \\ = \sin\theta \tan\alpha (-\cos\phi \sin\phi' + \frac{1}{\eta} \sin\phi \cos\phi') = 0 \end{aligned}$$

or

$$\sin\phi' = \frac{\sin\phi}{\sqrt{\sin^2\phi + \eta^2 \cos^2\phi}} ; \quad \cos\phi' = \frac{\cos\phi}{\sqrt{\sin^2\phi + \eta^2 \cos^2\phi}} . \quad (4.3.7)$$

Evaluation of the integration with respect to ϕ' by the method of stationary phase gives

$$\begin{aligned} g \approx \int_{L_1}^{L_2} \sqrt{\frac{\pi \eta z' \tan\alpha}{k \sin\theta \sqrt{\sin^2\phi + \eta^2 \cos^2\phi}}} \left(\frac{\sin\theta}{\sqrt{\sin^2\phi + \eta^2 \cos^2\phi}} - \frac{1}{\eta} \cos\theta \tan\alpha \right) \\ \times \left(e^{-2ikz' \left(\frac{1}{\eta} \sin\theta \tan\alpha \sin^2\phi + \eta^2 \cos^2\phi + \cos\theta \right) - \frac{\pi i}{4}} \right) dz' . \end{aligned} \quad (4.3.8)$$

Unless the factor $\frac{1}{\eta} \sin\theta \tan\alpha \sin^2\phi + \eta^2 \cos^2\phi + \cos\theta$ is nearly zero (normal incidence) we may integrate this by parts and neglect the new integral compared with the constant terms (this is a way of evaluating the two contributions which come from the points $z = L_1$ and $z = L_2$) to obtain

$$\begin{aligned} g \approx \sqrt{\frac{\pi \eta z' \tan\alpha}{k \sin\theta \sqrt{\sin^2\phi + \eta^2 \cos^2\phi}}} \left(\frac{\sin\theta}{\sqrt{\sin^2\phi + \eta^2 \cos^2\phi}} - \frac{1}{\eta} \cos\theta \tan\alpha \right) \\ \times \left(\frac{e^{-2ikz' \left(\frac{1}{\eta} \sin\theta \tan\alpha \sqrt{\sin^2\phi + \eta^2 \cos^2\phi} + \cos\theta \right) - \frac{\pi i}{4}}}{-2ik \left(\frac{1}{\eta} \sin\theta \tan\alpha \sqrt{\sin^2\phi + \eta^2 \cos^2\phi} + \cos\theta \right)} \right) \Bigg|_{L_1}^{L_2} . \end{aligned} \quad (4.3.9)$$

Evaluation at the two limits gives the two contributions to the cross section. At normal incidence the phase factor is a constant and equation (4.3.8) integrates to give:

$$g \approx \frac{2(L_2^{3/2} - L_1^{3/2})}{3} \sqrt{\frac{\pi \eta \tan \alpha}{k \sin \theta \sqrt{\sin^2 \phi + \eta^2 \cos^2 \phi}}} \left(\frac{\sin \theta}{\sqrt{\sin^2 \phi + \eta^2 \cos^2 \phi}} - \frac{1}{\eta} \cos \theta \tan \alpha \right). \quad (4.3.10)$$

From the above we obtain expressions for the cross section which are applicable only for $\sin \theta > \sin \alpha$. At normal incidence the cross section is given

by

$$\sigma = \frac{8\pi (L_2^{3/2} - L_1^{3/2})^2 \tan^4 \alpha}{9\lambda \eta^2 |\cos^3 \theta|} \quad (4.3.11)$$

where normal incidence is defined to be the direction given by

$$\tan \theta = - \frac{\eta}{\tan \alpha \sqrt{\sin^2 \phi + \eta^2 \cos^2 \phi}}. \quad (4.3.12)$$

For non-normal incidence there are two independent scatterers, the ends of the cone. If one of the ends of the cone is smoothly rounded then at non-normal incidence its contribution would have to be computed by means of a formula for the rounded end (for example the ellipsoid formula). The two contributions are given by

$$\sigma = \frac{\lambda L \eta^3 \tan \alpha}{8\pi \sin \theta \sqrt{\sin^2 \phi + \eta^2 \cos^2 \phi}} \left\{ \frac{\frac{\sin \theta}{\sqrt{\sin^2 \phi + \eta^2 \cos^2 \phi}} - \frac{1}{\eta} \cos \theta \tan \alpha}{\sin \theta \tan \alpha \sqrt{\sin^2 \phi + \eta^2 \cos^2 \phi} + \eta \cos \theta} \right\}^2 \quad (4.3.13)$$

where L has the value L_1 or L_2 depending on whether the contribution is from the small end or the large end of the cone.

For the truncated circular cone ($\eta = 1$), equations (4.3.11) and (4.3.12)

become

$$\sigma = \frac{8\pi}{9\lambda} \left[L_2^{3/2} - L_1^{3/2} \right]^2 \frac{\sin\alpha}{\cos^4\alpha} \quad (4.3.14)$$

and

$$\sigma = \left[\frac{\lambda L \tan \alpha}{8 \pi \sin \theta} \right] \tan^2 (\theta - \alpha) \quad (4.3.15)$$

A graphical presentation of equation (4.3.14) is given in Figure 4.3.2 and a graphical presentation of the relation between normal aspect to a cone and the angles α , θ , and ϕ is given in Figure 4.3.3.

4.4 The Cylinder and the Thin Wire

The cylinder has proved to be very useful in modeling portions of a fuselage, a wing tank, an engine nacelle, etc. Very thin cylinders, that is circular cylinders whose radii are very small in comparison with the wavelength, have been extremely useful in modeling the sharp edges of some wing surfaces; these very thin cylinders are referred to here as thin wires.

For the case in which the wavelength is small in comparison with both the length and the radius of the cylinder, the cross section formulas can be obtained as limiting cases of the results obtained for the truncated elliptic cone (i.e., equations (4.3.11) and (4.3.13)). To accomplish this let $\tan \alpha = \frac{a}{L_2}$, $L_1 = L_2 - L$, $L_2 \rightarrow \infty$. The results obtained are for the cylinder at normal incidence ($\theta = 90^\circ$)

$$\sigma = \frac{2\pi L^2 a^2 b^2}{\lambda \left[a^2 \cos^2\phi + b^2 \sin^2\phi \right]^{3/2}} \quad (4.4.1)$$

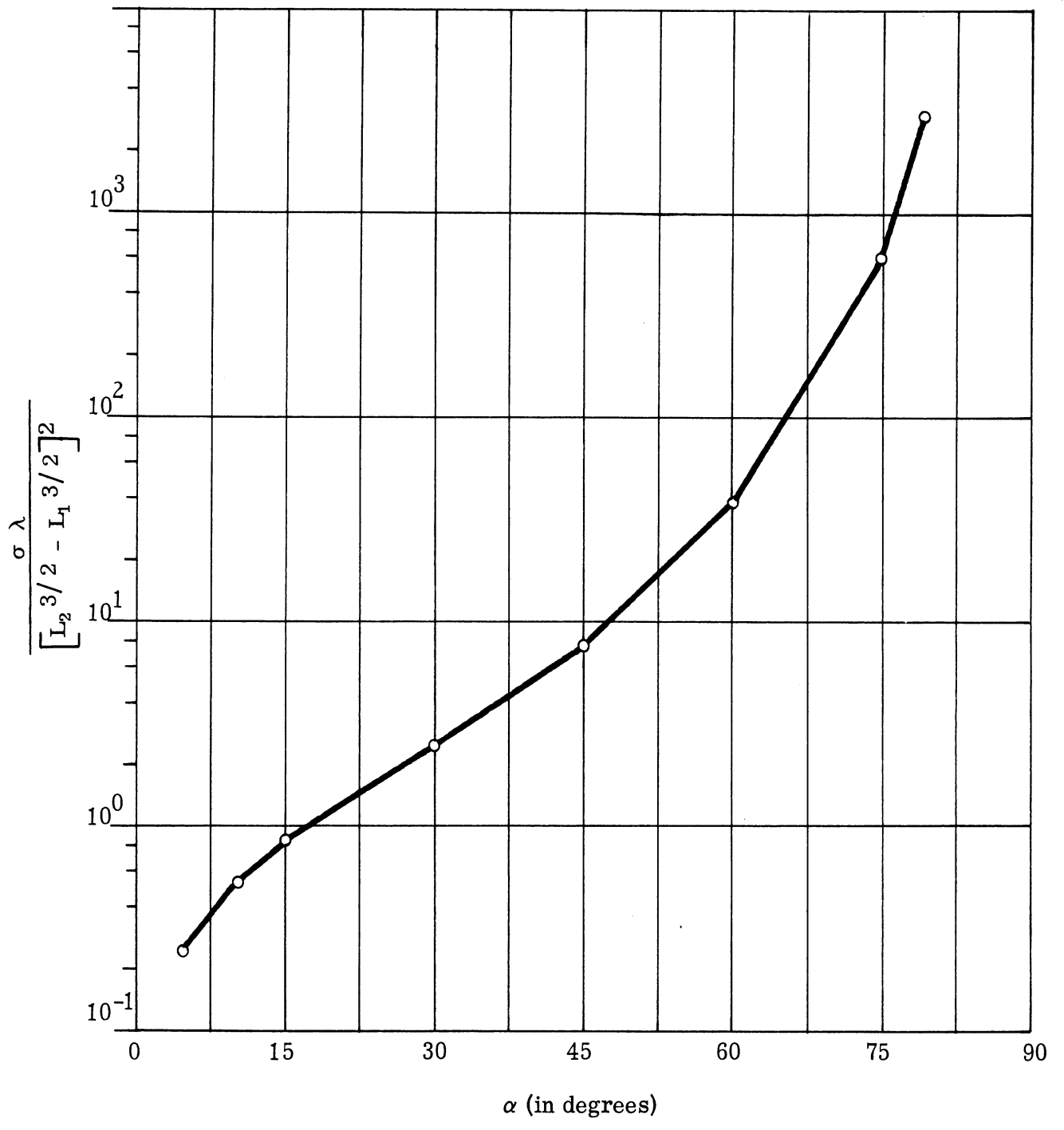


FIG. 4.3-2: CROSS SECTION OF A TRUNCATED CIRCULAR CONE AT NORMAL ASPECT AS A FUNCTION OF THE HALF-ANGLE α

$$-\tan \theta \tan \alpha = \frac{\eta}{\sin^2 \phi + \eta^2 \cos^2 \phi}$$

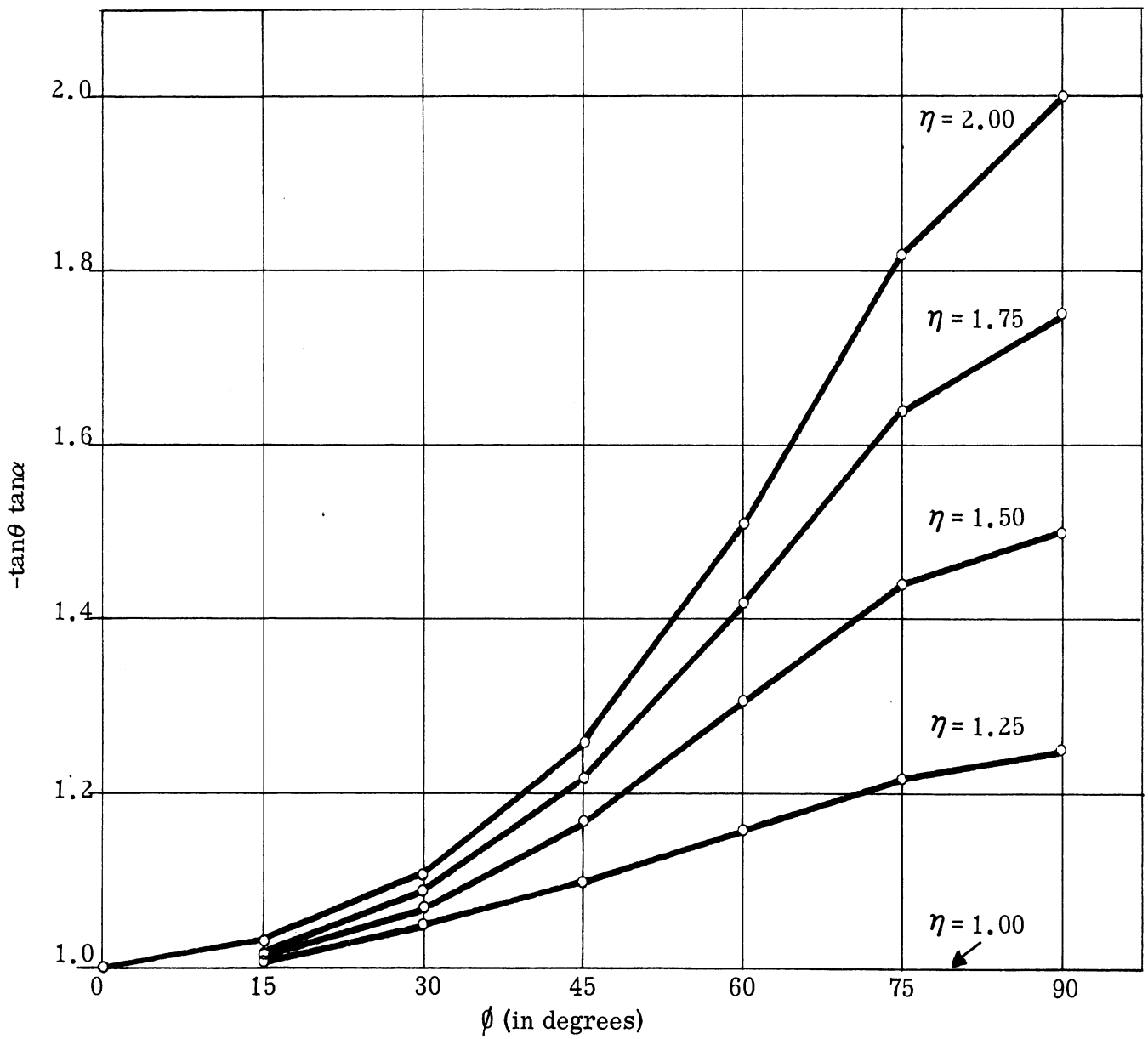


FIG. 4.3-3: NORMAL ASPECT TO A TRUNCATED ELLIPTIC CONE - RELATION BETWEEN THE ASPECT ANGLES θ AND ϕ AND THE CONE ANGLE α

and for non-normal incidence we have two components (assuming that the ends are not rounded or smoothed in any manner) each equal to

$$\sigma = \frac{\lambda a^2 b^2 \sin\theta}{8\pi \cos^2\theta \left[a^2 \cos^2\phi + b^2 \sin^2\phi \right]^{3/2}} \quad (4.4.2)$$

For a circular cylinder these expressions reduce to

$$\sigma = \frac{2\pi L^2 a}{\lambda} \quad (4.4.3)$$

and

$$\sigma = \frac{\lambda a \sin\theta}{8\pi \cos^2\theta} \quad (4.4.4)$$

respectively.

The application of equation (3.17) will yield an expression for the cross section at the off-normal aspects which incorporates the phase between the contributions from the two ends of the cylinder. The expression is more complicated and not so convenient to apply as those given above, but if knowledge of the oscillations in the cross section as a function of aspect is required, this result can prove to be extremely valuable. The expression so obtained for a circular cylinder of length L and radius a is

$$\sigma = \pi a^2 \sin^2\theta \left(\frac{\sin(kL \cos\theta)}{\cos\theta} \right)^2 (A^2 + B^2) \quad (4.4.5)$$

where

$$A = J_1(2ka \sin\theta) \text{ with } J_1 \text{ the Bessel function of the first order,}$$

$$B = (2/\pi) - S_1(2ka \sin\theta) \text{ with } S_1 \text{ the Struve function of the first order,}$$

$$\theta = \text{the angle between the cylinder axis and the direction of incidence.}^*$$

*As an aid to computation the expression $(A^2 + B^2)$ is presented graphically as a function of $(a \sin\theta / \lambda)$ in Figures 4.4-1 and 4.4-2.

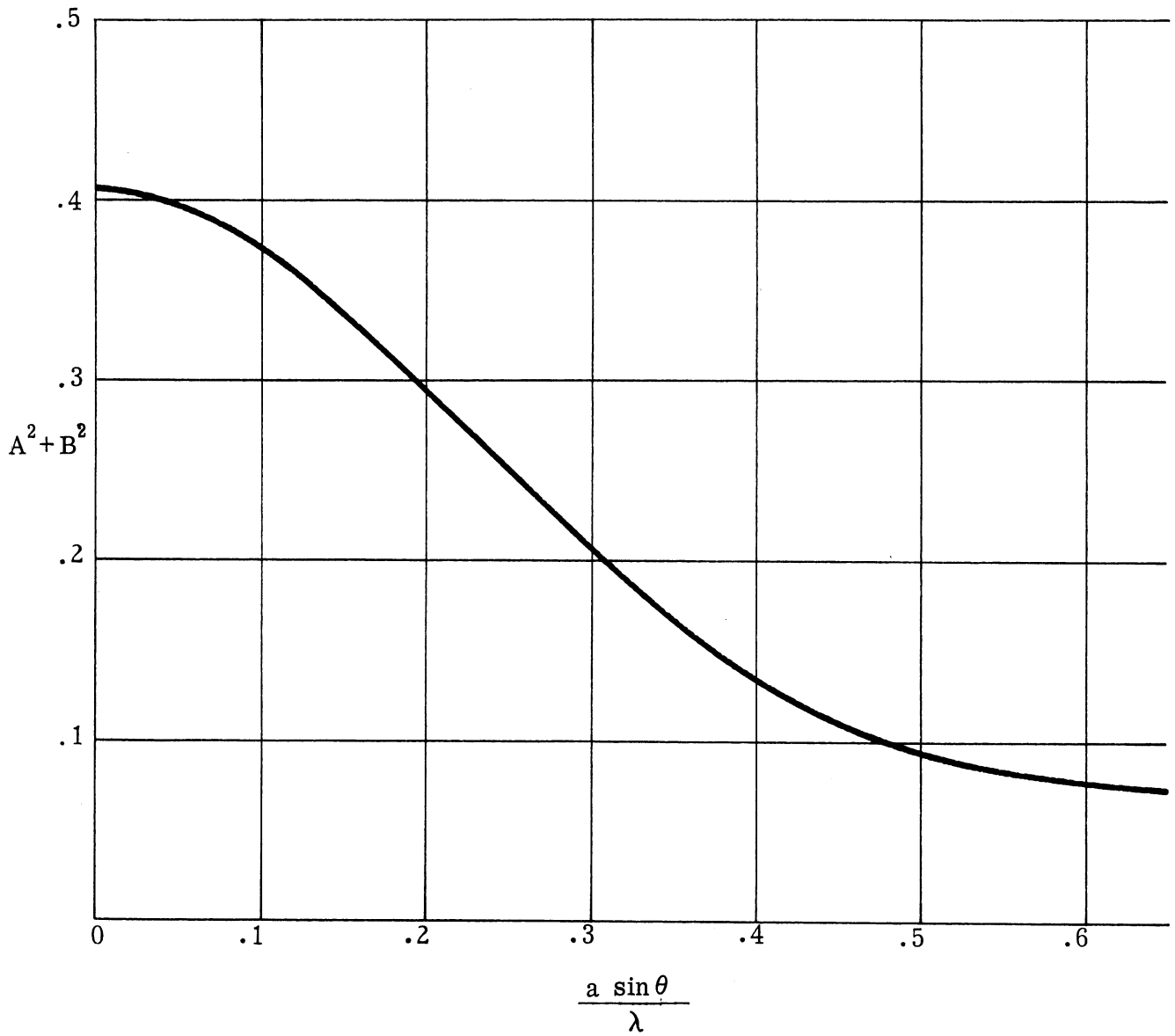


FIG. 4.4-1: THE EXPRESSION $(A^2 + B^2)$ OF EQUATION (4.4.5) - I

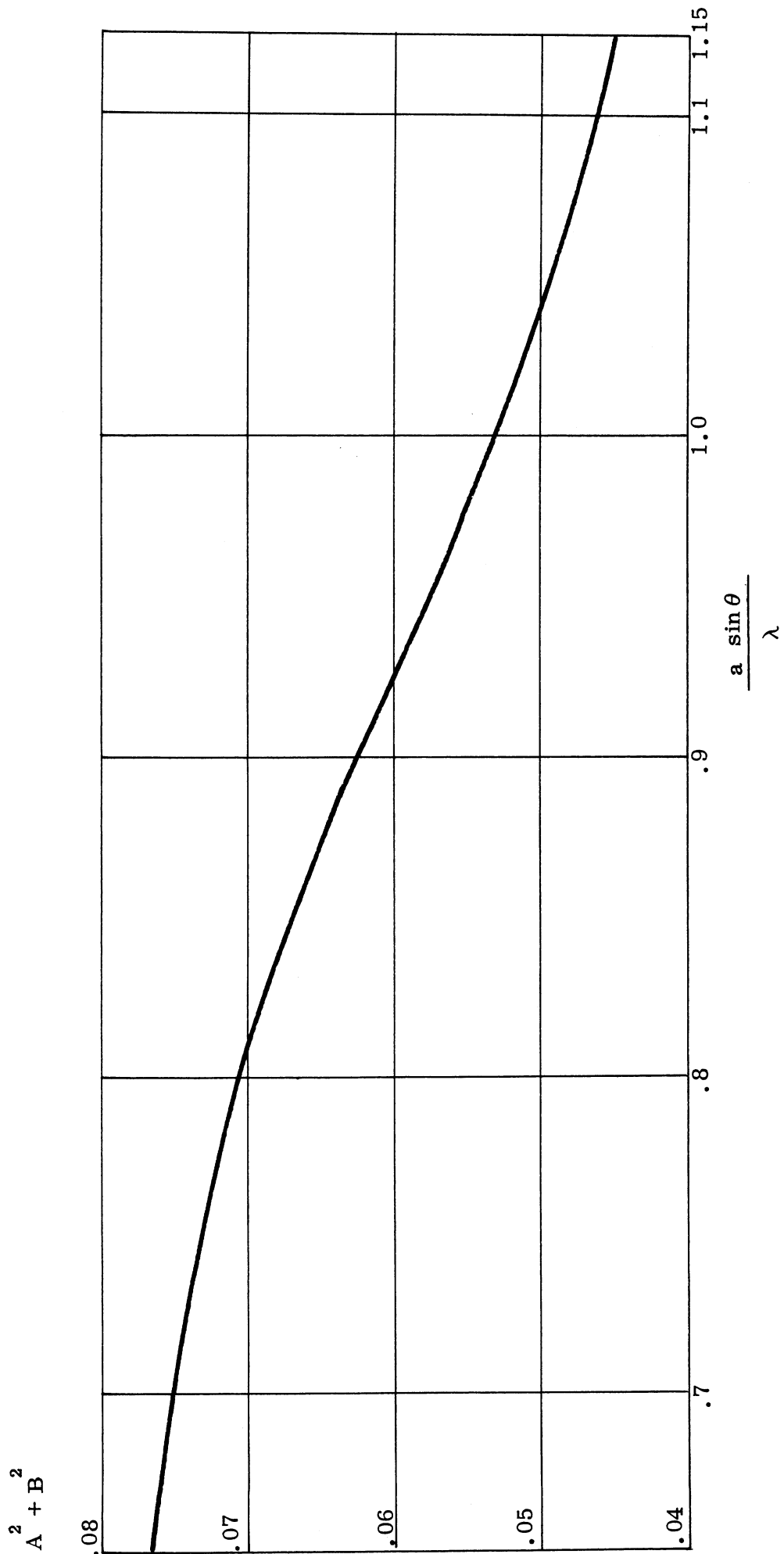


FIG. 4.4-2: THE EXPRESSION ($A^2 + B^2$) OF EQUATION (4.4.5) - II

The above is for cylinders whose dimensions are large in comparison with the wavelength; let us now turn our attention to the case in which the radius, a , is very small in terms of the wavelength; i.e., to the thin wire case.

We will consider first the cross section of a perfectly conducting wire which is many wavelengths long but only a fraction of a wavelength thick. Perhaps the simplest formula which is in good agreement with experiment is Chu's formula (Ref. 9)

$$\sigma_e = \sigma \cos^2\phi = \frac{\pi L^2 \sin^2\theta \left[\frac{\sin\left(\frac{2\pi L}{\lambda} \cos\theta\right)}{\frac{2\pi L}{\lambda} \cos\theta} \right]^2}{\left(\frac{\pi}{2}\right)^2 + \left(\ln \frac{\lambda}{\gamma \pi a \sin\theta}\right)^2} \cos^4\phi \quad (4.4.6)$$

where L is the length of the wire, a is the radius of the wire, $\gamma = 1.78\dots$, θ is the angle between the wire and the direction of incidence, and ϕ is the angle between the polarization direction and the plane formed by the wire and the direction of incidence. No attempt will be made here to derive this formula. Except for θ near 90° the two tips of the wire scatter essentially independently. A slight change in θ has a pronounced effect on the relative phase of the two components so that there is a rapid oscillation, the components sometimes adding and sometimes cancelling. When we approximate a part of the aircraft by a thin wire we will not be able to determine the relative phase of the two components accurately so that the proper picture is to replace the wire by two independent scatterers (except for θ near 90°) each having an effective cross section given by

$$\sigma_e = \frac{\lambda^2 \tan^2 \theta \cos^4 \phi}{16\pi \left[\left(\frac{\pi}{2}\right)^2 + \left(\ln \frac{\lambda}{\gamma\pi a \sin\theta}\right)^2 \right]} . \quad (4.4.7)$$

At $\theta = 90^\circ$ equation (4.4.7) diverges while equation (4.4.6) does not.

The reason for this is that at this one aspect the wire acts as a single scatterer.

For $\theta = 90^\circ$ then we must use equation (4.4.6) which reduces to:

$$\sigma_e = \frac{\pi L^2 \cos^4 \phi}{\left(\frac{\pi}{2}\right)^2 + \left(\ln \frac{\lambda}{\gamma\pi a}\right)^2} . \quad (4.4.8)$$

Now let us turn our attention to the case of wires whose length is comparable to the wavelength. The approximation technique employed here is derived from the work of Van Vleck, Bloch, and Hammermesh (Ref. 9). In Reference 9, the radar cross section, σ , the average return for fixed direction of incidence but random polarization, $\sigma(\theta)$, and the average cross section for all aspects and polarizations, $\bar{\sigma}$, are related by the following equations:

$$\bar{\sigma} = \frac{1}{4\pi} \iint \sigma \sin\theta \, d\theta \, d\phi \quad , \quad (4.4.9)$$

$$\sigma(\theta) = \frac{1}{2\pi} \int \sigma \, d\phi \quad , \quad (4.4.10)$$

$$\bar{\sigma} = \int_0^{\pi/2} \sigma(\theta) \sin\theta \, d\theta \quad , \text{ and} \quad (4.4.11)$$

$$\sigma = \frac{8}{3} \cos^4 \phi \, \sigma(\theta) \quad (4.4.12)$$

where the angle θ is as shown in Figure 4.4-3. The angle ϕ is the angle between the electric field of the incident wave and the plane formed by the direction of incidence and the wire (i.e. the plane of Figure 4.4-3).

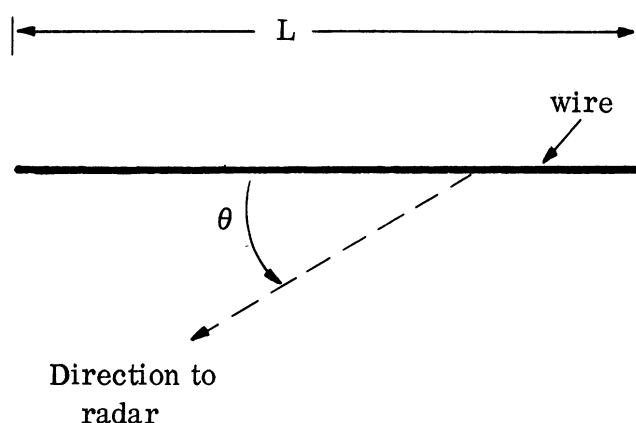
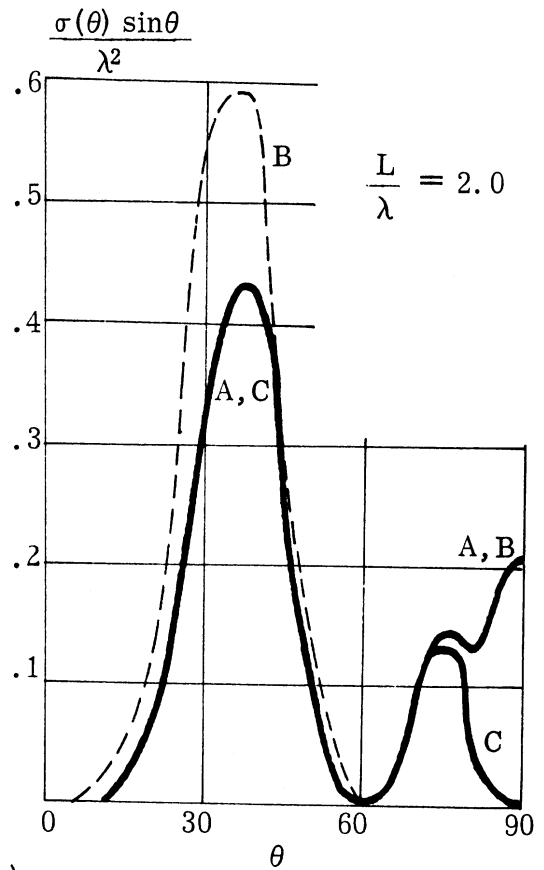
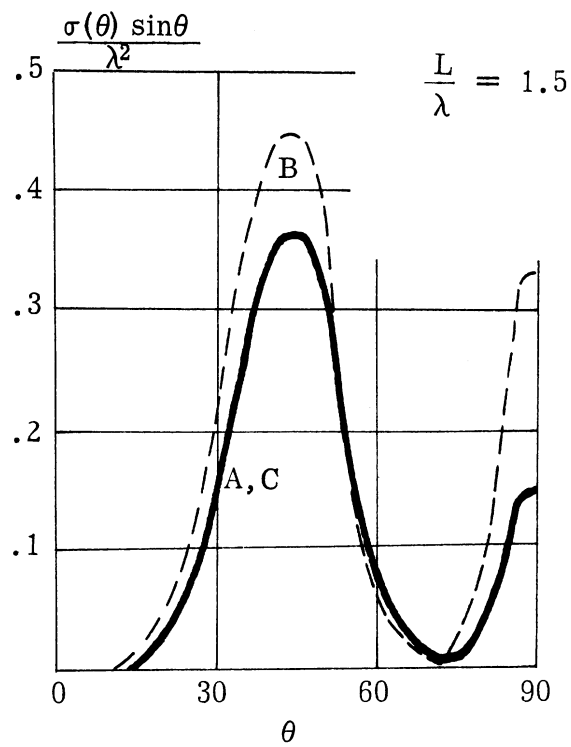
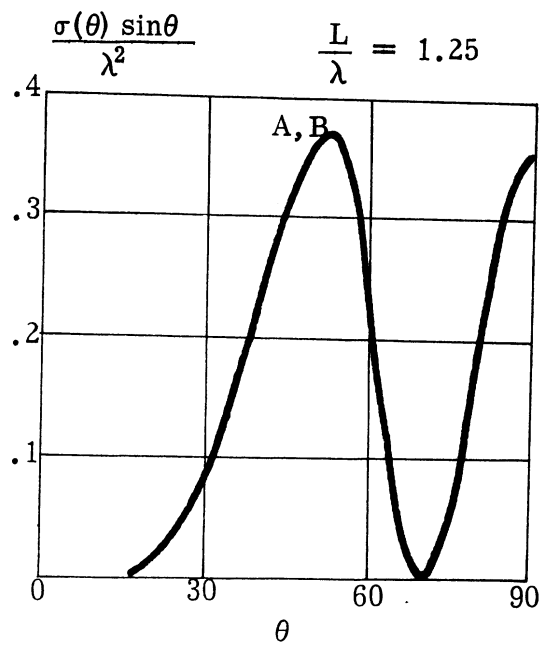
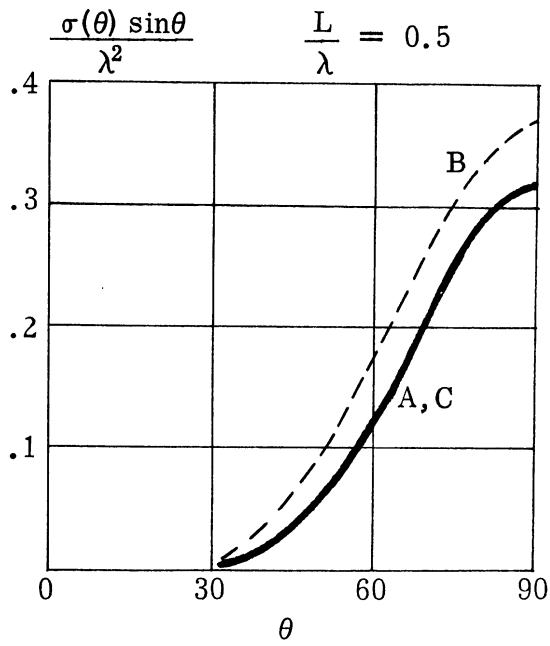


FIG. 4.4-3: THE THIN WIRE COORDINATE SYSTEM

Reference 9 contains plots of $\frac{\sigma(\theta)}{\lambda^2}$ vs θ for the case of $\frac{L}{\lambda}$ equal to 0.5, 1.5, 2.0, and 1.25. If the wire in question is one of these in size then direct readings from these plots combined with the application of equation (4.4.12) will yield the desired estimate of the cross section; these four plots are reproduced in Figure 4.4-4.

A complete presentation of Methods A and B will be found in Reference 9. All of the data presented in Figure 4.4-4 is for a wire of radius equal to $1/900$ of its length; it can be expected, however, that over a wide range of radius values these angular distributions of wire response will be appropriate. This is illustrated in Reference 9 in the determination of $\frac{\bar{\sigma}}{\lambda^2}$ for wires of three different radii: their Figure 2, which contains these results, is reproduced in Figure 4.4-5.



θ (in degrees)

FIG. 4.4-4: ANGULAR DISTRIBUTION OF RESPONSE OF WIRES (REF. 9)

($L/a = 900$ where $a =$ radius of wire; A--Method A, B--Method B, C--Chu's formula)

If other wire lengths are of interest in a specific problem one can employ either Method A or Method B as given in Reference 9, the Chu formula, or one can apply an approximation process based upon the material of Reference 9. This approximation procedure involves using the plot of $\frac{\sigma(\theta)}{\lambda^2}$, ($\theta = 90^\circ$) given in Reference 9 combined with the information presented in Reference 10 relative to angular variation in response together with equations (4.4.9) through (4.4.12).

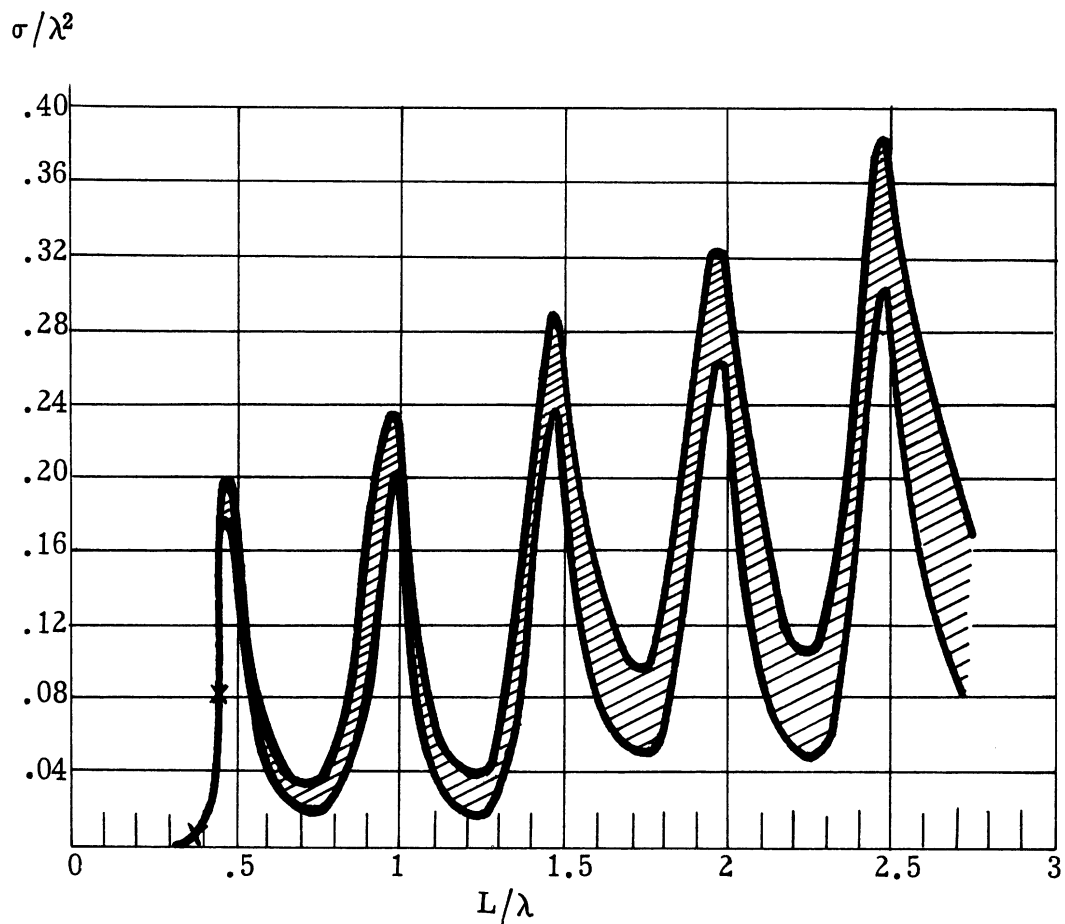


FIG. 4.4-5: RADAR RESPONSE OF WIRES - AVERAGE CROSS SECTION
($225 < L/a < 900$)

The 90° plot referred to above is shown in Figure 4.4-6 where the data of Reference 9 is compared with the Chu estimate. We see that the Chu formula suffices for wires which are more than two to three wavelengths long. The cases of wires which are one wavelength and three-fourths of a wavelength long, will be discussed to illustrate the approximation process referred to above.

For the wire of length λ we know from Reference 9 that

$$\frac{\bar{\sigma}}{\lambda^2} \approx 0.163 \quad \text{and} \quad \frac{\sigma(\theta) \sin\theta}{\lambda^2} \approx 0.04 \quad \text{at} \quad \theta = 90^\circ .$$

From Reference 10 we find that $\frac{\sigma(\theta) \sin\theta}{\lambda^2}$ takes on its maximum value at $\theta \approx 54^\circ$. Using this information together with data about the location (in θ) of the half-power points (Ref. 10), a broken line graph approximation of the curve $\frac{\sigma(\theta) \sin\theta}{\lambda^2}$ vs θ can be obtained. In doing this we employ the knowledge that

$$\int_0^{\pi/2} \frac{\sigma(\theta) \sin\theta}{\lambda^2} d\theta \approx 0.163 . \quad (4.4.13)$$

For the wire of length $3\lambda/4$ we find (from Ref. 5) that

$$\int_0^{\pi/2} \frac{\sigma(\theta) \sin\theta}{\lambda^2} d\theta \approx 0.023 \quad (4.4.14)$$

and

$$\frac{\sigma(\theta) \sin\theta}{\lambda^2} \approx 0.04 \quad \text{at} \quad \theta = 90^\circ .$$

Since a wire which is three-fourths of a wavelength long is a 'non-resonant' wire we can employ equation (19) of Reference 9 to obtain values of $\frac{\sigma(\theta) \sin\theta}{\lambda^2}$ at a few values of θ (say 30° , 60° , and 75°) and then fair a curve through these

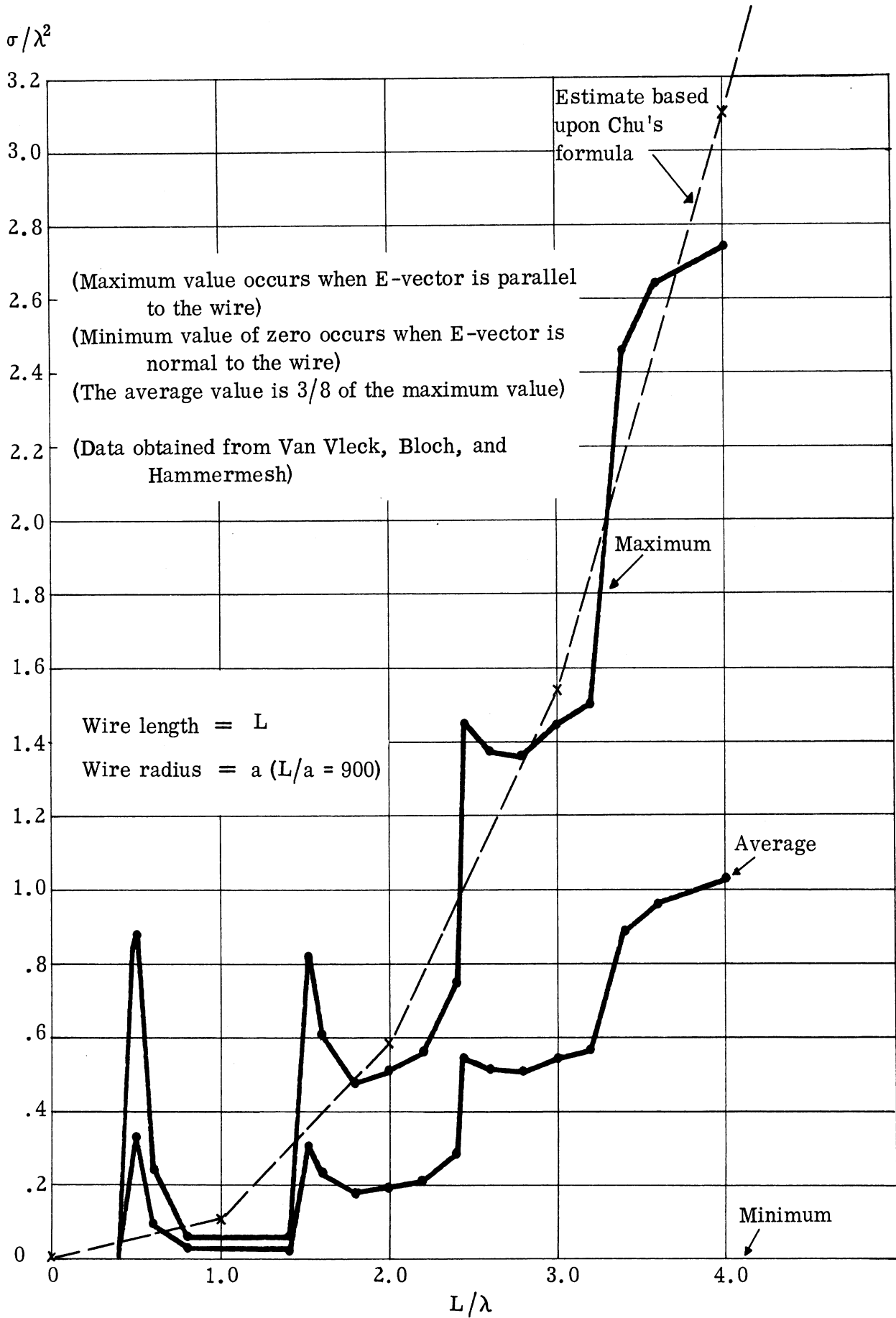


FIG. 4.4-6: RADAR CROSS SECTION OF THIN WIRES AS A FUNCTION OF WIRE LENGTH, L , ($\theta = 90^\circ$)

points using the area integral in equation (4.4.14) as a check on the resulting curve. Figure 4.4-7 shows the results obtained for these two cases; the half-wavelength wire is also included in the figure.

It should be repeated that the above considerations are based upon the analysis of wires for which $L/a = 900$. In view of the data presented in Figure 4.4-5, however, it can be concluded that these estimates should still be appropriate for a wide range of wire radii. To investigate this point further, the cross section of a thin wire is plotted as a function of wire radius for $\theta = 90^\circ$ in Figure 4.4-8. In addition to the wire estimate, the optics expression for a cylinder is extended into this region of wire radius space as well as the cylinder data obtained from Mentzer (Ref. 11). We see from Figure 4.4-8 that the cross section of a wire of given length does not change rapidly with changes in wire radius and thus that the methodology presented here for a wire whose radius is $1/900$ of its length can be considered appropriate for almost all "wire" computations which arise in connection with problems of estimating the cross section of an aircraft or a missile.

The work of Weber (Ref. 12) is also very useful in the consideration of wires whose lengths are less than 0.8λ , both for the monostatic and bistatic cases. This point will be discussed in Section 5.

Van Vleck, Bloch, and Hammermesh in Reference 9 also give some consideration to the very short wire case, a wire whose length is such that $\lambda/L \gg 10$. The expression they obtain for the cross section is (in the notation employed here)

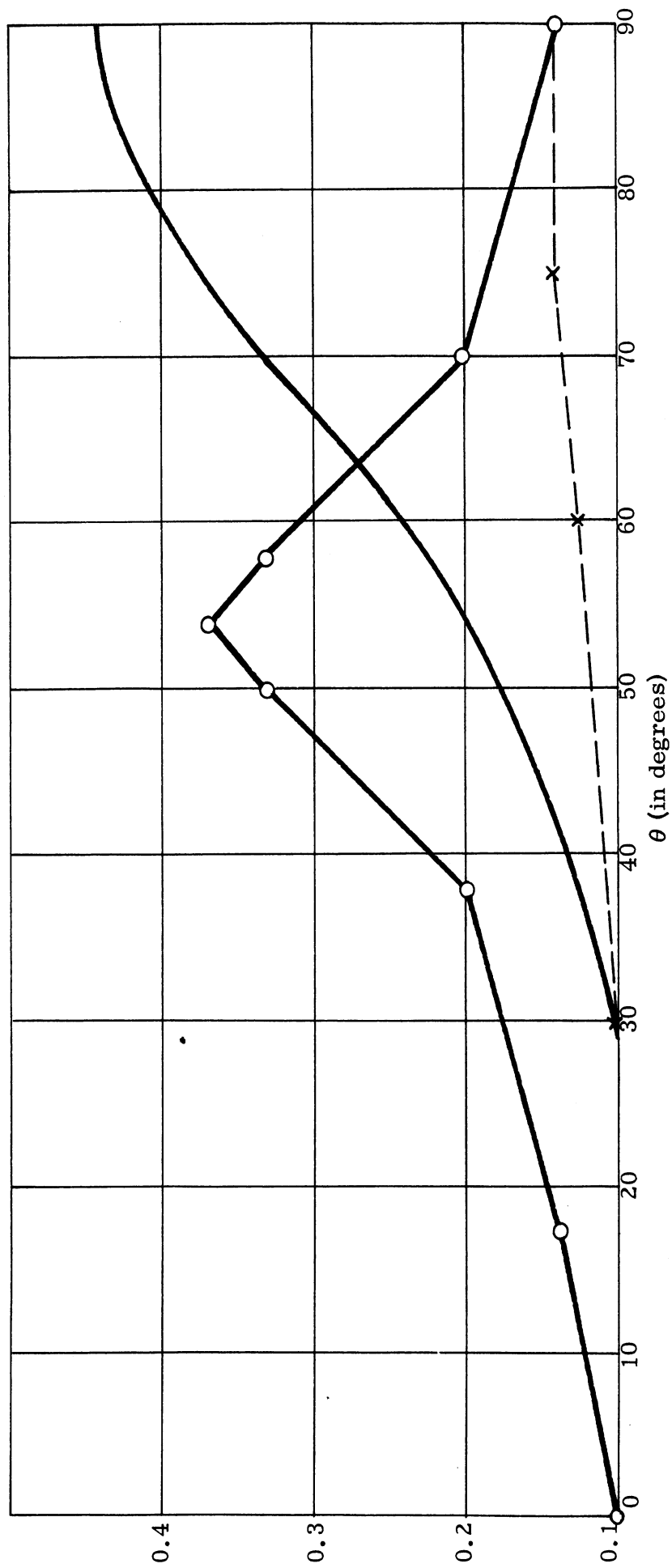
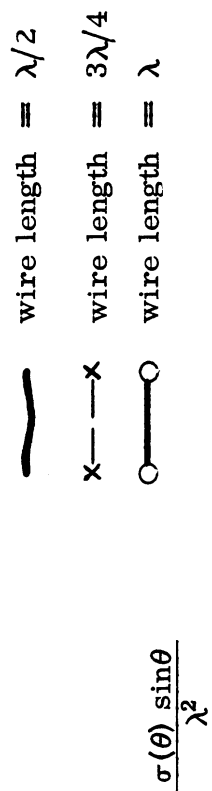


FIG. 4.4-7: $\sigma(\theta) \sin\theta/\lambda^2$ VS θ FOR THREE THIN WIRES

Wire or cylinder radius = a
 Wire or cylinder length = L

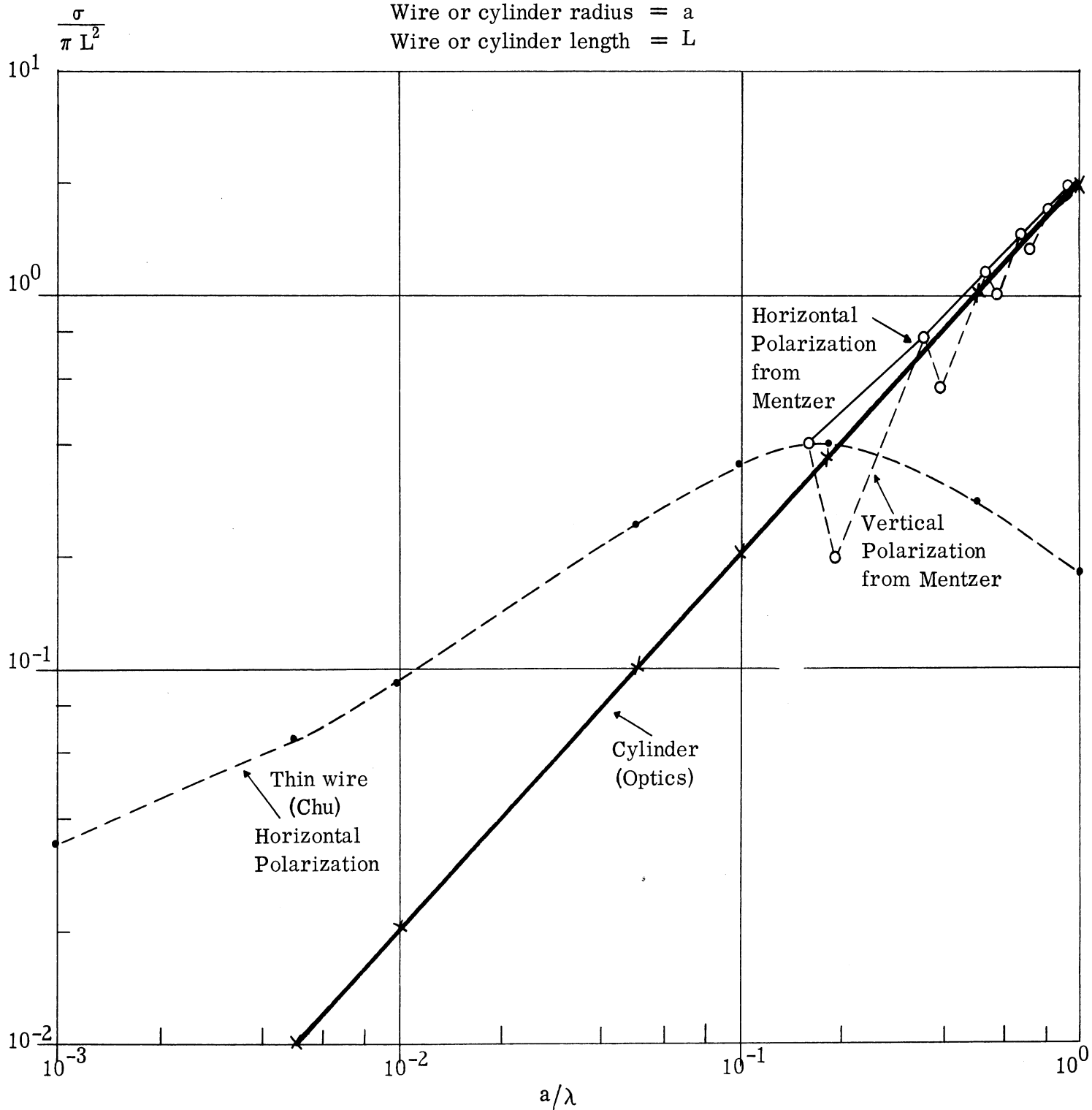


FIG. 4.4-8: BROADSIDE RETURN FROM THIN WIRES AND CYLINDERS AS A FUNCTION OF THE RADIUS

$$\sigma = \frac{(\lambda^2/9\pi) (\pi L/\lambda)^6 \cos^4 \theta \sin^4 \theta}{[1 - \ln(2L/a)]^2} \quad (4.4.15)$$

From this expression we see that if $\lambda/L \geq 10$ and $L/a \geq 10$, then it follows that $\sigma/\lambda^2 \leq 8.5 \times 10^{-6}$. The magnitude of the return from such wires is relatively so small as to make it possible to neglect such wires in most problems of determining the cross section of an aircraft or missile.

4.5 The Torus and the Wire Loop

The coordinate system employed in the analysis of the wire loop and the general torus is as shown in Figure 4.5-1; the polar angles are as given in Figure 4.2-1.

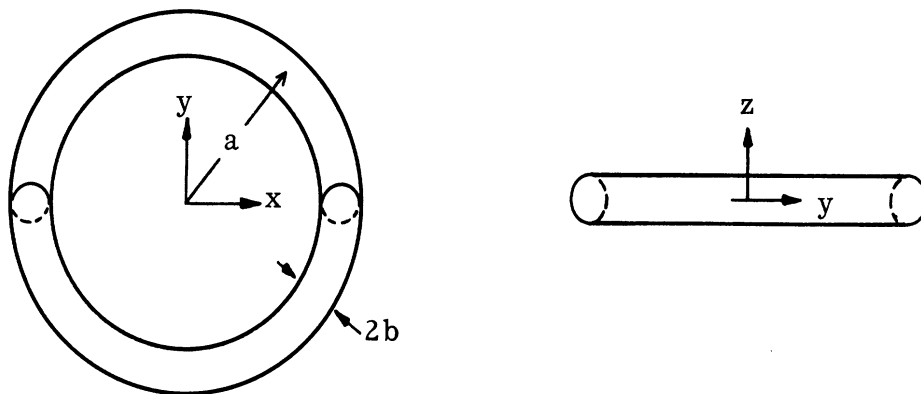


FIG. 4.5-1: TWO VIEWS OF THE TORUS (WIRE LOOP)

When the wavelength is small in comparison with both a and b we proceed as follows: For off-normal incidence the cross section is obtained by use of equations (3.25) and (3.29). The equation of the torus is taken as

$$(\rho - a)^2 + z^2 = b^2 \quad (4.5.1)$$

From equation (4.5.1) we find the ρ'' needed for equation (3.29). There are two contributions to the cross section, one where the incident wave hits the "outside" of the torus and the other where the wave hits the "inside" of the torus. In the two cases we have $\rho = a + b \sin\theta$ and $\rho = a - b \sin\theta$ respectively. Substitution in the resulting form of equation (3.29) yields the two contributions (it should be noted that the second contribution exists only if the inside of the torus is not shadowed by the outside; i.e. only if $b/(2a) < |\cos\theta|$). To obtain the expression for the normal aspect we make use of equation (3.17).

Thus, for the short wavelength case we have at normal incidence ($\theta = 0^\circ$)

$$\sigma = \frac{8\pi^3 b a^2}{\lambda} \quad (4.5.2)$$

and for $\theta > 0$ we have the two contributions

$$\sigma = \pi \left(\frac{ba}{\sin\theta} + b^2 \right) \quad (4.5.3)$$

and

$$\sigma = \pi \left(\frac{ba}{\sin\theta} - b^2 \right) . \quad (4.5.4)$$

In the range $0 \leq |\cos\theta| < b/(2a)$ the second contribution (eq. 4.5.4) is no longer present.

If b is very small in comparison to the wavelength the torus takes on the form of a wire loop. The cross section of a wire loop takes on a resonant peak in the vicinity of $ka = 1$ and the magnitude of the cross section at this peak is relatively independent of the wire radius. To obtain an estimate of the cross section of a wire loop on the optics side of this resonant peak we extend the methods used on the "straight thin wire". We shall do this first for a wire

which has a radius of about $1/85$ of a wavelength (a value chosen for convenience in computation) after which we shall consider the case for arbitrary (but small) values of b .

The scattered field from a small straight piece of a thin wire is like that of a dipole so that it has the form

$$\mathbf{E}_s = C \, d\ell \, \hat{\mathbf{R}} \times (\hat{\mathbf{R}} \times \hat{\boldsymbol{\ell}}) \frac{e^{ikR}}{R} \quad (4.5.5)$$

where C is a constant to be determined, $d\ell$ is the length of the piece of wire, $\hat{\mathbf{R}}$ is the vector from the piece of wire to the field point, and $\hat{\boldsymbol{\ell}}$ is a unit vector along the piece of wire. At normal incidence with the polarization parallel to $\hat{\boldsymbol{\ell}}$, the cross section is

$$\sigma = \lim_{r \rightarrow \infty} 4\pi r^2 \left| \frac{\hat{\mathbf{E}}_s}{\hat{\mathbf{E}}_i} \right|^2 = \frac{(d\ell)^2}{\pi}. \quad (4.5.6)*$$

If $\hat{\mathbf{p}}$ is the polarization vector then C is proportional to $\hat{\mathbf{p}} \cdot \hat{\boldsymbol{\ell}}$. Thus let $C = C_1 (\hat{\mathbf{p}} \cdot \hat{\boldsymbol{\ell}})$. For the case to which equation (4.5.6) applies we have $\hat{\mathbf{p}} \cdot \hat{\boldsymbol{\ell}} = |\hat{\mathbf{R}} \times (\hat{\mathbf{R}} \times \hat{\boldsymbol{\ell}})| = 1$. Substitution of equation (4.5.5) into equation (4.5.6) gives

$$\frac{(d\ell)^2}{\pi} = \frac{4\pi |C_1|^2 (d\ell)^2}{|\hat{\mathbf{E}}_i|^2} \quad (4.5.7)$$

*

It is here that the assumption that the wire radius is $\lambda/85$ is made. The expression on the right side of the equation is obtained from the Chu formula for a wire radius set equal to $\lambda/85$.

Substitution back finally gives (taking into account the phase leg in making the round trip from the radar to the wire and back to the radar)

$$\vec{E}_s = \frac{\hat{p} \cdot \hat{\ell}}{2\pi} |\vec{E}_i| d\ell \frac{\hat{R} \times (\hat{R} \times \hat{\ell})}{R} e^{2ikR} \quad (4.5.8)$$

Thus, corresponding to the physical optics formula for the cross section (equation 3.17), we have, in the case of a thin wire

$$\sigma = \frac{1}{\pi} |\vec{g}|^2; \quad \sigma_e = \frac{1}{\pi} |\hat{p} \cdot \vec{g}|^2$$

where,

$$\vec{g} = \int (\hat{p} \cdot \hat{\ell}) \hat{R} \times (\hat{R} \times \hat{\ell}) e^{2i\vec{k} \cdot \vec{r}'} d\ell \quad (4.5.9)$$

Due to the relation $\hat{p} \cdot \hat{R} = 0$ we can also write

$$\sigma_e = \frac{1}{\pi} \left| \int (\hat{p} \cdot \hat{\ell})^2 e^{2i\vec{k} \cdot \vec{r}'} d\ell \right|^2 \quad (4.5.10)$$

The integration in both equation (4.5.9) and (4.5.10) is taken along the wire. The edge of a truncated ogive gives a thin wire contribution where the thin wire is a loop in the x-y plane as shown in Figure 4.5-2. The thin wire contribution is given in general by equation (4.5.10). To evaluate this for a loop consider that on the wire we have $x' = a \cos\phi'$, $y' = a \sin\phi'$, and $d\ell = \sqrt{dx'^2 + dy'^2} = a d\phi'$, $\hat{k} = \hat{i}_x \sin\theta + \hat{i}_z \cos\theta$. The direction of the dipole is $\hat{\ell} = -\sin\phi' \hat{i}_x + \cos\phi' \hat{i}_y$. We have $\hat{k} \cdot \vec{r}' = (x' \hat{i}_x + y' \hat{i}_y) \cdot \hat{k} = a \sin\theta \cos\phi'$. The polarization vector is $\hat{p} = -\cos\theta \sin\gamma \hat{i}_x + \cos\gamma \hat{i}_y + \sin\theta \sin\gamma \hat{i}_z$, where γ is the angle between the polarization vector and the y-axis. Substitution into equation (4.5.10) gives finally

$$\sigma_e = \frac{1}{\pi} \left| a \int_0^{2\pi} e^{2ika \sin\theta \cos\phi'} (\cos^2\theta \sin^2\phi' \sin^2\gamma + 2\cos\theta \sin\phi' \cos\phi' \sin\gamma \cos\gamma + \cos^2\phi' \cos^2\gamma) d\phi' \right|^2 \quad (4.5.11)$$

$$= \pi a^2 \left| (\cos^2\theta \sin^2\gamma + \cos^2\gamma) J_0(2ka \sin\theta) + \left[(\cos^2\theta \sin^2\gamma - \cos^2\gamma) J_2(2ka \sin\theta) \right] \right|^2.$$

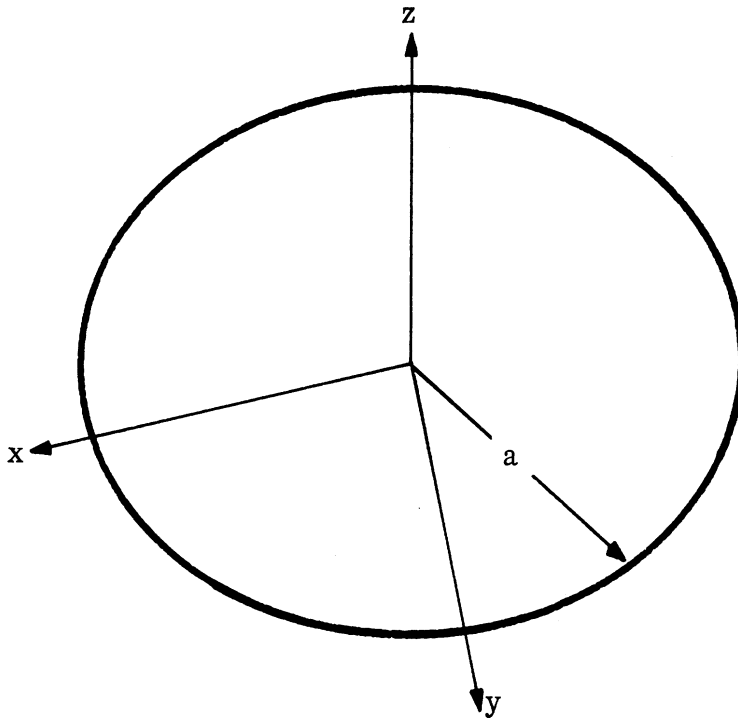


FIG. 4.5-2: WIRE LOOP

For $\theta = 0$, equation (4.5.11) gives $\sigma_e = \pi a^2$. For θ enough greater than zero that $2ka \sin\theta \gg 1$, we can use the asymptotic expansions for the Bessel functions:

$$J_0(z) \sim \sqrt{\frac{2}{\pi z}} \left[\cos(z - \pi/4) + \frac{1}{8z} \sin(z - \pi/4) - \frac{9}{128z^2} \cos(z - \pi/4) + \dots \right] \quad (4.5.12)$$

$$J_2(z) \sim \sqrt{\frac{2}{\pi z}} \left[-\cos(z - \pi/4) + \frac{15}{8z} \sin(z - \pi/4) + \frac{105}{128z^2} \cos(z - \pi/4) + \dots \right].$$

Using equation (4.5.12) and the average values of $\sin^2(2ka \sin\theta - \pi/4)$, $\sin(2ka \sin\theta - \pi/4)\cos(2ka \sin\theta - \pi/4)$, and $\cos^2(2ka \sin\theta - \pi/4)$ (which are $1/2$, 0 , and $1/2$ respectively) in equation (4.5.11) we obtain

$$\text{Average } \sigma_e \sim \frac{a\lambda}{\pi \sin\theta} \left\{ \cos^4 \gamma + \frac{8\cos^4\theta \sin^4\gamma - 8\cos^2\theta \sin^2\gamma \cos^2\gamma - \cos^4\gamma}{32 (ka \sin\theta)^2} \right\}. \quad (4.5.13)$$

Except when $\cos \gamma$ is nearly zero the first term in braces is sufficient and the cross section becomes $\beta \pi a^2$ for

$$\theta \sim \frac{\lambda \cos^4 \gamma}{\pi^2 a \beta}. \quad (4.5.14)$$

For $\cos \gamma = 0$, the cross section becomes $\beta \pi a^2$ when

$$\theta \sim \frac{\lambda}{(2\pi)^{4/3} a \beta^{1/3}}. \quad (4.5.15)$$

The above analysis is carried out for a wire of radius equal to about $1/85$ of a wavelength; an approximation for a wire of arbitrary radius can be obtained by replacing the right hand member of equation (4.5.6) by one which involves the wire radius; that is, for example, Chu's formula. This substitution into equation (4.5.6) results, upon the application of the steps outlined in the equations following (4.5.6), in the following expression for the cross section when $\theta = 0^\circ$

$$\frac{\sigma}{\pi a^2} \sim \frac{(\pi/2)^2 + (\ln(85/\gamma\pi))^2}{(\pi/2)^2 + (\ln(\lambda/\gamma \pi b))^2} \quad (4.5.16)^*$$

where b = the wire radius, a = the loop radius, and $\gamma = 1.78\dots$

*A plot of equation (4.5.16) is given in Figure 4.5-3; one will observe that the cross section is not critically dependent upon the radius of the wire for small values of b .

$$\frac{\sigma}{\pi a^2} = \frac{(\pi/2)^2 + (\ln(85/\gamma\pi))^2}{(\pi/2)^2 + (\ln(\lambda/b\gamma\pi))^2}$$

a = loop radius; b = wire radius; $\gamma = 1.78$

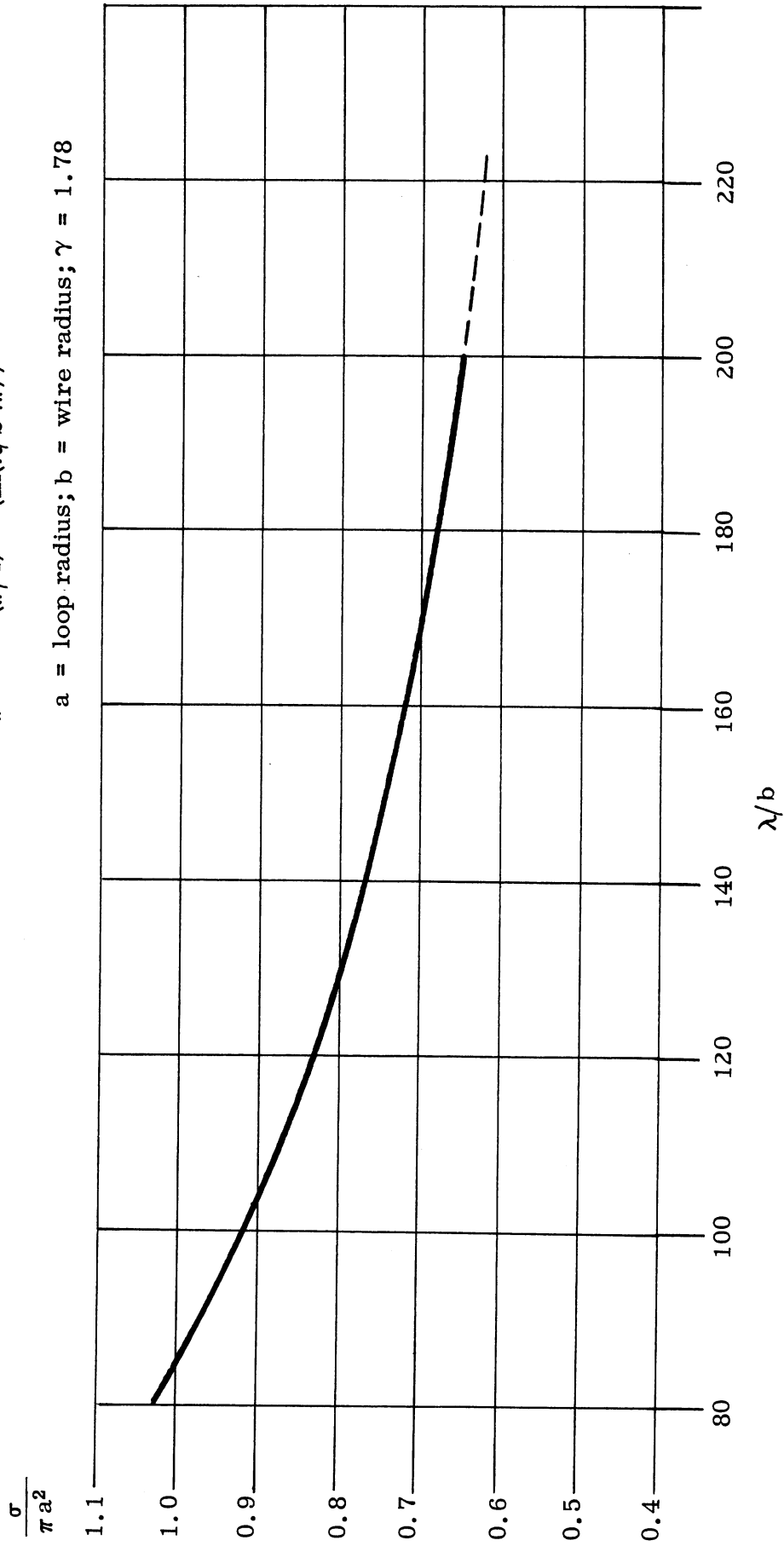


FIG. 4.5-3: THE RADAR CROSS SECTION OF A WIRE LOOP AS A FUNCTION OF THE WIRE RADIUS

The situation for $\theta = 0^\circ$ for various sized wires has been investigated by Kouyoumjian (Ref. 13). Kouyoumjian's results are shown in Figure 4.5-4 together with the corresponding values derived from equation (4.5.16).

Kouyoumjian in his paper, "The Calculation of the Echo Area of Several Scatterers of Simple Geometry by the Variational Method," which he presented at the Symposium on Microwave Optics at McGill University in June 1953 gives us a relation between the return from a wire loop at $\theta = 0^\circ$ and at $\theta = 90^\circ$. This relationship is displayed in Figure 4.5-5 where we note that if the loop radius is about 0.10 of a wavelength we can expect a return like that from a small sphere.

4.6 The Ogive

4.6.1 The Complete Ogive

Methods for obtaining the cross section of an ogive in the Rayleigh region are discussed in Appendix B. Thus, let us first consider the case of the cross section for very small wavelengths. The coordinate system employed in this discussion is shown in Figure 4.6-1. We see from Figure 4.6-1 that the ogive is obtained by rotating an arc of a circle of radius R_1 about a chord located a distance $R_1 - a$ from the center of the circle. This results in an ogive of length L and half-angle α which are related to R_1 and a by the equations

$$\cos \alpha = 1 - (a/R_1) \quad \text{and} \quad \frac{L}{2} = \sqrt{R_1^2 - (R_1 - a)^2} \quad . \quad (4.6.1)$$

Using the cylindrical coordinates (w, ϕ, z) the equation of the surface is

$$(w + R_1 - a)^2 + z^2 = R_1^2 \quad , \quad (4.6.2)$$

with $|z| \leq L/2$ and $0 \leq w \leq a$.

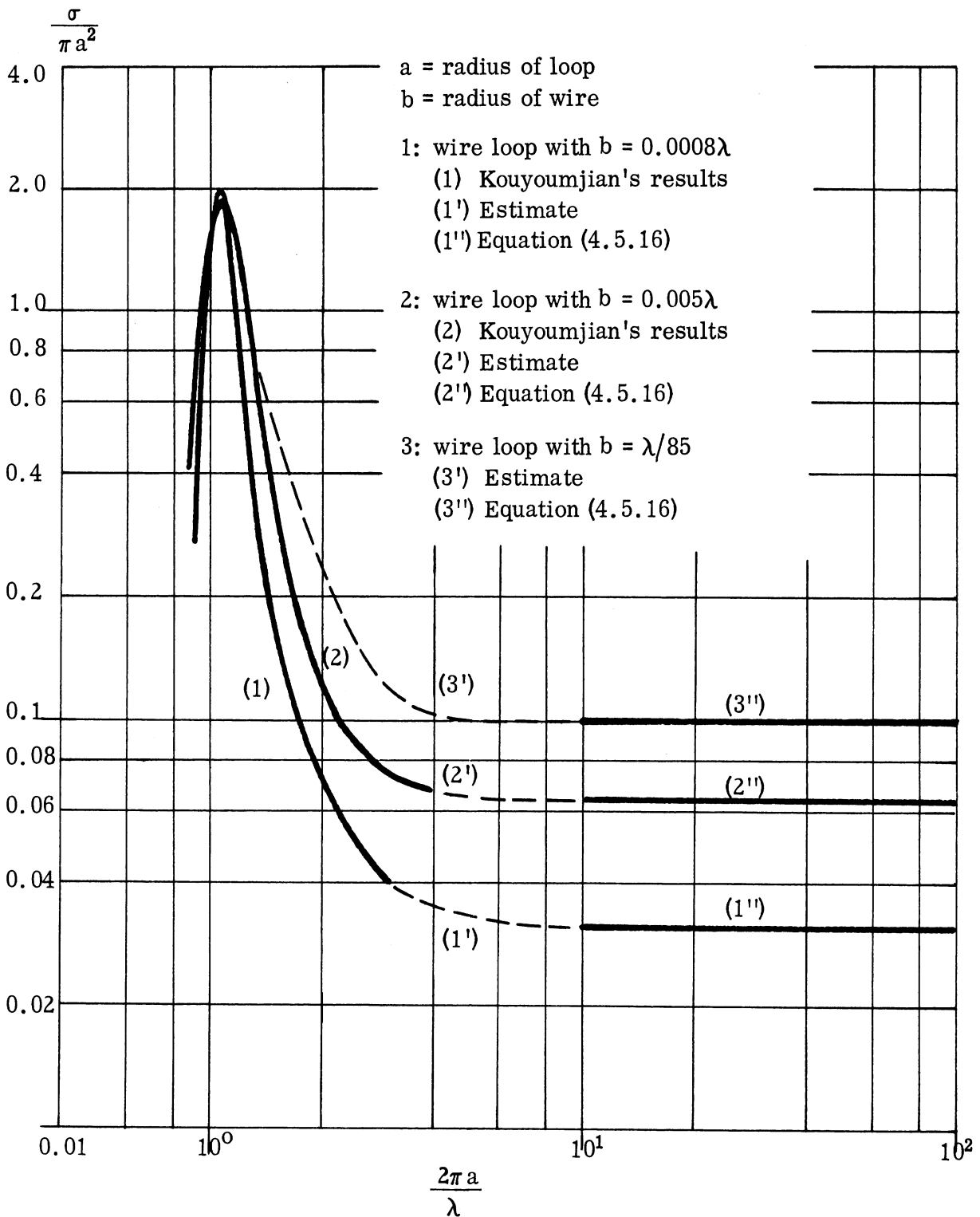


FIG. 4.5-4: RADAR CROSS SECTION OF WIRE LOOPS AT THE NORMAL ASPECT $\theta = 0^\circ$

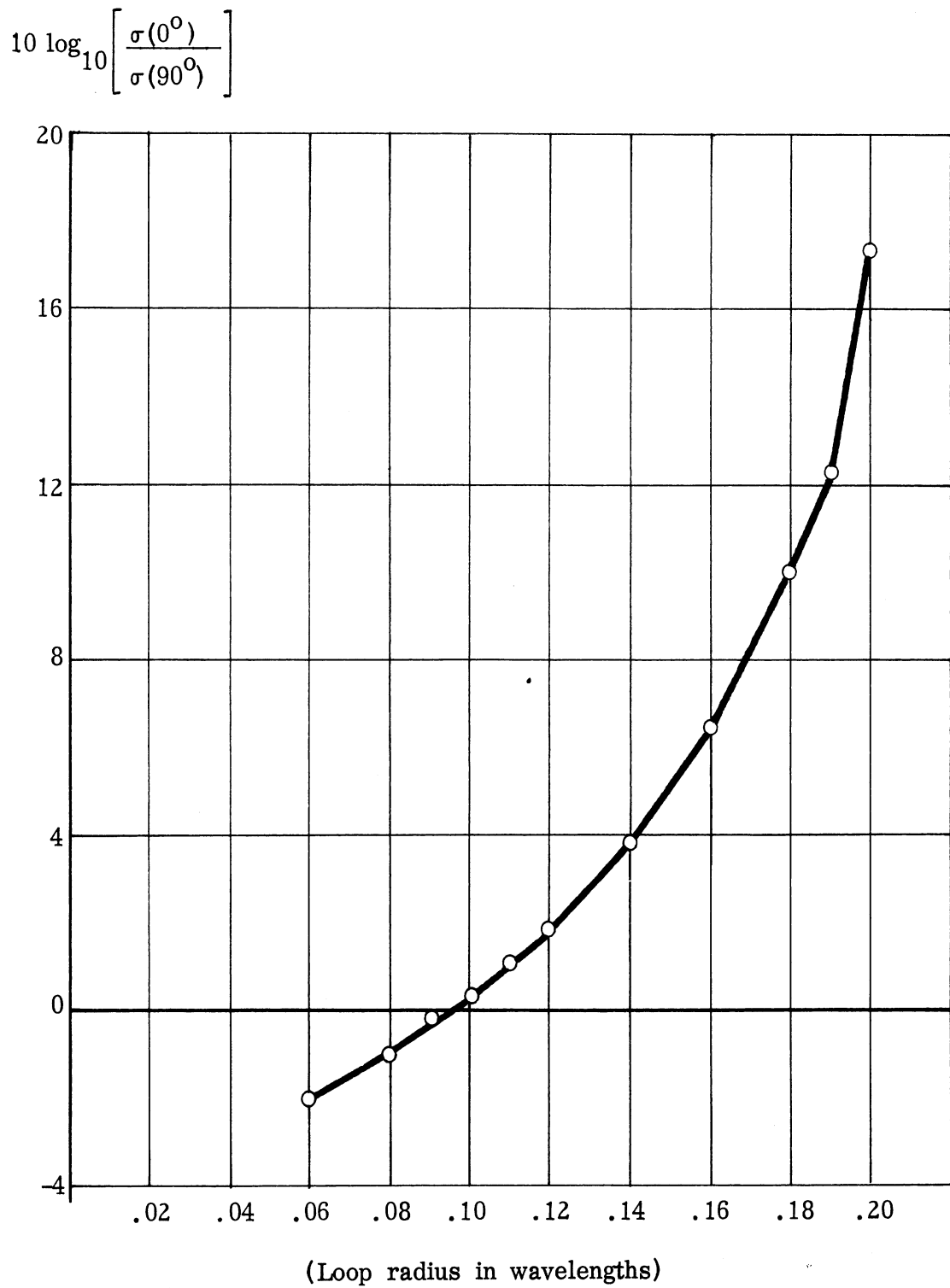


FIG. 4.5-5: RADAR CROSS SECTION OF A WIRE LOOP - RATIO OF THE CROSS SECTION AT $\theta = 0^\circ$ TO THE CROSS SECTION AT $\theta = 90^\circ$
(Wire radius of $.005 \lambda$)

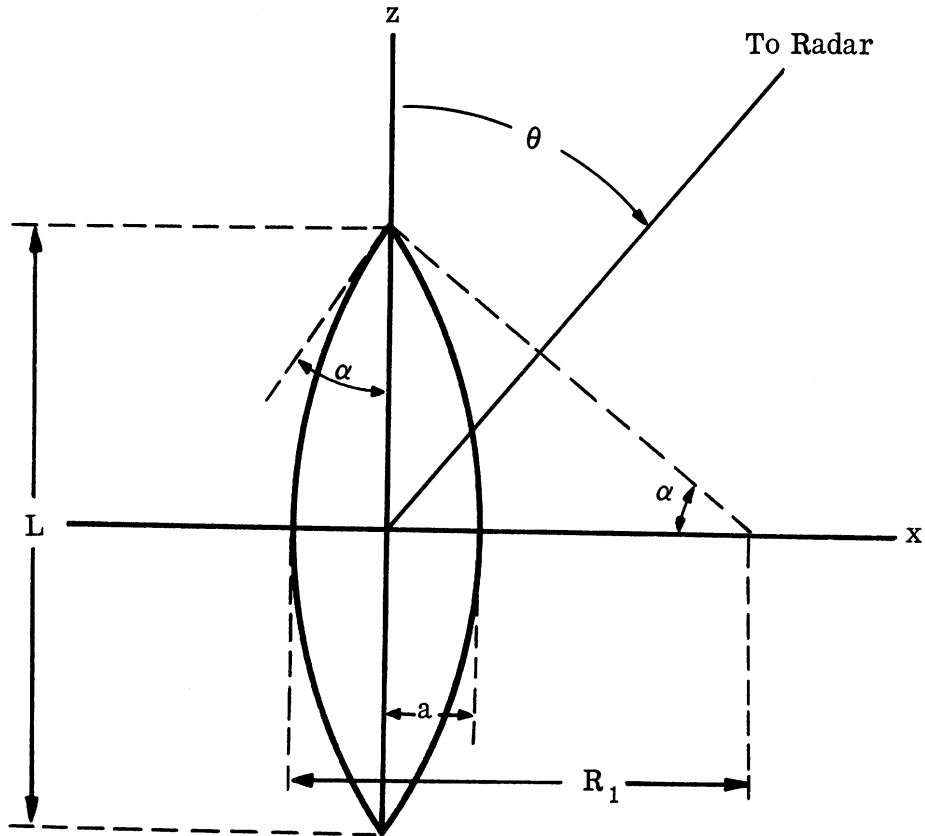


FIG. 4.6-1: THE OGIVE - GRAPHICAL DEFINITION OF THE COORDINATE SYSTEM

Applying the optics approach defined by equation (3.17) and ignoring all contributions except that from the tip we find that for $0^\circ \leq \theta < (90^\circ - \alpha)$ we have

$$\sigma(\theta) = \frac{\lambda^2 \tan^4 \alpha}{16\pi \cos^4 \theta (1 - \tan^2 \alpha \tan^2 \theta)^3} \quad (4.6.3)$$

with $\sqrt{\lambda/4\pi R_1} < \alpha < (\pi/2) - \sqrt{\lambda/4\pi R_1}$.

At $\theta = 90^\circ - \alpha$ we find that the cross section is given by

$$\sigma(90^\circ - \alpha) = \frac{(R_1^2 \sin^2 \alpha)}{4\pi} = \frac{a^2}{(4\pi \tan^2(\alpha/2))} \quad (4.6.4)$$

In the region $(90^\circ - \alpha) < \theta \leq 90^\circ$, the application of equation (3-25) yields the expression

$$\sigma(\theta) = \pi R_1^2 \left(1 - \frac{R_1 - a}{R_1 \sin \theta}\right). \quad (4.6.5)$$

The symmetry of the body is such that we have $\sigma(\theta) = \sigma(\pi - \theta)$.

It is of interest to check the behavior of equation (4.6.3) at $\theta = 0^\circ$ for large half-angle ogives since as the half-angle approaches 90° the body takes on the shape of a sphere.

Since πR_1^2 is the cross section of the sphere (at these small wavelengths), let us consider the ratio $\sigma_{ogive}(0^\circ)/\pi R_1^2$ using the expression in equation (4.6.3). Employing the maximum value of α indicated under equation (4.6.3), we find that

$$\frac{\sigma(0^\circ)}{\pi R_1^2} = \left[\sqrt{\frac{\lambda}{4\pi R_1}} \cot\left(\sqrt{\frac{\lambda}{4\pi R_1}}\right) \right]^4. \quad (4.6.6)$$

Since the limit of $x \cot(x)$ is 1 as x approaches zero, it follows that the maximum value of the nose-on cross section for an ogive predicted by equation (4.6.3) is πR_1^2 .

As pointed out in Reference 4, a better approximation for the near nose-on aspects of thin ogives is given by

$$\sigma(\theta) = \left(2/(-1 + \text{Cin}(kL))\right)^2 (f(\theta))^4 \lambda^2/4\pi, \quad (4.6.7)$$

where

$$f(\theta) = \left[\frac{\sin \theta}{(1 - \cos \theta)} \right] \sin \left[(kL/2) (1 - \cos \theta) \right],$$

and

$$\text{Cin}(x) = \text{modified cosine integral of argument } x.$$

As an aid to the application of equation (4.6.7) a plot of $F' = 1/\left\{\pi(-1 + \text{Cin}(kL))^2\right\}$

is presented in Figure 4.6-2. This substitution results in equation (4.6.7)

being condensed into the form

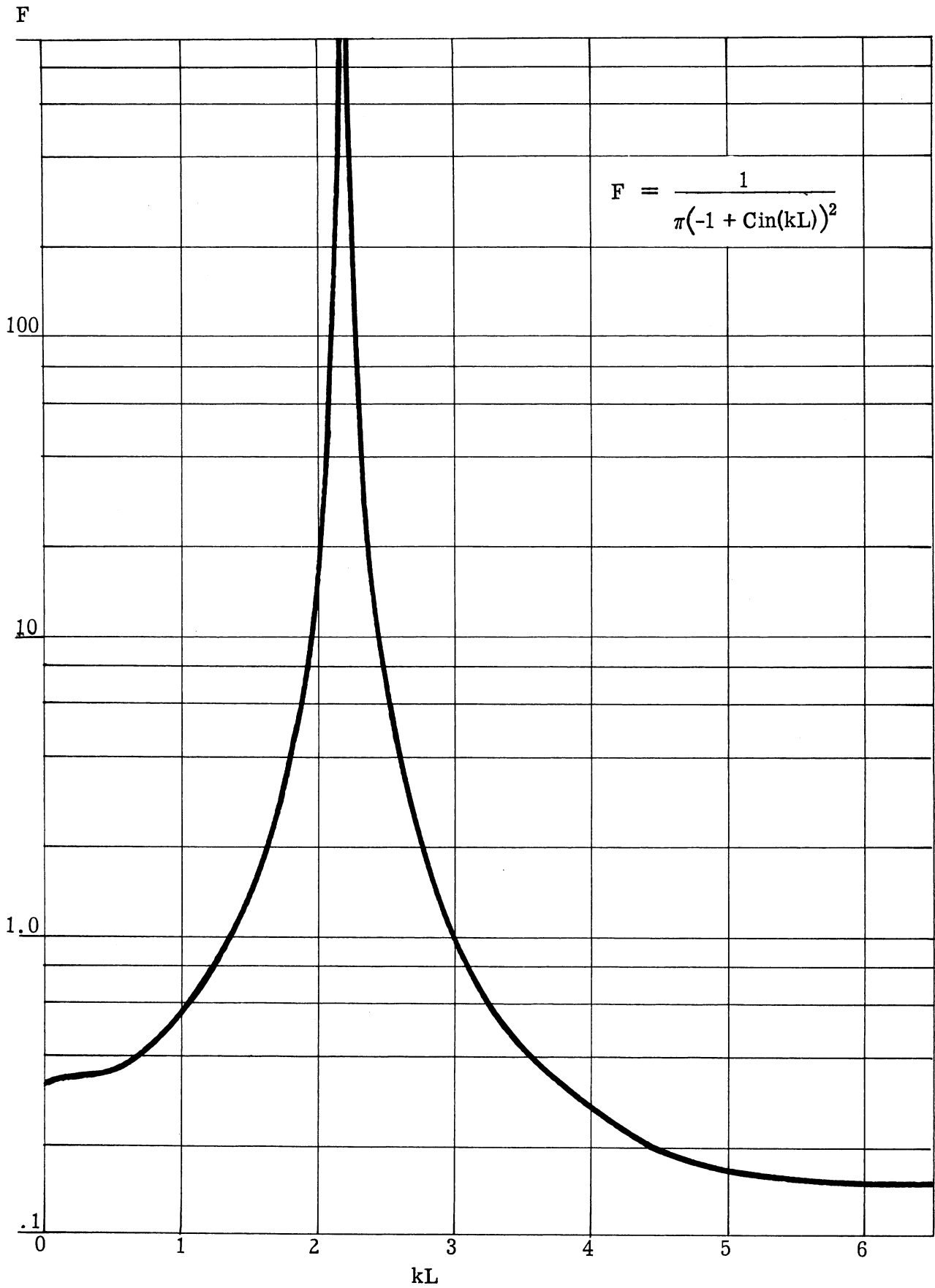


FIG. 4.6-2: THE FUNCTION F IN EQUATION 4.6.8

$$\sigma(\theta) = F'(f(\theta) \frac{4}{\lambda^2}). \quad (4.6.8)$$

For the nose-on case we again note from Reference 4 that in the resonance region for thin ogives a better approximation to the cross section is given by

$$\sigma(0^0) = \frac{\lambda^2 \tan^4 \alpha}{16\pi} + \frac{a\lambda}{2}. \quad (4.6.9)$$

From the work of Fock (Ref. 14) an estimate can be found for a lower bound of ka for which the current on the rear has attenuated sufficiently to justify the neglect of the contribution from the rear. It is assumed that an attenuation of the current reaching the rear tip to less than one-tenth of the current at the shadow boundary is required to insure that the front tip contribution dominates. Using Fock's expressions for the current on the rear of the sphere, the minimum kR_1 for which attenuation to one-tenth takes place is plotted against the half-angle of the ogive in Figure 4.6-3. It is seen that for thin ogives (say $\alpha < 30^0$) kR_1 must be greater than 200 in order for the tip contribution to dominate (that is, in order for equation (4.6.3) to be appropriate at $\theta = 0^0$).

4.6.2 The Truncated Ogive

Let us consider an ogive truncated in the manner shown in Figure 4.6-4.

That is, z is limited by the relation

$$|z| \leq b < \frac{L}{2}. \quad (4.6.10)$$

Let the radius of the circle cut by this truncation plane $z = b$ from the ogive have a radius = a' . The application of the optics methods defined by equation (3.17) indicates that for incidence along the z -axis the cross section is given by

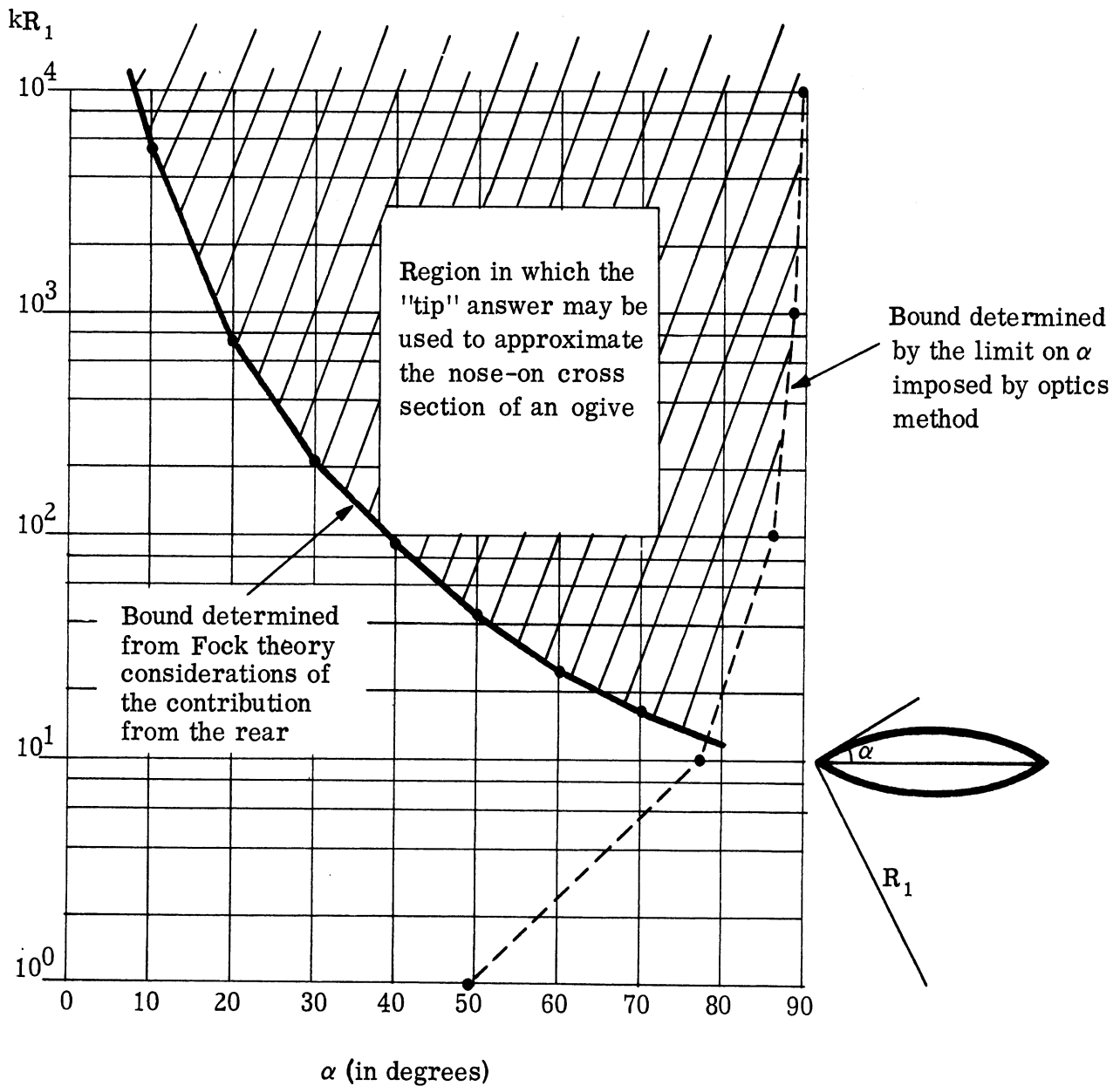


FIG. 4.6-3: REGION OF APPLICABILITY OF THE OGIVE TIP ANSWER FOR NOSE-ON INCIDENCE

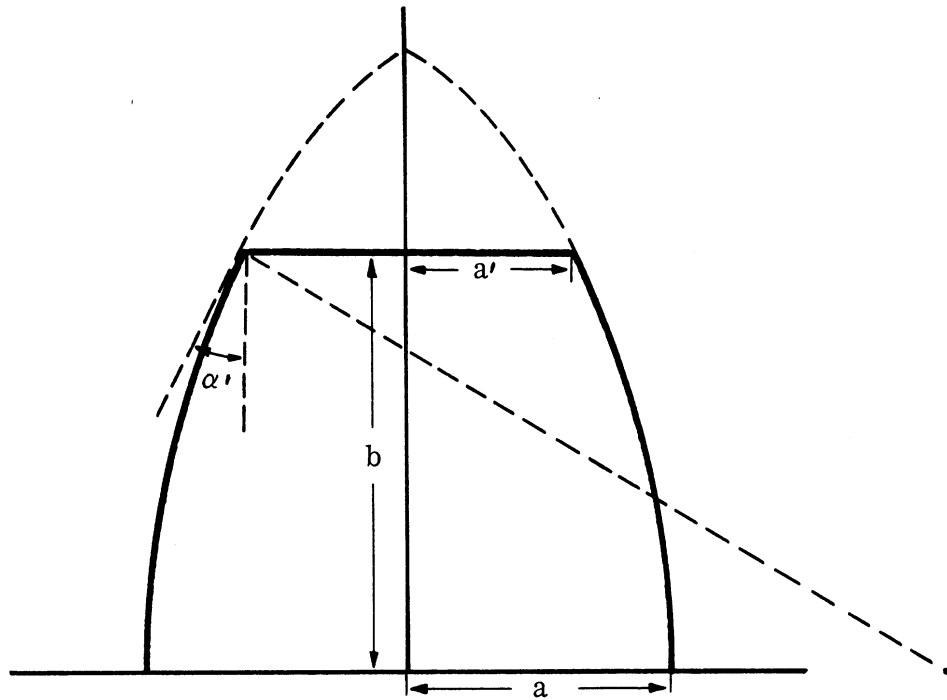


FIG. 4.6-4: THE TRUNCATED OGIVE

$$\sigma = \pi(a')^2 \tan^2(\alpha') \quad (4.6.11)$$

where α' is the angle between the z-axis and the ogive tangent plane where the ogive is truncated. For $0 < \theta < \alpha'$ and $\theta < (90^\circ - \alpha')$ there are two contributions to the cross section given by

$$\frac{\lambda a' \tan^2(\theta + \alpha')}{8\pi \sin\theta} \quad \text{and} \quad \frac{\lambda a' \tan^2(\theta - \alpha')}{8\pi \sin\theta} \quad (4.6.12)$$

For $\alpha' \leq \theta \leq 90^\circ - \alpha'$ (a range which exists only when $\alpha' < 45^\circ$), the second of these contributions is absent. For the remaining values of θ ($\theta < 90^\circ$) the approach used for the entire ogive in Section 4.6.1 is applicable (i.e., equation 4.6.5).

The expressions given above for the cross section of a truncated ogive are those obtained by physical optics through the application of equation (3.17). If the truncation of the ogive results in an opening then this also must be treated. If the rim is sharp, then the wire loop contribution should be added to the contribution obtained from equations (4.6.11) and (4.6.12); this can be done using the methods given in Section 4.5. If this truncation leaves a flat plate, then the methods discussed in Section 4.7 should be used.

Often one is confronted with an ogival shape which is truncated with a sphere (see Fig. 4.6-5). The approach one can use for this body is similar to that used for the complete ogive and in fact results in the upper bound for the "creeping wave" contribution from the rear of the ogive given in equation (4.6.9).

The sphere cross section can be decomposed into a geometrical optics term plus a diffraction term; the optics term comes from the region of specular reflection and the diffraction term from the effects of the currents induced in the shadow region and near the shadow boundary. This consideration leads us to attempt to approximate the "contribution from the rear" for a shape like that shown in Figure 4.6-5 by using known sphere results. Reading values of the cross section from the exact sphere curve (see Fig. 4.2-2) we obtain the following estimate for this rear contribution

$$\frac{\sigma_{\text{rear}}}{\pi a^2} = 1.03 (ka)^{-5/2} \quad (4.6.13)$$

where the a is as shown in Figure 4.6-5. Experience has shown this to be a good estimate for values of ka from 1 up to about 15. For larger values of ka let us employ the physical optics expression for the cross section of a sphere.

Although physical optics does not accurately predict the location of the relative maxima and minima it does predict with reasonable accuracy the amplitude of these relative maxima. The sphere cross section in the physical optics region is given by equation (4.2.5). This expression takes on a maximum value whenever $2ka = (4n+3)\pi/2$. With the approximation πa^2 used for the contribution from the first Fresnel zone, we have

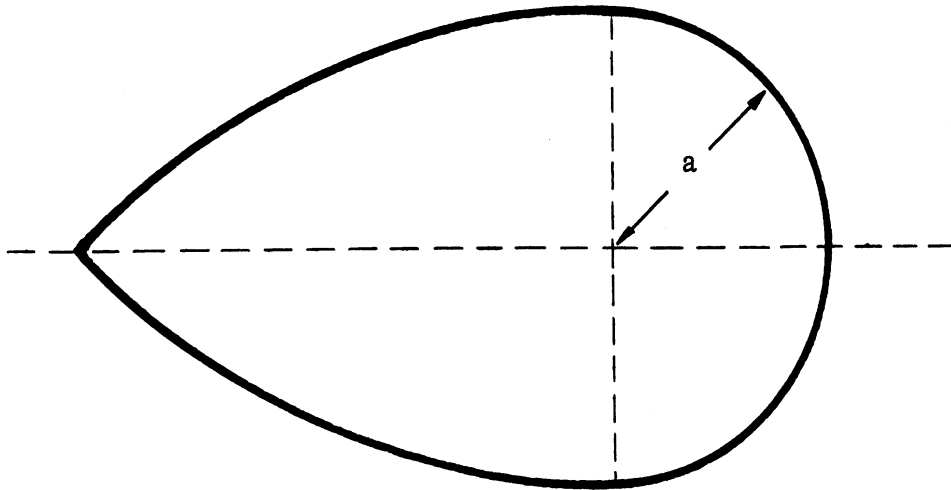


FIG. 4.6-5: AN OGIVE CAPPED BY A SPHERE

$$\left(\sqrt{\pi a^2} + \sqrt{\sigma_{\text{rear}}} \right)^2 \approx \pi a^2 \left(1 + \frac{1}{2ka} \right)^2 \quad (4.6.14)$$

from which is obtained

$$\sigma_{\text{rear}} \approx \frac{\pi a^2}{4(ka)^2} \quad (4.6.15)$$

$$\approx \frac{\lambda^2}{16\pi} . \quad (4.6.16)$$

A maximum value for the contribution from the rear can be obtained by assuming that $\sigma = \pi a^2 + \sigma_{\text{rear}}$ in equation (4.2.5) and maximizing the right hand side of the equation; this results in the $a\lambda/2$ estimate of equation (4.6.9).

As an aid in computation a plot of equation (4.6.13) is given below in Figure 4.6-6. A much more detailed computation of this "contribution from the rear" was made by V. E. Pound of the Cornell Aeronautical Laboratory, Incorporated (in C. A. L. Internal Memorandum No. 830-141). The results of Pound's computation is also shown in Figure 4.6-6.

4.7 The Flat Plate

In this consideration of a flat plate let us assume that the plate is located in the x-y plane with the polar angles defining the direction of incidence as indicated in Figure 4.2-1.

4.7.1 The Rectangular Flat Plate

Employing the physical optics approach of equation (3.17) we find that for a rectangular flat plate 2a by 2b (the 2a dimension along the x-axis and the 2b dimension along the y-axis) we have for $\theta = 0^\circ$

$$\sigma = \frac{64\pi a^2 b^2}{\lambda^2} \quad (4.7.1)$$

In the y-z plane ($\phi = 90^\circ$ or 270°) there are two components each given by

$$\sigma = \frac{a^2}{\pi \sin^2 \theta} \quad (4.7.2)$$

In the x-z plane ($\phi = 0^\circ$ or 180°) there are two components each given by

$$\sigma = \frac{b^2}{\pi \sin^2 \theta} \quad (4.7.3)$$

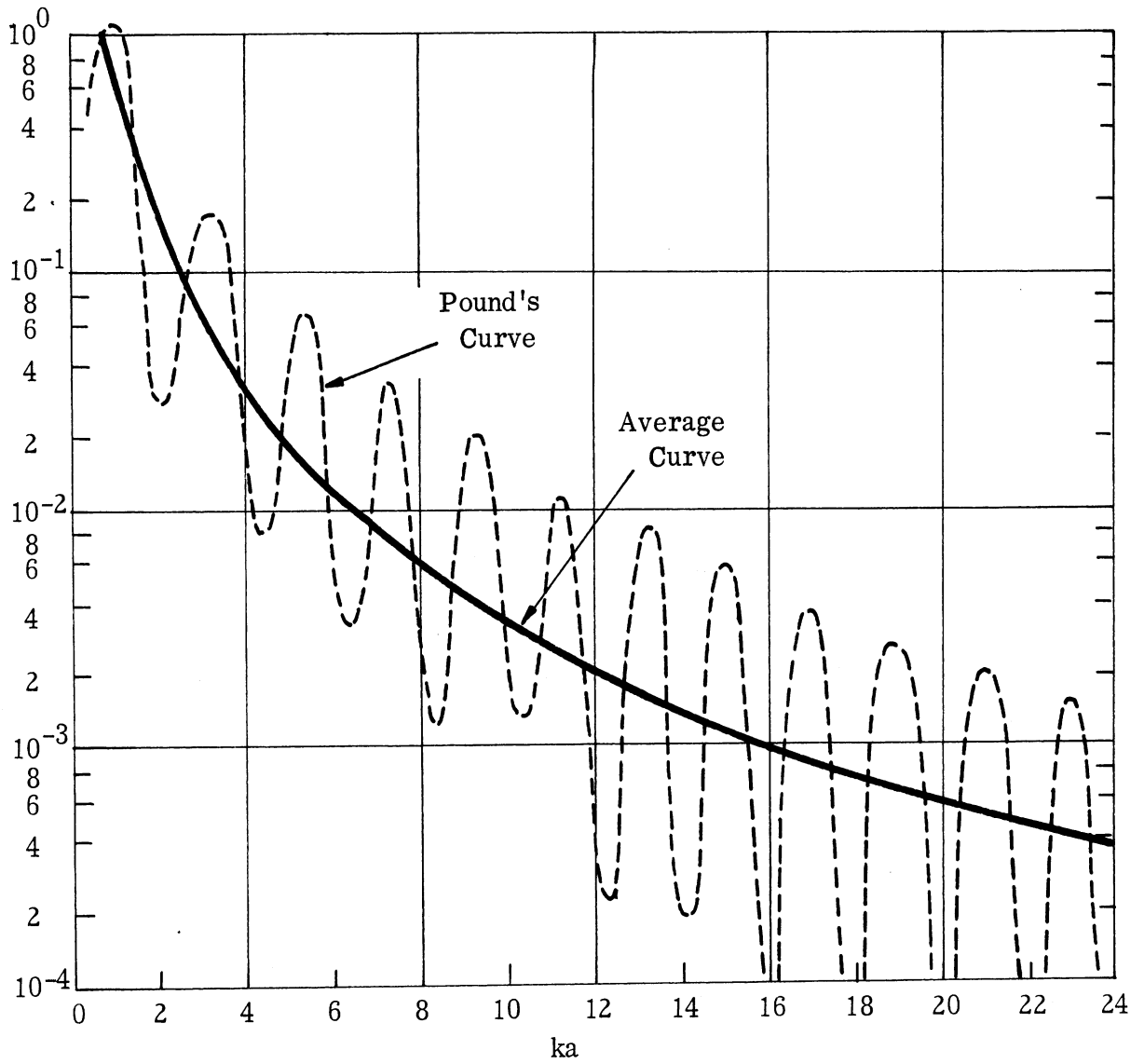


FIG. 4.6-6: RADAR CROSS SECTION CONTRIBUTION FROM THE REAR OF A SPHERE OF RADIUS a

For other aspects there are four components each given by

$$\sigma = \frac{\lambda^2 \cos^2 \theta}{64\pi^3 \sin^4 \theta \sin^2 \phi \cos^2 \phi} . \quad (4.7.4)$$

4.7.2 The Circular Flat Plate

The circular flat plate or disc cross section formula is

$$\sigma = \frac{\pi a^2}{\tan^2 \theta} \left[J_1 \left(\frac{4\pi a \sin \theta}{\lambda} \right) \right]^2 , \quad (4.7.5)$$

where a = the radius of the disc and $J_1(x)$ is the Bessel function of the first kind. When the asymptotic formula for the Bessel function is used ($ka \sin \theta \gg 1$) it is found that the scattering is due to two components with the magnitudes

given by
$$\frac{a \lambda}{8\pi \sin \theta \tan^2 \theta} . \quad (4.7.6)$$

4.7.3 The General Flat Plate

With the flat plate located in the xy -plane we have for normal incidence ($\theta = 0^\circ$)

$$\sigma = \frac{4\pi A^2}{\lambda^2} , \quad (4.7.7)$$

where A is the area of the plate. For non-normal incidence we have by extending the results obtained for the circular disc that there is a contribution to the cross section from each point on the boundary of the plate at which the boundary is perpendicular to the direction of incidence. If a is the radius of curvature of the boundary at this point (and a is finite) then the contribution is as given in equation (4.7.6). If a is infinite then the plate in question would be,

at least in part, rectangular and the approach of Section 4.7.1 would apply.

In the case of an elliptical disc defined by the equation

$$\left(\frac{x}{a}\right)^2 + \left(\frac{y}{b}\right)^2 = 1 \quad , \quad (4.7.8)$$

we find for $\theta > 0^\circ$

$$\sigma = \frac{\lambda a^2 b^2}{8\pi \sin\theta \tan^2\theta (a^2 \cos^2\phi + b^2 \sin^2\phi)^{3/2}} \quad . \quad (4.7.9)$$

4.8 The Tapered Wedge

We shall postpone the consideration of the tapered wedge (shown in Figure 4.8-1) for the present; it is discussed in Appendix A in considerable detail for general polarizations (see Section 6.6). We will remark, however, that over a wide range of aspects the return is dominated by the sharp edge of the tapered wedge, which may be treated as a thin wire. It will be observed that for

$$(1/\tan \alpha) < \tan\theta \cos\phi$$

the tapered wedge looks like a cylinder for short wavelengths.

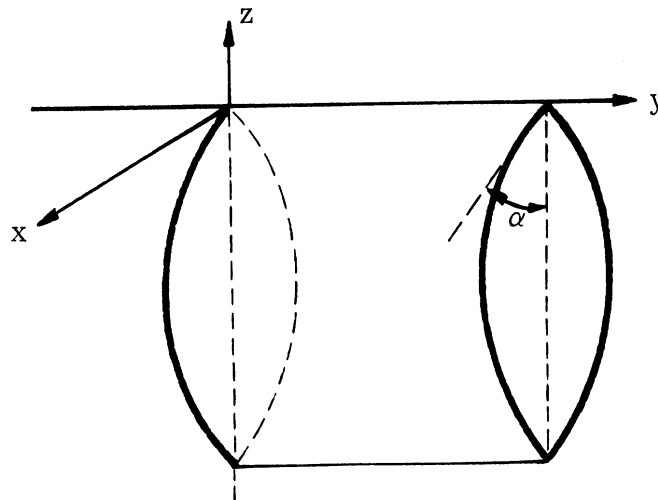


FIG. 4.8-1: THE TAPERED WEDGE

4.9 Corner Reflectors and Multiple Reflectors

The subject of corner reflectors and multiple reflectors in general has been discussed in a previous University of Michigan Report. We are including the material of that report in its entirety as Appendix C to this report and thus the reader is referred to Appendix C for the discussion of corner reflectors.* We will, however, in the present section make a few comments on double reflections.

The methods of geometric optics are applied in this analysis of multiple reflections and the case of multiple scattering by N bodies is discussed in Appendix C. Here we restrict our attention to the case of N = 2. Approximating each pair of aircraft components in the vicinity of the reflecting points by the surfaces

$$\frac{x_i^2}{2\rho_{i1}} + \frac{y_i^2}{2\rho_{i2}} = -z_i \quad (i = 1 \text{ and } 2) \quad (4.9.1)$$

where the z_i axes are oriented in the direction of the normals to the surfaces

(thus $\hat{i}_{z_1} \cdot \hat{i}_{z_2} = 0^{**}$) and

$$\hat{i}_{x_1} \cdot \hat{i}_{x_2} = 1; \hat{i}_{x_1} \cdot \hat{i}_{y_1} = \hat{i}_{y_1} \cdot \hat{i}_{x_2} = \hat{i}_{y_1} \cdot \hat{i}_{y_2} = 0 ,$$

the material of Appendix C indicates that the double-reflection contribution to the cross section is given by

* Additional comments on corner reflectors will be found in Appendix D.

** In order for the reflected ray to return in the direction from which it came it is necessary that the normals to the two surfaces at the reflecting points be perpendicular.

(4.9.2)

$$\sigma = \frac{\pi \rho_{11} \rho_{12} \rho_{21} \rho_{22}}{b^2 \sin(2\zeta) \left[\sin(2\zeta) + \frac{\rho_{21}}{b} \cos \zeta + \frac{\rho_{11}}{b} \sin \zeta \right] \left[2 + \frac{\rho_{12}}{b} \cos \zeta + \frac{\rho_{22}}{b} \sin \zeta \right]}$$

The geometry of the situation as well as graphical definitions of the parameters ζ and b are given in Figure 4.9-1.

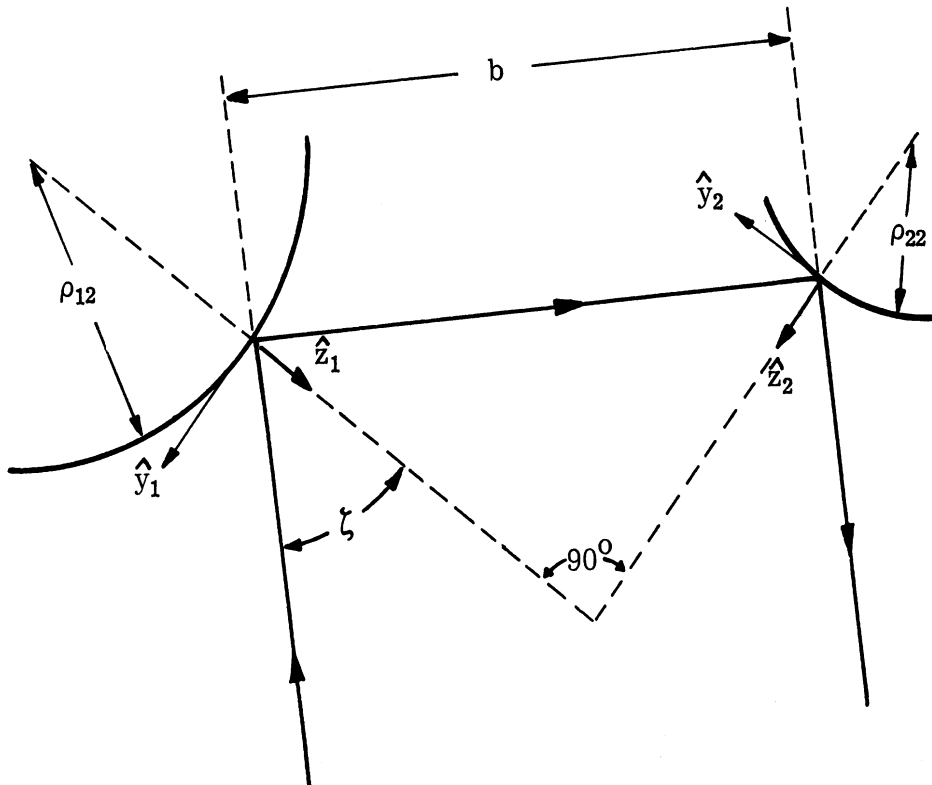


FIG. 4.9-1: DOUBLE REFLECTIONS (showing one of the two rays; the other ray follows the reverse path)

In the cases corresponding to $\zeta = 0^\circ$ or 90° , one body is in the shadow of the other, or a triple reflection is involved. For these reasons it is thought to be desirable to limit the application of equation (4.9.2) to the range $15^\circ \leq \zeta \leq 75^\circ$. With this restriction we see that the double-reflection contribution is bounded by the relation

$$\sigma < \frac{2\pi \rho_{11} \rho_{12} \rho_{21} \rho_{22}}{b^2} . \quad (4.9.3)$$

This inequality is extremely useful in determining the question of whether double reflections need be considered in the problem of estimating the cross section of a given aircraft. Often one is presented with a situation in which the b is zero. The above expression can be made to yield an estimate of the cross section in such a case if one of the ρ 's is infinite. For example suppose that $b = 0$ and $\rho_{22} = \infty$. Equation (4.9.2) can be rewritten in the form

$$\sigma = \frac{\pi \rho_{11} \rho_{12} \rho_{21}}{\sin(2\zeta) \left[b \sin(2\zeta) + \rho_{21} \cos\zeta + \rho_{11} \sin\zeta \right] \left[2 \frac{b}{\rho_{22}} + \frac{\rho_{12}}{\rho_{22}} \cos\zeta + \sin\zeta \right]} \quad (4.9.4)$$

from which it follows that

$$\lim_{\substack{b \rightarrow 0 \\ \rho_{22} \rightarrow \infty}} \sigma = \frac{\pi \rho_{11} \rho_{12} \rho_{21}}{\sin\zeta \sin(2\zeta) \left[\rho_{21} \cos\zeta + \rho_{11} \sin\zeta \right]} . \quad (4.9.5)$$

4.10 The Paraboloid

For a paraboloid defined by the equation $x^2 + y^2 = -4pz$ and with the direction to the radar defined as in Figure 4.2-1 the methods of geometric optics yield

$$\begin{aligned} \sigma(\theta) &= \frac{16 \pi p^2}{(1 + \cos(2\theta))^2} \\ &= 4 \pi p^2 \sec^4 \theta . \end{aligned} \quad (4.10.1)$$

The above gives the value of the cross section of the infinite paraboloid. In using a paraboloid to model the nose section of a fuselage or a wing tank one, of course, is dealing with a truncated or smoothed paraboloid and care must be taken to add the contributions from the truncated rear of the paraboloid.

It is shown in Reference 18 (and in Reference 15) that equation (4.10.1) yields the exact cross section for incidence along the axis of symmetry; that is, for $\theta = 0^\circ$.

4.11 Summary

In this section we have presented the methods of approach to be used in determining the radar cross sections of the simple shapes used in modeling the components of an aircraft or a missile. As stated earlier our knowledge of radar cross sections, even for simple shapes, is far from being complete; the state of the art is such that good approximations are available in the optics region and in the Rayleigh region but the knowledge of the behavior of the cross section of a given shape in the resonance region is, by comparison, quite meager. Thus, it is not surprising that from time to time one will be confronted with a complex shape for which the methods and formulas presented here are not completely adequate. In such a case it is often possible to obtain the necessary information from a judicious analysis of existing experimental data on shapes of "similar" size and shape. That is, apply the methods given here to the study of the "experimental configuration" and by working backwards obtain an estimate of the contribution of the simple shape component of the "experimental configuration".

We shall close this discussion of simple shape cross sections in the optics region (and that has been the region of primary concern in this section) with a brief examination of the peak width method of approach.

To obtain an estimate of peak width (i. e. the aspects at which the cross section is only $1/2$, $1/10$, $1/100$, etc. of its value at the 'normal' aspect) we require that the average cross section for non-normal incidence be $(1/N)$ times the cross section at normal incidence, solve the resulting equation for the aspect angle and thus obtain solutions θ_N at which the cross section is only $(1/N)$ th of the value at the peak.

This situation arises when the body in question has one principal radius of curvature which is infinite; the bodies discussed in this section having this property are the Cone, the Cylinder, the Thin Wire, the Torus, the Wire Loop, and the Flat Plate. The thin wire situation is discussed in Section 4.1 and the case of the wire loop in Section 4.5 (equations 4.5.14 and 4.5.15); here we shall restrict our attention to the cone, the cylinder, the torus, and the circular flat plate.

The Cylinder: The cross section of an elliptic cylinder at normal aspect ($\theta = 90^\circ$) is given by equation (4.4.1) and the cross section contribution of each end of the cylinder is given by equation (4.4.2). Thus, if the sum of the two non-normal-incidence cross sections is to be $(1/N)$ th of the cross section at $\theta = 90^\circ$, we have

$$\frac{2\pi L^2 a^2 b^2}{\lambda(a^2 \cos^2\phi + b^2 \sin^2\phi)^{3/2}} = 2N \left\{ \frac{\lambda a^2 b^2 \sin\theta_N}{8\pi \cos^2\theta_N (a^2 \cos^2\phi + b^2 \sin^2\phi)^{3/2}} \right\}. \quad (4.11.1)$$

This expression reduces to

$$\frac{(\sin\theta)_N}{\cos^2\theta_N} = \frac{8L^2\pi^2}{N\lambda^2}, \quad (4.11.2)$$

and for small $\lambda(\theta_N$ close to 90°) this is approximately equivalent to

$$\cos^2\theta_N = (N/2) (\lambda/2\pi L)^2. \quad (4.11.3)$$

From the above we obtain

$$\theta_N = (\pi/2) \pm (N/2)^{1/2} (\lambda/2\pi L) \quad (4.11.4)$$

as the measure of the peak width; i. e., the angles at which the cross section is down by a factor of N from its value at $\theta = 90^\circ$.

It should be noted that the above assumes that both ends of the cylinder are sharply terminated. If one end is smoothly faired into another body (such as a sphere or an ogive) then equation (4.11.1) would have to be appropriately modified.

The Truncated Cone: The cross section at normal aspect (defined by eq. 4.3.12) is given by equation (4.3.11) and the cross section contributions at the non-normal aspects are given by equation (4.3.13). If we assume that the truncated cone is sharply terminated at each end, then the equation we obtain for the determination of the θ_N is

$$\frac{8\pi(L_2^{3/2} - L_1^{3/2})^2 \tan^4 \lambda}{9\lambda\eta^2 |\cos^3\theta|} = \left\{ \frac{N\lambda(L_1+L_2)\eta^3 \tan \alpha}{8\pi \sin\theta_N (\sin^2\phi + \eta^2 \cos^2\phi)^{1/2}} \right\} \times \left\{ \frac{\frac{\sin\theta_N}{(\sin^2\phi + \eta^2 \cos^2\phi)^{1/2}} - \frac{\cos\theta_N \tan \alpha}{\eta}}{\sin\theta_N \tan \alpha (\sin^2\phi + \eta^2 \cos^2\phi)^{1/2} + \eta \cos\theta_N} \right\}. \quad (4.11.5)$$

Making use of the expression for θ_{\perp} given in equation (4.3.12), we find that

equation (4.11.5) may be rewritten in the form

$$\frac{64 \pi^2 (L_2^{3/2} - L_1^{3/2})^2}{9N \lambda^2 (L_1 + L_2)} (\eta^2 + \tan^2 \alpha (\sin^2 \phi + \eta^2 \cos^2 \phi)) = \frac{\eta^2}{\tan^2(\theta_N - \theta_{\perp})} \quad (4.11.6)$$

from which we obtain the measure of the peak width

$$\theta_N - \theta_{\perp} = \frac{3\eta\lambda \sqrt{N(L_1 + L_2)}}{8\pi (L_2^{3/2} - L_1^{3/2})} (\eta^2 + \tan^2 \alpha (\sin^2 \phi + \eta^2 \cos^2 \phi))^{-1/2}. \quad (4.11.7)$$

For the case of a circular cone ($\eta = 1$) we have

$$\theta_N - \theta_{\perp} = \frac{3\lambda \sqrt{N(L_1 + L_2)} \cos \alpha}{8\pi (L_2^{3/2} - L_1^{3/2})}. \quad (4.11.8)$$

The Torus: The cross section at normal incidence ($\theta = 0^\circ$) for the torus is given by equation (4.5.2) and the non-normal incidence contributions are given by equations (4.5.3) and (4.5.4). Thus to determine θ_N we have

$$\frac{8\pi^3 ba^2}{\lambda} = N(2ba \pi / \sin \theta_N). \quad (4.11.9)$$

From which we readily obtain (for small λ)

$$|\theta_N| = N(\lambda/4\pi^2 a). \quad (4.11.10)$$

The Circular Flat Plate: To determine θ_N for a circular flat plate (for small λ)

we employ the expressions given in Section 4.7 to obtain

$$\frac{4\pi (\pi a^2)^2}{\lambda^2} = \frac{2N}{8\pi} \cdot \frac{a^4}{\sin \theta_N \tan^2 \theta_N (a^2)^{3/2}}, \quad (4.11.11)$$

from which we obtain

$$|\theta_N| = \sqrt[3]{(N/2\pi)} (\lambda/\pi a) \quad . \quad (4.11.12)$$

The peak width results for the cylinder, the torus, and the circular flat plate are shown graphically in Figures 4.11-1 through 4.11-3 (where the magnitude of $(\theta_N - \theta)$ is plotted against N for four different values of the ratio of wavelength-to-body dimension. The material of these figures will make it possible to obtain a good estimate of the peak width for almost all cylinders, torii, and circular flat plates as long as the wavelength is no greater than 0.3 times the critical body dimension.

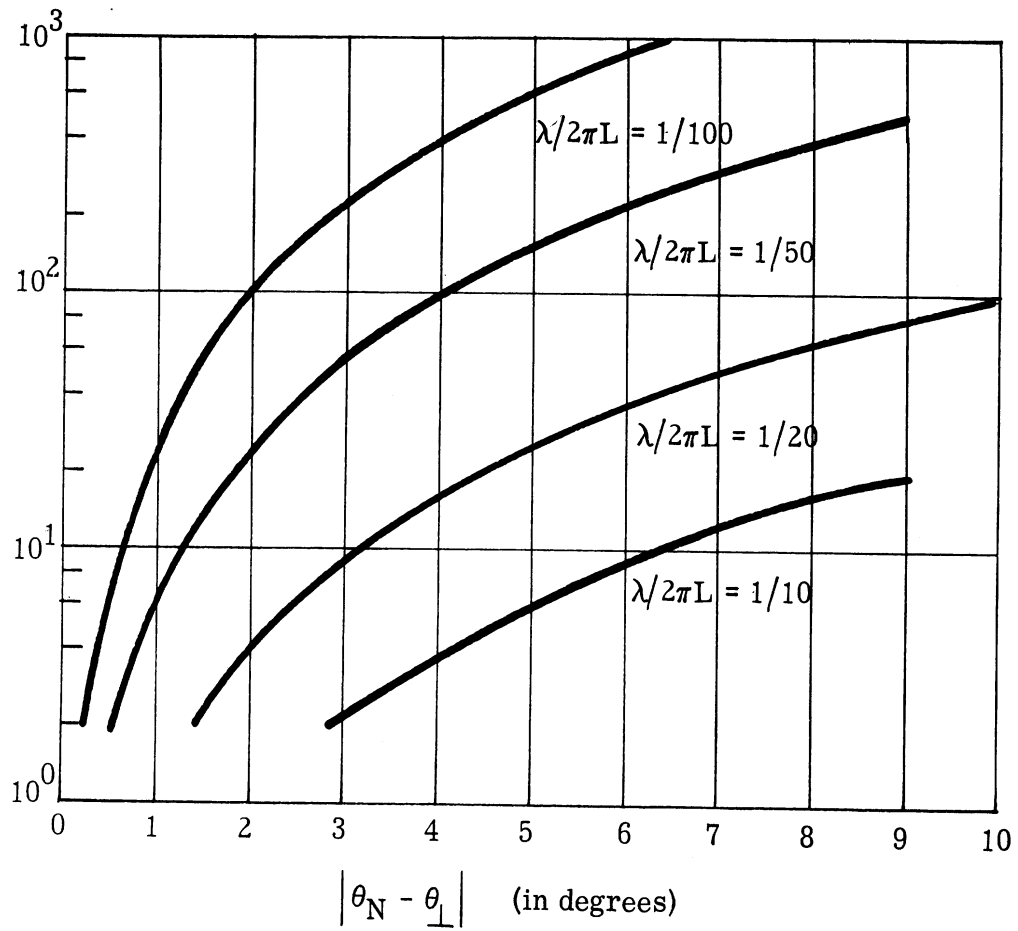


FIG. 4.11-1: PEAK WIDTHS FOR THE CYLINDER

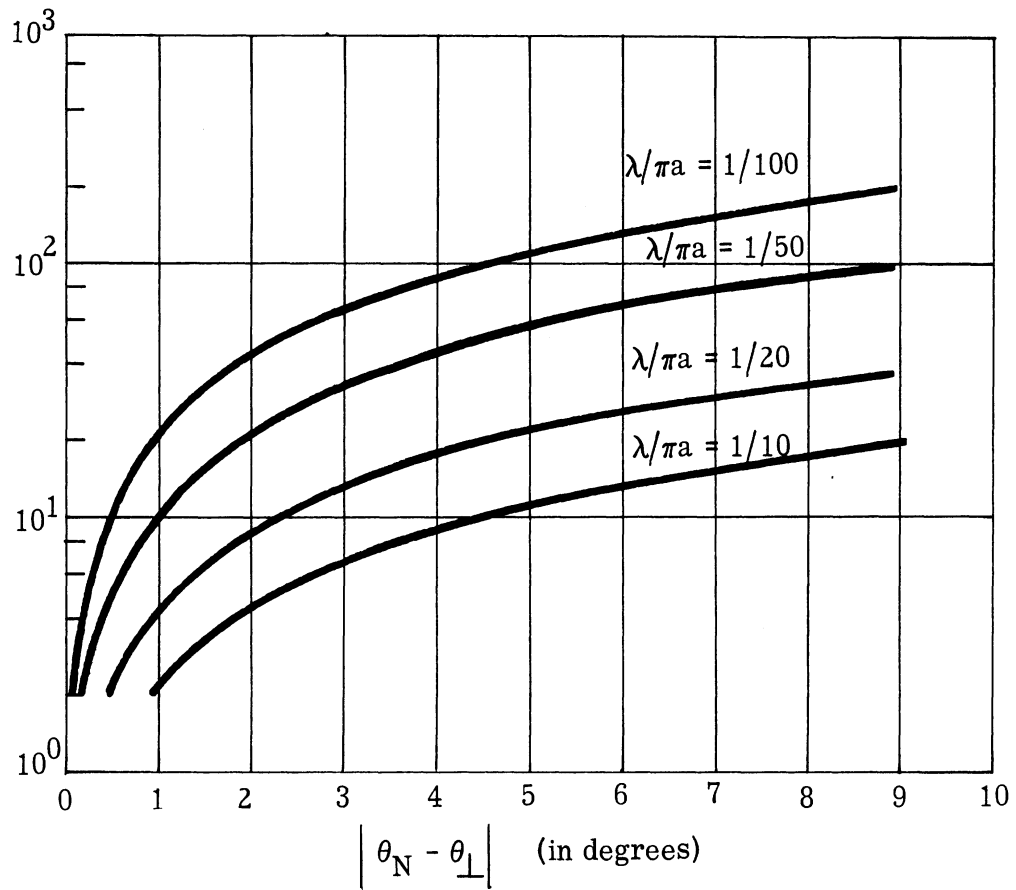


FIG. 4.11-2: PEAK WIDTHS FOR A TORUS

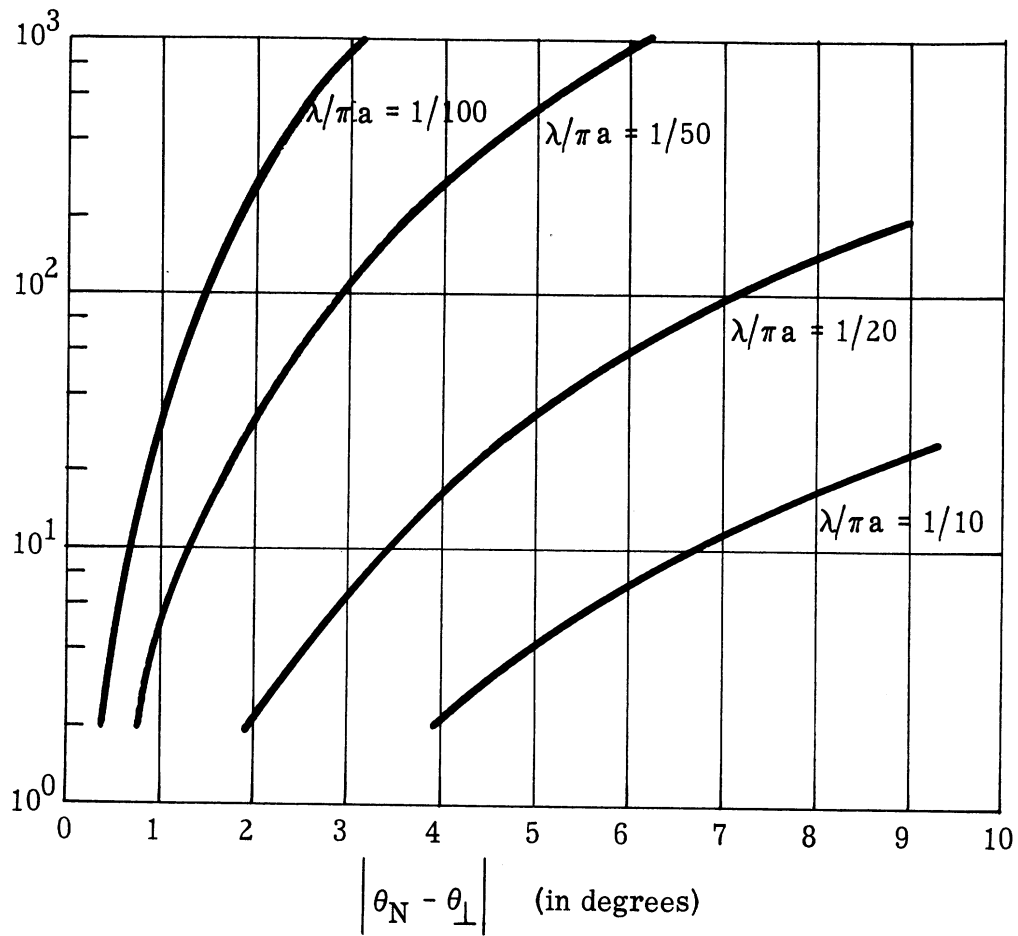


FIG. 4.11-3: PEAK WIDTHS FOR THE CIRCULAR FLAT PLATE

BISTATIC RADAR CROSS SECTIONS

5.1 Bistatic Cross Sections For Angles of Separation Less Than 180°

Bistatic cross sections for small wavelengths have been discussed in considerable detail in Reference 15 where the cross sections of several simple shapes are presented. There is, however, a very simple relationship which exists between the monostatic and bistatic cross sections that permits the determination of the bistatic cross section in terms of the monostatic results presented elsewhere in this report. Thus, we shall direct our attention to this relationship which we shall present in the form of a theorem:

IN THE LIMIT OF VANISHING WAVELENGTH THE BISTATIC CROSS SECTION FOR TRANSMITTER DIRECTION \hat{k} AND RECEIVER DIRECTION \hat{n}_0 IS EQUAL TO THE MONOSTATIC CROSS SECTION FOR THE TRANSMITTER-RECEIVER DIRECTION $\hat{k} + \hat{n}_0$ WITH $\hat{k} \neq \hat{n}_0$ FOR BODIES WHICH ARE SUFFICIENTLY SMOOTH

PROOF: From page 12 of Reference 15 we have the cross section as a function of receiver and transmitter positions given by

$$\sigma = 4\pi \left[|F_x|^2 + |F_y|^2 + |F_z|^2 \right] \quad (5.1.1)$$

where

$$\vec{F} = \frac{ik}{2\pi} \left[(\hat{n}_0 \cdot \hat{a}) \vec{f} - (\hat{n}_0 \cdot \vec{f}) \hat{a} \right] \quad (5.1.2)$$

$$\text{with } \vec{f} = \int_{S'} \hat{n} \exp [+ ik\vec{r}' \cdot (\hat{n}_o + \hat{k})] dS \quad (5.1.3)$$

$$i = \sqrt{-1}$$

$$k = 2\pi/\lambda, \quad (\lambda = \text{the wavelength}),$$

$$\hat{n}_o = \text{unit vector directed from the receiver to the origin,}$$

$$\hat{a} = \text{unit vector defining the incident magnetic field direction,}$$

$$S' = \text{illuminated region of the body,}$$

$$\hat{n} = \text{unit outward normal to the surface,}$$

$$\vec{r}' = \text{radius vector from origin to a point on the surface of the reflecting body, and}$$

$$\hat{k} = \text{unit vector directed from the transmitter to the origin.}$$

Let the origin of a rectangular coordinate system be located inside the reflecting surface. Since the body is not specified in what follows there will be no loss in generality if the transmitter in the bistatic case be placed on the z-axis of the coordinate system and the receiver be restricted to lie in the y-z plane. Thus, the geometry we shall employ in the bistatic case is defined by

$$\begin{aligned} \hat{n}_o &= (\sin 2\theta) \hat{i}_y - (\cos 2\theta) \hat{i}_z, \\ \hat{k} &= -\hat{i}_z, \text{ and} \\ \hat{a} &= \cos \phi_t \hat{i}_x + \sin \phi_t \hat{i}_y; \end{aligned} \quad (5.1.4)$$

and in the corresponding monostatic case by

$$\begin{aligned}
\hat{n}_o &= (\sin \theta) \hat{i}_y - (\cos \theta) \hat{i}_z, \\
\hat{k} &= (\sin \theta) \hat{i}_y - (\cos \theta) \hat{i}_z, \text{ and} \\
\hat{a} &= \cos \phi_t \hat{i}_x + \sin \phi_t \cos \theta \hat{i}_y + \sin \phi_t \sin \theta \hat{i}_z.
\end{aligned}
\tag{5.1.5}$$

This geometry is illustrated in Figure 5.1-1. Also, θ is restricted to be less than 90° ; i.e. $\hat{n}_o + \hat{k} \neq 0$.

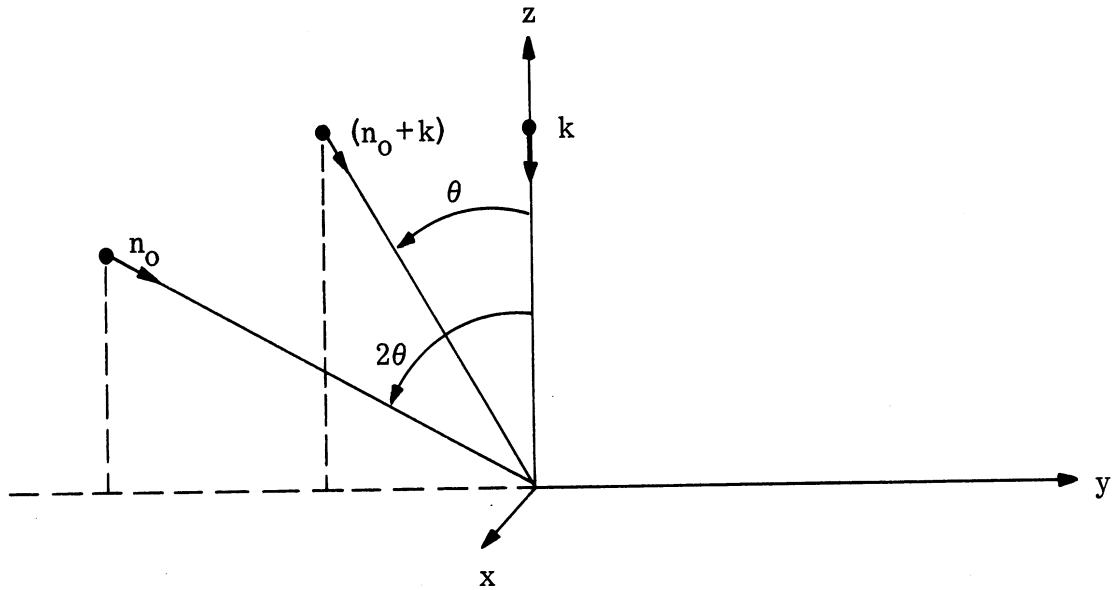


FIG. 5.1-1: BISTATIC GEOMETRY USED IN PROOF OF RELATIONSHIP BETWEEN BISTATIC AND MONOSTATIC CROSS SECTIONS

First let us consider the vector \vec{f} . We have, in the limit of vanishing wavelength (Ref. 15, p. 16)

$$\vec{f} = \frac{-(\hat{n}_o + \hat{k})}{|\hat{n}_o + \hat{k}|} \int_{S'} \exp \left[+ik\vec{r}' \cdot (\hat{n}_o + \hat{k}) \right] dS, \tag{5.1.6}$$

where the integral is evaluated by stationary phase. Thus, in the monostatic

case we have

$$\vec{f} = \hat{p} \int_{S'} \exp \left[ik\vec{r}' \cdot (2\hat{p}) \right] dS, \quad (5.1.7)$$

where

$$\hat{p} = (\sin \theta) \hat{i}_y - (\cos \theta) \hat{i}_z,$$

and in the bistatic case we have

$$\vec{f} = -\hat{p} \int_{S'} \exp \left[-ik\vec{r}' \cdot (2\hat{p} \cos \theta) \right] dS. \quad (5.1.8)$$

Thus, evaluating these integrals by stationary phase (page 14), Ref. 15 we obtain expressions of the form:

in the monostatic case

$$\vec{f} = \left[(A \sin \theta) \hat{i}_y - (A \cos \theta) \hat{i}_z \right] \exp(ikC), \quad (5.1.9)$$

and in the bistatic case

$$\vec{f} = \left[(A \tan \theta) \hat{i}_y - (A) \hat{i}_z \right] \exp(ikC \cos \theta). \quad (5.1.10)$$

Therefore, in the monostatic case under consideration we have

$$\vec{F} = \frac{ik}{2\pi} \left[(Ae^{ikC}) (\hat{i}_x \cos \phi_t + \hat{i}_y \sin \phi_t \cos \theta + \hat{i}_z \sin \phi_t \sin \theta) \right] \quad (5.1.11)$$

from which it follows that

$$\left| F_x \right|^2 + \left| F_y \right|^2 + \left| F_z \right|^2 = \left| kA/2\pi \right|^2. \quad (5.1.12)$$

In the bistatic case under consideration we have

$$\vec{F} = \frac{ik}{2\pi} \left\{ +Ae^{ikC\cos\theta} \right\} \left\{ (\sin\phi_t \sin 2\theta)(\hat{i}_y \tan\theta - \hat{i}_z) - (\tan\theta \sin 2\theta + \cos 2\theta)(\hat{i}_x \cos\phi_t + \hat{i}_y \sin\phi_t) \right\}. \quad (5.1.13)$$

Thus,

$$\begin{aligned} |F_x|^2 + |F_y|^2 + |F_z|^2 &= |kA/2\pi|^2 \left[(\tan\theta \sin 2\theta + \cos 2\theta)^2 \cos^2 \phi_t + \sin^2 \phi_t \cos^2 2\theta + \sin^2 \phi_t \sin^2 2\theta \right] \\ &= |kA/2\pi|^2. \end{aligned} \quad (5.1.14)$$

From the definition of σ it follows that for both cases under consideration

$$\sigma = |kA|^2 / \pi \quad (5.1.15)$$

and thus if the body is smooth the bistatic cross section corresponding to a transmitter direction, \hat{k} , and a receiver direction, \hat{n}_0 , is equal to the monostatic cross section corresponding to the transmitter-receiver direction, $\hat{n}_0 + \hat{k}$, in the limit of vanishing wavelength.

Thus, if the wavelength is small in comparison with the dimensions of the body, we can determine the bistatic cross section by applying the above theorem together with the monostatic results of Section 4.*

For the thin wire an approximation procedure based upon the material of References 9, 11, and 12 is as follows:

If $R(\theta)$ is the angular factor predicted by Terman's graphs (Ref. 10),

*

Recent experimental work (Ref. 16) has indicated that this procedure will give good results even for comparatively large wavelengths, wavelength to body dimensions that one would find in considering the B-47 aircraft at 250 Mc.

then we have in the monostatic case

$$\sigma(\theta_r, \theta_t) = K [R(\theta)]^4 \lambda^2 \quad (5.1.16)$$

where by $\sigma(\theta_r, \theta_t)$ we mean that θ_r denotes the direction to the receiver and θ_t the direction to the transmitter, and K is independent of aspect and the wavelength depending only on the wire parameters. In the bistatic case we would have

$$\sigma(\theta_r, \theta_t) = K [R(\theta_r)]^2 [R(\theta_t)]^2 \lambda^2 \quad (5.1.17)$$

Equations (5.1.16) and (5.1.17) imply that

$$\sigma(\theta_r, \theta_t) = \sqrt{\sigma(\theta_r, \theta_r) \times \sigma(\theta_t, \theta_t)} \quad (5.1.18)$$

i. e. that the bistatic cross section is equal to the square root of the product of the two corresponding monostatic cross sections. A study of Weber's work (Ref. 12) indicates that this approach is appropriate for the case of the half-wavelength wire.

It is important to note that in the bistatic case the reciprocity theorem permits the determination of complete patterns with a reduction in the computational effort. The theorem states that the effective cross section is unchanged if the positions of the transmitter and receiver are interchanged.

5.2 Bistatic Cross Sections For An Angle of Separation of 180° - Forward Scattering

Here we shall concentrate on the case of an angle of separation of 180° , the case in which $\hat{n}_o + \hat{k} = 0$ (see Figure 5.1-1). This case, as will be recalled, is not covered by the theorem of Section 5.1.

This case is of considerable importance and warrants special attention for two reasons. One is due to its nature which we will find is considerably different than the type of bistatic scattering discussed in the preceding section. The other is due to what might be termed a misuse of the term. This type of scattering phenomena is only observed for an angle of separation, β , such that $\beta = 180^\circ$. (Experimentally, of course, the phenomena of forward scattering will be observed over an interval around $\beta = 180^\circ$, however this is a small interval.)

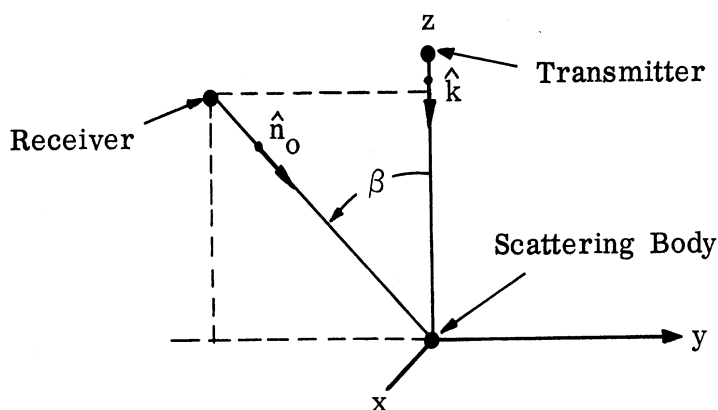


FIG. 5.2-1: GEOMETRY FOR ANALYSIS OF BISTATIC CASE

For the geometry shown in Figure 5.2-1 we have from equation (3.2.6) of Reference 15 that the cross section in the bistatic case is given by

$$\sigma(\beta) = 4\pi \left| \vec{F} \cdot \hat{d} \right|^2 \quad (5.2.1)$$

where

$$\vec{F} = \frac{+ik}{2\pi} \left[(\hat{n}_0 \cdot \hat{a}) \vec{f} - (\hat{n}_0 \cdot \vec{f}) \hat{a} \right]$$

with

$\hat{\mathbf{d}}$ = direction of receiver polarization ,

$\hat{\mathbf{a}}$ = direction of incident magnetic field,

$k = 2\pi/\lambda$,

$\hat{\mathbf{n}}_0$ = direction from receiver to the origin ,

$\hat{\mathbf{k}}$ = direction from transmitter to the origin ,

$$\vec{\mathbf{f}} = \int_{S'} \hat{\mathbf{n}} \exp [ik \vec{\mathbf{r}}' \cdot (\hat{\mathbf{n}}_0 + \hat{\mathbf{k}})] dS,$$

S' = illuminated portion of the body,

$\vec{\mathbf{r}}'$ = radius vector from the origin to any point on the surface of the scattering body, and

$\hat{\mathbf{n}}$ = the unit outward normal to the surface.

If in our discussion we do not specify the body geometry of the scatterer there will be no loss in generality in our consideration of this optics case if we restrict the receiver to lie in the yz-plane and the transmitter to be located on the z-axis (as shown in Figure 5.2-1).

With the above we may rewrite equation (5.2.1) in the form

$$\sigma(\beta) = \frac{4\pi}{\lambda^2} \left| (\hat{\mathbf{n}}_0 \cdot \hat{\mathbf{a}}) (\vec{\mathbf{f}} \cdot \hat{\mathbf{d}}) - (\hat{\mathbf{n}}_0 \cdot \vec{\mathbf{f}}) (\hat{\mathbf{a}} \cdot \hat{\mathbf{d}}) \right|^2. \quad (5.2.2)$$

Restricting our attention to the case of $\beta = 180^\circ$, we have

$$\hat{\mathbf{n}}_0 = \hat{\mathbf{i}}_z, \quad \hat{\mathbf{k}} = -\hat{\mathbf{i}}_z, \quad (\cos \phi_t) \hat{\mathbf{i}}_x + (\sin \phi_t) \hat{\mathbf{i}}_y = \hat{\mathbf{a}},$$

$$\text{and} \quad \hat{\mathbf{d}} = \cos \phi_r \hat{\mathbf{i}}_x + \sin \phi_r \hat{\mathbf{i}}_y.$$

from which we obtain upon substitution into equation (5.2.2)

$$\sigma (\pi) = \frac{4\pi}{\lambda^2} \left| (\cos \phi_t \cos \phi_r + \sin \phi_t \sin \phi_r) \left[\int_{S'} n_z dS \right] \right|^2. \quad (5.2.3)$$

The integral in equation (5.2.3) is merely the projected area in the xy-plane and if we represent this area by A we obtain

$$\sigma (\pi) = \frac{4\pi A^2 \cos^2 (\phi_t - \phi_r)}{\lambda^2}. \quad (5.2.4)$$

If the polarizations are chosen so as to obtain the maximum return then this expression reduces to

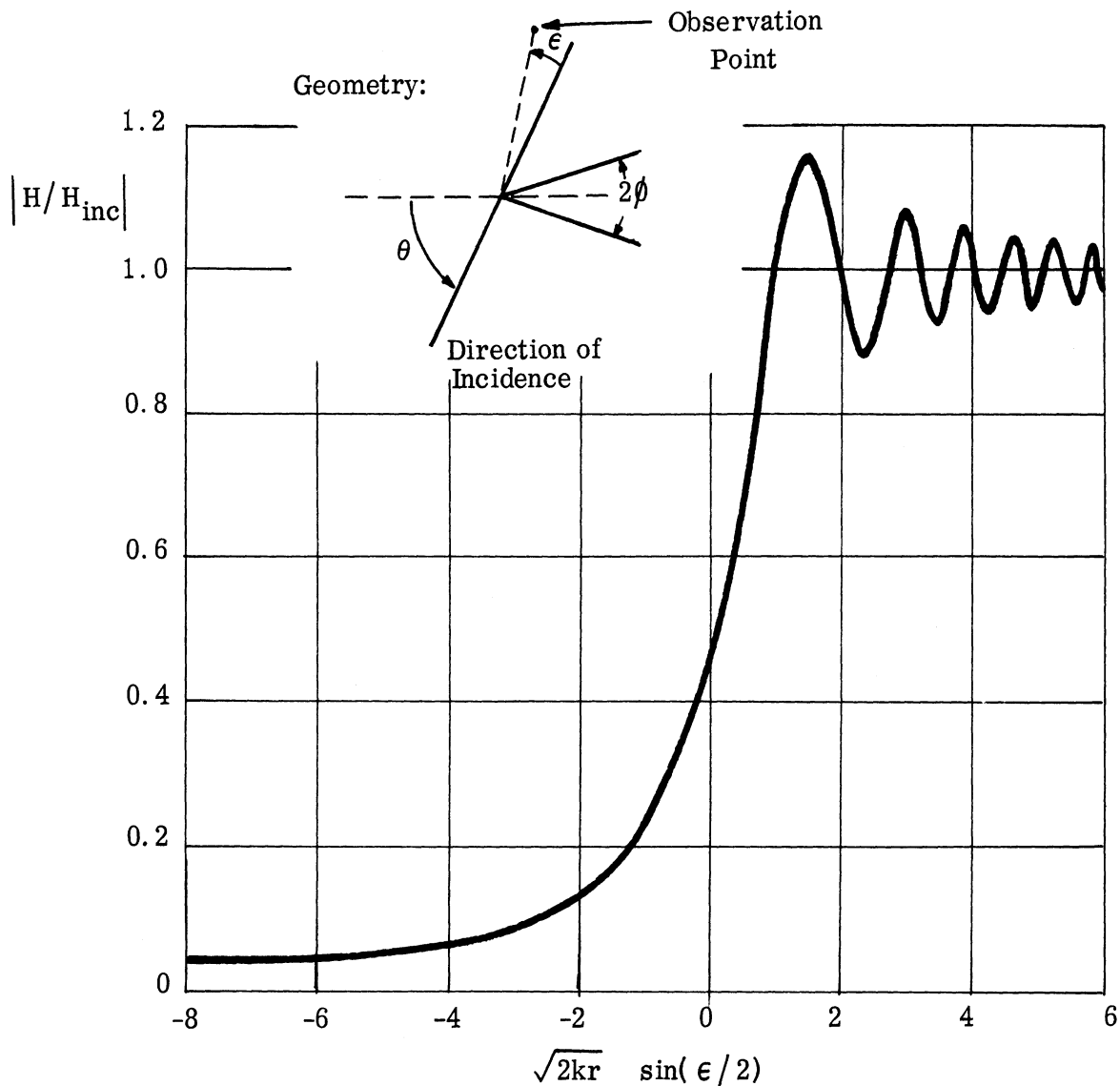
$$\sigma (\pi) = \frac{4\pi A^2}{\lambda^2}. \quad (5.2.5)$$

The case of forward scattering by a sharp edge can be handled in terms of the material of Reference 17; the ratio of $\left| \vec{H}_s \right|$ to $\left| \vec{H}_i \right|$ is displayed graphically in Figure 5.2-2.

The subject of forward scattering is discussed in more detail in Appendix E.

5.3 Bistatic Cross Sections - Illustrative Examples

Several examples of bistatic cross sections for simple shapes can be found in References 18 and 15; here, to serve as an illustration of the application of the material of Section 5.1 and also to give the reader a feeling for the relative magnitudes of monostatic and bistatic cross sections, we shall consider the following simple situation.



- (1) Field is independent of θ for $\theta > \phi$
- (2) $|H/H_{inc}| = (\pi)^{-1/2} \cdot |F(-\sqrt{2kr} \sin(\epsilon/2))|$ where $F(x) = \int_x^{\infty} \exp(-i\lambda^2) d\lambda$
- (3) This neglects an edge wave which is effectively uniform over the values of ϵ considered and decreases with increasing distance from the edge.
- (4) Except for the approximation (3), the result is exact for the half-plane and within 1% for wedges of angle $\phi < 15^\circ$.

FIG. 5.2-2: $|H/H_{inc}|$ AS A FUNCTION OF ANGLE FROM SHADOW EDGE FOR A WEDGE

Let a transmitter (and receiver) be located at the origin of a rectangular coordinate system and let a receiver be located at the point $(0, 2d, 0)$. Let a body in the shape of a 10:1 prolate spheroid move "between" these two points at an altitude equal to z_0 following a flight path defined by the vector $\hat{v} = (\cos \phi) \hat{i}_x + (\sin \phi) \hat{i}_y$. This flight path will cross the yz -plane at the point $(0, y, z_0)$ with $0 \leq y \leq 2d$. This geometry is shown in Figure 5.3-1.

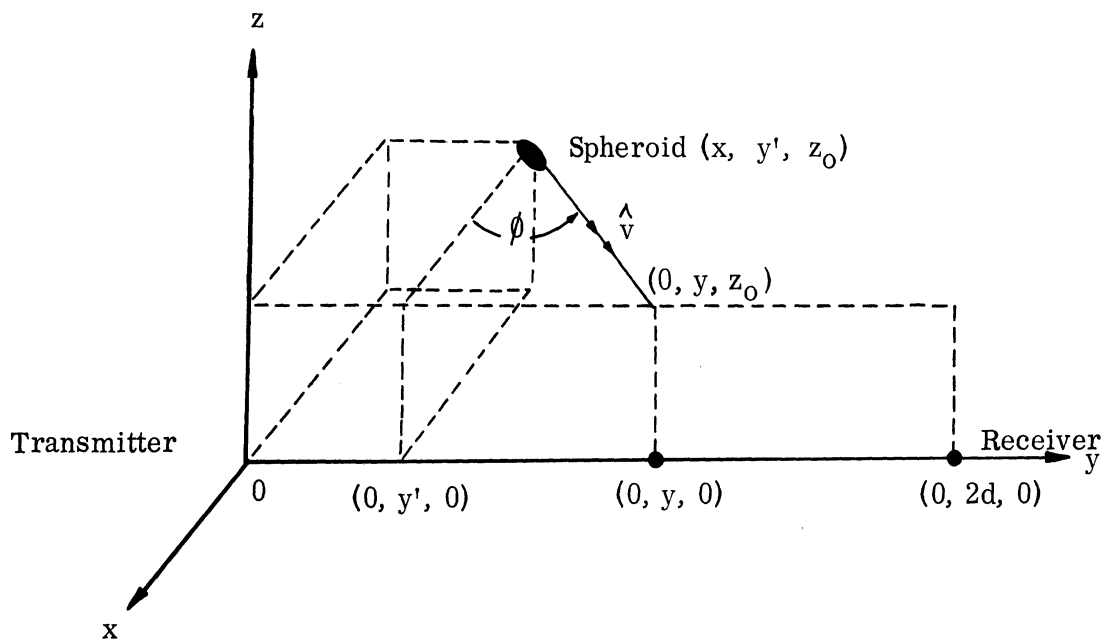


FIG. 5.3-1: GEOMETRY FOR BISTATIC ILLUSTRATIONS

In these examples we will assume that the vector \hat{v} lies along the major axis of the spheroid. We shall consider the cross sections as a function of the altitude z_0 , the cross-over-point y , and the flight direction ϕ . In each case the monostatic cross section (receiver at origin) and the bistatic cross section corresponding to the transmitter at the origin and

the receiver at the point $(0, 2d, 0)$ is determined. Specifically, we shall consider the following three cases:

(1) $z_0/d = 0.04$ and $\phi = 0$; $y = 0, d, \text{ and } 2d$; $-0.4 \leq x/d \leq 0.4$.

(2) $x/d = -0.2$ and $\phi = 0$; $z_0/d = .12$; $0 \leq y \leq 2d$.

(3) $x = 0, z_0/d = 0.2$.

In each case we make use of the theorem of Section 5.1 to determine the cross sections for the bistatic case from the material of Section 4 which of course also yields the monostatic data. The results obtained are shown in Figures 5.3-2 through 5.3-4 for the above three cases respectively.

We see from Figure 5.3-2 that for flight paths which are normal to the base line the bistatic return is appreciably larger than the monostatic if the object passes over the transmitter, there is little or no difference in the two returns if the flight path is over the bistatic receiver, and that if the flight path is over the midpoint of the base line then the monostatic return tends to be the larger.

From Figure 5.3-3 we note that for detection at a given distance from the base line the bistatic return is larger if the path is over the transmitter, the monostatic is considerably larger for flight paths over the midpoint of the base line, and that for other parallel flight paths the monostatic return tends to be slightly larger.

Figure 5.3-4 gives information about the relative magnitudes of the bistatic and monostatic returns at the moment the object passes over the

base line; we see from the figure that if the object passes over the base line with $\phi = 0$ or at $y/d = 0.5$ then the two cross sections are equal. If y/d is less than $1/2$ then the monostatic return is either the same or greater than the bistatic. For $y/d > 0.5$ and $\phi \neq 0$ the bistatic return is larger, and if y/d is close to one then the bistatic return can be considerably larger.

The situation becomes more complex if the body in question is not of this simple form; for example, if the prolate spheroid discussed above should have wing, rudder, and stabilizer surfaces attached, then the comparisons would be somewhat different. For most of the aspects one would consider (assuming a similar flight path) the contributions from the fuselage (the spheroid) would dominate, but there would be aspects at which peaks in the return would result due to contributions from the edges of the wing surfaces.

In comparing the radar cross section in the bistatic case with a corresponding monostatic case it is important to note that shadowing effects can play a dominant role. The theorem of Section 5.1 might lead one to think that the relationship given there for simple shapes would also hold for cross section studies on such shapes as aircraft. If the wavelength is sufficiently small and if none of the contributions are shadowed out, then the theorem of Section 5.1 would be applicable to the complex body problem. However, it will often happen that components which are dominant for the monostatic case will be completely shadowed in the bistatic case and conversely. This situation is illustrated in Figures 5.3-5 and 5.3-6.

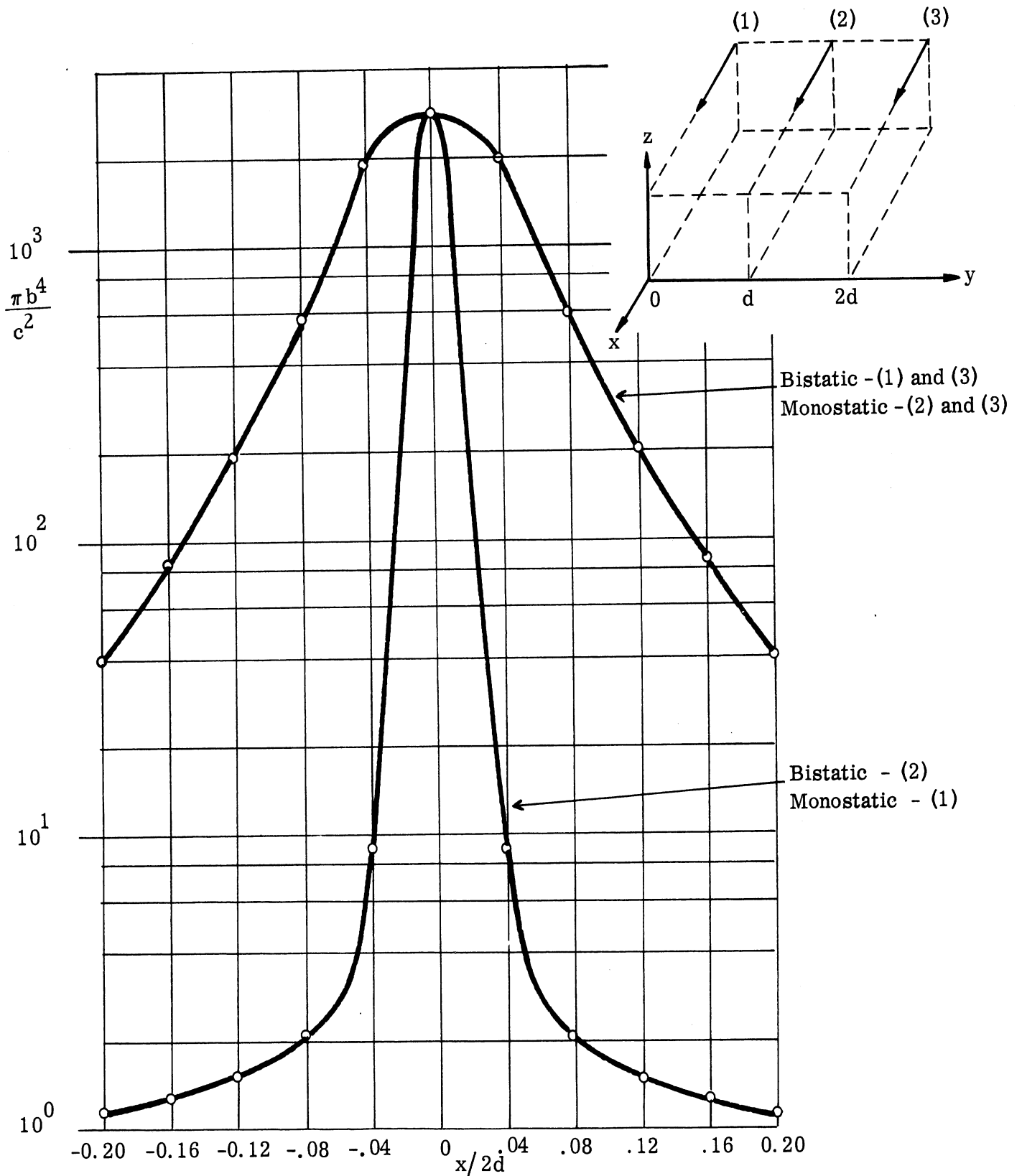


FIG. 5.3-2: COMPARISON BETWEEN BISTATIC AND MONOSTATIC CROSS SECTIONS OF A TEN TO ONE ($c/b = 10$) PROLATE SPHEROID FOR THREE FLIGHT PATHS NORMAL TO LINE JOINING TRANSMITTER AND RECEIVER (Altitude = $d/25$)

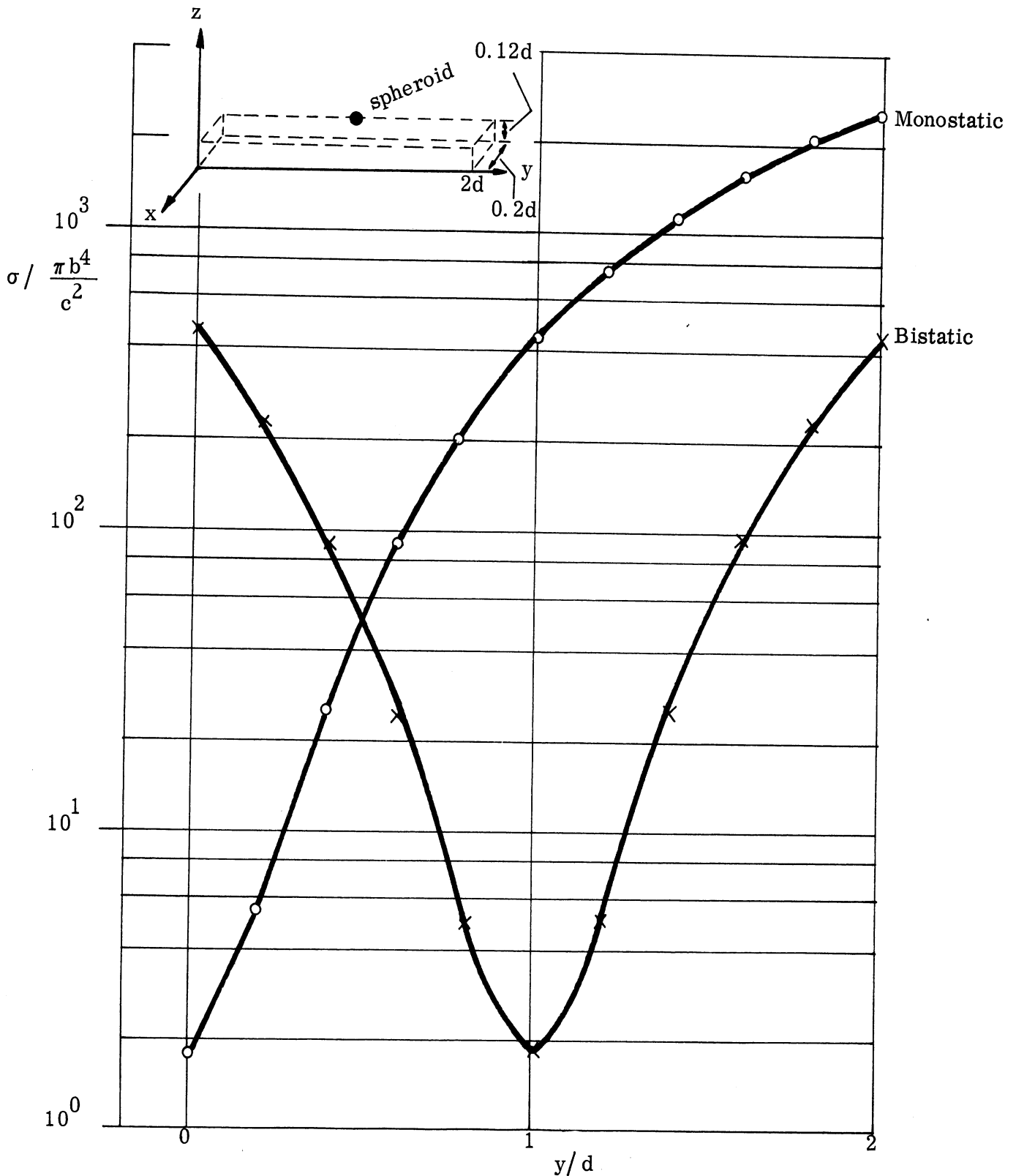


FIG. 5.3-3: COMPARISON BETWEEN BISTATIC AND MONOSTATIC CROSS SECTION OF A TEN TO ONE ($c/b = 10$) PROLATE SPHEROID FOR LOCATIONS RESTRICTED TO AN ALTITUDE EQUAL TO 0.06 TIMES THE DISTANCE BETWEEN TRANSMITTER AND RECEIVER AND AT A FIXED DISTANCE FROM THE "CROSS OVER" LINE

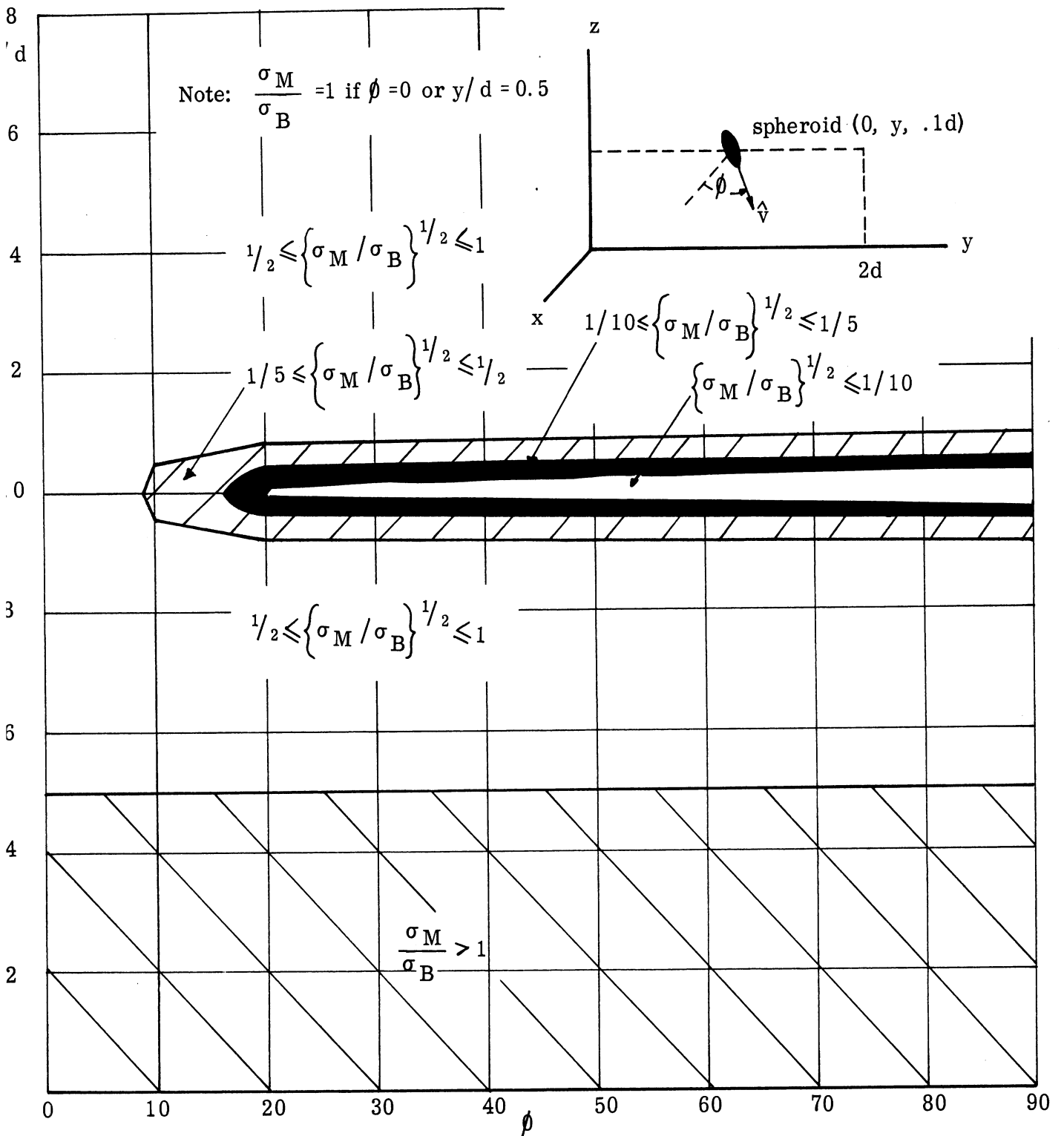


FIG. 5.3-4: COMPARISON OF BISTATIC AND MONOSTATIC CROSS SECTIONS OF A TEN TO ONE ($c/b = 10$) PROLATE SPHEROID FOR LOCATIONS ABOVE THE LINE JOINING THE TRANSMITTER AND RECEIVER AT AN ALTITUDE OF $0.1d$ WHERE THE DISTANCE BETWEEN TRANSMITTER AND RECEIVER EQUALS $2d$ AS A FUNCTION OF THE "CROSS OVER POINT" AND THE ASPECT

In Figure 5.3-5 we show the case in which shadowing leads to a larger bistatic return than the monostatic return. We see from the Figure that in the bistatic case reflections are received from both the fuselage and the wing tank while in the monostatic case the fuselage is in the shadow of the wing tank.

Figure 5.3-6 displays the type of situation which will lead to a much larger monostatic cross section than the bistatic cross section. We see from the figure that for the nose-on case (monostatic) reflections will be received from the fuselage, all the engines, and all of the wing tanks. In the bistatic case illustrated; however, only the return from the fuselage is received. The energy which is incident upon the wing engines and tanks on the left is reflected away from the bistatic receiver by the fuselage and the fuselage shields the wing surfaces on the right so that none of the incident energy reaches these surfaces. Thus we see that, in this case, if the bistatic angle is much larger than 40° (it is about 90° in Figure 5.3-6) we would expect shadowing to greatly reduce the bistatic return.

These two Figures (5.3-5 and 5.3-6) indicate why one must be careful in applying the theorem of Section 5.1 to a problem involving the determination of the bistatic cross section of a complex shape.

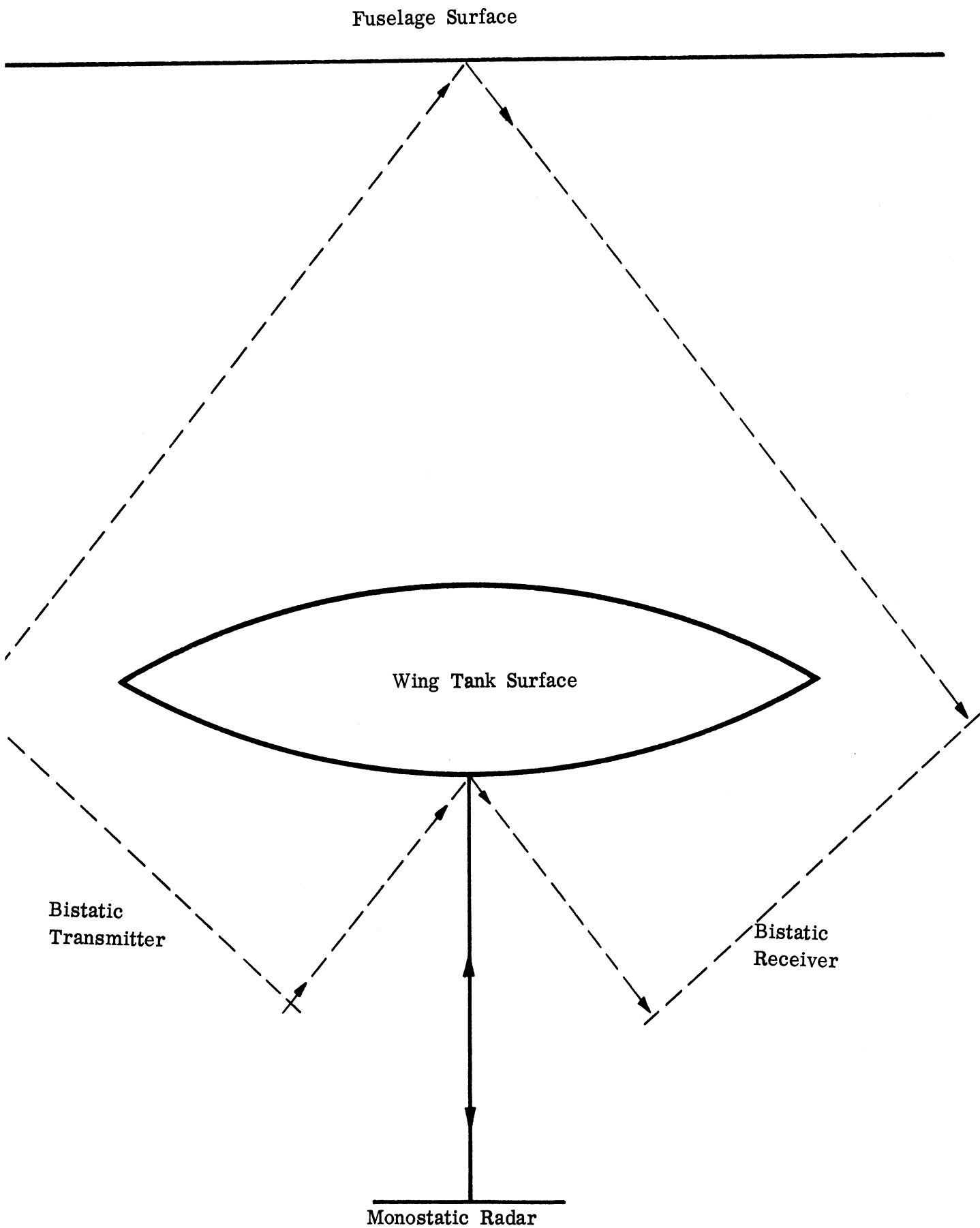


FIG. 5.3.5: SHADOWING EFFECT ON BISTATIC VS: MONOSTATIC CROSS SECTIONS - ILLUSTRATION I

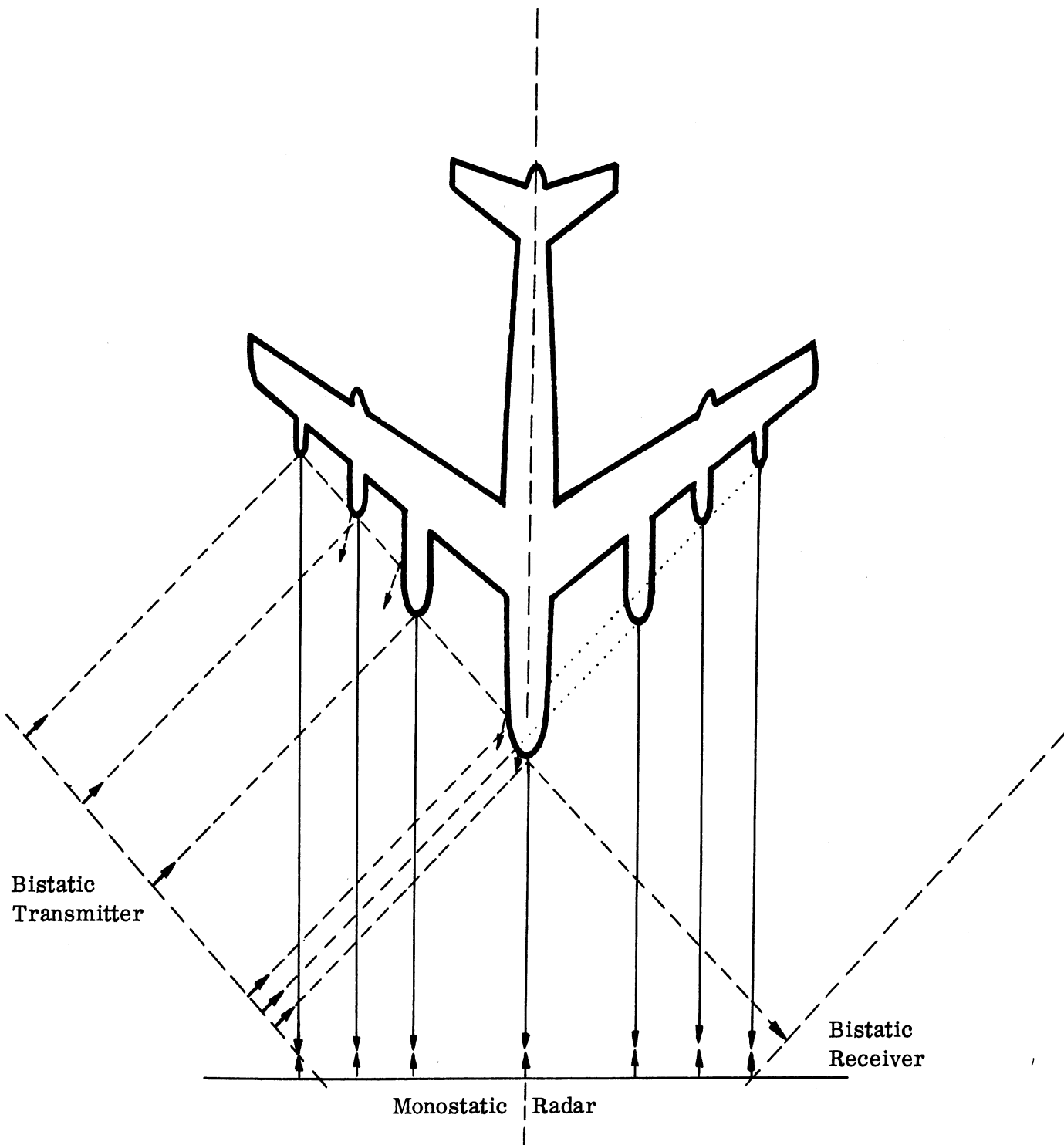


FIG. 5.3.6: SHADOWING EFFECT ON BISTATIC VS. MONOSTATIC CROSS SECTIONS - ILLUSTRATION II

THE COMBINATION OF THE COMPONENT CROSS SECTIONS

Having completed the first two steps of the theoretical method, one is then presented with the problem of properly combining these component cross sections to obtain the estimate of the cross section of the complex body itself. As a result of the first two steps we have, for any given combination of aspect angle, wavelength, and polarization, N components for which cross sections have been computed, i. e., we have the set of values

$$\sigma_1, \sigma_2, \sigma_3, \dots, \sigma_N.$$

In considering the proper manner in which these component cross sections should be combined we first must consider the question of shadowing effects.

When one body is in the shadow of another, the effect that the shadow has on the scattering properties depends upon the parts of the body which are in shadow. In general, the cross section of a body is mainly determined by the returns from those parts of the body giving specular reflections and/or from the discontinuities on the body surface. Thus, if these portions of the body are in shadow, then that component will not contribute significantly to the cross section of the complex of simple shapes making up the aircraft or missile under study. Conversely, if these critical portions of the body are not in shadow, then that component will contribute to the cross section of the aircraft (or missile) just as if there were no shadowing at all.

Having taken shadowing effects into account, we then have N scatterers to consider and thus N values of cross section to consider. There are two methods of combination which we shall consider; both of them have their limitations and both have been found to yield results which are in good agreement with experimental results. One of these methods of combination involves the consideration of the fact that these N scatterers are located at different distances from the radar and involves the attempt to determine the relative phase angles between the returns from these N scatterers. This approach leads to the following expression for the cross section of the entire body; we denote this expression for the cross section by σ_P (cross section by relative phase):

$$\sigma_P = \left| \sum_{j=1}^N (\sigma_j)^{1/2} \exp(i\phi_j) \right|^2 \quad (6.1)$$

where σ_j = the cross section of the j^{th} component and ϕ_j = the relative phase angle associated with the j^{th} component. The magnitudes of the ϕ_j are determined by the expression shown in Figure 6-1. Thus, in this approach it is necessary to determine estimates of many additional distances from the aircraft drawings. As can readily be seen from the expression for the ϕ_j , their values are directly dependent upon the ratios d_j/λ , and it is obvious that for a large aircraft at small wavelengths it might be impossible to measure the d_j from the aircraft drawings with sufficient precision. In addition to this difficulty in measuring the d_j (and thus the ϕ_j), it is to be noted

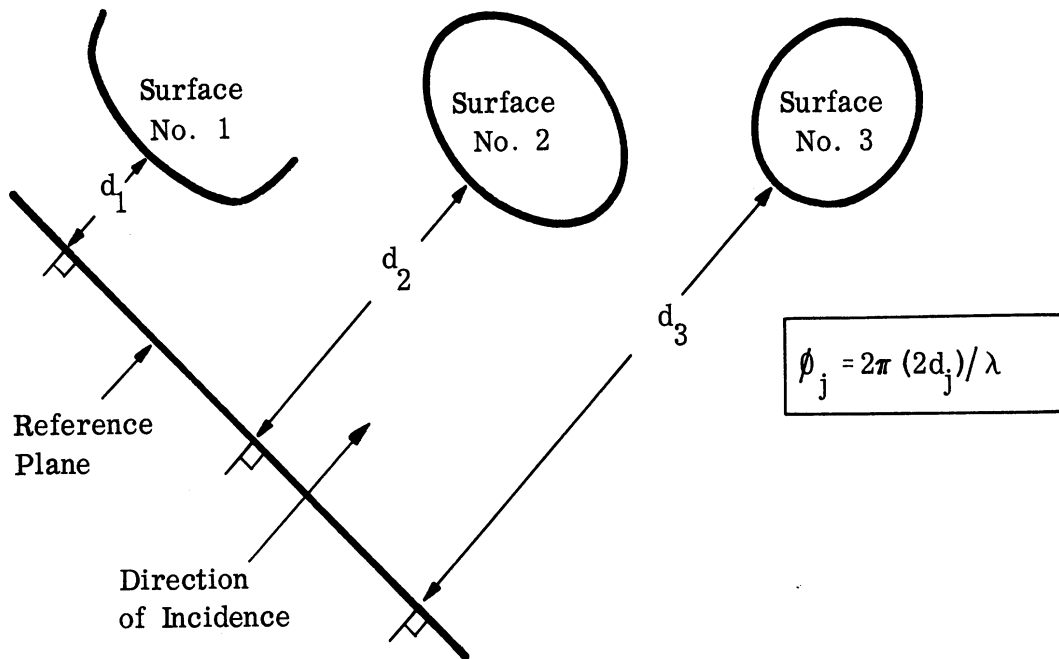


FIG. 6-1: DETERMINATION OF THE RELATIVE PHASE ANGLES

that an aircraft vibrates to some extent while in flight and this vibration could suffice, in many cases, to effectively change the values of the ϕ_j . Also, as pointed out in Section I in connection with the question of trying to obtain extreme precision in theoretical values for the radar cross sections of aircraft or missiles, minor variations between two aircraft of the same model designation might suffice to effectively change some of the ϕ_j . All of these facts tend to discourage the use of this method of combination.

As an alternative to this method of combination we have what we refer to as the random phase method of combination which yields the

"average" radar cross section. This method is based upon the assumption that the many different ϕ_j are randomly distributed between 0 and 2π (after each ϕ_j has been placed in its equivalently smallest form using the fact that $\exp(i\phi_j) = \exp(i\phi_j - 2i\pi)$); then upon averaging over the ϕ_j we obtain as our expression for the "average" cross section

$$\sigma' = \sum_{j=1}^N \sigma_j. \quad (6.2)$$

Associated with this method of approach we can estimate the amount of possible deviation from the average cross section, σ' , by employing the RMS spread. This measure of the possible variation in cross section due to relative phase effects leads to the following bounds on the cross section

$$\sigma' \pm S \quad (6.3)$$

where

$$S^2 = \left(\sum_{j=1}^N \sigma_j \right)^2 - \sum_{j=1}^N \sigma_j^2.$$

The random phase method which uses the average cross section and the RMS spread is designed to give estimates of the amount by which the cross section might deviate from the average value due to phase effects. On the other hand, the relative phase method of combination is designed as a means of estimating not only the amount by which the cross

section deviates from the average value but also the location (in aspect or wavelength) of the relative peaks and nulls.

Which of these two methods of combination to be chosen for a particular problem would depend upon the purpose of the calculation. If one were interested in finding an order-of-magnitude estimate of the cross section as a function of aspect for some fixed wavelength or as a function of wavelength at some fixed aspect, then the random phase method should be adequate. If, on the other hand, one should happen to be interested in determining the manner in which the cross section might vary (due to phase changes) with aspect at a given wavelength or with wavelength at a fixed aspect, then the relative phase method can provide information of considerable interest. It is true that the precise determination of the ϕ_j is often impossible and in such a case one could not place much confidence in the results obtained. However, even in this case one can obtain some idea of how the ϕ_j will change with aspect (at a fixed wavelength) or wavelength (at a fixed aspect) and thus, if one is only interested in determining the type of oscillation in cross section to be expected, the relative phase method can yield useful data even though precision is lacking in the determination of the ϕ_j . Of course, if the ratios, d_j/λ , can be determined with sufficient accuracy so that the ϕ_j were known to, say, two decimal places, then the relative phase method will yield fairly good estimates as to the location of the relative peaks and nulls.

The random phase method of combination has been applied in the past to the determination of the radar cross sections of many different aircraft and missiles and the results have been found to be in good agreement with experimental data (the two sets of results, theory and experiment, agreeing in almost all cases to within 2 to 10 db with differences greater than 6 db occurring, for the most part, only in the vicinity of an experimentally determined peak or null - a situation which can usually be traced to an extreme type of phase effect).

The basic premise that the cross section of an aircraft (or missile) can be estimated by (1) breaking up the aircraft into its components, (2) determining the radar cross sections of the components, and (3) adding the component cross sections to obtain the cross section of the entire body, has been checked out experimentally. The Air Force Cambridge Research Center applied this process on a missile shape (about three wavelengths long and 1.25 wavelengths thick). The cross section of the entire missile was first determined experimentally, then the cross sections of the components were determined (again by experiment); it was found that the sum of the component cross sections (upon taking shadowing effects into account) was approximately the same as the cross section of the entire body.

To obtain some idea of how the relative magnitudes of the σ_j effect the estimates of oscillation due to phase changes either through the use of the random phase method or the relative phase method let us give a little

attention to the cases $N = 2, 3, 4$. In doing this let us assume that the σ_j have been ordered according to magnitude as follows:

$$\begin{aligned}\sigma_1 &\leq \sigma_2, \\ \sigma_1 &\leq \sigma_2 \leq \sigma_3, \text{ or} \\ \sigma_1 &\leq \sigma_2 \leq \sigma_3 \leq \sigma_4\end{aligned}$$

with the cross sections normalized so that $\sigma_1 = 1 \text{ m}^2$.

For the case of $N = 2$ we have considered the cases of $\sigma_2 = 1, 1.5, 2, 4,$ and 9 m^2 . The average cross sections, the RMS spread, the relative phase maximums, and the relative phase minimums have been computed; the results obtained are shown in Table 6.1. We see from the table that the magnitude of the possible variation from the average is adequately predicted by the RMS spread in all cases if $\sigma_2 / \sigma_1 \geq 4$ and is not adequate in other cases only if the ϕ_j are such that $\cos(\phi_2 - \phi_1)$ is negative and close to -1 .

For the $N = 3$ case we have examined a variety of different values of the σ_j and in addition to the quantities determined for the $N = 2$ case we have also determined the relative phase minimum for the special case of $\cos(\phi_2 - \phi_3) = 0$. These results are shown in Table 6.2. An examination of this data indicates that the maximum is adequately predicted through the use of the RMS spread and that the minimum values are also adequately predicted by the RMS spread if the phase angles ϕ_2 and ϕ_3 are such that $\cos(\phi_2 - \phi_3)$ is non-negative.

The $N = 4$ case was considered in a similar manner and the results obtained are shown in Table 6.3; in this case only the relative phase minimums

were calculated in the relative phase consideration of the problem since it has already been observed in the $N = 3$ case that the greatest differences in the two sets of estimates occur in the vicinity of relative nulls.

σ_1	σ_2	The RMS Spread	σ'	The Relative-Phase Spread
1	1	0.59 - 3.4	2	0 - 4.0
1	1.5	0.77 - 4.2	2.5	0.05 - 4.9
1	2	1.0 - 5.0	3	0.17 - 5.8
1	4	2.2 - 7.8	5	1.0 - 9.0
1	9	5.8 - 14.2	10	4.0 - 16.0

TABLE 6.1: RELATIVE PHASE AND RANDOM PHASE FOR $N = 2$ (σ in m^2)

σ_1	σ_2	σ_3	The RMS Spread	σ'	The Relative-Phase Spread	Relative Phase Min. $\cos(\phi_2 - \phi_3) = 0$
1	1	1	0.55 - 5.45	3	0 - 9.0	0.18
1	1	9	4.84 - 17.2	11	1 - 25	4.7
1	1	49	36.9 - 65.1	51	25 - 81	37
1	2	2	1.0 - 9.0	5	0 - 15	1.0
1	2	9	4.38 - 19.6	12	.36 - 29	5.4
1	2	49	34.7 - 69.3	52	21 - 89	38
1	4	4	2.07 - 15.9	9	0 - 25	3.3
1	4	9	4.10 - 23.9	14	0 - 36	6.9
1	4	49	31.5 - 76.5	54	16 - 100	40

TABLE 6.2: RELATIVE PHASE AND RANDOM PHASE FOR $N = 3$
(σ in m^2)

σ_1	σ_2	σ_3	σ_4	σ'	RMS Spread	Relative Phase Minimum	Other Relative Phase Minima	
							$\cos(\phi_3 - \phi_4) = 0$	$\cos(\phi_3 - \phi_4) = 1$
1	4	81	100	186	52 - 320	0	130	256
1	4	64	100	169	49 - 289	0	113	225
1	4	49	100	154	48 - 260	0	98	196
1	4	36	100	141	48 - 234	1	85	169
1	4	25	100	130	51 - 209	4	74	144
1	4	16	100	121	55 - 187	9	65	121
1	4	9	100	114	60 - 168	16	58	100

TABLE 6.3: RELATIVE PHASE AND RANDOM PHASE FOR N = 4

The relative phase minima appearing in Table 6.3 were determined by employing equation (6.1) to obtain

$$\sigma_P = \left| 10 + \sqrt{\sigma_3} e^{i(\phi_3 - \phi_4)} + 2 e^{i(\phi_2 - \phi_4)} + e^{i(\phi_1 - \phi_4)} \right|^2 .$$

Thus, if $\phi_3 - \phi_4 = 2n\pi$, we have

$$\sigma_P \geq \left| 7 + \sqrt{\sigma_3} \right|^2 ; \text{ and}$$

if $\phi_3 - \phi_4 = (2n+1)\pi/2$, we have

$$\sigma_P \geq \left| 7 + i\sqrt{\sigma_3} \right|^2 .$$

The material presented in these three tables clearly indicates how highly dependent the relative phase estimate of the cross section is on the

phase angle between the two largest contributors. If one is sure that the relative phase angle between the two largest contributors is such that its cosine is non-negative, then the random phase method of combination (average cross section plus the RMS spread) will suffice as a means of estimating the range of the possible variation in the cross section.

It is of some interest to consider the case in which the two largest contributions are of equal magnitude. Let us assume that of the set of N values of cross section the two largest are σ_1 and σ_2 and that $\sigma_1 = \sigma_2$. We may place equation (6.1) in the form

$$\sigma_P = \sum_{n=1}^N \sigma_n + 2 \sum_{n=1}^{N-1} \sum_{k=n+1}^N \sqrt{\sigma_n \sigma_k} \cos(\phi_n - \phi_k). \quad (6.4)$$

Under the conditions we have imposed, equation (6.4) may be placed in the form

$$\begin{aligned} \sigma_P = & 2\sigma_1 + 2\sigma_1 \cos(\phi_1 - \phi_2) + 2\sqrt{\sigma_1} \sum_{k=3}^N \sqrt{\sigma_k} (\cos(\phi_1 - \phi_k) + \cos(\phi_2 - \phi_k)) \\ & + \sum_{n=3}^N \sigma_n + \sum_{n=3}^{N-1} \sum_{k=n+1}^N 2\sqrt{\sigma_n \sigma_k} \cos(\phi_n - \phi_k). \end{aligned} \quad (6.5)$$

We readily see that if $\phi_1 - \phi_2 = (2n+1)\pi$, then the entire first row of the right side of equation (6.5) will reduce to zero and the magnitude of σ_P is determined by the role played by the remaining σ_n ($n = 3, 4, \dots, N$).

ILLUSTRATIVE EXAMPLES

7.1 Radar Cross Section of a Missile

In this section we shall illustrate the theoretical method for the calculation of the radar cross section of a missile or an aircraft by determining the radar cross section of the fictitious missile shown in Figure 7.1-1. We will note from Figure 7.1-1 that this missile consists of a paraboloid faired into an ogive which in turn is faired into a cylinder; four fins are mounted in the back. The fins are taken to be rectangular in shape in the form of flat plates with sharp edges (for simplicity we shall assume that these edges are in the form of wires having a radius of $\lambda/85$). The calculation shall be performed at a wavelength of 1 ft (this choice of wavelength will permit us to illustrate both methods of treating wires discussed in Section 4.4). We shall consider two polarizations: vertical polarization - the case in which the E-vector is in the plane determined by the direction of incidence and the z-axis, and horizontal polarization - the case in which the E-vector is normal to this plane. The cross section will be determined for two different values of ϕ ($\phi = 0^\circ$ and $\phi = 45^\circ$) as a function of θ .

We observe from Figure 7.1-1 that there are the following components to be considered:

- (1) the paraboloid section of the fuselage, σ_1 (This component will contribute for $0^\circ \leq \theta < \sim 76^\circ$),

- (2) the ogive section of the fuselage, σ_2 (This component will contribute for $\sim 76^\circ < \theta < 90^\circ$),
- (3) the cylinder section of the fuselage, σ_3 (This component will contribute for $90^\circ \leq \theta \leq 180^\circ$ when $\phi = 0^\circ$ and for $0^\circ < \theta \leq 180^\circ$ when ϕ is between 0° and 90° ; we shall assume that the rear of the fuselage consists of one sharp rim in the form of a loop of radius 3 ft. with the "wire" having a radius = $\lambda/85$.),
- (4) the fin in the + x, z-plane, σ_4 ; there are four parts of this component to be considered:

$\sigma_{4,1}$ = the contribution from the leading edge,

$\sigma_{4,2}$ = the contribution from the side edge,

$\sigma_{4,3}$ = the contribution from the trailing edge, and

$\sigma_{4,4}$ = the contribution from the flat surface,

- (5) the fin in the + y, z-plane, σ_5 (We have the same four parts to consider as in σ_4 .),
- (6) the fin in the -x, z-plane, σ_6 (We have the same four parts to consider as in σ_4 .), and
- (7) the fin in the -y, z-plane, σ_7 . (We have the same four parts to consider as in σ_4 .)

To determine the magnitude of σ_1 we make use of equation (4.10.1) and we see that this contribution is independent of both wavelength and polarization. Thus we have

Description of Geometry of Surface:

A: Paraboloid: $x^2 + y^2 = -z$

B: Ogive: Radius = 33

C: Cylinder: $L = 24$, $a = 3$

D: Flat Plate

(all dimensions are in feet)

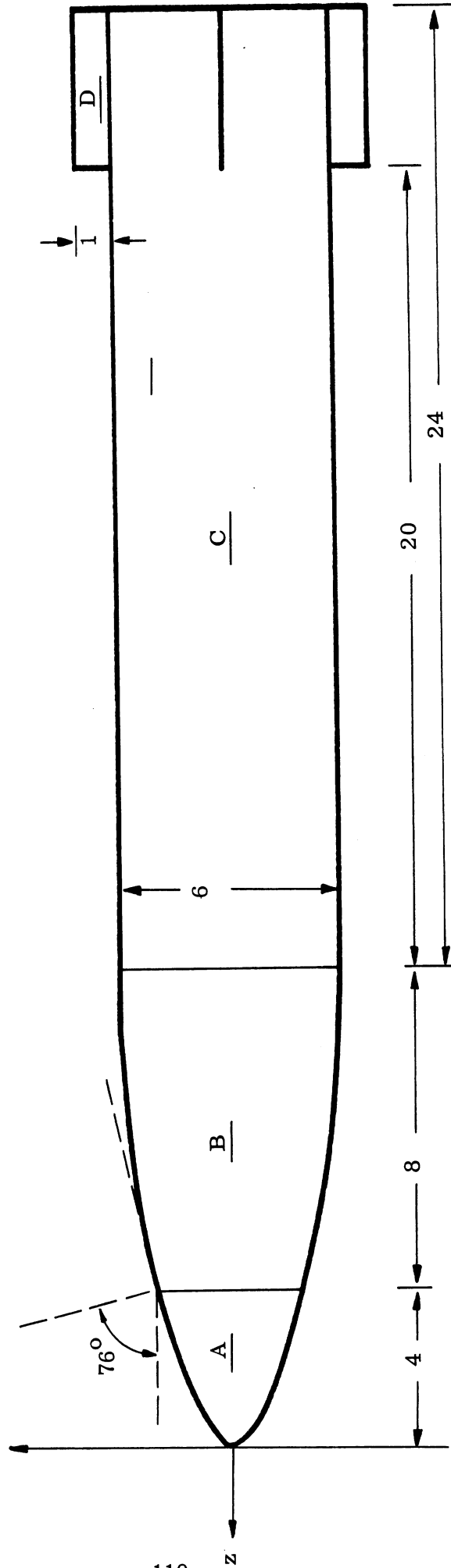
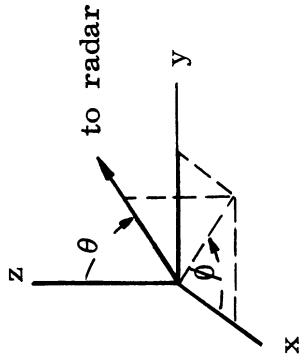


FIG. 7.1-1: FICTITIOUS MISSILE USED IN ILLUSTRATIVE EXAMPLE

$$\sigma_1 = (\pi/4)\sec^4 \theta \text{ ft}^2 \quad \text{for } 0^\circ \leq \theta < 76^\circ. \quad (7.1.1)$$

For σ_2 we make use of equation (4.6.5) and again we see that the contribution is independent of both wavelength and polarization. We have

$$\sigma_2 = 33\pi (33 - 30 \csc \theta) \text{ ft}^2 \quad \text{for } \sim 76^\circ < \theta < 90^\circ. \quad (7.1.2)$$

To determine the magnitude of σ_3 we must consider three cases; $\theta = 90^\circ$, $\theta \approx 180^\circ$, and $\theta \neq 90^\circ$ (but less than 180°). For $\theta = 90^\circ$ we employ equation (4.4.3) and thus we have (since $a = 3 \text{ ft.}$ and $\lambda = 1 \text{ ft.}$)

$$\sigma_3 = 6\pi L^2 \quad \text{for } \theta = 90^\circ. \quad (7.1.3)$$

When $\theta = 0^\circ$, $L = 20 \text{ ft.}$ and when $0^\circ < \theta < 90^\circ$, $L = 24 \text{ ft.}$

For $\theta \neq 90^\circ$ (but near the broadside aspect) we make use of equation (4.4.4); we note that since the front of the cylinder is faired into the ogive, we have only one such contribution. Thus for this range of θ we have (since $\lambda = 1 \text{ ft.}$ and $a = 3 \text{ ft.}$)

$$\sigma_3 = \frac{3 \sin \theta}{8\pi \cos^2 \theta} \text{ ft}^2. \quad (7.1.4)$$

We observe from Figure 4.4-8 that the size of the cylinder (in terms of λ) is such that these contributions are essentially independent of polarization. The return from the rear of the cylinder (the sharp wire loop rim) is not independent of polarization as can be seen from the material of Section 4.5. The magnitude of this contribution is determined using equations (4.5.14) and (4.5.15).

A graphical presentation of the contributions from these first three components is given in Figure 7.1-2. The data shown in this figure will serve as a guide in our considerations of the fin contributions.

For convenience in the following consideration of the fin contributions we shall use the notation $\sigma_i(\theta, \phi)$. Let us first consider the flat plate contributions which will appear only for $\phi = 0^\circ$ and $\theta = 90^\circ$. We have from equation (4.7.1) that

$$\begin{aligned} \sigma_{5,4}(90^\circ, 0^\circ) &= \sigma_{7,4}(90^\circ, 0^\circ) = 64\pi (1)^2 (4)^2 / (1)^2 \text{ ft}^2 \\ &= 3.22 \times 10^3 \text{ ft}^2. \end{aligned} \tag{7.1.5}$$

In the consideration of the wire contributions we note that for the shorter wavelengths we could use either the material of Section 4.7.1 or the thin wire material of Section 4.4 since both are based on the Chu formula. However since we are dealing here with wires which are either one wavelength or four wavelengths long we must use the wire theory of Section 4.4. Before we examine the individual magnitudes of σ_4 , σ_5 , σ_6 , and σ_7 , let us consider the two wires involved.

Employing the Chu formula with the radius of the wire equal to $1/85$ of a wavelength and assuming that the E-vector is in the plane determined by the direction of incidence and the wire we obtain an estimate of the maximum return from the side edges of the fins, that is from the 4 ft. edges. This result is shown in Figure 7.1-3 as a function of the "wire aspect angle" α .

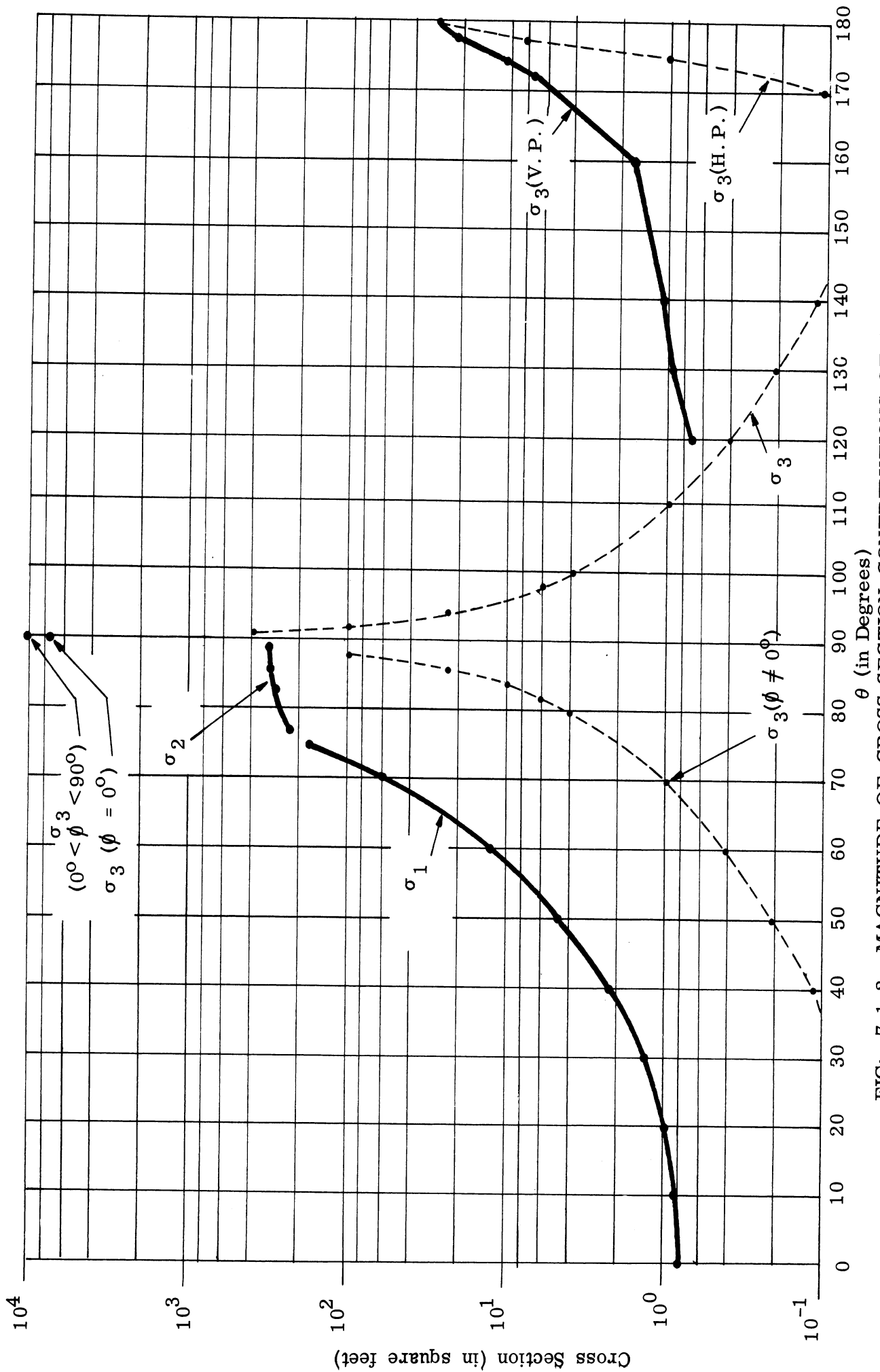


FIG: 7.1-2: MAGNITUDE OF CROSS SECTION CONTRIBUTIONS OF FIRST THREE COMPONENTS OF FICTITIOUS MISSILE

(As is shown in Figure 7.1-3 the angle α is the angle between the direction of incidence and the wire.)

The leading and trailing edges are 1 ft. long (that is they are considered as one wavelength wires). Thus we can employ the estimate of the return given in Figure 4.4-7 together with equation 4.4.9 to obtain the estimate from these 1 ft. edges. This estimate (for the case in which the E-vector is in the plane determined by the direction of incidence and the wire) is also shown in Figure 7.1-3.

The curves shown in Figure 7.1-3 suffice to determine the edge contributions for the aspects confined to the $\phi = 0^\circ$ plane. In the horizontal polarization case we can obtain $\sigma_{4,2}$, $\sigma_{5,2}$, and $\sigma_{7,2}$ directly from the 4 ft. wire curve of Figure 7.1-3 noting that for these edges $\alpha = \theta$; the magnitude of $\sigma_{4,1}$ we obtain from the 1 ft. wire curve noting that $\alpha = 90^\circ - \theta$ ($\sigma_{6,1} = \sigma_{4,1}$ contributes only at $\theta = 0^\circ$); the magnitude of $\sigma_{4,3}$ and $\sigma_{6,3}$ we can read from the 1 ft. curve noting that $\alpha = 90^\circ + \theta$. In the vertical polarization case for $\phi = 0^\circ$ the only edge contributions come from the leading and trailing edges of the fins in the yz-plane, i.e. $\sigma_{5,1}$, $\sigma_{5,3}$, $\sigma_{7,1}$, and $\sigma_{7,3}$ these four contributions are constant for all θ in the interval $0^\circ \leq \theta \leq 180^\circ$ and are given by the $\alpha = 90^\circ$ case for the 1 ft. wire in Figure 7.1-3. (We note that $\sigma_{5,3}$ and $\sigma_{7,3}$ must be taken as zero at $\theta = 0^\circ$, due to shadowing, and for similar reasons $\sigma_{5,1}$ and $\sigma_{7,1}$ must be taken as zero at $\theta = 180^\circ$.)

The $\phi = 45^\circ$ case requires a little more analysis due to more complicated relations between the θ and α aspect angles and the variation in the polarization angle. In the horizontal polarization case we can determine the magnitudes of $\sigma_{4,2}$ and $\sigma_{5,2}$ as was done above. The treatment of the leading and trailing edges is done as follows. First we determine the aspect angle α as a function of θ . A brief examination of the geometry indicates that the relation required is $\cos \alpha = \frac{\sin \theta}{\sqrt{2}}$. This relation is shown graphically in Figure 7.1-4. The polarization factor, we note from Section 4.4, is the fourth power of the cosine of the angle between the E-vector and the plane determined by the wire and the direction of incidence. To determine the magnitude of this polarization factor we first find the unit normal to the plane of the wire and the direction of incidence and then by taking the dot product of this vector with the E-vector (unit vector) we obtain the cosine of the complement of the angle we are seeking. The final polarization factor so obtained is presented graphically in Figure 7.1-5. These two relations (Figures 7.1-4 and 7.1-5) together with the data presented in Figure 7.1-3 makes it possible for us to quickly determine the magnitude of the contributions of the leading and trailing edges for this $\phi = 45^\circ$ case. We have to consider $\sigma_{4,1}$ and $\sigma_{5,1}$ for $0^\circ \leq \theta < 180^\circ$, $\sigma_{4,3}$ and $\sigma_{5,3}$ for $0^\circ < \theta \leq 180^\circ$, and we must take into account $\sigma_{6,3}$ and $\sigma_{7,3}$ for all θ between 90° and 180° . The magnitude of these contributions as a function of the aspect angle θ and the polarization is shown in Figure 7.1-6.

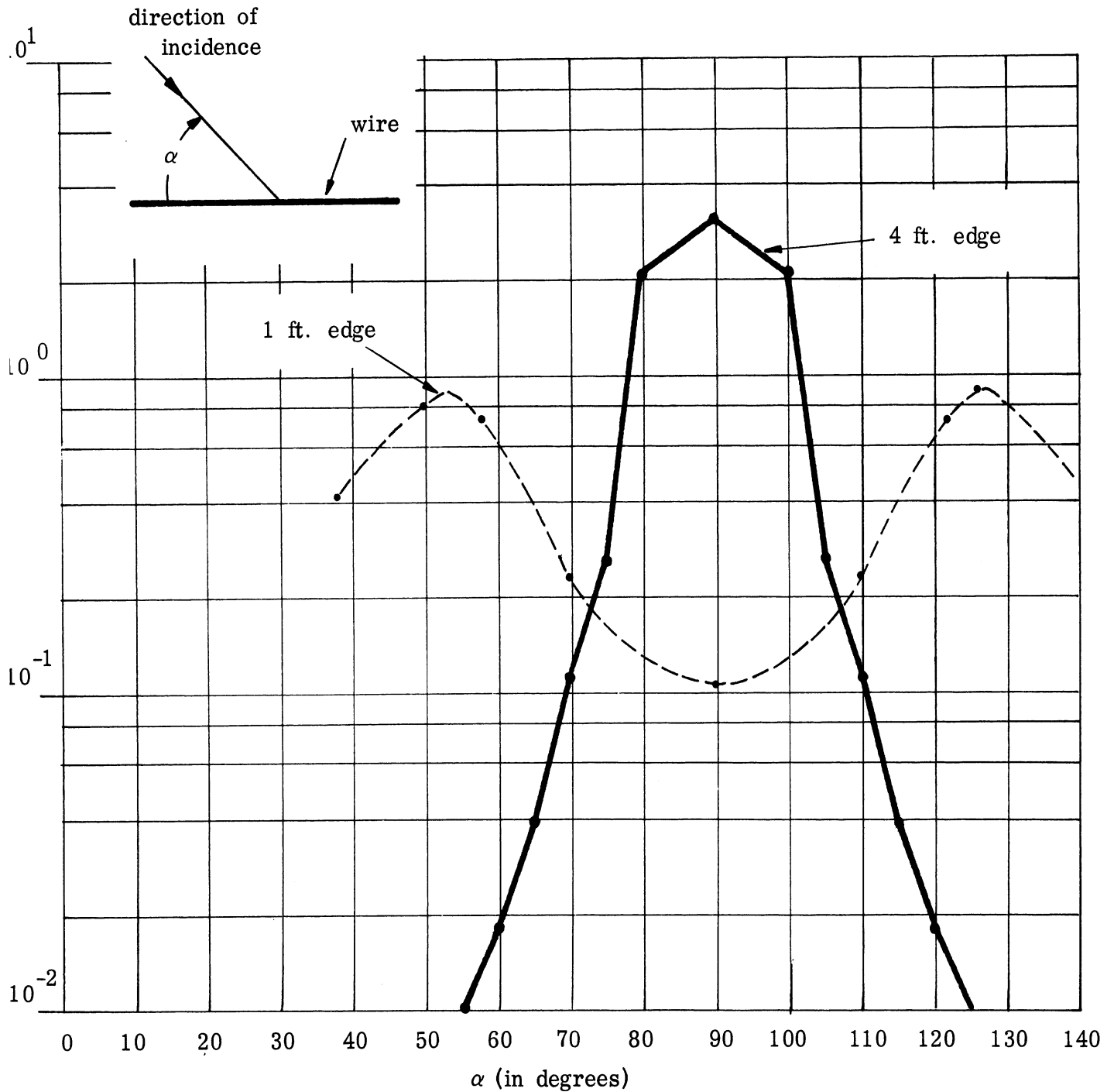


FIG. 7.1-3: MAGNITUDE OF EDGE CONTRIBUTIONS FOR THE FICTITIOUS MISSILE ($\lambda = 1$ ft. and E-vector in plane of wire and direction of incidence)

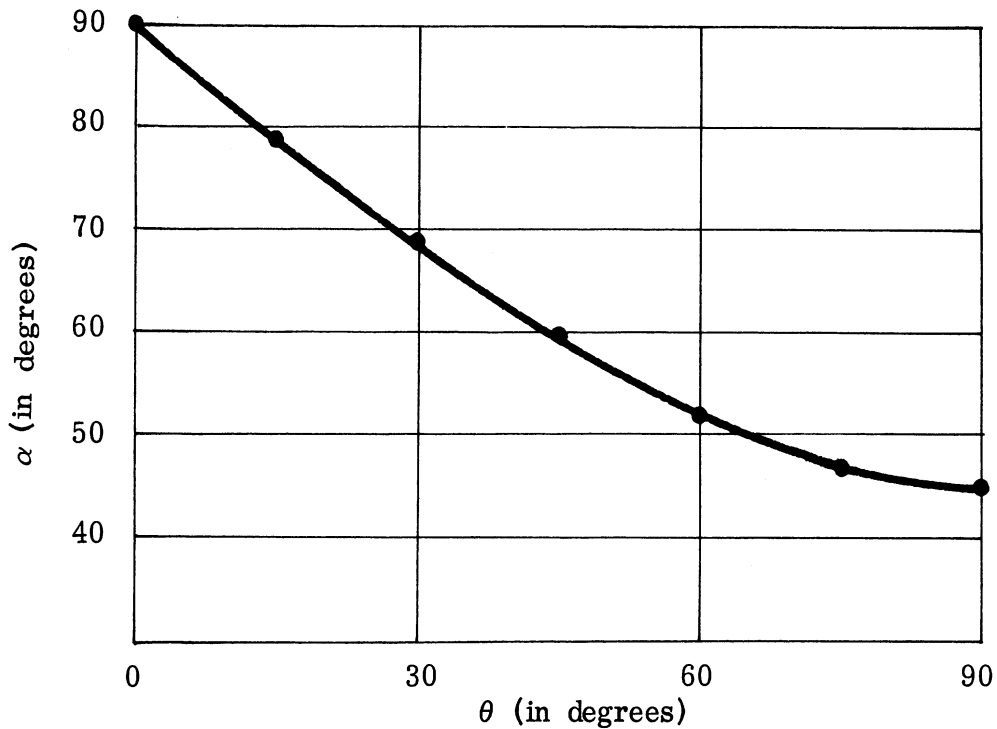


FIG. 7.1-4: θ VS α FOR THE TREATMENT OF THE LEADING AND TRAILING EDGES FOR THE $\phi = 45^\circ$ CASE

With the above information we are now in a position to assemble these component cross sections to obtain the estimate of the cross section of the entire missile. The summaries of the component cross sections are given in Tables 7.1.1 through 7.1.4. In this illustration we shall not go beyond this point; the "average" or "random phase" cross sections are given in the tables. An illustration of the relative phase approach and the RMS spread will be given in Section 7.1.2 where an illustrative example for a manned aircraft is discussed.

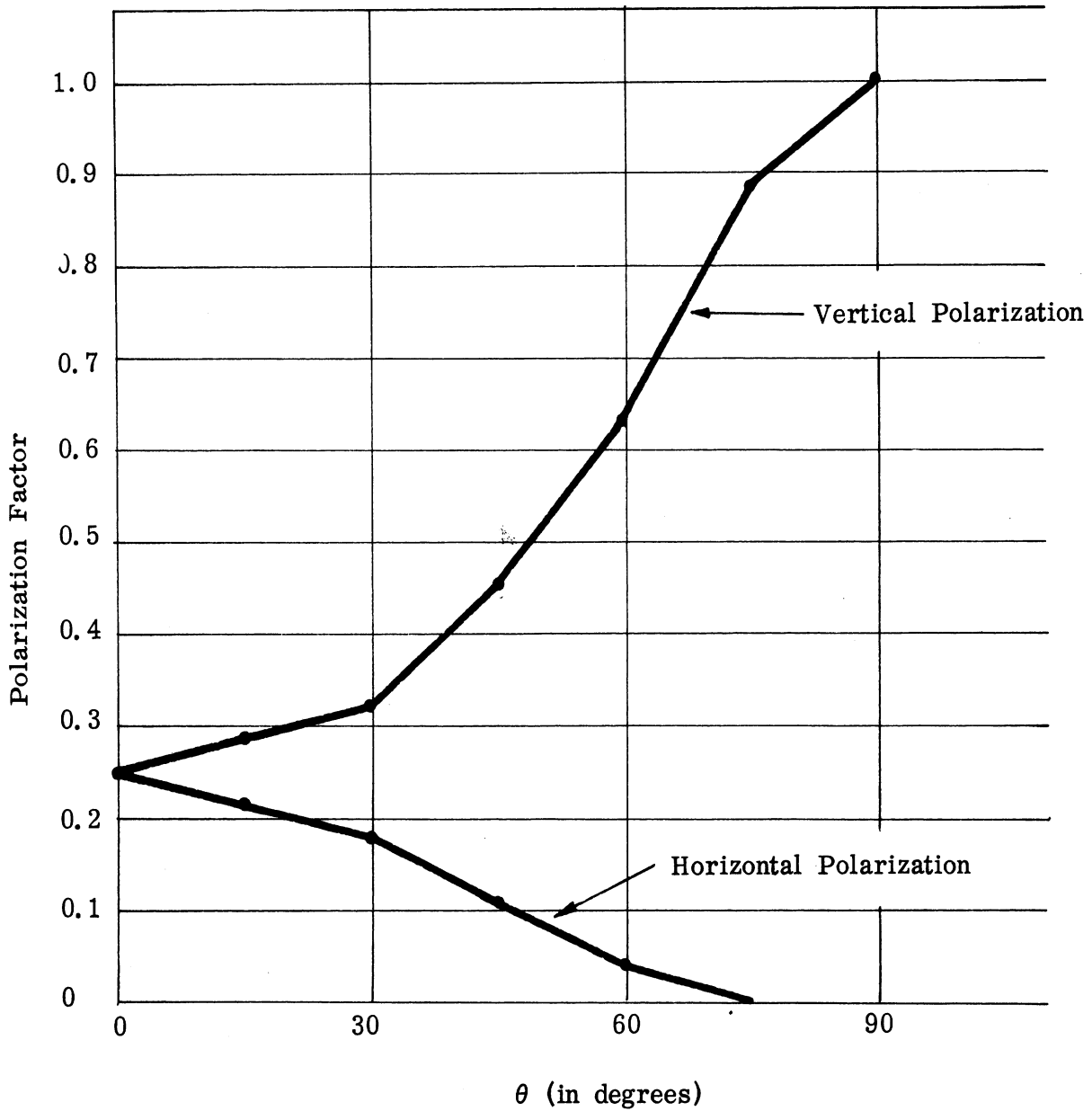


FIG. 7.1-5: POLARIZATION FACTORS IN $\phi = 45^\circ$ TREATMENT OF LEADING AND TRAILING EDGES

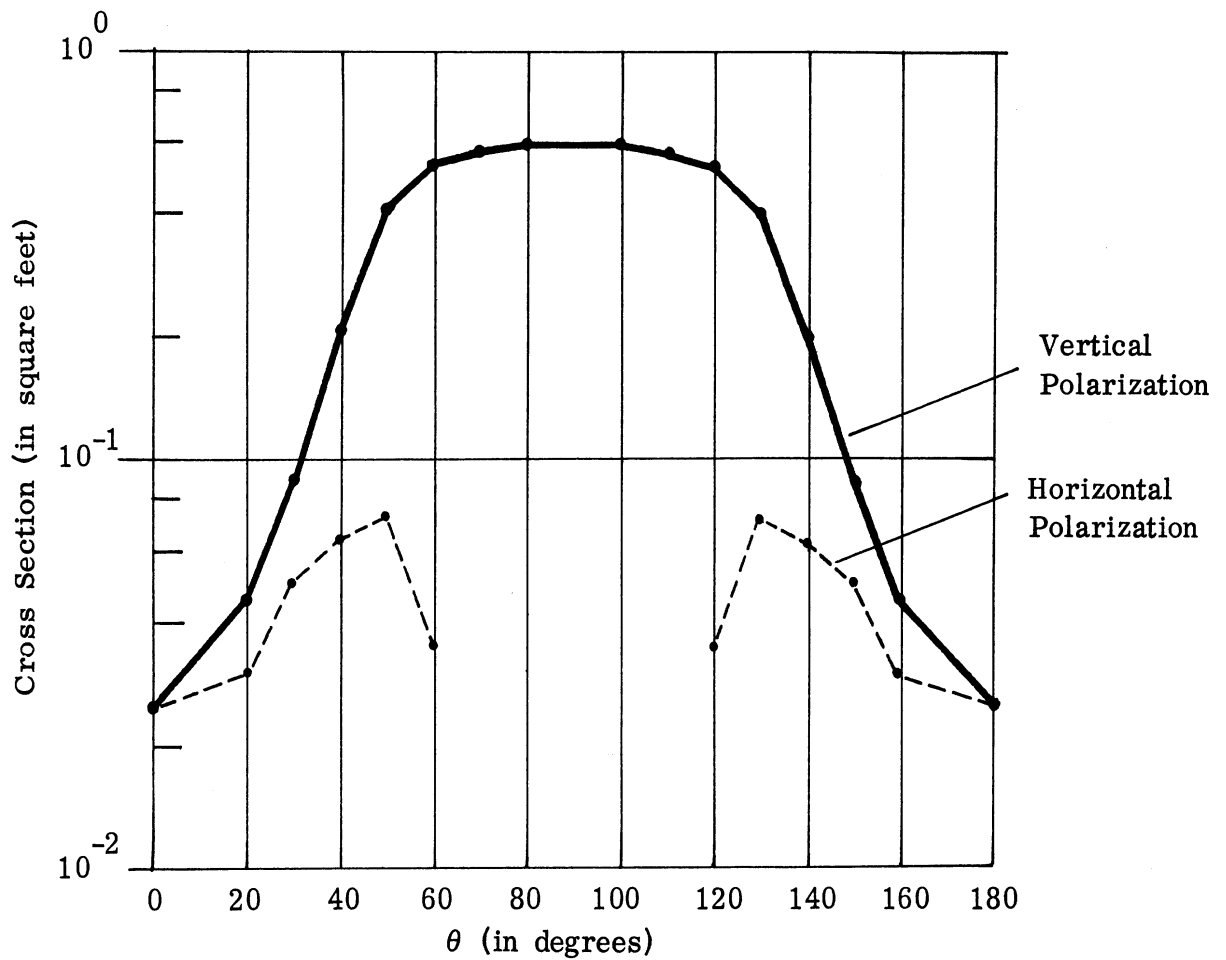


FIG. 7.1-6: CROSS SECTION CONTRIBUTION FROM LEADING (OR TRAILING) EDGE OF FIN FOR ASPECTS IN $\phi = 45^\circ$ PLANE

7.2 Radar Cross Section of an Aircraft

In the illustration given in Section 7.1 we started with a drawing of the configuration and went through the entire operation up to the point of combining the component cross sections. Here, in the aircraft illustration we shall start with the component cross sections and discuss the combination of these component cross sections.

θ	Cross Section (in Square feet)																σ			
	σ_1	σ_2	σ_3	$\sigma_{4,1}$	$\sigma_{4,2}$	$\sigma_{4,3}$	$\sigma_{4,4}$	$\sigma_{5,1}$	$\sigma_{5,2}$	$\sigma_{5,3}$	$\sigma_{5,4}$	$\sigma_{6,1}$	$\sigma_{6,2}$	$\sigma_{6,3}$	$\sigma_{6,4}$	$\sigma_{7,1}$		$\sigma_{7,2}$	$\sigma_{7,3}$	$\sigma_{7,4}$
0	.78			.11								.11								1.0
10	.83			.13																.96
20	.98			.23																1.2
30	1.4			.60																2.0
40	2.2			.80																3.0
50	4.6			.47																5.1
60	13				.018				.018								.018			13
70	57				.11				.11								.11			57
80		260			2.1				2.1								2.1			270
90			7500		3.0					3200									3200	14,000
100			3.9		2.1				2.1								2.1			10
110			.96		.11				.11								.11			1.3
120			.41		.018				.018								.018			.46
130			.22			.47								.47						1.2
140			.13		.80									.80						1.7
150			.08		.60									.60						1.3
160			.05		.23									.23						.51
170			.13		.13									.13						.39
180			28		.11									.11						28

TABLE 7.1.1: SUMMARY OF CROSS SECTION DATA FOR FICTITIOUS MISSILE
($\lambda = 1$ ft, $\phi = 0^\circ$, and Horizontal Polarization)

Cross Section (in Square feet)																				
θ	σ_1	σ_2	σ_3	$\sigma_{4,1}$	$\sigma_{4,2}$	$\sigma_{4,3}$	$\sigma_{4,4}$	$\sigma_{5,1}$	$\sigma_{5,2}$	$\sigma_{5,3}$	$\sigma_{5,4}$	$\sigma_{6,1}$	$\sigma_{6,2}$	$\sigma_{6,3}$	$\sigma_{6,4}$	$\sigma_{7,1}$	$\sigma_{7,2}$	$\sigma_{7,3}$	$\sigma_{7,4}$	σ
0	.78							.11								.11				1.0
10	.83							.11		.11						.11	.11			1.3
20	.98							.11		.11						.11	.11			1.4
30	1.4							.11		.11						.11	.11			1.8
40	2.2							.11		.11						.11	.11			2.6
50	4.6							.11		.11						.11	.11			5.0
60	13							.11		.11						.11	.11			13
70	57							.11		.11						.11	.11			57
80		260						.11		.11						.11	.11			260
90			7500					.11		.11	3200					.11	.11	3200		14,000
100			3.9					.11		.11						.11	.11			4.3
110			.96					.11		.11						.11	.11			1.4
120			.70					.11		.11						.11	.11			1.1
130			.90					.11		.11						.11	.11			1.3
140			1.1					.11		.11						.11	.11			1.5
150			1.3					.11		.11						.11	.11			1.7
160			1.8					.11		.11						.11	.11			2.2
170			5.4					.11		.11						.11	.11			5.8
180			28							.11							.11			28

TABLE 7.1.2: SUMMARY OF CROSS SECTION DATA FOR FICTITIOUS MISSILE
 $(\lambda = 1 \text{ ft}, \phi = 0^\circ, \text{ and Vertical Polarization})$

θ	Cross Section (in Square feet)																			
	σ_1	σ_2	σ_3	$\sigma_{4,1}$	$\sigma_{4,2}$	$\sigma_{4,3}$	$\sigma_{4,4}$	$\sigma_{5,1}$	$\sigma_{5,2}$	$\sigma_{5,3}$	$\sigma_{5,4}$	$\sigma_{6,1}$	$\sigma_{6,2}$	$\sigma_{6,3}$	$\sigma_{6,4}$	$\sigma_{7,1}$	$\sigma_{7,2}$	$\sigma_{7,3}$	$\sigma_{7,4}$	σ
0	.78			.025				.025				.025				.025				.88
10	.83		.021	.028		.028		.028		.028										.96
20	.98		.046	.030		.030		.030		.030										1.1
30	1.4		.079	.050		.050		.050		.050										1.7
40	2.2		.13	.065		.065		.065		.065										2.6
50	4.6		.22	.072		.072		.072		.072										5.1
60	13		.41	.035	.018	.035		.035	.018	.035										14
70	57		.96		.11				.11											58
80		260	3.9		2.1				2.1											270
90			11000		3.0				3.0											11,000
100			3.9		2.1				2.1											8.1
110			.96		.11				.11											1.2
120			.41	.035	.018	.035		.035	.018	.035				.035				.035		.66
130			.22	.072		.072		.072		.072				.072				.072		.65
140			.13	.065		.065		.065		.065				.065				.065		.52
150			.079	.050		.050		.050		.050				.050				.050		.38
160			.046	.030		.030		.030		.030				.030				.030		.23
170			.13	.028		.028		.028		.028				.028				.028		.30
180			28			.025				.025				.025				.025		28

TABLE 7.1.3: SUMMARY OF CROSS SECTION DATA FOR FICTITIOUS MISSILE
($\lambda = 1$ ft, $\phi = 45^\circ$, and Horizontal Polarization)

θ	Cross Section (in Square feet)																			
	σ_1	σ_2	σ_3	$\sigma_{4,1}$	$\sigma_{4,2}$	$\sigma_{4,3}$	$\sigma_{4,4}$	$\sigma_{5,1}$	$\sigma_{5,2}$	$\sigma_{5,3}$	$\sigma_{5,4}$	$\sigma_{6,1}$	$\sigma_{6,2}$	$\sigma_{6,3}$	$\sigma_{6,4}$	$\sigma_{7,1}$	$\sigma_{7,2}$	$\sigma_{7,3}$	$\sigma_{7,4}$	σ
0	.78			.025				.025				.025				.025				.88
10	.83		.021	.035		.035		.035		.035										.99
20	.98		.046	.045		.045		.045		.045										1.2
30	1.4		.079	.089		.089		.089		.089										1.8
40	2.2		.13	.21		.21		.21		.21										3.2
50	4.6		.22	.41		.41		.41		.41										6.5
60	13		.41	.55		.55		.55		.55										16
70	57		.96	.57		.57		.57		.57										60
80		260	3.9	.60		.60		.60		.60										270
90			11000	.60		.60		.60		.60										11,000
100			3.9	.60		.60		.60		.60				.60				.60		7.5
110			.96	.57		.57		.57		.57				.57				.57		4.4
120			.70	.55		.55		.55		.55				.55				.55		4.0
130			.90	.41		.41		.41		.41				.41				.41		3.3
140			1.1	.21		.21		.21		.21				.21				.21		2.4
150			1.3	.089		.089		.089		.089				.089				.089		1.8
160			1.8	.045		.045		.045		.045				.045				.045		2.1
170			5.4	.035		.035		.035		.035				.035				.035		5.6
180			28			.025				.025				.025				.025		28

TABLE 7.1.4: SUMMARY OF CROSS SECTION DATA FOR FICTITIOUS MISSILE
($\lambda = 1$ ft, $\phi = 45^\circ$, and Vertical Polarization)

The only essential difference between the problem of determining the radar cross section of a manned aircraft and the corresponding problem for a missile is the number of components to be considered.

Figure 7.2-1 displays the results obtained for a typical large jet aircraft. One will note that there are many significant contributors to be considered and that over a wide range of aspects we do not have a single large contributor. In discussing the combination of these component cross sections we can use a fixed wavelength and let the aspect vary or we can consider a fixed aspect and let the wavelength vary. Let us use the latter approach and concentrate on the nose-on aspect, that aspect at which all of the contributors are of approximately the same magnitude. Let us assume that there are four engines a distance d_1 back from the nose and two other engines a distance d_2 back from the nose; thus from the data shown in Figure 7.2-1 we would have four essential contributions to consider:

- (1) the contribution from the fuselage, σ_1 ,
- (2) the contribution from the group of four engines, σ_2 ,
- (3) the contribution from the group of two engines, σ_3 , and
- (4) the contribution from the group of two wing tanks, σ_4 .

The type of variation one can obtain between the relative phase and the random phase methods will be adequately illustrated if we consider a wavelength variation from about $\lambda = 0.69$ m to $\lambda = .72$ m. Over a wavelength range of this magnitude the cross sections of the individual components will not change

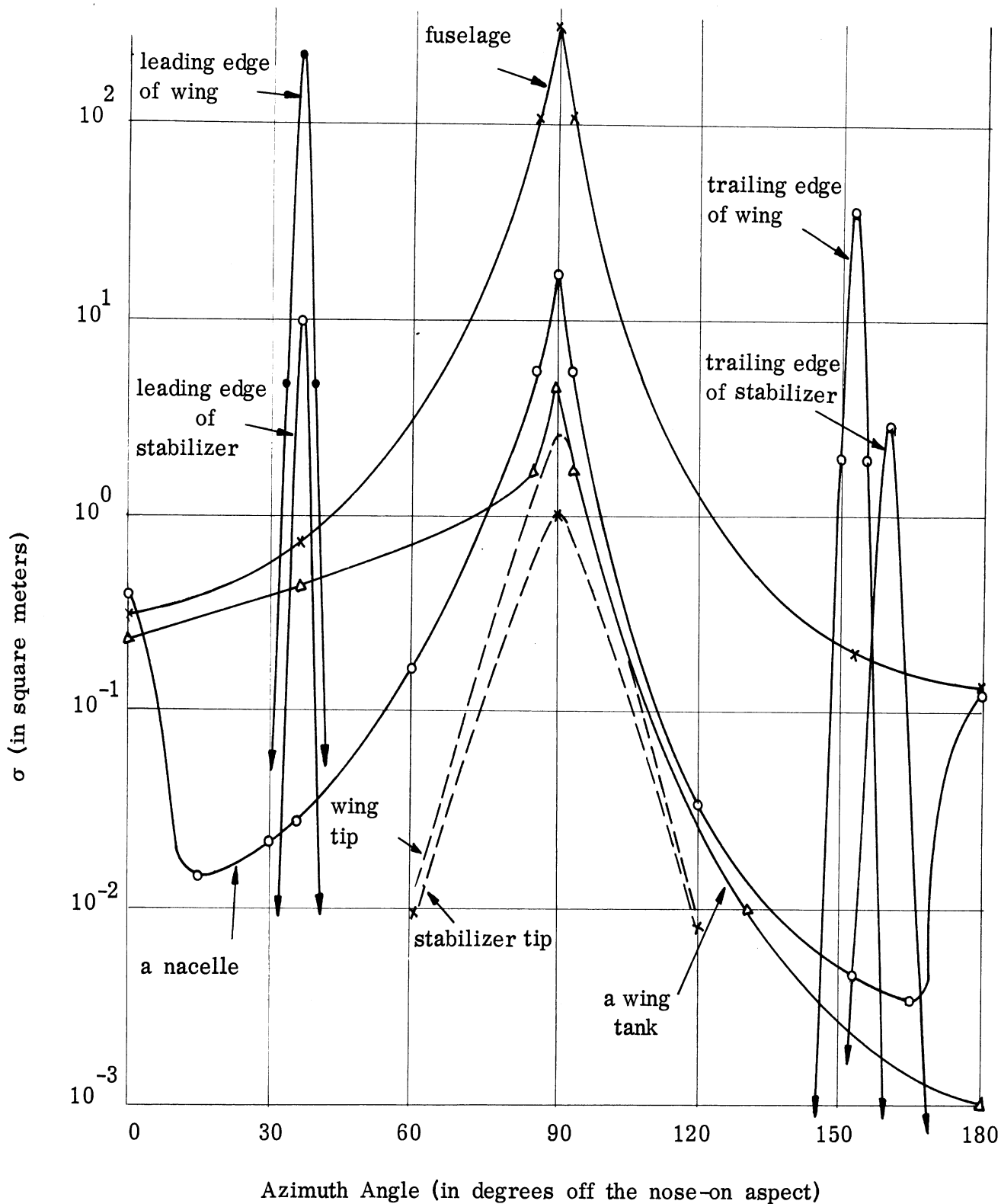


FIG. 7.2-1: RADAR CROSS SECTION PATTERN OF THE COMPONENTS OF A TYPICAL LARGE MANNED JET AIRCRAFT AT A WAVELENGTH OF 0.71 METERS

an appreciable amount; thus, let us assume that they are constant over this range of λ and have the following values:

$$\sigma_1 = 0.32 \text{ m}^2; \quad \sigma_2 = 6.9 \text{ m}^2; \quad \sigma_3 = 1.7 \text{ m}^2; \quad \sigma_4 = 1.0 \text{ m}^2.$$

Let us further assume that upon a study of the aircraft drawings (applying the method shown in Figure 6-1) the following values of the phase angles have been determined

$$\begin{aligned} |\phi_1 - \phi_2| &= 66.8\pi/\lambda; & |\phi_2 - \phi_3| &= 30.2\pi/\lambda \\ |\phi_1 - \phi_3| &= 36.6\pi/\lambda; & |\phi_2 - \phi_4| &= 14.8\pi/\lambda \\ |\phi_1 - \phi_4| &= 52.0\pi/\lambda; & |\phi_3 - \phi_4| &= 15.4\pi/\lambda. \end{aligned}^*$$

Applying equation (2.4) we can thus obtain the cross section as a function of wavelength taking these relative phase relations into account. The result so obtained (shown as $\sqrt{\sigma}$ vs. λ) is presented in Figure 7.2-2. The average cross section and the RMS spread is also shown in Figure 7.2-2 for comparison purposes. We see from Figure 7.2-2 that even for this case, in which we have a large number of contributors having approximately the same cross section, the variation due to changes in the relative phase very seldom exceeds the variation predicted by the RMS spread. Over the range shown in Figure 7.2-2 the cross section dips below the RMS minimum for only about 19% of the wavelengths considered. As an illustration of the manner in which the two

*Of course the wavelength is measured in the same units as the d_i , in this case the unit is meters.

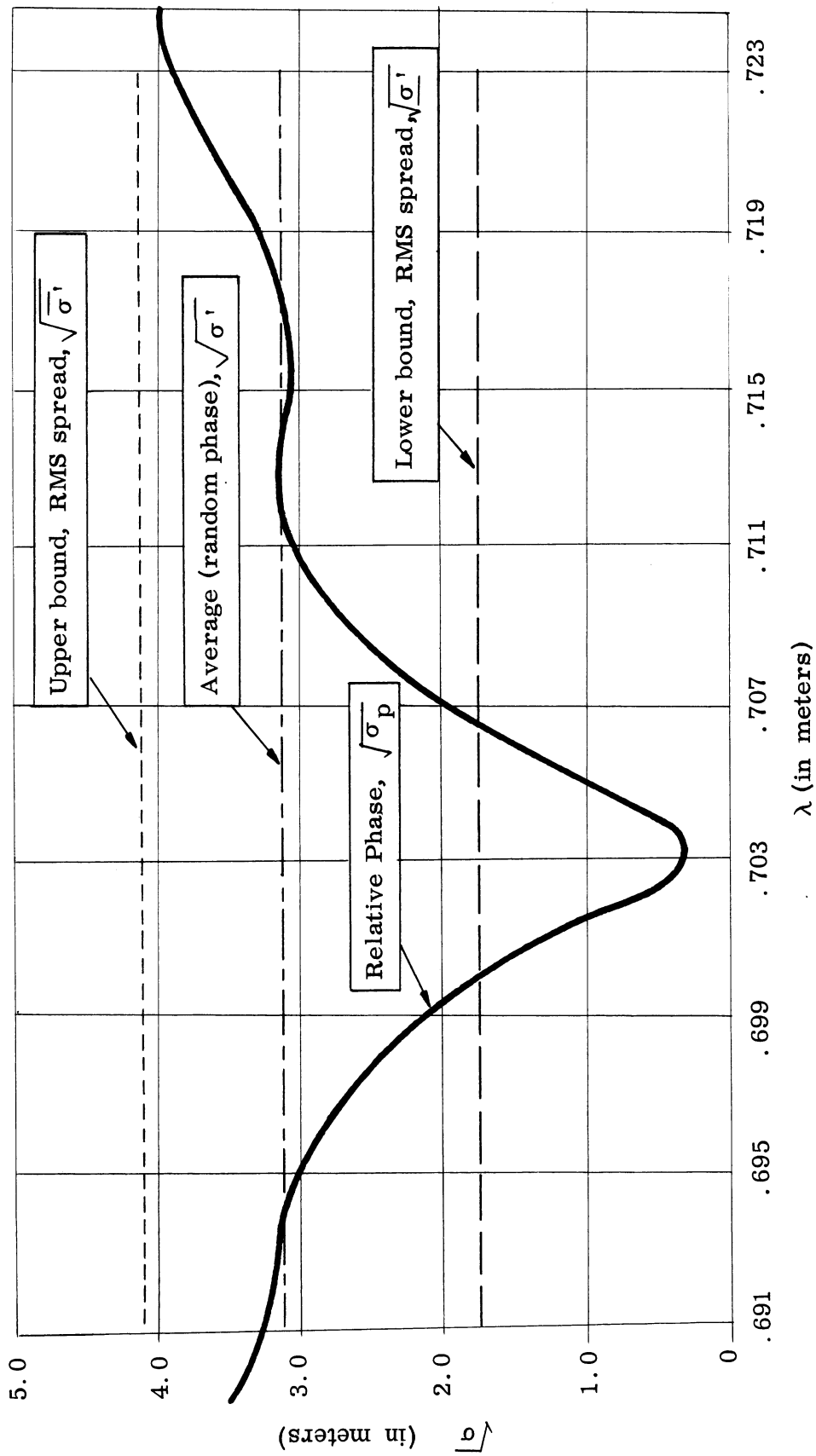


FIG. 7.2-2: CROSS SECTION AS A FUNCTION OF WAVELENGTH FOR THE NOSE ON ASPECT TO A LARGE JET AIRCRAFT

methods of combination (relative phase and random phase) compare for a fixed wavelength and varying aspect we present in Figure 7.2-3 the results obtained for a missile; the results are displayed on a relative scale as a function of aspect and it is obvious that the RMS spread calculation suffices for almost all of the aspects considered.

It is important to note that since a missile has fewer components than a manned aircraft it is to be expected that the relative phase results would lie outside the RMS spread more frequently in a missile calculation than they would in an aircraft calculation.

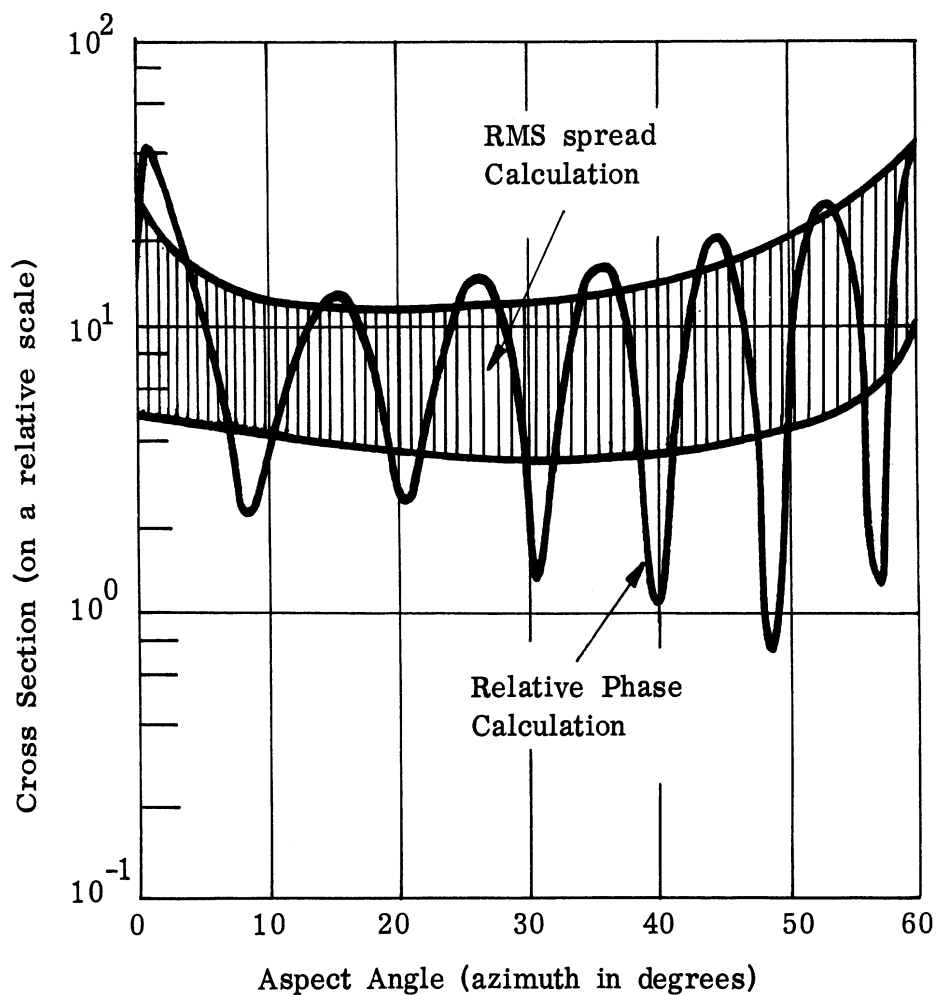


FIG. 7.2-3: RADAR CROSS SECTION OF A MISSILE - COMPARISON OF RELATIVE PHASE AND RANDOM PHASE (RMS SPREAD) RESULTS

CONCLUSIONS

We have attempted in this report to present a detailed outline of the procedure for calculating the radar cross sections of aircraft and missiles which has evolved at the Radiation Laboratory of The University of Michigan during the past several years. It is our hope that this report will serve as a handbook for the calculation of such radar cross sections.

Examples of the application of this process to the determination of the radar cross sections of various aircraft and missiles will be found in many of The University of Michigan reports in the Studies in Radar Cross Sections series and in the reports which supplement that series. Since each of these documents is at present classified we have included the illustrative examples in Section 7. It would be of considerable value to examine the details of some of these earlier computations. The documents which contain these examples are Studies in Radar Cross Sections XII, XIV, XV, XVII, XVIII, XIX, XX, XXI, and XXIV. The documents in the supplementary series which would be of interest in this connection are the reports 2476-1-F, 2541-1-F, 2550-1-F, 2200(01)-1-T, 2500-1-T, and 2660-1-F. (See Appendix H.)

It should be noted again that this process is designed for use when the cross sections are desired to within 2 to 10 db and experience has indicated that the method will yield results which differ from experimentally determined

values by less than 6 db for almost all combinations of wavelength, polarization, and aspect. This is illustrated in Figures 8-1 and 8-2. The first displays a comparison between theory and experiment for a missile shape and the second displays a comparison for a manned aircraft. A 10 db spread is shown in Figure 8-2 since (1) there is a 20 % difference in the frequencies employed in the theoretical and experimental work, (2) the theoretical analysis on this aircraft was one of the first applications of the method and thus did not contain the refinements now available, and (3) the RMS spread was not computed in this particular theoretical study. Figure 8-2 also contains an interesting observation relative to the experimental approach. One will note that experimentally one can obtain as much as an 8 or 9 db difference between the cross section on one side of the aircraft and the cross section on the other. That is, in terms of the coordinate system shown in Figure 8-3, one finds experimentally that $\sigma(\theta', \phi')$ and $\sigma(\theta', -\phi')$ may differ by as much as 8 or 9 db even though the aircraft is symmetric with respect to the xz-plane. The theoretical approach would, of course, imply that for an aircraft which was symmetric with respect to the xz-plane $\sigma(\theta', \phi') = \sigma(\theta', -\phi')$.

The material presented in this report applies for perfect conductors. If the surface was not a perfect conductor but one having a dielectric constant equal to ϵ , then we could employ the following relations:

In the geometric optics region:

$$\frac{\sigma_{\text{diel.}}}{\sigma_{\text{p. cond.}}} = \left(\frac{\sqrt{\epsilon} - 1}{\sqrt{\epsilon} + 1} \right)^2, \quad \omega \neq \epsilon \gg 1 \quad (8.1)$$

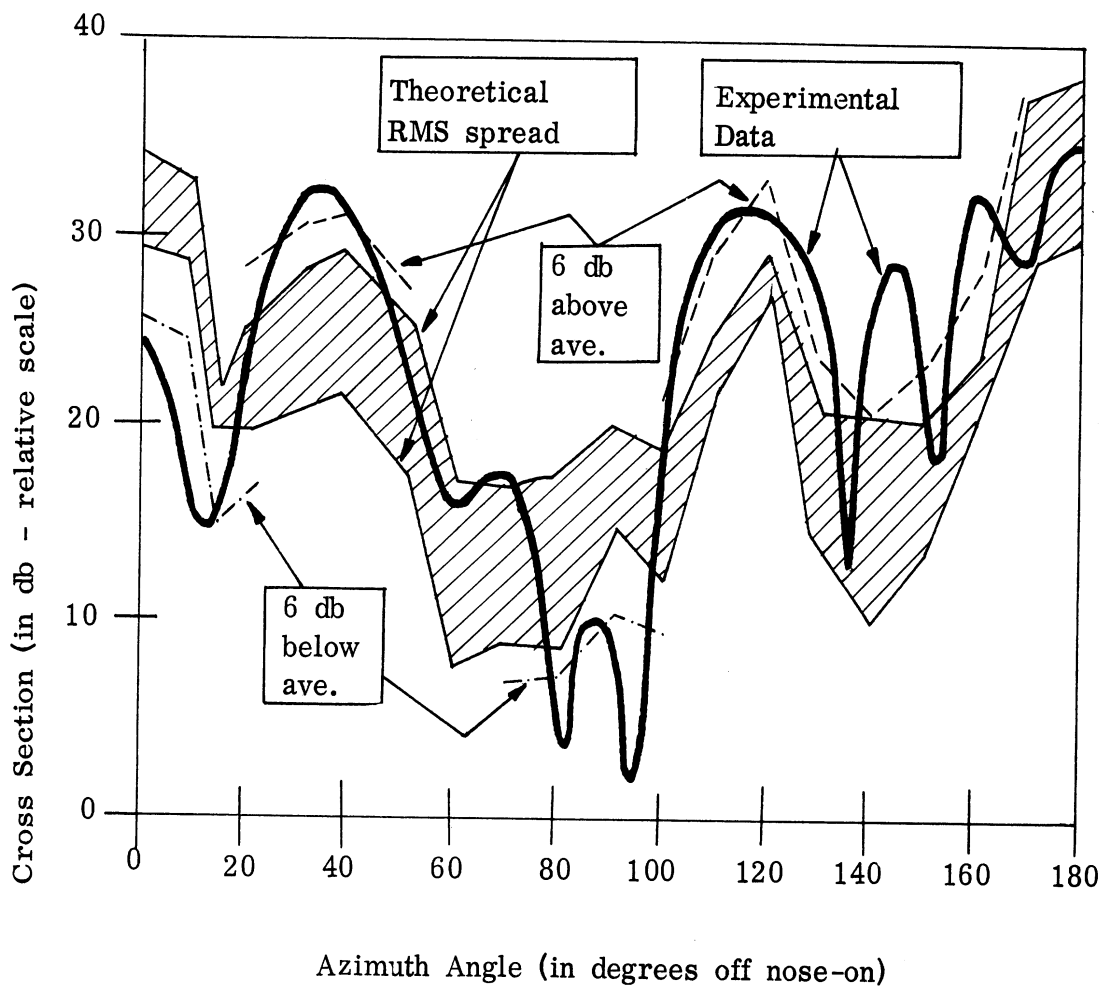






FIG. 8-1: RADAR CROSS SECTION OF A MISSILE BODY - A COMPARISON BETWEEN THEORY AND EXPERIMENT


Experimental Data (1200 Mc) indicating range of values for both sides of aircraft:

Theoretical Data (1000 Mc): "average" cross section

10 db above "average"

10 db below "average"

Cross Section
(in db - relative scale)

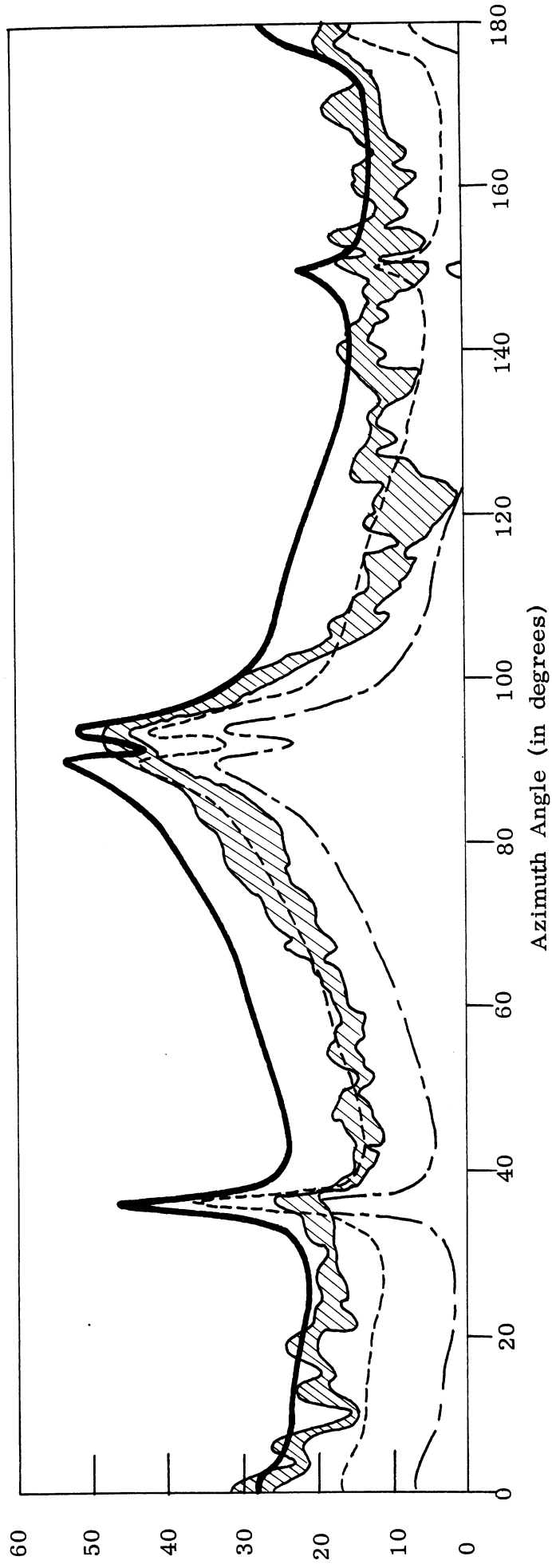


FIG. 8-2: RADAR CROSS SECTION OF A MANNED AIRCRAFT - A COMPARISON BETWEEN THEORY AND EXPERIMENT

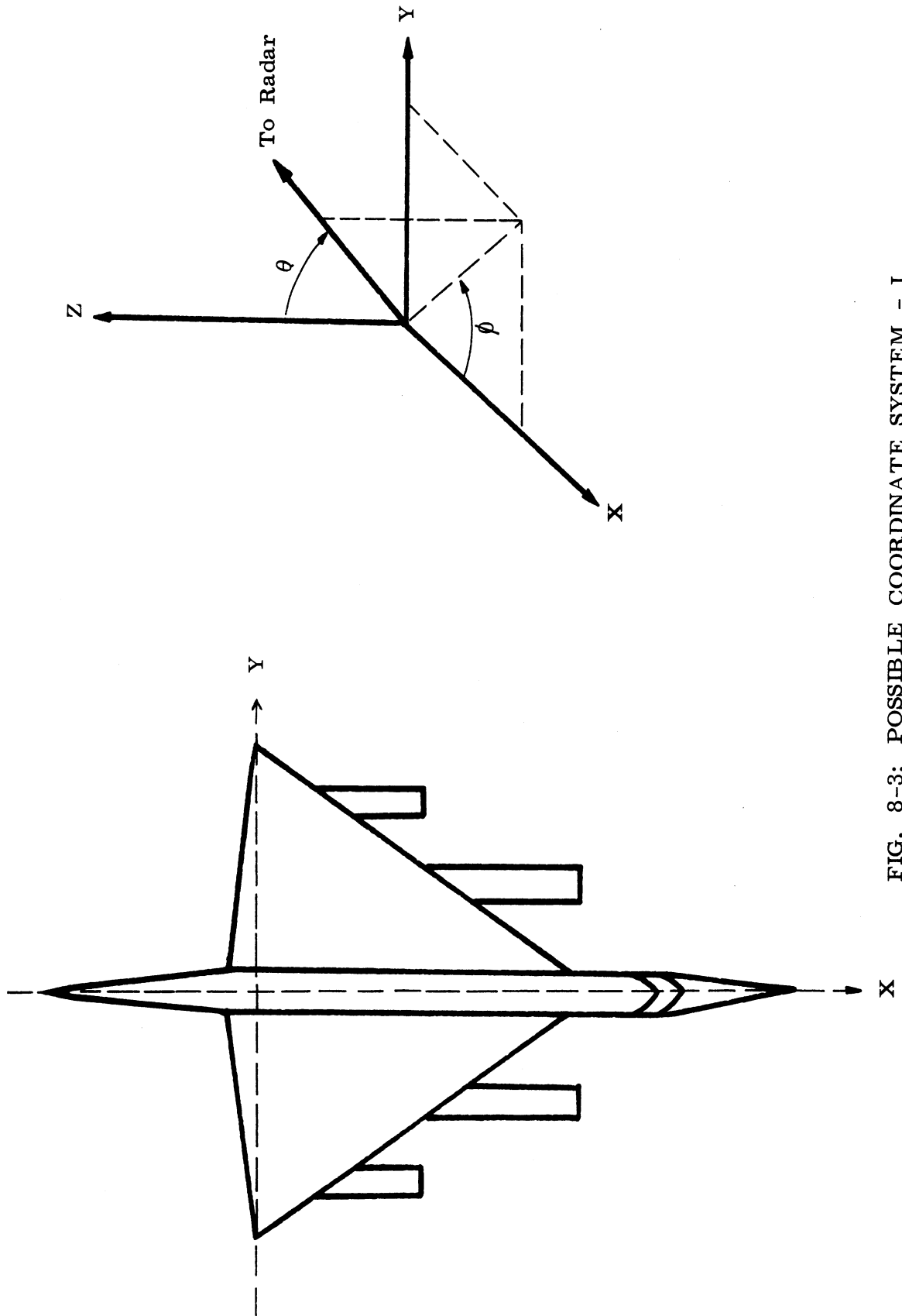


FIG. 8-3: POSSIBLE COORDINATE SYSTEM - I

In the Rayleigh Region (sphere result):

$$\frac{\sigma_{\text{diel.}}}{\sigma_{\text{p. cond.}}} = \frac{4}{9} \left| \frac{\epsilon - 1}{\epsilon + 1} \right|^2 \quad (8.2)$$

A plot of equation (8.1) is given in Figure 8-4 from which we see that in order for the cross section of a dielectric surface to be a factor of ten less than that for a surface which is geometrically the same but a perfect conducting surface, the dielectric constant must be greater than about 0.5 but less than about 2.

In the case of equation (8.2) it is of interest to note that for large values of ϵ the ratio approaches $4/9$ and as $\epsilon \rightarrow 0$ the ratio $\sigma_{\text{diel.}} / \sigma_{\text{p. cond.}}$ approaches the value $1/9$. Since in the application of this theoretical method most of the body components considered are in the optics region, the information presented in Figure 8-3 will suffice for most cases.

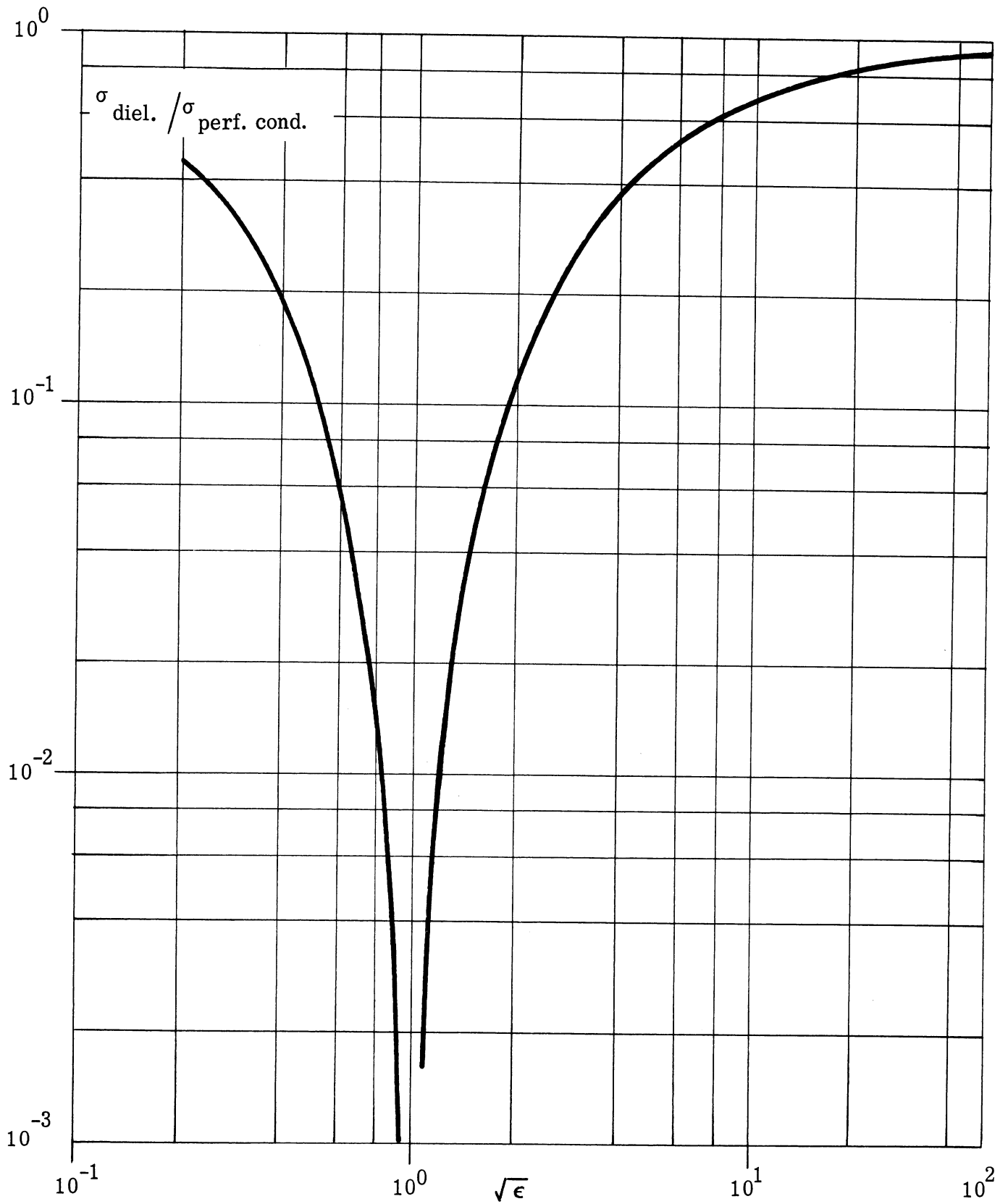


FIG. 8-4: CROSS SECTION OF A PERFECT CONDUCTOR COMPARED TO THE CROSS SECTION OF THE SAME BODY MADE OF A DIELECTRIC (CONSTANT = ϵ) AS A FUNCTION OF THE DIELECTRIC CONSTANT (GEOMETRIC OPTICS REGION)

ACKNOWLEDGEMENT

The material presented here covers the efforts of many scientists, engineers, computers and secretaries of The Radiation Laboratory of The University of Michigan. These past and present members of The Radiation Laboratory are: H. A. Alperin, M. E. Anderson, M. L. Barasch, R. R. Bonkowski, H. Brysk, W. E. Burdick, J. W. Crispin, Jr., R. E. Doll, B. H. Gere, R. F. Goodrich, B. A. Harrison, T. A. Kaplan, R. E. Kleinman, A. L. Maffett, I. Marx, W. C. Orthwein, D. M. Raybin, N. E. Reitlinger, C. E. Schensted, I. V. Schensted, F. V. Schultz, F. B. Sleator, K. M. Siegel and H. Weil.

REFERENCES

1. J. A. Stratton, *Electromagnetic Theory*, McGraw-Hill Book Company, Inc., New York (1941).
2. C. H. Wilcox, "Debye Potentials", Jour. Appl. Math. and Mech., 6, 167 (1957).
3. G. Mie, "Beiträge zur Optik trüber Medien speziell kolloidaler Metal-lösungen", Annalen der Physik, 25, 377-445 (1908).
4. K. M. Siegel, "Far Field Scattering From Bodies of Revolution", Appl. Sci. Res., Sec. B, 7, 293-328 (1958).
5. G. N. Watson, "The Diffraction of Electric Waves by the Earth", Proc. Roy. Soc., Series A, 95, 83-99 (1918).
6. H. Weil, M. L. Barasch, and T. A. Kaplan, "Studies in Radar Cross Sections X - Scattering of Electromagnetic Waves by Spheres", University of Michigan, Report No. 2255-20-T (July 1956).
7. F. V. Schultz, "Studies in Radar Cross Sections I - Scattering by a Prolate Spheroid", University of Michigan, Report No. UMM-42 (March 1950).
8. K. M. Siegel, B. H. Gere, I. Marx and F. B. Sleator, "Studies in Radar Cross Sections XI - The Numerical Determination of the Radar Cross Section of a Prolate Spheroid", University of Michigan, Report No. UMM-126 (December 1953).
9. J. H. Van Vleck, F. Bloch and M. Hammermesh, "Theory of Radar Reflection from Wires or Thin Metallic Strips", Jour. Appl. Phys., 18, 274 (1947).
10. F. E. Terman, Radio Engineer's Handbook, McGraw-Hill Book Company, Inc., New York 1943).
11. J. R. Mentzer, Scattering and Diffraction of Radio Waves, Pergamon Press (1955).
12. J. Weber, "Scattering of Electromagnetic Waves by Wires and Plates", Proc. IRE, 43, 82 (January 1955).

13. R. Kouyoumjian, "The Back Scattering from a Circular Loop", Appl. Sci. Res., B6, 165 (1956).
14. V. A. Fock, "The Field of a Plane Wave Near the Surface of a Conducting Body", Jour. of Phys., X, No. 5, 399 (1946).
15. K. M. Siegel, H. A. Alperin, R. R. Bonkowski, J. W. Crispin, Jr., A. L. Maffett, C. E. Schensted and I. V. Schensted, "Studies in Radar Cross Sections VIII - Theoretical Cross Section as a Function of Separation Angle Between Transmitter and Receiver at Small Wavelengths", University of Michigan, Report No. UMM-115 (October 1953).
16. W. E. Bulman, "Investigation of Angular Scattering Cross Sections of the B-47 Aircraft at a Simulated Frequency of 250 Megacycles", The Ohio State University Research Foundation, Report No. 601-27 (30 November 1957). CONFIDENTIAL
17. T. B. A. Senior, "Studies in Radar Cross Sections **XXV** - Diffraction by an Imperfectly Conducting Wedge", University of Michigan, Report No. 2591-2-T, ASTIA Document AD 133746, AFCRC-TN-57-791 (October 1957).
18. K. M. Siegel, H. A. Alperin, R. R. Bonkowski, J. W. Crispin, Jr., A. L. Maffett, C. E. Schensted and I. V. Schensted, "Bistatic Radar Cross Sections of Surfaces of Revolution", Jour. Appl. Phys., 26, No. 3, 297-305 (March 1955).

APPENDIX A

COMPLETE SCATTERING MATRICES AND CIRCULAR POLARIZATION CROSS SECTIONS

1

SCATTERING MATRICES

In general, in radar scattering problems we deal with transverse fields, i. e. vector fields whose components in the direction of propagation vanish, in that first the incident radiation and finally the scattered radiation at large distance from the scattering center are described in terms of such fields. There is a certain freedom in the description of these transverse fields which we will investigate in more detail.

The scattering of electromagnetic radiation may be described quite generally as follows: For simplicity, assume an incident plane wave and choose a coordinate system such that the negative z-axis is in the direction of propagation of the incident wave (Fig. A-1). Since the incident electric and magnetic vectors lie in a plane perpendicular to the direction of propagation, the incident radiation is completely specified in free space by the direction of propagation and the x- and y-components of either the electric or magnetic field. After diffraction by an obstacle the scattered radiation in the "far zone" is then completely determined by the configuration of the scatterer, its electrical properties, and by the incident radiation. If \hat{k} is a unit vector in the direction of the incident wave and \hat{k}_o is a unit vector in the direction of the observation point,

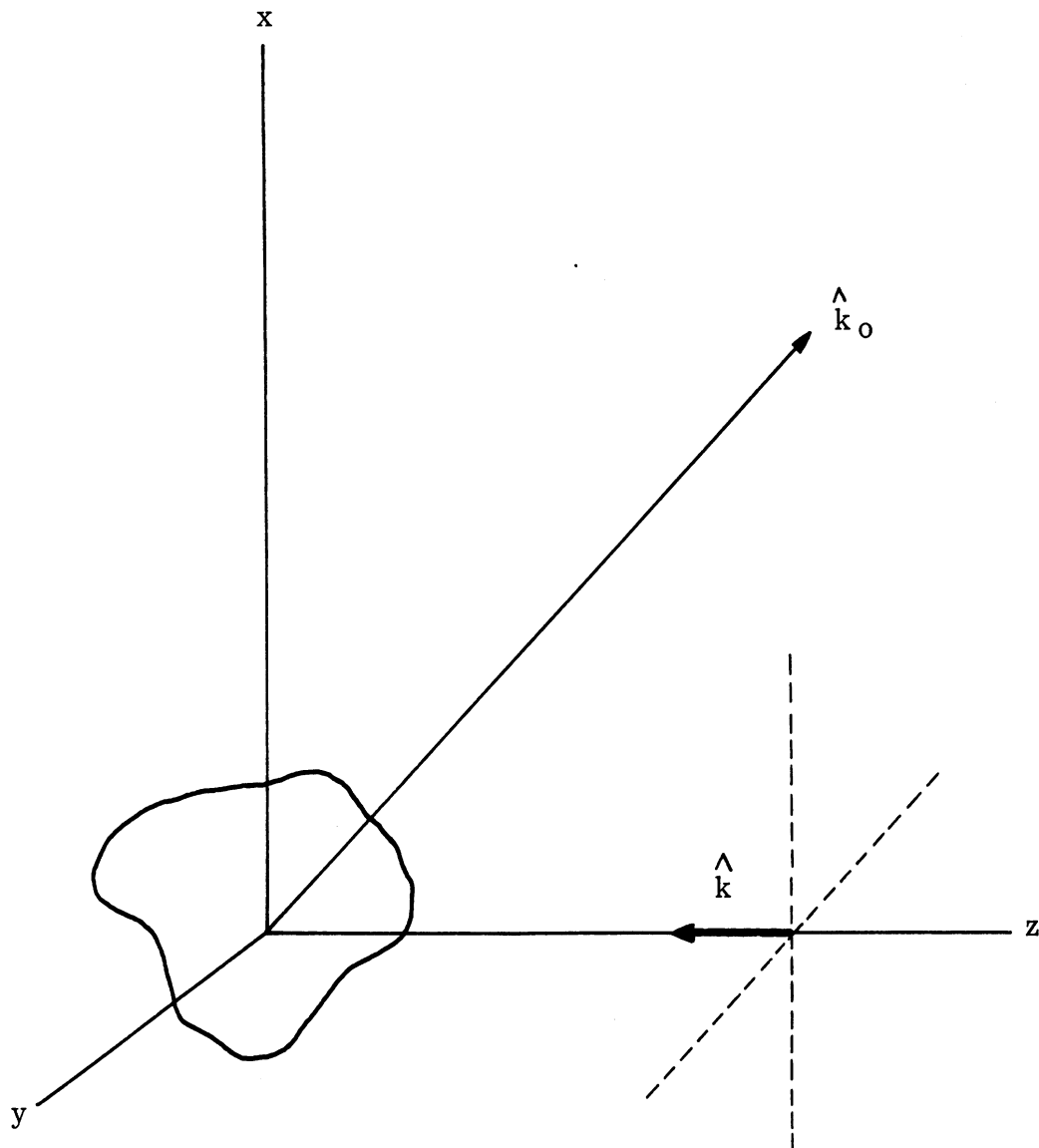


FIG. A-1: ASSUMED GEOMETRY FOR \hat{k} AND \hat{k}_0

the far field in the direction \hat{k}_0 is determined by the type of obstacle and the incident radiation, or, in symbols,

$$\vec{E}_{\hat{k}_0}^S = S(\hat{k}_0, \hat{k}) \vec{E}_{\hat{k}}^i, \quad (1.1)$$

where $\vec{E}_{\hat{k}}^i$ is the incident field moving in the direction \hat{k} , $\vec{E}_{\hat{k}_0}^S$ is the scattered field moving in the direction \hat{k}_0 and $S(\hat{k}_0, \hat{k})$ is a matrix with continuous indices \hat{k}_0 and \hat{k} which depends on the obstacle and the wavelength of the radiation.

From its analog in quantum mechanics, the matrix S is called the scattering matrix or, more briefly, S -matrix.

1.1 Scattered Field in S-Matrix Notation

If the coordinate system is rotated so that the new z -axis lies along the direction \hat{k}_0 the incident field will be specified by three components, but the scattered field in the direction \hat{k}_0 will be specified simply by the x - and y -components since the radiation field is transverse. Symbolically, this rotation

R is expressed as

$$R \vec{E}_{\hat{k}_0}^S = \begin{pmatrix} \alpha \\ \beta \\ 0 \end{pmatrix} = R S(\hat{k}_0, \hat{k}) R^{-1} \left(R \vec{E}_{\hat{k}}^i \right). \quad (1.1.1)$$

An immediate condition on the new S -matrix RSR^{-1} is then that it leads to zero z -component of the scattered field.

The maximum advantage of using the S -matrix notation is obtained when circularly or elliptically polarized incident radiation is considered.

Before going into this, however, it is desirable to give a brief review of the polarization phenomenon.

Consider a plane wave moving along the z-axis as in Figure A-2. If the electric vector is restricted to lie in one plane through the z-axis, say the yz-plane, the wave is said to be plane or linearly polarized since the projection of the locus of the electric vector on the xy-plane is a straight line.

If the electric vector is no longer required to lie in a single plane, then its projection on the xy-plane will no longer be a straight line but will in general describe an ellipse in time as shown in Figure A-3. The case of circular polarization occurs when the ellipse degenerates into a circle as shown in Figure A-4.

In particular, for backscattering, $\hat{k}_0 = -\hat{k}$. An incident elliptically polarized field can be expressed in terms of Cartesian coordinates and hence, as before:

$$\vec{E}_{-\hat{k}}^s = S(-\hat{k}, \hat{k}) \vec{E}_{\hat{k}}^i \quad (1.1.2)$$

It is possible to express the fields in terms of an elliptic basis by a coordinate transformation, U, such that

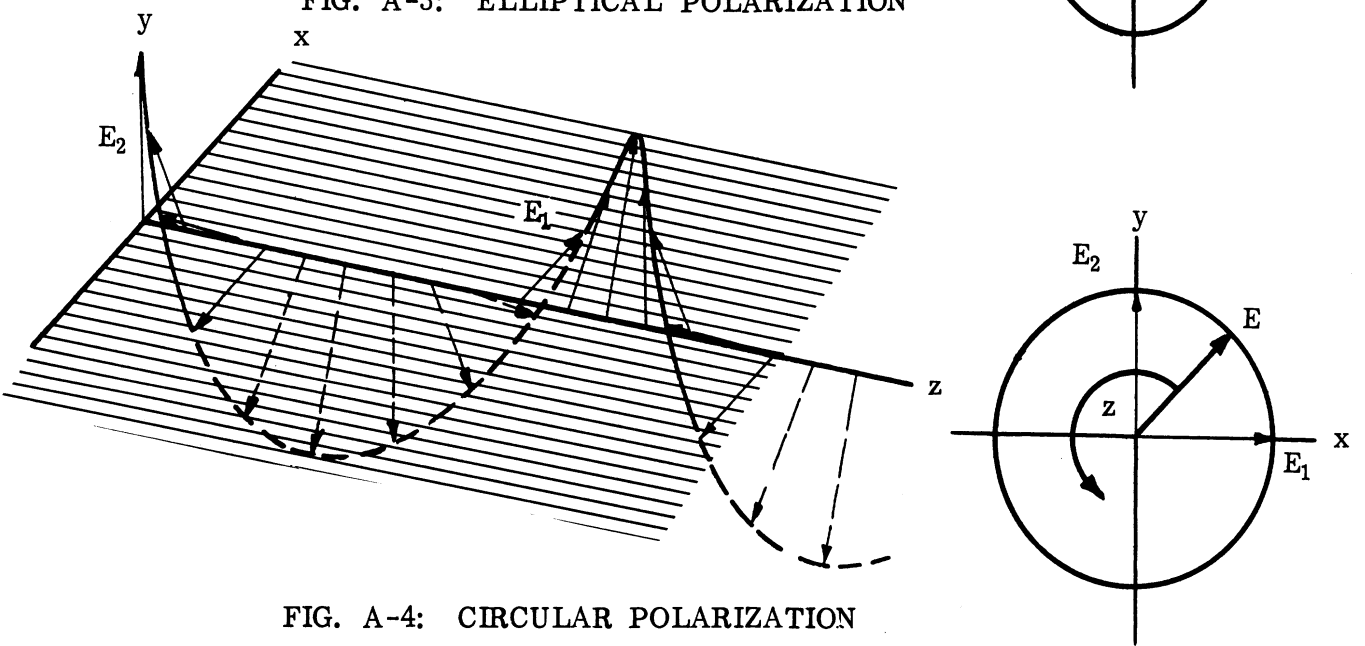
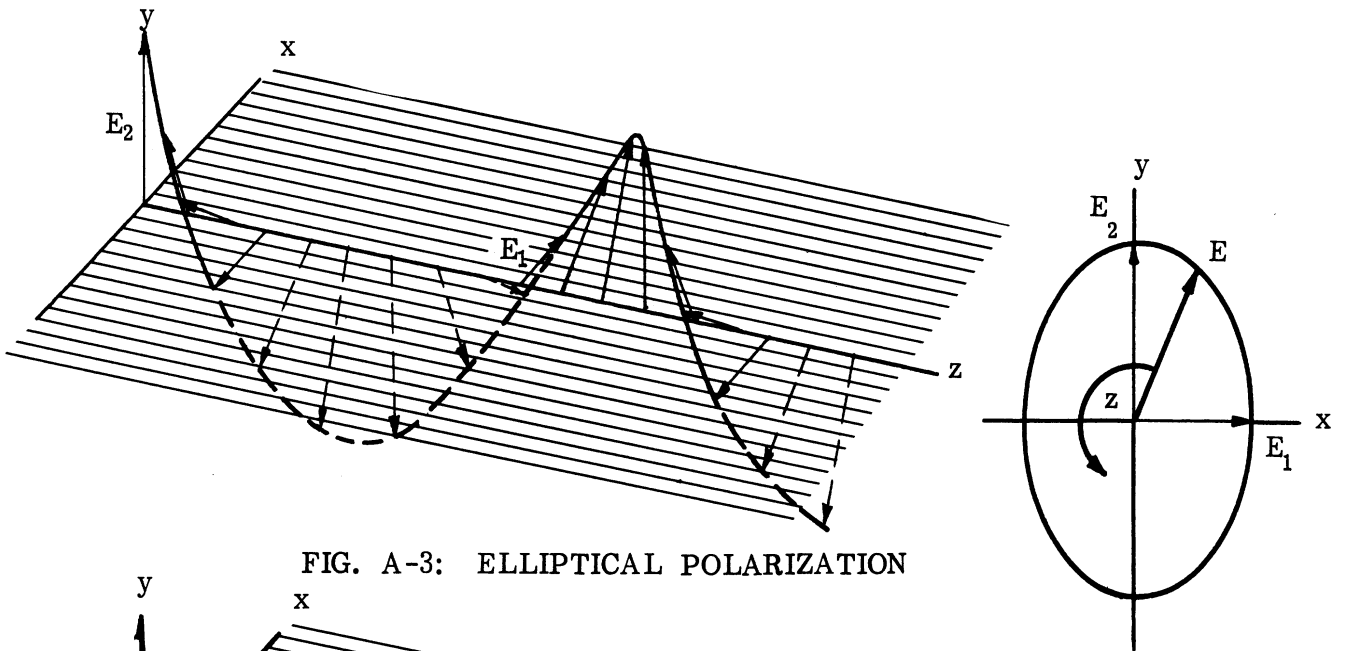
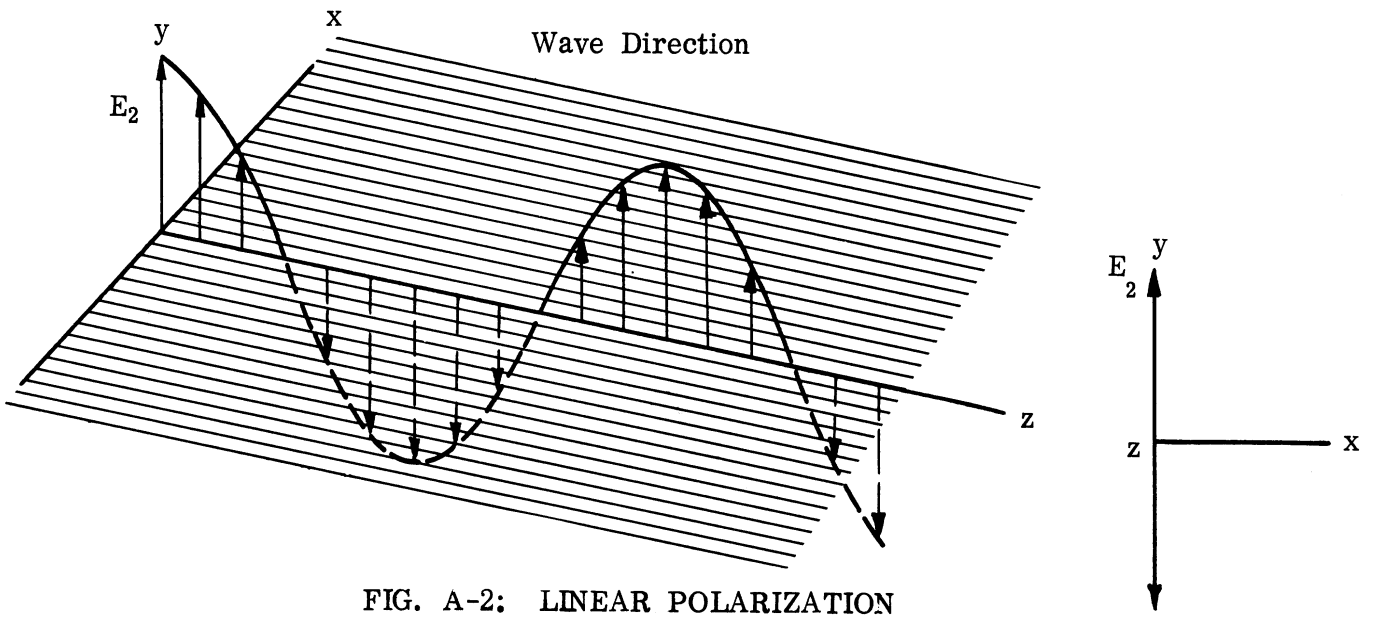
$$\vec{E}_{\hat{k}}^i = U \vec{E}_{\hat{k}}^i, \quad (1.1.3)$$

where $\vec{E}_{\hat{k}}^i$ is the incident vector in an elliptic basis. Then

$$\vec{E}_{-\hat{k}}^s = S(-\hat{k}, \hat{k}) U^{-1} U \vec{E}_{\hat{k}}^i = S(-\hat{k}, \hat{k}) U^{-1} \vec{E}_{\hat{k}}^i \quad (1.1.4)$$

The scattered field is transformed by the same transformation so that in the elliptic basis,

$$\vec{E}_{-\hat{k}}^s = U \vec{E}_{-\hat{k}}^s = U S(-\hat{k}, \hat{k}) U^{-1} \vec{E}_{\hat{k}}^i \quad (1.1.5)$$



This then gives a new scattering matrix $U S U^{-1}$ which is used for the case in which the incident and scattered fields are referred to an elliptic basis. Since the fields describing the incident and backscattered radiation lie in the same plane the two-dimensional transformation U gives the change of basis from linear to elliptic for both the incident and backscattered fields.

Thus, by using the S-matrix formalism, it is necessary to determine only the scattering for linear polarization and the transformation giving the change of basis to the particular basis of interest.

1.2 S-Matrix in Terms of Fixed but Arbitrary Basis

In order to be explicit, let $\hat{p}(H)$ and $\hat{p}(V)$ be unit orthogonal vectors*; these vectors define, respectively, directions of horizontal** and vertical polarization of an electric vector. A vector \vec{E} may be written in terms of this basis as

$$\vec{E} = E(H) \hat{p}(H) + E(V) \hat{p}(V) = \begin{pmatrix} E(H) & E(V) \end{pmatrix} \begin{pmatrix} \hat{p}(H) \\ \hat{p}(V) \end{pmatrix} = E'(HV) \hat{p}(HV),$$

where $E'(HV)$ designates the transpose of the column $\begin{pmatrix} E(H) \\ E(V) \end{pmatrix}$.

If $\hat{p}(A)$ and $\hat{p}(B)$ are an arbitrary pair of unit orthogonal vectors co-planar with $\hat{p}(H)$ and $\hat{p}(V)$, then they must be obtainable from $\hat{p}(H)$ and $\hat{p}(V)$ by a unitary transformation***

*

Orthogonal is to be interpreted in the sense that two vectors $\hat{p}(A)$ and $\hat{p}(B)$ are orthogonal if their product $\hat{p}(A) \cdot \hat{p}^*(B)$ is zero, where the asterisk indicates complex conjugate; unit in the sense that a vector $\hat{p}(A)$ is a unit vector if the product $\hat{p}(A) \cdot \hat{p}^*(A)$ is 1.

** Horizontal will mean tangent to the earth with horizontal, vertical, and direction of propagation being mutually orthogonal.

*** $u(IJ)$ is defined as the product $\hat{p}(I) \cdot \hat{p}^*(J)$. Note here also that $u^*(IJ) = u(JI)$.

$$\begin{pmatrix} u(AH) & u(AV) \\ u(BH) & u(BV) \end{pmatrix} = U(AB;HV), \quad U^{-1}(AB;HV) = U^{*'}(AB;HV) = U(HV;AB),$$

i. e., $\hat{p}(AB) = U(AB;HV) \hat{p}(HV)$, where the asterisk indicates complex conjugate of each element of the matrix and the prime indicates the transpose of the matrix.

Since the AB system will in general be used to describe some elliptical polarization, it is preferable to use distinct systems of unit vectors to specify the incident and scattered fields. This is done so that right-hand elliptical polarization may have the same sense with regard to the coordinate system for incident radiation as it does with regard to the coordinate system for scattered radiation. So if

$$\hat{p}^i(AB) = U(AB;HV) \hat{p}(HV)$$

is prescribed for the incident system, the desired similarity of sense for the two coordinate systems is accomplished by writing

$$\hat{p}^s(AB) = U^{*'}(AB;HV) \hat{p}(HV)$$

for the scattered system. Thus $\hat{p}^s(AB) = \hat{p}^{i*}(AB)$.

An incident vector \vec{E}^i may be written in terms of either the basis $\hat{p}(HV)$ or the basis $\hat{p}^i(AB)$:

$$\vec{E}^i = E^{i(HV)} \hat{p}(HV) = E^{i(AB)} \hat{p}^i(AB).$$

From this relation it easily follows that the two sets of components of \vec{E}^i are connected by

$$E^{i(AB)} = U^{*'}(AB;HV) E^{i(HV)}. \quad (1.2.1a)$$

Similarly for a scattered vector \vec{E}^s the relation between components is

$$E^s(AB) = U(AB;HV) E^s(HV). \quad (1.2.1b)$$

Since both the incident and scattered electric vectors are expressible in terms of either unit vector basis, there will be four transformations; i. e., scattering matrices, relating the components of the incident vector for either basis to the components of the scattered vector for either basis.

$$E^S(HV) = S(HV; HV) E^i(HV) , \quad (1.2.2)$$

$$E^S(AB) = S(AB; HV) E^i(HV) , \quad (1.2.3)$$

$$E^S(HV) = S(HV; AB) E^i(AB) , \quad (1.2.4)$$

$$E^S(AB) = S(AB; AB) E^i(AB) , \quad (1.2.5)$$

where the two indices in front of and following the semicolon indicate respectively rows and columns of the scattering matrix. For example; if equation (1.2.3) were written in detail, it would read*

$$\begin{pmatrix} E^S(A) \\ E^S(B) \end{pmatrix} = \begin{pmatrix} s(AH) & s(AV) \\ s(BH) & s(BV) \end{pmatrix} \begin{pmatrix} E^i(H) \\ E^i(V) \end{pmatrix} .$$

The elements of these matrices are associated with effective radar cross section σ by the following definition:

$$\sigma = \lim_{r \rightarrow \infty} 4\pi r^2 \left| \frac{\vec{E}^S \cdot \hat{p}}{\vec{E}^i} \right|^2 , \quad (1.2.6)$$

where \hat{p} is a unit vector denoting receiver polarization. For example, if

$\vec{E}^i = \hat{p}(H)$ and $\hat{p} = \hat{p}(V)$, then

$$\vec{E}^S = E^S(H) \hat{p}(H) + E^S(V) \hat{p}(V) = s(HH) \hat{p}(H) + s(VH) \hat{p}(V) ,$$

* In $s(IJ)$, $\hat{p}(J)$ designates the incident polarization.

and

$$\sigma(\text{VH}) = \lim_{r \rightarrow \infty} 4\pi r^2 \left| \frac{\hat{\mathbf{E}}^{\text{S}} \cdot \hat{\mathbf{p}}(\text{V})}{\hat{\mathbf{p}}(\text{H})} \right|^2 = \lim_{r \rightarrow \infty} 4\pi r^2 |s(\text{VH})|^2 . \quad (1.2.7a)$$

In a similar fashion it can be shown that

$$\sigma(\text{IJ}) = \lim_{r \rightarrow \infty} 4\pi r^2 |s(\text{IJ})|^2 . \quad (1.2.7b)$$

These $\sigma(\text{IJ})$ will be called CROSS POLARIZATION cross sections.

Using equation (1.2.1) in conjunction with equations (1.2.2) through (1.2.5), it follows that any three of the scattering matrices can be expressed in terms of the fourth. Thus, for example,

$$S(\text{AB}; \text{HV}) = U(\text{AB}; \text{HV}) S(\text{HV}; \text{HV}) U^*(\text{HV}; \text{HV}) , \quad (1.2.8)$$

$$S(\text{HV}; \text{AB}) = U(\text{HV}; \text{HV}) S(\text{HV}; \text{HV}) U^*(\text{HV}; \text{AB}) , \quad (1.2.9)$$

$$S(\text{AB}; \text{AB}) = U(\text{AB}; \text{HV}) S(\text{HV}; \text{HV}) U^*(\text{HV}; \text{AB}) . \quad (1.2.10)^*$$

This means that if $S(\text{HV}; \text{HV})$ is known completely any scattering matrix can be calculated from it. Since the elements of $S(\text{HV}; \text{HV})$ are complex numbers, there will be eight real numbers (four magnitudes, four phases) required to specify $S(\text{HV}; \text{HV})$ completely. This is reduced from eight to seven because only relative phase differences can be calculated. It is further reduced to five

* More generally, $S(\text{AB}; \text{JK}) = U(\text{AB}; \text{HV}) S(\text{HV}; \text{HV}) U^*(\text{HV}; \text{JK})$, where JK indicates an arbitrary basis. $U(\text{HV}; \text{HV})$ and $U^*(\text{HV}; \text{HV})$ have been included above for consistency. (They are each equal to the identity matrix).

for backscattering because of the reciprocity theorem* and the conservation of energy principle.**

To recapitulate, assume that $|s(\text{HH})|$, $|s(\text{HV})|$, $|s(\text{VV})|$, $|s(\text{AH})|$, $|s(\text{AV})|$ are known; from these quantities the differences of phases (or relative arguments) of $s(\text{HH})$, $s(\text{HV})$, $s(\text{VH})$, and $s(\text{VV})$ can be determined; i. e., the complete matrix

$$S(\text{HV}; \text{HV}) = \begin{pmatrix} s(\text{HH}) & s(\text{HV}) \\ s(\text{VH}) & s(\text{VV}) \end{pmatrix} \quad (1.2.11)$$

can be found.

Since $s(\text{IJ})$ and $u(\text{IJ})$ may be written:

$$\begin{aligned} s(\text{IJ}) &= |s(\text{IJ})| e^{i\theta(\text{IJ})} , \\ u(\text{IJ}) &= |u(\text{IJ})| e^{i\phi(\text{IJ})} , \end{aligned} \quad (1.2.12)$$

* If \vec{E}_1^i and \vec{E}_2^i are two given incident electric vectors, and \vec{E}_1^s and \vec{E}_2^s are the respective scattered electric vectors, then the reciprocity theorem states that

$$\vec{E}_1^s \cdot \vec{E}_2^i = \vec{E}_2^s \cdot \vec{E}_1^i , \text{ or}$$

$$E_1^s(\text{H}) E_2^i(\text{H}) + E_1^s(\text{V}) E_2^i(\text{V}) = E_2^s(\text{H}) E_1^i(\text{H}) + E_2^s(\text{V}) E_1^i(\text{V}) .$$

If equation (1.2.2) is used to state this theorem entirely in terms of the components of the incident vectors, it follows that

$$s(\text{HV}) \left(E_1^i(\text{V}) E_2^i(\text{H}) - E_2^i(\text{V}) E_1^i(\text{H}) \right) = \left(s(\text{VH}) E_1^i(\text{V}) E_2^i(\text{H}) - E_2^i(\text{V}) E_1^i(\text{H}) \right) ,$$

or

$$s(\text{HV}) = s(\text{VH}) .$$

From this equality and equations (1.2.8), (1.2.9), and (1.2.10), it follows that $s(\text{IJ}) = s(\text{JI})$ for $I \neq J$.

**

Because energy must be conserved, it follows that

$$\sigma(\text{KA}) + \sigma(\text{KB}) = \sigma(\text{KH}) + \sigma(\text{KV}) ,$$

where K may be H, V, A, or B.

it follows from equation (1.2.8) that

$$\begin{aligned}
|s(AH)|^2 &= |u(AH) s(HH) + u(AV) s(VH)|^2 \\
&= |u(AH) s(HH)|^2 + |u(AV) s(VH)|^2 + 2|u(AH) u(AV) s(HH) s(VH)| \\
&\quad \times \cos [\theta(HH) - \theta(VH) + \phi(AH) - \phi(AV)] .
\end{aligned} \tag{1.2.13}$$

Therefore,

$$\cos [\theta(HH) - \theta(VH) + \phi(AH) - \phi(AV)] = \frac{|s(AH)|^2 - |u(AH) s(HH)|^2 - |u(AV) s(VH)|^2}{2|u(AH) u(AV) s(HH) s(VH)|} , \tag{1.2.14}$$

where $\theta(IJ) = \arg s(IJ)$ and $\phi(IJ) = \arg u(IJ)$.

Similarly,

$$\cos [\theta(HV) - \theta(VV) + \phi(AH) - \phi(AV)] = \frac{|s(AV)|^2 - |u(AH) s(HV)|^2 - |u(AV) s(VV)|^2}{2|u(AH) u(AV) s(HV) s(VV)|} . \tag{1.2.15}$$

An expression for the difference $\theta(HH) - \theta(VV)$ may be obtained from equations (1.2.14) and (1.2.15). A check for this difference can be obtained by assuming that $\sigma(AA)$ is known; then the difference $\theta(HH) - \theta(VV)$ can be calculated directly as a function of $|s(AA)|$, $|s(HH)|$, $|s(VV)|$, and the $u(IJ)$.

The above argument may be summarized in the theorem: If $\sigma(HH)$, $\sigma(HV)$, $\sigma(VV)$, $\sigma(AH)$, and $\sigma(AV)$ are given, then the matrix $S(HV; HV)$ can be determined to within an arbitrary phase factor; and from $S(HV; HV)$ any scattering matrix can be found.

APPROACH TO THE MULTIPLE-COMPONENT BODY PROBLEM

In Section 1 it was shown that for a single simple geometric shape, or a complex shape considered as a unit, the scattering matrix $S(HV; HV)$ can be completely specified from a knowledge of the five radar cross sections $\sigma(HH)$, $\sigma(HV)$, $\sigma(VV)$, $\sigma(AH)$, and $\sigma(AV)$.

However, in an analytic treatment of the scattering matrix for a complex configuration consisting of many components, each of which is a simple geometric shape, a somewhat different approach must be used since component-wise calculation of cross sections does not furnish information as to phase differences between different parts of the target. It is reasonable to assume that for each component of the scattering body expressions for certain of the $s(IJ)$ may be obtained directly from expressions for the scattered fields in terms of the incident fields. Then, to find certain $\sigma(IJ)$, to be specified below, as fairly smooth functions of aspect and to minimize computational labor, an average with respect to phase is made over the set of components of the scatterer. Such an averaging procedure assumes random phase relations among scattered fields of the components, and requires a knowledge of nine* real numbers for the determination of arbitrary $\sigma(IJ)$.

*

By the reciprocity relation; without reciprocity, 16 real numbers would have to be known.

That only nine real numbers are needed may be seen as follows: Let

$$s(IJ) = (u(IH) \ u(IV)) \ S(HV; HV) \begin{pmatrix} u^*(HJ) \\ u^*(VJ) \end{pmatrix} \quad (2.1)$$

represent, for the entire scattering body, any of the linear relations among elements indicated by equations (1.2.8), (1.2.9), or (1.2.10). The averaged quantity $\overline{|s(IJ)|^2}$ is then

$$\begin{aligned} \overline{|s(IJ)|^2} &= \overline{s(IJ) \ s^*(IJ)} \\ &= (u(IH) \ u(IV)) \ \otimes \ (u^*(IH) \ u^*(IV)) \ \overline{S(HV; HV) \ x \ S^*(HV; HV)} \\ &\quad \begin{pmatrix} u^*(HJ) \\ u^*(VJ) \end{pmatrix} \ \otimes \ \begin{pmatrix} u(HJ) \\ u(VJ) \end{pmatrix} \end{aligned} \quad (2.2)$$

where \otimes indicates a direct (or Kronecker) matrix product^{*,**} and the bar indicates phase-averaged matrix elements. Let α, β denote any of the combinations

* The definition of a direct (or Kronecker) matrix product is illustrated by the example

$$\begin{bmatrix} a_{11} & a_{12} & a_{13} \\ a_{21} & a_{22} & a_{23} \end{bmatrix} \otimes \begin{bmatrix} b_{11} & b_{12} \\ b_{21} & b_{22} \end{bmatrix} = \begin{bmatrix} a_{11}b_{11} & a_{11}b_{12} & a_{12}b_{11} & a_{12}b_{12} & a_{13}b_{11} & a_{13}b_{12} \\ a_{11}b_{21} & a_{11}b_{22} & a_{12}b_{21} & a_{12}b_{22} & a_{13}b_{21} & a_{13}b_{22} \\ a_{21}b_{11} & a_{21}b_{12} & a_{22}b_{11} & a_{22}b_{12} & a_{23}b_{11} & a_{23}b_{12} \\ a_{21}b_{21} & a_{21}b_{22} & a_{22}b_{21} & a_{22}b_{22} & a_{23}b_{21} & a_{23}b_{22} \end{bmatrix}$$

**

In equation (2.2) the following theorem has been used:

$$(ABC) \ \otimes \ (DEF) = (A \ \otimes \ D) \ (B \ \otimes \ E) \ (C \ \otimes \ F)$$

where A, B, C, D, E, F are matrices of suitable dimensions. As applied in equation (2.2) it should be noted that $s(IJ) \ s^*(IJ) = s(IJ) \ \otimes \ s^*(IJ)$.

HH, HV, VH, VV; if $s(\alpha) = \sum_m s_m(\alpha)$ where the sum is taken over the set of components of the entire scattering body, then the expressions $s(\alpha)s^*(\beta)$ in the right-hand member of equation (2.2) are given by

$$\begin{aligned} \overline{s(\alpha)s^*(\beta)} &= \overline{\sum_{m,n} s_m(\alpha)s_n^*(\beta)} = \sum_{m,n} \overline{s_m(\alpha)s_n^*(\beta)} \\ &= \sum_{m,n} |s_m(\alpha)s_n(\beta)| e^{i[\theta_m(\alpha) - \theta_n(\beta)]}. \end{aligned} \quad (2.3)$$

Since it is assumed that random phase relations obtain among scattered fields of the components, the last sum is zero for $m \neq n$. Hence, equation (2.3)

becomes

$$\overline{s(\alpha)s^*(\beta)} = \sum_n s_n(\alpha)s_n^*(\beta). \quad (2.4)$$

Thus to obtain an element of the form $\overline{|s(IJ)|^2} = \sigma(IJ)$ it is necessary and sufficient to know a certain set of quantities $s_n(\alpha)s_n^*(\beta)$ for each component.

Since α and β may take any of the values HH, HV, VH, VV it will be necessary to know a set of six quantities, three of which are real, three complex (eq. 2.5).

The matrix

$$\overline{\mathbf{S}(\text{HV}; \text{HV})} \otimes \overline{\mathbf{S}^*(\text{HV}; \text{HV})} = \begin{bmatrix} \overline{s(\text{HH}) s^*(\text{HH})} & \overline{s(\text{HH}) s^*(\text{HV})} & \overline{s(\text{HV}) s^*(\text{HH})} & \overline{s(\text{HV}) s^*(\text{HV})} \\ \overline{s(\text{HH}) s^*(\text{VH})} & \overline{s(\text{HH}) s^*(\text{VV})} & \overline{s(\text{HV}) s^*(\text{VH})} & \overline{s(\text{HV}) s^*(\text{VV})} \\ \overline{s(\text{VH}) s^*(\text{HH})} & \overline{s(\text{VH}) s^*(\text{HV})} & \overline{s(\text{VV}) s^*(\text{HH})} & \overline{s(\text{VV}) s^*(\text{HV})} \\ \overline{s(\text{VH}) s^*(\text{VH})} & \overline{s(\text{VH}) s^*(\text{VV})} & \overline{s(\text{VV}) s^*(\text{VH})} & \overline{s(\text{VV}) s^*(\text{VV})} \end{bmatrix} \quad (2.5)$$

is of course not a scattering matrix. It is made up of the direct product of two scattering matrices, and will be called an $\overline{S \otimes S^*}$ - MATRIX.

Assuming reciprocity, and taking into account that $\left[s_n(\alpha) s_n^*(\beta) \right]^* = s_n^*(\alpha) s_n(\beta)$, it follows from equations (2.4) and (2.5) that it is necessary and sufficient to know the six numbers

$$s_n(HH) s_n^*(HH) , \quad s_n(VH) s_n^*(VH) , \quad s_n(VV) s_n^*(VV) ,$$

$$s_n(HH) s_n^*(VH) , \quad s_n(HH) s_n^*(VV) , \quad s_n(VV) s_n^*(VH)$$

for each n (component of the body) in order to determine an $\overline{S \otimes S^*}$ - MATRIX and hence the elements $\overline{|s(LJ)|^2}$.

INDEPENDENT CROSS SECTIONS APPROPRIATE TO
MULTIPLE-COMPONENT BODIES

It was shown in Section 2 that $\overline{\sigma(IJ)}$ could be obtained from the independent set $|\overline{s(HH)}|^2, |\overline{s(HV)}|^2, |\overline{s(VV)}|^2, \overline{s(HH) s^*(HV)}, \overline{s(HV) s^*(VV)},$ and $\overline{s(VV) s^*(HH)}$. In this section it will be shown how $\overline{\sigma(IJ)}$ can be obtained from a basic set of nine average effective cross sections.

To do so, it is necessary to determine the most general set of basis vectors $\hat{p}(A), \hat{p}(B)$, in terms of $\hat{p}(H)$ and $\hat{p}(V)$. The normalization of $\hat{p}(A)$ and $\hat{p}(B)$ requires that $\hat{p}(A) \cdot \hat{p}^*(A) = 1$ and $\hat{p}(B) \cdot \hat{p}^*(B) = 1$. The most general vectors satisfying these requirements are:

$$\begin{aligned}\hat{p}(A) &= e^{i\phi_1} \cos \alpha \hat{p}(H) + e^{i\phi_2} \sin \alpha \hat{p}(V) \quad , \\ \hat{p}(B) &= -e^{i\phi_3} \sin \beta \hat{p}(H) + e^{i\phi_4} \cos \beta \hat{p}(V) \quad .\end{aligned}$$

There is the additional orthogonality requirement $\hat{p}(A) \cdot \hat{p}^*(B) = 0$, or

$$-e^{i(\phi_1 - \phi_3)} \cos \alpha \sin \beta + e^{i(\phi_2 - \phi_4)} \sin \alpha \cos \beta = 0 .$$

Thus, $\phi_1 - \phi_3 = \phi_2 - \phi_4$, and $\alpha = \beta^*$. The values of the cross sections $\sigma(AJ)$ and $\sigma(BJ)$ are not affected by multiplying $\hat{p}(A)$ and $\hat{p}(B)$ by $e^{-i\phi_1}$ and $e^{-i\phi_3}$ respectively. As a result, the most general basis vectors which need be considered are of the form

$$\begin{aligned}\hat{p}(A) &= \cos \alpha \hat{p}(H) + e^{i\gamma} \sin \alpha \hat{p}(V) \quad , \\ \hat{p}(B) &= -\sin \alpha \hat{p}(H) + e^{i\gamma} \cos \alpha \hat{p}(V) \quad .\end{aligned}\tag{3.1}$$

* Actually there are other solutions but they do not result in increased generality.

The corresponding transformation matrices are:

$$U(AB; HV) = \begin{pmatrix} \cos \alpha & e^{i\gamma} \sin \alpha \\ -\sin \alpha & e^{i\gamma} \cos \alpha \end{pmatrix}; \quad U(HV; AB) = \begin{pmatrix} \cos \alpha & -\sin \alpha \\ e^{-i\gamma} \sin \alpha & e^{-i\gamma} \cos \alpha \end{pmatrix}. \quad (3.2)$$

Using equations (1.2.8), (1.2.9), and (1.2.10), it follows that

$$\begin{aligned} s(AH) &= \cos \alpha s(HH) + e^{i\gamma} \sin \alpha s(HV) , \\ s(AV) &= \cos \alpha s(HV) + e^{i\gamma} \sin \alpha s(VV) , \\ s(AB) &= -\frac{1}{2} \sin 2\alpha s(HH) + e^{i\gamma} \cos 2\alpha s(HV) + \frac{1}{2} e^{2i\gamma} \sin 2\alpha s(VV) . \end{aligned} \quad (3.3)$$

Taking the squares of the magnitudes of equation (3.3) yields:

$$\begin{aligned} |s(AH)|^2 &= \cos^2 \alpha |s(HH)|^2 + \sin^2 \alpha |s(HV)|^2 + \sin 2\alpha \cos \gamma \operatorname{Re} s^*(HH) s(HV) \\ &\quad - \sin 2\alpha \sin \gamma \operatorname{Im} s^*(HH) s(HV) , \\ |s(AV)|^2 &= \cos^2 \alpha |s(HV)|^2 + \sin^2 \alpha |s(VV)|^2 + \sin 2\alpha \cos \gamma \operatorname{Re} s^*(HV) s(VV) \\ &\quad - \sin 2\alpha \sin \gamma \operatorname{Im} s^*(HV) s(VV) , \\ |s(AB)|^2 &= \frac{1}{4} \sin^2 2\alpha |s(HH)|^2 + \cos^2 2\alpha |s(HV)|^2 + \frac{1}{4} \sin^2 2\alpha |s(VV)|^2 \\ &\quad - \frac{1}{2} \sin 4\alpha \cos \gamma \operatorname{Re} s^*(HH) s(HV) + \frac{1}{2} \sin 4\alpha \sin \gamma \operatorname{Im} s^*(HH) s(HV) \\ &\quad - \frac{1}{2} \sin^2 2\alpha \cos 2\gamma \operatorname{Re} s^*(HH) s(VV) + \frac{1}{2} \sin^2 2\alpha \sin 2\gamma \operatorname{Im} s^*(HH) s(VV) \\ &\quad + \frac{1}{2} \sin 4\alpha \cos \gamma \operatorname{Re} s^*(HV) s(VV) - \frac{1}{2} \sin 4\alpha \sin \gamma \operatorname{Im} s^*(HV) s(VV) , \end{aligned} \quad (3.4)$$

where Re and Im refer respectively to the real and imaginary part of the quantity they precede.

The squares of the magnitudes of the other elements are obtained from the conservation of energy relations, together with the reciprocity relation

$s(IJ) = s(JI)$:

$$\begin{aligned}
 |s(BH)|^2 &= |s(HH)|^2 + |s(HV)|^2 - |s(AH)|^2 \\
 |s(BV)|^2 &= |s(HV)|^2 + |s(VV)|^2 - |s(AV)|^2 \\
 |s(AA)|^2 &= |s(AH)|^2 + |s(AV)|^2 - |s(AB)|^2 \\
 |s(BB)|^2 &= |s(BH)|^2 + |s(BV)|^2 - |s(AB)|^2 .
 \end{aligned} \tag{3.5}$$

For $\alpha = 45^\circ$, $\gamma = 90^\circ$, let $A = L$ and $B = R$. For $\alpha = 45^\circ$, $\gamma = 0^\circ$, let $A = +$ and $B = -$. For $\alpha = 45^\circ$, $\gamma = 45^\circ$, let $A = \wedge$, $B = P$. The polarizations $H, V, L, R, +, -, \wedge, P$, being considered are shown in Figure A-5.

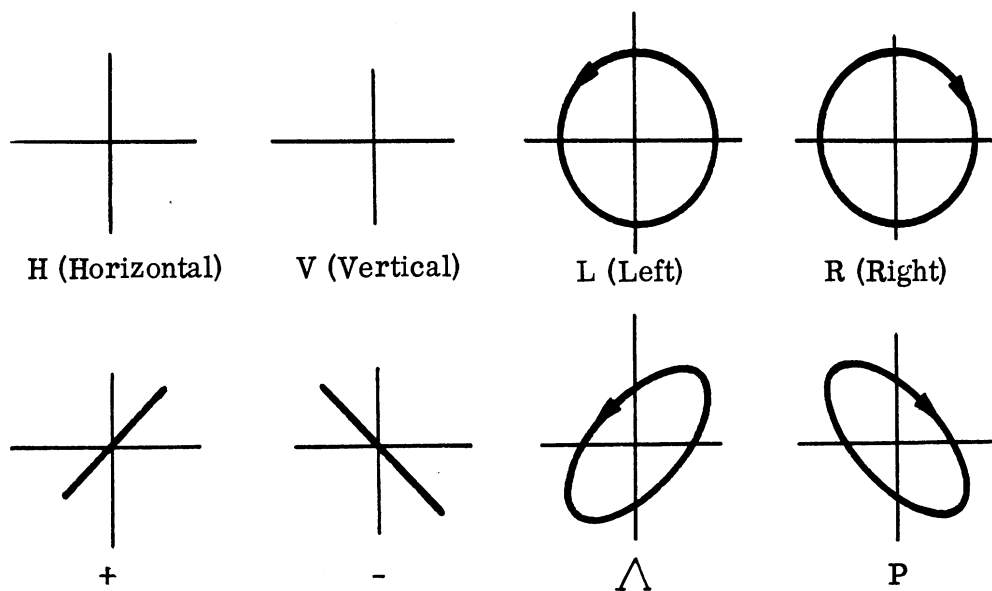


FIG. A-5: POLARIZATIONS $H, V, L, R, +, -, \wedge, P$

Then it follows from equation (3.4) that

$$\begin{aligned}
|s(\text{LH})|^2 &= \frac{1}{2} |s(\text{HH})|^2 + \frac{1}{2} |s(\text{HV})|^2 - \text{Im } s^*(\text{HH}) s(\text{HV}) \\
|s(\text{LV})|^2 &= \frac{1}{2} |s(\text{HV})|^2 + \frac{1}{2} |s(\text{VV})|^2 - \text{Im } s^*(\text{HV}) s(\text{VV}) \\
|s(\text{LR})|^2 &= \frac{1}{4} |s(\text{HH})|^2 + \frac{1}{4} |s(\text{VV})|^2 + \frac{1}{2} \text{Re } s^*(\text{HH}) s(\text{VV}) \\
|s(+\text{H})|^2 &= \frac{1}{2} |s(\text{HH})|^2 + \frac{1}{2} |s(\text{HV})|^2 + \text{Re } s^*(\text{HH}) s(\text{HV}) \\
|s(+\text{V})|^2 &= \frac{1}{2} |s(\text{HV})|^2 + \frac{1}{2} |s(\text{VV})|^2 + \text{Re } s^*(\text{HV}) s(\text{VV}) \\
|s(\Delta\text{P})|^2 &= \frac{1}{4} |s(\text{HH})|^2 + \frac{1}{4} |s(\text{VV})|^2 + \frac{1}{2} \text{Im } s^*(\text{HH}) s(\text{VV}) . \quad (3.6)
\end{aligned}$$

If the scattering matrix $S(\text{HV}; \text{HV})$ has been obtained, then from S and equation (3.6), the cross sections $\sigma(\text{HH})$, $\sigma(\text{HV})$, $\sigma(\text{VV})$, $\sigma(\text{LH})$, $\sigma(\text{LV})$, $\sigma(\text{LR})$, $\sigma(+\text{H})$, $\sigma(+\text{V})$, and $\sigma(\Delta\text{P})$ can be found. From these nine cross sections the cross sections for all other polarization combinations may be obtained by using equations (3.4), (3.5), and (3.6). Use of equation (3.6) in equation (3.4) gives

$$\begin{aligned}
\sigma(\text{AH}) &= \left[\cos^2 \alpha - \frac{1}{2} \sin 2\alpha (\sin \gamma + \cos \gamma) \right] \sigma(\text{HH}) \\
&+ \left[\sin^2 \alpha - \frac{1}{2} \sin 2\alpha (\sin \gamma + \cos \gamma) \right] \sigma(\text{HV}) \\
&+ \sin 2\alpha \cos \gamma \sigma(+\text{H}) + \sin 2\alpha \sin \gamma \sigma(\text{LH}) , \\
\sigma(\text{AV}) &= \left[\cos^2 \alpha - \frac{1}{2} \sin 2\alpha (\sin \gamma + \cos \gamma) \right] \sigma(\text{HV}) \\
&+ \left[\sin^2 \alpha - \frac{1}{2} \sin 2\alpha (\sin \gamma + \cos \gamma) \right] \sigma(\text{VV}) \\
&+ \sin 2\alpha \cos \gamma \sigma(+\text{V}) + \sin 2\alpha \sin \gamma \sigma(\text{LV}) , \quad (3.7)
\end{aligned}$$

$$\begin{aligned}
\sigma(\text{AB}) &= \frac{1}{4} \sin^2 2\alpha (1 + \cos 2\gamma - \sin 2\gamma) [\sigma(\text{HH}) + \sigma(\text{VV})] \\
&+ \frac{1}{4} \sin 4\alpha (\sin \gamma + \cos \gamma) [\sigma(\text{HH}) - \sigma(\text{VV})] + \frac{1}{2} \sin 4\alpha \cos \gamma [\sigma(+\text{V}) - \sigma(+\text{H})] \\
&+ \frac{1}{2} \sin 4\alpha \sin \gamma [\sigma(\text{LV}) - \sigma(\text{LH})] + \cos^2 2\alpha \sigma(\text{HV}) + \sin^2 2\alpha \sin 2\gamma \sigma(\text{LP}) \\
&- \sin^2 2\alpha \cos 2\gamma \sigma(\text{LR}) .
\end{aligned}$$

From equation (3.5):

$$\begin{aligned}
\sigma(\text{BH}) &= \sigma(\text{HH}) + \sigma(\text{HV}) - \sigma(\text{AH}) , \\
\sigma(\text{BV}) &= \sigma(\text{HV}) + \sigma(\text{VV}) - \sigma(\text{AV}) , \\
\sigma(\text{AA}) &= \sigma(\text{AH}) + \sigma(\text{AV}) - \sigma(\text{AB}) , \\
\sigma(\text{BB}) &= \sigma(\text{BH}) + \sigma(\text{BV}) - \sigma(\text{AB}) ; \tag{3.8}
\end{aligned}$$

and by reciprocity,

$$\begin{aligned}
\sigma(\text{HA}) &= \sigma(\text{AH}) , & \sigma(\text{HB}) &= \sigma(\text{BH}) , \\
\sigma(\text{VA}) &= \sigma(\text{AV}) , & \sigma(\text{VB}) &= \sigma(\text{BV}) , \\
\sigma(\text{BA}) &= \sigma(\text{AB}) . \tag{3.9}
\end{aligned}$$

Equations (3.7), (3.8), and (3.9) give all of the cross-polarization cross sections of interest except ones of the form $\sigma(\text{AJ})$ where A and J are polarization vectors from different bases. These can be obtained by using the $\overline{\text{S} \otimes \text{S}^*}$ - MATRIX defined in the preceding section. The elements of the $\overline{\text{S} \otimes \text{S}^*}$ - MATRIX can be obtained from equation (3.6) and the cross section can be obtained from the $\overline{\text{S} \otimes \text{S}^*}$ - MATRIX defined in equation (2.5).

POLARIZATION EFFECTS AND THE PHYSICAL OPTICS APPROXIMATION

No REPOLARIZATION* effects obtain when physical optics is used in computing the monostatic single scattering cross sections. However, the physical optics approximation does yield repolarization effects for monostatic multiple scattering cross sections.

Since the assumptions**, of physical optics are employed in this report, according to the methods of Reference A-1, to obtain cross sections for many simple shapes representing component parts of an aircraft, it is necessary to consider the degree to which the physical optics approximation agrees with experiment and with exact solutions when available.

For arbitrary directions of incidence on a general body, if any radius of curvature of the body is of the order of a wavelength in the neighborhood of a stationary phase point, neither the physical optics prediction of no repolarization

* Repolarization is said to occur when $S(HV;HV)$ is not of the form $\begin{pmatrix} q & 0 \\ 0 & q \end{pmatrix}$.

** A simple and commonly used assumption for a body possessing principal radii of curvature R_1 and R_2 which are everywhere large compared to a wavelength is, as stated in Reference A-2, p. 462, that "... the induced currents and fields radiated from any infinitesimal unit of area are very nearly those which would be obtained from the same area if it were part of an infinite plane, tangent to the surface at the location of the element of area. The currents and fields on the surface are determined by the boundary condition that the surface magnetic field is entirely tangential and is twice the tangential component of the magnetic field of the incident wave".

For a detailed discussion of the assumptions of physical optics see Reference A-16, p. 9.

nor its prediction of magnitude should be accepted without further investigation. Likewise in those cases where any radius of curvature is less than the wavelength, the assumptions of physical optics make the results suspect, although other considerations for a particular case may show the results to be quite acceptable. For example, for the Poynting vector incident along the axis of symmetry of a perfectly conducting surface of revolution, the physical optics indications of no repolarization are valid. Such validity may most easily be seen from an analysis of the boundary value problem involved.

Since the boundary conditions may be given in terms of \vec{E} alone, and since \vec{H} is given in terms of \vec{E} by Maxwell's equations, the problem of a perfect conductor may be stated in terms of \vec{E} alone. The wave equation for \vec{E} and the boundary conditions are unchanged by reflection in the plane P containing the incident Poynting vector and the incident electric field. Therefore, to any solution for \vec{E}^s with components normal to P, there must correspond another solution with normal components cancelling these. Since two solutions are impossible by uniqueness, \vec{E}^s must lie in P. Thus there is no repolarization. So the validity of the application of physical optics for the Poynting vector incident along the axis of symmetry of a perfectly conducting surface of revolution will be a question of magnitude only.

It has been observed that for the case of a cone or a paraboloid of revolution with the transmitter and receiver on the axis of symmetry the physical optics answer agrees both with experimental results and with the exact theory, as illustrated in References A-7 and A-16. Further, it has been found (Ref. A-8)

that the geometric optics fields for the infinite dihedral agree with the exact fields for dihedral angles of π/n , $n = 1, 2, \dots$, and that the geometric and physical optics fields are in agreement for these cases.

These results suggest that the physical optics cross section may be expected to agree fairly well with the exact solution for a wider range of objects than the large-principal-radii criterion would indicate.

It is, of course, not necessary to be limited to the particular method discussed above. A different assumption (as in Kerr's example of the finite cylinder) is that the exact solution for a similar problem (in Kerr's case the infinite cylinder) may be used as a guide for the assumed field at the surface of the scatterer. It would seem reasonable to expect this solution to be a good approximation as long as it is used advisedly.

Another approximate method has been suggested by Fock (Ref. A-9). It is limited only by the restrictions that the scatterer be convex and the radii of curvature be much greater than the wavelength, so that it is applicable to a wide variety of scatterers and will yield both scattered magnitude and polarization information.

For those components of a scattering body to which physical optics applies it may be assumed that the scattering matrix $S(HV; HV)$ has the form

$$S(HV; HV) = \begin{pmatrix} 1 & 0 \\ 0 & 1 \end{pmatrix} S(HH) . \quad (4.1)$$

From this relation the scattering matrices $S(LR; HV)$, $S(HV; LR)$, and $S(LR; LR)$ may be determined from equations (1.2.8), (1.2.9), (1.2.10), and (3.2) by putting

$A = L$, $B = R$, $\alpha = 45^\circ$ and $\gamma = 90^\circ$. The unitary transformation matrices $U(LR; HV)$ and $U(HV; LR)$ involved here are given by [from equation (3.2) with $\alpha = 45^\circ$, $\gamma = 90^\circ$],

$$U(LR; HV) = \frac{1}{\sqrt{2}} \begin{pmatrix} 1 & i \\ -1 & i \end{pmatrix}; \quad U(HV; LR) = \frac{1}{\sqrt{2}} \begin{pmatrix} 1 & -1 \\ -i & -i \end{pmatrix}. \quad (4.2)$$

Hence,

$$S(LR; HV) = \begin{pmatrix} 1 & i \\ -1 & i \end{pmatrix} \frac{s(HH)}{\sqrt{2}}, \quad (4.3a)$$

$$S(HV; LR) = \begin{pmatrix} 1 & -1 \\ i & i \end{pmatrix} \frac{s(HH)}{\sqrt{2}}, \quad (4.3b)$$

$$S(LR; LR) = \begin{pmatrix} 0 & -1 \\ -1 & 0 \end{pmatrix} s(HH). \quad (4.3c)$$

It follows from equations (4.3) and (3.6) that, for the nine cross sections of interest (as given in Sec. 3), the following relations hold where physical optics reasoning is applied:

$$\sigma(HH) = \sigma(VV) = \sigma(LR), \quad (4.4a)$$

$$\sigma(HV) = 0, \quad [\sigma(RR) = \sigma(LL) = 0 \text{ also}], \quad (4.4b)$$

$$\sigma(LH) = \sigma(LV) = \sigma(+H) = \sigma(+V) = \sigma(\Lambda P) = \frac{1}{2} \sigma(HH). \quad (4.4c)$$

CROSS-POLARIZATION CROSS SECTIONS OF WEDGES

The trailing edges of wing and tail assemblies of modern aircraft, in particular the B-47 aircraft, are thin and sharp enough to warrant simulation by wedge, or tapered wedge, shapes. Since sharp edges will, in general, give rise to repolarization, such edges are considered in this section.

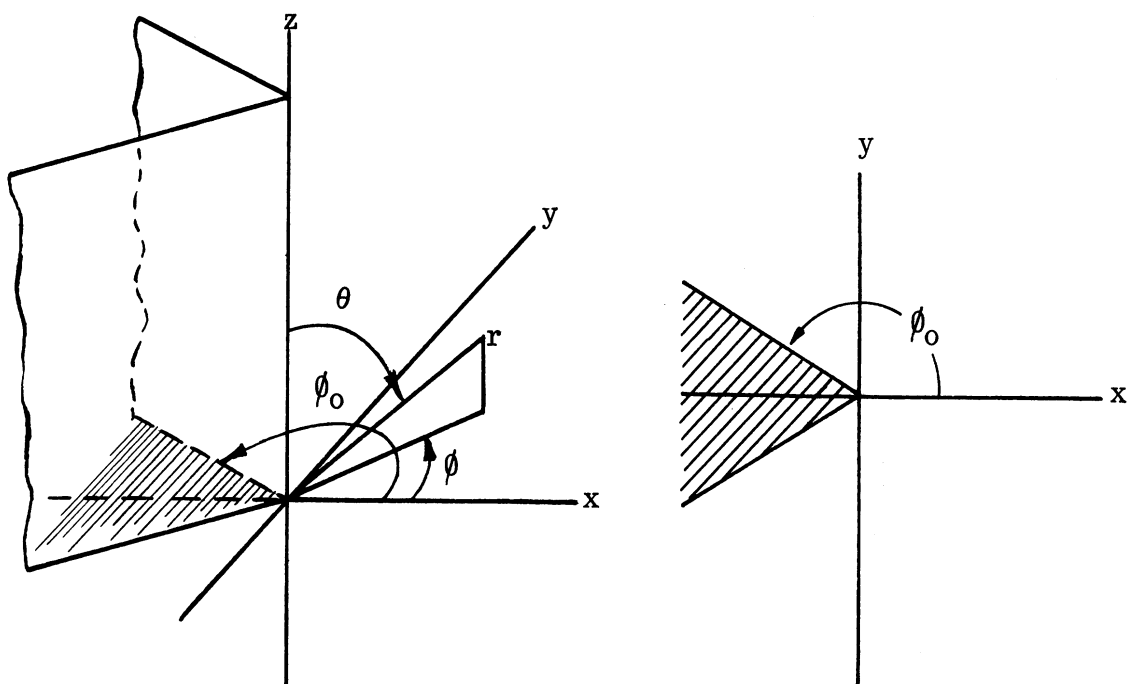


FIG. A-6: WEDGE COORDINATE SYSTEM

5.1 General Theory

Consider an infinite perfectly conducting wedge whose edge lies along the z -axis and whose intersection with the xy -plane makes an angle ϕ_0 with the positive x -axis.

To find the total electric field for arbitrary incidence it is necessary to solve the equation

$$(\nabla^2 + k^2) \vec{E} = 0 , \quad (5.1.1)$$

subject to a radiation condition at infinity and to the conditions

$$\nabla \cdot \vec{E} = 0 , \quad \text{in space} , \quad (5.1.2)$$

$$\hat{n} \times \vec{E} = 0 , \quad \text{at the body} , \quad (5.1.3)$$

where \hat{n} is a unit outward normal to the body.

Let the direction of incidence be restricted to the xy-plane with polarizations (a) perpendicular to , and (b) parallel to the edge of the wedge.

Then equations (5.1.1) and (5.1.2) are satisfied if \vec{E} has the form

$$\hat{i}_z \psi (r, \phi)$$

or

$$-\frac{1}{ik} \text{curl} \hat{i}_z \psi (r, \phi) ,$$

where

$$(\nabla^2 + k^2) \psi (r, \phi) = 0^* . \quad (5.1.4)$$

The form $\vec{E} = -1/ik \text{curl} \hat{i}_z \psi (r, \phi)$ suffices for case (a) with equation (5.1.3)

implying the condition

$$\frac{\partial}{\partial n} \psi (r, \pm \phi_0) = 0 . \quad (5.1.5)$$

* A cylindrical coordinate system, r, ϕ, z , is used throughout this section. Unit vectors for these directions are $\hat{i}_r, \hat{i}_\phi, \hat{i}_z$. The unit vector designating polarization perpendicular to the edge of the wedge is $\hat{p}(a) = \hat{i}_\phi$, and the unit vector designating polarization parallel to the edge of the wedge is $\hat{p}(b) = \hat{i}_z$.

Case (b) requires the form $\vec{E} = \hat{i}_z \psi(r, \phi)$ with equation (5.1.3) implying the condition

$$\psi(r, \pm\phi_0) = 0 . \quad (5.1.6)$$

In a recent paper (Ref. A-10) F. Oberhettinger obtained expressions for the Green's functions for the wave equation for the conditions (5.1.5) and (5.1.6). Let $Q(\rho, \gamma + \phi_0)$ be the intersection with the xy-plane of a line source parallel to the edge of the wedge and $P(r, \phi + \phi_0)$ be a point outside the wedge. Oberhettinger expresses the incident cylindrical wave in the form

$$\psi_{(i)} = H_0^{(2)}(-kR) = \frac{2i}{\pi} K_0(\beta R) = \frac{2i}{\pi} K_0 \left[\beta \left(r^2 + \rho^2 - 2r\rho \cos(\phi - \gamma) \right)^{1/2} \right] \quad (5.1.7)$$

where k has been put equal to $i\beta$. This equation is expanded in the form

$$\psi_{(i)} = \frac{4i}{\pi^2} \int_0^\infty K_{i\zeta}(\beta r) K_{i\zeta}(\beta \rho) \cosh \left[\zeta (\pi - |\phi - \gamma|) \right] d\zeta , \quad (5.1.8)$$

where $K_\mu(Z)$ is the modified Hankel function defined by

$$K_\mu(Z) = -\frac{1}{2} i\pi e^{\frac{-i\mu\pi}{2}} H_\mu^{(2)} \left(Z e^{\frac{-i\pi}{2}} \right) .$$

The total field $\psi_{(t)}$ is given as the sum of the incident field $\psi_{(i)}$ and the reflected field ψ :

$$\psi_{(t)} = \psi_{(i)} + \psi . \quad (5.1.9)$$

The reflected field can be represented in a form similar to equation (5.1.8)

$$\psi = \frac{4i}{\pi^2} \int_0^\infty K_{i\zeta}(\beta r) K_{i\zeta}(\beta \rho) \left[f_1(\zeta) e^{\zeta(\phi + \phi_0)} + f_2(\zeta) e^{-\zeta(\phi + \phi_0)} \right] d\zeta , \quad (5.1.10)$$

where, by using equations (5.1.8) and (5.1.9), f_1 and f_2 are given by

$$\begin{aligned} f_1(\xi) - f_2(\xi) &= -\sinh \left[\xi (\pi - \gamma - \phi_0) \right] \\ f_1(\xi) e^{2\xi\phi_0} - f_2(\xi) e^{-2\xi\phi_0} &= \sinh \left[\xi (\pi + \gamma - \phi_0) \right] , \end{aligned} \quad (5.1.11)$$

for condition (5.1.5), and by

$$\begin{aligned} f_1(\xi) + f_2(\xi) &= -\cosh \left[\xi (\pi - \gamma - \phi_0) \right] \\ f_1(\xi) e^{2\xi\phi_0} + f_2(\xi) e^{-2\xi\phi_0} &= -\cosh \left[\xi (\pi + \gamma - \phi_0) \right] , \end{aligned} \quad (5.1.12)$$

for condition (5.1.6).

To determine radar cross sections, the reflected fields must be found for conditions (5.1.5) and (5.1.6). In particular for condition (5.1.6) it follows from equation (5.1.12) that

$$\psi = -\frac{4i}{\pi^2} \int_0^\infty K_{i\xi}(\beta r) K_{i\xi}(\beta \rho) A(\xi) d\xi ,$$

where

$$A(\xi) = \frac{1}{\sinh 2\xi\phi_0} \left\{ \sinh \xi \pi \cosh \xi (\phi + \gamma) + \sinh \xi (2\phi_0 - \pi) \cosh \xi (\phi - \gamma) \right\}$$

or

$$\psi = i \int_0^\infty e^{-\xi\pi} H_{i\xi}^{(1)}(kr) H_{i\xi}^{(1)}(k\rho) A(\xi) d\xi . \quad (5.1.13)$$

If the point $Q(\rho, \gamma + \phi_0)$ defined above is moved to infinity, the Hankel function $H_{i\xi}^{(1)}(k\rho)$ may be replaced* by its asymptotic value

$$\sqrt{\frac{2}{\pi k\rho}} e^{ik\rho + \frac{\pi\xi}{2} - \frac{i\pi}{4}} .$$

* This is justified in Section 5.2.

To express equation (5.1.13) in a manner appropriate to the form $e^{-ikr \cos(\phi-\gamma)}$ for an incoming plane wave, the asymptotic expansion of $H_{1\xi}^{(1)}(k\rho)$ must be divided by the asymptotic expression

$$- \sqrt{\frac{2}{\pi k\rho}} e^{ik\rho - \frac{\pi i}{4} - ikr \cos(\phi-\gamma)}$$

of equation (5.1.7) and multiplied by $e^{-ikr \cos(\phi-\gamma)}$. Thus equation (5.1.13) becomes for incident polarization (b) parallel to the edge of the wedge,

$$\psi^{(b)} \approx -i \int_0^\infty e^{-\frac{\xi\pi}{2}} H_{1\xi}^{(1)}(kr) A(\xi) d\xi. \quad (5.1.14)$$

If it is further assumed that the value of r is very large, an asymptotic expansion can be substituted for the Hankel function in equation (5.1.14) giving*

$$\psi^{(b)} \approx - \sqrt{\frac{2}{\pi kr}} e^{ikr + \frac{\pi i}{4}} \int_0^\infty A(\xi) d\xi.$$

The remaining integral is convergent and may be evaluated for

$$\begin{aligned} 2\phi_0 &> \pi + |\phi + \gamma| \\ 2\phi_0 &> |2\phi_0 - \pi| + |\phi - \gamma| \end{aligned}$$

to give (Ref. A-11, page 55),

$$\psi^{(b)} \approx -\frac{1}{4\phi_0} \sqrt{\frac{2\pi}{kr}} e^{ikr + \frac{\pi i}{4}} \left[\frac{1}{A} + \frac{1}{B} \right] \sin \frac{\pi^2}{2\phi_0} \quad (5.1.15)$$

* This is justified in Section 5.2.

where

$$A = \cos \frac{\pi(\phi + \gamma)}{2\phi_0} + \cos \frac{\pi^2}{2\phi_0}$$

and

$$B = \cos \frac{\pi(\phi - \gamma)}{2\phi_0} - \cos \frac{\pi^2}{2\phi_0} .$$

Using condition (5.1.5) and equation (5.1.11) it can be shown for incident polarization (a) perpendicular to the edge of the wedge that

$$\psi^{(a)} \approx \frac{1}{4\phi_0} \sqrt{\frac{2\pi}{kr}} e^{ikr + \frac{\pi i}{4}} \left[\frac{1}{A} - \frac{1}{B} \right] \sin \frac{\pi^2}{2\phi_0} . \quad (5.1.16)$$

5.2 Remark on the Use of Asymptotic Expansions of Hankel Functions in the Integral Representation of the Scattered Field for a Wedge

The purpose of this section is the justification of the replacement of the Hankel functions by their asymptotic expansions in the integral

$$\int_0^\infty e^{-\xi\pi} H_{i\xi}^{(1)}(kr) H_{i\xi}^{(1)}(k\rho) A(\xi) d\xi . \quad (5.2.1)$$

Since the Hankel function $H_{i\xi}^{(1)}(kr)$ has the representation

$$H_{i\xi}^{(1)}(kr) = \frac{2 e^{\frac{\xi\pi}{2}}}{\pi i} \int_0^\infty e^{ikr \cosh t} \cos \xi t dt , \quad (5.2.2)$$

and since the asymptotic form

$$\sqrt{\frac{2}{\pi kr}} e^{ikr + \frac{\xi\pi}{2} - \frac{\pi i}{4}} \quad \text{of} \quad H_{i\xi}^{(1)}(kr)$$

has the representation

$$\begin{aligned}
\sqrt{\frac{2}{\pi kr}} e^{ikr + \frac{\zeta\pi}{2} - \frac{\pi i}{4}} &= e^{\frac{\zeta\pi}{2} + \frac{i\pi}{4}} H_{1/2}^{(1)}(kr) \\
&= \frac{2e^{\frac{\zeta\pi}{2}}}{\pi i} \int_0^\infty e^{ikr \cosh t} \cosh \frac{1}{2} t dt,
\end{aligned}
\tag{5.2.3}$$

it will suffice to consider the problem of obtaining a bound for the expression

$$\left| \int_0^\infty e^{ikr \cosh t} (\cosh t/2 - \cos \zeta t) dt \right|.
\tag{5.2.4}$$

More generally, if $f(t)$ and $g(t)$ are real valued functions such that $g(t)/f'(t)$ is of bounded variation and such that $g(\infty)/f'(\infty) = 0$, then

$$\begin{aligned}
\left| \int_0^\infty e^{if(t)} g(t) dt - i e^{if(0)} \frac{g(0)}{f'(0)} \right| &= \left| \int_0^\infty e^{if(t)} \frac{d}{dt} \left[\frac{g(t)}{f'(t)} \right] dt \right| \\
&\leq \int_0^\infty \left| \frac{d}{dt} \left[\frac{g(t)}{f'(t)} \right] \right| dt.
\end{aligned}
\tag{5.2.5}$$

Taking $f(t) = kr \cosh t$ and $g(t) = \cosh 1/2t - \cos \zeta t$ it follows that the problem of bounding the expression (5.2.4) becomes the problem of bounding

$$I = \frac{1}{kr} \int_0^\infty \left| \frac{d}{dt} \left[\frac{\cosh t/2 - \cos \zeta t}{\sinh t} \right] \right| dt;
\tag{5.2.6}$$

and this is done as follows:

$$\begin{aligned}
\text{kr I} &= \int_0^{\infty} \left| \frac{\sinh t \left(\frac{1}{2} \sinh \frac{1}{2} t + \zeta \sin \zeta t \right) - \cosh t \left(\cosh \frac{1}{2} t - \cos \zeta t \right)}{\sinh^2 t} \right| dt \\
&\leq \int_0^{\infty} \frac{\left| \frac{1}{2} \sinh \frac{1}{2} t \right| + \left| \zeta \sin \zeta t \right|}{\sinh t} dt + \int_0^{\infty} \frac{\left| \cosh \frac{1}{2} t - \cos \zeta t \right| \cosh t}{\sinh^2 t} dt \\
&\leq \int_0^{\infty} \frac{\frac{1}{2} \sinh \frac{1}{2} t dt}{2 \sinh \frac{1}{2} t \cosh \frac{1}{2} t} + \int_0^{\infty} \frac{\left| \zeta \sin \zeta t \right| dt}{2 \sinh \frac{1}{2} t \cosh \frac{1}{2} t} \\
&+ \int_0^{\infty} \frac{\left| \cosh \frac{1}{2} t - \cos \zeta t \right| \cosh t dt}{\sinh^2 t} = I_1 + I_2 + I_3 . \quad (5.2.7)
\end{aligned}$$

Each of I_1, I_2, I_3 may be either bounded or evaluated in finite form:

$$\begin{aligned}
I_1 &= \frac{1}{4} \int_0^{\infty} \frac{dt}{\cosh \frac{t}{2}} = \frac{\pi}{8} ; \quad I_2 \leq \zeta^2 \int_0^{\infty} \frac{t dt}{t \cosh \frac{1}{2} t} = \frac{\zeta^2 \pi}{2} ; \\
I_3 &= \int_0^{\infty} \frac{\left(\cosh \frac{1}{2} t - \cos \zeta t \right) \cosh t dt}{\sinh^2 t} = \frac{\pi}{4} + \frac{\zeta \pi}{2} \tanh \frac{\zeta \pi}{2} \leq \frac{\pi}{4} + \frac{\zeta \pi}{2} .
\end{aligned}$$

This integration is performed as follows: on pages 142 and 163 of

Reference A-11 the integrals

$$\begin{aligned}
\int_0^{\infty} \frac{\cos ax - \cos bx}{\sinh cx} \frac{dx}{x} &= \log \frac{\cosh \frac{b\pi}{2c}}{\cosh \frac{a\pi}{2c}} , \quad c > 0 , \\
\int_0^{\infty} \frac{\cosh ax - 1}{\sinh cx} \frac{dx}{x} &= -\log \left(\cos \frac{a\pi}{2c} \right) , \quad c > |a| , \text{ are given.}
\end{aligned}$$

Put $a = 0$ in the first of these formulas and add:

$$\int_0^{\infty} \frac{\cosh ax - \cos bx}{\sinh cx} \frac{dx}{x} = \log \frac{\cosh \frac{b\pi}{2c}}{\cosh \frac{a\pi}{2c}} ;$$

differentiate with respect to c and set $a = 1/2$, $b = \zeta$, $c = 1$:

$$\int_0^{\infty} \frac{\left(\cosh \frac{1}{2} t - \cos \zeta t\right) \cosh t}{\sinh^2 t} dt = \frac{\pi}{4} + \frac{\zeta \pi}{2} \tanh \frac{\zeta \pi}{2} .$$

Therefore,

$$e^{-\frac{\zeta \pi}{2}} \left| H_{i\zeta}^{(1)}(kr) - \sqrt{\frac{2}{\pi kr}} e^{ikr + \frac{\zeta \pi}{2} - \frac{\pi i}{4}} \right| \leq I \leq \frac{\pi}{8kr} (3 + 4\zeta + 4\zeta^2) . \quad (5.2.8)$$

A similar bound can be given in the case of the remaining Hankel function of equation (5.2.1) for the difference between it and its asymptotic expansion.

Finally, since every term of $A(\zeta)$ is of the form

$$\frac{e^{\mu \zeta} - e^{-\mu \zeta}}{e^{\nu \zeta} - e^{-\nu \zeta}} , \quad \nu > \mu \geq 0 ,$$

it can be seen by using equation (5.2.8) a bound which goes to zero as $1/r\rho$ for large r and ρ may be given for

$$\left| \int_0^{\infty} e^{-\zeta \pi} \left(H_{i\zeta}^{(1)}(kr) - \sqrt{\frac{2}{\pi kr}} e^{ikr + \frac{\zeta \pi}{2} - \frac{\pi i}{4}} \right) \left(H_{i\zeta}^{(1)}(k\rho) - \sqrt{\frac{2}{\pi k\rho}} e^{ik\rho + \frac{\zeta \pi}{2} - \frac{\pi i}{4}} \right) A(\zeta) d\zeta \right| .$$

5.3 Electric Fields for Linear Polarizations

Let the incident field be polarized perpendicular to the edge of the wedge.

Then the scattered electric field for the infinite wedge is given by

$$\vec{E}^{S(a)} = \frac{1}{ik} \hat{i}_z \times \nabla \psi^{(a)} \cong \left\{ \frac{1}{4\phi_0} \sqrt{\frac{2\pi}{kr}} e^{ikr + \frac{\pi i}{4}} \sin \frac{\pi^2}{2\phi_0} \left[\frac{1}{A} - \frac{1}{B} \right] \right\} \hat{i}_\phi, \quad (5.3.1a)$$

where A and B are given by equation (5.1.15).

If $\psi^{(a)}$ is written as $\psi^{(a)} = D \sqrt{\frac{2\pi}{kr}} e^{ikr + \frac{\pi i}{4}} f(\phi)$, then

$$\begin{aligned} \nabla \psi^{(a)} &= D f(\phi) \left[ik \sqrt{\frac{2\pi}{kr}} e^{ikr + \frac{\pi i}{4}} - \frac{1}{2} \sqrt{\frac{2\pi}{k}} r^{-\frac{3}{2}} e^{ikr + \frac{\pi i}{4}} \right] \hat{i}_r \\ &\quad + D \sqrt{\frac{2\pi}{k}} r^{-\frac{3}{2}} e^{ikr + \frac{\pi i}{4}} f'(\phi) \hat{i}_\phi \end{aligned}$$

can be approximated, for very large r, by

$$\nabla \psi^{(a)} \cong ikD \sqrt{\frac{2\pi}{kr}} e^{ikr + \frac{\pi i}{4}} f(\phi) \hat{i}_r = ik \psi^{(a)} \hat{i}_r$$

in equation (5.3.1a).

If the incident field is polarized parallel to the edge of the wedge, the scattered electric field for the infinite wedge is given by

$$\vec{E}^{S(b)} = \hat{i}_z \psi^{(b)} \cong \left\{ \frac{-1}{4\phi_0} \sqrt{\frac{2\pi}{kr}} e^{ikr + \frac{\pi i}{4}} \sin \frac{\pi^2}{2\phi_0} \left[\frac{1}{A} + \frac{1}{B} \right] \right\} \hat{i}_z. \quad (5.3.1b)$$

5.4 Electric Fields for Arbitrary Polarizations

If the incident field, with direction of incidence in a plane normal to the edge of the wedge, has an arbitrary polarization; i.e., if

$$\vec{E}^i = E(a)(-\hat{i}_x \sin \gamma + \hat{i}_y \cos \gamma) + E(b) \hat{i}_z = E(a) \hat{i}_\phi + E(b) \hat{i}_z, \quad (5.4.1a)$$

the scattered field is a linear combination of equations (5.3.1a) and (5.3.1b):

$$\vec{E}^s = \frac{1}{4\phi_0} \sqrt{\frac{2\pi}{kr}} e^{ikr + \frac{\pi i}{4}} \sin \frac{\pi^2}{2\phi_0} \left[\frac{E(a) \hat{i}_\phi - E(b) \hat{i}_z}{A} - \frac{E(a) \hat{i}_\phi - E(b) \hat{i}_z}{B} \right]. \quad (5.4.1b)$$

It was shown in Section A.2.8 of Reference A-1 that to go from the field for an infinite wedge to the field for the class of finite wedges whose current distributions are the same near the vertex involves only the multiplicative factor $\frac{L e^{-i\pi/4}}{\sqrt{r\lambda}}$, where L is the length of the finite wedge. Thus, if the incident electric field is of the form (5.4.1a), equation (5.4.1b) becomes for a wedge of length L:

$$\vec{E}^s = \frac{L e^{ikr}}{4r\phi_0} \sin \frac{\pi^2}{2\phi_0} \left[\frac{E(a) \hat{i}_\phi - E(b) \hat{i}_z}{A} - \frac{E(a) \hat{i}_\phi + E(b) \hat{i}_z}{B} \right]. \quad (5.4.2)$$

5.5 Cross Sections for Linear Polarizations

The effective cross sections σ for the finite wedge can now be given for the cases where the transmitted and received radiations are of arbitrary polarization and the direction of incidence still in a plane perpendicular to the edge of the wedge. The definition of effective cross section is, as given before by equation (1.2.6)

$$\sigma = \lim_{r \rightarrow \infty} 4\pi r^2 \left| \frac{\vec{E}^s \cdot \hat{p}}{\vec{E}^i} \right|^2, \quad (5.5.1)$$

where \hat{p} is a unit vector denoting the receiver polarization.

For example, if $\vec{E}^i = E(b)\hat{i}_z$ and $\hat{p} = \hat{p}(b) = \hat{i}_z$, then

$$\vec{E}^s = -\frac{L e^{ikr}}{4\phi_0 r} \sin \frac{\pi^2}{2\phi_0} \left[\frac{1}{A} + \frac{1}{B} \right] E(b)\hat{i}_z \quad (5.5.2)$$

and

$$\sigma(bb) = \frac{\pi L^2}{4\phi_0^2} \sin^2 \frac{\pi^2}{2\phi_0} \left[\frac{1}{A} + \frac{1}{B} \right]^2, \quad (5.5.3)$$

where $\sigma(bb)$ indicates that both the transmitted and received polarizations are in a direction parallel to the edge of the wedge.

If $\vec{E}^i = E(b)\hat{i}_z$ and $p = p(a) = -\hat{i}_x \sin \gamma + \hat{i}_y \cos \gamma$, then \vec{E}^s is as in equation

(5.5.2) and

$$\sigma(ab) = 0, \quad (5.5.4)$$

where $\sigma(ab)$ means that the transmitted and received polarizations are respectively parallel and perpendicular to the edge of the wedge. When the transmitted and received polarizations are both in a direction perpendicular to the edge of the wedge; i. e., when $\vec{E}^i = E(a)(-\hat{i}_x \sin \gamma + \hat{i}_y \cos \gamma)$ and $\hat{p} = \hat{p}(a) = -\hat{i}_x \sin \gamma + \hat{i}_y \cos \gamma$, then

$$\vec{E}^s = \frac{L e^{ikr}}{4\phi_0 r} \sin \frac{\pi^2}{2\phi_0} \left[\frac{1}{A} - \frac{1}{B} \right] E(a)\hat{i}_\phi \quad (5.5.5)$$

and

$$\sigma(aa) = \frac{\pi L^2}{4\phi_0^2} \sin^2 \frac{\pi^2}{2\phi_0} \left[\frac{1}{A} - \frac{1}{B} \right]^2 \cos^2(\phi - \gamma). \quad (5.5.6)$$

5.6 Cross Sections for Circular Polarizations

For circularly polarized transmitted and received polarizations it suffices to find $\sigma(Rb)$, $\sigma(Ra)$, and $\sigma(RR)$, where R indicates right circular

polarization. For incident radiation, unit vectors indicating right and left circular polarization are respectively,

$$\hat{i}(R) = \frac{1}{\sqrt{2}} \left[(-\hat{i}_x \sin \gamma + \hat{i}_y \cos \gamma) + i \hat{i}_z \right] \quad (5.6.1a)$$

$$\hat{i}(L) = \frac{1}{\sqrt{2}} \left[(-\hat{i}_x \sin \gamma + \hat{i}_y \cos \gamma) - i \hat{i}_z \right] \quad (5.6.1b)$$

For scattered radiation, the unit vector system is interchanged; i.e.,

$$\hat{i}^S(R) = \hat{i}(L) \quad \text{and} \quad \hat{i}^S(L) = \hat{i}(R).$$

If $\vec{E}^i = E(R) \hat{i}(R)$ and $\hat{p} = \hat{p}(R) = \hat{i}^S(R)$, then

$$\vec{E}^S = \frac{E(R)}{\sqrt{2}} \cdot \frac{L e^{ikr}}{4\phi_0 r} \sin \frac{\pi^2}{2\phi_0} \left\{ \hat{i}_\phi \left[\frac{1}{A} - \frac{1}{B} \right] - i \hat{i}_z \left[\frac{1}{A} + \frac{1}{B} \right] \right\} \quad (5.6.2)$$

and

$$\sigma(RR) = \frac{\pi L^2}{16 \phi_0^2} \sin^2 \frac{\pi^2}{2\phi_0} \left[\left(\frac{1}{A} - \frac{1}{B} \right) \cos(\phi - \gamma) + \left(\frac{1}{A} + \frac{1}{B} \right) \right]^2. \quad (5.6.3)$$

If $\vec{E}^i = E(b) \hat{k}$ and $\hat{p} = \hat{p}(R) = \left[(-\hat{i}_x \sin \gamma + \hat{i}_y \cos \gamma) - i \hat{i}_z \right] \sqrt{\frac{1}{2}}$, then \vec{E}^S is as in equation (5.5.2) and

$$\sigma(Rb) = \frac{\pi L^2}{8\phi_0^2} \sin^2 \frac{\pi^2}{2\phi_0} \left[\frac{1}{A} + \frac{1}{B} \right]^2 = \frac{1}{2} \sigma(bb). \quad (5.6.4)$$

Finally, if \vec{E}^i is given by $\vec{E}^i = E(a) (-\hat{i}_x \sin \gamma + \hat{i}_y \cos \gamma)$ and \hat{p} by $\hat{p}(R) =$

$1/\sqrt{2} \left[(-\hat{i}_x \sin \gamma + \hat{i}_y \cos \gamma) - i \hat{i}_z \right]$, then \vec{E}^S is given by equation (5.5.5) and

$$\sigma(Ra) = \frac{\pi L^2}{8\phi_0^2} \sin^2 \frac{\pi^2}{2\phi_0} \left[\frac{1}{A} - \frac{1}{B} \right]^2 \cos^2(\phi - \gamma) = \frac{1}{2} \sigma(aa). \quad (5.6.5)$$

5.7 Summary of Formulas

For backscattering, $\phi = \gamma$ (direction of incidence still perpendicular to the edge of the wedge) the effective cross sections obtained in Sections 5.5 and 5.6 become:

$$\left. \begin{aligned}
 1. \quad \sigma(\text{bb}) &= M \left[\frac{1}{C} + \frac{1}{D} \right]^2 \\
 2. \quad \sigma(\text{ab}) &= 0 \\
 3. \quad \sigma(\text{aa}) &= M \left[\frac{1}{C} - \frac{1}{D} \right]^2 \\
 4. \quad \sigma(\text{RR}) &= \frac{M}{4C^2} \\
 5. \quad \sigma(\text{Rb}) &= \frac{1}{2} \sigma(\text{bb}) \\
 6. \quad \sigma(\text{Ra}) &= \frac{1}{2} \sigma(\text{aa})
 \end{aligned} \right\} \begin{aligned}
 M &= \frac{\pi L^2}{4\phi_0^2} \sin^2 \frac{\pi^2}{2\phi_0} \\
 C &= \cos \frac{\pi\gamma}{\phi_0} + \cos \frac{\pi^2}{2\phi_0} \\
 D &= 1 - \cos \frac{\pi^2}{2\phi_0}
 \end{aligned} \quad (5.7.1)$$

C and D are respectively the values of A and B of equation (5.1.15) for $\phi = \gamma$.

5.8 Coordinate Systems

To apply the formulas of Section 5.7 to wedge-shaped components of an airplane, the relations between the polar angles of the wedge and of the airplane coordinate systems must be known. These relations are derived in this section.

Let $\hat{i}_x^*, \hat{i}_y^*, \hat{i}_z^*$ be a unit orthogonal set describing the airplane x^*, y^*, z^* -axes, with ϕ^* and θ^* as polar angles in this system. Let $\hat{i}_x, \hat{i}_y, \hat{i}_z$ be a unit orthogonal set describing the wedge axes, with ϕ and θ as polar angles

in this system; and suppose that the edge of the wedge lies along the z-axis and that the wedge is symmetric with regard to the xz-plane.

For a fixed aspect θ^* it is desired to find the azimuth, ϕ_{\perp}^* , for which the direction of incidence, $\phi = \gamma$, is perpendicular to the edge of the wedge.

Let

$$\hat{i}_x^* = a_{11} \hat{i}_x + a_{12} \hat{i}_y + a_{13} \hat{i}_z$$

$$\hat{i}_y^* = a_{21} \hat{i}_x + a_{22} \hat{i}_y + a_{23} \hat{i}_z \quad (5.8.1)$$

$$\hat{i}_z^* = a_{31} \hat{i}_x + a_{32} \hat{i}_y + a_{33} \hat{i}_z .$$

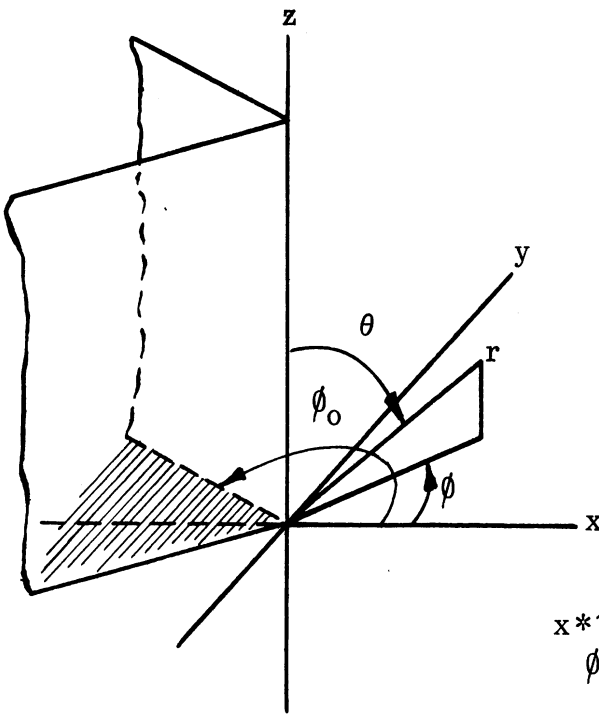


FIG. A-7:
WEDGE COORDINATE SYSTEM

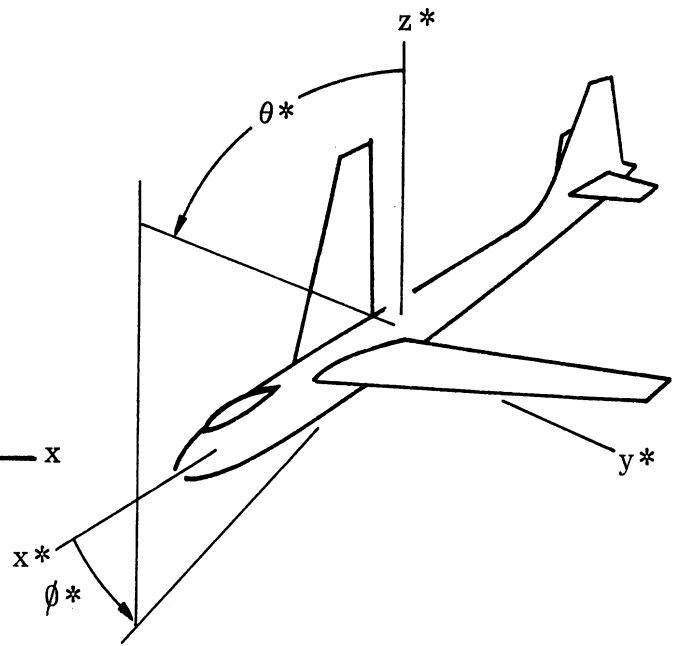


FIG. A-8:
AIRCRAFT COORDINATE SYSTEM

Let the unit vector \hat{i}_z in the direction of the edge of the wedge be given by

$$\begin{aligned}\hat{i}_z &= \sin \alpha \cos \beta \hat{i}_x^* + \sin \alpha \sin \beta \hat{i}_y^* + \cos \alpha \hat{i}_z^* \\ &= a_{13} \hat{i}_x^* + a_{23} \hat{i}_y^* + a_{33} \hat{i}_z^* .\end{aligned}\quad (5.8.2)$$

If the direction \hat{v} of incidence is expressed by

$$\hat{v} = \sin \theta^* \cos \phi^* \hat{i}_x^* + \sin \theta^* \sin \phi^* \hat{i}_y^* + \cos \theta^* \hat{i}_z^* , \quad (5.8.3)$$

then for some specified aspect θ^* , the azimuth ϕ_{\perp}^* for which incidence is perpendicular to the edge of the wedge ($\hat{i}_z \cdot \hat{v} = 0$) is

$$\cos (\phi_{\perp}^* - \beta) = -\cot \theta^* \cot \alpha , \quad (5.8.4)$$

where $\alpha = \arccos a_{33}$ and $\beta = \arctan a_{23}/a_{13}$.

The angle $\phi = \gamma$ for which incidence is perpendicular to the edge of the wedge is given by

$$\tan \gamma = \frac{a_{12} \sin \theta^* \cos \phi_{\perp}^* + a_{22} \sin \theta^* \sin \phi_{\perp}^* + a_{32} \cos \theta^*}{a_{11} \sin \theta^* \cos \phi_{\perp}^* + a_{21} \sin \theta^* \sin \phi_{\perp}^* + a_{31} \cos \theta^*} . \quad (5.8.5)$$

For incidence slightly out of the normal plane, say by an amount δu , the cross section will drop off approximately $\lambda^2/8\pi^2 L^2 (\delta u)^2$ (Cf. Ref. A-1, p. 129), that is

$$\frac{\sigma_{\text{non-normal}}}{\sigma_{\text{normal}}} = g^2 \cong \frac{\lambda^2}{8\pi^2 L^2 (\delta u)^2} . \quad (5.8.6)$$

Thus it is possible to find δu for which σ_{normal}^* drops off by a given amount ;

it is, from equation (5.8.6),

$$\delta u \cong \frac{\lambda}{2 \sqrt{2\pi} L g} . \quad (5.8.7)$$

* The amounts used for the computations later are $g^2 = 1/2, 1/10, 1/100$.

It is now necessary to find the change in azimuth angle $\delta\phi^*$ for which σ_{normal} drops off by the fraction g^2 ; that is, find $\delta\phi^*$ in terms of δu .

From

$$\sin \delta u = a_{13} \sin\theta^* \cos(\phi_{\perp}^* + \delta\phi^*) + a_{23} \sin\theta^* \sin(\phi_{\perp}^* + \delta\phi^*) + a_{33} \cos\theta^* , \quad (5.8.8)$$

it follows that

$$\begin{aligned} \delta u &\cong a_{13} \sin\theta^* \cos\phi_{\perp}^* \left(1 - \frac{\delta\phi^{*2}}{2}\right) - a_{13} \sin\theta^* \sin\phi_{\perp}^* \delta\phi^* \\ &\quad + a_{23} \sin\theta^* \sin\phi_{\perp}^* \left(1 - \frac{\delta\phi^{*2}}{2}\right) + a_{23} \sin\theta^* \cos\phi_{\perp}^* \delta\phi^* + a_{33} \cos\theta^* \\ &\cong a_{33} \cos\theta^* \frac{\delta\phi^{*2}}{2} + \delta\phi^* \left[-a_{13} \sin\theta^* \sin\phi_{\perp}^* + a_{23} \sin\theta^* \cos\phi_{\perp}^* \right] \end{aligned}$$

$$\delta u \cong a_{33} \cos\theta^* \frac{\delta\phi^{*2}}{2} + \delta\phi^* \sqrt{\sin^2\theta^* - a_{33}^2} . \quad (5.8.9)$$

Solving equation (5.8.9) for $\delta\phi^*$ yields

$$\delta\phi^* \cong \frac{-\sqrt{\sin^2\theta^* - a_{33}^2} + \sqrt{\sin^2\theta^* - a_{33}^2 + 2a_{33} \cos\theta^* (\delta u)}}{a_{33} \cos\theta^*} , \quad (5.8.10)$$

and if $\sin^2\theta^* - a_{33}^2 \gg 2a_{33} \cos\theta^* (\delta u)$, equation (5.8.10) gives

$$\delta\phi^* \cong \frac{\delta u}{\sqrt{\sin^2\theta^* - a_{33}^2}} . \quad (5.8.11)$$

5.9 Wedge S-Matrices in the Airplane Coordinate System

Let the designation of axes be as given in Section 5.8 and the direction of incidence of energy on the airplane be as given by equation (5.8.3). Horizontal polarization is taken to be polarization parallel to the ground; i. e., in the x^*y^* -plane of the airplane coordinate system:

$$\hat{p}(H) = -\hat{i}_x^* \sin\phi^* + \hat{i}_y^* \cos\phi^* . \quad (5.9.1)$$

Vertical polarization is perpendicular to horizontal polarization; hence

$$\hat{p}(V) = \hat{v} \times \hat{p}(H) = -\cos\theta^* \cos\phi^* \hat{i}_x^* - \cos\theta^* \sin\phi^* \hat{i}_y^* + \sin\theta^* \hat{i}_z^* . \quad (5.9.2)$$

The polarization directions $\hat{p}(a)$ and $\hat{p}(b)$ of Section 5.5 may be written in the airplane system as

$$\hat{p}(b) = \sin\alpha \cos\beta \hat{i}_x^* + \sin\alpha \sin\beta \hat{i}_y^* + \cos\alpha \hat{i}_z^* \left[= \hat{i}_z^* = a_{13} \hat{i}_x^* + a_{23} \hat{i}_y^* + a_{33} \hat{i}_z^* \right], \quad (5.9.3)$$

$$\begin{aligned} \hat{p}(a) = \hat{v} \times \hat{p}(b) &= (\sin\theta^* \sin\phi^* \cos\alpha - \cos\theta^* \sin\alpha \sin\beta) \hat{i}_x^* \\ &+ (\cos\theta^* \sin\alpha \cos\beta - \sin\theta^* \cos\phi^* \cos\alpha) \hat{i}_y^* \\ &+ (\sin\theta^* \cos\phi^* \sin\alpha \sin\beta - \sin\theta^* \sin\phi^* \sin\alpha \cos\beta) \hat{i}_z^* . \end{aligned} \quad (5.9.4)$$

The matrix

$$U = \begin{pmatrix} u(Ha) & u(Hb) \\ u(Va) & u(Vb) \end{pmatrix}$$

can now be given explicitly as

$$U = \begin{pmatrix} -\sin\theta^* \cos\alpha + \cos\theta^* \sin\alpha \cos(\phi^* - \beta) & -\sin\alpha \sin(\phi^* - \beta) \\ -\sin\alpha \sin(\phi^* - \beta) & \sin\theta^* \cos\alpha - \cos\theta^* \sin\alpha \cos(\phi^* - \beta) \end{pmatrix}, \quad (5.9.5)$$

where the elements $u(IJ)$ of the matrix are determined from the previously given relation $u(IJ) = p(I) \cdot p^*(J)$. Since the direction of incidence is to be

perpendicular to the edge of the wedge; i. e., \hat{v} is perpendicular to $\hat{p}(b)$, the angle ϕ_{\perp}^* for which such perpendicularity occurs (for fixed θ^* , α , β) is given by equation (5.8.4)

$$\cos(\phi_{\perp}^* - \beta) = -\cot \theta^* \cot \alpha . \quad (5.8.4)$$

For each such angle ϕ_{\perp}^* , U reduces to

$$U = \begin{pmatrix} -\cos \alpha \csc \theta^* & -\sin \alpha \sin(\phi_{\perp}^* - \beta) \\ -\sin \alpha \sin(\phi_{\perp}^* - \beta) & \cos \alpha \csc \theta^* \end{pmatrix} . \quad (5.9.6)$$

From equation (5.4.2) the S-matrix S(ab; ab) can be read off as

$$S(ab; ab) = \frac{L e^{ikr}}{4r\phi_0} \sin \frac{\pi^2}{2\phi_0} \begin{bmatrix} \left(\frac{1}{C} - \frac{1}{D}\right) & 0 \\ 0 & -\left(\frac{1}{C} + \frac{1}{D}\right) \end{bmatrix} . \quad (5.9.7)$$

Using equation (5.9.7) in conjunction with equations (5.9.5) and (1.2.10), the matrix S(HV; HV) = U S(ab; ab) U¹ in the airplane coordinate system for any wedge component of the airplane is

$$S(HV; HV) = \frac{1}{2} \left(\frac{M}{\pi}\right)^{1/2} \frac{e^{ikr}}{r} \begin{bmatrix} \frac{2\cos^2 \alpha}{C \sin^2 \theta^*} - \left(\frac{1}{C} + \frac{1}{D}\right) & \frac{\sin \alpha \cos \alpha \sin(\phi^* - \beta)}{C \sin \theta^*} \\ \frac{\sin \alpha \cos \alpha \sin(\phi^* - \beta)}{C \sin \theta^*} & \left(\frac{1}{C} - \frac{1}{D}\right) - \frac{2\cos^2 \alpha}{C \sin^2 \theta^*} \end{bmatrix} , \quad (5.9.8)$$

where M, C, D are given by equation (5.7.1).

CROSS-POLARIZATION CROSS SECTIONS OF WIRE LOOPS

In addition to those sharp edges on an aircraft which must be represented by wedges there are, particularly for jet aircraft, sharp edges of a circular or loop shape. Such circular sharp edges are represented by wire loops which are discussed in this section.

6.1 General Theory

As pointed out in Section A.2.10 of Reference A-1, the scattered field from a small straight piece of thin wire is similar to the field of a dipole. It is of the form

$$\vec{E}^s = K \frac{\hat{r} \times (\hat{r} \times \hat{d})}{r} e^{ikr} d\ell, \quad (6.1.1)$$

where $d\ell$ is the length of the wire, \hat{r} is the unit vector to the field point, r is the distance to the field point, and \hat{d} is a unit vector along the wire. K is a proportionality factor given by,

$$K = K_1 (\hat{p}^i \cdot \hat{d}), \quad (6.1.2)$$

where \hat{p}^i is a unit vector giving the direction of polarization of the incident electric field and K_1 is a constant to be determined.

From the definition of cross section given by equation (1.2.6) the cross section of a small straight piece of thin wire is

$$\sigma = 4\pi r^2 \frac{K_1^2 (\hat{p}^i \cdot \hat{d})^2}{|\vec{E}^i|^2} \frac{(\hat{p}^r \cdot \hat{d})^2}{r^2} (d\ell)^2, \quad (6.1.3)$$

where superscripts i and r denote transmitter and receiver polarizations respectively. If \hat{p} (for both i and r) is parallel to the wire, $(\hat{p} \cdot \hat{d}) = 1$; for this case ($\phi_0 = \pi$, $\gamma = 0$) equation (5.5.3) gives for the cross section

$$\sigma = \frac{(d\ell)^2}{\pi} , \quad (6.1.4)$$

where, in equation (5.5.3), L has been replaced by $d\ell$. Comparison of equations (6.1.3) and (6.1.4) for this case (i.e., \hat{p} parallel to wire) yields:

$$K_1 = \frac{|\vec{E}^i|}{2\pi} .$$

Hence the field equation (6.1.1) may be written as

$$\frac{\vec{E}^s}{d\ell} = \frac{|\vec{E}^i|}{2\pi} (\hat{p}^i \cdot \hat{d}) \cdot \frac{\hat{r} \times (\hat{r} \times \hat{d})}{r} \cdot e^{2ikr} d\ell . \quad (6.1.5)^*$$

To find the scattered field for a wire loop, an integration is made over the loop:

$$\vec{E}^s = \frac{|\vec{E}^i|}{2\pi} \int_{\text{loop}} (\hat{p}^i \cdot \hat{d}) \frac{\hat{r} \times (\hat{r} \times \hat{d})}{r} e^{2ikr} d\ell .$$

The effective cross section of a wire loop is then, since $\hat{p} \cdot \hat{r} = 0$,

$$\sigma = 4\pi r^2 \left| \frac{\vec{E}^s \cdot \hat{p}^r}{E^i} \right|^2 = \frac{1}{\pi} \left| \int_{\text{loop}} (\hat{p}^i \cdot \hat{d}) (\hat{p}^r \cdot \hat{d}) e^{2ik\rho} d\ell \right|^2 , \quad (6.1.6)$$

where ρ is the distance measured in the direction of incidence.

* To take into account the phase lag in making the round trip from radar to wire and back, equation (6.1.1) has been multiplied by e^{ikr} to obtain equation (6.1.5).

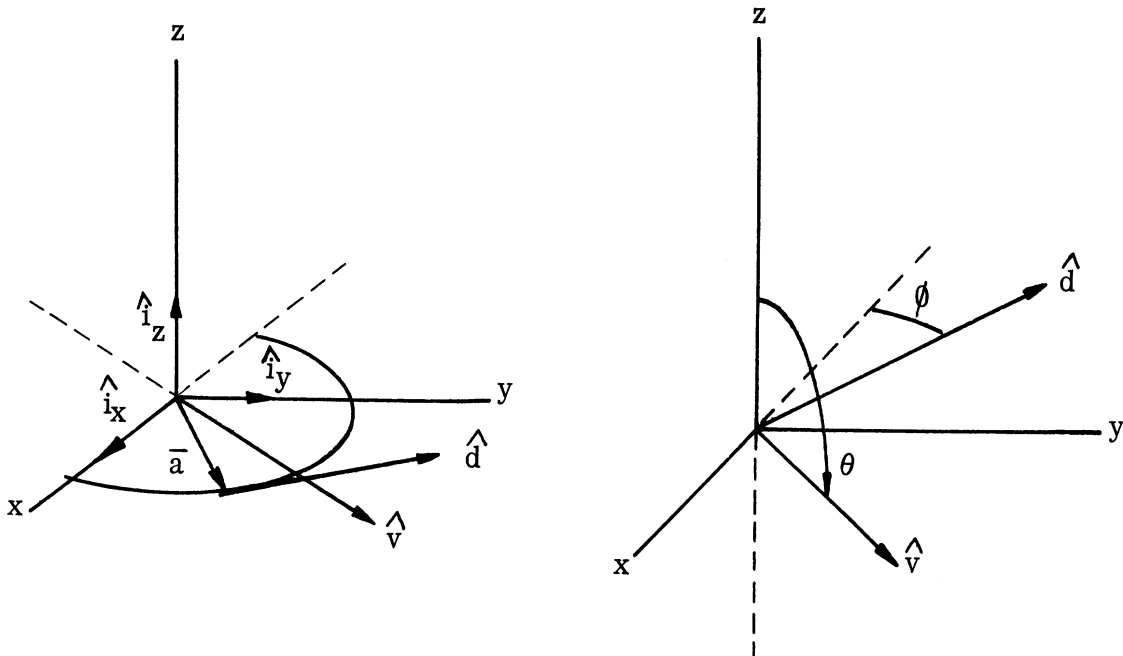
Consider a loop of radius a in the xy -plane with center at the origin

Figure A-9. On the wire $x = a \cos\phi$, $y = a \sin\phi$; thus $d\mathcal{L} = a d\phi$; and the direction of the dipole is $\hat{d} = -\hat{i}_x \sin\phi + \hat{i}_y \cos\phi$. Let the direction of incidence be in the xz -plane and be given by $\hat{v} = \hat{i}_x \sin\theta - \hat{i}_z \cos\theta$; this makes $\rho = (x\hat{i}_x + y\hat{i}_y) \cdot \hat{v} = a \sin\theta \cos\phi$.

Let two perpendicular directions of polarization be given by:

$$\hat{p}(A) = \hat{i}_x \cos\theta \sin\gamma + \hat{i}_y \cos\gamma + \hat{i}_z \sin\theta \sin\gamma, \quad (6.1.7)$$

$$\hat{p}(B) = \hat{i}_x \cos\theta \cos\gamma - \hat{i}_y \sin\gamma + \hat{i}_z \sin\theta \cos\gamma, \quad (6.1.8)$$



a = radius of loop

\hat{d} = direction of dipole

\hat{v} = direction of propagation of incident plane wave

$$\hat{d} = -\hat{i}_x \sin\phi + \hat{i}_y \cos\phi$$

$$\hat{v} = -\hat{i}_x \sin\theta + \hat{i}_z \cos\theta$$

$$\bar{a} = a (\hat{i}_x \cos\phi + \hat{i}_y \sin\phi)$$

FIG. A-9: COORDINATE SYSTEMS FOR A WIRE LOOP

where γ is the angle between the polarization vector and the y-axis. Right- and left-circular polarization directions can then be given respectively by:

$$\hat{p}(R) = \frac{1}{\sqrt{2}} e^{-i\gamma} \left[\hat{i}_x(i \cos\theta) + \hat{i}_y + \hat{i}_z(i \sin\theta) \right], \quad (6.1.9)$$

$$\hat{p}(L) = \frac{1}{\sqrt{2}} e^{i\gamma} \left[-\hat{i}_x(i \cos\theta) + \hat{i}_y - \hat{i}_z(i \sin\theta) \right]. \quad (6.1.10)$$

6.2 Cross Section Formulas

Formulas for the following effective cross sections have been determined: $\sigma(AA)$, $\sigma(BB)$, $\sigma(AB)$, $\sigma(AR)$, $\sigma(BR)$, and $\sigma(RR)$; in $\sigma(IJ)$, I and J denote receiver and transmitter polarization respectively. For example, using equations (6.1.6) and (6.1.7), $\sigma(AA)$ is given by:

$$\begin{aligned} \sigma(AA) &= \frac{a^2}{\pi} \left| \int_0^{2\pi} (\cos\phi \cos\gamma - \sin\phi \sin\gamma \cos\theta)^2 e^{2ika \sin\theta \cos\phi} d\phi \right|^2 \\ &= \pi a^2 \left| (\sin^2\gamma \cos^2\theta + \cos^2\gamma) J_0(2ka \sin\theta) \right. \\ &\quad \left. + (\sin^2\gamma \cos^2\theta - \cos^2\gamma) J_2(2ka \sin\theta) \right|^2, \end{aligned} \quad (6.2.1)$$

where J_n is the Bessel function of order n.

In a similar fashion the remaining formulas are found to be

$$\begin{aligned} \sigma(BB) &= \pi a^2 \left| (\cos^2\theta \cos^2\gamma - \sin^2\gamma) J_2(2ka \sin\theta) \right. \\ &\quad \left. + (\cos^2\theta \cos^2\gamma + \sin^2\gamma) J_0(2ka \sin\theta) \right|^2, \end{aligned} \quad (6.2.2)$$

$$\sigma(AB) = \pi a^2 \sin^2\gamma \cos^2\gamma \left| (1 + \cos^2\theta) J_2(2ka \sin\theta) - \sin^2\theta J_0(2ka \sin\theta) \right|^2, \quad (6.2.3)$$

$$\begin{aligned} \sigma(\text{AR}) = & \frac{\pi a^2}{2} \left| (i \cos^2 \theta \sin \gamma - \cos \gamma) J_2(2ka \sin \theta) \right. \\ & \left. + (i \cos^2 \theta \sin \gamma + \cos \gamma) J_0(2ka \sin \theta) \right|^2, \end{aligned} \quad (6.2.4)$$

$$\begin{aligned} \sigma(\text{BR}) = & \frac{\pi a^2}{2} \left| (i \cos^2 \theta \cos \gamma + \sin \gamma) J_2(2ka \sin \theta) \right. \\ & \left. + (i \cos^2 \theta \cos \gamma - \sin \gamma) J_0(2ka \sin \theta) \right|^2, \end{aligned} \quad (6.2.5)$$

$$\sigma(\text{RR}) = \frac{\pi a^2}{4} \left| (-\cos^2 \theta - 1) J_2(2ka \sin \theta) + (-\cos^2 \theta + 1) J_0(2ka \sin \theta) \right|^2. \quad (6.2.6)$$

DIHEDRAL SCATTERING

7.1 Wing-Body Dihedral Scattering in the Dihedral Coordinate System

Let the surfaces representing the wing and body be such that for each surface one of the two principal radii of curvature is infinite and the other is neither infinite nor zero. The scattered field is computed in this section for the dihedral formed by the wing and body by Fock's formulation of geometric optics (Ref. A-17).

Consider the conditions on a ray which is reflected back to the point whence it came: Let \hat{k} be the initial direction of the ray and let \hat{n}_w and \hat{n}_b be the normals of the wing and body, respectively, at the points where the ray hits them. Suppose the ray hits the wing first. After hitting the wing the ray is traveling in a direction

$$\hat{k} - 2(\hat{k} \cdot \hat{n}_w) \hat{n}_w ; \quad (7.1.1)$$

after hitting the body the ray will be traveling in a direction

$$\hat{k} - 2(\hat{k} \cdot \hat{n}_w) \hat{n}_w - 2 \left\{ \left[\hat{k} - 2(\hat{k} \cdot \hat{n}_w) \hat{n}_w \right] \cdot \hat{n}_b \right\} \hat{n}_b = -\hat{k} . \quad (7.1.2)$$

The equality is required in order that the ray be reflected back to the source.

Since equation (7.1.2) may be rewritten as:

$$\hat{k} + 2(\hat{k} \cdot \hat{n}_w) (\hat{n}_w \cdot \hat{n}_b) \hat{n}_b = (\hat{k} \cdot \hat{n}_w) \hat{n}_w + (\hat{k} \cdot \hat{n}_b) \hat{n}_b , \quad (7.1.3)$$

it is apparent that \hat{k} is a linear combination of \hat{n}_w and \hat{n}_b , and thus lies in the plane of these two vectors. Further, the scalar product of equation (7.1.3) with \hat{n}_w and \hat{n}_b respectively yields:

$$\begin{aligned}
(\hat{n}_w \cdot \hat{n}_b) \left[2(\hat{k} \cdot \hat{n}_w)(\hat{n}_w \cdot \hat{n}_b) - (\hat{k} \cdot \hat{n}_b) \right] &= 0 \quad , \\
(\hat{k} \cdot \hat{n}_w)(\hat{n}_w \cdot \hat{n}_b) &= 0 \quad .
\end{aligned}
\tag{7.1.4}$$

Thus, $\hat{n}_w \cdot \hat{n}_b = 0$. The same conclusions would have been reached if the ray had hit the body first.

The above results allow a coordinate system to be chosen such that $\hat{n}_w = \hat{i}_z$ and $\hat{n}_b = \hat{i}_x$ (Fig. A-10). The ray is reflected from the xy-plane at $x = R' \sin\theta$, and from the yz-plane at $z = R' \cos\theta$, where R' is the distance between the two points from which the ray is reflected.

Since the geometric optics field depends only on local properties of the scatterer, the wing and body surfaces may be replaced by parabolic cylinders having the same radii of curvature. These are, for the wing and body, respectively,

$$\begin{aligned}
z &= - \frac{(y \cos\beta - x \sin\beta + R' \sin\theta \sin\beta)^2}{2R_w} \quad , \\
x &= - \frac{(z \cos\alpha - y \sin\alpha - R' \cos\theta \cos\alpha)^2}{2R_b} \quad ,
\end{aligned}
\tag{7.1.5}$$

where R_w and R_b are the radii of curvature of the wing and the body.

Fock's formulation of geometric optics will be used. Since the pertinent formulas are given in Section 3.1 of Reference A-17, the detail involved to obtain reflected fields will be omitted.

Consider the case shown in Figure A-10 where the ray hits the wing before it hits the body. (The reverse case can then be obtained from the symmetries of the problem.) If the incident electric field is taken to be

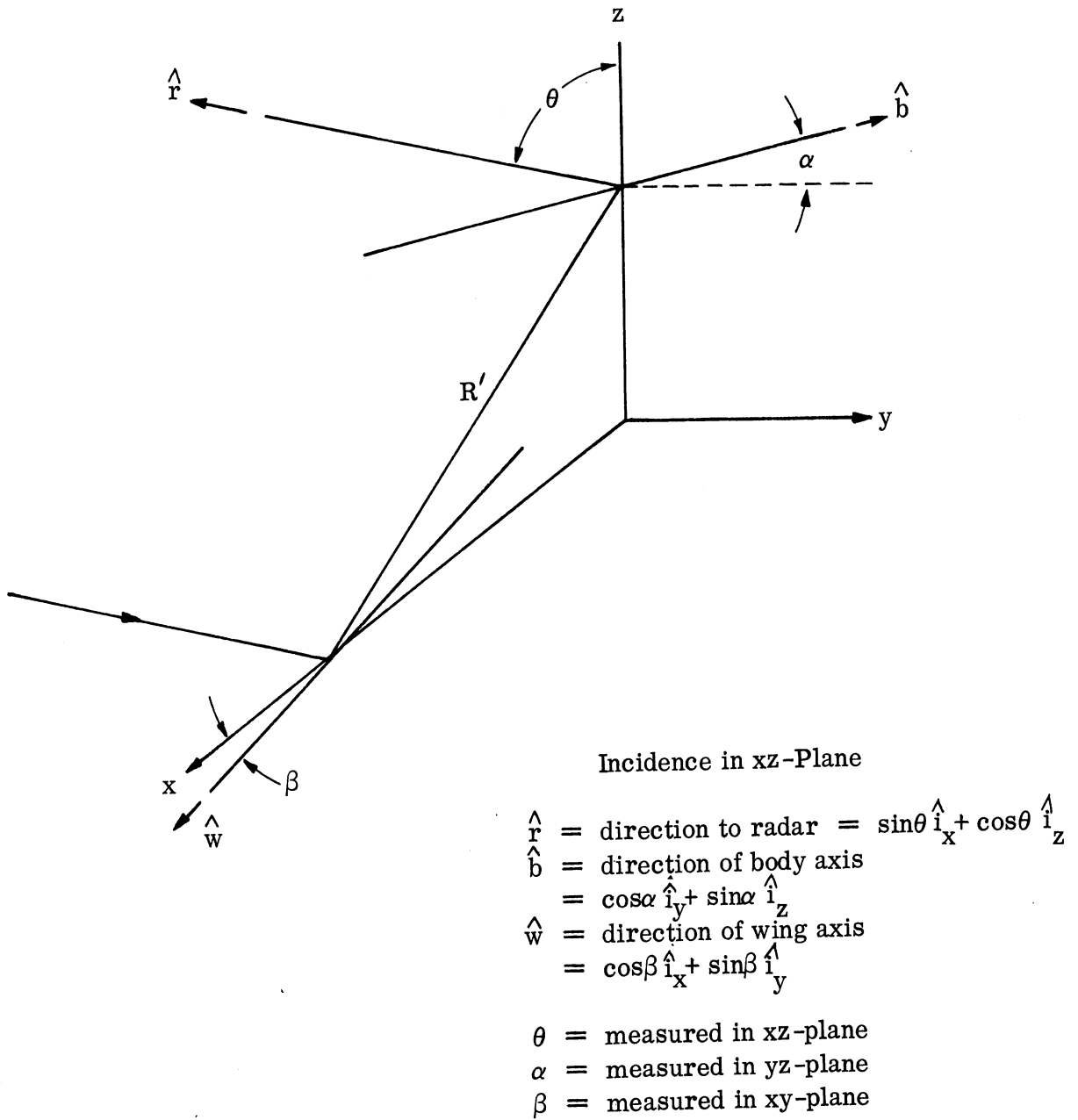


FIG. A-10: COORDINATE SYSTEM FOR WING-BODY DIHEDRAL

$$\vec{E}_i = \left[\hat{i}_y \cos \gamma + (-\hat{i}_x \cos \theta + \hat{i}_z \sin \theta) \sin \gamma \right] e^{-ik(x \sin \theta + z \cos \theta)}, \quad (7.1.6)$$

the field reflected from the wing at the reflection point on the body is

(following the procedure of the above-mentioned reference),

$$\vec{E} = (\sin \gamma \cos \theta \hat{i}_x - \cos \gamma \hat{i}_y + \sin \gamma \sin \theta \hat{i}_z) \frac{e^{ikR' \cos^2 \theta}}{\sqrt{1 + 2 \frac{R'}{R_w} \frac{1 - \sin^2 \theta \cos^2 \beta}{\cos \theta}}}. \quad (7.1.7)$$

After reflection from the body the scattered field for large R_0 is

$$\vec{E}_s = \frac{\sqrt{R_w R_b \sin \theta \cos \theta} (\sin \gamma \cos \theta \hat{i}_x + \cos \gamma \hat{i}_y - \sin \gamma \sin \theta \hat{i}_z)}{2 R_0 |\cos \alpha \cos \beta \cos \theta - \sin \alpha \sin \beta \sin \theta|} e^{ik(R' \cos^2 \theta + R_0)},$$

where R_0 is the distance from the reflector to the radar. Thus the scattered

field of wing-to-body plus body-to-wing is

$$\vec{E}_s = \frac{\sqrt{R_w R_b \sin \theta \cos \theta} (\sin \gamma \cos \theta \hat{i}_x + \cos \gamma \hat{i}_y - \sin \gamma \sin \theta \hat{i}_z) e^{ik(R' \cos^2 \theta + R_0)}}{R_0 |\cos \alpha \cos \beta \cos \theta - \sin \alpha \sin \beta \sin \theta|}. \quad (7.1.1)$$

If the polarization basis vectors are taken to be

$$\begin{aligned} \hat{p}(A) &= \hat{i}_y, \\ \hat{p}(B) &= -\cos \theta \hat{i}_x + \sin \theta \hat{i}_z, \end{aligned} \quad (7.1.9)$$

then the scattering matrix $S(AB; AB)$ is given by:

$$S(AB; AB) = \frac{Q e^{i\mu}}{R_0} \begin{pmatrix} 1 & 0 \\ 0 & -1 \end{pmatrix}, \quad (7.1.10)$$

where

$$Q = \frac{\sqrt{R_w R_b \sin\theta \cos\theta}}{|\cos\alpha \cos\beta \cos\theta - \sin\alpha \sin\beta \sin\theta|} ,$$

and μ is a phase factor which is unimportant for the calculation of cross sections.

The form of equation (7.1.10) indicates that the incident wave has been re-polarized (Sec. 4) by the wing-body dihedral.

7.2 Transformation to the Aircraft Coordinate System

In Figure A-10 let \hat{r} be the direction to the radar, \hat{b} be the direction of the body axis, and \hat{w} be the direction of the wing axis. The direction of incidence is taken to be in the xz-plane so that θ is measured in the xz-plane; α and β are measured in the yz- and xy-planes, respectively.

Put

$$\begin{aligned} \hat{w} &= \cos\beta \hat{i}_x + \sin\beta \hat{i}_y , \\ \hat{b} &= \cos\alpha \hat{i}_y + \sin\alpha \hat{i}_z , \\ \hat{r} &= \sin\theta \hat{i}_x + \cos\theta \hat{i}_z . \end{aligned} \quad (7.2.1)$$

As before, asterisks are used to denote the aircraft coordinate system.

The tie-up between the two coordinate systems is made through \hat{r} , \hat{b} , and \hat{w} which can be expressed in both coordinate systems. In the aircraft coordinate system \hat{b} and \hat{w} are constant vectors for a given aircraft while

$$\hat{r} = \sin\theta * \cos\phi * \hat{i}_x * + \sin\theta * \sin\phi * \hat{i}_y * + \cos\theta * \hat{i}_z * . \quad (7.2.2)$$

The expressions of equation (7.2.1) for \hat{w} , \hat{b} , and \hat{r} can be inverted to give

$$\begin{aligned}
\hat{i}_x &= \frac{\cos\alpha \cos\theta \hat{w} - \sin\beta \cos\theta \hat{b} + \sin\alpha \sin\beta \hat{r}}{\hat{w} \cdot \hat{b} \times \hat{r}} \\
\hat{i}_y &= \frac{\sin\alpha \sin\theta \hat{w} + \cos\beta \cos\theta \hat{b} - \sin\alpha \cos\beta \hat{r}}{\hat{w} \cdot \hat{b} \times \hat{r}} \\
\hat{i}_z &= \frac{-\sin\theta \cos\alpha \hat{w} + \sin\beta \sin\theta \hat{b} + \cos\alpha \cos\beta \hat{r}}{\hat{w} \cdot \hat{b} \times \hat{r}}
\end{aligned} \tag{7.2.3}$$

where $\cos\alpha \cos\beta \cos\theta + \sin\alpha \sin\beta \sin\theta$ has been replaced by $\hat{w} \cdot \hat{b} \times \hat{r}$. If the expressions for \hat{w} , \hat{b} , and \hat{r} in terms of \hat{i}_x^* , \hat{i}_y^* , \hat{i}_z^* are substituted into equation (7.2.3), the vectors \hat{i}_x , \hat{i}_y , and \hat{i}_z will be given in terms of \hat{i}_x^* , \hat{i}_y^* , and \hat{i}_z^* except that α , β , and θ are unknown. These angles can be determined from

$$\begin{aligned}
\hat{w} \cdot \hat{b} &= \sin\beta \cos\alpha = s, \\
\hat{b} \cdot \hat{r} &= \sin\alpha \cos\theta = t, \\
\hat{r} \cdot \hat{w} &= \sin\theta \cos\beta = u;
\end{aligned} \tag{7.2.4}$$

they are

$$\begin{aligned}
\cos 2\alpha &= \frac{s^2 - t^2 + D}{1 - u^2}, \\
\cos 2\beta &= \frac{u^2 - s^2 + D}{1 - t^2}, \\
\cos 2\gamma &= \frac{t^2 - u^2 + D}{1 - s^2}.
\end{aligned} \tag{7.2.5}$$

where $D^2 = (1 - s^2 - t^2 - u^2)^2 - (2stu)^2$. The sign of D must be chosen so as to obtain the correct physical setup of the wing-body combination. α , β , and θ are used not only in the expressions for \hat{i}_x , \hat{i}_y , and \hat{i}_z , but also in the expression for Q .

The transformation from the scattering matrix for the AB basis to that for the HV basis is accomplished by

$$S(HV; HV) = U(HV; AB) S(AB; AB) U'(HV; AB) , \quad (7.2.6)$$

where

$$U(HV; AB) = \begin{pmatrix} \hat{p}(H) \cdot \hat{p}(A) & \hat{p}(H) \cdot \hat{p}(B) \\ \hat{p}(V) \cdot \hat{p}(A) & \hat{p}(V) \cdot \hat{p}(B) \end{pmatrix} , \quad (7.2.7)$$

since $\hat{p}(A)$ and $\hat{p}(B)$ are real. Here,

$$\begin{aligned} \hat{p}(H) &= -\sin\phi * \hat{i}_x^* + \cos\phi * \hat{i}_y^* , \\ \hat{p}(V) &= -\cos\theta * \cos\phi * \hat{i}_x^* - \cos\theta * \sin\phi * \hat{i}_y^* + \sin\theta * \hat{i}_z^* . \end{aligned} \quad (7.2.8)$$

The only unknowns remaining in the determination of $S(HV; HV)$ are R_w and R_b . From Figure A-10 the normals to the wing and body at the reflection point are:

$$\begin{aligned} \hat{n}_w &= \hat{i}_z , \\ \hat{n}_b &= \hat{i}_x , \end{aligned}$$

which are known in terms of \hat{i}_x^* , \hat{i}_y^* , and \hat{i}_z^* . From the direction of the normal at the reflection point the radius of curvature can be determined from the formula

$$\text{radius of curvature} = \frac{a^2 b^2}{[(a \hat{n} \cdot \hat{M})^2 + (b \hat{n} \cdot \hat{m})^2]^{3/2}} , \quad (7.2.9)$$

where a and b are the semi-major and semi-minor ellipse axes and \hat{M} and \hat{m} are unit vectors along these axes, respectively.

CROSS-POLARIZATION CROSS SECTIONS FOR CYLINDERS

In this section the limitations on the use of the physical optics current distribution method are considered. That such limitations exist is evident from the fact that there is no repolarization of incident radiation in monostatic single reflection situations according to physical optics. However, this is not an essential limitation in computing the cross sections for various aircraft components.

For example, consider the scattering from the wing-fuselage combination illustrated in Figure A-11.

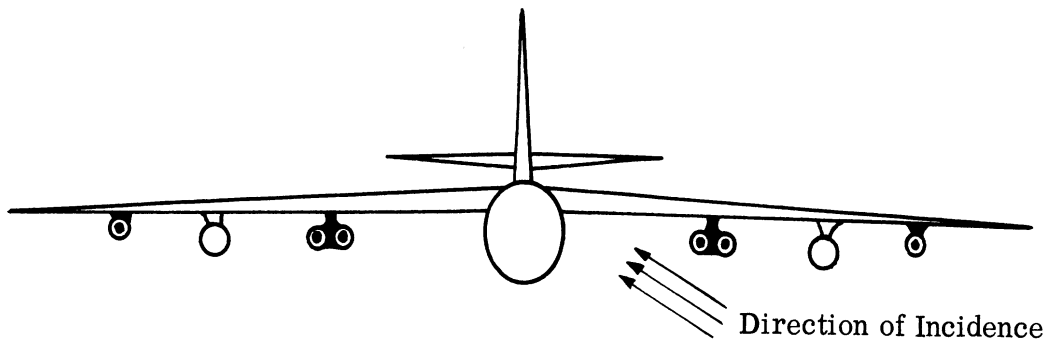


FIG. A-11: WING-BODY DIHEDRAL

For broadside aspects the wing-fuselage combination was treated as a dihedral which gives rise to double scattering (Sec. 7). Moreover, the single-scattering contributions, principally from the fuselage, have been included.

In the case of circularly polarized radiation, an analysis in terms of the characteristic dimensions of the wing and fuselage for the aspects considered indicates that for double scattering the dominant components will be $\sigma(\text{RR})$ and $\sigma(\text{LL})$, while for single scattering the dominant components are $\sigma(\text{RL})$ and $\sigma(\text{LR})$. That is, the characteristic dimensions are such as to insure the validity of the physical optics approximation. It is then possible to set up the following rule of thumb for the application of the physical optics approximation in determining the scattering properties of a target for circularly polarized radiation:

1. The double-scattering contribution to $\sigma(\text{RR})$ must be much greater than that of single scattering to $\sigma(\text{RR})$; i. e., the repolarization effect of the single scattering is small with respect to the double scattering.
2. The single-scattering contribution to $\sigma(\text{RL})$ must be much greater than that of double scattering to $\sigma(\text{RL})$.

On the other hand, viewing, for example, the leading edge of the wing there may be a measurable contribution to $\sigma(\text{RR})$ arising principally from a single-scattering repolarization effect. Although in this case the physical optics approximation may give a sufficiently accurate measure of $\sigma(\text{HH})$ and $\sigma(\text{VV})$, it can give no indication of the contribution to $\sigma(\text{RR})$. To take into account such cases the polarization-dependent current-distribution method of V. A. Fock

(Ref. A-9) is introduced. It is, in effect, a modification of the physical optics method and can best be illustrated by a comparison with physical optics.

In the physical optics approximation, the tangential component of the magnetic field on the surface is taken to be twice the tangential component of the incident field on the illuminated side and zero on the shadow side of the scatterers. Thus, the tangential component of the incident magnetic field can be written:

$$H_t = H_t^0 G(\xi) , \quad (8.1)$$

where $G(\xi)$ is a function of a certain reduced distance from the shadow boundary; ξ is positive on the shadow side, negative on the illuminated side of the scatterer.

Hence, for the physical optics approximation

$$\begin{aligned} G(\xi) &= 2 \text{ for } \xi < 0 , \\ &= 0 \text{ for } \xi > 0 . \end{aligned} \quad (8.2)$$

By considering the local fields on the shadow boundary, Fock had obtained a continuous function $G(\xi)$ such that

$$\begin{aligned} G(\xi) &\xrightarrow{\xi \rightarrow +\infty} 0 , \\ G(\xi) &\xrightarrow{\xi \rightarrow -\infty} 2 . \end{aligned} \quad (8.3)$$

Fock's value for the field on the surface becomes the first approximation of the method of Franz and Depperman (Refs. A-12 and A-13) applied to the circular cylinder or sphere.

The details of Fock's method applied to the particular surface chosen to approximate the wing surface are given below.

Consider a finite cylinder whose cross section is made up of one-half an ellipse and one-half an ogive. Let the major and minor semi-axes of the ellipse be designated by a and b respectively. Let the ogive have radius of curvature $R_0 = a^2/b$, and a semi-minor axis b .

Attach the half ogive at the point of maximum radius of curvature of the ellipse; i.e., at the minor axis. The cross-section is then a smooth curve having an elliptic 'nose' and an ogival 'tail'. Let the length of the cylinder be L .

Under the assumption that plane radiation is incident at or near 'nose-on'; i.e., the direction of propagation \hat{k} is in the XY-plane making a small angle α with the negative X-axis, the cross section is computed using a current distribution method as follows:

After Fock (Ref. A-9) it is assumed that the characteristic dimensions of the cylinder are sufficiently large with respect to the wavelength of the incident radiation that the current on the surface is given by the geometrical optics current modified by a shape factor which is a universal function of a certain reduced distance from the shadow boundary. It is further assumed that the cylinder is of sufficient length L that edge effects may be neglected and that the same current distribution can be used along the entire length of the cylinder.

In general the magnetic field scattered from a finite perfectly conducting closed surface is given by the expression (Ref. A-1),

$$\vec{H}_s = \frac{1}{4\pi} \int_S (\hat{n} \times \vec{H}_t) \times \nabla \frac{e^{-ikR}}{R} dS, \quad (8.4)$$

where S is the surface of the cylinder, \hat{n} is the unit outward normal vector to S , R is the distance from the integration element on S to the field point, and \vec{H}_t is the tangential component of the total magnetic field on the surface. In particular, for the backscattered far field,

$$\vec{H}_s = \frac{ik}{4\pi r} \int_S \hat{k} \times (\hat{n} \times \vec{H}_t) e^{ikR} dS, \quad (8.5)$$

where r is the distance from the field point to the center of the scatterer and \hat{k} is a unit vector in the direction of propagation of the incident plane wave.

For the scatterer under consideration put the origin of coordinates on the upper shadow boundary midway between the ends of the cylinder. Let the X -axis be in the direction of the incoming radiation, the Z -axis perpendicular to the cylinder surface and the Y -axis in the direction of the cylinder axis (Fig. A-12).

First consider the case of incidence along the X -axis and the electric vector polarized perpendicular to the cylinder axis (Fig. A-13).

In this case

$$\vec{H}_t = (0, H_t, 0); \quad (8.6)$$

hence,

$$\hat{k} \times (\hat{n} \times \vec{H}_t) = (0, n_x H_t, 0), \text{ and} \quad (8.7)$$

$$e^{ikR} \cong e^{ikr} e^{i\vec{k} \cdot \vec{r}'} \quad (8.8)$$

where,

$$\vec{k} = \hat{k} k, \quad (8.9)$$

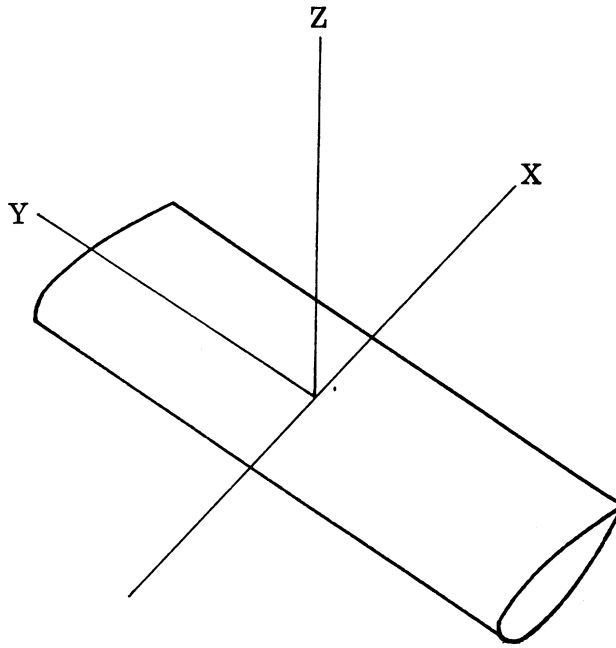


FIG. A-12: ORIENTATION OF COORDINATE AXES

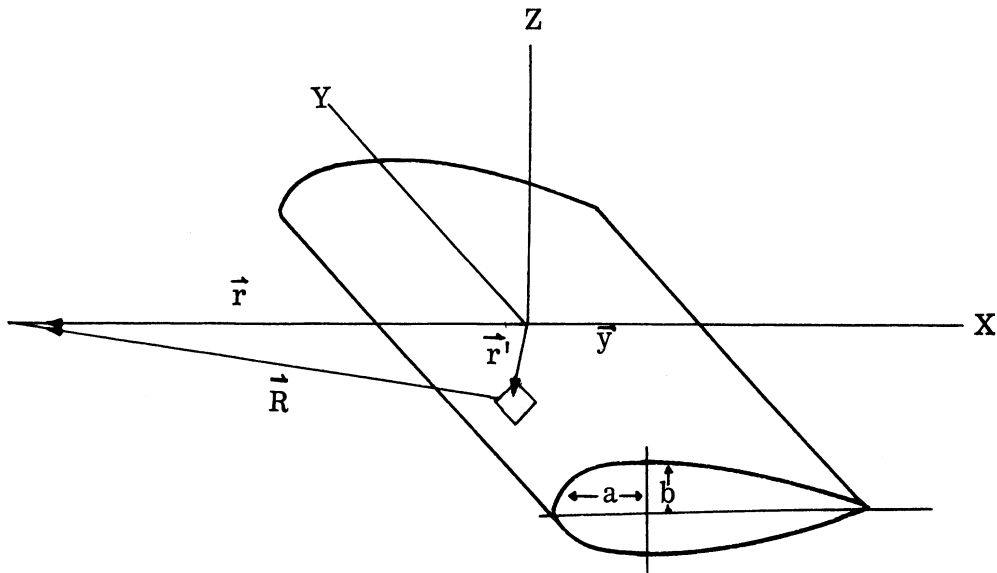


FIG. A-13: DEFINITION OF PARAMETERS

so that

$$H_s = \frac{ik}{4\pi} \frac{e^{ikr}}{r} \int_s n_x H_t e^{i\vec{k} \cdot \vec{r}'} dS . \quad (8.10)$$

After Fock (Ref. A-9), write

$$H_t = H_t^0 G(\xi) , \quad (8.11)$$

where $H_t^0 = e^{i\vec{k} \cdot \vec{R}}$. The function $G(\xi)$ is determined numerically and tabulated for $\xi = -4.5 (0.1) 4.5$ by Fock (Ref. A-9).

The integration over the y direction of the integral gives simply

$$H_s = \frac{ikL}{4\pi} \frac{e^{2ikr}}{r} \int n_x e^{2i\vec{k} \cdot \vec{r}'} G(\xi) d\ell , \quad (8.12)$$

where $d\ell$ is the element of path around the cross section of the cylinder. To facilitate the computation divide the integral into two parts, that over the ellipse, and that over the ogive. Let these parts be designated by I_e and I_o for the integration over the ellipse and ogive respectively. Because of the symmetry of the nose-on case, only the integral over 1/2 the cross section, from nose to tail need be calculated. Thus,

$$H_s = \frac{ikL}{4\pi} \frac{e^{2ikr}}{r} (2 I_e + 2 I_o) , \quad (8.13)$$

where

$$I_{e/o} = \int_{\ell_{e/o}} n_x e^{2i\vec{k} \cdot \vec{r}'} G(\xi) d\ell . \quad (8.14)$$

Now

$$n_x d\ell = -\frac{bx}{a^2} \frac{dx}{\sqrt{1 - \frac{x^2}{a^2}}} \text{ on } \ell_e, \text{ and} \quad (8.15)$$

$$\xi = \left(\frac{kb^2}{2a}\right)^{1/3} \frac{x}{a}; \quad (8.16)$$

hence,

$$I_e = \int_0^0 \frac{\xi d\xi}{\sqrt{1 - \left(\frac{2a}{kb^2}\right)^{2/3} \xi^2}} e^{i\left(\frac{4ka^2}{b}\right)^{2/3} \xi} G(\xi) \left(\frac{4a^2}{k^2 b}\right)^{1/3}, \quad (8.17)$$

while $n_x d\ell = \frac{a^2}{b} \cos\theta d\theta$ on ℓ_o and ξ is given above; hence

$$I_o = \left(4 \frac{a^2}{bk^2}\right)^{1/3} \int_0^{\left(\frac{ka^2}{2b}\right)^{1/3}} \frac{\xi d\xi}{\sqrt{1 - \left(\frac{2b}{ka^2}\right)^{2/3} \xi^2}} e^{i\left(\frac{4ka^2}{b}\right)^{2/3} \xi} G(\xi). \quad (8.18)$$

The cross section is then given by:

$$\begin{aligned} \sigma &= 4\pi \left(\frac{Lk}{2\pi}\right)^2 \left| I_e + I_o \right|^2, \\ &= \frac{k^2 L^2}{\pi} \left| I_e + I_o \right|^2. \end{aligned} \quad (8.19)$$

For incidence at some angle α to the X-axis, the same current distribution technique is applicable provided:

1. The radius of curvature, R_0 , at the shadow boundary remains sufficiently large,
2. The minimum distance from the shadow boundary to the "tail" is large enough for the shape factors to assume the asymptotic value, zero.

It is required that the radius of curvature at A be much larger than a wavelength and that the reduced distance from the shadow curve at B to the tail C be so great as to be in the asymptotic range of the function $G(\xi)$.

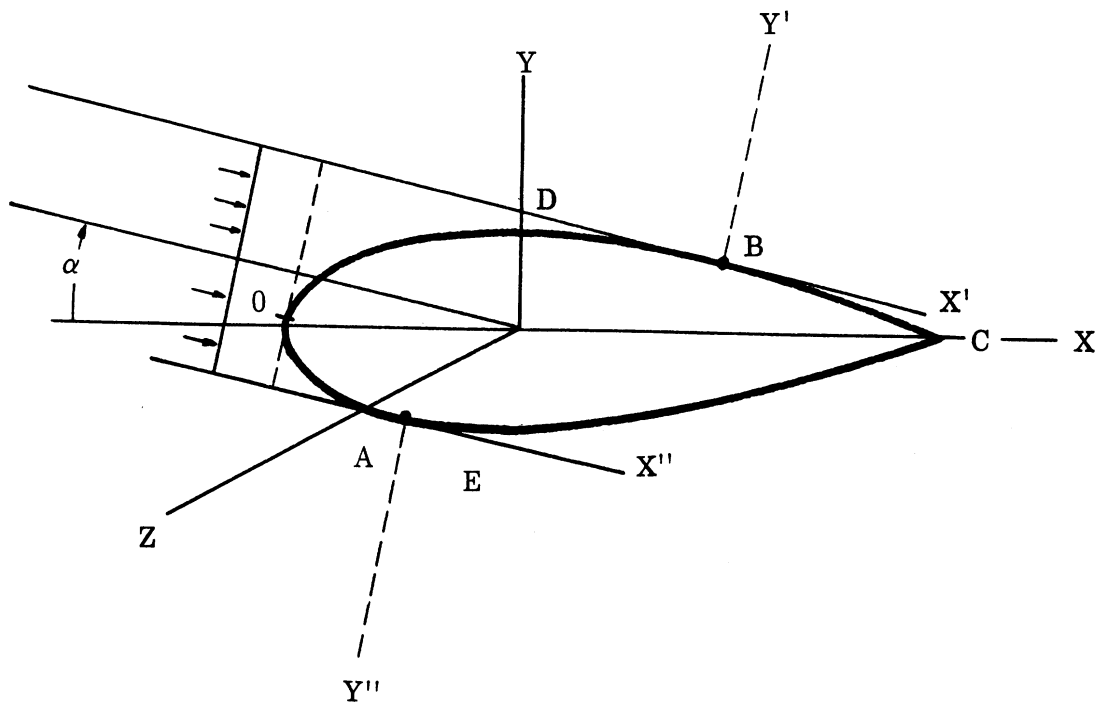


FIG. A-14: COORDINATE AXES FOR INCIDENCE AT ANGLES α

As before erect the coordinate axis with the shadow boundary as the origin. Since there is no longer the symmetry of the 'nose-on' case, it is necessary to divide the surface into two parts and determine the contributions from the two sides of the specular reflection point separately. With this in mind two coordinate systems as indicated are used and the procedure is the same as before.

In the case of parallel polarization, after Fock (Ref. A-9), make the approximation that on the surface

$$H_z = 0 \quad , \quad (8.20)$$

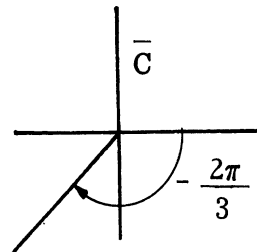
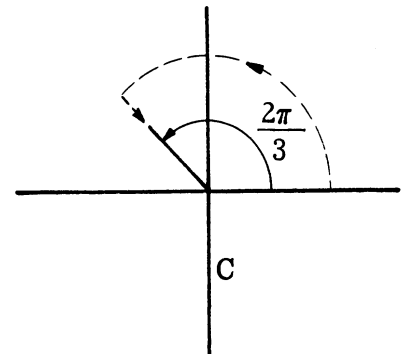
$$H_x = \frac{i}{m} H_z^0 e^{ikx} F(\xi) \quad , \quad (8.21)$$

where

$$m = \left(\frac{ka^2}{2b} \right)^{1/3} = \left(\frac{kR_0}{2} \right)^{1/3} \quad ,$$

$$F(\xi) = \frac{1}{\sqrt{\pi}} e^{\frac{i\xi^3}{3}} \int_C \frac{e^{i\xi t}}{w(t)} dt \quad ,$$

$$w(t) = \frac{1}{\sqrt{\pi}} \int_{\bar{C}} e^{zt - \frac{1}{3}z^3} dz \quad .$$



(8.22)

Asymptotically for large negative ξ , $F(\xi)$ is evaluated by the method of stationary phase; thus,

$$\left| F(\xi) \right| \cong 2 \xi \quad , \quad (8.23)$$

which gives the geometrical optic field

$$H_x = 2i e^{ikx} H_z^0 \frac{xb}{a^2} = 2i H_z^0 e^{ikx} \frac{x}{R_0} . \quad (8.24)$$

For positive ξ , the function $F(\xi)$ may be evaluated by closing the contour C and obtaining the sum of residues,

$$F(\xi) = 2\pi i \sum \frac{e^{i\xi t_s}}{w'(t_s)} , \quad (8.25)$$

where the t_s are the zeros of $w(t)$.

The zeros of $w(t)$ are given by Fock (Ref. A-9) and by Franz (Ref. A-13).

The values of $w'(t_s)$ are given by Franz in the form of those of a related function.

The function $F(\xi)$ must be evaluated by quadratures for $\xi < 0$ and as is in-

dicated above, may be evaluated by the method of stationary phase for $\xi \ll -1$.

The function $F(\xi)$ has been computed and appears in Tables A-1 and A-2.

By an analysis analogous to the above the scattered magnetic field is found to be in the Z direction, and is given by

$$H_s = \frac{ik}{4\pi} \frac{e^{ikr}}{r} \int_S n_z H_x e^{i\vec{k} \cdot \vec{r}'} dS . \quad (8.26)$$

Substituting for H_x ,

$$H_s = \left(\frac{ik}{4\pi} \right) \left(\frac{i}{m} \right) \frac{e^{ikr}}{r} \int_S e^{2ikx} n_z F(\xi) dS , \quad (8.27)$$

where $n_z = \sqrt{1 - n_x^2}$ and n_x is given above.

TABLE A-1: VALUES OF $F(\xi)$, $0(0.1) 2.1$

ξ	$\text{Re} [F(\xi)]$		$\text{Im} [F(\xi)]$	
	Numerical Integration	Residues	Numerical Integration	Residues
0	0.38791		-0.67188	
.1	0.38569		-0.56098	
.2	0.37880		0.45779	
.3	0.36699		-0.36257	
.4	0.35013	0.34876	-0.27557	-0.27526
.5	0.32825	0.32747	-0.19712	-0.19747
.6	0.30153	0.30120	-0.12754	-0.12793
.7	0.27040	0.27027	-0.06721	-0.06291
.8	0.23547	0.23550	-0.01648	-0.01665
.9	0.19762	0.19768	+0.02432	+0.02432
1.0	0.15799	0.15777	0.05496	0.05480
1.1	0.11797	0.11793	0.07539	0.07526
1.2	0.07918	0.07920	0.08582	0.08575
1.3	0.04341	0.04343	0.08683	0.08681
1.4	0.01247	0.01249	0.07951	0.07950
1.5		-0.01193		0.06546
1.6		-0.02852		0.04689
1.7		-0.03660		0.02651
1.8		-0.03644		0.00722
1.9		-0.02937		-0.00815
2.0		-0.01785		-0.01748
2.1		-0.00512		-0.01986
2.2				
2.3				
2.4				
2.5				
2.6				
2.7				

TABLE A-2: VALUES OF $F(\xi)$, $-2.7(0.1)0$

ξ	Re $[F(\xi)]$		Im $[F(\xi)]$	
	Numerical Integration	Asymptotic	Numerical Integration	Asymptotic
0	0.38791		-0.67188	
- .1	0.38582		-0.79024	
- .2	0.37987		-0.91585	
- .3	0.37052		-1.04845	
- .4	0.35838		-1.18775	
- .5	0.34392		-1.33347	
- .6	0.32771		-1.48526	
- .7	0.31027		-1.64276	
- .8	0.29209		-1.80557	
- .9	0.27355		-1.97328	
-1.0	0.25509	0.15972	-2.14544	-2.13348
-1.1	0.23697	0.16006	-2.32164	-2.30150
1.2	0.21948	0.15162	-2.50144	-2.47517
-1.3	0.20285	0.13924	-2.68455	-2.65543
-1.4	0.18718	0.12599	-2.87050	-2.84129
-1.5		0.11340		-3.03128
-1.6		0.10205		-3.22414
-1.7		0.09207		-3.41898
-1.8		0.08336		-3.61514
-1.9		0.07576		-3.81216
-2.0		0.06912		-4.00998
-2.1		0.06328		-4.20819
-2.2		0.05810		-4.40675
-2.3		0.05352		-4.60557
-2.4		0.04942		-4.80461
-2.5		0.04575		-5.00388
-2.6		0.04245		-5.20322
-2.7		0.03947		-5.40270

REFERENCES

- A-1. C. Schensted, J. Crispin, K. Siegel, "Studies in Radar Cross Sections XV - Radar Cross Sections of B-47 and B-52 Aircraft", University of Michigan Radiation Laboratory Report No. 2260-1-T, (1954).
- A-2. D. Kerr, "Propagation of Short Radio Waves", Vol. 13, Massachusetts Institute of Technology Radiation Laboratory Series, McGraw-Hill Book Company (1951),
- A-3. W.D. White, "Circular Polarization Study", Report No. 392-1, Airborne Instruments Laboratory Inc. (1950).
- A-4. "Effects of Type of Polarization in Echo Characteristics", Second Quarterly Progress Report under Contract No. AF 28(099)-90, The Ohio State University Research Foundation, Antennas Laboratory (1949).
- A-5. "Quarterly Progress Report", Division 2 - Aircraft Control and Warning, Massachusetts Institute of Technology, Lincoln Laboratory (15 August 1954).
- A-6. Project Report 389-4, The Ohio State University Research Foundation, Antenna Laboratory, Prepared under Contract AF 28(099)-90 (June 1950).
- A-7. K.M. Siegel, H.A. Alperin, J.W. Crispin, Jr., H.E. Hunter, R.E. Kleinman, W.C. Orthwein, and C.E. Schensted, "Studies in Radar Cross Sections IV - Comparison between Theory and Experiment of the Cross Section of a Cone", University of Michigan Radiation Laboratory Report No. UMM-92, (February 1953).
- A-8. W.W. Granneman, C.W. Horton, and R.B. Watson, "Diffraction of Electromagnetic Waves by a Metallic Wedge of Acute Dihedral Angle", Presented at the 1954 Austin (Texas) Meeting of the American Physical Society, February 26-27, 1954.
- A-9. V. Fock, "The Field of a Plane Wave near the Surface of a Conducting Body", Journal of Physics, Vol. X, pp. 399-409 (1946).
- "The Distribution of Currents Induced by a Plane Wave on the Surface of a Conductor", Journal of Physics, Vol. X, pp. 130-136 (1946).
- A-10. F. Oberhettinger, "Diffraction of Waves by a Wedge", Communications on Pure and Applied Mathematics, Vol. VII, pp. 551-563 (1954).

REFERENCES

- A-11. W. Gröbner and N. Hofreiter, Integraltafel, zweiter teil, Springer-Verlag (1950).
- A-12. W. Franz and K. Depperman, "Theory of Diffraction by a Cylinder as Affected by the Surface Wave", Annalen der Physik, 10, 361 (1952).
- A-13. W. Franz, "On the Green's Functions of the Cylinder and Sphere", Zeitschrift für Naturforschung, 9a, pp. 705-716 (1954).
- A-14. G. Walters, "Final Engineering Report on Effect of Polarization of the Radar Return from Ground Target and Rain", Dalmo-Victor - R-135-697 (AF-20926) (30 May 1952).
- A-15. S.D. Wanlass, G. Tanielian, D.M. Jacob, "X-Band Radar Cross Section Measurements", Hughes Aircraft Company, TM 371 (1 August 1954).
- A-16. K.M. Siegel, H.A. Alperin, R.R. Bonkowski, J.W. Crispin, Jr., A.L. Maffett, C.E. Schensted, and I.V. Schensted, "Studies in Radar Cross Sections VIII - Theoretical Cross Sections as a Function of Separation Angle between Transmitter and Receiver at Small Wavelengths", University of Michigan Radiation Laboratory Report No. UMM-115 (October 1953).
- A-17. R.R. Bonkowski, C.R. Lubitz, and C.E. Schensted, "Studies in Radar Cross Sections VI - Cross Sections of Corner Reflectors and other Multiple Scatterers at Microwave Frequencies", University of Michigan Report No. UMM-106 (October 1953).
- A-18. Private communication from Mr. William R. Hutchins, Radar and Missile Division, Raytheon Manufacturing Company, Boston, Massachusetts.

APPENDIX B

FAR FIELD SCATTERING FROM BODIES OF REVOLUTION *

1

SUMMARY

By use of approximations based on physical reasoning, radar cross section results for bodies of revolution are found. In the Rayleigh region (wavelength large in respect to the object's dimensions) approximate solutions are found. Examples given include a finite cone, a lens, elliptic ogive, a spindle and a finite cylinder. In the physical optics region (wavelength very small in respect to all radii of curvature) Kirchhoff theory and also geometric optics can be used. When the body dimensions are only moderately large in respect to the wavelength then Fock or Franz theory can be applied and examples of the circular and elliptic cylinder are presented. In the region where some dimensions of the body are large in respect to the wavelength and other dimensions are small in respect to the wavelength, special techniques are used. One example, the finite cone, is solved by appropriate use of the wedge-like fields locally at the base. Another example is the use of traveling wave theory for obtaining approximate solutions for the prolate spheroid and the ogive. Other results are obtained for cones the base perimeter of which is of the order of a wavelength by using known results for rings of the same perimeter.

* Applied Sci. Res., Sect. B., Vol. 7, 293-328 (1958). (Errata have been corrected and slight revisions have been made.)

INTRODUCTION

It is the intent in this appendix to use different mathematical techniques to obtain approximate results for the far zone scattering of plane electromagnetic waves by perfectly conducting bodies of revolution for all ratios of body dimension to wavelength. In places speculation based on physical reasoning has replaced mathematical rigor. We shall first discuss the Rayleigh region, then the physical optics region, and then the resonance region.

RAYLEIGH CROSS SECTION OF BODIES OF REVOLUTION

Rayleigh scattering (Ref. B-1) describes the scattering of electromagnetic radiation by a body whose dimensions are much smaller than the wavelength of the radiation. Thus the Rayleigh limit describes the scattered field, due to an incident plane wave, approximated at a large distance from the body by the field of radiating electric and magnetic dipoles located at the scatterer (the magnetic dipole contribution is comparable to that of the electric dipole only for a perfect conductor). To evaluate the electric (magnetic) dipole moment, the static electric (magnetic) field induced on the body by an applied constant field must be known. In other words, the electrodynamic boundary-value problem has been reduced to a corresponding static problem.

Although the solution of the Laplace equation is in principle simpler than the solution of the Maxwell equations, there are very few geometrical cases for which even the former is manageable. The question, therefore, arises whether any approximate information can be obtained as to the Rayleigh cross section when a solution of the Laplace equation is not available. That this should be possible is heuristically plausible. When the wavelength is much longer than the dimensions of a body, one cannot discern details of the structure of the body - the observed effect depends more on the size of the body than on its shape. Thus, knowledge of the size of the body modified by a rough indication of shape, should suffice for a description of the body in finding the Rayleigh cross section. It is the purpose of the present discussion to explore this possibility.

As background, it might be helpful to bear in mind a couple of features of the Rayleigh approximation itself. The solution to an electromagnetic scattering problem can be expressed as a multipole expansion. The relative importance of terms in the expansion differs according to the distance of the observer from the scatterer (as well as on the dimensions of the body relative to the wavelength), so that a small error in describing the field in one region can result in completely misrepresenting the corresponding field elsewhere. For a scatterer much smaller than the wavelength, retaining only the dipole terms gives a good approximation to the far zone, though the field in the near zone may be entirely wrong. Specifying the dipole moments of the body does not determine the body uniquely (i. e. different bodies may have the same dipole moments). Thus the Rayleigh cross section alone cannot identify the body fully. On the other hand, the finer details of the structure of the body, which would be exhibited by the higher moments (and seriously affect the cross section at small wavelengths), do not affect the Rayleigh cross section.

For simplicity, consider the scatterer to be a body of revolution, make it a perfect conductor (this is a rather trivial limitation), and examine backscattering of a plane wave incident along the axis of symmetry. There is then no polarization dependence. Thus, the direction of incidence will be denoted by z , the incident electric vector direction by x , the incident magnetic vector direction by y , and the length of the body along the symmetry axis by ℓ . The electric dipole moment \vec{p} is given by

$$\vec{p} = \int_S \omega \vec{r}' dS \quad (3.1)$$

where ω is the charge density, S the surface of the body, and \vec{r}' the vector, to a point on the surface. The boundary condition yields

$$\omega = \epsilon \vec{E} \cdot \hat{n} = \epsilon E \quad (3.2)$$

where ϵ = dielectric constant, \hat{n} = outward normal to the surface, and \vec{E} = electric field strength. Using cylindrical coordinates,

$$dS = \rho \sqrt{1 + (d\rho/dz)^2} d\phi dz \quad (3.3)$$

where ρ is a function of z but not of ϕ so that

$$\vec{p} = \epsilon \int_0^{\ell} dz \rho \sqrt{1 + \left(\frac{d\rho}{dz}\right)^2} \int_0^{2\pi} d\phi E \vec{r}' \quad (3.4)$$

From uniqueness and symmetry considerations, we can write

$$E = \sum_{n=0}^{\infty} a_n(z) \cos n\phi \quad (3.5)$$

Then $p_y = 0$, $p_z = 0$, and

$$p_x = \epsilon \int_0^{\ell} dz \rho^2 \sqrt{1 + \left(\frac{d\rho}{dz}\right)^2} \int_0^{2\pi} d\phi \cos \phi \left(\sum_{n=0}^{\infty} a_n(z) \cos n\phi \right) \quad (3.6)$$

$$= \epsilon \int_0^{\ell} \pi dz \rho^2 a_1(z) \sqrt{1 + \left(\frac{d\rho}{dz}\right)^2} = \epsilon \int_0^{\ell} \pi dz \rho^2 a_1'(z).$$

Apart from the factor $a_1'(z)$, the integral is just the volume of the body, V . In fact, the whole determination of the electric dipole moment resolves itself into

the determination of the factor $a(z)$ in

$$E = a(z) \cos \phi \quad (3.7)$$

since the other terms in the series do not contribute. If the body is elongated along the axis of symmetry (i. e., if $l \gg \rho$), $a_1'(z)$ will be a slowly varying function of z and can be removed from the integral and replaced by a mean value (or actually by an estimate of its value). To estimate $a(z)$, we resort to an analogy with reflection from a plane. In the latter case, the amplitude of the total field is twice that of the incident field. Thus we choose $a = 2E_0$ (phase differences in the incident field at various points on the body can be neglected) to obtain

$$\vec{p} = \hat{x} 2 \epsilon E_0 V. \quad (3.8)$$

The far zone electric field at a point on the z -axis due to the electric dipole is (Ref. B-2)

$$\vec{E} = - \frac{k^2}{4\pi\epsilon} \hat{z} \times (\hat{z} \times \vec{p}) \frac{e^{i(kz-\omega t)}}{z}. \quad (3.9)$$

The form of the magnetic dipole far-zone field is the same as that for the electric dipole if the electric and magnetic fields are interchanged (Ref. B-2). The symmetry of the problem insures that the magnetic dipole is along the y -axis, just as the electric dipole is along the x -axis. Consequently, the far-zone fields due to the two dipoles have the same orientation and phase. If we again resort to a cylinder-like model for approximation (with the amplitude of the total field at the surface twice that of the incident field), it is obvious from the complete symmetry of occurrence of the electric and magnetic interactions that the two contributions are equal.

Altogether, we have in the far zone on the z-axis

$$\vec{E} = \hat{x} \frac{k^2}{\pi} E_0 V \frac{e^{i(kz - \omega t)}}{z} \quad (3.10)$$

The back-scattering cross section is given by

$$\sigma = 4 \pi z^2 \lim_{z \rightarrow \infty} \left| \frac{\vec{E}}{\vec{E}_0} \right|^2 = \frac{4}{\pi} k^4 V^2 \quad (3.11)$$

This, then, is the value of the cross section to be expected for an elongated body of revolution.* As the flatness of the scatterer increases, the approximation is expected to get worse, in fact an infinitely flat body (i. e. a disc) has zero volume but a non-zero cross section. To anticipate the discussion below, for prolate spheroids the error incurred in the cross section varies from zero for extreme elongation to 13 per cent for the sphere.

Let us now compare this pseudo-derivation in detail with the exact answer for the special case we do know, the spheroid (Ref. B-1.) Let us define for convenience the quantity

$$F = \frac{\pi z \left| \vec{E} \right|}{k^2 E_0 V} \quad (3.12)$$

$F = 1$ yields the magnitude of \vec{E} given by Equation (3-10). Modifying Rayleigh's notation slightly,

$$F = \frac{1}{2} \left(\frac{1}{L} + \frac{1}{2-L} \right) = \frac{1}{L(2-L)} \quad (3.13)$$

where for a prolate spheroid, (Ref. B-1),

$$L = \frac{1}{e^2} - \frac{1-e^2}{2e^3} \ln \frac{1+e}{1-e} \quad (3.14)$$

* It should be noted that for the acoustic case the treatment would be equivalent except that instead of the two components (electric and magnetic) there would be only one, and thus the cross section would be $\sigma = (1/\pi) k^4 V^2$.

where $e =$ eccentricity -- i.e. the semi-axes are $a, a, \frac{a}{\sqrt{1-e^2}}$. For an elongated spheroid ($e \rightarrow 1$), $L \rightarrow 1$ and $F \rightarrow 1$, checking the approximation.

Next, let us inquire into the shape correction by first examining its form for the spheroid. We already know the prolate result; for the oblate spheroid,

$$L = \left(\frac{\sqrt{1-e^2}}{e^3} \sin^{-1} e - \frac{1-e^2}{e^2} \right) \quad (\text{Ref. B-1}) \quad (3.15)$$

where the semi-axes are now $a, a, a\sqrt{1-e^2}$. As these expressions are quite complicated, it is profitable to examine their limiting values. Consider a sphere ($e = 0$): From (3.14)

$$\log\left(\frac{1+e}{1-e}\right) = 2 \left(e + \frac{1}{3} e^3 + \dots \right) \quad (3.16)$$

$$\begin{aligned} L &= \frac{1}{e^2} \left[1 - (1-e^2) \left(1 + \frac{1}{3} e^2 + \dots \right) \right] \\ &= \frac{1}{e^2} \left[1 - 1 + e^2 - \frac{1}{3} e^2 + \dots \right] \rightarrow \frac{2}{3} \end{aligned} \quad (3.17)$$

$$F = \left[\frac{2}{3} \left(2 - \frac{2}{3} \right) \right]^{-1} = \left[\frac{2}{3} \cdot \frac{4}{3} \right]^{-1} = \frac{9}{8}. \quad (3.18)$$

It is easily demonstrated that F is monotone decreasing as we progress from a sphere to an elongated prolate spheroid. Hence, it ranges from $9/8$ to 1 -- very nearly constant, of the form $1 +$ decaying term.

Examine the disc limit ($e \rightarrow 1$ for oblate spheroid): Let

$$e = \sin x. \quad (3.19)$$

Then

$$L = \cos x \csc^2 x (x \csc x - \cos x). \quad (3.20)$$

Let

$$y = \frac{\pi}{2} - x. \quad (3.21)$$

Then

$$L = \sin y \sec^2 y \left[\left(\frac{\pi}{2} - y \right) \sec y - \sin y \right]. \quad (3.22)$$

Expand near $y = 0$ (equivalent to $e \rightarrow 1$):

$$L \approx y \left[\left(\frac{\pi}{2} - y \right) - y \right] = \frac{\pi y}{2} - 2y^2 = \frac{\pi}{2} y \left(1 - \frac{4}{\pi} y \right) \quad (3.23)$$

$$F = \frac{1}{L(2-L)} \approx \frac{1}{\frac{\pi}{2} y \left(1 - \frac{4}{\pi} y \right) \left(2 - \frac{\pi}{2} y \right)} \approx \frac{1}{\pi y} \left(1 + \frac{4}{\pi} y + \frac{\pi}{4} y \right). \quad (3.24)$$

For small y , $y \approx \sqrt{1-e^2}$; if we call the semi-axes a , a , b , then $y \simeq b/a$.

Combine the information about F . In the oblate case, F is again monotone, increasing toward the disc limit. The prolate spheroid discussion indicates that we should split off from F a unity term, and that the remaining term should decay as $b/a \rightarrow \infty$. Thus we write

$$F \approx 1 + \frac{1}{\pi y} \left[1 + \left(\frac{4}{\pi} + \frac{\pi}{4} - \pi \right) y \right] \approx 1 + \frac{1}{\pi y} (1-y) \approx 1 + \frac{1}{\pi y} e^{-y}. \quad (3.25)$$

We now postulate that for all spheroids (with semi-axes a , a , b), the shape correction factor is approximately

$$F = 1 + \frac{1}{\pi y} e^{-y} \quad (3.25)$$

where $y = b/a$. Numerical comparison indicates that the approximation is valid to within one per cent. The Rayleigh cross section of a spheroid for backscattering along the axis of symmetry is

$$\sigma = \frac{4}{\pi} k^4 V^2 \left[1 + \frac{1}{\pi y} e^{-y} \right]^2. \quad (3.26)$$

The cross section of the spheroid depends on its volume and on a correction factor involving $y = b/a$. Except for very flat oblate spheroids, the shape correction factor can be neglected. Where it is not neglected, the shape correction factor is a simple function of y , which is a measure of the elongation.

The natural extension of the discussion is to postulate that for all bodies of revolution the Rayleigh cross section for backscattering along the axis of symmetry can be expressed as

$$\sigma = \frac{4}{\pi} k^4 V^2 \left(1 + \frac{1}{\pi y} e^{-y} \right)^2 \quad (3.26)$$

where y is a measure of the elongation (characteristic dimension along the axis of symmetry)/(characteristic dimension in the perpendicular direction). For elongated bodies, the term in y drops out and there is no ambiguity. For flattened bodies, the answer is sensitive to the choice of characteristic dimensions, but a good approximation should still be attainable. The ambiguity can be eliminated in a number of cases by imposing a restriction on the choice of characteristic dimensions: in the limit of extreme flattening, the cross section must tend to the value for the appropriate disc.

Illustration I: Finite Cone

Consider a right circular cone of altitude h and radius of base a . As $h \rightarrow 0$, the cross section of the cone must go into the cross section of a disc of radius r -- i.e., we must have

$$VF = \frac{1}{3} \pi a^2 h \left(1 + \frac{1}{\pi y} e^{-y}\right) \rightarrow \frac{a^2 h}{3y} = \frac{4}{3} a^3. \quad (3.27)$$

Thus, the appropriate ratio of characteristic dimensions to be used in equation (3.26) is

$$y = h/4a. \quad (3.28)$$

Hence, the cone has the same cross section as a spheroid of equal volume whose semi-axes are $(a, a, h/4)$.

Illustration II: Lens

Consider a symmetrical convex lens of radius of curvature R_1 (the body of revolution obtained by rotating the shaded area in Figure B-1 about the η -axis). In the disc limit (d constant, $c \rightarrow 0$),

$$VF \rightarrow \frac{V}{\pi y} = \frac{4}{3} d^3. \quad (3.29)$$

Hence, we take for the lens

$$y = \frac{3V}{4\pi d^3} = \frac{3V}{4\pi R_1^3 \sin^3 \theta}. \quad (3.30)$$

The volume of the lens is

$$V = \frac{2\pi}{3} R_1^3 (1 - \cos \theta)(1 - \cos \theta + \sin^2 \theta). \quad (3.31)$$

As $\theta \rightarrow \pi/2$ (sphere limit), we reproduce the previous spheroid result, as expected.

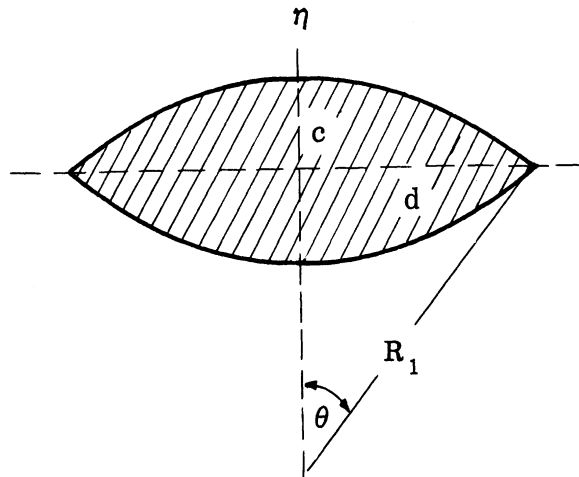


FIG. B-1: THE LENS

Illustration III: Elliptic Ogive

Inasmuch as the circular ogive is more elongated than a sphere, the argument from the disc limit cannot be applied to it directly.

Instead, we consider the elliptic ogive obtained by rotating the shaded area of Figure B-2 (a portion of an ellipse) about the η -axis (which is taken parallel to the minor axis). For this body, in the disc limit (d constant, $c \rightarrow 0$):

$$VF \rightarrow \frac{V}{\pi y} = \frac{4}{3} d^3 . \quad (3.32)$$

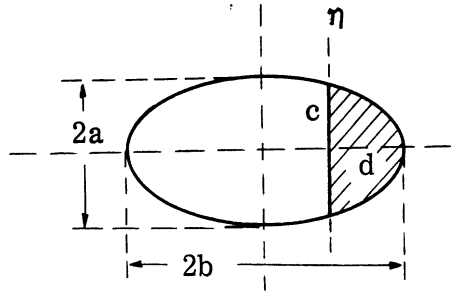


FIG. B-2: THE ELLIPTIC OGIVE

The equation for the ellipse is

$$\frac{c^2}{a^2} + \frac{(b-d)^2}{b^2} = 1, \quad (3.33)$$

which suggests use of the parameter θ ,

$$\sin \theta = c/a \quad (3.34)$$

Then

$$y = \frac{3V}{4\pi d^3} = \frac{3V}{4\pi b^3 (1-\cos \theta)^3} \quad (3.35)$$

The volume of the elliptic ogive is

$$V = 2\pi ab^2 \left(\sin \theta - \theta \cos \theta - \frac{1}{3} \sin^3 \theta \right). \quad (3.36)$$

As $\theta \rightarrow \pi/2$, we reproduce the previous spheroid result, as expected.

Special Case: Circular Ogive . To obtain the cross section of the circular ogive, we now merely take the special case of the elliptic ogive with $a = b$. From geometry, θ can then be identified with the ogive half-angle. Now

$$y = \frac{3}{2} \frac{\sin \theta - \theta \cos \theta - \frac{1}{3} \sin^3 \theta}{(1 - \cos \theta)^3} \quad (3.37)$$

Illustration IV: Spindle

Consider the body of revolution obtained by rotating the shaded area of Figure B-3 (bounded by a parabola and a straight line perpendicular to the axis of the parabola) about the η -axis. Using the disc limit just as before, we have

$$y = \frac{3V}{4\pi d^3} \quad (3.38)$$

where the volume is

$$V = \frac{16}{15} \pi c d^2 \quad (3.39)$$

so that

$$y = \frac{4}{5} \frac{c}{d} \quad (3.40)$$

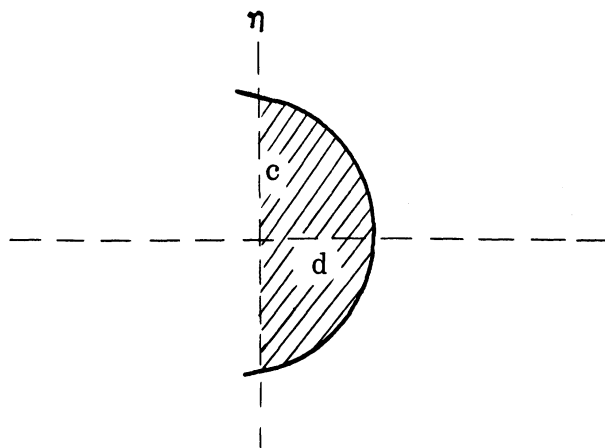


FIG. B-3: THE SPINDLE

Illustration V: Finite Cylinder

Consider a cylinder of radius a and height h . From the disc limit,

$$y = \frac{3V}{4\pi a^3} = \frac{3h}{4a} \quad (3.41)$$

By further exploitation of this approach we can go on to obtain the Rayleigh cross section of a body of revolution for arbitrary separation between transmitter and receiver and for all aspects and all polarizations. The most direct extension is to replace the body by an equivalent spheroid and take over the spheroid results. The equivalent spheroid is a spheroid with the same volume and the same elongation factor as the body. The simplified expression found for backscattering along the symmetry axis provides a reasonable way to arrive at an elongation factor for many bodies. The logical ultimate extension in the spirit of this approach is to formulate the Rayleigh scattering of a body of revolution at all aspect combinations and polarizations in terms of the following parameters only: the volume, the elongation factor, and the aspect and polarization angles.

THE OPTICS REGION

By the optics region we mean, generally, that region, in wavelength, wherein the techniques of geometric and physical optics yield good approximations to the radar cross section of a body. The extent of the optics region thus depends on the particular body being studied. By the geometric optics cross section we mean $\pi R_1 R_2$ where R_1 and R_2 are the principal radii of curvature of the body at the point where a ray is reflected toward the receiver. We use physical optics (Kirchhoff) theory to denote the scattered far field, and the cross section thus defined, given by the following expression

$$\vec{H}_s = (1/4\pi) \int_{\text{illuminated area}} (\hat{n} \times \vec{H}) \times \nabla \frac{e^{ikR}}{R} dS$$

where \vec{H} = twice the tangential component of the incident magnetic field,

R = the distance from the integration point to the field point,

\hat{n} = the unit outward normal to the surface at the integration point,

and in which the far field approximations for $\nabla \frac{e^{ikR}}{R}$ are used. That is, with the receiver at a very great distance from the body and if the body

is finite we have

$$\nabla \left(\frac{e^{ikR}}{R} \right) \approx \frac{ik}{r} \left(e^{ikR} \right) \hat{n}_o$$

where $R = r + (\hat{n}_o \cdot \vec{r}')$, r = the distance from the origin to the field point

(receiver), r' = the distance from the origin to the integration point on the scatterer (\vec{r}' = the corresponding vector) and \hat{n}_0 = the unit vector directed from the receiver to the origin.

When the wavelength is small with respect to all of the dimensions of the scatterer, the geometric optics cross section is an excellent approximation to the exact result. When a body is infinite in extent, then geometric optics can be the exact solution. Examples of such exact solutions are the paraboloid of revolution, when we are considering plane wave illumination along the axis of symmetry, and the wedge for particular wedge angles and for particular angles of incidence and polarization.

Let us now consider a body which has one radius of curvature which is small with respect to the wavelength. In three dimensions we can consider the infinite cone and in two dimensions we can consider the wedge. By purely dimensional analysis we find that the tip far field behaves like $1/k$ and the edge in two dimensions behaves like $(1/k)^{1/2}$. We find that physical optics not only predicts these types of k -dependence but also (for large and small cone angles) that it predicts the leading term of a rapidly convergent expansion in the angle parameter as long as the transmitter or receiver is on the axis of symmetry.

Kirchhoff theory will give poor results for problems in which the major contribution to the cross section comes from an edge. For example, consider the case in which the transmitter and receiver are located at a

point along the face of a wedge but far from the edge, with Poynting's vector, \vec{P} , parallel to the face of the wedge and normal to the edge (see Fig. B-4).

For the \vec{E} -vector perpendicular to the surface, the exact result is:

$$\sigma_{\perp} = 2\pi \left| f(\phi) \right|^2 = \frac{\pi \lambda}{2\phi_0^2} \tan^2 \frac{\pi}{2\phi_0}$$

where the cross section, in two dimensions, is given by

$$\sigma = \lim_{r \rightarrow \infty} 2\pi r \left| \frac{E_s}{E_i} \right|^2$$

while the Kirchhoff answer is zero.

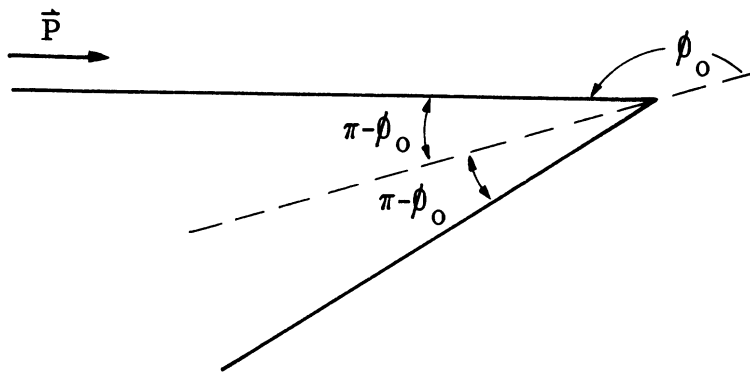


FIG. B-4: THE WEDGE FOR INCIDENCE ALONG ONE FACE OF THE WEDGE AND NORMAL TO THE EDGE

This leads one to the realization of why Kirchhoff theory would give poor results for a finite thin cone. The major contribution to the cross section

in the non-specular directions for small wavelengths comes from the rear circular edge. The field, locally, would be like that for a wedge. Thus, we need to use an improvement on Kirchhoff theory to obtain good cone answers. We will show this improvement and also how we obtain approximate results for thin cones in the resonance region. Thus we will show how to obtain, approximately, a complete cone cross section curve.

Kirchhoff theory gives excellent first order approximations for bodies with dimensions large with respect to the wavelength and the results are too well known to warrant their discussion here.

In the region to which we must give the vague characterization as lying somewhere between the resonance region and the optics region there has been a rapid and fruitful development of new ideas recently.

We begin with the remarkable paper of V. A. Fock (Ref. B-3) in which he presented a method which we will describe as a local order analysis of the field near the shadow boundary. He succeeds in giving the fields on the diffracting surface near the shadow boundary in terms of one or the other of two "universal" functions according as the incident polarization direction lies parallel or perpendicular to the shadow curve. Strictly, these are solutions of the two dimensional (scalar) problems and depend on the radius of curvature at the shadow boundary and the wavelength of the radiation. These functions are of the form

$$\begin{aligned}
 g(\xi) &= \frac{1}{\sqrt{\pi}} \int_{\Gamma} \frac{e^{i\xi t}}{\omega'(t)} dt \\
 f(\xi) &= \frac{1}{\sqrt{\pi}} \int_{\Gamma} \frac{e^{i\xi t}}{\omega(t)} dt
 \end{aligned}
 \tag{4.1}$$

where

$$\omega(t) = \frac{1}{\sqrt{\pi}} \int_{\Gamma'} e^{zt - \frac{1}{3} z^3} dz \quad (4.2)$$

with the contours shown in Figure B-5.

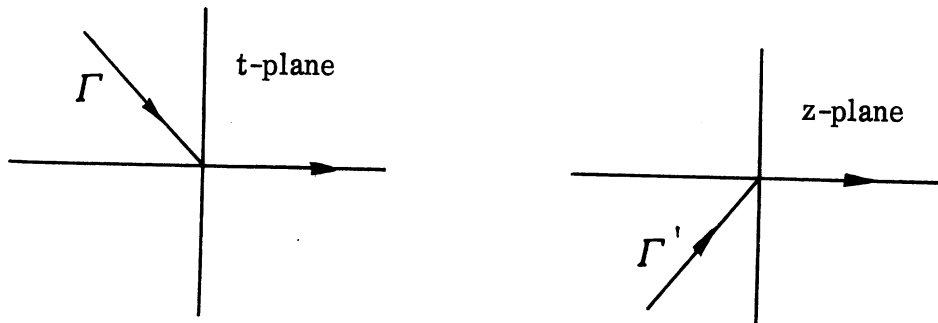


FIG. B-5: CONTOURS

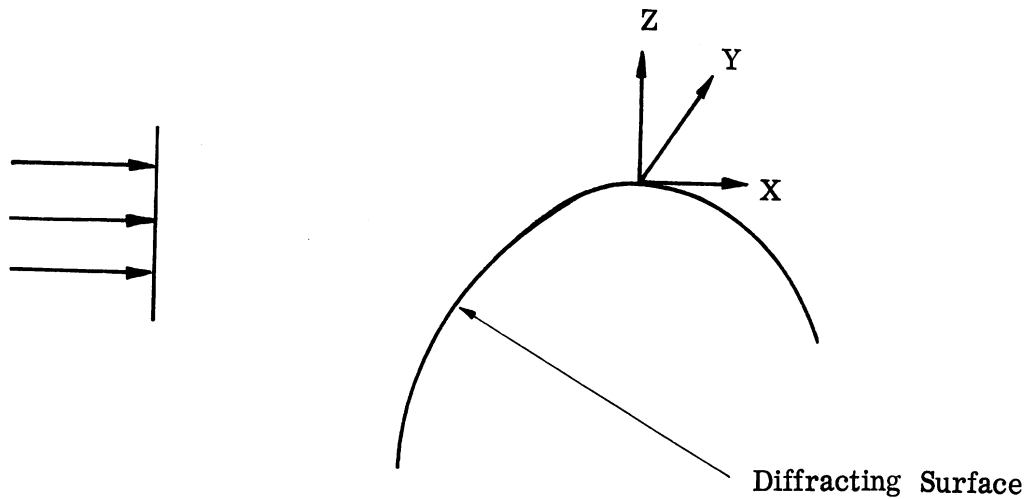


FIG. B-6: GEOMETRY

The arguments used are certain reduced distances measured from the

geometrical shadow boundary, i. e., near the origin as indicated in Figure B-6 we have

$$\zeta = \left[\frac{kR}{2} \right] \frac{1}{3} \frac{X}{R} \quad (4.3)$$

where R is the radius of curvature and $k = \frac{2\pi}{\lambda}$.

These same functions appear in the approximate solutions of specific problems. There are two which we particularly wish to note. The fields induced on a parabolic cylinder (Ref. B-4) and on a circular cylinder (Ref. B-5) are given, in a sense, by these same functions. These are not remarkably similar surfaces.

In these examples for the solution continued into the shadow we must modify the arguments of the universal functions as follows. The motivation for this stems from the "generalized ray optics" of Keller (Ref. B-6). In place of Equation (4.3) we write

$$\zeta = \int_0^S \left[\frac{kR(s)}{2} \right] \frac{1}{3} \frac{ds}{R(s)} \quad (4.4)$$

where S is path length measured along the surface of the obstacle from the shadow boundary into the shadow, ds is the element of path length, and $R(s)$ is the radius of curvature at the position s .

Franz and Deppermann (Ref. B-7), however, have given the connection between the two in the concept of "creeping waves". We can meaningfully

speak of the continuation of the penumbra solution into the shadow of the parabolic cylinder, but in the case of the circular cylinder we find we are wrapping our solution around the cylinder if we allow the argument of the universal functions to continue increasing. This latter concept is made meaningful if we understand the field in the shadow as arising from waves "launched" at the shadow boundary and "creeping" around the rear and eventually back to the front, etc. The physical interpretation has been justified by Friedlander (Ref. B-8) while the underlying mathematical structure has been illuminated by Wu (Ref. B-9) with his concept of a universal covering space.

In the following is given an account of the general procedure. Let a convex closed surface S , $f(x, y, z) = 0$ be illuminated by a plane wave incident in the direction of the x -axis. The geometrical shadow is then given by the two equations $f(x, y, z) = 0$, $\frac{\partial f}{\partial x} = 0$. Let the origin be located at a point on the shadow boundary with the z -axis the outward directed normal to S and the y -axis chosen to form a right-handed system. Using the geometric assumption that the surface can be approximated by a paraboloid at any point, i. e.,

$$z + 1/2 (ax^2 + 2bxy + cy^2) = 0, \quad (4.5)$$

so that $\frac{\partial f}{\partial x} = ax + by$, and the physical assumption that the variation of this field in the z -direction is much larger than that in either the x - or y -direction for sufficiently small λ , Fock obtains an approximation to Maxwell's

equations which leads to the solutions:

$$\begin{aligned}
 H_y &= H_y^0 G(\zeta) \\
 H_x &= \left(\frac{2a}{k}\right)^{1/3} i H_z^0 e^{ikx} F(\zeta) \\
 H_z &= 0
 \end{aligned} \tag{4.6}$$

on the surface. The incident field is given by

$$\vec{H}_0 = (0, H_y^0, H_z^0) \tag{4.7}$$

while the functions G and F have the asymptotic behavior

$$\begin{aligned}
 \lim_{\zeta \rightarrow \mp \infty} G(\zeta) &= \begin{cases} 2 \\ 0 \end{cases} \\
 \lim_{\zeta \rightarrow \mp \infty} F(\zeta) &= \begin{cases} 2\zeta \\ 0 \end{cases}
 \end{aligned} \tag{4.8}$$

where ζ is a reduced distance from the shadow boundary given by

$$\zeta = \left(\frac{k}{2a}\right)^{1/3} (ax + by). \tag{4.9}$$

In Figure B-7 we compare the result using the Fock-Franz method with the sum of the harmonic series for a circular cylinder (e.g., Bailin's work in Reference 10) with $ka = 12$. In Figure B-8 we compare the method with the experimental measurements of Wetzel and Brick (Ref. B-11) on an elliptic cylinder of $ka = 12$ and $kb = 7.5$.

In the case of the three-dimensional problem of scattering by finite obstacles we have an additional complication which appears in both the scalar and vector problems. Since there is a caustic at the rear of the obstacle, we must take account of the fact that the energy converges on the caustic and, in fact, the "creeping waves" lose their identity in this region.

This behavior is apparent from the work of Fock (Ref. B-12), Franz (Ref. B-5) and, more recently, Belkina and Weinstein (Ref. B-13) and N. Logan (Ref. B-14) who have given a thorough treatment of this approach for the sphere.

However, Fock theory can be used to determine a partial creeping wave type field and if we can find another way to handle the partial field due to the small radii of curvature, we can again obtain good far-field approximations for moderate values of ka . The value of Fock theory is twofold: (1) when the wavelength is very small with respect to the characteristic dimensions of the body, it yields an approximation to the true field in the shadow region where the Kirchhoff result would predict a zero field, and (2) it is a procedure which is easily applied to sphere and cylinder problems for moderate values of ka ($ka > 5$). One finds upon applying this process to spheroids that the values of ka required in order to obtain good results may be very large.

In the three dimensional problems we see that the sphere solution with the interpretation of creeping waves and behavior of the caustic serves as a prototype from which we infer the solution for other shapes provided the

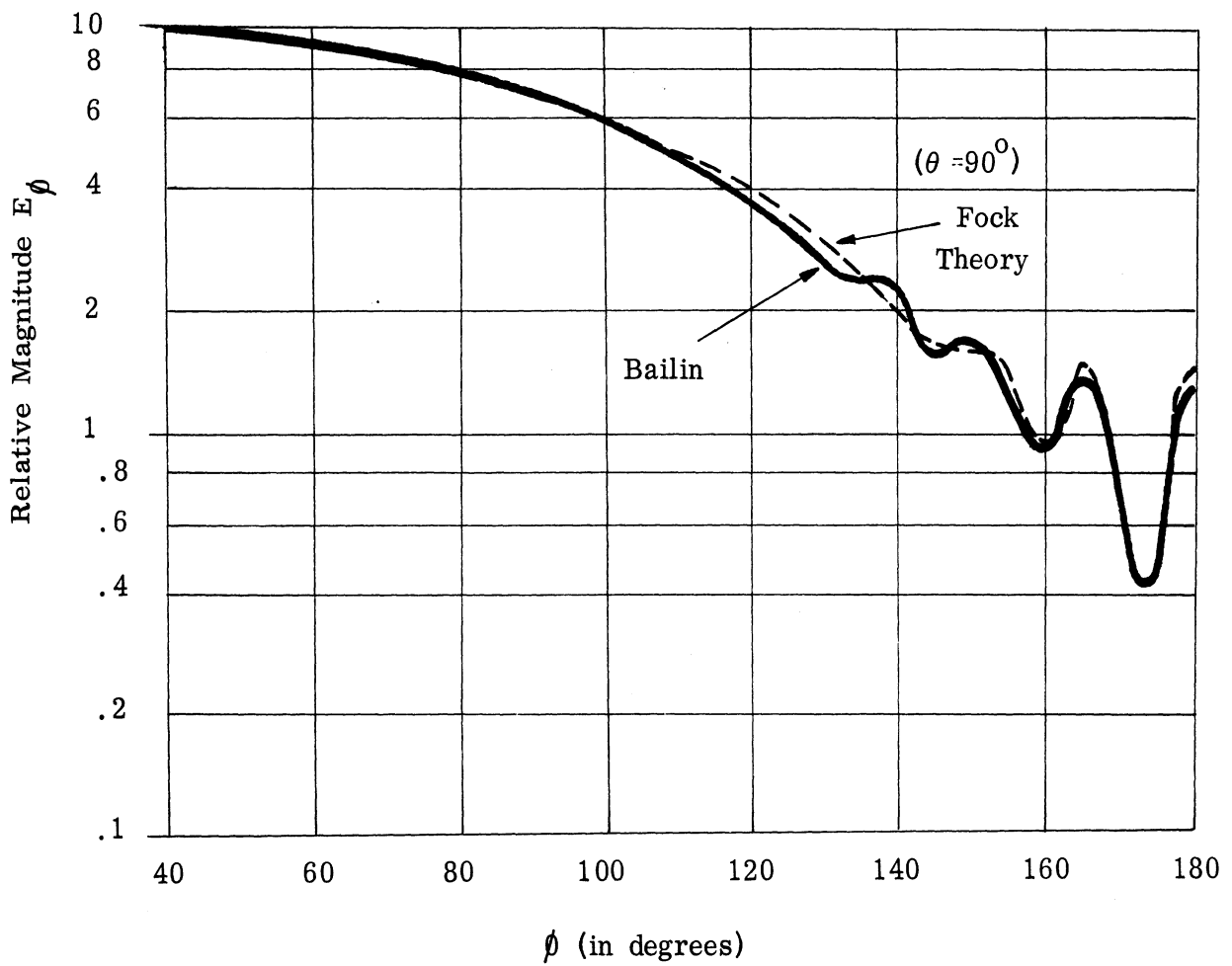


FIG. B-7: COMPARISON OF AMPLITUDES FROM EXACT SERIES AND FOCK'S CURRENT DISTRIBUTION FOR A CIRCULAR CYLINDER WITH $ka = 12$

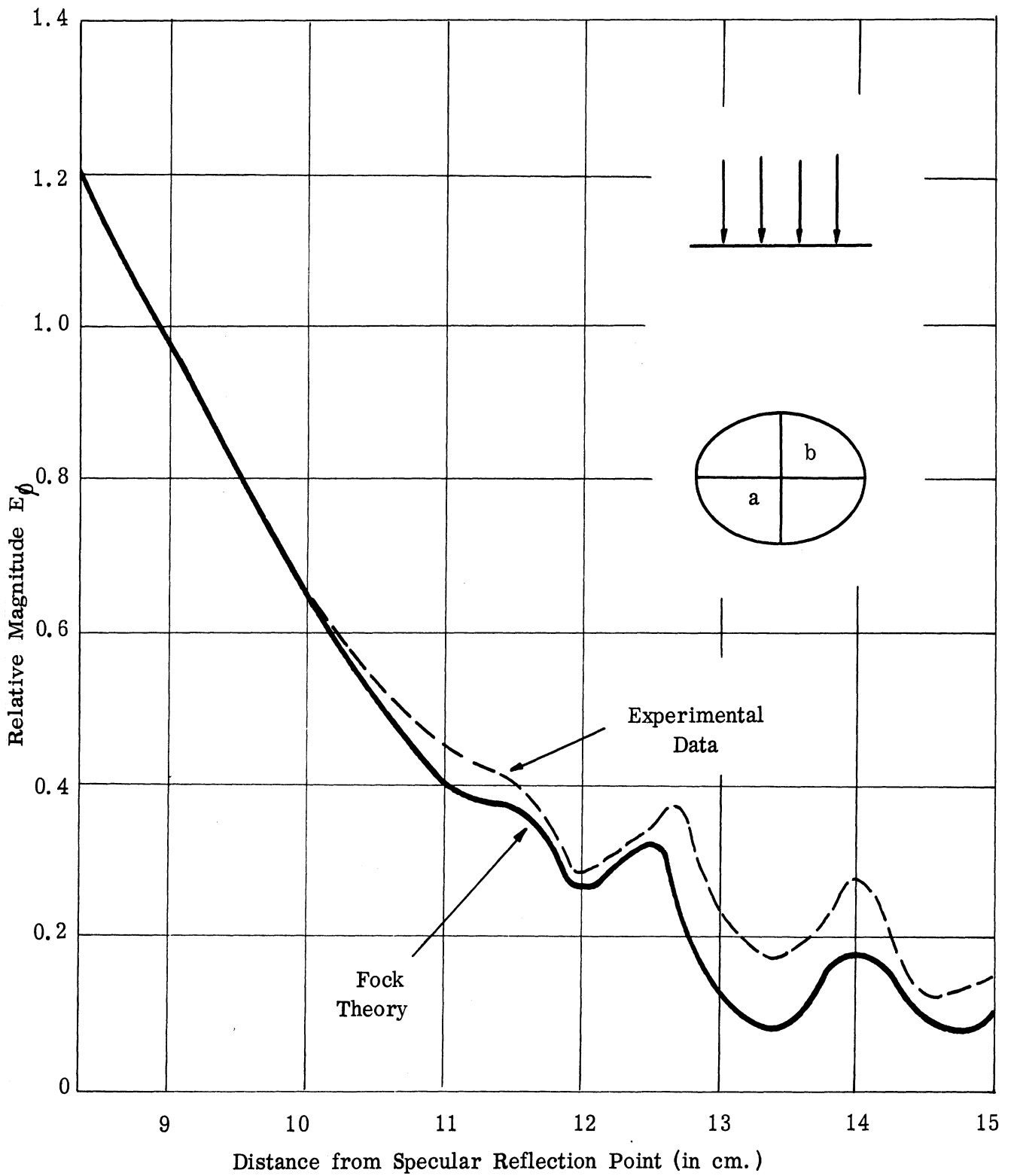


FIG. B-8: COMPARISON OF AMPLITUDES FROM EXPERIMENTAL DATA AND FOCK'S CURRENT DISTRIBUTION FOR AN ELLIPTIC CYLINDER OF ECCENTRICITY 0.780 WITH $ka = 12$ AND $kb = 7.5$

characteristic parameters are sufficiently large with respect to the wavelength. For example, a symmetrically illuminated spheroid of large enough dimensions should be an easy generalization.

Suppose we consider a prolate spheroid in somewhat more detail. Let the semi-major and semi-minor axes be denoted by a and b respectively. The condition we require for the application of the Fock-Franz theory is that

$$k R_{\min} \text{ be large where } k = \frac{2\pi}{\lambda} \text{ and } R_{\min} \text{ is the minimum radius of curvature,}$$

$$R_{\min} = \frac{b^2}{a} .$$

As an example of this limitation we note that for a prolate spheroid of $\frac{a}{b} = 10$ the requirement $k R_{\min} \sim 5$ would imply $ka > 500$. This was pointed out by Belkina and Weinstein (Ref. B-13).

If we let $k R_{\min}$ decrease while we keep ka , kb large we approach a body which is "large" but which has "sharp" ends. We illuminate this object along the symmetry axis and consider a limited application of our "creeping wave" theory. Certainly for $k R_{\min} < 1$ the forward tip will scatter more like an infinite cone than like a sphere of radius b , hence, our theory is not applicable. In the penumbra region all requirements are met and we feel justified in making a creeping wave analysis. Granted this, we have launched a wave which is creeping toward this effective discontinuity, the rear tip. Here we must again have recourse to another description and consider the wave to be reflected from the rear tip and again launched along the surface.

An example of this would be the thin cone radiation problem when the source is far from the tip (a = distance from tip to source). The Green's

function for this case is approximated by that for a cylinder and thus Fock theory should give excellent results. If an infinitesimal slot is along a generatrix of the cone, the Fock answer should be excellent for all ka . If one can obtain a tip answer to add to the Fock result, then one can handle all kinds of slots on cones.

We postpone our discussion of the ogive, finite cone, and the spheroid approximations (for moderate values of ka) until we reach the resonance region discussion of Section 5.

In addition to the Fock theory, small wavelength approximations can be improved by making use of known results. Just as Artmann, in his solution for the thick half plane (Ref. B-15), replaced the cylindrical edge with a polygon, we can obtain an approximation for the thin finite cone by replacing the cone with a regular pyramid. The base, locally, will be a wedge and to calculate the field scattered by the cone base, we will add up the fields scattered by all the wedge-like segments into which the cone base has been decomposed. We shall consider the cone in some detail, hence it might be valuable to first present the physical optics approximation.

The problem we shall consider is that of determining the radar cross section of a thin finite cone when both transmitter and receiver are situated on the axis of symmetry of the cone in the far zone. We will treat the case where the wavelength of the incident radiation is much smaller than the altitude, z_0 , and the base radius, a , of the cone. The geometry of the problem is as shown in Figure B-9.

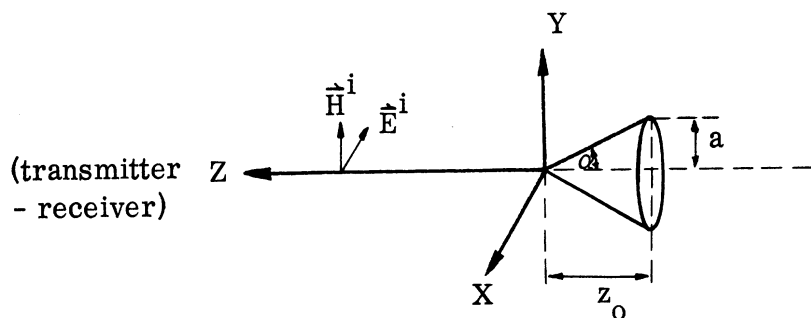


FIG. B-9: CONE GEOMETRY

We shall also utilize polar variables in the x-y plane as shown in Figure B-10.

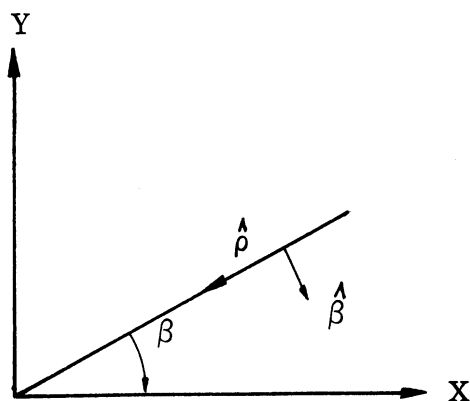


FIG. B-10: POLAR VARIABLES

The following definitions of radar cross section (of perfect conductors) will be used,

$$\sigma = \lim_{r \rightarrow \infty} 4\pi r^2 \left| \frac{\vec{E}_s}{\vec{E}_i} \right|^2 = \lim_{r \rightarrow \infty} 4\pi r^2 \left| \frac{\vec{H}^s}{\vec{H}^i} \right|^2 \quad (4.10)$$

The Kirchhoff (physical optics) expression for the scattered magnetic field is (Ref. B-16)

$$\vec{H}^s = \frac{ik}{2\pi} \frac{e^{+ikr}}{r} \left[(\hat{n}_o \cdot \hat{a}) \vec{f} - (\hat{n}_o \cdot \vec{f}) \hat{a} \right] \quad (4.11)$$

where

$$\vec{f} = \int_{S'} \hat{n} e^{+ik\vec{r}'} \cdot (\hat{n}_o + \hat{k}) dS$$

S' = illuminated area of scatterer
 \hat{n} = unit outward normal to S
 r' = position vector of point on S
 \vec{r} = position vector of field point
 \hat{a} = direction of incident magnetic field
 \hat{n}_o = direction of receiver to origin
 \hat{k} = direction of transmitter to origin.

Note. We assume $|H^i| = |E^i| = 1$. In this case, the following relations hold.

$$\begin{aligned} \hat{n} &= \sin \alpha \hat{i}_z + \cos \alpha (\hat{i}_x \cos \beta + \hat{i}_y \sin \beta) \\ \vec{r}' &= x' \hat{i}_x + y' \hat{i}_y + z' \hat{i}_z \\ \hat{a} &= \hat{i}_y \\ \hat{n}_o &= -\hat{i}_z \\ \hat{k} &= -\hat{i}_z \\ dS &= \frac{z' \tan \alpha}{\cos \alpha} dz' d\beta. \end{aligned} \quad (4.12)$$

Hence

$$\hat{n}_o \cdot \hat{a} = -\hat{i}_z \cdot \hat{i}_y = 0, \quad (4.13)$$

and

$$\hat{n}_o \cdot \vec{f} = \int_{S'} \hat{n}_o \cdot \hat{n} e^{+ik\vec{r}' \cdot (\hat{n}_o + \hat{k})} dS$$

which becomes

$$= -\tan^2 \alpha \int_0^{2\pi} \int_0^{-z_o} z' e^{-2ikz'} dz' d\beta. \quad (4.14)$$

The integration with respect to β yields

$$\hat{n}_o \cdot \vec{f} = -2\pi \tan^2 \alpha \int_0^{-z_o} z' e^{-2ikz'} dz' \quad (4.15)$$

This integration can also be performed yielding

$$\hat{n}_o \cdot \vec{f} = +2\pi \tan^2 \alpha \left(\frac{e^{-2ikz'}}{(2ik)^2} + \frac{ze^{-2ikz'}}{2ik} \right) \Bigg|_0^{-z_o},$$

or

$$\hat{n}_o \cdot \vec{f} = -2\pi \tan^2 \alpha \left[\frac{e^{+2ikz_o}}{4k^2} + \frac{z_o e^{+2ikz_o}}{2ik} - \frac{1}{4k^2} \right]. \quad (4.16)$$

Hence

$$\vec{H}^s = \frac{ie^{+ikr}}{r} \tan^2 \alpha k \hat{i}_y \left[\frac{e^{+2ikz_o}}{4k^2} + \frac{z_o e^{+2ikz_o}}{2ik} - \frac{1}{4k^2} \right] \quad (4.17)$$

which can be written

$$\vec{H}^s = \frac{ie^{+ik(r+2z_o)}}{2kr} \tan^2 \alpha \hat{i}_y \left[\frac{1}{2} - ikz_o - \frac{e^{-2ikz_o}}{2} \right]. \quad (4.18)$$

Since $|kz_0| > 1$ (small wavelength approximation)

$$\vec{H}^s \approx \frac{-ie^{+ik(r+2z_0)}}{2kr} \tan^2 \alpha \hat{i}_y (ikz_0) \quad (4.19)$$

$$= + \frac{e^{+ik(r+2z_0)}}{2r} z_0 \tan^2 \alpha \hat{i}_y .$$

Now using the definition of radar cross section we have

$$\sigma = \lim_{r \rightarrow \infty} 4\pi r^2 \left| \frac{\vec{H}^s}{\vec{H}^i} \right|^2 = \pi z_0^2 \tan^4 \alpha$$

or

$$\sigma = \pi a^2 \tan^2 \alpha. \quad (4.20)$$

We will now approximate the cone with a pyramid and determine the field scattered by the wedge segments that constitute the base. To illustrate the technique we will first use the physical optics approximation for the field scattered by the wedges. We use the Kirchhoff expressions for the scattered field previously presented where in this case (incidence perpendicular to the back face of the wedge - see Figure B-11) we have

$$\begin{aligned} \hat{n} &= \sin \gamma \hat{i}_\eta - \cos \gamma \hat{i}_\xi \\ \vec{r}' &= \xi \hat{i}_\xi + \eta \hat{i}_\eta + \zeta \hat{i}_\zeta \\ \hat{a} &\text{ has no } \xi \text{ component, i.e., } \hat{a} \cdot \hat{i}_\xi = 0 \\ \hat{n}_0 &= \hat{i}_\xi \\ \hat{k} &= \hat{i}_\xi \\ dS &= \frac{d\xi d\zeta}{\sin \gamma} . \end{aligned} \quad (4.21)$$

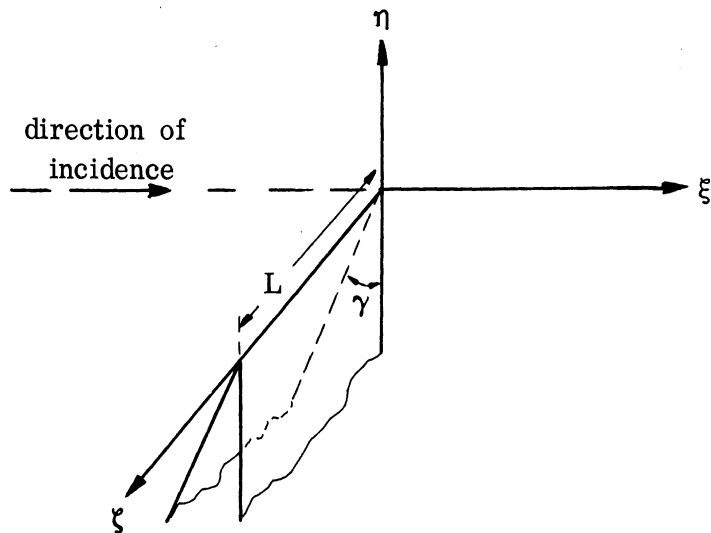


FIG. B-11: WEDGE GEOMETRY

Hence $\hat{n}_0 \cdot \hat{a} = \hat{i}_\xi \cdot \hat{a} = 0$, and

$$\hat{n}_0 \cdot \vec{f} = - \frac{\cos \gamma}{\sin \gamma} \int_0^L \int_0^{-\infty} e^{+2ik\xi} d\xi d\zeta . \quad (4.22)$$

Integrating with respect to ζ and letting $\xi \rightarrow -\xi$, we obtain

$$\hat{n}_0 \cdot \vec{f} = \frac{L}{\tan \gamma} \int_0^\infty e^{-2ik\xi} d\xi = \frac{-L}{\tan \gamma} \left. \frac{e^{-2ik\xi}}{2ik} \right|_0^\infty \quad (4.23)$$

Associating the edge contribution with the value at the lower limit (just as in the infinite cone case we obtain the "tip" contribution) we obtain

$$\hat{n}_0 \cdot \vec{f} = + \frac{L}{2ik \tan \gamma} . \quad (4.24)$$

Hence

$$\vec{H}^s = \frac{-L}{4\pi \tan \gamma} \frac{e^{+ikr}}{r} \hat{a} . \quad (4.25)$$

Now letting $L = a d\beta$, where $a =$ radius of base, and integrating around the base ($\hat{a} =$ constant vector), we have

$$\vec{H}^s = - \int_0^{2\pi} \frac{\hat{a} e^{+ikr}}{4\pi r \tan \gamma} a d\beta = \frac{-a \hat{a} e^{+ikr}}{2r \tan \gamma} \quad (4.26)$$

$$\begin{aligned} \sigma &= 4\pi r^2 \left| \frac{\vec{H}^s}{\vec{H}^i} \right|^2 \\ &= 4\pi r^2 \left| \frac{-ae^{+ikr}}{2r \tan \gamma} \hat{p} \right|^2 \\ &= \frac{a^2}{\tan^2 \gamma} \end{aligned} \quad (4.27)$$

But $\gamma = \frac{\pi}{2} - \alpha$ (see Fig. B-12) where α is half the cone angle; thus,

$$\begin{aligned} \tan \alpha &= \tan \left(\frac{\pi}{2} - \gamma \right) \\ &= \cot \gamma \end{aligned}$$

and finally

$$\sigma = \pi a^2 \tan^2 \alpha, \quad (4.28)$$

which is precisely the nose-on result obtained for the cone directly with physical optics.

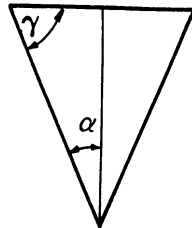


FIG. B-12: DEFINITIONS OF γ AND α

Now we are in a position to employ this technique to obtain a new finite cone result. We make use of the following expression for the electric field scattered by an infinite wedge:

$$\vec{E}^s = \frac{\sqrt{2\pi/kr}}{2(2\pi - \gamma)} e^{ikr + i\frac{\pi}{4}} \sin\left(\frac{2\pi}{2\pi - \gamma}\right) \left[\frac{E(a)\hat{\rho} - E(b)\hat{\beta}}{B} - \frac{E(a)\hat{\rho} + E(b)\hat{\beta}}{A} \right] \quad (4.29)$$

(Ref. B-17) where incidence is in a direction perpendicular to the edge of the wedge and

$E(a) = E_{\perp}^i$ = component of the incident field perpendicular to the edge of the wedge,

$E(b) = E_{\parallel}^i$ = component of the incident field parallel to the edge of the wedge,

$$A = \cos\left(\frac{2\pi\theta}{2\pi - \gamma}\right) + \cos\left(\frac{\pi}{2\pi - \gamma}\right)$$

$$B = 1 - \cos\left(\frac{\pi}{2\pi - \gamma}\right)$$

θ = angle of incidence measured from the bisector of the exterior angle of the wedge, and $\hat{\rho}$ and $\hat{\beta}$ are unit vectors perpendicular and parallel, respectively, to the edge of the wedge.

This expression is valid for an infinite wedge. In order to obtain an expression for a wedge of finite edge length, we again look at the current distribution integrals. We know that the integral over the edge length, will be, in the two-dimensional case,

$$\int_{-\infty}^{\infty} e^{ik\sqrt{r^2 + \zeta^2}} d\zeta \approx \sqrt{r\lambda} e^{i(kr + \frac{\pi}{4})} \quad (4.30)$$

and, in the three-dimensional case,

$$\int_0^L e^{ik\sqrt{r^2 + \zeta^2}} d\zeta \approx L e^{ikr}. \quad (4.31)$$

This is the only difference between the two- and three-dimensional problems so that the three-dimensional fields can be obtained from the two-dimensional fields by multiplying by

$$\frac{L e^{\frac{-\pi i}{4}}}{\sqrt{r\lambda}}.$$

Thus we obtain, for linear polarization, the following expression for the scattered field for a wedge of length L :

$$\vec{E}^s = \frac{L e^{ikr}}{2r(2\pi - \gamma)} \sin\left(\frac{\pi}{2\pi - \gamma}\right) \left[\frac{E(a)\hat{\rho} - E(b)\hat{\beta}}{B} - \frac{E(a)\hat{\rho} + E(b)\hat{\beta}}{A} \right]. \quad (4.32)$$

Again we are really considering the base of a cone and hence

$$\begin{aligned} \hat{\rho} &= -\hat{i}_x \cos \beta - \hat{i}_y \sin \beta \\ \hat{\beta} &= +\hat{i}_x \sin \beta - \hat{i}_y \cos \beta. \end{aligned}$$

\hat{E}^i , we recall, is equal to $-\hat{i}_x$, but

$$\hat{i}_x = -\hat{\rho} \cos \beta + \hat{\beta} \sin \beta.$$

Hence

$$E_{\perp}^i = \cos \beta \quad (4.33)$$

and

$$E_{\parallel}^i = -\sin \beta.$$

Thus, using these relations for E_{\perp}^i , E_{\parallel}^i , $\hat{\rho}$ and $\hat{\beta}$,

$$\begin{aligned} E_{\perp}^i \hat{\rho} - E_{\parallel}^i \hat{\beta} &= (\hat{\rho} \cos \beta + \hat{\beta} \sin \beta) \text{ which, in rectangular unit vectors, is} \\ &= -\hat{i}_x \cos 2\beta - \hat{i}_y \sin 2\beta, \end{aligned} \quad (4.34)$$

and similarly,

$$\begin{aligned} E_{\perp}^i \hat{\beta} + E_{\parallel}^i \hat{\rho} &= \hat{\rho} \cos \beta - \hat{\beta} \sin \beta, \text{ or simply} \\ &= -\hat{i}_x. \end{aligned} \quad (4.35)$$

Substituting in \vec{E}^S we obtain

$$\vec{E}^S = \frac{L e^{ikr}}{2r(2\pi - \gamma)} \sin\left(\frac{\pi}{2\pi - \gamma}\right) \left[\frac{\hat{i}_x \cos 2\beta + \hat{i}_y \sin 2\beta}{1 - \cos\left(\frac{\pi}{2\pi - \gamma}\right)} + \frac{\hat{i}_x}{\cos\left(\frac{2\pi\theta}{2\pi - \gamma}\right) + \cos\left(\frac{\pi}{2\pi - \gamma}\right)} \right]. \quad (4.36)$$

As before, we set ($L = a d\beta$) and integrate over β from 0 to 2π , obtaining

for the scattered field from the cone,

$$\vec{E}_{\text{cone}}^s = \frac{\pi a e^{ikr}}{r(2\pi - \gamma)} \sin\left(\frac{\pi^2}{2\pi - \gamma}\right) \frac{\hat{i}_x}{\cos\left(\frac{2\pi\theta}{2\pi - \gamma}\right) + \cos\left(\frac{\pi^2}{2\pi - \gamma}\right)}. \quad (4.37)$$

Now, using the following definition of σ ,

$$\sigma = \lim_{r \rightarrow \infty} 4\pi r^2 \left| \frac{\vec{E}^s}{\vec{E}^i} \right|^2$$

we obtain, remembering that $\theta = \pi/2 + \gamma/2$,

$$\sigma = \frac{4\pi^3 a^2}{(2\pi - \gamma)^2} \frac{\sin^2\left(\frac{\pi^2}{2\pi - \gamma}\right)}{\left[\cos\left(\frac{\pi^2}{2\pi - \gamma}\right) - \cos\left(\frac{3\pi^2}{2\pi - \gamma}\right) \right]^2}. \quad (4.38)$$

In terms of the cone angle α we have, since $\gamma = \frac{\pi}{2} - \alpha$,

$$\sigma = \frac{\pi^3 a^2}{(3\pi/2 + \alpha)^2} \operatorname{cosec}^2\left(\frac{4\pi^2}{3\pi + 2\alpha}\right). \quad (4.39)$$

This result is compared with the physical optics result in Figure B-13. The wedge solution must be restricted to cases where the ring singularity is dominant. As an example, for the cone with $ka \gg 1$, this obtains for α such that $kz_0 \gg 1$. Consider, for example, a cone-cylinder combination viewed nose-on (see Fig. B-14). The expression (4.37) still applies in this case, so that since $\theta = \gamma/2$ now, we have

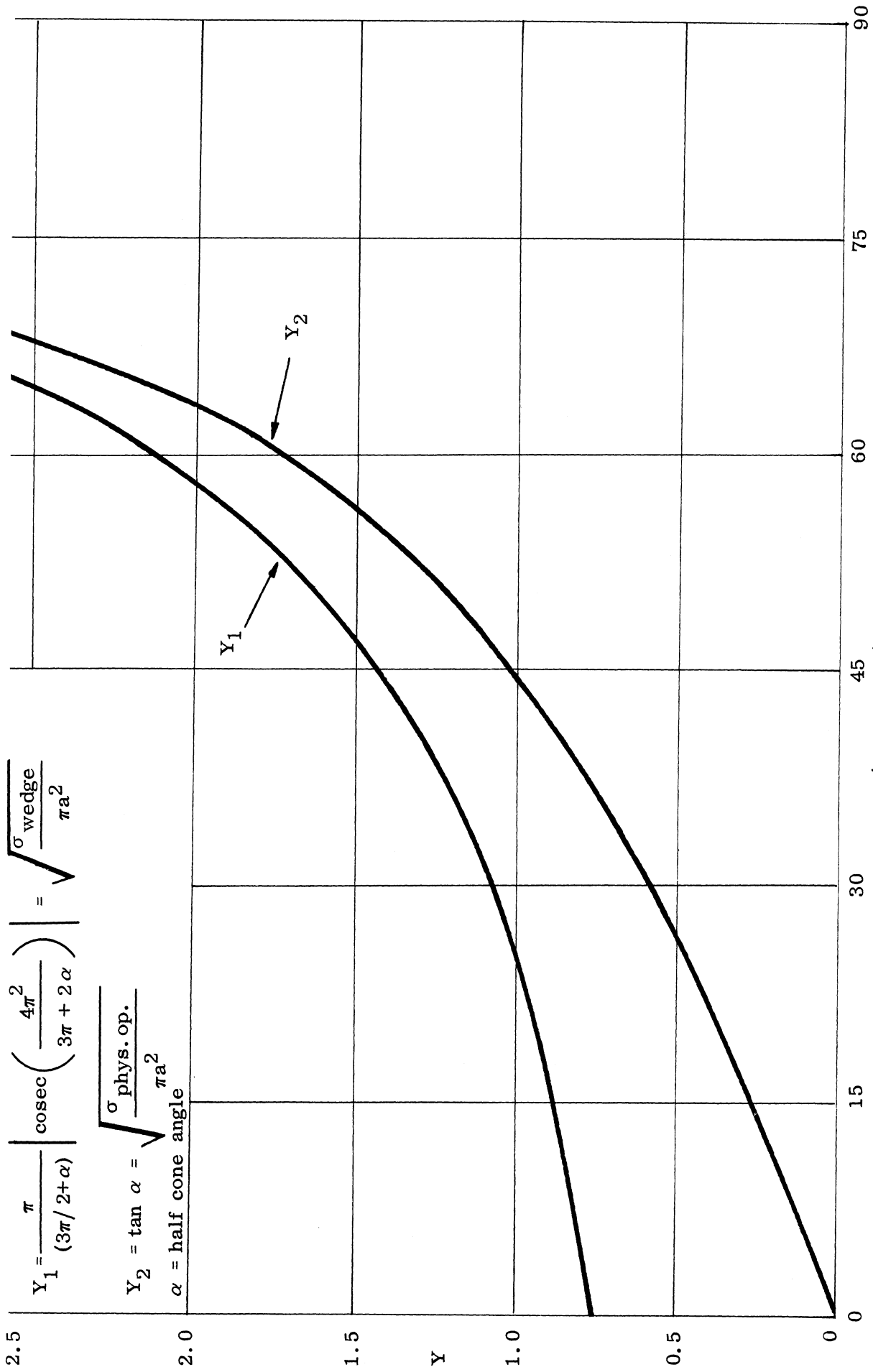


FIG. B-13: NOSE-ON FINITE CROSS SECTIONS AS COMPUTED BY PHYSICAL OPTICS AND CIRCULAR WEDGE APPROXIMATIONS

$$\frac{\sigma}{\pi a^2} = \frac{4\pi^2}{(2\pi - \gamma)^2} \frac{\sin^2 \left(\frac{\pi^2}{2\pi - \gamma} \right)}{\left[\cos \left(\frac{\pi^2}{2\pi - \gamma} \right) - \cos \left(\frac{2\pi^2}{2\pi - \gamma} \right) \right]^2} \quad (4.40)$$

In terms of the half cone angle, α , we have since $\alpha = \pi - \gamma$,

$$\frac{\sigma}{\pi a^2} = \frac{4\pi^2}{(\pi + \alpha)^2} \frac{\sin^2 \left(\frac{\pi^2}{\pi + \alpha} \right)}{\left[\cos \left(\frac{\pi^2}{\pi + \alpha} \right) - \cos \left(\frac{2\pi^2}{\pi + \alpha} \right) \right]^2} \quad (4.41)$$

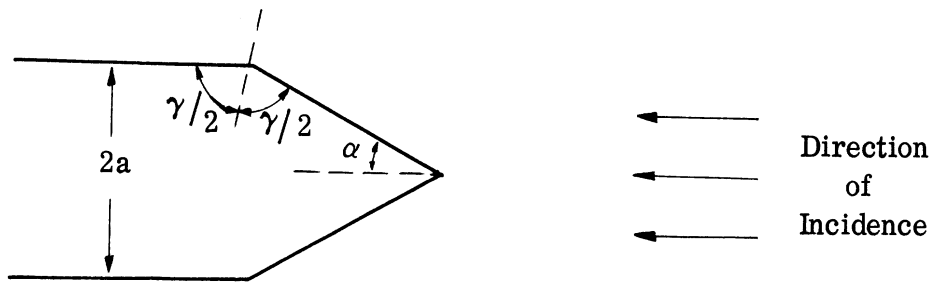


FIG. B-14: CONE-CYLINDER COMBINATION

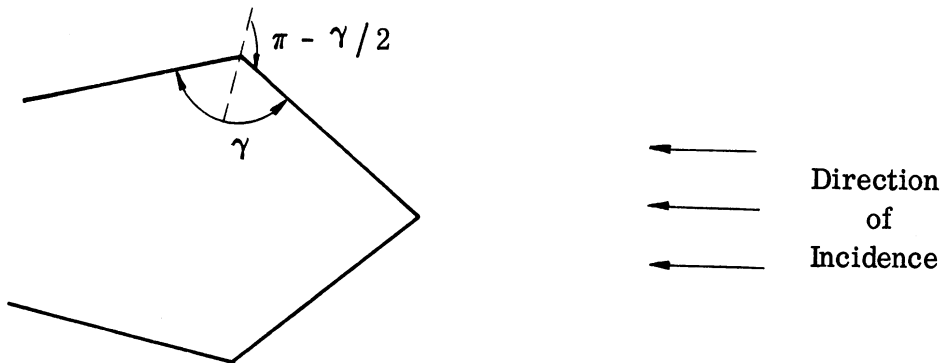


FIG. B-15: DEFINITION OF WEDGE ANGLE

Similarly, for the contribution from any ring singularity, equation (4.37)

holds where γ is the included wedge angle (Fig. B-15).

For $ka \gg 1$, $kz_0 \gg 1$ the ring singularity dominates. As kz_0 decreases with ka fixed the ring contribution diverges, approaching the first term of physical optics asymptotically; hence it is necessary to use physical optics for kz_0 small, i. e.,

$$\sigma \sim 4\pi \left[\frac{\pi a^2}{\lambda} \right]^2 .$$

Since the ring and first term physical optics are independent of wavelength (except for the implicit requirements $ka \gg 1$, $kz_0 \gg 1$), the graphing of the complete cross section dependence on cone angle (ka fixed) cannot be done in any two-dimensional curve without fixing λ .

A similar technique of decomposition into straight segments was employed by Artmann (Ref. B-15) in his solution of the problem of diffraction by a thick half-plane. He considered a half-plane of thickness $2a$ capped by a half-cylinder of radius a , as in Figure B-16. For $ka \gg 1$ and incidence as indicated he decomposed the cylindrical portion into a regular N -gon of length $L \gg \lambda$. Then by considering the conditions under which the rays striking near the apex S be diffracted onto the next side of the N -gon he determined the size of the penumbra region and hence the shift in the diffraction pattern as compared with the diffraction pattern of a completely black screen of like form. In order for rays diffracted from one polygonal face to have any effect on the next face, the following inequality must hold,

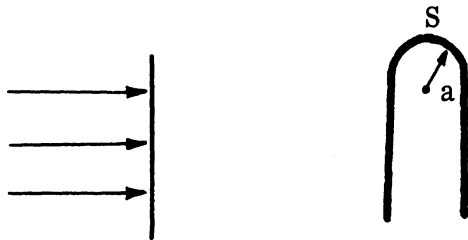


FIG. B-16: THICK HALF PLANE

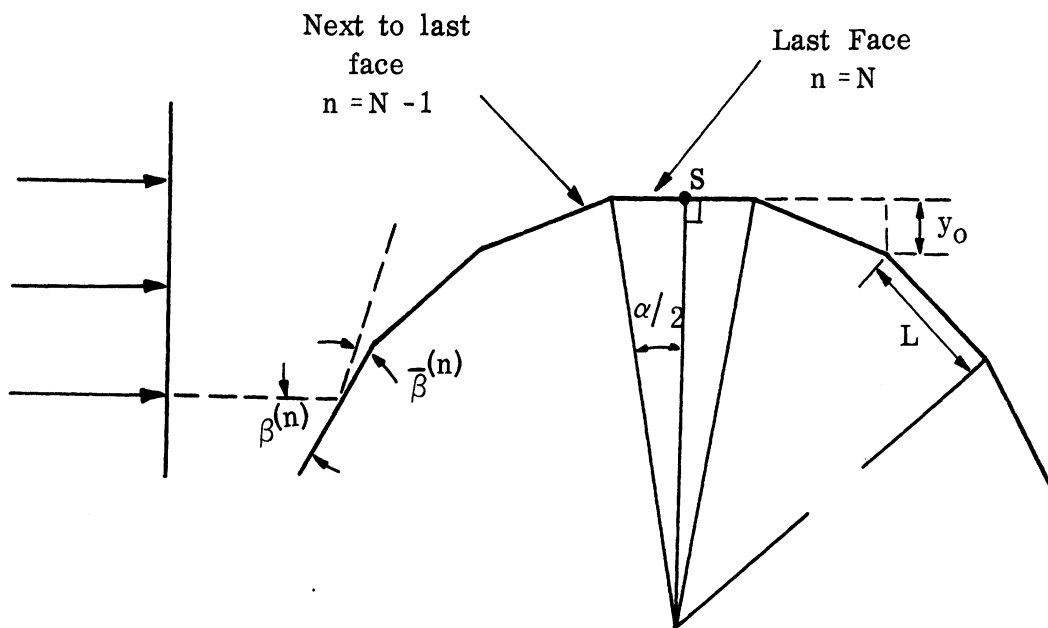


FIG. B-17: N-GON GEOMETRY

$$kL \left| \cos \beta^{(n)} - \cos \bar{\beta}^{(n)} \right| \lesssim 2\pi. \quad (4.42)$$

The quantities involved are shown in Figure B-17. To measure the penumbra width, or in this approximation the number and length of the polygonal sides that have any effect on succeeding sides, Artmann proceeds as follows. First he restricts the sides so that the only ones that affect the next one are the last and next to last where the last side contains the apex and naturally the next to last side immediately precedes it on the lit side (see Fig. B-17). In order that this be true

$$kL \left| \cos \beta^{(N-1)} - \cos \bar{\beta}^{(N-1)} \right| \approx 2\pi. \quad (4.43)$$

From Figure B-17 we see that

$$\beta^{(N-1)} = \alpha \quad (4.44)$$

Since the next to last face ($n = N-1$) is not affected by rays from the preceding face ($n = N-2$)

$$\bar{\beta}^{(N-1)} = 0.$$

Substituting these values in equation (4.43), (4.45) yields

$$kL \left| \cos \alpha - 1 \right| \approx 2\pi \quad (4.45)$$

but

$$\cos \alpha \approx 1 - \frac{\alpha^2}{2} \quad (4.46)$$

hence

$$kL \frac{\alpha^2}{2} \approx 2\pi. \quad (4.47)$$

Again referring to Figure B-17 we see that

$$\sin \frac{\alpha}{2} = \frac{L}{2a} \quad (4.48)$$

but

$$\sin \frac{\alpha}{2} \approx \frac{\alpha}{2} \quad (4.49)$$

hence

$$L \approx \alpha a \quad (4.50)$$

and

$$ka \alpha^3 \approx 4\pi \quad (4.51)$$

or

$$\alpha \approx \left(\frac{4\pi}{ka} \right)^{1/3} \quad (4.52)$$

Once more referring to Figure B-17 we see that

$$y_0 = L \sin \alpha \quad (4.53)$$

or employing the above results

$$y_0 \approx \alpha^2 a \approx \left(\frac{4\pi}{ka} \right)^{2/3} a. \quad (4.54)$$

Hence, reasons Artmann, the diffraction pattern of the thick screen is displaced by this distance, $\left(\frac{4\pi}{ka} \right)^{2/3} a$, perpendicular to the direction of

incidence as compared with the diffraction pattern of a completely black screen.

The above small wavelength approximations assist us in obtaining approximate far zone cross sections for many bodies of revolution. We must describe what can be done to obtain results in the resonance region.

THE RESONANCE REGION

To obtain answers for prolate spheroids when the radius of curvature at the tip ($\frac{b^2}{a}$) is small with respect to the wavelength and simultaneously when the wavelength is small with respect to the broadside radii of curvature, b and $\frac{a^2}{b}$, we must use another type of approximation. A point in electromagnetics is physically a region where all radii of curvature are small with respect to the wavelength. Thus the thin prolate spheroid looks very much like an ogive.

The approximate theory used by Belkina for thin spheroids, which she compares with her exact answers (Ref. B-18), and that used by Peters (Ref. B-19) for thin ogives, as one might expect, are for the problem under consideration almost equivalent. Belkina's approximate theory is a special case of Peters' more general considerations. However, she obtains physical information from exact theory, not obtained by Peters, on when the approximation is valid for spheroids.

For axially symmetric transmission, scattering from infinite cones is extremely small in all directions except the specular direction. Local analysis near the front tip and in the penumbra region for thin prolate spheroids or ogives (since the reradiation is tangent to the path) provides no big scattering effect except in the forward direction. A good portion of energy is guided towards the rear point and again there is, primarily, a reflection back. The

back flow of energy coming from the rear tip is again primarily in the forward direction (flow towards the front tip) which is in the direction back towards where it originally came from. Thus the backscattering near nose-on cross section of an ogive looks as if it is primarily due to the tip in the rear. This has been experimentally checked by Peters (Ref. B-19).

This suggested to Peters and Belkina that the thin body should act like a traveling wave antenna. Peters derives the results for certain ogives, and derives the cross section for such an antenna (both monostatic and bistatic) for aspects out to 40° off nose-on. The theory would fail exactly nose-on but provides excellent results for near nose-on aspects.

To illustrate the theory we shall concentrate on a specific example, the thin prolate spheroid with \vec{E} polarized field incident. The radar cross section of a long thin body is given by

$$\sigma = \frac{\gamma^2 \lambda^2}{\pi Q^2} \left\{ \frac{\sin \theta}{1 - p \cos \theta} \sin \left[\frac{kL}{2p} (1 - p \cos \theta) \right] \right\}^2 = \frac{\gamma^2 \lambda^2}{\pi Q^2} [f(\theta)]^2$$

where Q is given by

$$Q = -(2/p^2) + \frac{\text{Cin} [(kL/p)(1+p)] - \text{Cin} [(kL/p)(1-p)]}{p^3} + \frac{1}{2p^3} \left\{ (p-1)\cos [(kL/p)(1+p)] \right. \\ \left. + (p+1)\cos [(kL/p)(1-p)] + (p^2-1) \frac{kL}{p} \left(\text{Si} [(kL/p)(1+p)] - \text{Si} [(kL/p)(1-p)] \right) \right\}$$

with $\text{Cin}(x)$ being the modified cosine integral of argument x and Si the sine

integral. We see that there are three parameters besides the wavelength which serve to describe the body. They are the voltage reflection coefficients γ , the relative phase velocity p , and the length L .

Voltage reflection coefficients of thick ogives and thin rods have been experimentally determined by Peters who found that for a fairly thick ogive the reflection coefficient is about 0.7. For thin rods Peters found that the voltage reflection coefficient is about $1/3$. Physical reasoning indicates that the thin prolate spheroid, near nose-on, should be compared with a thin rod rather than an ogive and as a result for a thin prolate spheroid we use a voltage reflection coefficient of $1/3$. However, as θ increases from zero (the nose-on aspect), the point at which the traveling wave is reflected may be expected to move around the body and in this case will cause it to enter a region of larger radius of curvature. Thus we would expect the voltage reflection coefficient to increase to 1 as the aspect goes to broadside. The actual values used in the graph (Fig. B-18) are as given in the following table:

θ	$0^\circ - 40^\circ$	$40^\circ - 60^\circ$	$60^\circ - 75^\circ$
γ	0.33	0.7	1.0

The relative phase velocity (p) is defined as the ratio of the length of the body to that of the current path on the body. For this case it turns out that $p = 0.985$.

As the angle of incidence is increased from zero, a point is ultimately reached at which the traveling wave theory breaks down and the analogy with a thin wire is no longer possible. To deal with such values of θ (i.e., near broadside incidence) an alternative model is required. In this case the body is likened to a thick cylinder; the thick cylinder results are displayed for aspects in the range $\theta = 60^\circ$ to $\theta = 90^\circ$ in Figure B-18. The thick cylinder results are obtained from Reference B-20.

The excellent, but as yet unpublished, experimental results of J. Lotsof of the Cornell Aeronautical Laboratory are included in Figure B-18 for the purpose of comparison. Indeed, it was the existence of this experimental data which dictated the choice of the dimensions of the spheroid to be used in this illustrative example.

Before terminating this discussion of traveling wave theory, a few words about the \vec{H} polarization case for the same prolate spheroid are in order. At near nose-on incidence we should expect the same current to be induced, and thus the same cross section. However, with increasing θ , the spiralling of the current may be expected to lead to an appreciable reduction in the cross section; this has been confirmed by the above mentioned experiments.

Now we shall turn our attention to the problem of estimating the nose-on scattering cross section of thin finite cones for all values of ka .*

* The quantity "a" denotes the radius of the base of the cone and as usual $k = 2\pi/\lambda$.

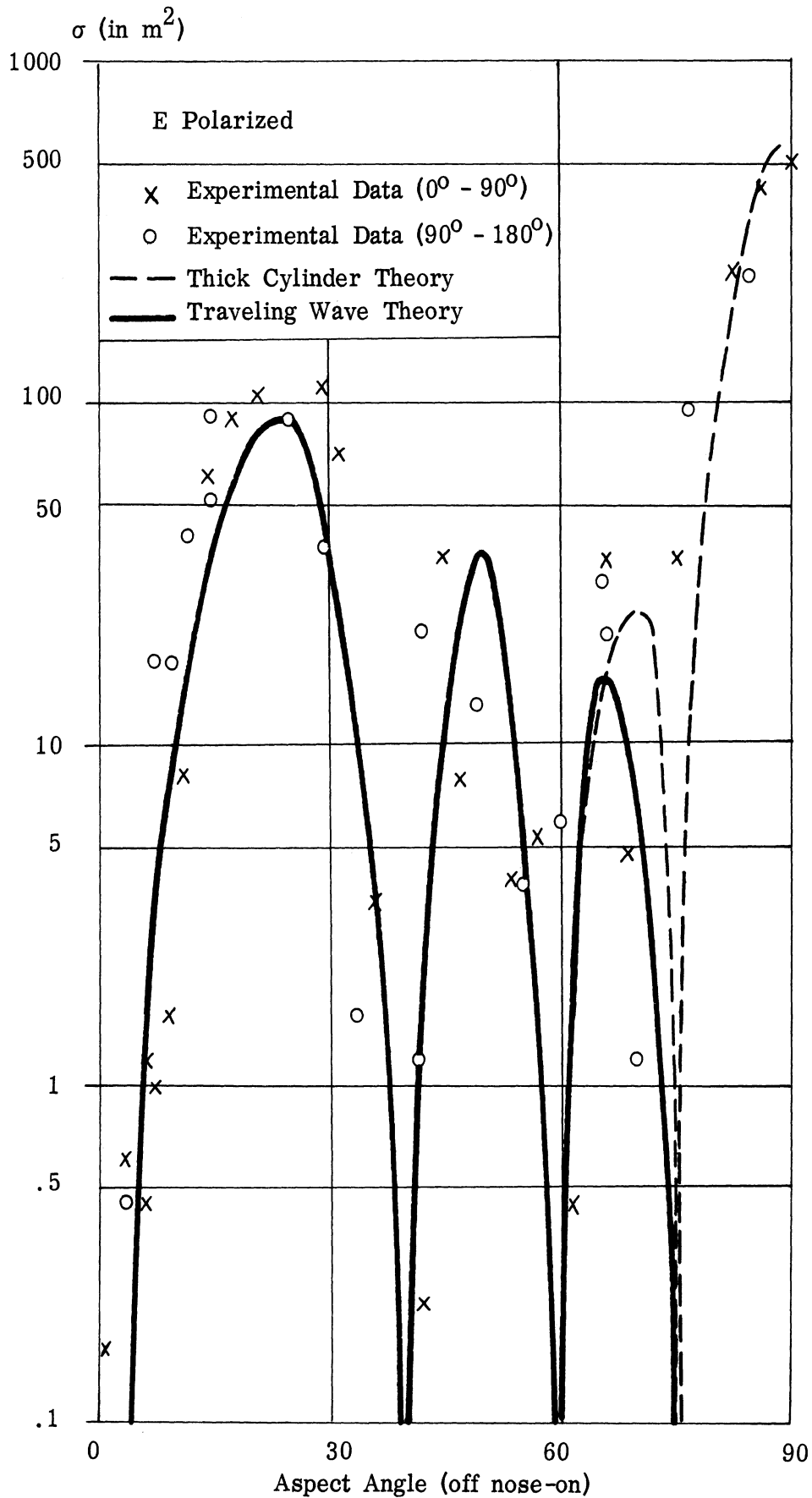


FIG. B-18: MONOSTATIC RADAR CROSS SECTION OF A 10:1 PROLATE SPHEROID WHICH IS $43 \text{ cm} = 4 \lambda$ IN LENGTH

We need the approximate behavior in the resonance region as we have already presented small and large wavelength approximations. This is obtained by assuming that the base is still the dominant feature as the resonance region is entered from the small wavelength side. The resonance maximum of the ring singularity would approximate, in both position and amplitude, the last large maximum of the cone. Since in any physically realizable situation, the edge of the base of a cone will have a non-zero radius of curvature, b , ($b \ll \lambda$), the only difference between it and a wire loop (wire radius $\ll \lambda$) relative to incident electromagnetic energy is that currents can exist "inside" the loop but not "inside" the base of the cone.

When one looks at the axially symmetric cross section of a ring as a function of wavelength, one finds that there are no minima. This then allows one to predict that the contribution of the inner edge is negligible in comparison to the outer edge when the wavelength is equal to the order of the loop radius but greater than the wire radius. (If there were non-negligible contributions from both the outer and inner edges, then at some wavelengths they would add in phase and at some wavelengths they would add out of phase. But there are no noticeable minima in this region!) Thus the cross section of a loop here looks like a Rayleigh type answer, depending only on the loop radius but not on the wire radius. This then, gives added justification for using an analogy between the conical base and the wire loop. Kouyoumjian's variational results (Ref. B-21) and Weston's exact results (Ref. B-22) for wire loops in the resonance region can then be utilized. Their results

(as a function of wire radius and loop radius) indicate that the resonant peak is fairly insensitive to changes in wire radius but that as the wavelength decreases the wire radius becomes important. However, when the wavelength decreases, we use the wedge approximation. There may be a region on the small wavelength side of the loop maximum where other, smaller in amplitude, maxima can occur. These lesser extrema are essentially averaged in this approximation.

On the Rayleigh side, we find that the Rayleigh line, which is an upper bound on the cross section, lies so close to the ring maximum (in fact may intersect the ring curve before the maximum) that the existence of any maxima greater than the ring maximum on the Rayleigh side is precluded. This is illustrated in the following figure (Fig. B-19) where the experimental results of S. Silver of the University of California, R. Kell of the Cornell Aeronautical Laboratory, and M. Ehrlich of the Microwave Radiation Company have been included for the purpose of comparison.

In order to obtain off-axis finite cone results and to check our assumptions concerning the different reflection coefficients at the two ends, we compare the off-axis results for the cone with the traveling wave antenna result. We add the Kirchhoff disc contribution to the results for backscattering near rear-on. These theoretical estimates are compared with the corresponding experimental data obtained by Ehrlich in Figures B-20 and B-21. We note that the null near the rear-on aspect is theoretically predicted to be too near to the $\theta = 180^\circ$ aspect. This could have been anticipated since we know from the resonance discussion of the importance of the disc contribution.

By using approximations based on a creeping wave type picture we augment the above theory for nose-on results where $f(\theta) = 0$. For ogives of $1/2$ angle α , $\alpha \leq 20^\circ$, and $ka \geq 15$ ($a = 1/2$ maximum minor dimension) we obtain a nose-on result of

$$\sigma(0) = \frac{\lambda^2 \tan^4 \alpha}{16 \pi} + \frac{a \lambda}{2} .$$

When the creeping wave contribution is negligible, then the $\frac{a \lambda}{2}$ augmentation disappears. This occurs for thick ogives. The above formula holds for all ogive experiments analyzed to date within a factor of two. A feeling for when to drop out the $\frac{a \lambda}{2}$ can be obtained from known sphere results.

The reader is now in a position to fill in roughly the complete cross section curves for ogives and spheroids.

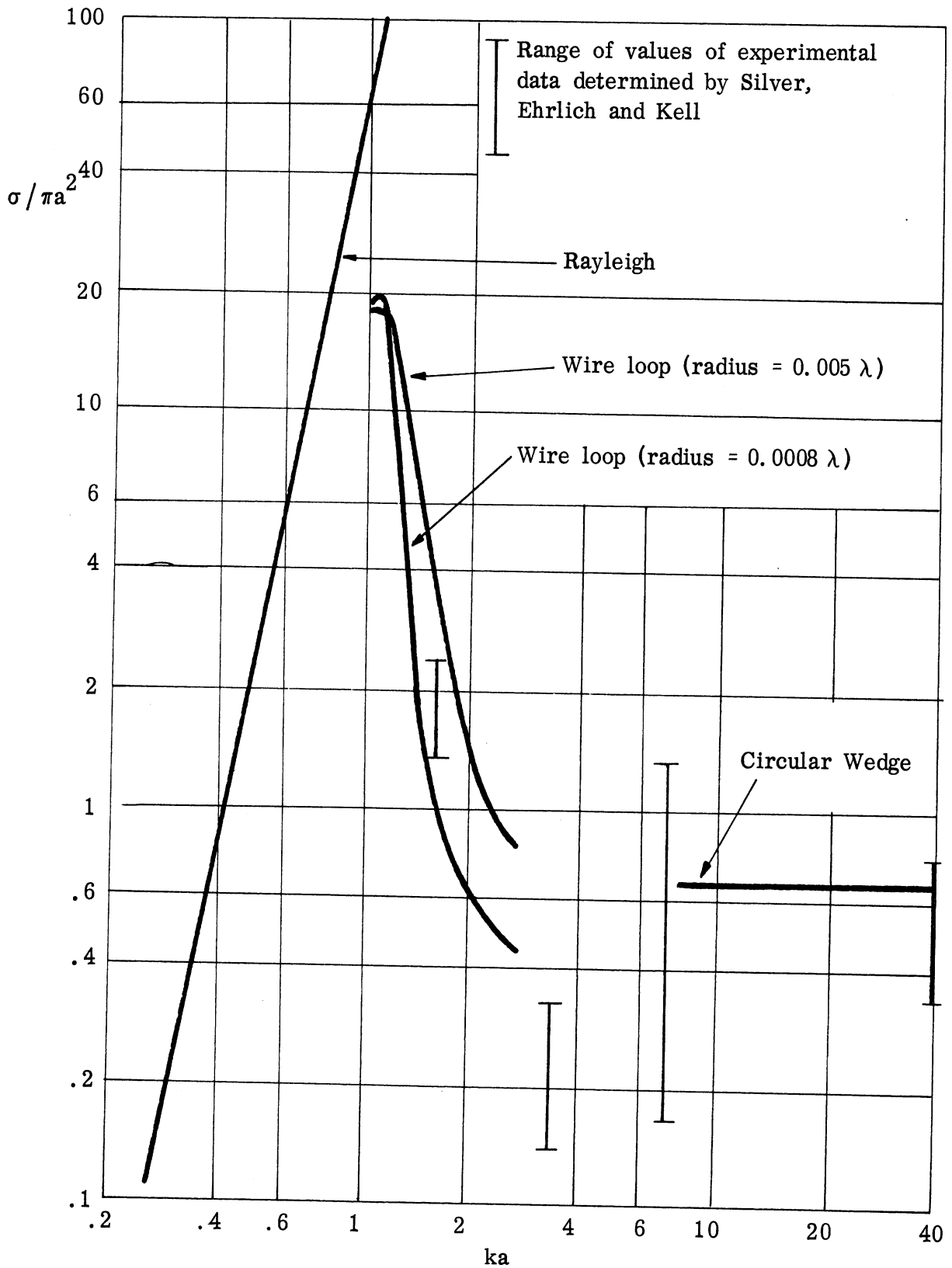


FIG. B-19: NOSE-ON CROSS SECTION OF THIN FINITE CONE ($\alpha = 7.5^\circ$)

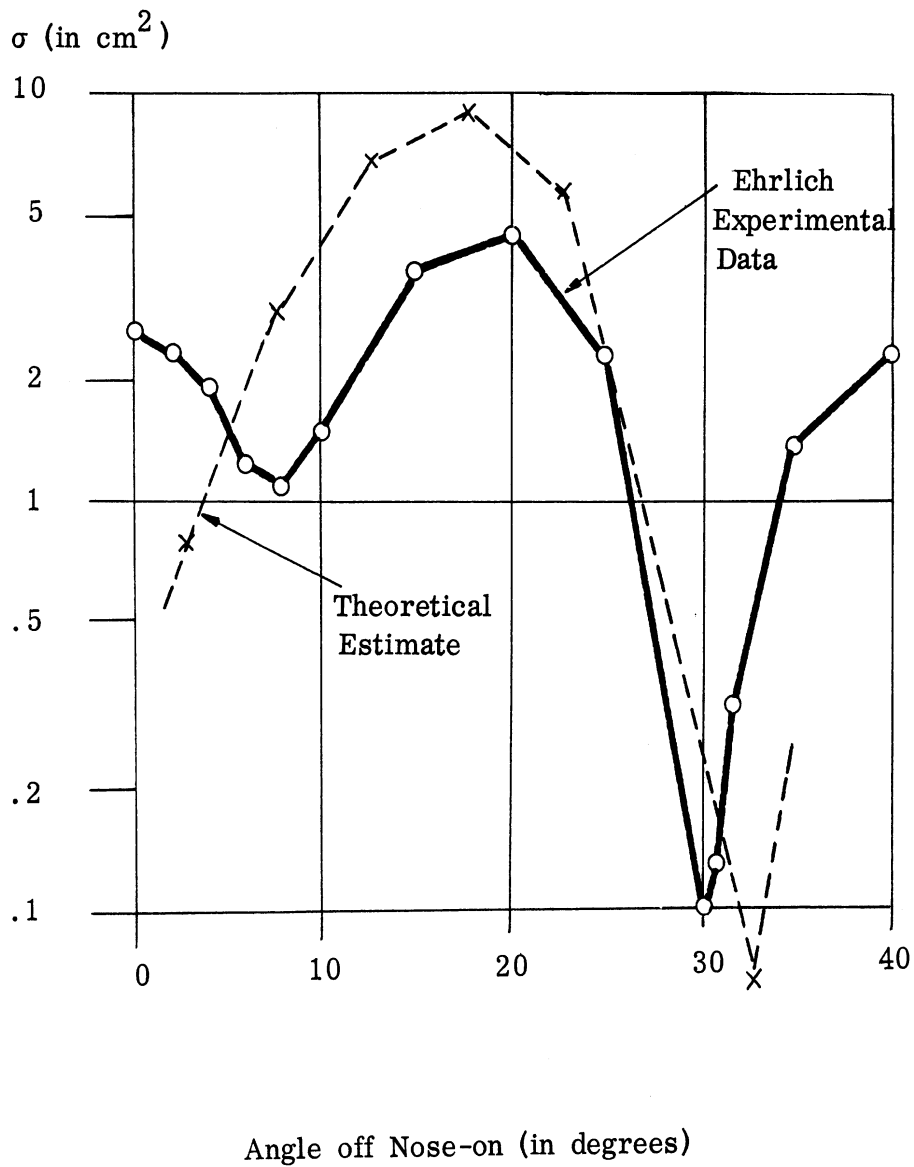


FIG. B-20: RADAR CROSS SECTION OF A FINITE CONE - A COMPARISON BETWEEN THEORY AND EXPERIMENT - I

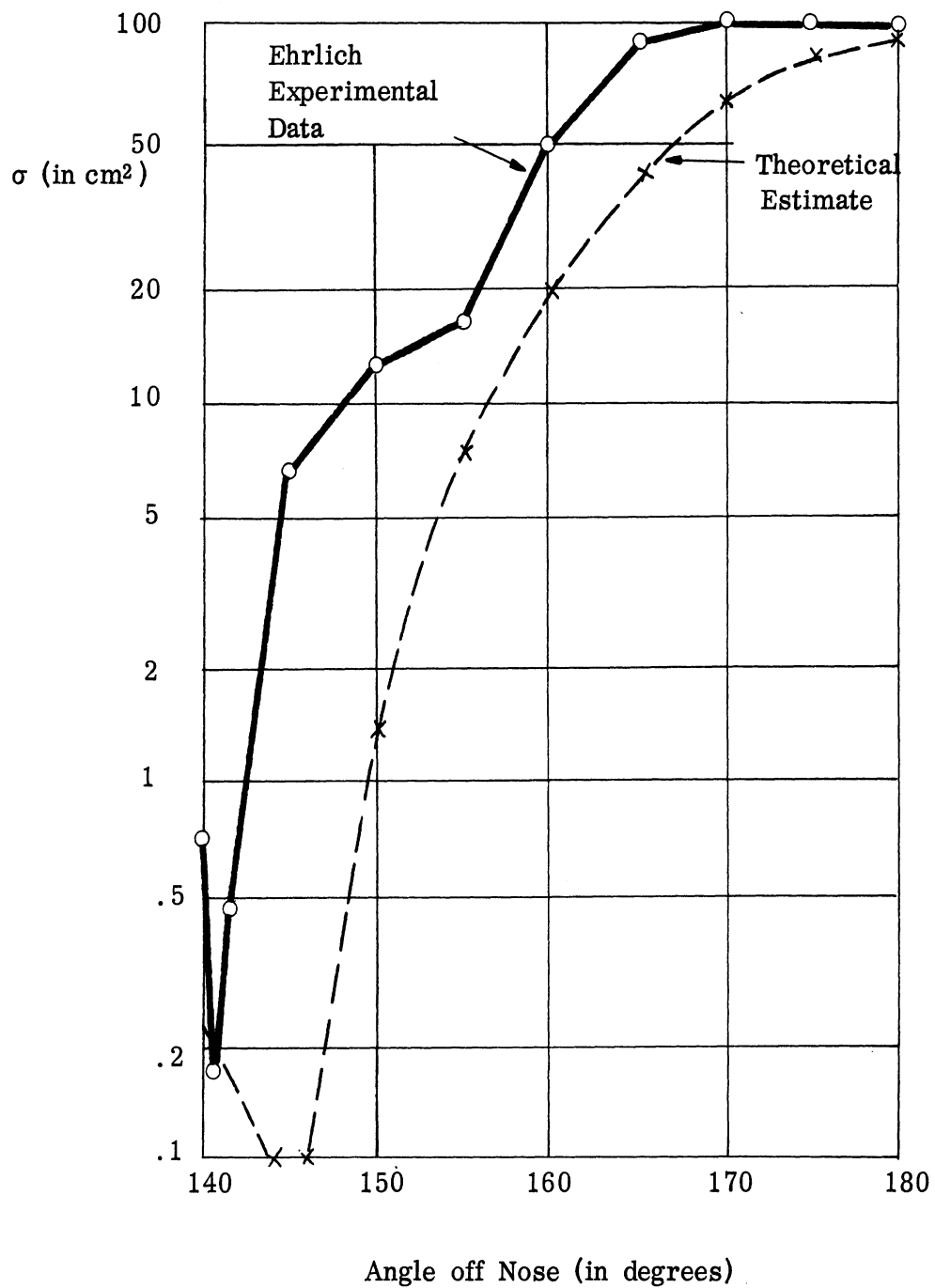


FIG. B-21: RADAR CROSS SECTION OF A FINITE CONE - A COMPARISON BETWEEN THEORY AND EXPERIMENT - II

REFERENCES

- B-1. J. W. Strutt, (Baron Rayleigh), "On the Incidence of Aerial and Electric Waves Upon Small Obstacles in the Form of Ellipsoids or Elliptic Cylinders and on the Passage of Electric Waves Through a Circular Aperture in a Conducting Screen", Phil. Mag., Vol. 44, 28, (1897).
- B-2. J. A. Stratton, Electromagnetic Theory, McGraw-Hill, New York, (1941).
- B-3. V. A. Fock, "The Field of a Plane Wave Near the Surface of a Conducting Body", Journal of Physics, Vol. X, No. 5, 399, (1946).
- B-4. S. O. Rice, "Diffraction of Plane Radio Waves by a Parabolic Cylinder-Calculation of Shadows Behind Hills", Bell Syst. Tech. J., Vol. XXXIII, 417, (1954).
- B-5. W. Franz, "On the Green's Functions of the Cylinder and the Sphere", Z. für Naturforschung, 9a, 705-716, (1954).
- B-6. J. B. Keller, "Diffraction by a Convex Cylinder", Trans. I.R.E., AP-4, 312, (1956).
- B-7. W. Franz, and K. Deppermann, "Theory of Diffraction By a Cylinder As Affected By the Surface Wave", Annalen der Physik, 10, 361 (1952).
- B-8. F. G. Friedlander, "Diffraction of Pulses by a Circular Cylinder", Comm. Pure and Appl. Math., VII, 705, (1954).
- B-9. T. T. Wu, "High Frequency Scattering", Phys. Rev., 104, 201, (1956).
- B-10. L. L. Bailin, "Field Produced by a Slot in a Large Circular Cylinder", IRE Trans. Antennas and Propagation, AP-3, 128-138, (1955).
- B-11. L. Wetzel, and D. B. Brick, "An Experimental Investigation of High-Frequency Current Distributions on Conducting Cylinders", Air Force Cambridge Research Center, Scientific Report No. 4, (Dec. 12, 1955).
- B-12. V. A. Fock, "Diffraction of Radio Waves Around the Earth's Surface", Journal of Physics, Vol. IX, No. 4, 255, (1945).
- B-13. M. G. Belkina, and L. A. Weinstein, "Radiation Characteristics of Spherical Surface Antennas", Appearing in Diffraction of Electromagnetic Waves on Certain Bodies of Rotation, Moscow, (1957).

- B-14. N. A. Logan, "The Role of Fock Functions in the Theory of Diffraction by Convex Surfaces", Air Force Cambridge Research Center, Paper presented at the URSI meeting held May 22-25, 1957, in Washington, D. C.
- B-15. K. Artmann, "Diffraction of Polarized Light by Screens of Finite Thickness in the Neighborhood of the Boundary of the Shadow", Zeitschrift für Physik, 127, 468-494, (1950).
- B-16. K. M. Siegel, H. A. Alperin, R. R. Bonkowski, J. W. Crispin, Jr., A. L. Maffett, C. E. Schensted, and I. V. Schensted, "Bistatic Radar Cross Sections of Surfaces of Revolution", Journal of Appl. Physics, Vol. 26, No. 3, 297-305, (March 1955).
- B-17. F. Oberhettinger, "Diffraction of Waves by a Wedge", Communications on Pure and Applied Math., Vol. VII, 551-563, (1954)
- B-18. M. G. Belkina, "Radiation Characteristics of an Elongated Rotary Ellipsoid", Appearing in Diffraction of Electromagnetic Waves On Certain Bodies of Revolution, Moscow, (1957).
- B-19. L. Peters, "End-Fire Echo Area of Long, Thin Bodies", IRE Transactions on Antennas and Propagation, Vol. AP-6, (Jan. 1958).
- B-20. J. R. Mentzer, Scattering and Diffraction of Radio Waves, Pergamon Press, (1955).
- B-21. R. Kouyoumjian, "The Back-Scattering From a Circular Loop", Appl. Sci. Res., B6, 165, (1956).
- B-22. V. H. Weston, Thesis, "Solutions of the Toroidal Wave Equation and Their Applications", University of Toronto, (1956).

APPENDIX C

CROSS SECTIONS OF CORNER REFLECTORS AND OTHER MULTIPLE SCATTERERS AT MICROWAVE FREQUENCIES

1

INTRODUCTION AND SUMMARY

If a body is not convex, radiation incident on it may be reflected a number of times from one part of the body to another before finally being reflected away from the body. These multiple reflections have an important effect on the radar cross section of a complicated body such as an airplane. Therefore, the following study of the radar cross sections of multiple scatterers at short wavelengths has been made. This paper presents a summary of known data on multiple scatterers, together with a few new formulas for special cases.

The best known and best understood example of a multiple scatterer is the corner reflector, which is widely used as a beacon and as a standard in experimental determinations of cross section. A corner reflector consists of sections of three mutually orthogonal planes, and has the characteristic property of giving a large monostatic cross section over a wide range of directions of incidence.*

A simple approximation to the bistatic cross section of a corner reflector is given in equations (2.1.5) and (2.1.6). An optical model to

* Certain closely related configurations are also commonly referred to as corner reflectors.

be used in conjunction with equation (2.1.5) for determining the monostatic cross section of a corner reflector is described in Section 2.2. Explicit expressions for the monostatic cross sections of square and triangular corner reflectors are given in Section 2.3. A study of the bistatic cross section of a square corner reflector with the transmitter on the axis of symmetry is made in Section 2.4. A discussion of the effects of constructional errors, compensation, and truncation is given in Section 2.5.

When the multiple scatterer has surfaces which are curved, the cross section may be obtained by applying equation (2.1.4). The application of this formula involves the geometrical optics approximation to the fields on the scattering surface and this is given in equation (3.1.1). In the special case when the radii of curvature of the scattering body are finite at all of the reflection points the cross section may be obtained by using equations (3.3.10) and (2.1.3). To illustrate the methods used, the cross sections of a biconical reflector and of a pair of spheres are obtained (Sec. 3.2 and 3.4).

A sampling of experimental data on corner reflectors is quoted in Section 4. The authors wish to express their appreciation for the kind permission of the Bell System Technical Journal to reproduce Figures C-16-C-20, and of Dr. R. D. O'Neal to reproduce Figures C-14 and C-15 and the figures in this appendix.

THE CORNER REFLECTOR*

2.1 Analytical Method for Determining the Radar Cross Section of the Corner Reflector

Although the simplest method for obtaining radar cross sections is the method of geometrical optics (References C-1 and C-2), this method is not directly applicable to corner reflectors because it predicts that the radar cross section is infinite in the directions in which radiation is specularly reflected and zero elsewhere. More explicitly, for a scattering body consisting only of plane surfaces, geometric optics predicts that the incident radiation is scattered into a region which, at large distances from the body, subtends a vanishingly small solid angle. Actually the radiation must be spread by diffraction over a region of solid angle $(\lambda/h)^2$ where λ is the wavelength of the radiation and h is the characteristic dimension of the body. Near the body this objection no longer exists so that geometrical optics can be used to obtain the fields on the surface of the scatterer when $\lambda \ll h$. When the magnetic field is known on the surface of a perfectly conducting body the following formula (Reference C-3, page 466) can be used to obtain the scattered magnetic field at any point in space:

$$\vec{H}_s = \frac{1}{4\pi} \int_{S'} (\hat{n} \times \vec{H}) \times \nabla \frac{e^{ikR}}{R} ds' \quad (2.1.1)$$

* Much of the material presented in this section appears in Reference C-4.

where \vec{H} is the magnetic field on the surface of integration,

\vec{H}_s is the scattered magnetic field,

\hat{n} is the outward unit normal to the surface,

$k = 2\pi/\lambda$,

R is the distance between the integration point and the field point.

The integration is performed over the illuminated surface, S' , of the body.

When the field point is at a large distance from the body, (2.1.1) can be approximated by

$$\vec{H}_s \approx \frac{ik}{4\pi} \frac{e^{-ikr}}{r} \int_{S'} (\hat{n} \times \vec{H}) \times \hat{r} e^{-ik\hat{r} \cdot \vec{r}'} dS' \quad (2.1.2)$$

where \hat{r} is the unit vector from the origin to the field point,

r is the distance from the origin to the field point, and

\vec{r}' is the radius vector from the origin to the integration point.

In this report the radar cross section σ is defined as

$$\sigma = \lim_{r \rightarrow \infty} 4\pi r^2 \left| \frac{\vec{H}_s}{\vec{H}_i} \right|^2 \quad (2.1.3)$$

where \vec{H}_i is the incident magnetic field. Throughout this paper $|\vec{H}_i|$ is

taken to be unity. In view of (2.1.2), (2.1.3) can be written as

$$\sigma = \frac{\pi}{\lambda^2} \left| \int_{S'} (\hat{n} \times \vec{H}) \times \hat{r} e^{-ik\hat{r} \cdot \vec{r}'} dS' \right|^2. \quad (2.1.4)$$

The integral in (2.1-4) is an elementary one since the surfaces are planes and the magnetic field on the surface is obtained by geometric optics.

However, these integrals are usually tedious to evaluate and provide more information than is required in most applications.

The scattered energy is concentrated in a number of beams, each of which is centered about a specular reflection direction. Ordinarily the most important information is the maximum radar cross section for each beam and the half-power widths of each beam. The evaluation of the part of (2.1.4) that corresponds to a particular beam gives nearly the same result as would be obtained for diffraction at normal incidence through an aperture having the shape of the projection of the part of the corner* that reflects rays in the direction of the beam. Therefore, the maximum radar cross section for each beam is approximately:

$$\sigma = 4\pi A^2 / \lambda^2 \quad (2.1.5)$$

where A is the area of the above-mentioned aperture.

The angle $\delta \psi$ between the beam direction and the direction in which the radar cross section has decreased by a factor of two is approximately (Ref. C-4)

$$\delta \psi = 7.5^\circ \lambda / B \quad (2.1.6)$$

where B is the radius of gyration of the aperture taken about an axis through the center of gravity of the aperture and perpendicular to the plane in which the deviation from the center of the beam is taken.

2.2 An Optical Model for Corner Reflectors

One of the beams in which the scattered energy is concentrated is

* It should be noted that the effective aperture area used here is not necessarily the same as the projected area which is used in a similar formula for the forward scattering cross section.

reflected back toward the transmitter. The value of A for this beam determines the monostatic cross section through (2.1.5). The task of obtaining A analytically can be avoided by use of an optical model which, looked at from any direction, presents an aperture whose projected area is A .

Such an optical model can be constructed by cutting appropriate openings in three mutually orthogonal opaque sheets (Ref. C-4 and C-5). For the corner reflector in Figure C-1, the openings are as shown in Figure C-2. Each of the three apertures shown in Figure C-2 is obtained by cutting one of the faces of the corner reflector out of each of the four quadrants so as to give a symmetrical figure. Figure C-3 shows the optical model consisting of the three apertures of Figure C-2. An optical model for any corner reflector can be constructed in precisely the same manner.

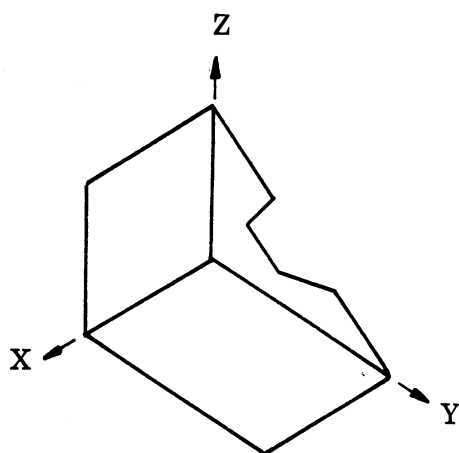


FIG. C-1: A CORNER REFLECTOR

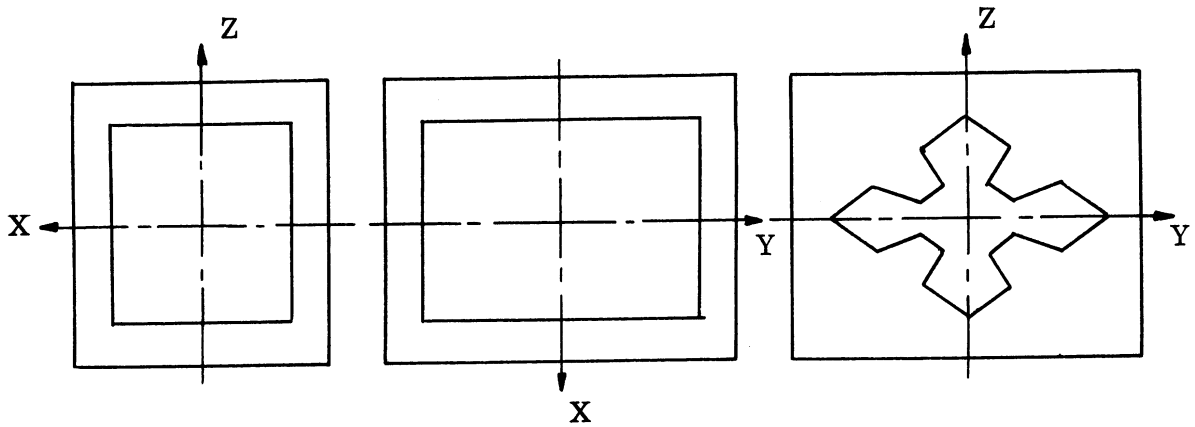
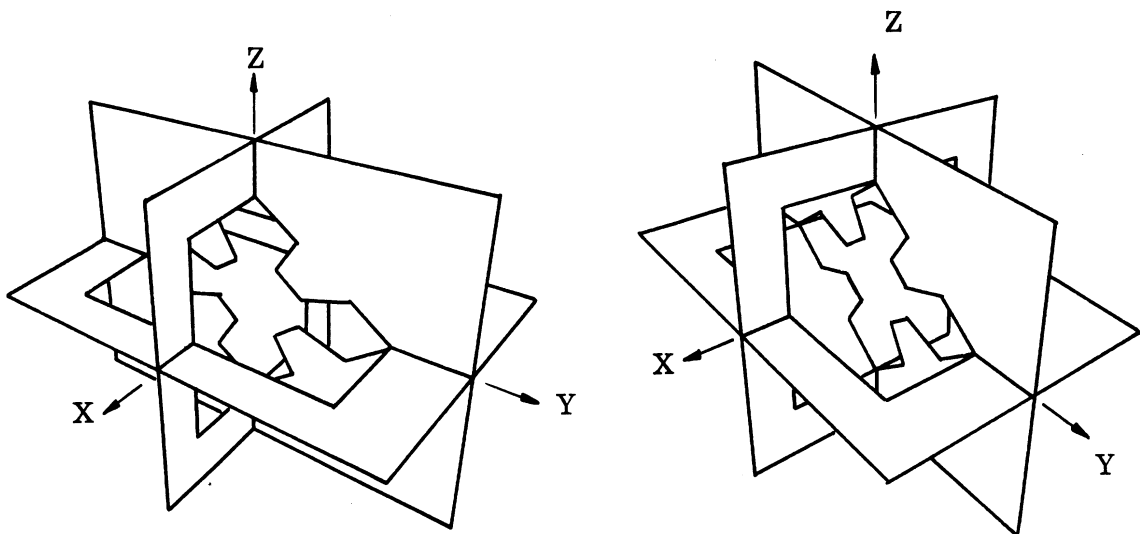


FIG. C-2: APERTURES IN OPTICAL MODEL OF CORNER REFLECTOR

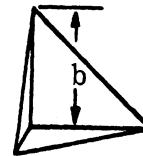
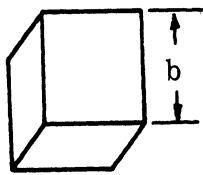


The two views form a stereo pair. A three dimensional effect may be obtained by focusing the right eye on the right view, the left eye on the left view, and then superposing the images. Alternatively a standard stereoscopic viewer may be used.

FIG. C-3: OPTICAL MODEL OF CORNER REFLECTOR

2.3 Monostatic Cross Section of Square and Triangular Corner Reflectors

In Reference C-4, the value of A for the beam reflected towards the transmitter has been determined analytically for both square and triangular corner reflectors (Fig. C-4).



Square Corner Reflector

Triangular Corner Reflector

FIG. C-4: SQUARE AND TRIANGULAR CORNER REFLECTORS

The value of A is expressed most simply in terms of the cosines of the angles between the axes of the corner reflector and the direction to the transmitter. If these cosines are $l \leq m \leq n$, then A is given by:

For a Square Corner Reflector:

$$\begin{aligned}
 A &= 4lm b^2 / n, \quad (m \leq n/2) \\
 A &= l \left(4 - \frac{n}{m}\right) b^2, \quad (m \geq n/2)
 \end{aligned}
 \tag{2.3.1}$$

For a Triangular Corner Reflector:

$$\begin{aligned}
 A &= 4 \frac{lm}{l+m+n} b^2, \quad (l+m \leq n) \\
 A &= \left(l+m+n - \frac{2}{l+m+n}\right) b^2, \quad (l+m \geq n).
 \end{aligned}
 \tag{2.3.2}$$

The transmitter direction making equal angles with the three axes is a symmetry axis for square and triangular corner reflectors. If δ is the angle, in degrees, between this symmetry axis and the direction to the transmitter, then, for small δ , A is given by:

For a Square Corner Reflector:

$$A \simeq \sqrt{3} (1 - 0.0274 \delta^2) b^2 \quad (2.3.3)$$

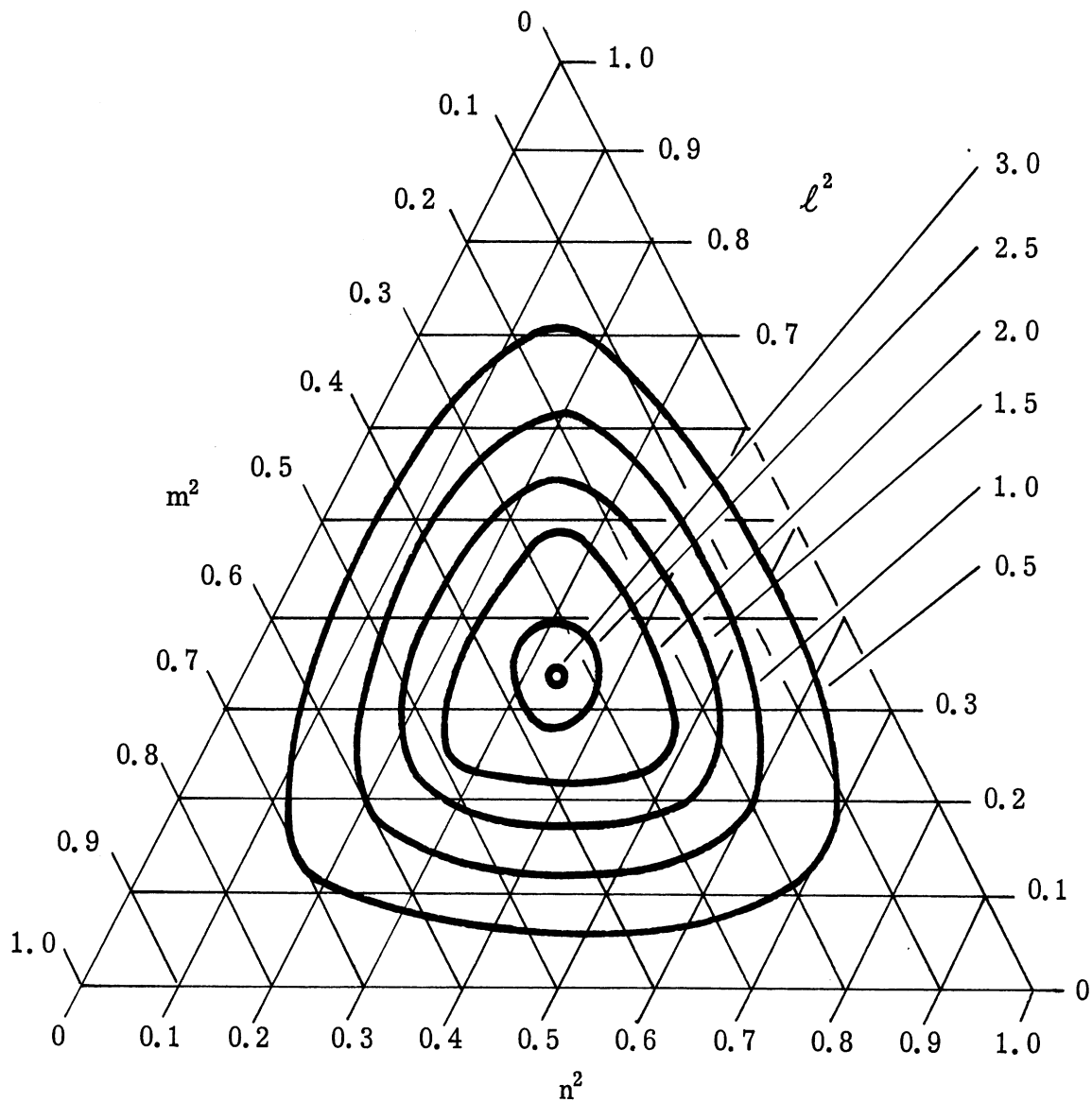
For a Triangular Corner Reflector:

$$A \simeq (1/\sqrt{3}) (1 - 0.00076 \delta^2) b^2. \quad (2.3.4)$$

From these equations and from (2.1.5) it follows that the dimensionless quantity $\sigma \lambda^2 / 4\pi b^4 = A^2 / b^4$ depends only on the direction to the transmitter. Curves of constant A^2 / b^4 are plotted in Figure C-5 for a square corner reflector using the trilinear coordinates ℓ^2 , m^2 , and n^2 . As can be seen from (2.1.5), (2.3.3), and (2.3.4) the maximum values of σ for square and triangular corner reflectors are $12 \pi b^4 / \lambda^2$ and $4\pi b^4 / 3\lambda^2$ respectively.

2.4 Bistatic Cross Section of a Square Corner Reflector for the Symmetric Case

The analytic methods described in Section 2.1 are applicable to both the monostatic and bistatic cross section problems by a suitable choice of the radius vector from the body to the field point. To illustrate the procedure for computing the bistatic cross section, consider the case of a square corner reflector of side length b . The orientation of the transmitter is as indicated in Figure C-6. The receiver is restricted to the first octant ($x \geq 0$, $y \geq 0$, $z \geq 0$).



The curves drawn here are for $\frac{\sigma \lambda^2}{4\pi b^4} = \text{constant}$

FIG. C-5: THE MONOSTATIC RADAR CROSS SECTION OF A SQUARE CORNER REFLECTOR

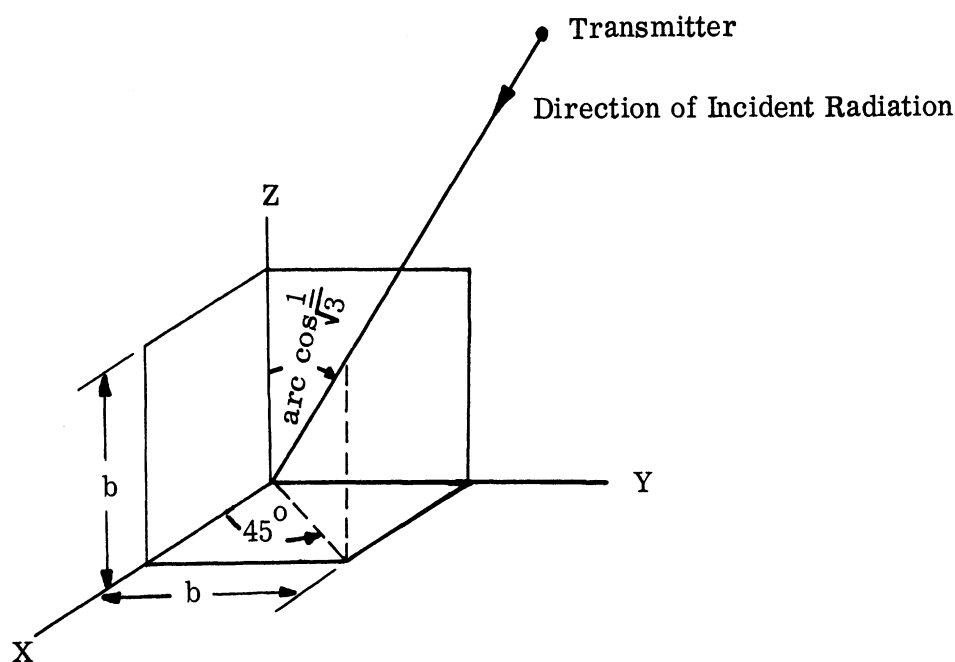


FIG. C-6: TRANSMITTER ORIENTATION FOR THE SYMMETRIC BISTATIC CASE

When the wavelength of the incident radiation is less than the side length b , the radar cross section is determined almost entirely by the triply reflected radiation. Thus to apply (2.1.1) it is only necessary to obtain the magnetic field \vec{H} for the triply reflected rays. Consider a ray reflected first from the x -plane, then from the y -plane, and finally from the z -plane, and let the incident magnetic field be

$$\vec{H}_i = \hat{a} e^{-i\omega \left(t - \frac{\hat{k} \cdot \vec{r}'}{c} \right)} \quad (2.4.1)$$

where \hat{a} is a unit vector. Suppressing the time factor $e^{-i\omega t}$, the magnetic field along the ray going from the y - z plane to the x - z plane is

$$\left[\hat{\mathbf{a}} - 2 (\hat{\mathbf{a}} \cdot \hat{\mathbf{i}}_x) \hat{\mathbf{i}}_x \right] e^{\left\{ ik \left[\hat{\mathbf{k}} - 2 (\hat{\mathbf{k}} \cdot \hat{\mathbf{i}}_x) \hat{\mathbf{i}}_x \right] \cdot \vec{\mathbf{r}} \right\}}, \quad (2.4.2)$$

where $\hat{\mathbf{i}}_x$ is the unit vector in the x direction. The magnetic field along the ray going from the x-z plane to the x-y plane is

$$\left[-\hat{\mathbf{a}} + 2 (\hat{\mathbf{a}} \cdot \hat{\mathbf{i}}_z) \hat{\mathbf{i}}_z \right] e^{\left\{ -ik \left[\hat{\mathbf{k}} + 2 (\hat{\mathbf{k}} \cdot \hat{\mathbf{i}}_z) \hat{\mathbf{i}}_z \right] \cdot \vec{\mathbf{r}} \right\}} \quad (2.4.3)$$

On the x-y plane $\vec{\mathbf{r}}' = x\hat{\mathbf{i}}_x + y\hat{\mathbf{i}}_y$, so that $\hat{\mathbf{i}}_z \cdot \vec{\mathbf{r}}' = 0$. If $\hat{\mathbf{n}}$ is a unit vector normal to this surface, then

$$\hat{\mathbf{n}} \times \vec{\mathbf{H}} = -2 \left(\hat{\mathbf{i}}_z \times \hat{\mathbf{a}} \right) e^{\left\{ -ik (\hat{\mathbf{k}} \cdot \vec{\mathbf{r}}) \right\}} \quad (2.4.4)$$

In general, for triply reflected radiation,

$$\hat{\mathbf{n}} \times \vec{\mathbf{H}} = -2 (\hat{\mathbf{n}} \times \hat{\mathbf{a}}) e^{\left\{ -ik (\hat{\mathbf{k}} \cdot \vec{\mathbf{r}}) \right\}} \quad (2.4.5)$$

on the scattering surface.

It is still necessary to determine how much of the corner is illuminated by such triply reflected radiation. A consideration of the optical model shows that the entire corner is illuminated for the transmitter orientation of Figure C-6. For orientations of the transmitter other than that in Figure C-6, the corner is not entirely illuminated. However, these orientations present no new problems, since the part of the corner that is illuminated in these cases may also be found from the optical model.

From (2.1.4) and (2.4.5) the cross section of the corner reflector is

$$\begin{aligned} \sigma = \frac{4\pi}{\lambda^2} & \left| \int_0^b \int_0^b (\hat{i}_z \times \hat{a}) \times \hat{r} e^{-ik(\hat{k} + \hat{r}) \cdot \hat{r}'} dx dy \right. \\ & + \int_0^b \int_0^b (\hat{i}_y \times \hat{a}) \times \hat{r} e^{-ik(\hat{k} + \hat{r}) \cdot \hat{r}'} dz dx \\ & \left. + \int_0^b \int_0^b (\hat{i}_x \times \hat{a}) \times \hat{r} e^{-ik(\hat{k} + \hat{r}) \cdot \hat{r}'} dy dz \right|^2 \end{aligned} \quad (2.4.6)$$

Let $\hat{r} = r_x \hat{i}_x + r_y \hat{i}_y + r_z \hat{i}_z$, $\hat{k} + \hat{r} = E\hat{i}_x + F\hat{i}_y + G\hat{i}_z$, and $\hat{a} = a_x \hat{i}_x + a_y \hat{i}_y + a_z \hat{i}_z$.

In this notation (2.4.6) becomes

$$\begin{aligned} \sigma = \frac{4\pi}{\lambda^2} & \left| \left[r_z a_x \hat{i}_x + r_z a_y \hat{i}_y - (r_x a_x + r_x a_y) \hat{i}_z \right] \int_0^b \int_0^b e^{-ik(Ex + Fy)} dx dy \right. \\ & + \left[r_x a_y \hat{i}_y + r_x a_z \hat{i}_z - (r_y a_y + r_z a_z) \hat{i}_x \right] \int_0^b \int_0^b e^{-ik(Fy + Gz)} dy dz \\ & \left. + \left[r_y a_z \hat{i}_z + r_y a_x \hat{i}_x - (r_z a_z + r_x a_x) \hat{i}_y \right] \int_0^b \int_0^b e^{-ik(Gz + Ex)} dz dx \right|^2. \end{aligned} \quad (2.4.7)$$

After performing the integration, (2.4.7) becomes

$$\begin{aligned}
\sigma = \frac{\lambda^2}{4\pi^3} & \left| \left[r_{z x x} \hat{i}_z + r_{z y y} \hat{i}_z - (r_{x x x} + r_{y y y}) \hat{i}_z \right] \frac{e^{-ikb(E+F)} - e^{-ikbE} - e^{-ikbF} + 1}{EF} \right. \\
& + \left[r_{x y y} \hat{i}_y + r_{x z z} \hat{i}_z - (r_{y y y} + r_{z z z}) \hat{i}_x \right] \frac{e^{-ikb(F+G)} - e^{-ikbG} - e^{-ikbE} + 1}{FG} \\
& \left. + \left[r_{y z z} \hat{i}_z + r_{y x x} \hat{i}_x - (r_{z z z} + r_{x x x}) \hat{i}_y \right] \frac{e^{-ikb(G+E)} - e^{-ikbG} - e^{-ikbE} + 1}{GE} \right|^2 .
\end{aligned} \tag{2.4.8}$$

To simplify (2.4.8), the following condensation symbols are introduced.

$$\begin{aligned}
c_1 &= \frac{\cos kb(F+G) - \cos kbF - \cos kbG - 1}{FG} , \\
c_2 &= \frac{\cos kb(G+E) - \cos kbG - \cos kbE - 1}{GE} , \\
c_3 &= \frac{\cos kb(E+F) - \cos kbE - \cos kbF - 1}{EF} , \\
s_1 &= \frac{\sin kb(F+G) - \sin kbF - \sin kbG}{FG} , \\
s_2 &= \frac{\sin kb(G+E) - \sin kbG - \sin kbE}{GE} , \\
s_3 &= \frac{\sin kb(E+F) - \sin kbE - \sin kbF}{EF} ,
\end{aligned} \tag{2.4.9}$$

In this notation, the radar cross section of the square corner reflector for

the symmetric case is given by

$$\begin{aligned}
 \sigma = \frac{\lambda^2}{4\pi^3} & \left\{ \left[\begin{aligned} & -(r_{yy}^a + r_{zz}^a) c_1 + r_{yx}^a c_2 + r_{zx}^a c_3 \end{aligned} \right]^2 \right. \\
 & + \left[\begin{aligned} & r_{xy}^a c_1 - (r_{xx}^a + r_{zz}^a) c_2 + r_{zy}^a c_3 \end{aligned} \right]^2 \\
 & + \left[\begin{aligned} & r_{xz}^a c_1 + r_{yz}^a c_2 - (r_{xx}^a + r_{yy}^a) c_3 \end{aligned} \right]^2 \\
 & + \left[\begin{aligned} & -(r_{yy}^a + r_{zz}^a) s_1 + r_{yx}^a s_2 + r_{zx}^a s_3 \end{aligned} \right]^2 \\
 & + \left[\begin{aligned} & r_{xy}^a s_1 - (r_{xx}^a + r_{zz}^a) s_2 + r_{zy}^a s_3 \end{aligned} \right]^2 \\
 & \left. + \left[\begin{aligned} & r_{xz}^a s_1 + r_{yz}^a s_2 - (r_{xx}^a + r_{yy}^a) s_3 \end{aligned} \right]^2 \right\}.
 \end{aligned} \tag{2.4.10}$$

This formula gives the radar cross section for any polarization of the incident electromagnetic wave. To show how the bistatic radar cross section varies as a function of receiver position for this symmetric case, (2.4.10) has been plotted in Figures C-8, C-9, C-10, and C-11 for a corner reflector of side length $b = 25$ cm., for three values of wavelength, and for the incident magnetic field vector parallel to one of the coordinate surfaces, that is

$$\hat{a}_H = -\frac{\hat{i}_x}{\sqrt{2}} + \frac{\hat{i}_y}{\sqrt{2}}.$$

The polar angles designating receiver position are indicated in Figure C-7.

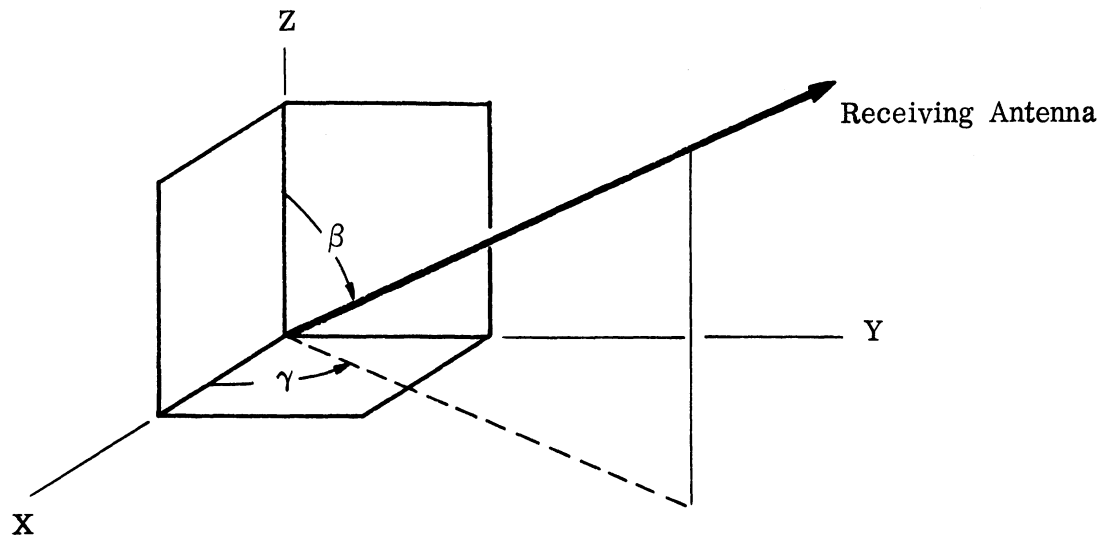


FIG. C-7: POLAR ANGLES β AND γ DESCRIBING RECEIVER POSITION

Figure C-8 shows the variation of σ with γ for $\beta = 54.74^\circ$ and for wavelengths of 3, 10, and 30 cm. The variation of σ with β for a wavelength of 3 cm, and $\gamma = 15^\circ$, 30° , and 45° is shown in Figure C-9. The $\gamma = 45^\circ$ values were obtained at two degree intervals while the $\gamma = 15^\circ$ and $\gamma = 30^\circ$ values were obtained at 10 degree intervals. Because the 10° interval is too large to show the variation of σ with β accurately, curves have not been drawn for a wavelength of 10 cm. Figures C-10 and C-11 show the variation of σ with β for $\gamma = 45^\circ$ and wavelengths of 10 and 30 cm, respectively.

As was noted in Section 2.1, the scattering pattern of a corner reflector is approximately the same as the diffraction pattern of an equivalent

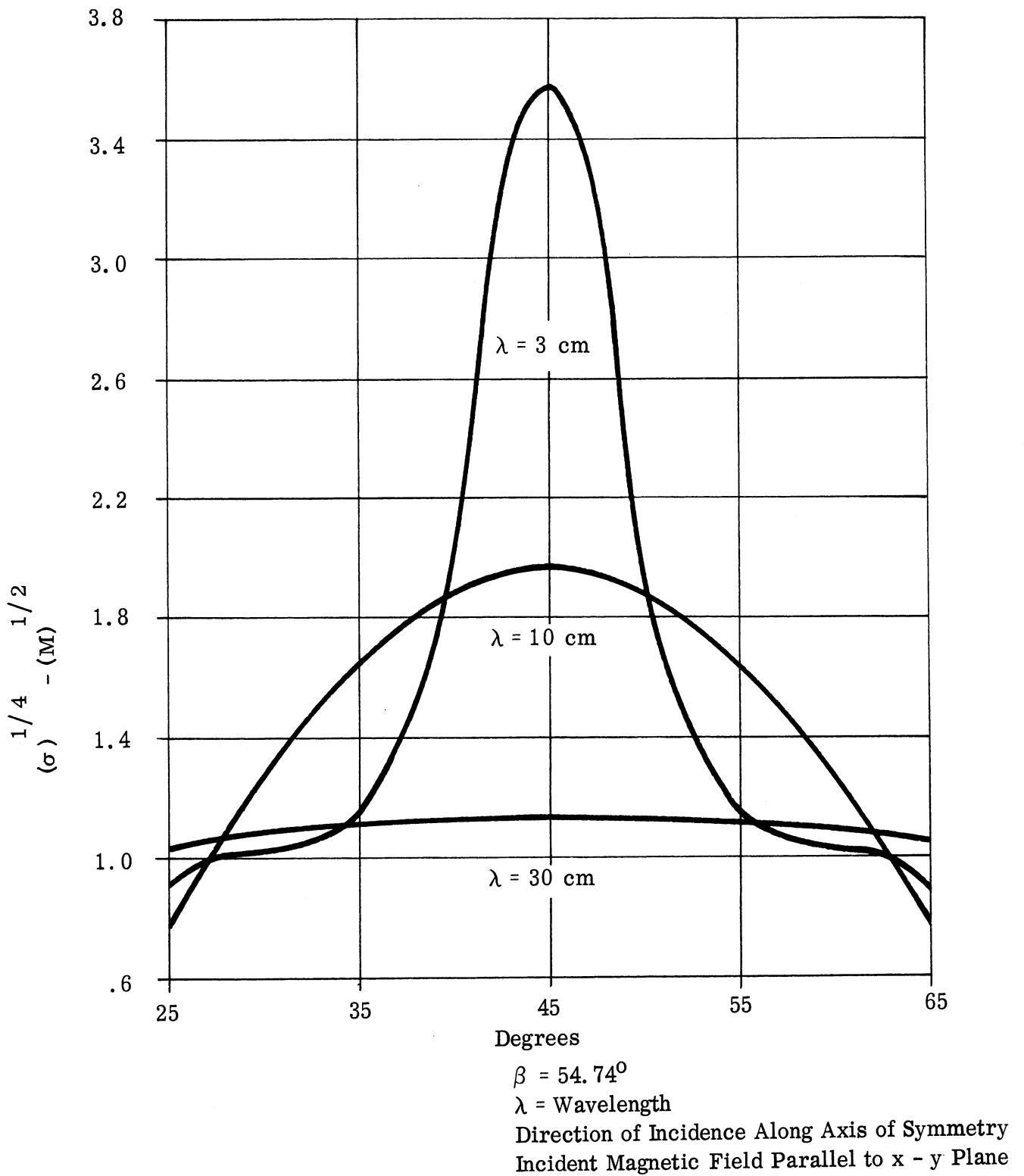


FIG. C-8: BISTATIC RADAR CROSS SECTION OF A SQUARE CORNER REFLECTOR AS A FUNCTION OF γ

Sidelength of Reflector = 25 cm
 Direction of Incidence: along Axis of Symmetry
 Incident Magnetic Field Parallel to x - y Plane

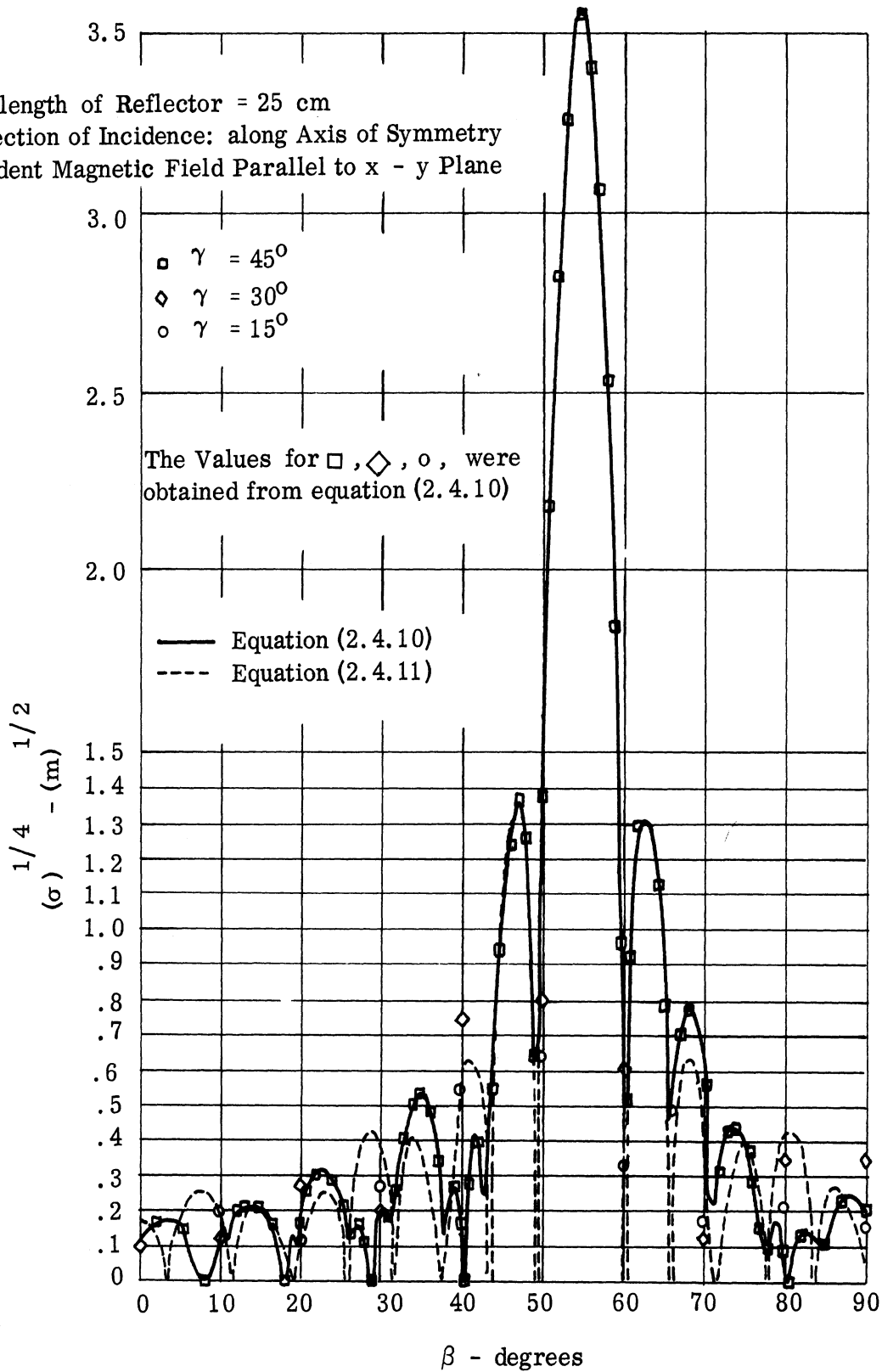


FIG. C-9: BISTATIC RADAR CROSS SECTION OF A SQUARE CORNER REFLECTOR AS A FUNCTION OF β FOR A WAVELENGTH OF 3 CM

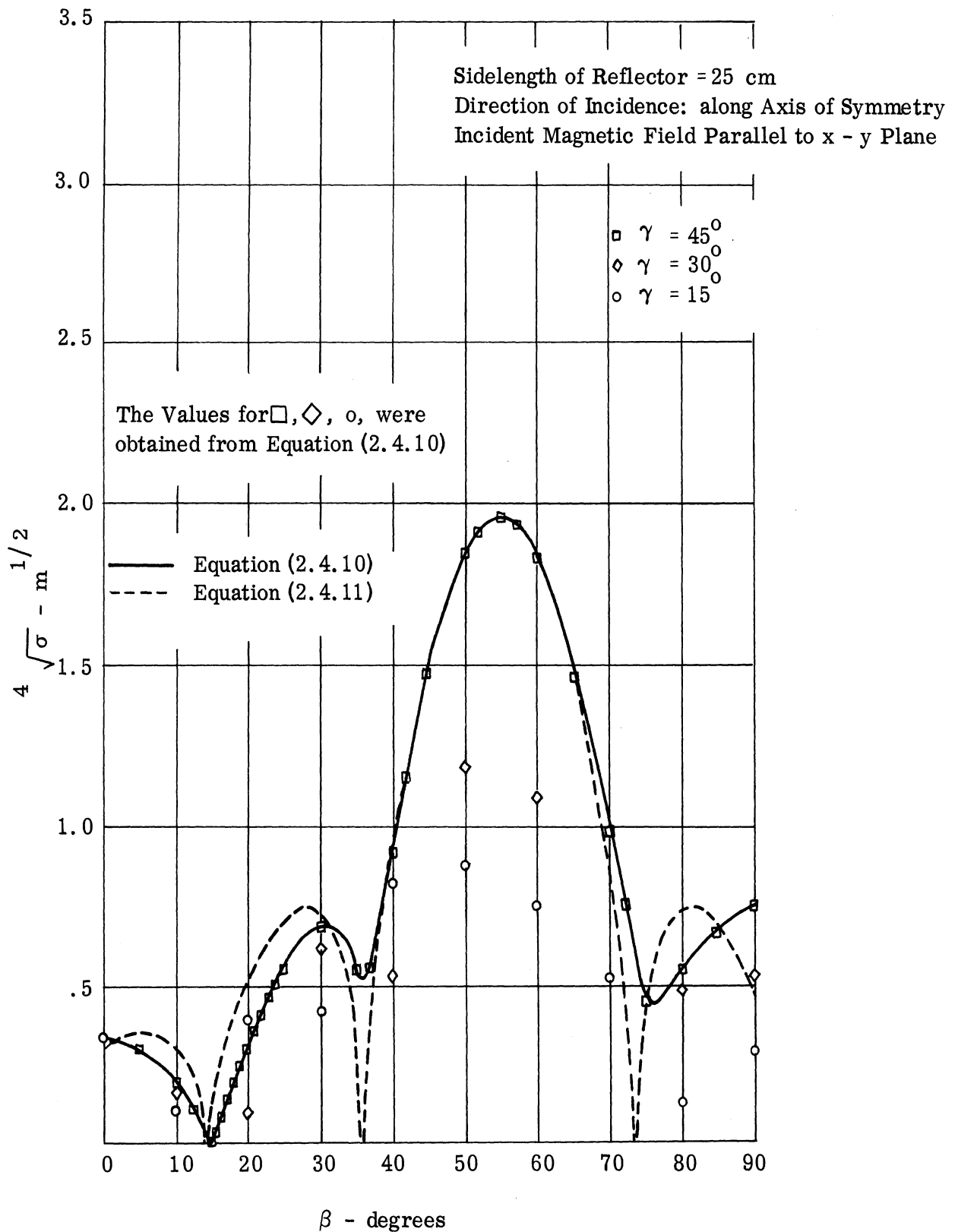


FIG. C-10: BISTATIC RADAR CROSS SECTION OF A SQUARE CORNER REFLECTOR AS A FUNCTION OF β FOR A WAVELENGTH OF 10 CM

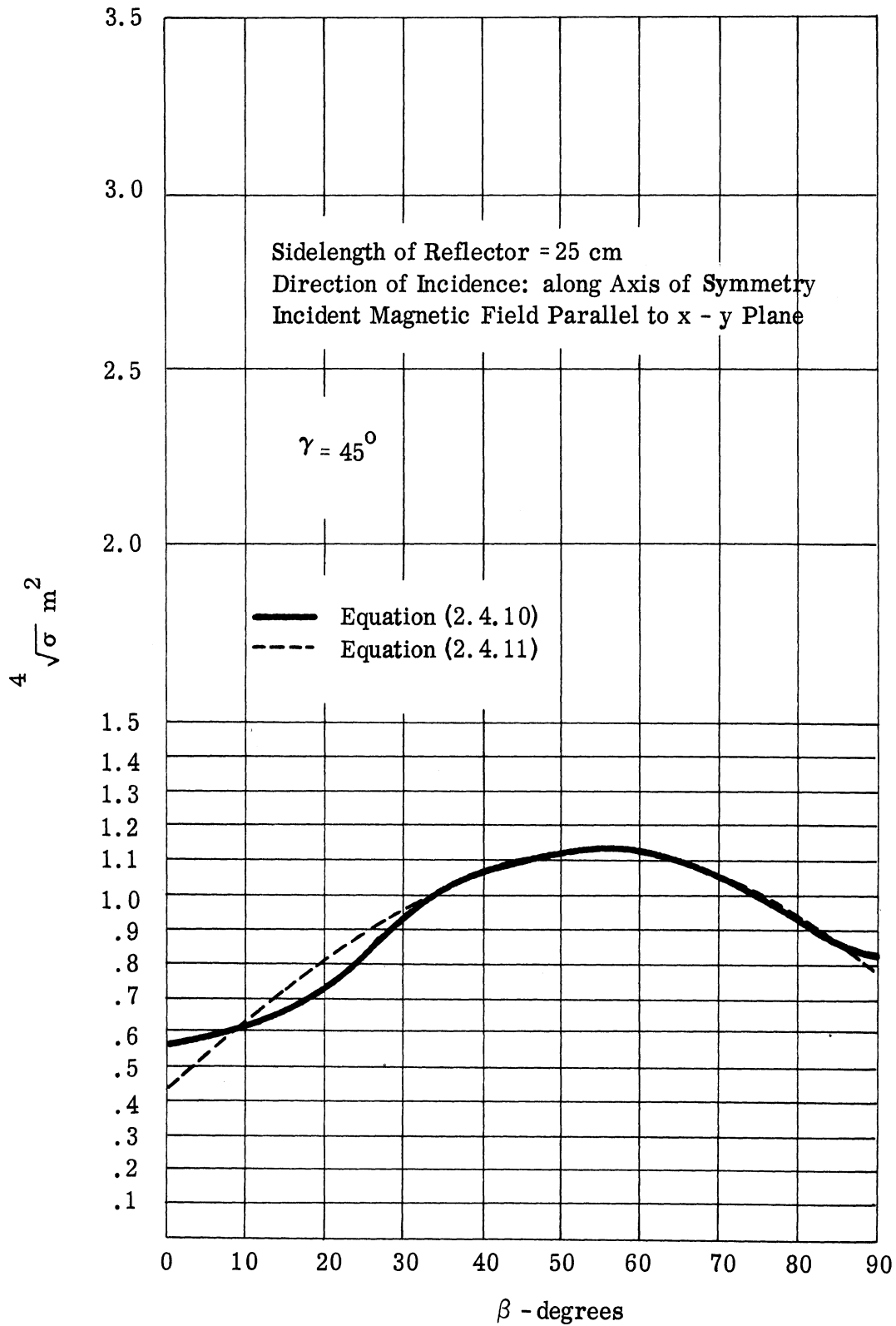


FIG. C-11: BISTATIC RADAR CROSS SECTION OF A SQUARE CORNER REFLECTOR AS A FUNCTION OF β FOR A WAVELENGTH OF 30 CM

aperture. For the symmetric case considered, the diffracting aperture is hexagonal. For $\gamma = 45^\circ$, the bistatic radar cross section for this aperture is

$$\sigma = \frac{108 \pi b^4}{\lambda^2 \tau^4} (\sin \tau \sin \tau / 3)^2 \quad (2.4.11)$$

where

$$\tau = \frac{\pi b}{\lambda} \left[\frac{1}{\sqrt{2}} \sin \beta - \cos \beta \right].$$

The values of radar cross section (2.4.11) as predicted by this equivalent aperture are also plotted in Figures C-9, C-10, and C-11 for comparison with the values obtained from (2.4.10). It should be noted that the half-power widths given by both (2.4.10) and (2.4.11) agree with the values predicted by (2.1.6).

Although the geometric optics and physical optics approximations are based on the assumption that the wavelength is small compared to the characteristic dimension of the body, there is reason to believe that the error introduced by the use of these approximation techniques when b/λ is approximately one is sometimes much less than an order of magnitude. Kouyoumjian (Ref. C-6), for example, has found that the monostatic radar cross section predicted by physical optics for a flat plate at normal incidence does not deviate from the exact electromagnetic solution by more than a factor of five for the range b/λ between 0.8 and 5. Since it is not likely that exact computations will be made of the cross sections of corner reflectors

in the near future, and since there is reason to believe that the approximation techniques do yield order of magnitude answers for the square corner reflector for $\lambda \approx b$, these techniques have been applied for a wavelength of 30 cm. (i. e. $\lambda / b = 1.2$).

2.5 Effect of Constructional Errors, Compensation, and Truncation.

Corner reflectors are generally used to direct a large signal back toward the transmitter. This large signal is reduced in intensity if the corner is not perfectly constructed. If the faces of a corner reflector do not meet at exactly 90° then the beam which would have been reflected back to the transmitter is divided into several beams, none of which, in general, are directed exactly toward the transmitter. As a result, there will be a reduction in signal received at the transmitter. In Reference C-4 the magnitudes of the errors which reduce the signal returned by square or triangular corners (Fig. C-4) to one half the maximum returned signal are calculated. This error, Δ , is measured as follows: if one of the faces of the corner is rotated about one of the coordinate axes through which it passes, then Δ is the distance which the part of the face farthest from the axis moves. These errors are independent of the size of the corner, and therefore are difficult to avoid for large corners and small wavelengths.

For incidence along the axis of symmetry these errors are

Square Corner:	one error, $\Delta = .40 \lambda$
	three equal errors, $\Delta = .24 \lambda$
Triangular Corner:	one error, $\Delta = .70 \lambda$
	three equal errors, $\Delta = .35 \lambda$

For some applications, such as a movable corner used as a beacon, it is desirable to sacrifice some of the strength of the returned signal in order to obtain a usable signal over a wider range of incidence angles on the corner. This flattening and widening of the monostatic response pattern can be accomplished by truncation or compensation (Ref. C-5), i. e., the removal of some of the reflecting surface (see Sec. 4).

OTHER MULTIPLE SCATTERERS

3.1 Formulas for Scattering from Curved Surfaces: Fock's Method

In Section 2 only scattering from surfaces having infinite radii of curvature was considered. In this section multiple scattering from surfaces having finite radii of curvature will be considered. In Reference C-7, formulas are developed for the scattering from curved surfaces. These formulas, which are useful for computing the cross section of bodies with curved surfaces, are summarized in this section.

The scattered electric and magnetic fields, as given by geometric optics, are

$$\begin{aligned} \vec{E}_s &= \left[\vec{E}_i - 2\hat{n} \times (\vec{E}_i \times \hat{n}) \right] \sqrt{\frac{D(0)}{D(r)}} e^{ikr}, \\ \vec{H}_s &= \left[\vec{H}_i - 2(\hat{n} \cdot \vec{H}_i) \hat{n} \right] \sqrt{\frac{D(0)}{D(r)}} e^{ikr} \end{aligned} \quad (3.1.1)$$

where $D(r)$ is the cross sectional area of a bundle of rays at a distance r from the specular reflection point, and \vec{E}_i , \vec{H}_i is the incident field at the specular reflection point.

The area of the bundle of rays at a distance r is given by

$$D(r) = \begin{vmatrix} T_u^u & T_v^u \\ T_u^v & T_v^v \end{vmatrix} \quad (3.1.2)$$

where T_q^p is the symmetrical tensor

$$T_q^p = g^{pu} T_{uq} + g^{pv} T_{vq} \quad (3.1.3)$$

and

$$T_{pq} = g_{pq} - \Omega_p \Omega_q + r (\Omega_{pq} - \cos \zeta G_{pq}), \quad (3.1.4)$$

where the summation convention is not being used. Here u and v are curvilinear coordinates on the scattering surface and g_{pg} is the metric tensor given by

$$d\sigma^2 = g_{uu} du^2 + 2g_{uv} du dv + g_{vv} dv^2 \quad (3.1.5)$$

where $d\sigma$ is an element of arc on the surface. The g^{pq} that appear in (3.1.3) are related to the g_{pq} by

$$\begin{bmatrix} g^{uu} & g^{uv} \\ g^{vu} & g^{vv} \end{bmatrix} = \frac{1}{g_{uu}g_{vv} - g_{uv}^2} \begin{bmatrix} g_{vv} & -g_{uv} \\ -g_{vu} & g_{uu} \end{bmatrix} \quad (3.1.6)$$

G_{pq} is the curvature tensor of the surface given by

$$-G_{pq} = \frac{\partial n_x}{\partial p} \frac{\partial x}{\partial q} + \frac{\partial n_y}{\partial p} \frac{\partial y}{\partial q} + \frac{\partial n_z}{\partial p} \frac{\partial z}{\partial q} \quad (3.1.7)$$

where n_x , n_y , and n_z are the components of the unit normal to the surface at a point x , y , z of the surface. The angle ζ is the angle between the

direction of incidence and the normal to the surface. Ω is defined in terms of the phase of the incident wave on the scattering surface $e^{ik\Omega(u, v)}$.

Ω_p is the ordinary derivative of Ω with respect to p .

$$\Omega_p = \frac{\partial \Omega}{\partial p}. \quad (3.1.8)$$

Ω_{pq} is the second covariant derivative

$$\Omega_{pq} = \frac{\partial^2 \Omega}{\partial p \partial q} - \Gamma_{pq}^u \frac{\partial \Omega}{\partial u} - \Gamma_{pq}^v \frac{\partial \Omega}{\partial v}. \quad (3.1.9)$$

Γ_{qw}^p is the Christoffel symbol of the second kind,

$$\Gamma_{qw}^p = g^{pu} [q, w; u] + g^{pv} [q, w; v] \quad (3.1.10)$$

and $[p, q; w]$ is the Christoffel symbol of the first kind

$$[p, q; w] = \frac{1}{2} \left(\frac{\partial g_{pw}}{\partial q} + \frac{\partial g_{qw}}{\partial p} - \frac{\partial g_{pq}}{\partial w} \right). \quad (3.1.11)$$

3.2 Scattering from Two Spheres

As an example of the application of the formulas in Section 3.1, consider the backscattering from two spheres of equal radius for an electric field $\hat{i}_x e^{-ikz}$ incident perpendicular to the common axis of the spheres.

(Positive x-axis points into the paper)

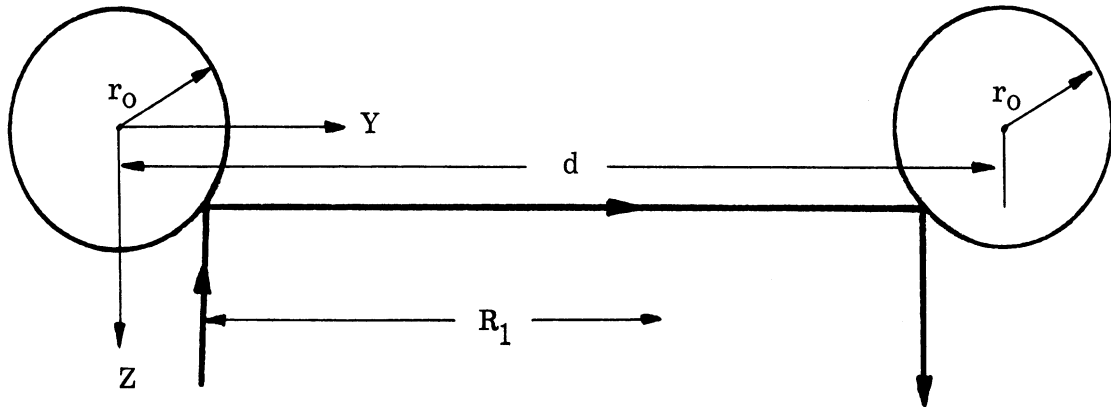


FIG. C-12: REFLECTION GEOMETRY FOR TWO SPHERES

First, consider the doubly reflected ray shown in Figure C-12. For the reflection from the first sphere the coordinates u and v are

$$\begin{aligned} u_1 &= \theta_1, \\ v_1 &= \phi_1 \end{aligned} \quad (3.2.1)$$

where θ_1 and ϕ_1 are related to the Cartesian coordinates by

$$\begin{aligned} x &= r_0 \sin \theta_1 \cos \phi_1, \\ y &= r_0 \sin \theta_1 \sin \phi_1, \\ z &= r_0 \cos \theta_1. \end{aligned} \quad (3.2.2)$$

The normal on the surface of the sphere is

$$\hat{n} = \sin \theta_1 \cos \phi_1 \hat{i}_x + \sin \theta_1 \sin \phi_1 \hat{i}_y + \cos \theta_1 \hat{i}_z. \quad (3.2.3)$$

Thus, by (3.1.7)

$$\begin{bmatrix} G_{\theta_1 \theta_1} & G_{\theta_1 \phi_1} \\ G_{\phi_1 \theta_1} & G_{\phi_1 \phi_1} \end{bmatrix} = \begin{bmatrix} r_0 & 0 \\ 0 & r_0 \sin^2 \theta_1 \end{bmatrix} \quad (3.2.4)$$

The square of the element of arc on the sphere is

$$d\sigma^2 = r_o^2 d\theta_1^2 + r_o^2 \sin^2 \theta_1 d\phi_1^2 \quad (3.2.5)$$

so that

$$\begin{bmatrix} g_{\theta_1 \theta_1} & g_{\theta_1 \phi_1} \\ g_{\phi_1 \theta_1} & g_{\phi_1 \phi_1} \end{bmatrix} = \begin{bmatrix} r_o^2 & 0 \\ 0 & r_o^2 \sin^2 \theta_1 \end{bmatrix} \quad (3.2.6)$$

and

$$\begin{bmatrix} \theta_1 \theta_1 & \theta_1 \phi_1 \\ \phi_1 \theta_1 & \phi_1 \phi_1 \end{bmatrix} = \begin{bmatrix} \frac{1}{r_o^2} & 0 \\ 0 & \frac{1}{r_o^2 \sin^2 \theta_1} \end{bmatrix} \quad (3.2.7)$$

The phase factor is

$$\Omega_1(\theta_1, \phi_1) = -z = -r_o \cos \theta_1 \quad (3.2.8)$$

and the first derivatives of the phase factor are

$$\begin{aligned} \Omega_{1 \theta_1} &= r_o \sin \theta_1, \\ \Omega_{1 \phi_1} &= 0 \end{aligned} \quad (3.2.9)$$

The Christoffel symbols of the first kind are

$$\begin{aligned} [\phi_1, \phi_1; \theta_1] &= -r_o^2 \sin \theta_1 \cos \theta_1, \\ [\phi_1, \theta_1; \phi_1] &= r_o^2 \sin \theta_1 \cos \theta_1, \end{aligned} \quad (3.2.10)$$

$$[\theta_1, \theta_1; \theta_1] = [\theta_1, \theta_1; \phi_1] = [\theta_1, \phi_1; \theta_1] = [\phi_1, \phi_1; \phi_1] = 0.$$

The Christoffel symbols of the second kind are

$$\begin{aligned}\Gamma_{\phi_1 \phi_1}^{\theta_1} &= -\sin \theta_1 \cos \theta_1, \\ \Gamma_{\phi_1 \theta_1}^{\phi_1} &= \cot \theta_1, \\ \Gamma_{\theta_1 \theta_1}^{\theta_1} &= \Gamma_{\theta_1 \theta_1}^{\phi_1} = \Gamma_{\theta_1 \phi_1}^{\theta_1} = \Gamma_{\phi_1 \phi_1}^{\phi_1} = 0.\end{aligned}\tag{3.2.11}$$

Therefore, by (3.1.9) the second covariant derivatives are

$$\begin{bmatrix} \Omega_{1\theta_1\theta_1} & \Omega_{1\theta_1\phi_1} \\ \Omega_{1\phi_1\theta_1} & \Omega_{1\phi_1\phi_1} \end{bmatrix} = \begin{bmatrix} -\Omega_1 & 0 \\ 0 & -\Omega_1 \sin^2 \theta_1 \end{bmatrix}.\tag{3.2.12}$$

Since $\xi_1 = \theta_1$, and $\Omega_1 = -r_o \cos \theta_1$ the symmetric tensor (3.1.4) is

$$\begin{bmatrix} T_{\theta_1\theta_1} & T_{\theta_1\phi_1} \\ T_{\phi_1\theta_1} & T_{\phi_1\phi_1} \end{bmatrix} = \begin{bmatrix} \Omega_1^2 - 2R_1\Omega_1 & 0 \\ 0 & (r_o^2 - \Omega_1^2)(1 - 2\frac{R_1\Omega_1}{r_o^2}) \end{bmatrix}.\tag{3.2.13}$$

The cross sectional area of a bundle of rays at a distance R_1 from the

specular reflection point is

$$D_1(R_1) = \begin{bmatrix} T_{\theta_1}^{\theta_1} & T_{\phi_1}^{\theta_1} \\ T_{\theta_1}^{\phi_1} & T_{\phi_1}^{\phi_1} \end{bmatrix} = \begin{bmatrix} \frac{\Omega_1^2 - 2R_1\Omega_1}{r_o^2} & 0 \\ 0 & 1 - \frac{2R_1\Omega_1}{r_o^2} \end{bmatrix}\tag{3.2.14}$$

$$= \cos \theta_1 \left(\cos \theta_1 + \frac{2R_1}{r_o} \right) \left(1 + 2\frac{R_1}{r_o} \cos \theta_1 \right).$$

The electric field (3.1.1) scattered from the first sphere is

$$-\hat{i}_x \sqrt{\frac{\cos \theta_1}{(\cos \theta_1 + 2 \frac{R_1}{r_0})(1 + 2 \frac{R_1}{r_0} \cos \theta_1)}} e^{ik(R_1 - r_0 \cos \theta_1)}. \quad (3.2.15)$$

For the ray shown in Figure C-12, $\theta_1 = \pi/4$ so that the electric field incident on the second sphere is

$$\frac{-\hat{i}_x e^{ik(d - \frac{3}{\sqrt{2}} r_0)}}{\sqrt{(2\sqrt{2} \frac{d}{r_0} - 3)(\sqrt{2} \frac{d}{r_0} - 1)}} \quad (3.2.16)$$

On the second sphere the coordinates u and v are taken to be $u_2 = \theta_2$ and $v_2 = \phi_2$. These coordinates are related to the Cartesian coordinates by

$$\begin{aligned} x &= r_0 \sin \theta_2 \cos \phi_2, \\ y &= d + r_0 \sin \theta_2 \sin \phi_2, \\ z &= r_0 \cos \theta_2. \end{aligned} \quad (3.2.17)$$

The metric and curvature tensors, and the Christoffel symbols, for the second sphere are obtained from those of the first sphere by replacing θ_1 and ϕ_1 by θ_2 and ϕ_2 .

The phase function on the second sphere is given by the simultaneous equations

$$(\Omega_2 - \Omega_1) \sin 2\theta_1 \cos \phi_1 = r_0 \sin \theta_2 \cos \phi_2 - r_0 \sin \theta_1 \cos \phi_1,$$

$$(\Omega_2 - \Omega_1) \sin 2\theta_1 \sin \phi_1 = d + r_0 \sin \theta_2 \sin \phi_2 - r_0 \sin \theta_1 \sin \phi_1, \quad (3.2.18)$$

$$(\Omega_2 - \Omega_1) \cos 2\theta_1 = r_0 \cos \theta_2 - r_0 \cos \theta_1,$$

where in this example $\theta_1 = \theta_2 = \frac{\pi}{4}$, $\phi_1 = \frac{\pi}{2}$, and $\phi_2 = \frac{3\pi}{2}$.

Hence, the phase factor and its derivatives for this example are

$$\begin{aligned} \Omega_2 &= d - \frac{3}{\sqrt{2}} r_0, \\ \Omega_{2\theta_2} &= -\frac{r_0}{\sqrt{2}}; \quad \Omega_{2\phi_2} = 0, \end{aligned} \quad (3.2.19)$$

$$\Omega_{2\theta_2\theta_2} = \frac{2d - \frac{r_0}{\sqrt{2}}}{2\sqrt{2} \frac{d}{r_0} - 3}, \quad \Omega_{2\phi_2\phi_2} = \frac{\frac{d}{2} + \frac{r_0}{2\sqrt{2}}}{\sqrt{2} \frac{d}{r_0} - 1}, \quad \Omega_{2\theta_2\phi_2} = 0.$$

The metric and curvature tensors at $\theta_2 = \pi/4$ and $\phi_2 = 3\pi/2$ are

$$\begin{bmatrix} g_{\theta_2\theta_2} & g_{\theta_2\phi_2} \\ g_{\phi_2\theta_2} & g_{\phi_2\phi_2} \end{bmatrix} = \begin{bmatrix} r_0^2 & 0 \\ 0 & \frac{r_0^2}{2} \end{bmatrix} \quad (3.2.20)$$

and

$$\begin{bmatrix} G_{\theta_2\theta_2} & G_{\theta_2\phi_2} \\ G_{\phi_2\theta_2} & G_{\phi_2\phi_2} \end{bmatrix} = \begin{bmatrix} -r_0 & 0 \\ 0 & -\frac{r_0}{2} \end{bmatrix}. \quad (3.2.21)$$

Since $\xi_2 = \pi/4$, the symmetrical tensor (3.1.4) is

$$\begin{bmatrix} T_{\theta_2 \theta_2} & T_{\theta_2 \phi_2} \\ T_{\phi_2 \theta_2} & T_{\phi_2 \phi_2} \end{bmatrix} = \begin{bmatrix} \frac{r_0^2}{2} + \frac{4d - 2\sqrt{2}r_0}{2\sqrt{2}d - 3r_0} - r_0 R_2 & 0 \\ 0 & \frac{r_0^2}{2} + \frac{dr_0 R_2}{\sqrt{2}d - r_0} \end{bmatrix}. \quad (3.2.22)$$

The cross sectional area of the bundle of rays at a distance R_2 from the specular reflection point is

$$D_2(R_2) = \left(\frac{1}{2} + \frac{R_2}{r_0} \frac{4d - 2\sqrt{2}r_0}{2\sqrt{2}d - 3r_0} \right) \left(1 + \frac{R_2}{r_0} \frac{2d}{\sqrt{2}d - r_0} \right). \quad (3.2.23)$$

Therefore, at a large distance from the scatterer, for the doubly reflected ray shown in Figure C-12, the scattered electric field is

$$\frac{r_0^2 e^{ik(z + d - 2\sqrt{2}r_0)}}{4 dz \sqrt{1 - \frac{r_0}{\sqrt{2}d}}} \hat{i}_x. \quad (3.2.24)$$

There is a second doubly reflected ray which gives a contribution equal to (3.2.24) and there are two singly reflected rays each of which contribute to the backscattered electric field by an amount

$$- \frac{r_0}{2z} e^{ik(z - 2r_0)} \hat{i}_x. \quad (3.2.25)$$

In addition there are backscattered rays which are reflected more than twice.

If the distance between the centers of the spheres is much larger than the radii of the spheres, the radiation which undergoes more than two reflections may be neglected and the total reflected field is approximately

$$\left[-r_0 e^{-2ikr_0} + \frac{r_0^2 e^{ik(d - 2\sqrt{2}r_0)}}{2d \sqrt{1 - \frac{r_0}{\sqrt{2}d}}} \right] \frac{e^{ikz}}{z} \hat{i}_x \quad (3.2.26)$$

3.3 Formulas for Scattering From Curved Surfaces: The Method of Stationary Phase

Another technique for finding the scattered fields when the wavelength is less than a characteristic dimension of the scatterer is the method of stationary phase. The field associated with a multiply reflected ray, as given by this method, depends upon the radii of curvature of the body at the specular reflection points. These radii of curvature are assumed to be finite.

A Cartesian coordinate system is used at each reflection point. The z-axis is taken along the normal to the surface, and the x- and y-axes are chosen so that the x and y planes are the principal sections of the surface, that is sections in which the principle radii of curvature are obtained. In the vicinity of the reflection points the equations of the surfaces are, approximately,

$$z_j = -\frac{x_j^2}{2\rho_{j1}} - \frac{y_j^2}{2\rho_{j2}} \quad (j = 1, 2, 3, \dots, N) \quad (3.3.1)$$

where ρ_{j1} and ρ_{j2} are the principle radii of curvature of the j'th surface.

Let θ_j and ϕ_j represent the polar angles at the j 'th reflection point, \vec{r}'_j represent the radius vector to a point on the j 'th surface from a fixed arbitrary reference point. Assume the incident magnetic field to be $\hat{a} e^{ik(\hat{k} \cdot \vec{r})}$ where \vec{r} is the radius vector from the reference point to an arbitrary point in space. From equation (2.1.1) the field scattered from the first surface is

$$\vec{H}_s = \frac{1}{2\pi} \int (\hat{n}_1 \times \hat{a}) \times \nabla \frac{e^{ik|\vec{r}-\vec{r}'_1|}}{|\vec{r}-\vec{r}'_1|} e^{ik\hat{k} \cdot \vec{r}'_1} ds_1 \quad (3.3.2)$$

and the multiply scattered field reflected from the N surfaces in succession is

$$\vec{H}_s = \frac{1}{(2\pi)^N} \int \dots \int \left\{ \hat{n}_N \times \left[\hat{n}_{N-1} \times \dots \times \left[\hat{n}_2 \times \left[\hat{n}_1 \times \hat{a} \right] \times \nabla \frac{e^{ik|\vec{r}'_2-\vec{r}'_1|}}{|\vec{r}'_2-\vec{r}'_1|} \right] \right] \right\} \times \dots \times \left[\nabla \frac{e^{ik|\vec{r}'_3-\vec{r}'_2|}}{|\vec{r}'_3-\vec{r}'_2|} \right] \times \dots \times \left[\nabla \frac{e^{ik|\vec{r}'_N-\vec{r}'_{N-1}|}}{|\vec{r}'_N-\vec{r}'_{N-1}|} \right] \times \nabla \frac{e^{ik|\vec{r}-\vec{r}'_N|}}{|\vec{r}-\vec{r}'_N|} e^{ik\hat{k} \cdot \vec{r}'_1} ds_1 \dots ds_N. \quad (3.3.3)$$

Assume the wavelength to be so short that $k|\vec{r}'_{j+1}-\vec{r}'_j| \gg 1$. For this case

$$\nabla \frac{e^{ik|\vec{r}'_{j+1}-\vec{r}'_j|}}{|\vec{r}'_{j+1}-\vec{r}'_j|} \approx -\frac{ike^{ik|\vec{r}'_{j+1}-\vec{r}'_j|}}{|\vec{r}'_{j+1}-\vec{r}'_j|^2} (\vec{r}'_{j+1}-\vec{r}'_j). \quad (3.3.4)$$

In the integrand of (3.3.3) all of the quantities except the exponential factor

can be replaced by their values at the specular reflection points. With this approximation, (3.3.3) becomes

$$\vec{H}_s = \left(\frac{k}{2\pi i} \right) \frac{N \left\{ \hat{n}_N \times \dots \times \left[\left\{ \hat{n}_2 \times \left[\left\{ \hat{n}_1 \times \hat{a} \right\} \times \hat{R}_1 \right] \right\} \times \hat{R}_2 \right] \right\} \times \dots \right\} \times \hat{R}_N}{R_1 R_2 \dots R_N} \quad (3.3.5)$$

$$\times \int \dots \int e^{ik \left[\hat{k} \cdot \vec{r}'_1 + \sum_{j=1}^N R_j \right]} dS_1 \dots dS_N$$

where

$$\vec{r}'_{j+1} - \vec{r}'_j = \vec{R}_j = R_j \hat{R}_j \quad \text{and} \quad \vec{r} - \vec{r}'_N = \vec{R}_N = R_N \hat{R}_N.$$

Let $\xi_1 = x_1$, $\xi_2 = y_1$, $\xi_3 = x_2$, $\xi_4 = y_2$, \dots , $\xi_{2N-1} = x_N$, $\xi_{2N} = y_N$,

and expand the phase factor in equation (3.3.5) in the ξ_j . The first order terms will vanish at the specular reflection points, leaving terms of second order as the leading terms in the expansion. Neglecting all but second order terms, (3.3.5) becomes

$$\vec{H}_s = \left(\frac{k}{2\pi i} \right)^N \frac{\cos \theta_1}{R_1} \frac{\cos \theta_2}{R_2} \dots \frac{\cos \theta_N}{R_N} \hat{H}_N e^{ik \left[\hat{k} \cdot \vec{r}' + \sum_{j=1}^N R_j \right]} I \quad (3.3.6)$$

where $I = \int_{-\infty}^{\infty} \dots \int_{-\infty}^{\infty} e^{ik \tilde{\xi} M \xi} d\xi_1 \dots d\xi_{2N}$ is a 2N-dimensional Fresnel

integral, \hat{H}_N is a unit vector giving the polarization of the scattered wave, and

ξ and M are the matrices

$$\xi = \begin{bmatrix} \xi_1 \\ \xi_2 \\ \vdots \\ \xi_{2N} \end{bmatrix}; \quad \tilde{\xi} = \left[\xi_1, \xi_2, \dots, \xi_{2N} \right] \quad (3.3.7)$$

$$M = \tilde{M} =$$

$$\begin{bmatrix} \frac{\cos\theta_1}{\rho_{11}} + \frac{1 - \sin^2\theta_1 \cos^2\phi_1}{2R_1} & -\frac{\sin^2\theta_1 \sin\phi_1 \cos\phi_1}{2R_1} & \frac{\sin\theta_2 \cos\phi_2 \sin\theta_1 \cos\phi_1 - \alpha_{111}}{2R_1} & \dots & 0 \\ -\frac{\sin^2\theta_1 \sin\phi_1 \cos\phi_1}{2R_1} & \frac{\cos\theta_1}{\rho_{12}} + \frac{1 - \sin^2\theta_1 \sin^2\phi_1}{2R_1} & \frac{\sin\theta_2 \cos\phi_2 \sin\theta_1 \sin\phi_1 - \alpha_{121}}{2R_1} & \dots & 0 \\ \frac{\sin\theta_2 \cos\phi_2 \sin\theta_1 \cos\phi_1 - \alpha_{111}}{2R_1} & \frac{\sin\theta_2 \cos\phi_2 \sin\theta_1 \sin\phi_1 - \alpha_{121}}{2R_1} & 2 \frac{\cos\theta_2}{\rho_{21}} + (1 - \sin^2\theta_2 \cos^2\phi_2) \left(\frac{1}{2R_1} + \frac{1}{2R_2} \right) & \dots & 0 \\ \frac{\sin\theta_2 \sin\phi_2 \sin\theta_1 \cos\phi_1 - \alpha_{112}}{2R_1} & \frac{\sin\theta_2 \sin\phi_2 \sin\theta_1 \sin\phi_1 - \alpha_{122}}{2R_1} & -\sin^2\theta_2 \sin\phi_2 \cos\phi_2 \left(\frac{1}{2R_1} + \frac{1}{2R_2} \right) & \dots & 0 \\ 0 & 0 & \frac{\sin\theta_3 \cos\phi_3 \sin\theta_2 \cos\phi_2 - \alpha_{211}}{2R_2} & \dots & 0 \\ 0 & 0 & \frac{\sin\theta_3 \sin\phi_3 \sin\theta_2 \cos\phi_2 - \alpha_{212}}{2R_2} & \dots & 0 \\ 0 & 0 & 0 & \dots & 0 \\ \cdot & \cdot & \cdot & \dots & \cdot \\ \cdot & \cdot & \cdot & \dots & \cdot \\ \cdot & \cdot & \cdot & \dots & \cdot \\ 0 & 0 & 0 & \dots & \frac{\sin^2\theta_N \sin\phi_N \cos\phi_N}{2R_{N-1} \left(\frac{R_N}{R_{N-1}} + R_N \right)} \\ 0 & 0 & 0 & \dots & \frac{\cos\theta_N}{\rho_{N2}} + \frac{1 - \sin^2\theta_N \sin^2\phi_N}{2R_{N-1} \left(\frac{R_N}{R_{N-1}} + R_N \right)} \end{bmatrix}$$

(3.3.8)

In (3.3.8) α_{j11} is the cosine of the angle between the x_j and the x_{j+1} axes, α_{j12} is the cosine of the angle between the x_j and the y_{j+1} axes, α_{j21} is the cosine of the angle between the y_j and the x_{j+1} axes, and α_{j22} is the cosine of the angle between the y_j and y_{j+1} axes.

Evaluation of the integral I yields

$$I = \left(\frac{\pi e^{\frac{\pi i}{2}}}{k} \right)^N \frac{1}{\sqrt{|M|}} \quad (3.3.9)$$

where $|M|$ is the determinant of M. Thus (3.3.6) becomes

$$\hat{H}_s = \hat{H}_N \frac{e^{ik(k \cdot \hat{r}'_1 + \sum_{j=1}^N R_j)}}{\sqrt{|M|}} \quad (3.3.10)$$

When the radii of curvature at the reflection points are finite, equation (3.3.10) is equivalent to equation (3.1.1). To illustrate this equivalence, the method of stationary phase will be applied to the problem of multiple scattering from two spheres treated by Fock's method in Section 3.2. In this problem

$$\begin{aligned} \rho_{11} &= \rho_{12} = \rho_{21} = \rho_{22} = r_0, \\ R_1 &= d - \sqrt{2} r_0, \\ R_2 &= z - \frac{r_0}{\sqrt{2}}, \\ \theta_1 &= \theta_2 = \frac{\pi}{4}, \\ \hat{k} \cdot \hat{r}'_1 &= -\frac{r_0}{\sqrt{2}}, \end{aligned} \quad (3.3.11)$$

and

$$\alpha_{111} = 1, \alpha_{112} = \alpha_{121} = \alpha_{122} = 0,$$

$$\phi_1 = \frac{\pi}{2}, \phi_2 = \frac{3\pi}{2}.$$

Assuming that $d - \frac{r_0}{\sqrt{2}} \ll z$, the substitution of (3.3.11) into (3.3.8) gives

$$|M| = \frac{(2d - \sqrt{2} r_0) d}{8 r_0^2 (d - \sqrt{2} r_0)^2} \quad (3.3.12)$$

The substitution of (3.3.11) and (3.3.12) into (3.3.10) gives

$$\vec{H}_s = \vec{H}_N \frac{r_0^2 e^{ik(z + d - 2\sqrt{2} r_0)}}{4d(z - \frac{r_0}{\sqrt{2}}) \sqrt{1 - \frac{r_0}{\sqrt{2}d}}} \quad (3.3.13)$$

If $\sqrt{2} z \gg r_0$, equation (3.3.13) reduces to equation (3.2.26).

3.4 The Biconical Reflector

In the examples considered thus far the radii of curvature of the scattering surfaces have either been all finite or all infinite. However, many problems that arise in practice involve both finite and infinite radii of curvature. Rather than attempt to give a general formula for all the cases that might arise, the scattering from a biconical reflector will be treated to illustrate the appropriate technique. A method of attack for this

problem has already been given, namely the use of (2.1-4) with the value of \vec{H} in the integrand given by the geometric optics formula (3.1.1). As with the examples which have already been treated, it is usually advantageous to make simplifying approximations in the evaluation of the integral appearing in (2.1.4). One approximation is to take into account only the current induced on the scattering surface by the last reflection of a multiply reflected ray. A second approximation is to use stationary phase in evaluating the integral whenever appropriate. In the following computation only the case of transmitter and receiver along the x-axis is considered (Figure C-13).

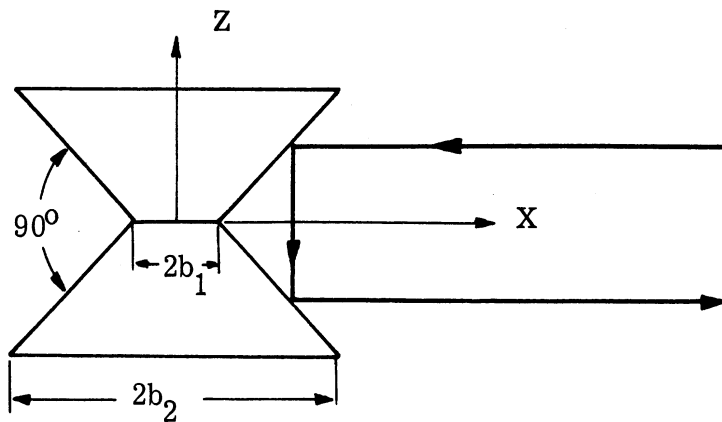


FIG. C-13: THE BICONICAL REFLECTOR

The equation of the upper cone is

$$x^2 + y^2 = (z + b_1)^2 \quad (3.4.1)$$

while the equation of the lower cone is

$$x^2 + y^2 = (z - b_1)^2. \quad (3.4.2)$$

Equation (3.1.1) can be used to obtain the field reflected from the upper cone to the lower cone. If the surface coordinates are z and ϕ , then

$$\begin{aligned}x &= (z + b_1) \cos \phi, \\y &= (z + b_1) \sin \phi, \\z &= z.\end{aligned}\tag{3.4.3}$$

The outward unit normal on the upper cone is

$$\hat{n} = \frac{\cos \phi}{\sqrt{2}} \hat{i}_x + \frac{\sin \phi}{\sqrt{2}} \hat{i}_y - \frac{1}{\sqrt{2}} \hat{i}_z.\tag{3.4.4}$$

Applying (3.1.7) yields

$$\begin{bmatrix} G_{zz} & G_{z\phi} \\ G_{\phi z} & G_{\phi\phi} \end{bmatrix} = \begin{bmatrix} 0 & 0 \\ 0 & \frac{z + b_1}{\sqrt{2}} \end{bmatrix}.\tag{3.4.5}$$

The arc element is given by

$$d\sigma^2 = 2 dz^2 + (z + b_1) d\phi^2\tag{3.4.6}$$

so that

$$\begin{bmatrix} g_{zz} & g_{z\phi} \\ g_{\phi z} & g_{\phi\phi} \end{bmatrix} = \begin{bmatrix} 2 & 0 \\ 0 & (z + b_1)^2 \end{bmatrix}.\tag{3.4.7}$$

The inverse of the metric tensor is

$$\begin{bmatrix} g^{zz} & g^{z\phi} \\ g^{\phi z} & g^{\phi\phi} \end{bmatrix} = \begin{bmatrix} 1/2 & 0 \\ 0 & \frac{1}{(z + b_1)^2} \end{bmatrix}.\tag{3.4.8}$$

The phase factor is

$$\Omega(z, \phi) = -x = -(z + b_1) \cos \phi. \quad (3.4.9)$$

The derivatives of the phase factor are

$$\begin{aligned} \Omega_z &= -\cos \phi, \\ \Omega_\phi &= (z + b_1) \sin \phi. \end{aligned} \quad (3.4.10)$$

The Christoffel symbols of the first kind are

$$\begin{aligned} [z, z; z] &= [z, z; \phi] = [z, \phi; z] = [\phi, \phi; \phi] = 0, \\ [\phi, \phi; z] &= -(z + b_1) = -[\phi, z; \phi]. \end{aligned} \quad (3.4.11)$$

The Christoffel symbols of the second kind are

$$\Gamma_{zz}^z = \Gamma_{zz}^\phi = \Gamma_{z\phi}^z = \Gamma_{\phi\phi}^\phi = 0, \quad (3.4.12)$$

$$\begin{aligned} \Gamma_{\phi\phi}^z &= -(1/2)(z + b_1), \\ \Gamma_{\phi z}^\phi &= \frac{1}{z + b_1} \end{aligned}$$

so that

$$\begin{bmatrix} \Omega_{zz} & \Omega_{z\phi} \\ \Omega_{\phi z} & \Omega_{\phi\phi} \end{bmatrix} = \begin{bmatrix} 0 & 0 \\ 0 & (1/2)(z + b_1) \cos \phi \end{bmatrix}. \quad (3.4.13)$$

Since $\cos \xi = \hat{i}_x \cdot \hat{n} = \cos \phi / \sqrt{2}$,

$$\begin{bmatrix} T_{zz} & T_{z\phi} \\ T_{\phi z} & T_{\phi\phi} \end{bmatrix} = \begin{bmatrix} 2 - \cos^2 \phi & (z + b_1) \sin \phi \cos \phi \\ (z + b_1) \sin \phi \cos \phi, & (z + b_1)^2 \cos^2 \phi + R_1 (z + b_1) \cos \phi \end{bmatrix}, \quad (3.4.14)$$

$$\begin{bmatrix} T_z^z & T_\phi^z \\ T_z^\phi & T_\phi^\phi \end{bmatrix} = \begin{bmatrix} 1 - (1/2)\cos^2 \phi & (1/2)(z + b_1) \sin \phi \cos \phi \\ \frac{\sin \phi \cos \phi}{z + b_1} & \cos^2 \phi + \frac{R_1 \cos \phi}{z + b_1} \end{bmatrix},$$

where R_1 is the distance from the specular reflection point on the upper cone.

Thus

$$D(R_1) = (1/2) \cos^2 \phi \left[1 + \frac{R_1}{z + b_1} \left(\frac{2}{\cos \phi} - \cos \phi \right) \right]. \quad (3.4.15)$$

If the magnetic field incident on the upper cone is $\hat{i}_y e^{-ikx}$, then the magnetic field scattered from the upper cone is

$$\frac{(-\sin \phi \cos \phi \hat{i}_x + \cos^2 \phi \hat{i}_y + \sin \phi \hat{i}_z) e^{ik[R_1 - (z + b_1) \cos \phi]}}{\sqrt{1 + \frac{R_1}{z + b_1} \left(\frac{2}{\cos \phi} - \cos \phi \right)}}. \quad (3.4.16)$$

For $\phi = \theta$ the reflected magnetic field on the surface of the lower cone is

$$\sqrt{\frac{z + b_1}{3z + b_1}} e^{ik(z - b_1)} \hat{i}_y \quad (3.4.17)$$

where z is the height at which the incident ray strikes the upper cone. If

(3.4.16) is written in terms of the coordinates x' , y' , z' on the lower cone

with

$$\begin{aligned} x' &= (b_1 - z') \cos \phi', \\ y' &= (b_1 - z') \sin \phi' \end{aligned} \quad (3.4.18)$$

it becomes

$$\sqrt{\frac{b_1 - z'}{b_1 - 3z'}} e^{ik \left[-b_1 - z' + (1/2) \left\{ \frac{(b_1 - z')^2}{b_1 - 3z'} \right\} \phi'^2 + O(\phi'^4) \right]} \left[\hat{i}_y + O(\phi') \right] \quad (3.4.19)$$

where $O(\mathbf{X})$ is a function for which $\lim_{x \rightarrow 0} O(x)/x = \text{constant}$ which is neither zero nor infinity. If (3.4.19) is used in (2.1.2) and the integration over ϕ'

is carried out by the method of stationary phase, it is found that the doubly scattered field at a large distance x is given by

$$\hat{i}_y \frac{ik}{2\pi} \frac{e^{ik(x - 2b_1)}}{x} \int_0^{b_2 - b_1} \frac{(b_1 + z)^{3/2}}{(b_1 + 3z)^{1/2}} \int_{-\infty}^{\infty} e^{ik \frac{(b_1 + z)(b_1 + 2z)}{b_1 + 3z}} \phi'^2 d\phi' dz \quad (3.4.20)$$

$$= \sqrt{\frac{k}{\pi}} \frac{1}{2} e^{\frac{3\pi i}{4}} \hat{i}_y \frac{e^{ik(x - 2b_1)}}{x} \int_0^{b_2 - b_1} \frac{b_1 + z}{\sqrt{b_1 + 2z}} dz.$$

Integrating the last expression with respect to z gives

$$\frac{1}{3} \sqrt{\frac{2}{\lambda}} e^{\frac{3\pi i}{4}} \frac{e^{ik(x - 2b_1)}}{x} (b_2 \sqrt{2b_2 - b_1} - b_1^{3/2}) \hat{i}_y. \quad (3.4.21)$$

Therefore, taking into account the radiation reflected from the lower cone to the upper cone, the radar cross section of the biconical reflector is

$$\sigma = \frac{32\pi}{9\lambda} \left(b_2 \sqrt{2b_2 - b_1} - b_1^{3/2} \right)^2. \quad (3.4.22)$$

Numerically, the cross section given by equation (3.4.22) is in excellent agreement with experimental results that appear in Reference C-5. Furthermore, the dependence on wavelength is in agreement with Robertson's experimental results.

EXPERIMENTAL DATA ON MULTIPLE SCATTERERS

Many experimental measurements have been made of the radar cross section of the corner reflector. Of the bodies considered in this paper, data are available for square and triangular corner reflectors (Ref. C-8) and for biconical reflectors (Ref. C-5). In addition, the effects of compensation (Sec. 2.5) are discussed in detail in Reference C-5. The material in this section is taken from these two references.

Theoretical curves and experimental points for the backscattering from square and triangular corner reflectors are shown in Figures C-14 and C-15 respectively. The results are plotted so as to be independent of the size of the corner. The experimental dependence of the cross section on the size of the reflector is shown in Table C-1 for a square corner reflector.

TABLE C-1

<u>Variation of Cross Section with Corner Side Length b</u>	
$(\lambda = 9.1 \text{ cm})$	
<u>Size of Reflector</u>	<u>Value of n in $\sigma = Kb^n$</u>
6 inch	3.3
2 foot	4.0
3 foot	3.8
4 foot	3.8

A one foot corner reflector was used to obtain the constant K. For the 6 inch

reflector, whose dimensions are of the same order of magnitude as the wavelength of the incident radiation, the cross section deviated from that predicted by physical optics by a factor of approximately 1.6. The discrepancies between physical optics theory and experiment for the 3 and 4 foot reflectors can be attributed to non-perpendicularity of the reflector sides.

Compensation, i. e., reduction of scattering surfaces, can be used to widen the response pattern of a corner reflector (Sec. 2.5). The response pattern of the compensated triangular reflector, shown in Figure C-16, is compared with the response pattern from an uncompensated reflector of the same dimensions in Figure C-17. A special case of the compensated corner reflector is the corner which has been modified so as to yield a minimum response along the axis of symmetry (which usually yields the maximum response). The response pattern from this corner (Fig. C-18) is shown in Figure C-19.

The response pattern from a biconical reflector is shown in Figure C-20. This response pattern is independent of azimuth since the biconical reflector is axially symmetric.

In conclusion it is felt that the profusion of multiple scatterers and the widespread use of corner reflectors warrants theoretical investigations, even though the corner reflector may be a poorer standard than the sphere since its exact solution is not known. It is shown here that when $\lambda < h$ the cross section of these bodies can be predicted within an order of magnitude.

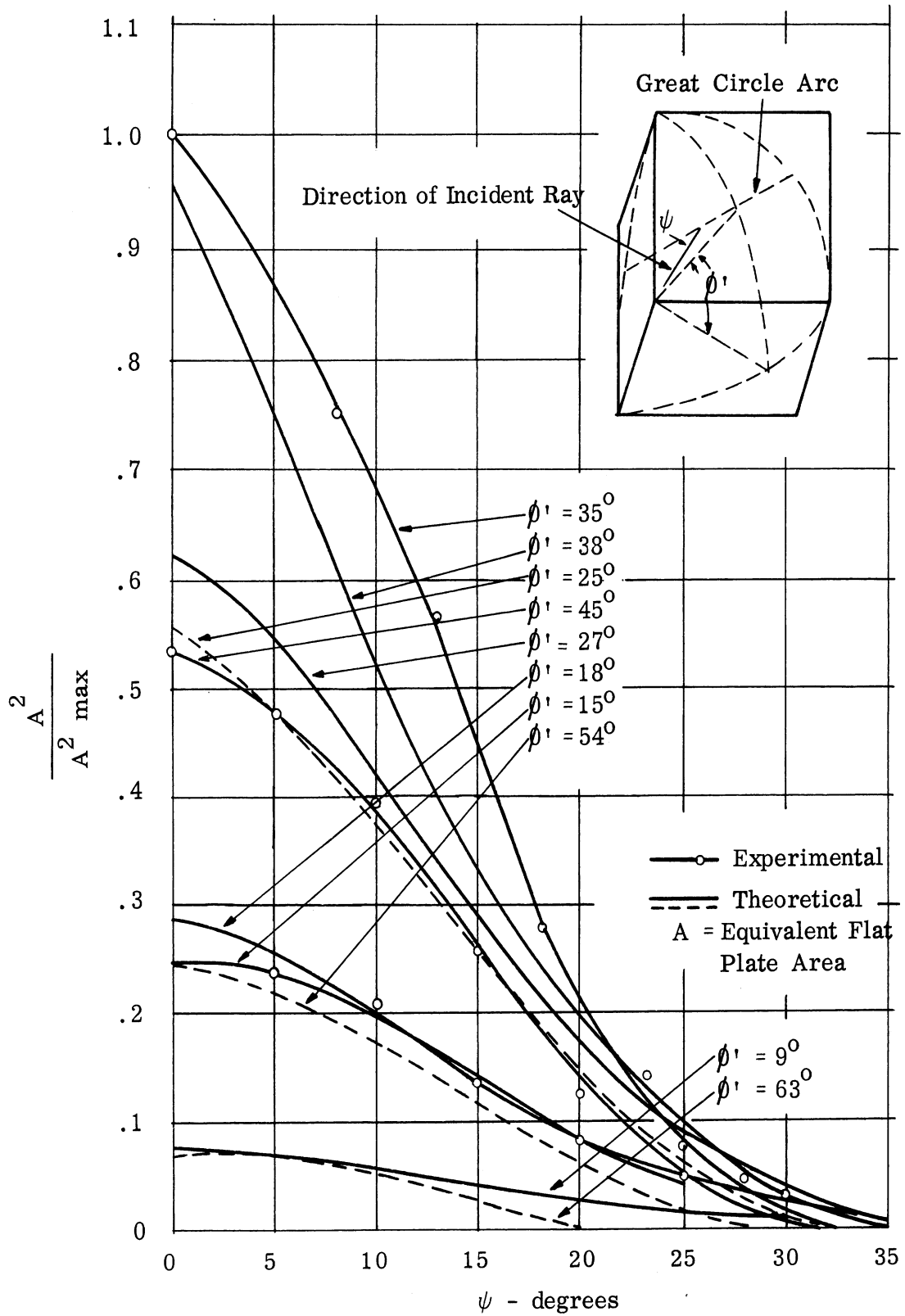


FIG. C-14: RELATIVE INTENSITY OF REFLECTION FROM SQUARE CORNER REFLECTOR

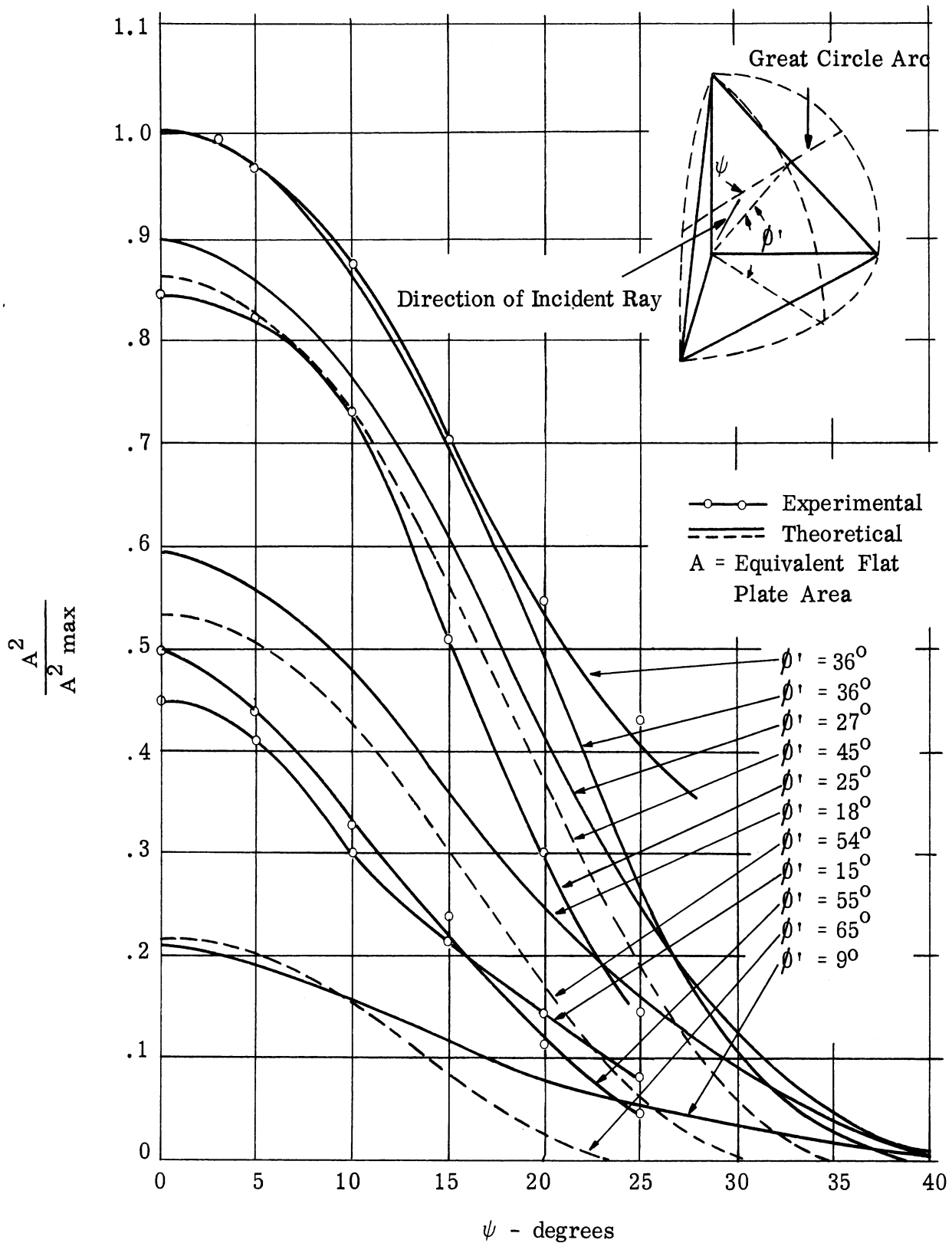
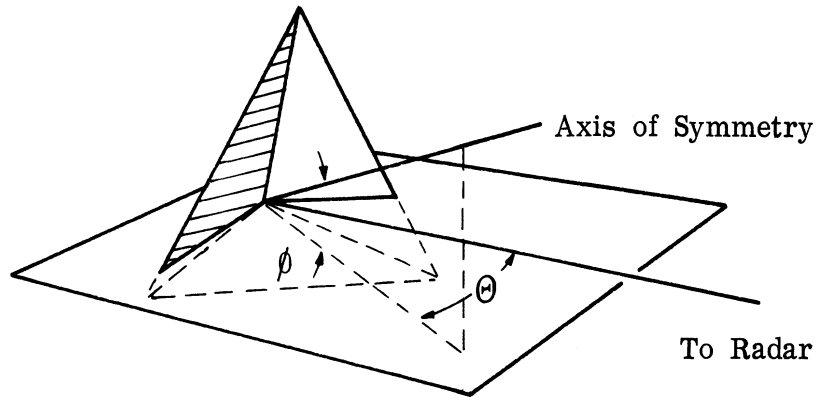
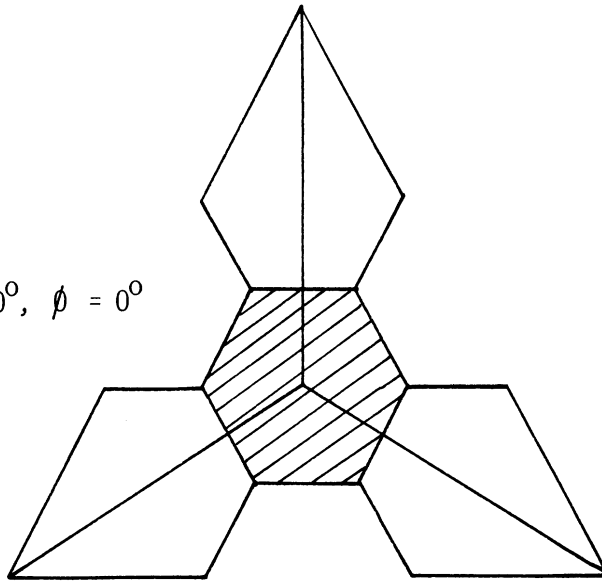


FIG. C-15: RELATIVE INTENSITY OF REFLECTION FROM TRIANGULAR CORNER REFLECTOR



(a)
Aspect $\Theta = 0^\circ$, $\phi = 0^\circ$



Shaded Region Represents
Effective Area A

(b)
Aspect $\Theta = 30^\circ$, $\phi = 0^\circ$

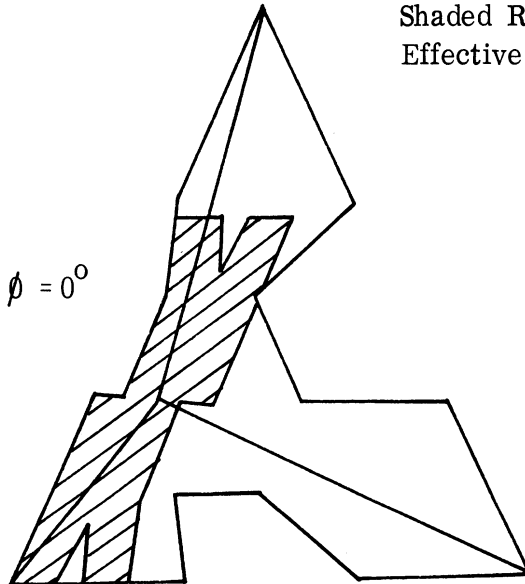


FIG. C-16: COMPENSATED TRIANGULAR CORNER REFLECTOR

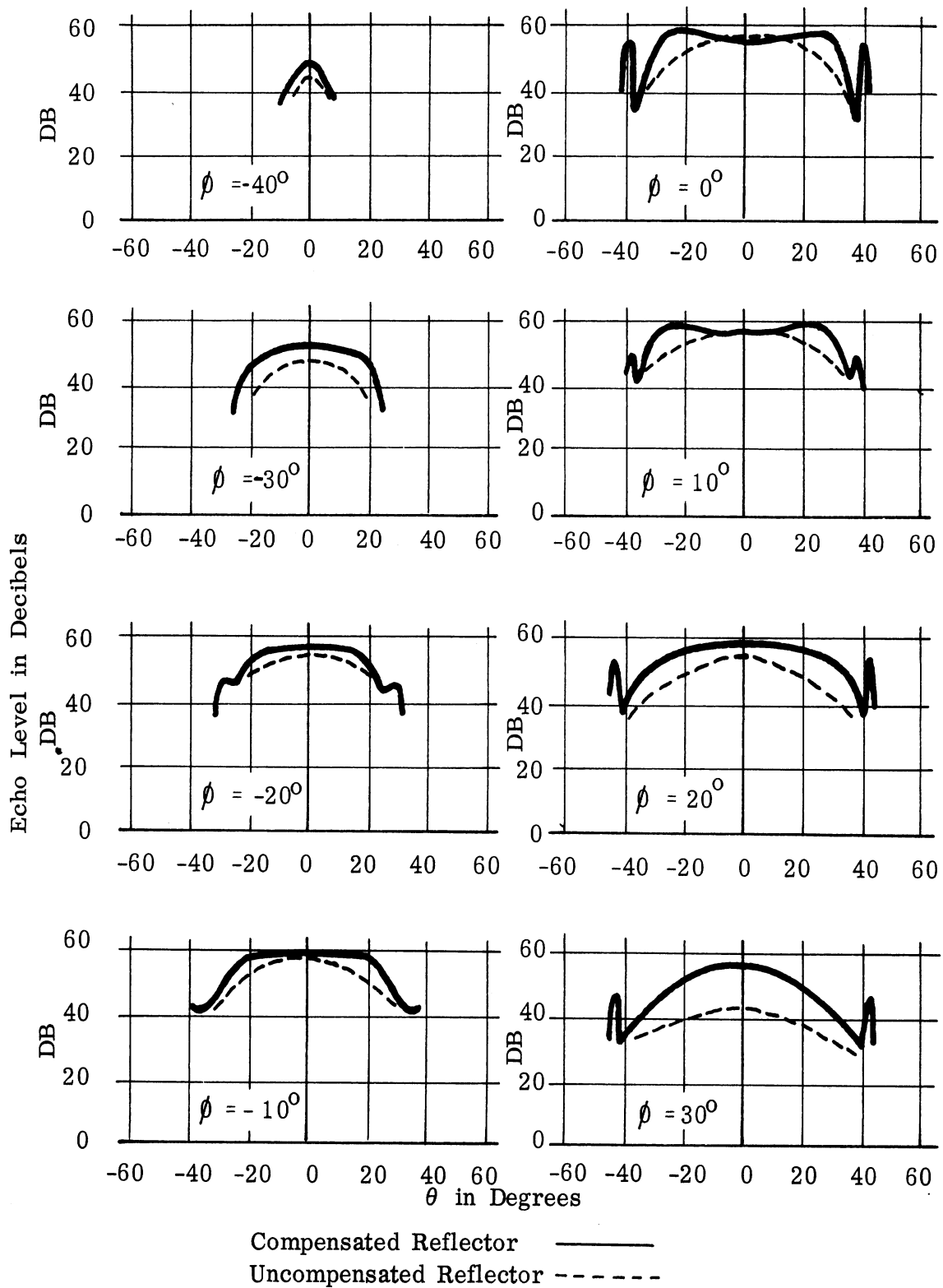
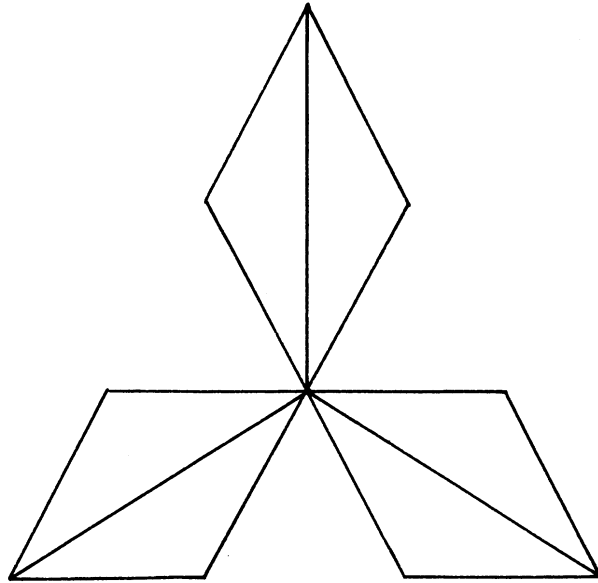
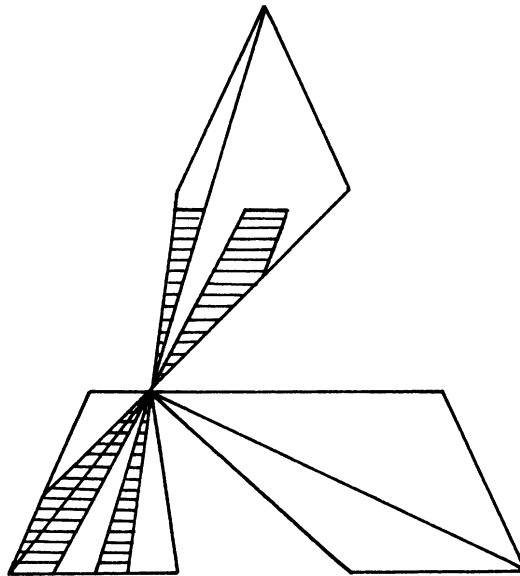


FIG. C-17: REFLECTION CHARACTERISTICS OF COMPENSATED TRIANGULAR CORNER REFLECTOR



Aspect $\Theta = 0^\circ$, $\phi = 0^\circ$
Effective Area, $A = 0$



Aspect $\Theta = 30^\circ$, $\phi = 0^\circ$
Shaded Region Represents Effective Area A

FIG. C-18: SPECIALLY COMPENSATED TRIANGULAR CORNER REFLECTOR
DESIGNED TO PRODUCE MINIMUM BACKSCATTERING ALONG AXIS OF SYMMETRY

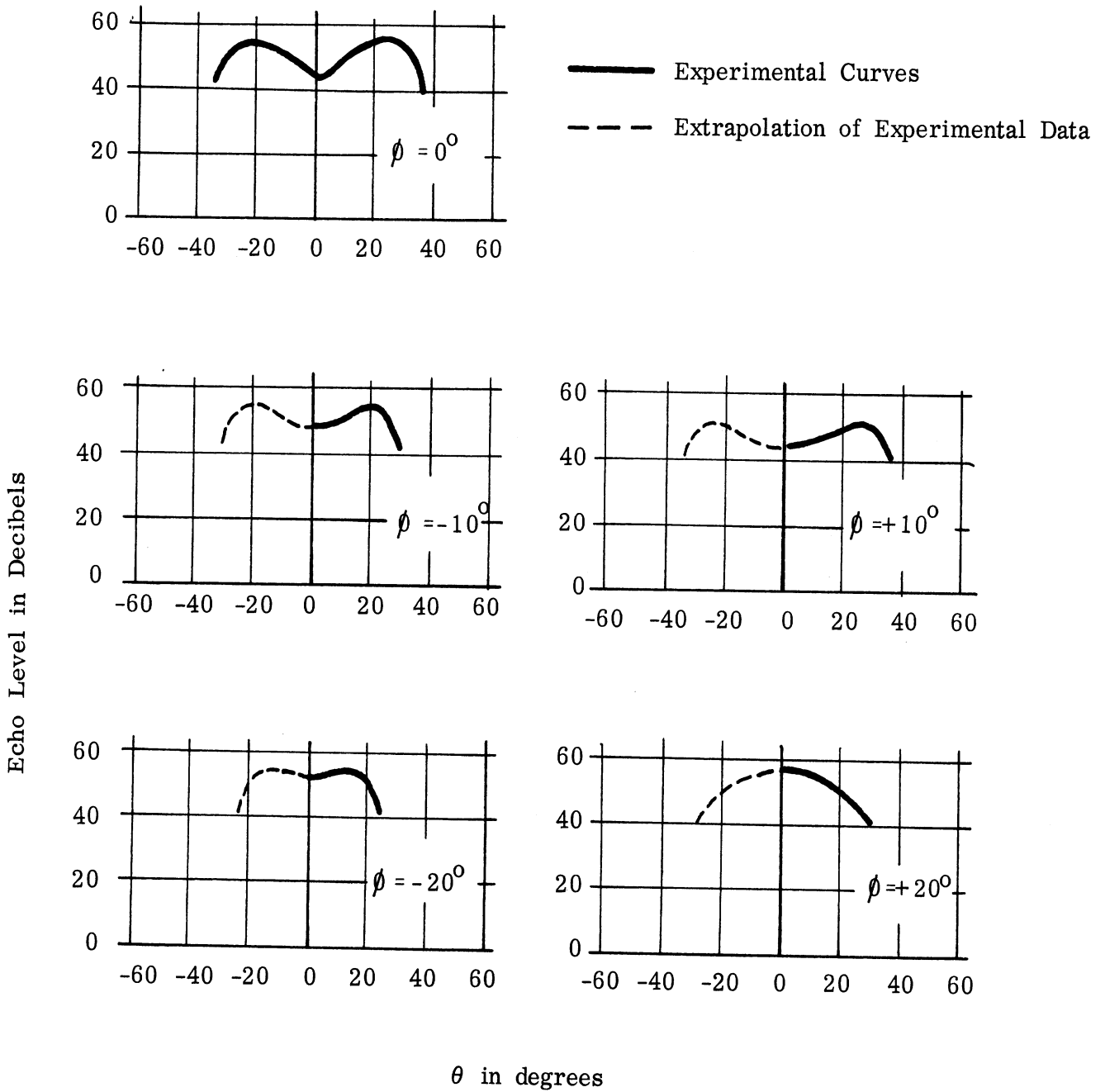


FIG. C-19: RESPONSE PATTERN OF CORNER REFLECTOR DESIGNED FOR MINIMUM ECHO ON THE AXIS

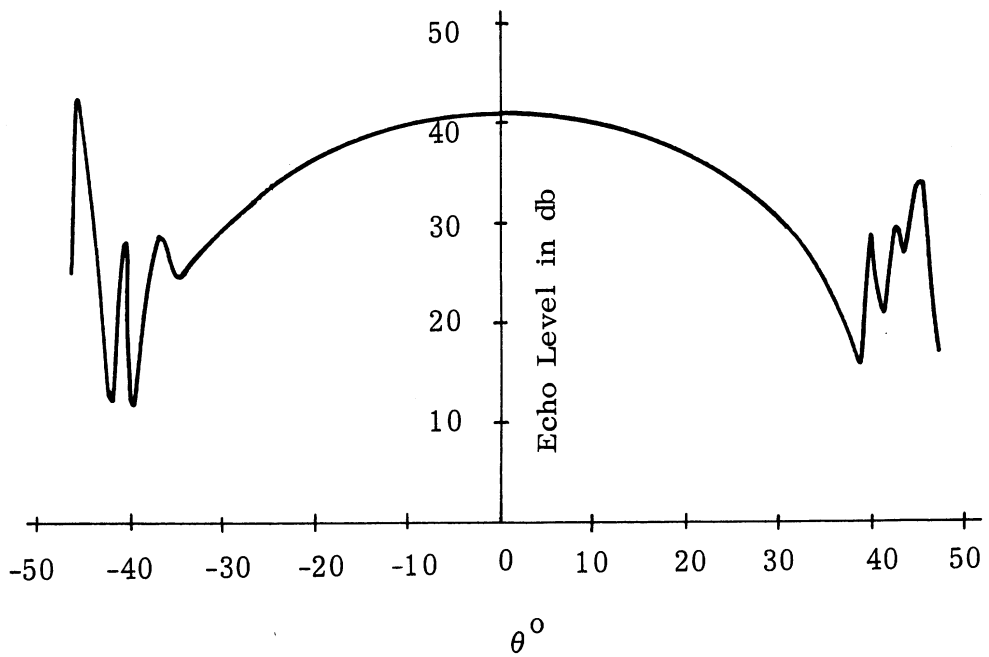
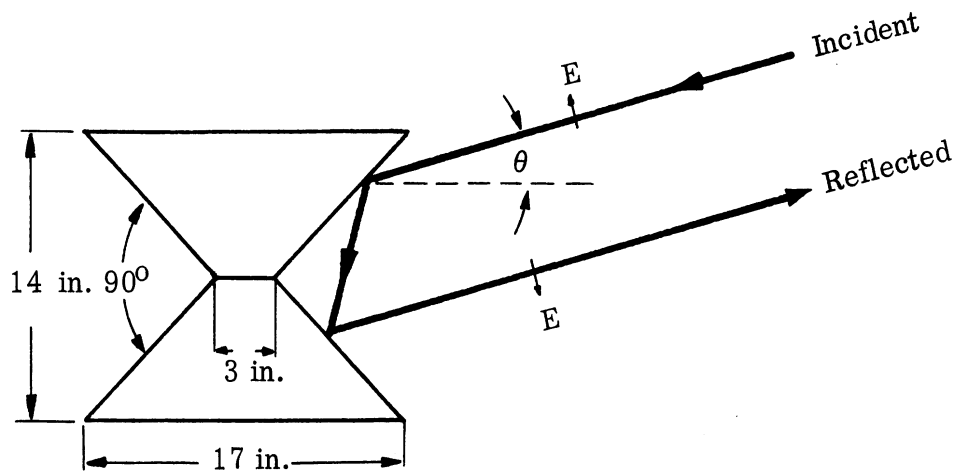


FIG. C-20: RESPONSE PATTERN OF BICONICAL REFLECTOR

REFERENCES

- C-1. R. K. Luneberg, "Mathematical Theory of Optics", Brown University, Providence, R. I. (1944).
- C-2. N. Arley, "A Note on the Foundations of Geometrical Optics", Det. Kgl. Danske Videnskabernes Selskab. Matematisk - fysiske Meddelelser, Vol. 22, No. 8, (1945-46).
- C-3. J. A. Stratton, Electromagnetic Theory, McGraw-Hill, New York, (1941).
- C-4. R. C. Spencer, "Optical Theory of the Corner Reflector", MIT Radiation Laboratory. (1944). ATI-5763.
- C-5. S. D. Robertson, "Targets for Microwave Radar Navigation", Bell System Technical Journal, 26, 852, (1947).
- C-6. "Symposium on Microwave Optics", Eaton Electronics Research Laboratory, McGill University. (June 1953).
- C-7. V. A. Fock, "Generalization of the Reflection Formulae to the Case of Reflection of an Arbitrary Wave from a Surface of Arbitrary Form", Zhurnal Eksperimental' noi i Teoreticheskoi Fiziki, 20, 961, (1950).
- C-8. R. D. O'Neal, "The Application of Corner Reflectors to Radar (Experimental)", M.I.T. Radiation Laboratory (1 July 1943).

APPENDIX D

MONOSTATIC RADAR CROSS SECTION OF THE ELLIPTICAL CORNER REFLECTOR*

1

INTRODUCTION

As discussed in Appendix C the monostatic radar cross section of a corner reflector is given by

$$\sigma = \frac{4 \pi A^2}{\lambda^2}, \quad (1.1)$$

in which A is the area of the projection of an equivalent aperture on a plane normal to the direction of incidence. A convenient aperture, as described in Appendix C may be constructed by cutting out of each of the four quadrants of each coordinate plane an aperture of the same shape as the leaf of the corner reflector associated with that plane. This A will be determined here for the elliptical corner reflector, a shape frequently employed in asymmetric and limited volumes; as a special case, the area A will also be given for the circular corner reflector. Only triply-reflected radiation will be considered.

* Appendix D (Unclassified) of The University of Michigan Report "Studies in Radar Cross Sections XVIII - Airborne Passive Measures and Countermeasures", by K. M. Siegel, M. L. Barasch, J. W. Crispin, R. F. Goodrich, A. H. Halpin, A. L. Maffett, W. C. Orthwein, C. E. Schensted, and C. J. Titus (2260-29-F, January 1956). SECRET.

PROJECTION OF THE EQUIVALENT APERTURE

The area A will be a function of ℓ/a , m/b , and n/c , where ℓ , m , and n are the direction cosines of the line-of-sight with the three coordinate axes, and a , b , c the edge-lengths of the ellipses along these axes. Because of the symmetry of the optical model, it is necessary to consider only the range of parameters

$$\ell/a \geq m/b \geq n/c, \quad (2.1)$$

where $1 > \ell, m, n > 0.$ (2.2)

The coordinate system may then be chosen in accordance with equation (2.1). Because of the invariance of the optical model under reflections in the coordinate planes, a right-handed system may always be chosen.

Consider the corner reflector of Figure D-1.

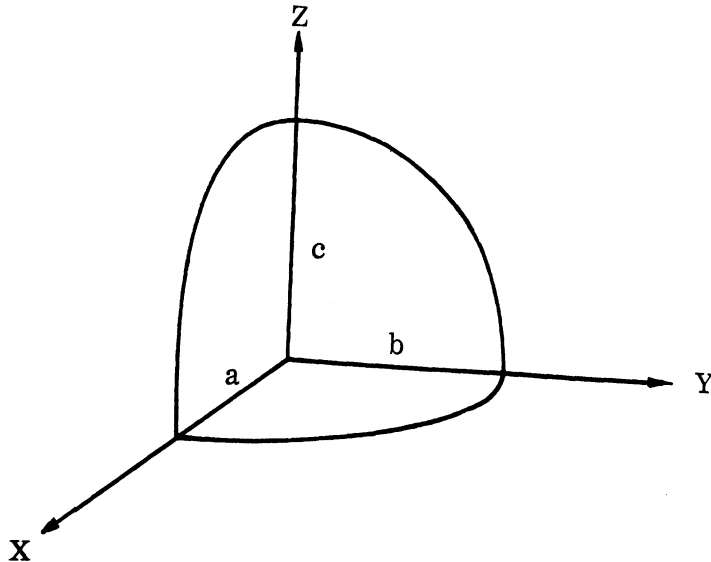


FIG. D-1: ORIENTATION OF CORNER REFLECTOR

The equations of the three ellipses are

$$\begin{aligned}
x^2/a^2 + y^2/b^2 &= 1 \\
x^2/a^2 + z^2/c^2 &= 1 \\
y^2/b^2 + z^2/c^2 &= 1
\end{aligned}
\tag{2.3}$$

Project these curves onto the X-Y plane along the line-of-sight, or (ℓ , m , n) direction. These equations of these projected curves are

$$\begin{aligned}
x^2/a^2 + y^2/b^2 &= 1 \\
x^2 - \frac{2\ell}{m} xy + y^2 \frac{(\ell^2 c^2 + n^2 a^2)}{m^2 c^2} &= a^2 \\
\frac{m^2 c^2 + n^2 b^2}{\ell^2 c^2} x^2 - \frac{2m}{\ell} xy + y^2 &= b^2.
\end{aligned}
\tag{2.4}$$

The area common to the three curves is to be determined, and then projected onto the plane normal to the line-of-sight. A is therefore the common area in the X-Y plane multiplied by n , the cosine of the angle between the normals to the two planes.

The procedure is simplified by an additional projection which transforms the first ellipse into a circle. If $b < a$, the projection introduces the transformation

$$x' = x \cos \psi = x \frac{b}{a}, \tag{2.5}$$

where ψ is the projecting angle. If $b > a$, use

$$y' = y \cos x = y \frac{a}{b}. \tag{2.6}$$

Either of these will lead to the same final result for A. The first is employed.

Equation (2.4) then becomes (dropping the primes on x and y)

$$x^2 + y^2 = b^2$$

$$x^2 - \frac{2\ell b}{ma} xy + y^2 \left[\frac{\ell^2 b^2 c^2 + n^2 a^2 b^2}{m^2 a^2 c^2} \right] = b^2 \quad (2.7)$$

$$\frac{m^2 a^2 c^2 + n^2 a^2 b^2}{\ell^2 b^2 c^2} x^2 - \frac{2ma}{\ell} xy + y^2 = b^2.$$

The area common to these three curves must be found, and multiplied by na/b to yield A.

THE INTERSECTIONS, SEMI-AXES, AND ORIENTATIONS OF THE CURVES

Using the condensation symbols

$$L = \ell^2 b^2 c^2, \quad M = m^2 a^2 c^2, \quad N = n^2 a^2 b^2, \quad (3.1)$$

Equations (2.7) become

$$(a) \quad x^2 + y^2 = b^2$$

$$(b) \quad x^2 - 2 \sqrt{\frac{L}{M}} xy + \frac{L+N}{M} y^2 = b^2 \quad (3.2)$$

$$(c) \quad \frac{M+N}{L} x^2 - 2 \sqrt{\frac{M}{L}} xy + y^2 = b^2.$$

The intersection points of these three curves are displayed in Table D-2 the key to which is Table D-1. In each block, the upper intersection is encountered first in a counter-clockwise circuit.

TABLE D-1

NOMENCLATURE FOR INTERSECTION POINTS

	1	2	3
1		P B	E F
2	C D		I J
3	G H	K L	

TABLE D-2

LOCATION OF INTERSECTION POINTS

	$\theta = 0$ $\theta = \pi$ $\rho = b$	$\theta = \frac{\pi}{2}$ $\theta = \frac{3\pi}{2}$ $\rho = b$
$\tan \theta = \frac{2\sqrt{LM}}{L - M + N}$ $\rho = b$		$\tan \theta = \sqrt{M/L}$ $= \sqrt{\frac{M+L}{N}}$
$\tan \theta = -\frac{L - (M+N)}{2\sqrt{LM}}$	$\tan \theta = \sqrt{M/L} \left[\frac{L - M - N}{L - M + N} \right]$ $\rho^2 = \frac{b^2}{N} \frac{(L+M)(L-M)^2 + 2N(L-M)^2 + N^2(L+M)}{(L-M)^2 + 2N(L+M) + N^2}$	

It follows from the inequality [equation (2.1)] which may be written

$$L \geq M \geq N \tag{3.3}$$

that the intersection points are ordered in the following fashion:

TABLE D-3

ORDERING OF INTERSECTION POINTS

	Case 1		L < M + N											
Quadrant	1				2				3				4	
Point:	P	G	I	C	E	K	B	H	J	D	F	L		
ρ :	b	a	>b	b	b	<b	b	b	>b	b	b	<b		

TABLE D-3 (Continued)

Case 2 $L > M + N$

Quadrant	1				2		3				4	
Point:	P	K	I	C	E	G	B	L	J	D	F	H
ρ :	b	b	$>\rho_k$	b	b	b	b	$>b$	$>\rho_L$	b	b	b

The curves may, therefore, be drawn as shown in Figures D-2 and D-3.

Now the area of a sector of an ellipse of semi-major axis r and semi-minor axis s between the angles α and β is given by

$$\text{Area} = \frac{rs}{2} \left[\arctan \left(\frac{r}{s} \tan \phi \right) \right]_{\alpha}^{\beta} \quad (3.4)$$

The semi-axes and orientation of the semi-major axes in our coordinate system must therefore be obtained. For the circle, of course,

$$r = s = b; \quad (3.5)$$

for ellipse (b) of equation (3.2)

$$\frac{r}{s} = \frac{2b^2M}{L+N+M \mp \sqrt{(L+N-M)^2 + 4LM}} \quad (3.6)$$

for ellipse (c)

$$\frac{r}{s} = \frac{2b^2L}{L+N+M \mp \sqrt{(L-M-N)^2 + 4ML}} \quad (3.7)$$

The angle between the semi-major axes of ellipse (b) and the x-axis is the first quadrant root of

$$\theta_2 = \frac{1}{2} \tan^{-1} \frac{2\sqrt{ML}}{L+N-M}. \quad (3.8)$$

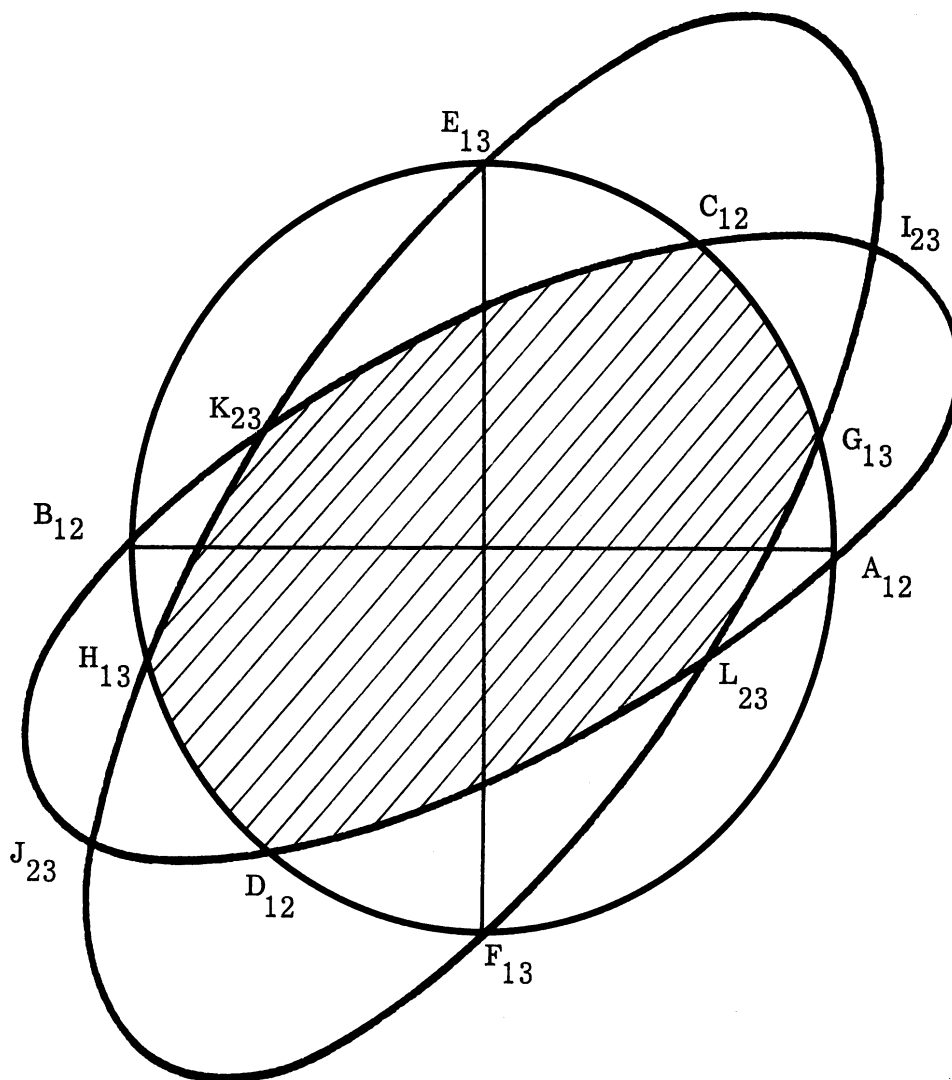


FIG. D-2: SIX-SIDED AREA FOR $L < M + N$

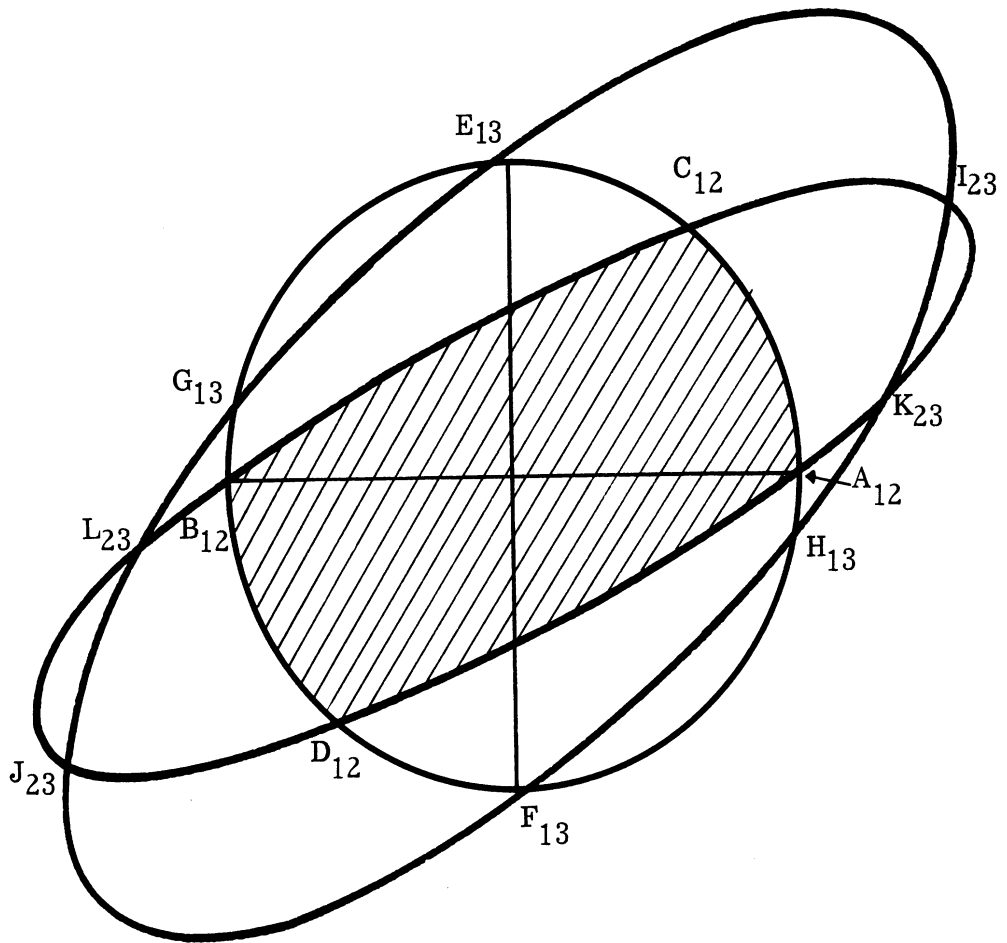


FIG. D-3: FOUR-SIDED AREA FOR $L > M + N$

The similar quantity for ellipse (c) is given by the first quadrant root of

$$\theta_3 = \frac{1}{2} \tan^{-1} \frac{2 \sqrt{ML}}{L - M - N}. \quad (3.9)$$

The final expressions for A, the shaded areas in Figure D-3 may also be given. They are, for $L < M + N$:

$$A = nab (C - G) + nab \sqrt{\frac{M}{N}} \arctan \frac{2 \sqrt{MN} \tan \phi}{L + M + N - \sqrt{(L - M + N)^2 + 4LM}} \left| \begin{array}{l} K - \theta_2 \\ C - \theta_2 \end{array} \right. +$$

$$nab \sqrt{\frac{L}{N}} \arctan \frac{2 \sqrt{LN} \tan \phi}{L + M + N - \sqrt{(L - M - N)^2 + 4LM}} \left| \begin{array}{l} H - \theta_3 \\ K - \theta_3 \end{array} \right. ; \quad (3.10)$$

for $L > M + N$:

$$A = nab (C - P) + nab \sqrt{M/N} \arctan \left(\frac{2 \sqrt{MN} \tan \phi}{L + M + N - \sqrt{(L - M + N)^2 + 4LM}} \right) \left| \begin{array}{l} B - \theta_2 \\ C - \theta_2 \end{array} \right. \quad (3.11)$$

When the values of P, B, C, G, H, and K from Tables D-1 and D-2 and the expressions for θ_2 and θ_3 from equations (3.8) and (3.9) are utilized in equations (3.10) and (3.11), these expressions for the common area become:

$$L > M + N, \quad \frac{A}{abc} = \sqrt{M} \tan^{-1} \left(\frac{2 \sqrt{LN}}{L + M - N} \right) + \sqrt{N} \tan^{-1} \left(\frac{2 \sqrt{LM}}{L + N - M} \right) ; \quad (3.12)$$

$$\begin{aligned}
L < M+N, \quad \frac{A}{abc} = \sqrt{L} \tan^{-1} \left(\frac{(M+N)^2 - L^2}{4 L \sqrt{MN}} \right) + \sqrt{M} \tan^{-1} \left(\frac{(L+N)^2 - M^2}{4 M \sqrt{LN}} \right) \\
\hspace{15em} (3.13) \\
+ \sqrt{N} \tan^{-1} \left(\frac{(L+M)^2 - N^2}{4 N \sqrt{LM}} \right).
\end{aligned}$$

We may simplify the form of these equations by making use of the symmetric functions

$$\begin{aligned}
S &= \frac{1}{2} (L+M+N) \\
T &= L M N.
\end{aligned}$$

Then we have

$$\begin{aligned}
L \geq M+N, \quad \frac{A}{abc} &= \sqrt{M} \tan^{-1} \left(\frac{\sqrt{\frac{T}{M}}}{S-N} \right) + \sqrt{N} \tan^{-1} \left(\frac{\sqrt{\frac{T}{N}}}{S-M} \right); \quad (3.14) \\
L \leq M+N, \quad \frac{A}{abc} &= \sqrt{L} \tan^{-1} \left(\frac{S(S-L)}{\sqrt{LT}} \right) + \sqrt{M} \tan^{-1} \left(\frac{S(S-M)}{\sqrt{MT}} \right) + \\
\hspace{15em} (3.15) \\
&\quad \sqrt{N} \tan^{-1} \left(\frac{S(S-N)}{\sqrt{NT}} \right).
\end{aligned}$$

This form is the easiest for numerical computation.

DISCUSSION OF RESULTS

It is to be noted that for the transition point $L = M + N$, $G = P = 0$ and $E = B = H = \pi$, so that equations (3.12) and (3.13) become identical, as they should.

Further, the transition point corresponds to that of $\ell^2 = 1/2$ for a circular reflector. For a circular corner reflector of edge length R , equations (3.12) and (3.13) reduce to

$$\ell^2 \geq \frac{1}{2}, \quad \frac{A}{R^2} = m \tan^{-1} \left(\frac{2\ell n}{1-2n^2} \right) + n \tan^{-1} \left(\frac{2\ell m}{1-2m^2} \right). \quad (4.1)$$

$$\ell^2 \leq \frac{1}{2}, \quad \frac{A}{R^2} = \ell \tan^{-1} \left(\frac{1-2\ell^2}{4\ell^2 mn} \right) + m \tan^{-1} \left(\frac{1-2m^2}{4\ell m^2 n} \right) + n \tan^{-1} \left(\frac{1-2n^2}{4\ell mn^2} \right). \quad (4.2)$$

The values of A/R^2 for a circular corner reflector of unit radius have been computed from equations (4.1) and (4.2). A is plotted as a function of m^2 (or n^2) for fixed values of ℓ^2 from 0.01 to 0.99 in steps of 0.01 (Fig. D-4 to D-23). Of course, ℓ^2 , m^2 , and $n^2 = 1 - \ell^2 - m^2$ may be permuted in any convenient way in using these graphs. σ is determined from the graphs as

$$\sigma = \frac{4\pi A^2}{\lambda^2}. \quad (4.3)$$

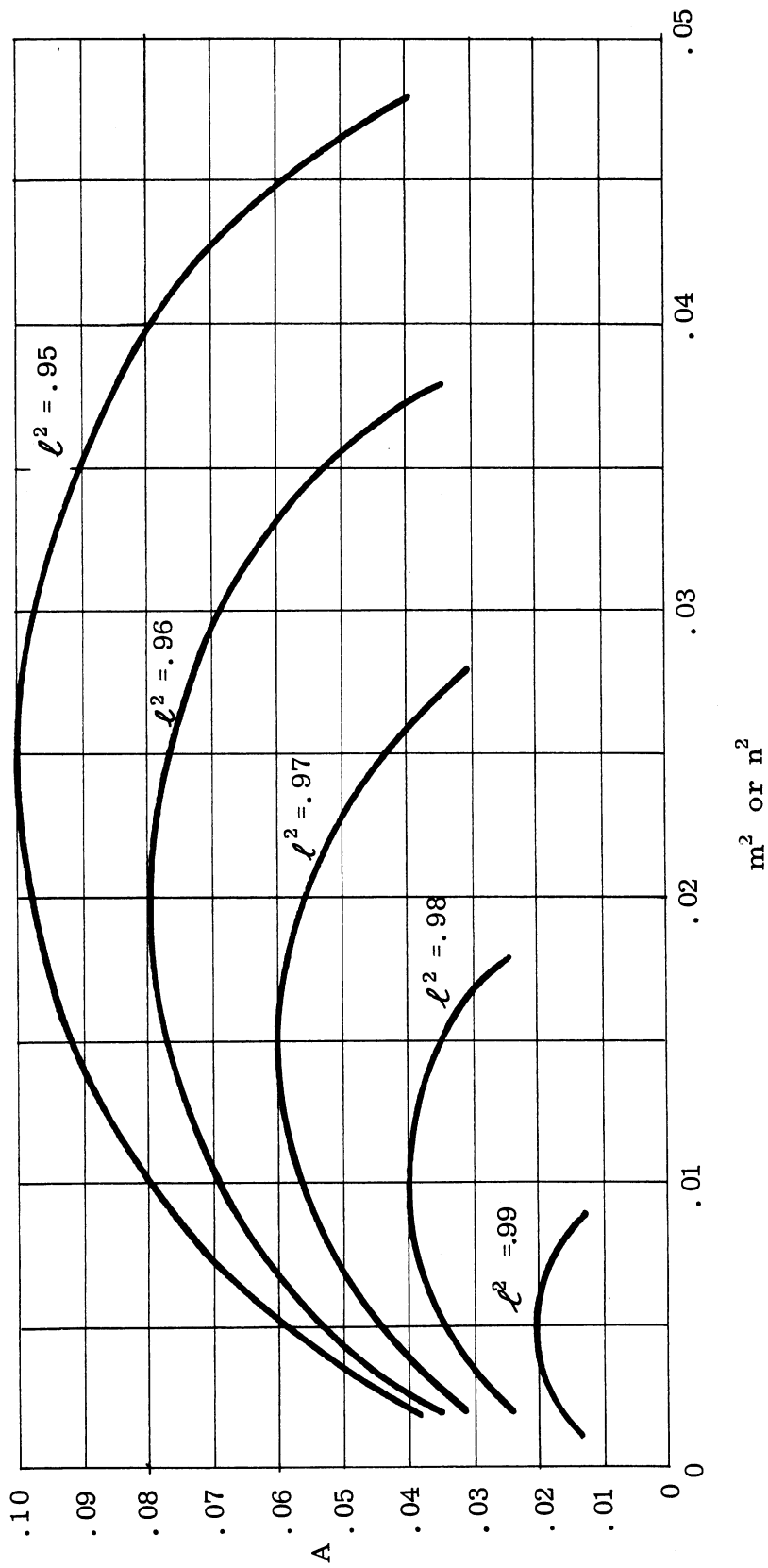


FIG. D-4: A, FOR UNIT EDGE CIRCULAR CORNER REFLECTOR, VS. m^2 OR n^2 FOR $\ell^2 = .99(.01).95$

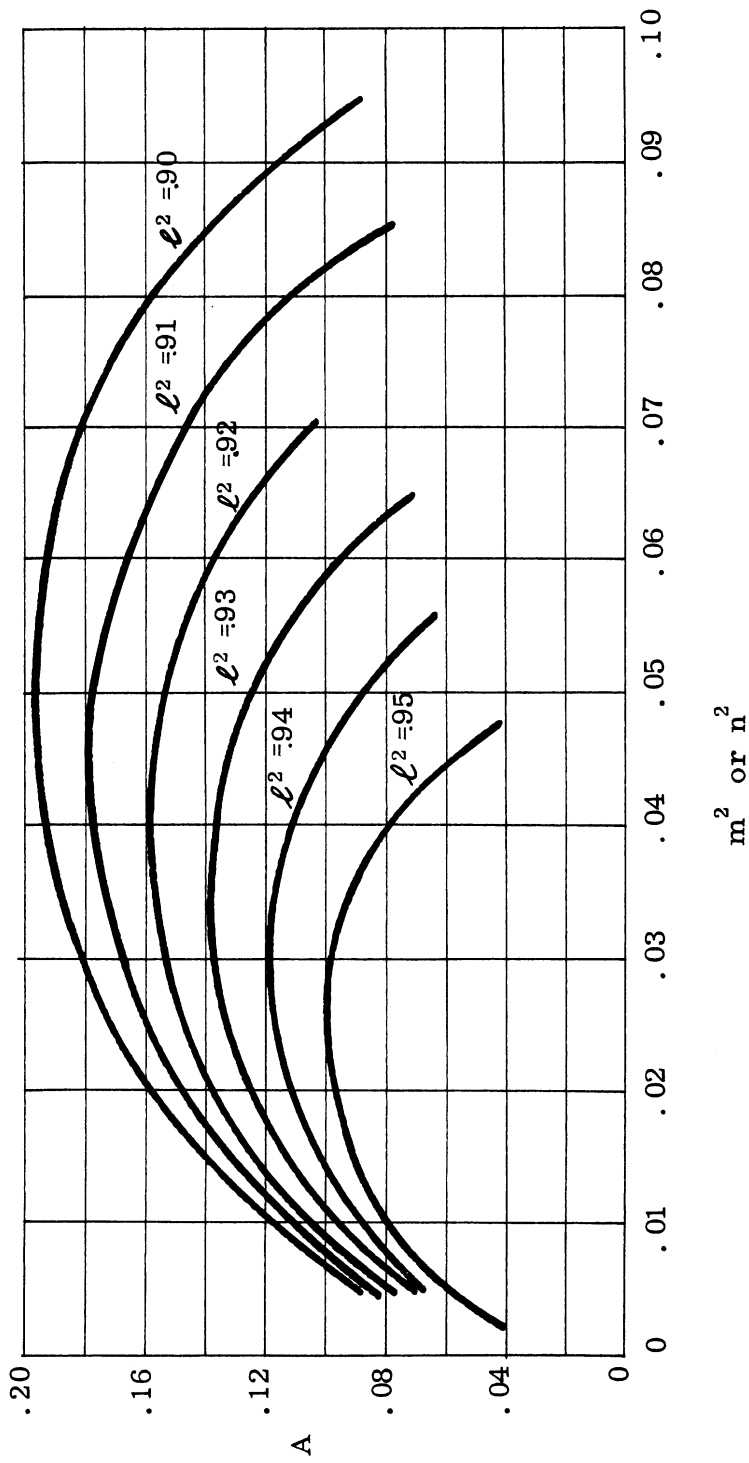


FIG. D-5: A, FOR UNIT EDGE CIRCULAR CORNER REFLECTOR,
 VS. m^2 OR n^2 FOR $l^2 = .95$ (.01).90

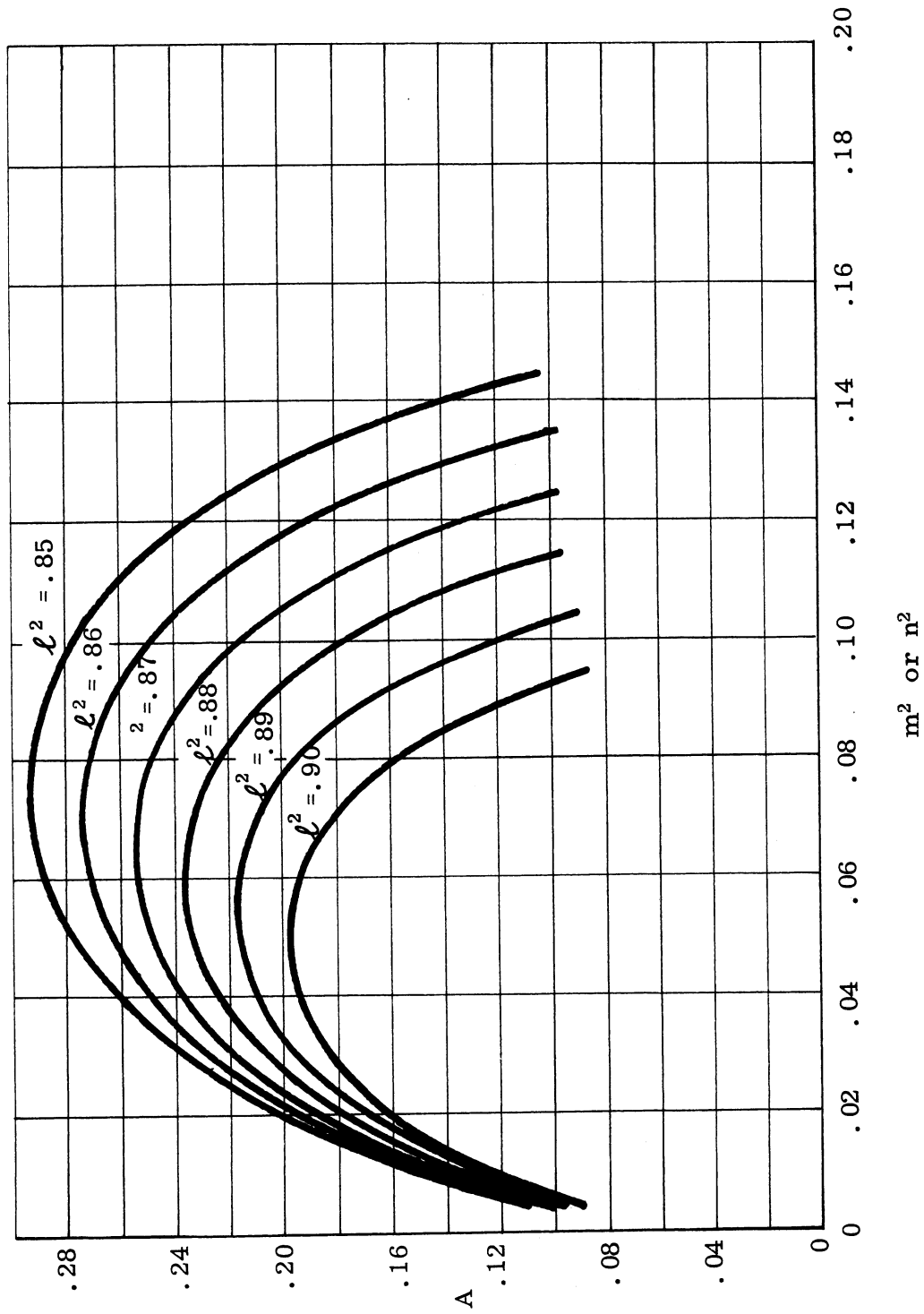


FIG. D-6: A, FOR UNIT EDGE CIRCULAR CORNER REFLECTOR,
 VS. m^2 OR n^2 FOR $l^2 = .90(.01) .85$

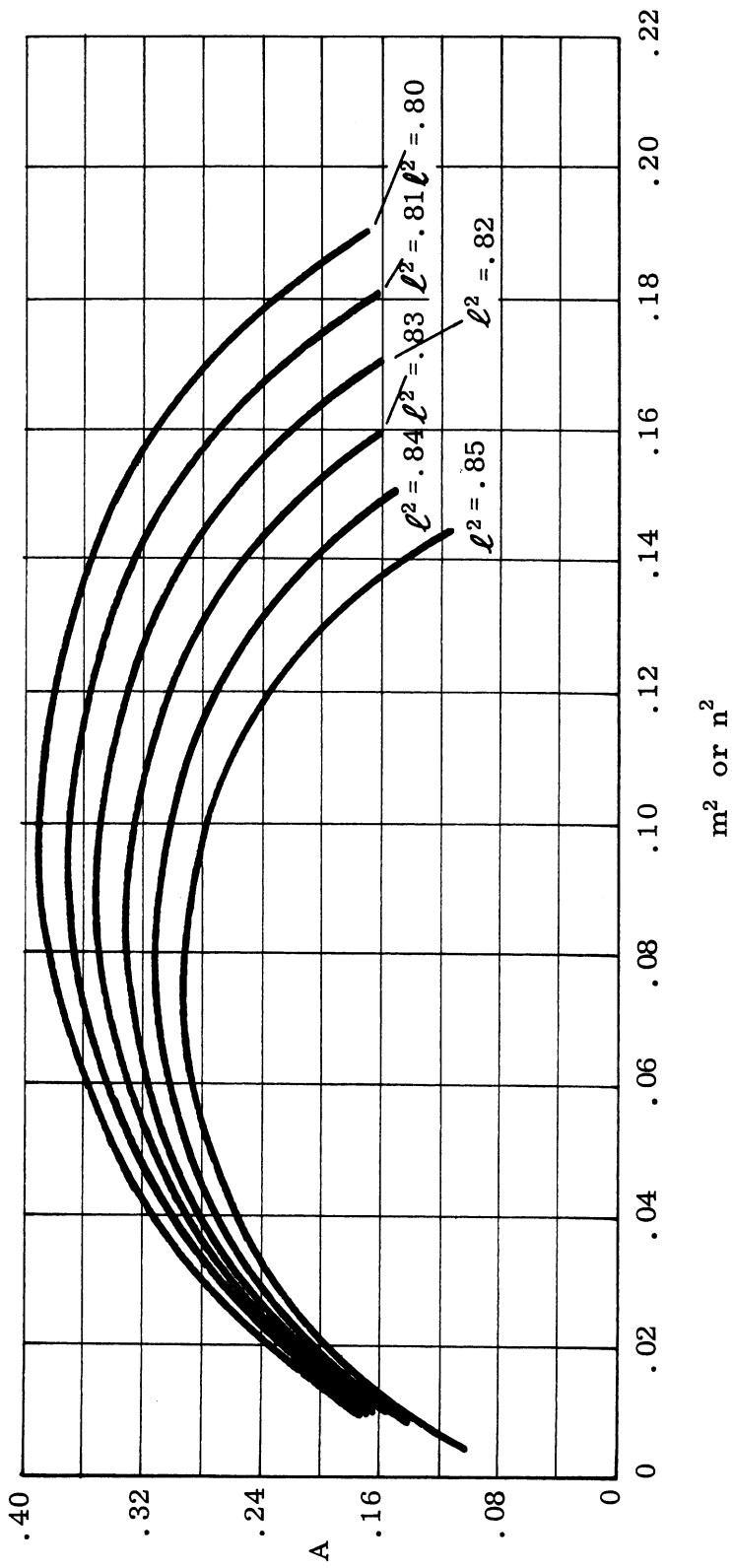


FIG. D-7: A, FOR UNIT EDGE CIRCULAR CORNER REFLECTOR,
VS. m^2 OR n^2 FOR $l^2 = .85(.01).80$

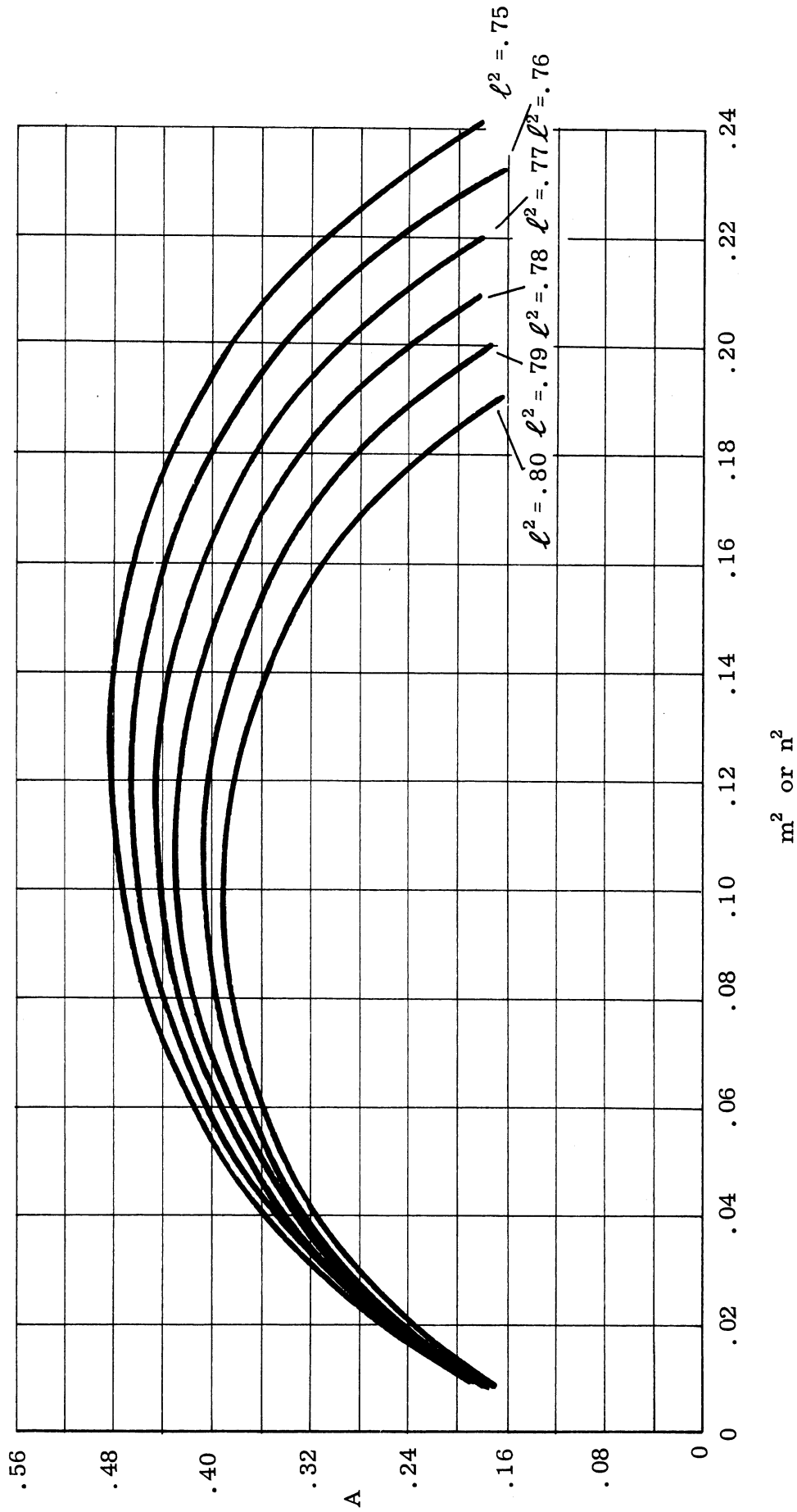


FIG. D-8: A, FOR UNIT EDGE CIRCULAR CORNER REFLECTOR,
 VS. m^2 OR n^2 FOR $\ell^2 = .80(.01).75$

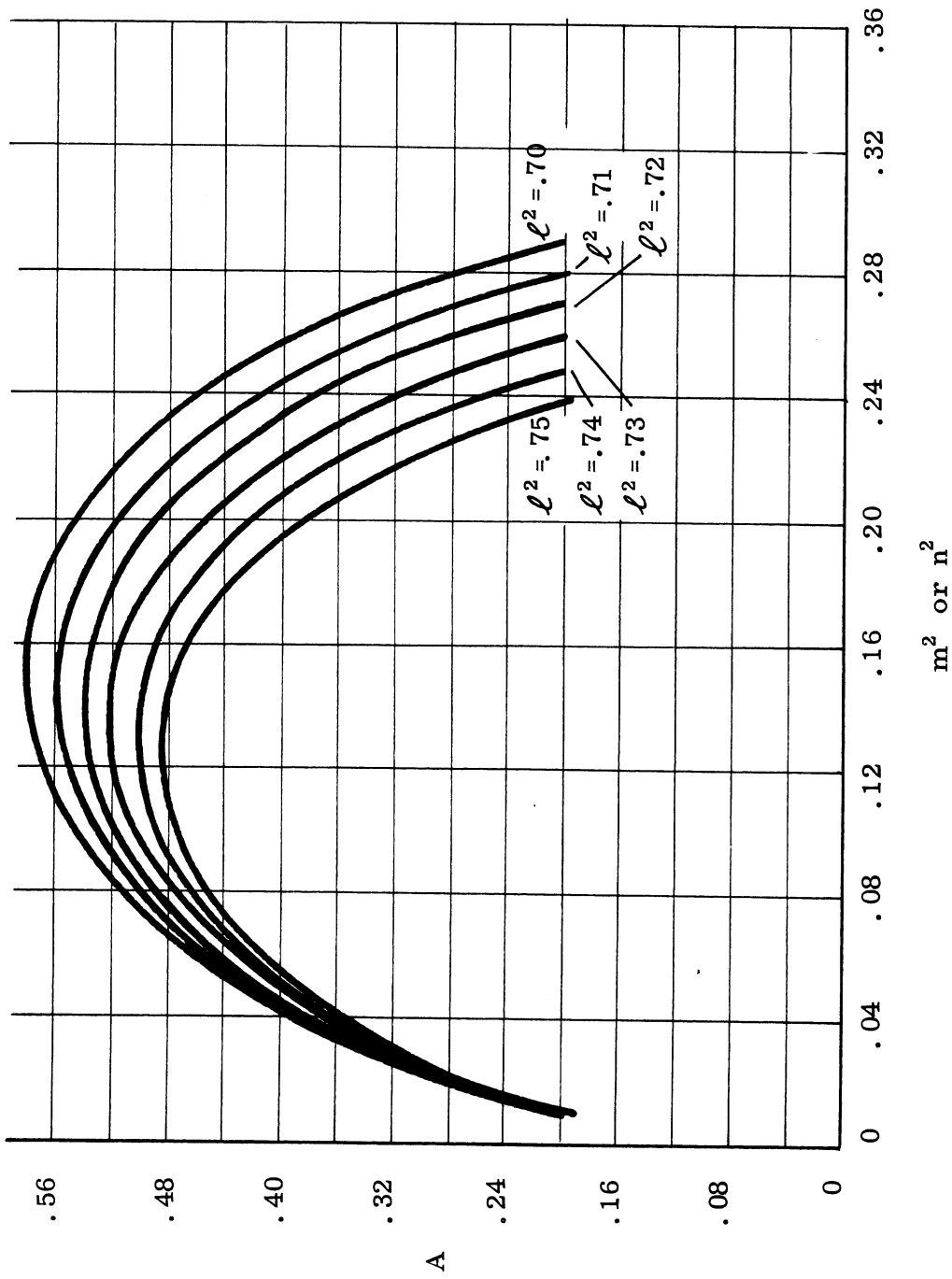


FIG. D-9: A, FOR UNIT EDGE CIRCULAR CORNER REFLECTOR,
VS m^2 OR n^2 FOR $\ell^2 = .75$ (.01) .70

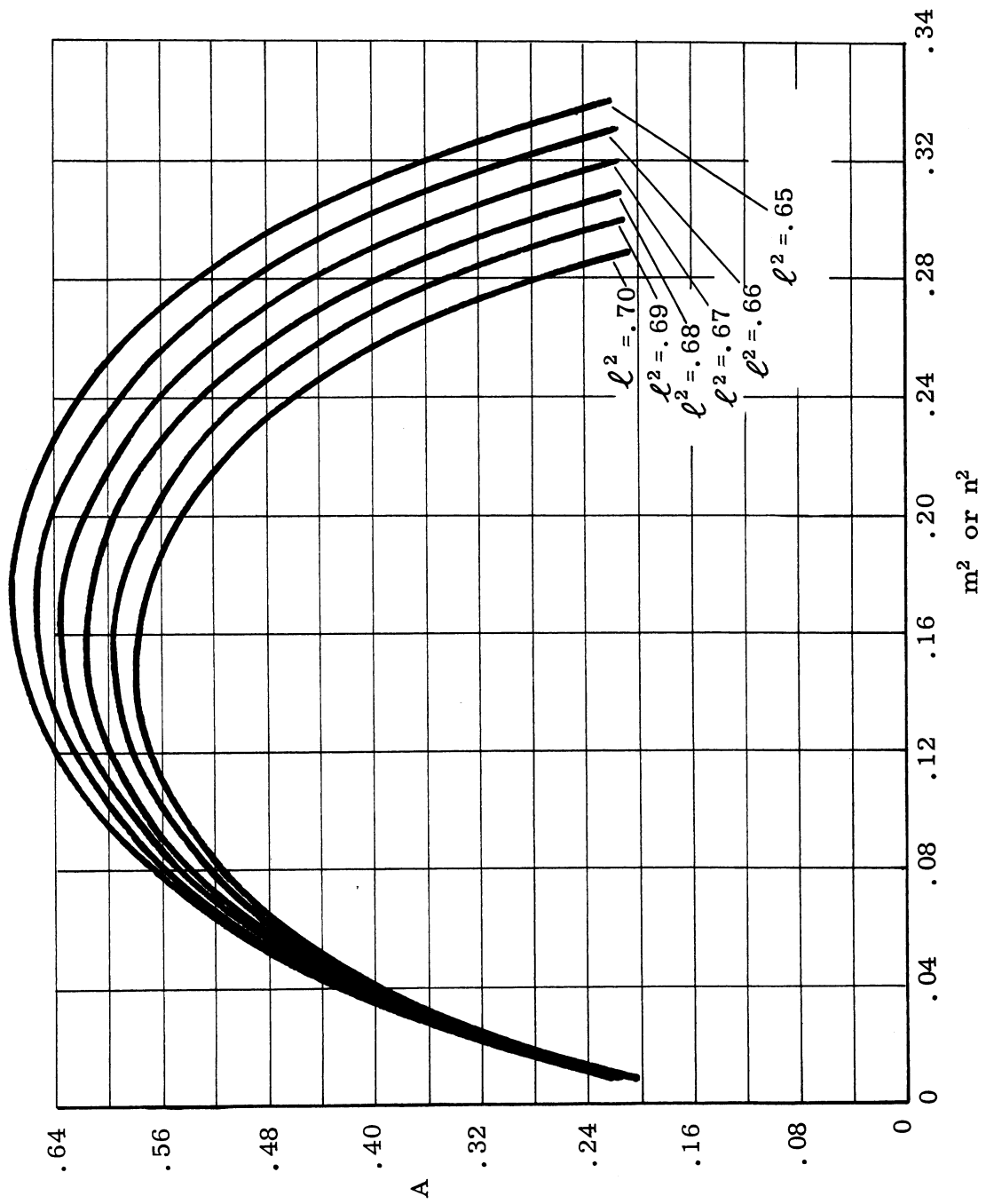


FIG. D-10: A, FOR UNIT EDGE CIRCULAR CORNER REFLECTOR,
VS. m^2 OR n^2 FOR $\ell^2 = .70(.01).65$

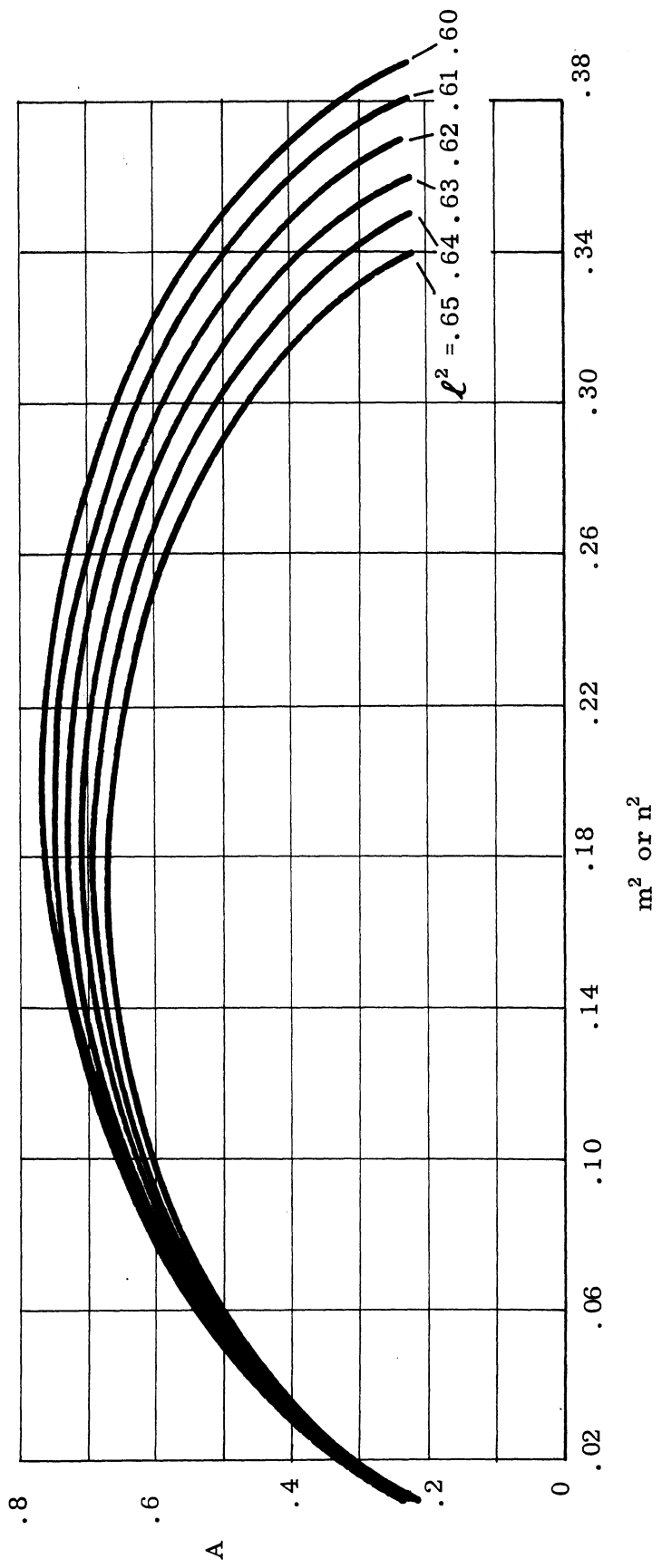


FIG. D-11: A, FOR UNIT EDGE CIRCULAR CORNER REFLECTOR,
 VS. m^2 OR n^2 FOR $L^2 = .65(.01).60$

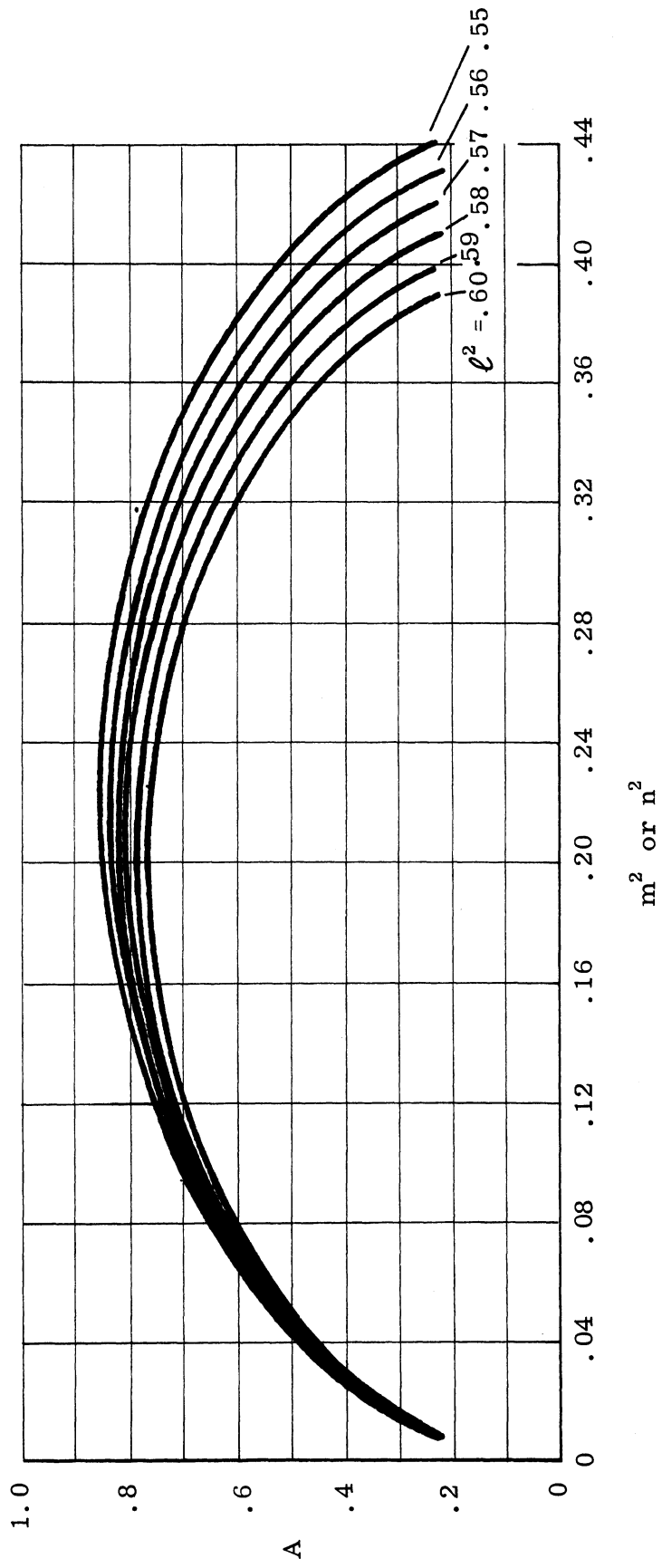


FIG. D-12: A, FOR UNIT EDGE CIRCULAR CORNER REFLECTOR,
 VS. m^2 OR n^2 FOR $l^2 = .60(.01).55$

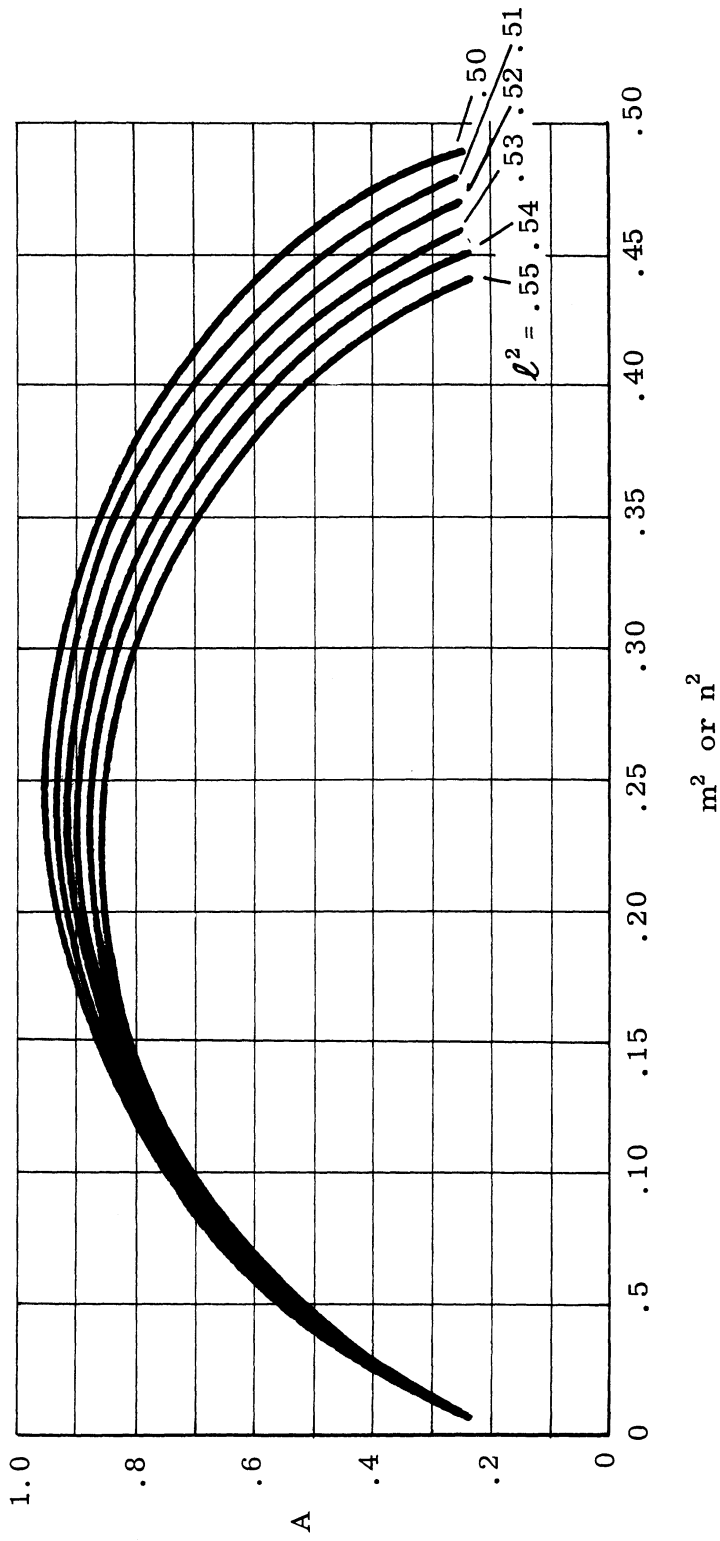


FIG. D-13: A, FOR UNIT EDGE CIRCULAR CORNER REFLECTOR, VS. m^2 OR n^2 FOR $l^2 = .55(.01).50$

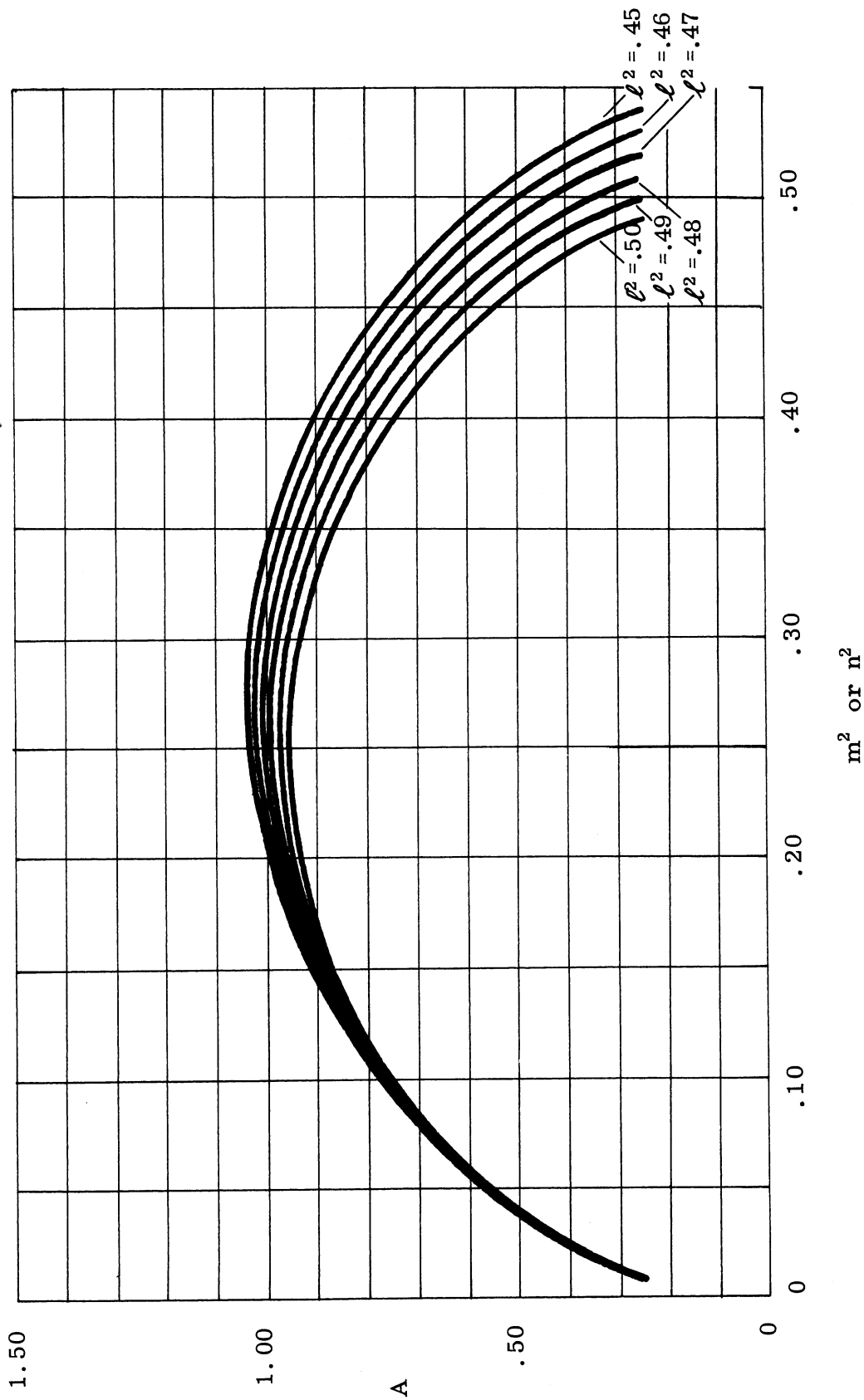


FIG. D-14: A, FOR UNIT EDGE CIRCULAR CORNER REFLECTOR, VS. m^2 OR n^2 FOR $\ell^2 = .50(.01).45$

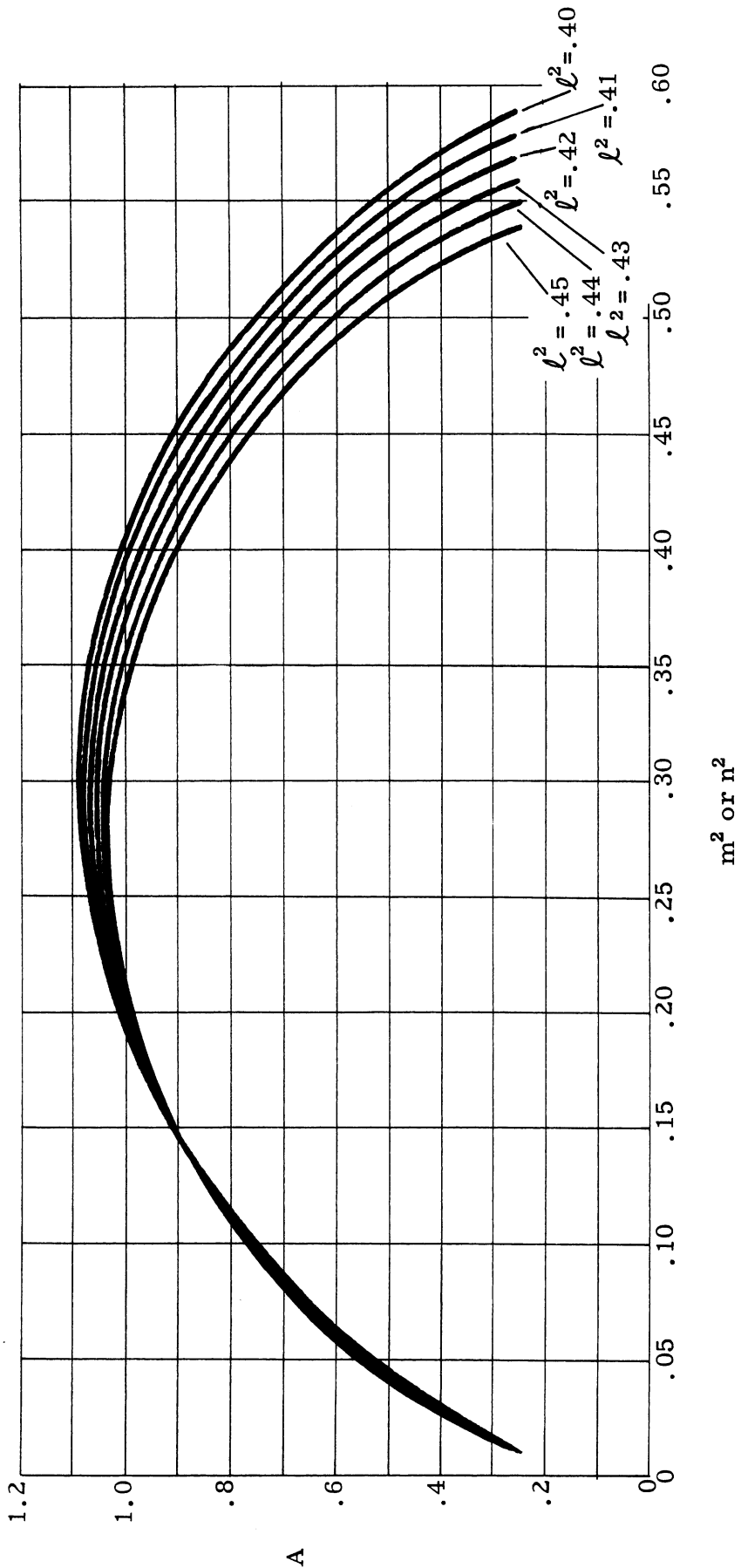


FIG. D-15: A, FOR UNIT EDGE CIRCULAR CORNER REFLECTOR, VS. m^2 OR n^2 FOR $\ell^2 = .45(.01).40$

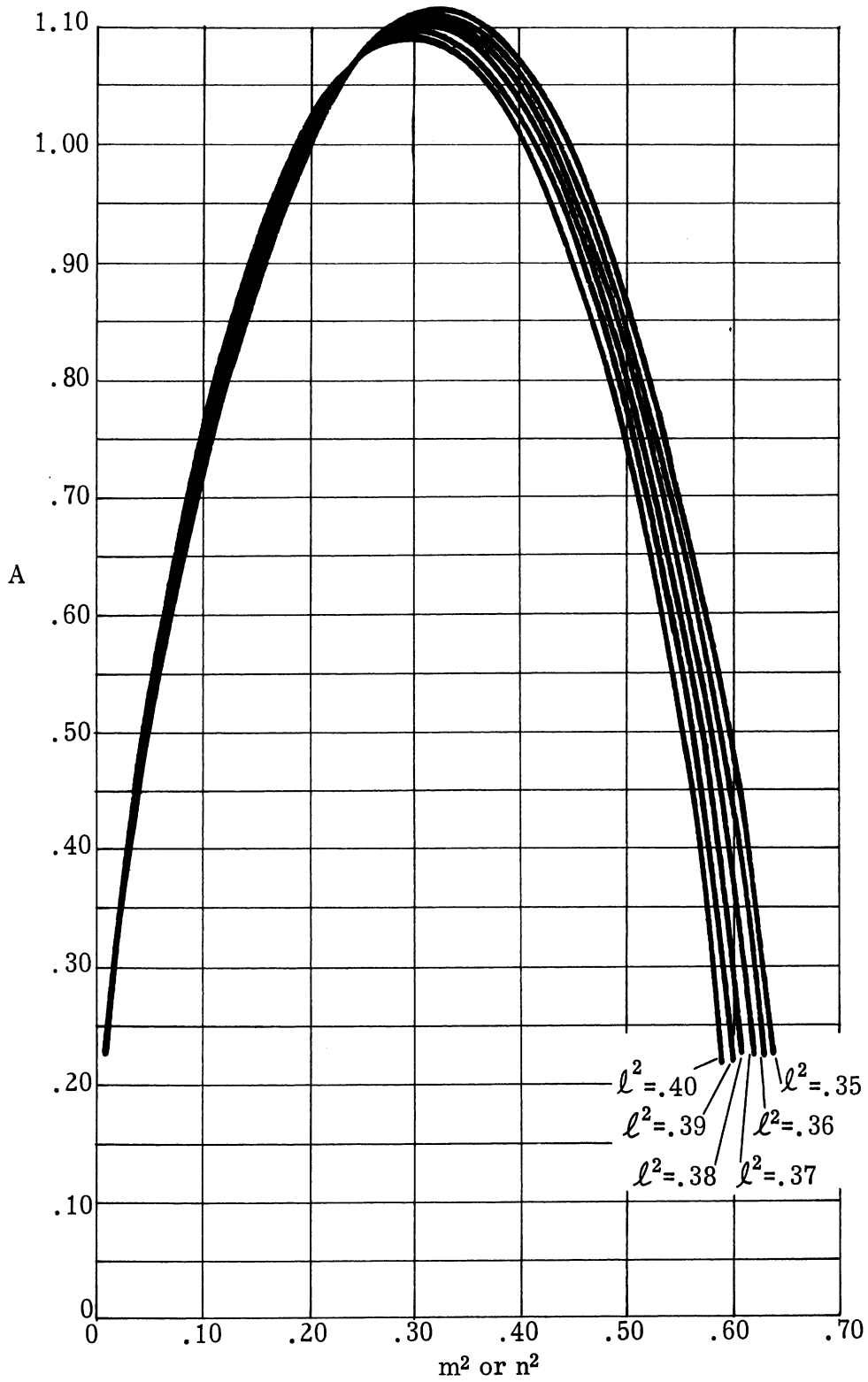


FIG. D-16: A, FOR UNIT EDGE CIRCULAR CORNER REFLECTOR VS. m^2 OR n^2 FOR $l^2 = .40(.01).35$

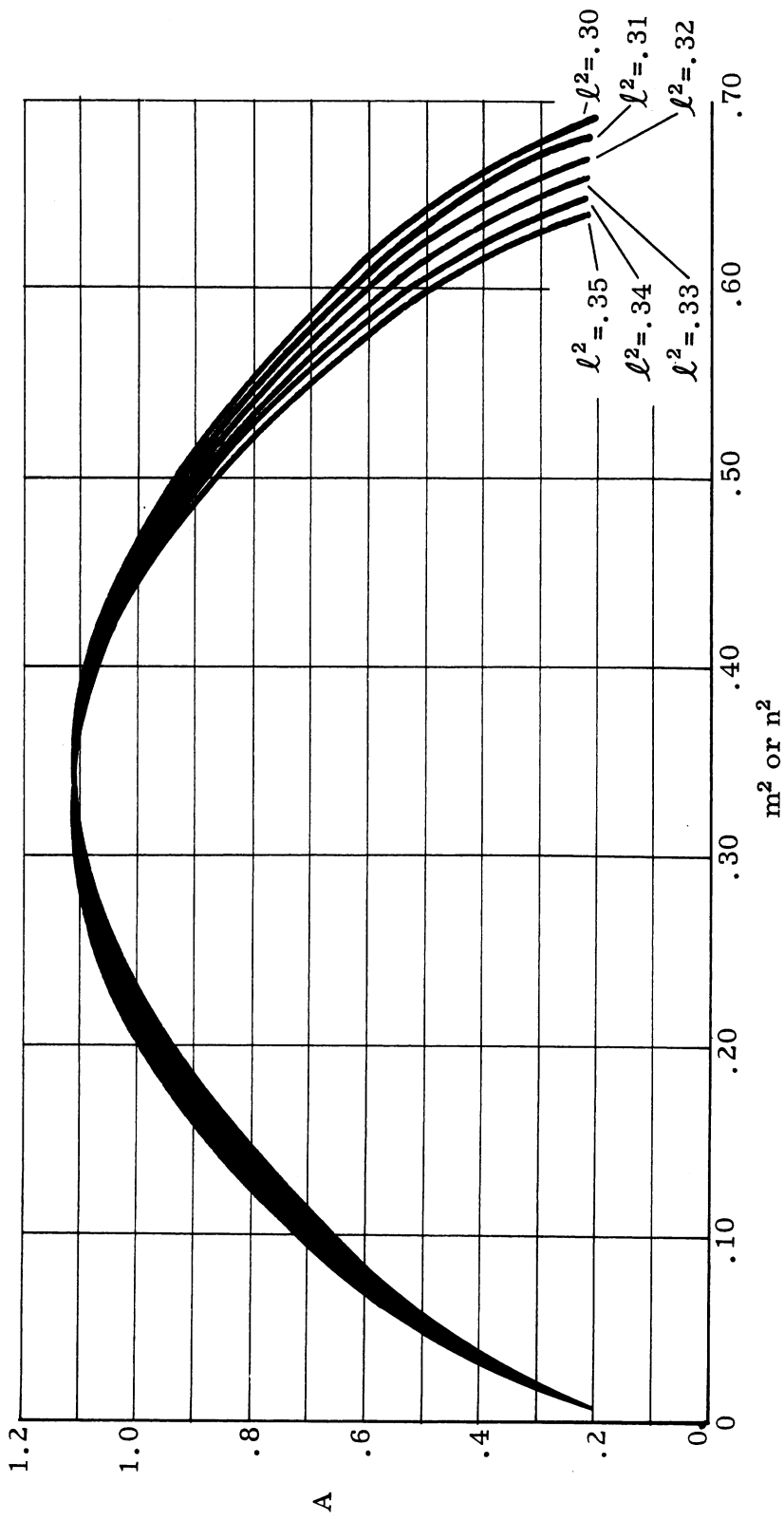


FIG. D-17: A, FOR UNIT EDGE CIRCULAR CORNER REFLECTOR, VS. m^2 OR n^2 FOR $\ell^2 = .35(.01).30$

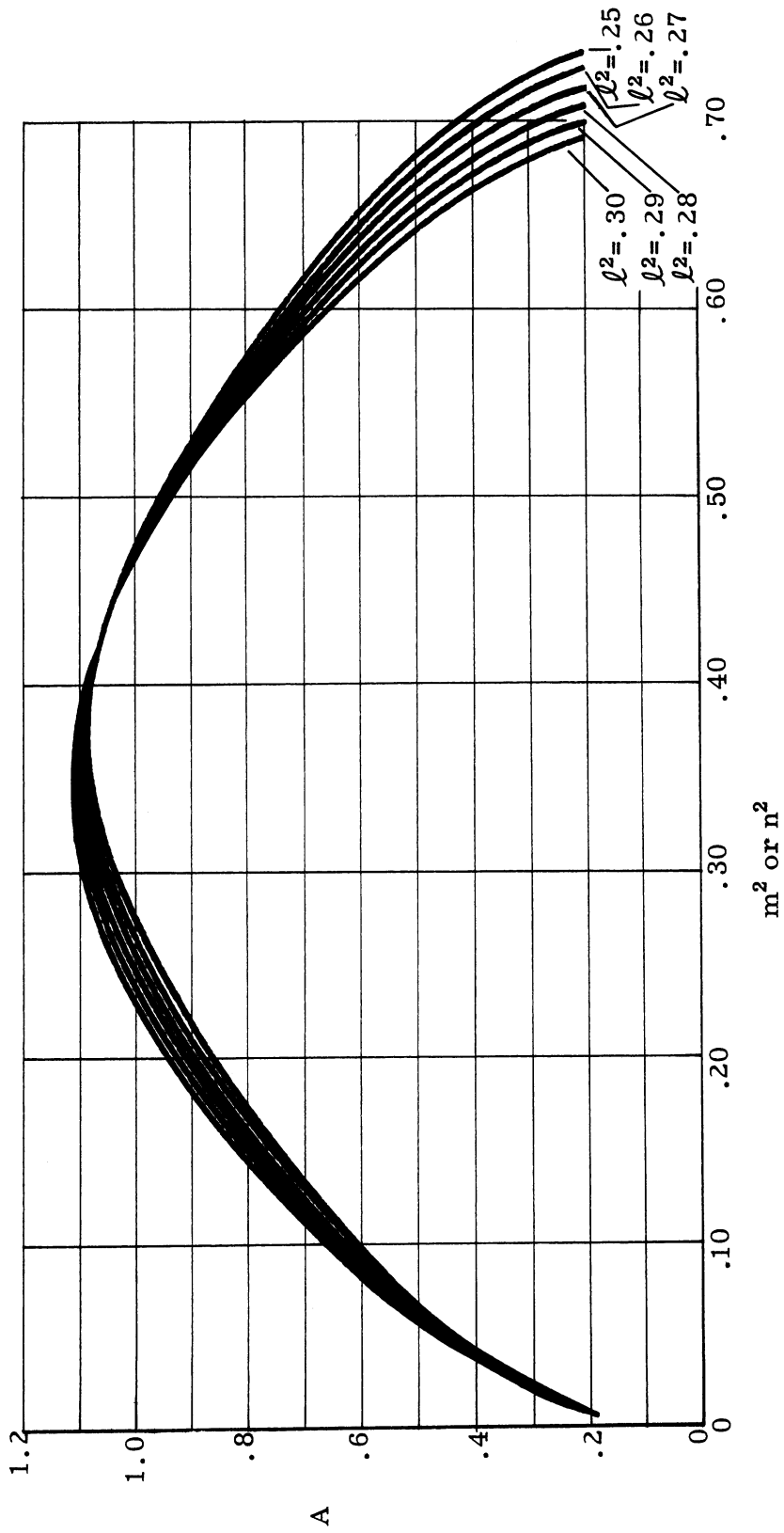


FIG. D-18: A, FOR UNIT EDGE CIRCULAR CORNER REFLECTOR, VS. m^2 OR n^2 FOR $\ell^2 = .30(.01).25$

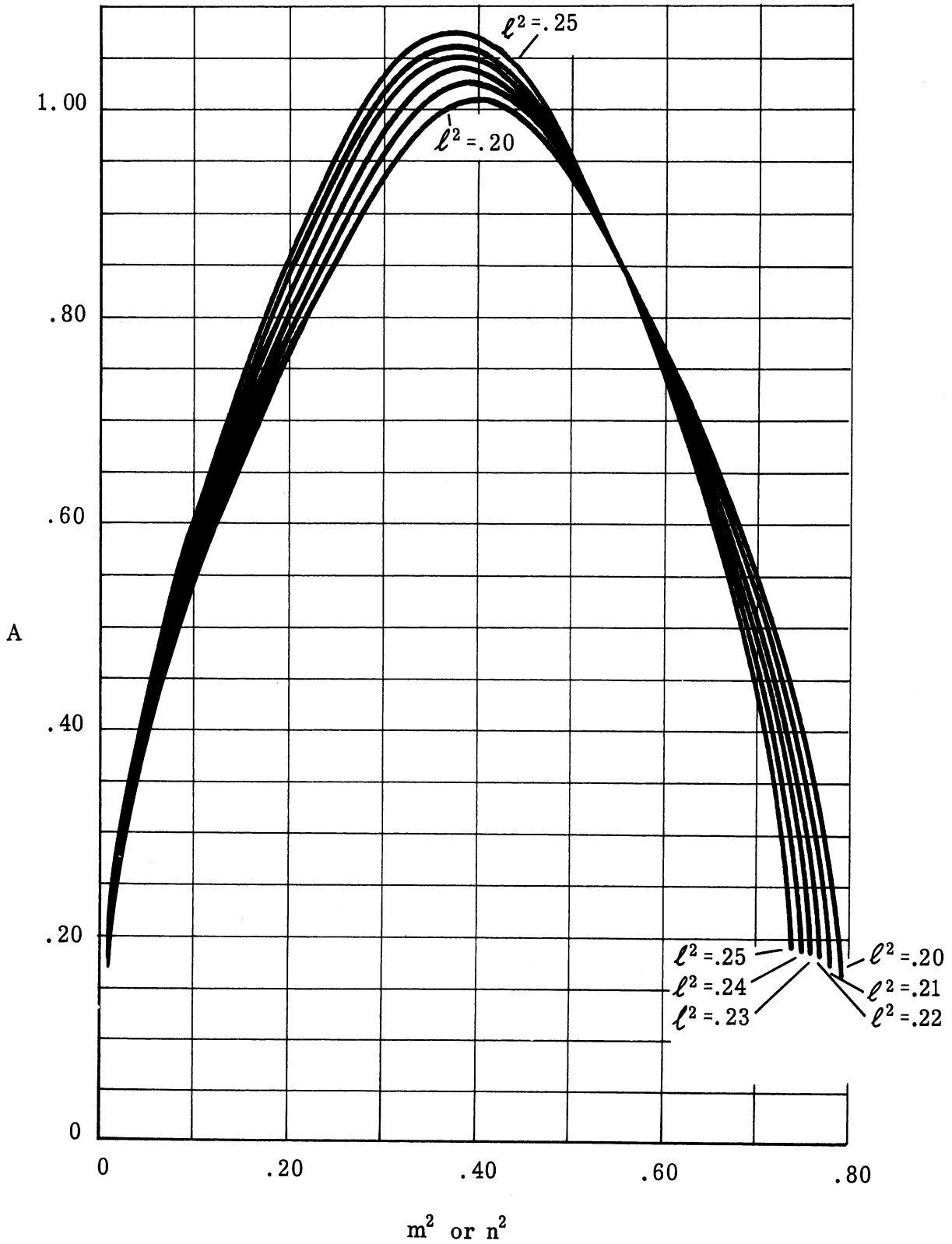


FIG. D-19: A, FOR UNIT EDGE CIRCULAR CORNER REFLECTOR,
 VS. m^2 OR n^2 FOR $l^2 = .25(.01).20$

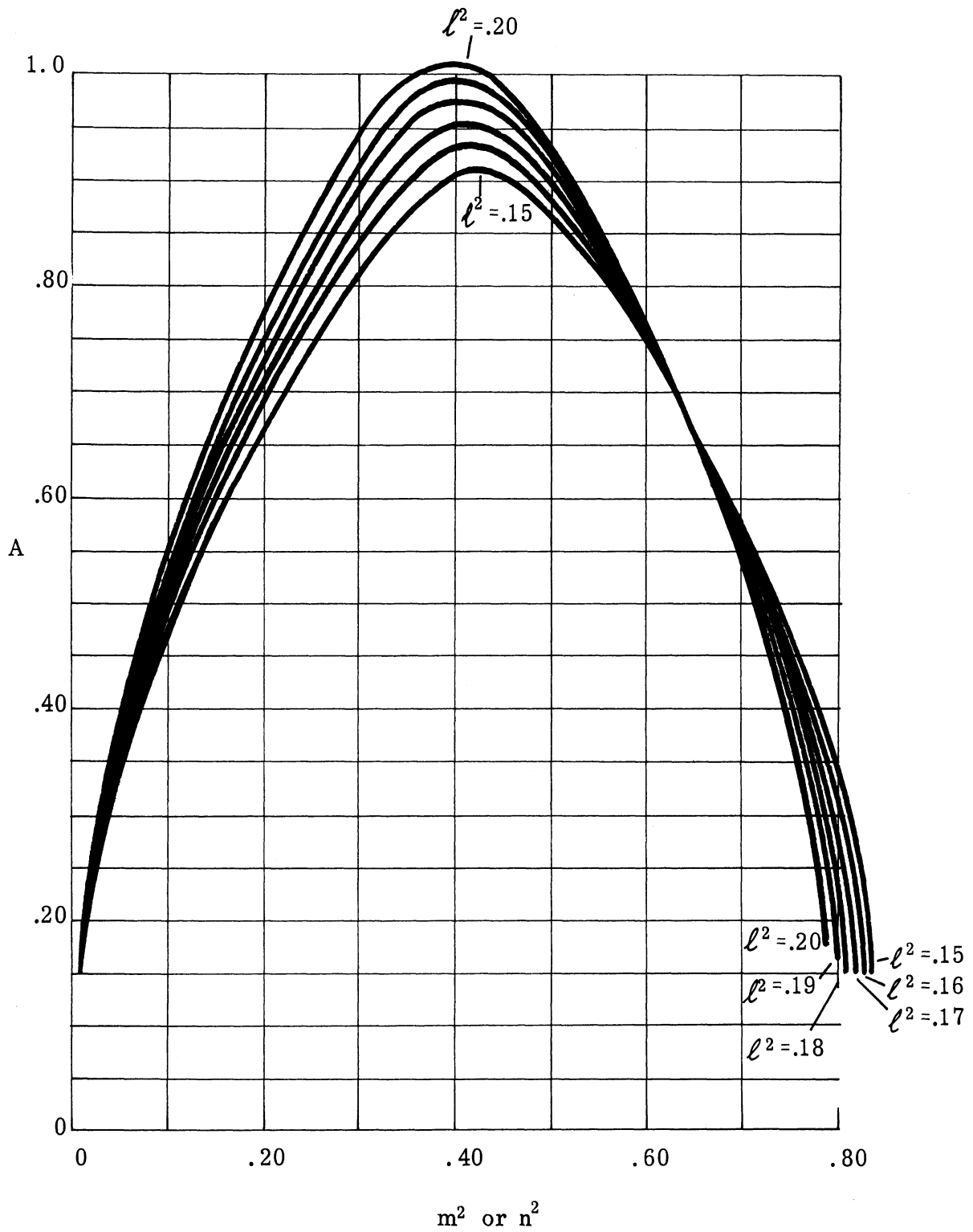


FIG. D-20: A, FOR UNIT EDGE CIRCULAR CORNER REFLECTOR, VS. m^2 OR n^2 FOR l^2 .20(.01).15

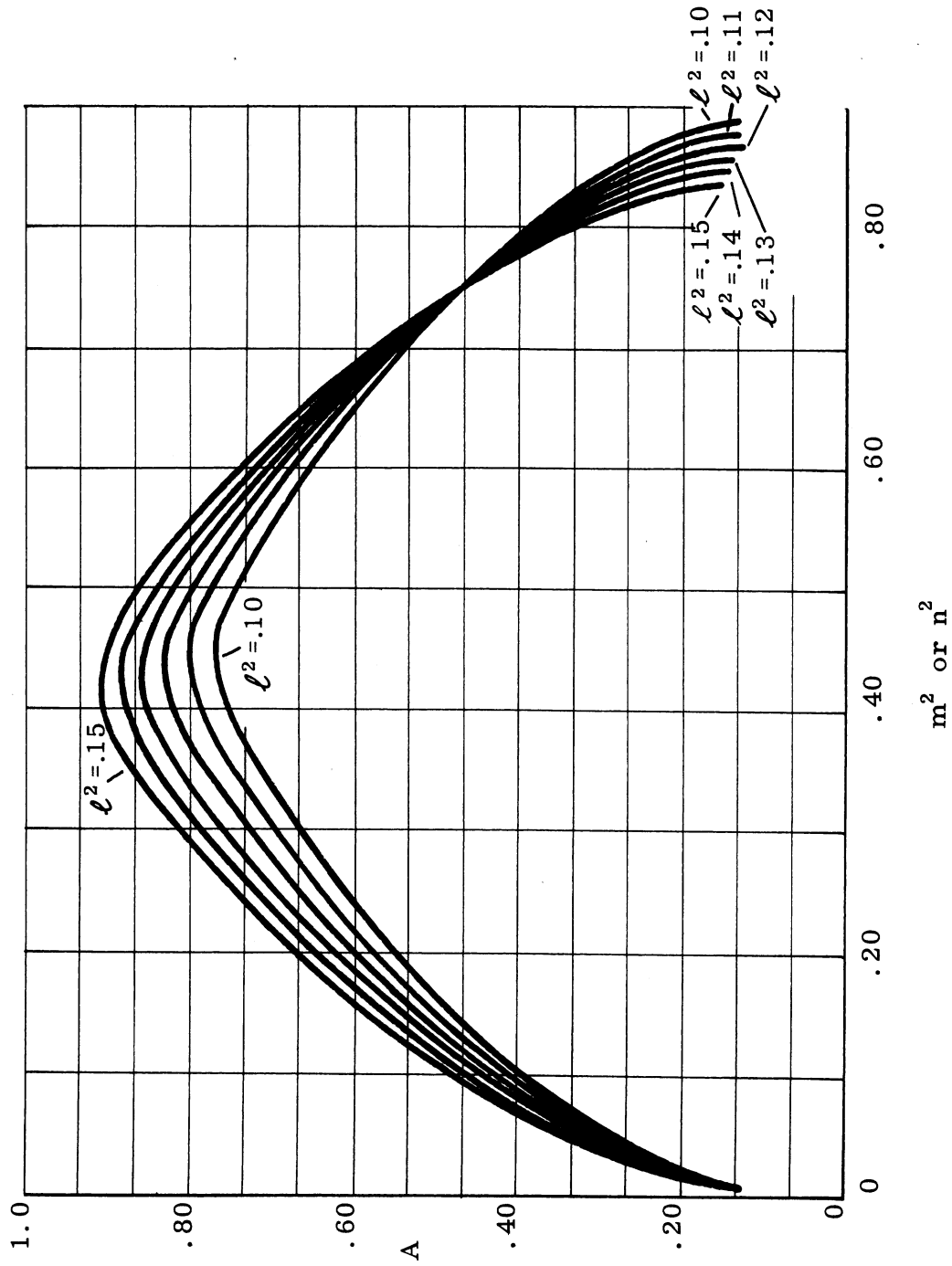


FIG. D-21: A, FOR UNIT EDGE CIRCULAR CORNER REFLECTOR,
 VS. m^2 OR n^2 FOR $l^2 = .15(.01).10$

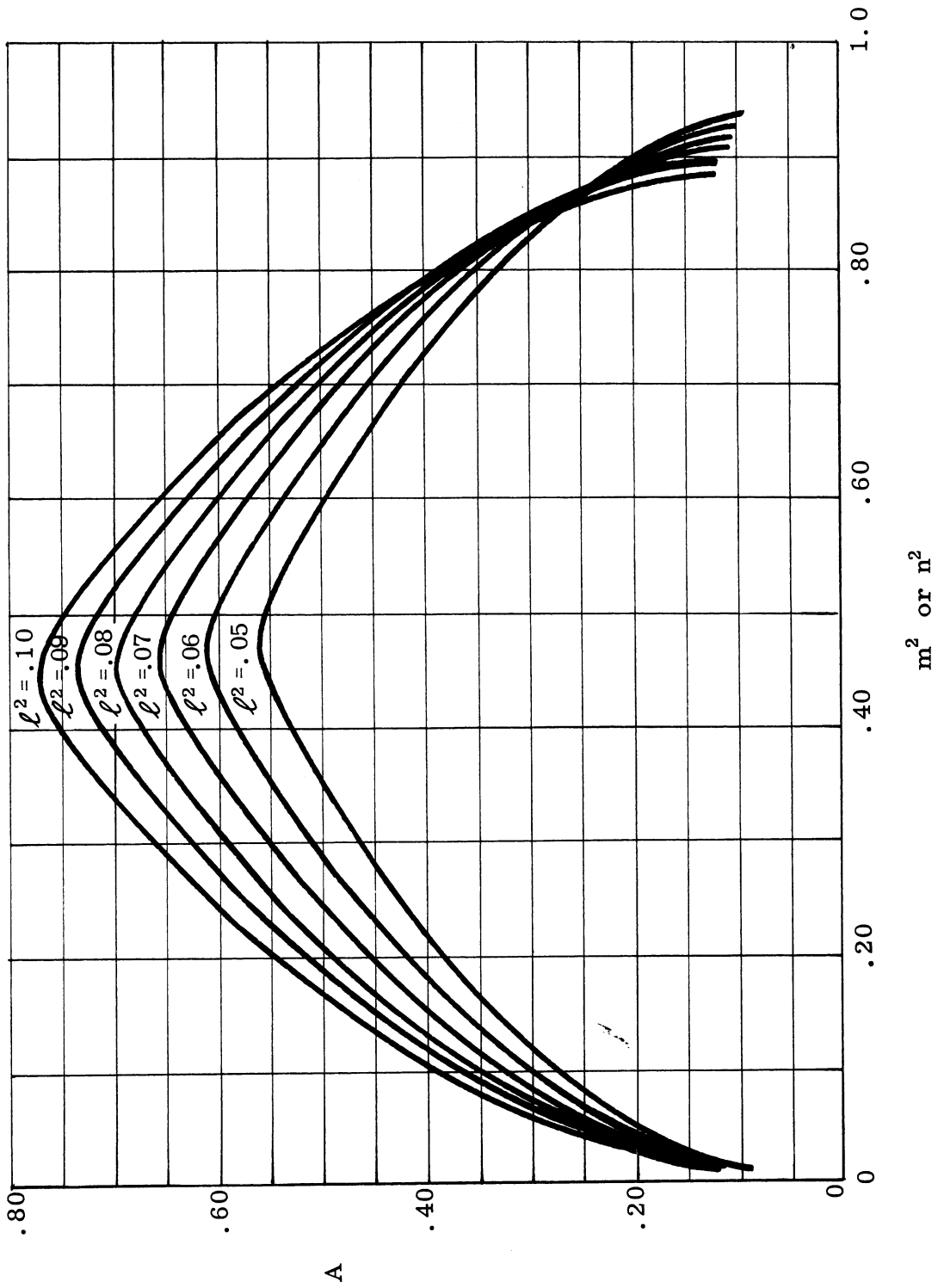


FIG. D-22: A, FOR UNIT EDGE CIRCULAR CORNER REFLECTOR, VS. m^2 OR n^2 FOR $l^2 = .10(.01).05$

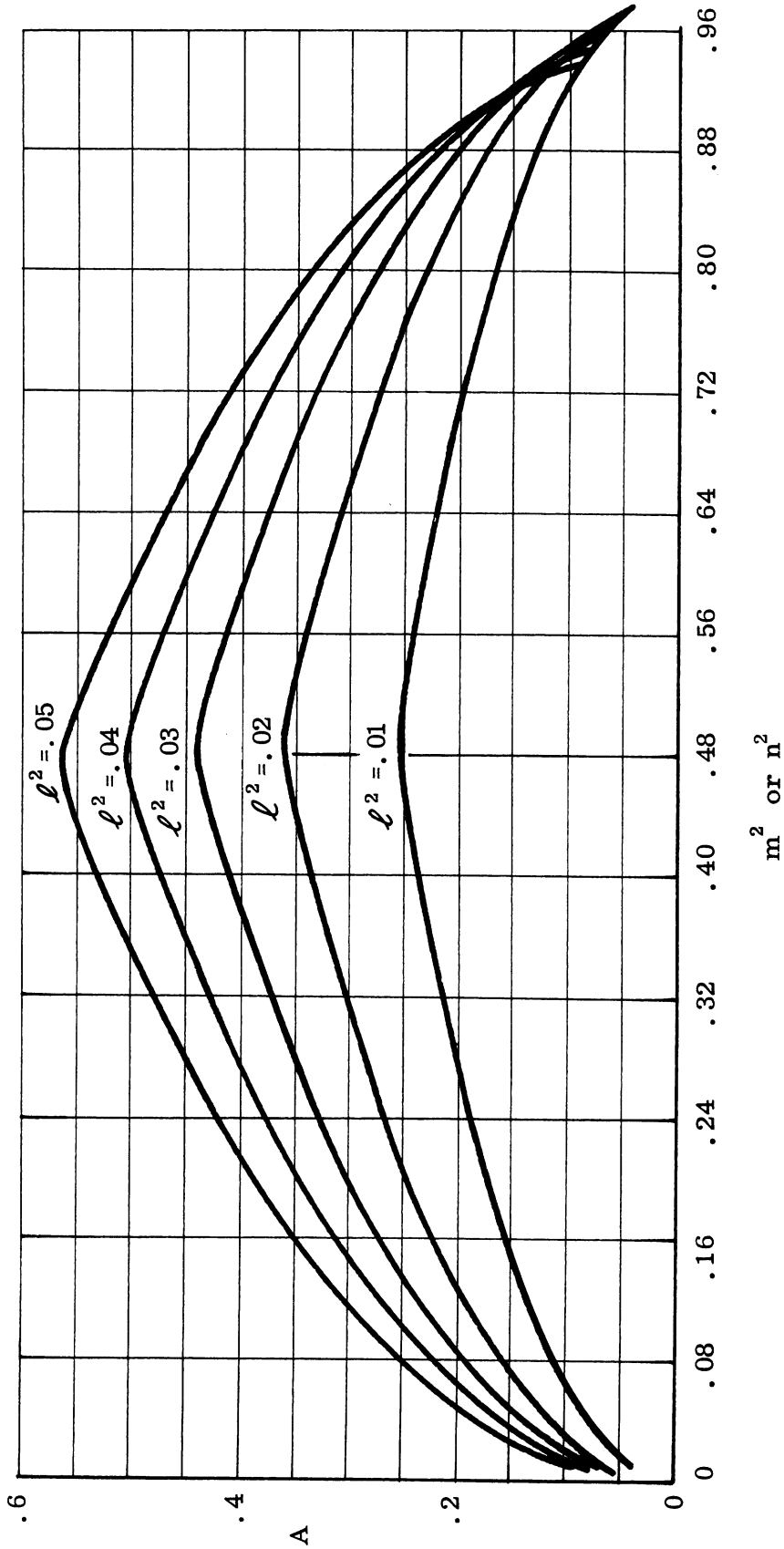


FIG. D-23: A, FOR UNIT EDGE CIRCULAR CORNER REFLECTOR, VS. m^2 OR n^2 FOR $\ell^2 = .05$ ($.01$). $.01$

APPENDIX E

BISTATIC RADARS AND FORWARD SCATTERING*

1

SUMMARY

The radar cross section results which are least understood by radar experimenters are in the area of forward scattering. It is here that a scattering maximum exists when the wavelength is small in respect to the dimensions of the body, and the theorist who wants precise results is most apt to question another's conclusions. It is here that the experimenter finds he "observes" the incident beam in his results.

New theoretical results for forward scattering are presented, and it is shown that physical optics results do predict this forward scattering maximum correctly even for complex shapes.

* A paper presented by K. M. Siegel at the IRE meeting in Dayton, Ohio, on the 13th of May 1958.

INTRODUCTION

During the early 1950's one of the authors (K. M. Siegel) commenced an investigation of radars whose transmitters and receivers were separated by large distances. Other theoretical analyses along these lines were made by Professor R. V. Pound of Harvard and Professor G. E. Valley of M. I. T., and excellent work was also performed at McGill University under the direction of Professor G. A. Woonton. In June 1952, R. E. Machol and the above author coined the name "bistatic radars" to describe radars of this type. The name came about because Sir Watson-Watt used the word "monostatic" to describe his recommendation to put transmitters and receivers in one place. It was to emphasize the desirability (for certain applications) that transmitters and receivers be spaced far apart that we decided on the word "bistatic". Intended applications primarily considered situations where the target was blown or driven between the transmitter and the receiver. If the physics of the problem allows it, the positions of the transmitter and receiver should be chosen so that the target lies exactly on the line joining them. Moreover, the method to be used should subtract off the incident field vectorially. If this can be done then a bistatic radar operating at high microwave frequencies is always better (in the following sense) than a monostatic radar. It is better because when the wavelength is small in respect to the

dimensions of a target, the forward scattering cross section increases in direct proportion to increasing frequency while the backscattering cross section of convex targets of major interest remains essentially constant with increasing frequency. Thus for the spectrum of usual radar interest (that is, for wavelengths small in respect to the dimensions of the scatterer) the forward scattering return dominates the convex target's return at all other aspects.

FORWARD SCATTERING AND RADAR CROSS SECTIONS OF ARBITRARY
CONVEX SHAPES

For separation angles such that the receiver is not near to, or in, the shadow region, the leading term of the asymptotic expansion of the exact electromagnetic cross section for convex shapes is given by the geometric optics. (For reference to asymptotic expansions pertaining to electromagnetics one should refer to the many excellent New York University reports on the subject.)

The radar cross section is defined as

$$\sigma(\theta, \phi) = \lim_{r \rightarrow \infty} 4\pi r^2 \left| \frac{E^s}{E^i} \right|^2 \quad (\text{Ref. E-1}) \quad (3.1)$$

where E^s is the scattered field and E^i is the incident field. For far fields

$$E^s = E_0 \frac{e^{ikr}}{r} f(\theta, \phi),$$

$$E^i = E_0 e^{ikz},$$

and

$$\sigma(\theta, \phi) = 4\pi |f|^2. \quad (3.2)$$

The total cross section is given by two formulas

$$\sigma_T = \int |f|^2 d\Omega \quad (\text{Ref. E-2}) \quad (3.3)$$

$$\sigma_{\text{T}} = \frac{4\pi}{k} \text{Im } f(\pi) \quad (\text{Ref. E-3}) \quad (3.4)$$

where Im means "imaginary part", and the argument π refers to forward scattering (in some references the angle π is used to denote backscattering).

The cross section given by geometric optics is wavelength independent.

Let us therefore write the exact cross section σ_{T} in the form

$$\sigma_{\text{T}} = G + \lambda^p Q + \text{higher powers of } \lambda$$

where G and Q are wavelength independent. If $p > 0$, then G is the leading term of the asymptotic expansion at high frequencies. If $p = 0$, then G and Q can be combined to form a new G. If $p < 0$, the limit of σ_{T} as $\lambda \rightarrow \infty$ is infinite, in violation of the conservation of energy. Thus the leading term of the asymptotic expansion of the total cross section σ_{T} is wavelength independent. Hence from equation (3.4)

$$\text{Im } f(\pi) \sim \frac{Gk}{4\pi} = \frac{G}{2\lambda}$$

for small λ . This means that the leading term in the expansion for the scattering function f must be either $G/2\lambda$ or M/λ^q , where $q > 1$ and M is wavelength independent. In either case the forward scattering cross section is such that

$$\sigma(\pi) \geq 4\pi \left| \frac{G}{2\lambda} \right|^2$$

(for small wavelengths). But for receivers not in or near the shadow region the cross sections are wavelength independent as regards the leading term of

the asymptotic expansion for small wavelengths and for convex bodies. Thus for backscattering or for receivers not near or in the shadow region the cross sections are of higher order (much smaller in magnitude) than the forward scattering cross sections.

By straight applications of Kirchhoff theory (Ref. E-4) the forward scattering cross section is $4\pi A^2/\lambda^2$ where A is the area under the curve separating the lit region and the shadow region on the body. The method which is used is equivalent to applying a Maggi transformation to the integral equation (Ref. E-2) and then evaluating both integrals. Since the Kirchhoff answer for forward scattering is pure imaginary, we have (from equation (3.4))

$$f(\pi) = i \frac{A}{\lambda} .$$

This actually turns out to be the correct leading term of the asymptotic expansion and hence the leading term in the expansion for the total cross section σ_T is $2A$. An analysis proving this fact is presented in Reference E-5.

The result of $\sigma_T \sim 2A$ is well known from scattering work in modern physics. The interpretation of the factor 2 is as follows: the energy scattered in the small angle forward direction is exactly equal to the scattered through large angles all over. In the short wavelength limit the small angle forward direction becomes the geometric shadow. The cross section for this term is the geometrical cross section A. Hence the total cross section is

$2A$ in the short wavelength limit. Thus, physical reasoning alone would have given us that $\text{Im } f(\pi) = A/\lambda$ and this term is the dominant term in the expression for $f(\pi)$ for small λ . This same reasoning forces $f(\pi)$ to be pure imaginary to this order and enables us to recognize that the Kirchhoff forward scattering answer is exact. Nevertheless, the result can be derived from purely mathematical principles and this is done in Reference E-5.

We shall now attempt to push these results towards wavelengths which are almost equal to the maximum size of the scattering object. Asymptotic theory should not be used in general in such cases and each individual shape of target has to be considered separately. Let us examine the results for a sphere.

Hamren (Ref. E-6) has studied scattering by a conducting sphere both theoretically and experimentally. He compares (Figure E-1) experimental values of the scattered field with theoretical points obtained by summing the Mie series. This is done for a wavelength of 3.2 cm for a sphere of 4.75λ diameter (i.e., $ka \cong 14.8$, where a is the radius). The measurements and computations were made at a distance $R = 1.5 M$ from the center of the sphere, and give the amplitude of the component of the scattered E-field parallel to the incident field as a function of the angle off axis in the equatorial plane behind the sphere. His measurements of E_{θ} are such that the zero degree location corresponds to true forward scattering. It is interesting to note that his forward scattered field which he computed yields a cross section differing by only about seven per cent from the value $4\pi(\pi a^2)^2/\lambda^2$.

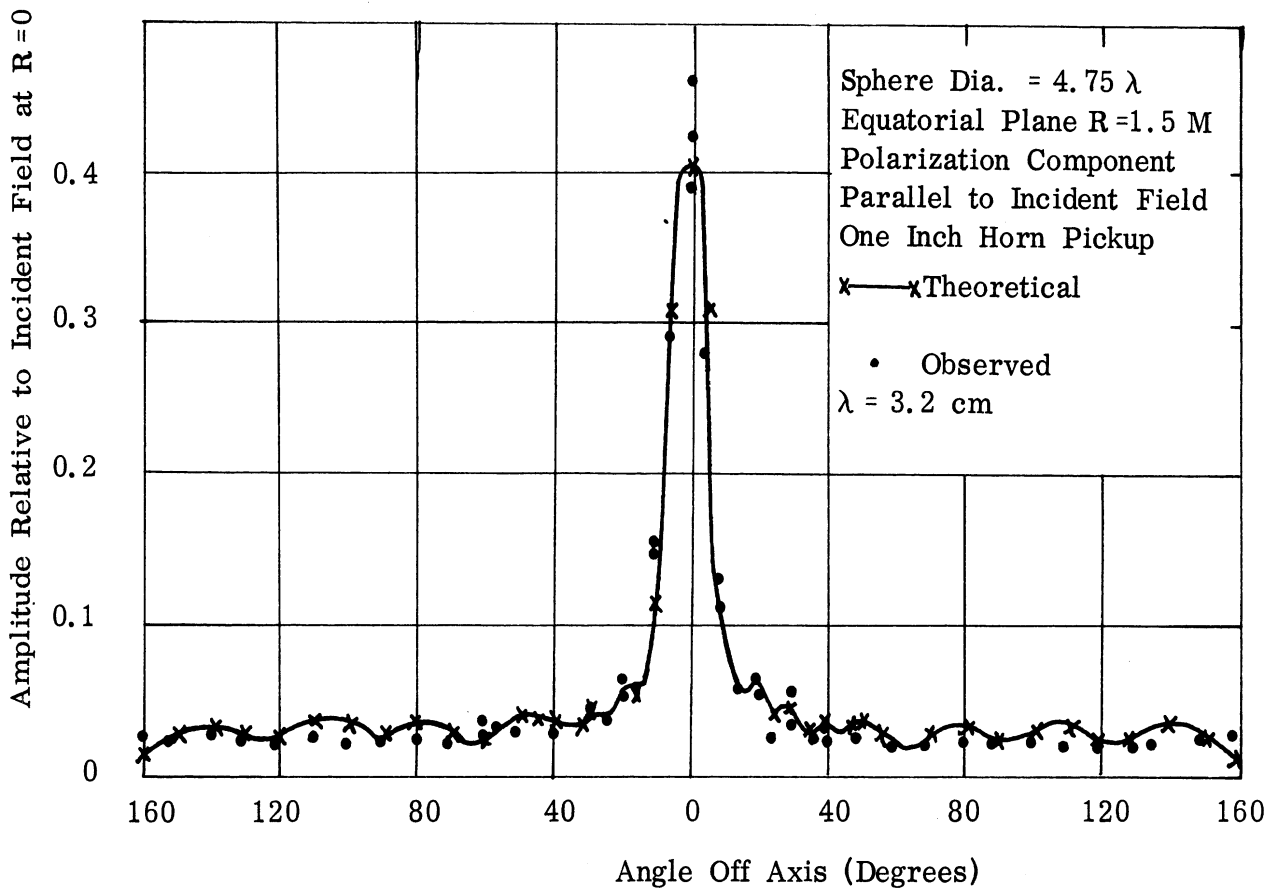


FIG. E-1: AMPLITUDE OF SCATTERED E - FIELD VERSUS ANGLE

The error one can tolerate in calculations determines the smallest ka that can be used when applying $4 \pi A^2 / \lambda^2$. In radar applications an error of seven per cent is of course negligible. Thus, for a sphere, one could use much smaller values of ka than 15.

In order to obtain a feeling for forward scattering and the region for which this type of cross section applies, an example will be given showing

how to compute the approximate small angle beam width for the sphere. The total scattering cross section is given by equation (3.3). If the half width of the small angle beam is denoted by ℓ/ka , where ℓ is a constant, then

$$\sigma_T = \int_0^{2\pi} \int_0^{\pi - \frac{\ell}{ka}} \frac{\pi a^2}{4\pi} \sin \theta \, d\theta \, d\phi$$

$$+ \int_0^{2\pi} \int_{\pi - \frac{\ell}{ka}}^{\pi} \frac{(\pi a^2)^2}{\lambda^2} \sin \theta \, d\theta \, d\phi,$$

since, by geometric optics, $\sigma = \pi R_1 R_2$ where R_1 and R_2 are principal radii of curvature. For a sphere $R_1 = R_2 = a$, giving $\sigma(\theta, \phi) = \pi a^2$ for θ not within the forward scattering cone. Within this cone the formula

$$\sigma(\pi) = \frac{4\pi A^2}{\lambda^2}$$

has been used. Hence

$$\sigma_T = -2\pi \left[\frac{\pi a^2}{4\pi} \cos \theta \right]_{\pi - \frac{\ell}{ka}}^{\pi},$$

for large angle scattering

$$\sigma_T = -2\pi \left[\frac{(\pi a^2)^2}{\lambda^2} \cos \theta \right]_{\pi - \frac{\ell}{ka}}^{\pi}$$

for small angle (or forward) scattering giving

$$\sigma_{\text{T}} = \frac{\pi a^2}{2} \left\{ 1 - \cos \left(\pi - \frac{\ell}{ka} \right) \right\} - \frac{2\pi (\pi a^2)^2}{\lambda^2} \left\{ \cos \pi - \cos \left(\pi - \frac{\ell}{ka} \right) \right\}.$$

By expanding $\cos \theta$ about $\theta = \pi$ and noting that ka is large

$$\sigma_{\text{T}} = \frac{\pi a^2}{2} + \frac{2\pi (\pi a^2)^2}{\lambda^2} \frac{\ell^2}{2 (ka)^2} = \pi a^2 + \pi a^2 \frac{\ell^2}{4}.$$

Hence, the assumption of the beam of half width $\frac{\ell}{ka}$ does not lead to a contradiction. For the sphere

$$\sigma_{\text{T}} = 2\pi a^2$$

so that $\ell = 2$, and the small angle beam width is then $4/ka$. It should be noted that this is an approximate answer, since it has been assumed that the cross section changes abruptly at the angle $\theta = \pi - \frac{\ell}{ka}$.

ILLUSTRATION OF RESULTS FOR AN ARBITRARY SHAPE BY SCALAR THEORY

To illustrate the method used in Reference E-2, S. Stone of The University of Michigan Radiation Laboratory has applied it to obtaining the total cross section.

Using Green's Theorem together with the Neumann boundary condition for the problem, an integral expression for the scattered wave has been derived in Reference E-2, in terms of the value of the incident wave on the surface and the appropriate Green's function. In the following discussion \hat{k} = direction of the incident plane wave, \hat{n} is the outward normal at the surface, \vec{r} is the spherical vector from the origin to the field point and \vec{r}' is the vector from the origin to the source point. If

$$\psi = \psi_i + \psi_s \text{ and } \psi_i = e^{i\vec{k} \cdot \vec{r}} \text{ with } \vec{k} = -\hat{i}_z k,$$

then according to Green's theorem

$$\psi_s(\vec{r}) = \frac{1}{4\pi} \int_S \left[\psi_s(\vec{r}') \frac{\partial}{\partial n} g_k(\vec{r}, \vec{r}') - g_k(\vec{r}, \vec{r}') \frac{\partial}{\partial n} \psi_s(\vec{r}') \right] dS. \quad (4.1)$$

Since $\frac{\partial \psi}{\partial n} = 0$ at the surface of the scatterer,

$\frac{\partial \psi_s}{\partial n}$ must equal $-\frac{\partial \psi_i}{\partial n}$ there, giving

$$\psi_s(\vec{r}) = \frac{1}{4\pi} \int_S \left[\psi_s(\vec{r}') \frac{\partial}{\partial n} g_k(\vec{r}, \vec{r}') + g_k(\vec{r}, \vec{r}') \frac{\partial}{\partial n} \psi_i(\vec{r}') \right] dS.$$

For very short waves we know that the part of the surface for which $\hat{n} \cdot \hat{k}$ is positive (if the surface is everywhere convex) as in the "shadow", whereas those parts for which $\hat{n} \cdot \hat{k}$ is negative are "illuminated" by the incident wave. What is meant by "shadow" is that ψ_s almost completely cancels ψ_i , in value as well as in normal derivative there. In the "illuminated" part, on the other hand, while $\partial \psi_s / \partial n$ cancels $\partial \psi_i / \partial n$, ψ_s is approximately equal to ψ_i at the surface. Therefore, the scattered wave can be represented approximately by integrals of the product of the Green's function and the incident wave, but with different combinations for the two portions of the surface;

$$\begin{aligned} \psi_s(\vec{r}) \approx & \frac{1}{4\pi} \int_{S'} \left[\psi_i(\vec{r}') \frac{\partial}{\partial n} g_k(\vec{r}, \vec{r}') \right. \\ & \left. + g_k(\vec{r}, \vec{r}') \frac{\partial}{\partial n} \psi_i(\vec{r}') \right] dS \\ & + \frac{1}{4\pi} \int_{S''} \left[g_k(\vec{r}, \vec{r}') \frac{\partial}{\partial n} \psi_i(\vec{r}') \right. \\ & \left. - \psi_i(\vec{r}') \frac{\partial}{\partial n} g_k(\vec{r}, \vec{r}') \right] dS, \end{aligned} \tag{4.2}$$

where the subscript S' indicates integration over the illuminated portion and the subscript S'' indicates integration over the shadow area.

These two integrands have very different behavior. The first represents the "reflected wave", the second is the "shadow forming" wave, which is needed to cancel the incident wave.

The second integral may be simplified by means of a Maggi transformation. The vector

$$\vec{A} = (\vec{g}_k \nabla' \psi_i(\vec{r}') - \psi_i(\vec{r}') \nabla' \vec{g}_k),$$

considered as a function of \vec{r}' , has zero divergence (except when \vec{r} is on the surface also). Thus we write

$$\begin{aligned} \text{div}' \vec{A} &= \vec{g}_k \nabla'^2 \psi_i - \psi_i \nabla'^2 \vec{g}_k \\ &= 4\pi \psi_i(\vec{r}') \delta(\vec{r} - \vec{r}'), \end{aligned}$$

and \vec{A} can be considered to be a curl of a vector \vec{B} . Using Stokes' theorem,

$$\frac{1}{4\pi} \int_S \nabla' \times \vec{B} \cdot \vec{dS} = \frac{1}{4\pi} \oint \vec{B} \cdot \vec{ds}$$

where the line integral of \vec{B} is along the line which separates the shadow from the illuminated part of the surface. It follows that the integral does not depend on the shape of the shadow surface (only on the shape of the shadow line). To

the degree of approximation represented by equation (4.1), the shadow forming wave is the same for all surfaces having the same shadow line.

The first integral in equation (4.1) cannot be calculated so easily and for short wavelengths it is usually evaluated by the method of steepest descent. It will now be shown that this approach predicts the same total cross section as the Kirchhoff method.

The Green's function

$$g_k = \frac{e^{ikR}}{R} \approx \frac{e^{ikr}}{r} e^{-ik(\hat{\mathbf{r}} \cdot \hat{\mathbf{r}}')},$$

where the approximation is to take $R \simeq r - (\hat{\mathbf{r}} \cdot \hat{\mathbf{r}}')$ in the phase factor and

$R \simeq r$ in the amplitude. This is true for large r . The incident wave is $\psi_i = e^{i\vec{k}_i \cdot \vec{r}}$ and for incidence along the z axis, $\vec{k}_i = -\hat{i}_z k$. On the surface $\vec{r} = \vec{r}'$, giving

$$\psi_i(\vec{r}') = e^{-ikr'(\hat{i}_z \cdot \hat{\mathbf{r}}')}.$$

For forward scattering $\hat{\mathbf{r}} = -\hat{i}_z$ so the Green's function becomes

$$g_k = \frac{e^{ikr}}{r} e^{ikr'(\hat{i}_z \cdot \hat{\mathbf{r}}')}.$$

Equation (4.1) may now be written

$$\begin{aligned} \psi_s(\vec{r}) = & \frac{1}{4\pi} \int_{S'} \left[e^{-ikr' \cos\theta'} \nabla' \left(\frac{e^{ikr}}{r} e^{ikr' \cos\theta'} \right) \right. \\ & \left. + \frac{e^{ikr}}{r} e^{ikr' \cos\theta'} \nabla' \left(e^{-ikr' \cos\theta'} \right) \right] \cdot d\vec{S} \\ & + \frac{1}{4\pi} \int_{S''} \left[\frac{e^{ikr}}{r} e^{ikr' \cos\theta'} \nabla' \left(e^{-ikr' \cos\theta'} \right) \right. \\ & \left. - e^{-ikr' \cos\theta'} \nabla' \left(\frac{e^{ikr}}{r} e^{ikr' \cos\theta'} \right) \right] \cdot d\vec{S}. \end{aligned}$$

This can be found from (4.2) by replacing $\partial / \partial n$ with $\hat{n} \cdot \nabla$ and $(\hat{z} \cdot \hat{r})$ by $\cos \theta'$.

If the indicated operations are performed, the integrand of the first is found to be zero, while the second integrand is

$$\vec{A} = \frac{e^{ikr}}{r} 2ik \left[-\cos\theta' \hat{r}' + \sin\theta' \hat{\theta}' \right].$$

This is the vector obtained by the Maggi transformation. If $\nabla' \cdot \vec{A}$ is computed, it is seen to vanish everywhere except when \vec{r} is on the surface.

The scattered wave is then

$$\psi_s(\vec{r}) = \frac{1}{4\pi} 2ik \frac{e^{ikr}}{r} \int_{S'} \left[-\cos\theta' \hat{r}' + \sin\theta' \hat{\theta}' \right] \cdot \vec{dS}$$

or

$$\psi_s(\vec{r}) = \frac{1}{4\pi} 2ik \frac{e^{ikr}}{r} \int_S -\hat{i}_z \cdot \hat{n} \, dS.$$

This may be rewritten as

$$\psi_s(\vec{r}) = \frac{1}{4\pi} 2ik \frac{e^{ikr}}{r} \int_A dA$$

where A is the projected area, giving

$$\psi_s(\vec{r}) = \frac{ik}{2\pi} A \frac{e^{ikr}}{r}.$$

Examining this expression it is seen that

$$f(\pi) = \frac{ikA}{2\pi}$$

and

$$\sigma_T = \frac{4\pi}{K} \operatorname{Im} f(\pi)$$
$$= 2A ,$$

which is the total cross section predicted by the Kirchhoff method. As previously stated, this is the result "well known" to theoretical physicists working on scattering problems.

CONCLUSIONS

If the wavelength is small compared with the dimensions of the target and the physical situation is such that one can measure forward scattering returns, then these bistatic cross sections are always greater than the monostatic ones for targets of convex shape. Of course, forward scattering applies only to positions of the receiver within the forward scattering cone. For flat shapes (neither concave nor convex) there is one aspect of the body for which the monostatic cross section equals the forward scattering cross section; at all other aspects the forward scattering result dominates. But for all convex shapes the particular bistatic cross sections corresponding to the forward scattering direction dominate the scattering pattern.

REFERENCES

- E-1. D. E. Kerr, Propagation of Short Radio Waves, Vol. 13, p. 33, Radiation Laboratory Series, McGraw-Hill Book Company, New York (1951).
- E-2. P. Morse, and H. Feshbach, Methods of Theoretical Physics, Vol. II, pp. 1066 and 1551-4, McGraw-Hill Book Company, New York (1953).
- E-3. L. I. Schiff, Quantum Mechanics, p. 105, McGraw-Hill Book Company, New York (1955).
- E-4. K. M. Siegel, H. A. Alperin, R. R. Bonkowski, J. W. Crispin, Jr., A. L. Maffett, C. E. Schensted and I. V. Schensted, "Bistatic Radar Cross Sections of Surfaces of Revolution", Journal of Applied Physics, Vol. 26, No. 3, 297-305 (March 1955).
- E-5. D. M. Raybin, T. B. A. Senior, K. M. Siegel, S. E. Stone and H. Weil, "Forward Scattering (Electromagnetics)". Presented at Joint Meeting, U. S. A. National Committee, International Scientific Radio Union, Institute of Radio Engineers, Washington, D. C., (24 - 26 April 1958).
- E-6. S. D. Hamren, "Scattering From Spheres", University of California Reoprt 171, Antenna Laboratory (15 June 1950).

APPENDIX F

POWER SPECTRA FOR EXPERIMENTAL DATA

1

INTRODUCTION

We have observed from the text and the other appendices that the radar cross section of a given aircraft or missile is a function of aspect and wavelength. In practice, however, the observed variation in the cross section will be a variation with time. This time dependence will be due naturally to changes in aspect with time, changes in frequency with time, and changes in the relative positions of the scattering surfaces (due to vibration, etc.) with time.

It is thus apparent that in the study of the radar reflection characteristics of a given target one's interest could be directed toward the time distribution of the amplitudes. In the belief that one may be able to find something characteristic of the target in this "fine structure" of the return the method of study becomes a statistical one. A common approach involves the study of the autocorrelation function and the power spectrum associated with the time varying quantities. In this appendix and in the following appendix (Appendix G) we shall illustrate this approach; that is, we illustrate the approach to follow in performing this statistical study of the function $\sigma(t)$, the cross section at time t . In this appendix we shall turn our attention to an approach used for experimental data and in Appendix G we shall consider a purely theoretical problem.

The experimental study involved the determination of the power spectra and the autocorrelation functions from dynamic data; the results of this study have been reported in References F-1 and F-2. A study such as this one deals with finite samples while the classical theory is based upon a sample of infinite size. A certain amount of arbitrariness is thus involved when the theory is modified for application to a finite sample. Alternative definitions of the power spectrum and autocorrelation function have been given in the literature (Refs. F-3 and F-4)

Even though the main contribution to the radar cross section of V-2 type missiles usually comes from the fins, the variation in the shapes of the curves found for missiles with swept-back fins appeared to be as great as the variation between these and the curves for missiles with rectangular shaped fins. In fact, there appeared to be little difference between the spectra found for missiles and those obtained for a B-57 aircraft (Ref. F-5).

THE DEFINITIONS OF THE AUTOCORRELATION FUNCTION, $R(\tau)$,
AND THE POWER SPECTRUM, $S(\omega)$, USED IN THE COMPUTATIONS

In this section a brief summary of pertinent facts concerning the usual $R(\tau)$ and $S(\omega)$, the definitions of $R(\tau)$ and $S(\omega)$ used in the computations, the relationship between $R(\tau)$ and $S(\omega)$, and one aspect of the significance of the definitions are presented.

When a real random function $y(t)$ is known for all times t from 0 to ∞ , the autocorrelation function $R_{\infty}(\tau)$ and power spectrum, $S_{\infty}(\omega)$, are defined as

$$R_{\infty}(\tau) = \lim_{T \rightarrow \infty} \frac{1}{T} \int_0^T y(t) y(t + \tau) dt, \quad (2.1)$$

and

$$S_{\infty}(\omega) = \lim_{T \rightarrow \infty} \frac{2 |A(\omega, T)|^2}{T}, \quad (2.2)$$

where

$$A(\omega, T) = \frac{1}{\sqrt{2\pi}} \int_0^T y(t) e^{-i\omega t} dt. \quad (2.3)$$

Note that

$$S_{\infty}(\omega) \geq 0, \quad |R_{\infty}(\tau)| \leq R(0), \quad (2.4)$$

and

$$S_{\infty}(\omega) = \frac{2}{\pi} \int_0^{\infty} R_{\infty}(\tau) \cos(\omega \tau) d\tau. \quad (2.5)$$

The last equation is known as the Wiener-Khinchine Theorem.

For a random function $y(nT_0)$, $n = 0, 1, \dots, N$ (that is, for a finite set of data), the autocorrelation function, $R(\tau, T)$, and the power spectrum, $S(\omega)$, will be defined here by

$$R(\tau_s, T) = \frac{1}{N} \sum_{n=0}^{N-s} y(nT_0) y(nT_0 + \tau_s), \text{ where } 0 \leq \tau_s \leq NT_0$$

and

$$R(\tau_s, \tau) = 0, \text{ if } \tau_s < 0 \text{ or } \tau_s > NT_0, \quad (2.6)$$

where

$$\tau_s = sT_0, \quad s = 0, 1, \dots, N, \quad \text{and} \quad S(\omega) = \frac{2}{T} \left| F(\omega, T) \right|^2, \quad (2.7)$$

where

$$F(\omega, T) = \frac{T_0}{\sqrt{2\pi}} \sum_{n=0}^N y(nT_0) e^{-i\omega nT_0}. \quad (2.8)$$

Note that the summation in $R(\tau_s, T)$ is divided by N , the total number of values for $y(nT_0)$, rather than by $N-s$, the number of values of $y(nT_0) \times y(nT_0 + \tau_s)$ in the summation. The reason for this is to preserve the relation

$$S(\omega) = \frac{2T_0}{\pi} \left\{ \sum_{s=0}^N R(sT_0, T) \cos(\omega sT_0) - \frac{1}{2} R(0, T) \right\}, \quad (2.9)$$

which is the analogue of the Wiener-Khinchine relation. A proof of equation (2.9) is the following:

Using the definition of $F(\omega, T)$ given in equation (2.8),

$$\begin{aligned}
|F(\omega, T)|^2 &= \frac{T_0^2}{2\pi} \sum_{n=0}^N \sum_{m=0}^N y(nT_0) y(mT_0) e^{i\omega(n-m)T_0} \\
&= \frac{T_0^2}{2\pi} \sum_{n=0}^N \sum_{s=n}^{n-N} y(nT_0) y[(n-s)T_0] e^{i\omega s T_0} \\
&= \frac{T_0^2}{2\pi} \left\{ \sum_{s=0}^N \sum_{n=s}^N y(nT_0) y[(n-s)T_0] e^{i\omega s T_0} \right. \\
&\quad \left. + \sum_{s=-N}^{-1} \sum_{n=0}^{N+s} y(nT_0) y[(n-s)T_0] e^{i\omega s T_0} \right\} \\
&= \frac{T_0^2}{2\pi} \left\{ \sum_{n=0}^N y^2(nT_0) + 2 \sum_{s=1}^N \sum_{n=s}^N y(nT_0) y[(n-s)T_0] \cos(\omega s T_0) \right\}.
\end{aligned}$$

From the definition of $R(\tau_s, T)$

$$R(sT_0, T) = \left(\frac{T_0}{T}\right) \sum_{n=s}^N y(nT_0) y[(n-s)T_0],$$

where

$$T = NT_0.$$

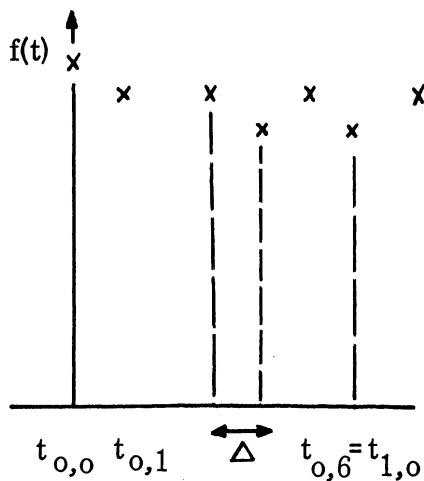
Thus

$$S(\omega) \equiv \frac{2}{T} |F(\omega, T)|^2 = \frac{T_0}{\pi} \left\{ R(0, T) + 2 \sum_{s=1}^N R(sT_0, T) \cos(\omega s T_0) \right\}$$

from which equation (2.9) immediately follows.

One aspect of the significance of the definition of $F(\omega, T)$ may be seen from the following considerations. $R(\gamma_s, T)$ and $S(\omega)$ were computed (in the missile calculation) according to the above equations, using for $y(nT_0)$

Set of Discrete Data $M = 5$



an averaged value of cross section; that is, each $\bar{\sigma}$ is the average over six successive values of σ with no overlap in neighboring $\bar{\sigma}$'s. Consider the Fourier analysis of an arbitrary function $f(t)$ which passes through a given set of points $f_{n,m}$ defined at the times $t_{n,m}, m = 0, 1, \dots, M, n = 0, 1, \dots, N$, and $f(t) = 0$ for $t < t_{0,0}$ and $t > t_{N, M+1}$. (The $f_{n,m}$ correspond

to the σ values, $M+1$ of these being used to obtain a value of $\bar{\sigma}$.) The Fourier transform of $f(t)$ is given by

$$F(\omega) = \frac{1}{\sqrt{2\pi}} \int_{t_{0,0}}^{t_{N, M+1}} f(t) e^{-i\omega t} dt = \frac{1}{\sqrt{2\pi}} \sum_{n=0}^N \sum_{m=0}^M \int_{t_{n,m}}^{t_{n,m+1}} f(t) e^{-i\omega t} dt,$$

the latter expression being valid provided $t_{n, M+1} = t_{n+1, 0}$ (this insures that the whole integration range be covered).

If

$$t_{n, m+1} - t_{n, m} = \Delta \quad \text{and} \quad t_{0,0} = 0,$$

then

$$t_{n,m} = n(M+1)\Delta + m\Delta,$$

and

$$t_{n,m+1} = n(M+1)\Delta + (m+1)\Delta,$$

$$\int_{t_{n,m}}^{t_{n,m+1}} f(t) e^{-i\omega t} dt = e^{-i\omega t_{n,m}} \int_0^{\Delta} f(t' + t_{n,m}) e^{-i\omega t'} dt'.$$

If $\omega\Delta \ll 1$,

$$F(\omega) \cong \left(\frac{\Delta}{\sqrt{2\pi}}\right) \sum_{n=0}^N \sum_{m=0}^M e^{-i\omega [n(M+1)\Delta + m\Delta]} \tilde{f}_{n,m},$$

where

$$\tilde{f}_{n,m} = \left(\frac{1}{\Delta}\right) \int_{t_{n,m}}^{t_{n,m+1}} f(t) dt.$$

If further $\omega M\Delta \ll 1$,

$$F(\omega) \cong \frac{T_0}{\sqrt{2\pi}} \sum_{n=0}^N \bar{f}_n e^{-i\omega n T_0},$$

where

$$T_0 = (M+1)\Delta$$

and

$$\bar{f}_n = \frac{1}{M+1} \sum_{m=0}^M \tilde{f}_{n,m}.$$

The formal similarity between this expression for $F(\omega)$ and $F(\omega_1 T)$ as defined in equation (2.8) is apparent. If now $f(t)$ is slowly varying over time intervals of length Δ (i. e., $f(t)$ is band limited with $\omega_{\text{maximum}} \ll 1/\Delta$), then $\tilde{f}_{n,m} \cong f_{n,m} \cong \tilde{f}_{n,m+1}$; that is, $\tilde{f}_{n,m}$ may be replaced by $f_{n,m}$ in which case \bar{f}_n is merely the average of the $M+1$ values: $f_{n,0}, f_{n,1}, \dots, f_{n,M}$. Thus, the definition of $F(\omega, T)$ given above and used in the computations gives the power spectrum, for $\omega \ll 1/T_0$ (T_0 is the interval over which the data are averaged), of a function which is zero outside the observation interval and which passes through all the points of the data before averaging. It is assumed that the function is band limited with maximum frequency $\ll 1/\Delta$ (Δ is the pulse repetition period of the radar used in obtaining the original data). In this case, $\Delta = 1/409.75$ sec and $T_0 = 6\Delta$ ($M = 5$).

In actual practice, the following procedure was used:

$$R(\mathcal{T}) = R(sT_0) = \left(\frac{1}{N}\right) \sum_{n=0}^{N-s} \bar{\sigma}(nT_0) \bar{\sigma}((n+s)T_0),$$

where values of s used were

$$s = 0(5)150(25)1250 \quad \text{for S-band ,}$$

$$s = 0(5)200(25)1250 \quad \text{for X-band .}$$

These are the values shown on the accompanying list.

Then $S(\omega)$ for $\omega \leq 2\pi$ was approximated as

$$S(\omega) = \frac{2T_0}{\pi} \sum_{s=0}^N a_s R(sT_0) \cos(\omega s T_0),$$

where

$$\begin{aligned}
 a_0 &= 5/2, \\
 a_s &= 5 \quad \text{for } \begin{cases} 5 \leq s \leq 145 & \text{for S-band} \\ 5 \leq s \leq 195 & \text{for X-band} \end{cases}, \\
 a_s &= 15 \quad \text{for } \begin{cases} s = 150 & \text{for S-band} \\ s = 200 & \text{for X-band} \end{cases}, \\
 a_s &= 25 \quad \text{for } \begin{cases} 175 \leq s \leq 1250 & \text{for S-band} \\ 225 \leq s \leq 1250 & \text{for X-band} \end{cases}.
 \end{aligned}$$

This procedure was used to obtain $S(\omega)$ for $\omega/2\pi = 0(.1)1.0$ cycles per second; for larger values of ω , the method must be altered, inasmuch as taking s at intervals of 25 does not yield sufficient accuracy. In the interest of economy of time and money, it was decided to return to the basic definition of the power spectrum, namely

$$S(\omega) \equiv \frac{2}{T} |F(\omega, T)|^2.$$

Numerically, this means

$$S(\omega) = \frac{25T_0}{\pi N} \left\{ \left[\sum_{n=0}^{\lfloor N/5 \rfloor} \bar{\sigma}(5nT_0) \cos(5n\omega T_0) \right]^2 + \left[\sum_{n=0}^{\lfloor N/5 \rfloor} \bar{\sigma}(5nT_0) \sin(5n\omega T_0) \right]^2 \right\}.$$

This is the formula used to obtain $S(\omega)$ for $\omega/2\pi = 1.1, 1.2, 1.5, 2.0, 3.0, 4.0, 5.5, 6.0, 6.5, 7.5$ cycles per second. To get $S(\omega)$ for higher values of ω would require taking more than every fifth value of $\bar{\sigma}$ which was not considered warranted.

REFERENCES

- F-1. K.M. Siegel, M.L. Barasch, H. Brysk, J.W. Crispin, Jr., T.B. Curtz and T.A. Kaplan, "Studies in Radar Cross Sections XIX - Radar Cross Section of a Ballistic Missile II", University of Michigan Report 2428-3-T (AF-04(645)-33), January 1956. (SECRET)
- F-2. K.M. Siegel, W.E. Burdick, J.W. Crispin, Jr. and S. Chapman, "Studies in Radar Cross Sections XX - Radar Cross Section of Aircraft and Missiles", University of Michigan Report WR-31-J, March 1956. (SECRET)
- F-3. J.L. Lawson and G.E. Uhlenbeck, Threshold Signals, McGraw-Hill (1950).
- F-4. James, Nichols, and Phillips, Theory of Servomechanism, Radiation Laboratory Series, Vol. 25, McGraw-Hill.
- F-5. B.L. Lewis, "Radar Characteristics of Jet Exhaust Gases", Tracking Branch, Radar Division, Naval Research Laboratories, Report 4438, December 1954.

APPENDIX G

DETERMINATION OF POWER SPECTRA FROM THEORETICAL ESTIMATES OF THE RADAR CROSS SECTION

1

INTRODUCTION

In Appendix F we have considered a procedure for determining power spectra from experimental data; here we shall consider the approach one can use in determining the power spectra from theoretically determined values of the radar cross section. Here we shall consider the case in which the aspect remains fixed and the frequency changes. As an illustration we shall assume that the nominal frequency is 425 Mc, the pulse repetition frequency is 300 cycles per second, the pulse length is 6 microseconds, and the frequency scan rate is 5 cycles per second. We shall assume that the frequency scan waveform is sawtooth and we shall restrict our attention to two modes of frequency: $\pm 1\%$ and $\pm 2.5\%$.

In fact we shall consider two different approaches: one is the spectrum of the cross sections and the other is the spectrum of the square root of the cross sections. Section 2 is devoted to the consideration of the first case and Section 3 is devoted to the consideration of the second.

SPECTRUM OF THE CROSS SECTION

The problem here is to determine the power spectrum of the radar return from a given aircraft for a specified aspect when the transmitting radar is both pulsed and frequency-modulated. Since the frequency modulation sweeps at a rate of 5 cycles per second, harmonics of this frequency are expected in the return. The importance of these harmonics may be assessed through the determination of the power spectrum.

The radar cross section, σ , has a period of 5 cycles per second by virtue of its frequency dependence. Since there exists no time axis, in general, about which $\sigma(t)$ is either even or odd, $\sigma(t)$ should be expanded in a general Fourier series. Specifically, using the series in complex exponentials, $\sigma(t)$ is written

$$\sigma(t) = \sum_{-\infty}^{\infty} C_n \exp(i 10n \pi t) \quad (2.1)$$

where $i = \sqrt{-1}$ and t is measured in seconds.

Determination of the power spectrum from the constant term through the first thirty harmonics consists in obtaining $|C_n|$ for $\pm n = 0, 1, 2, \dots, 30$. However, since $\sigma(t)$ is real, it follows that

$$C_{-n} = C_n^* \quad \text{and} \quad |C_{-n}| = |C_n|.$$

It is therefore sufficient to consider only those cases for which $0 \leq n$.

For $n > 0$, the contribution to σ (which measures the power return) at the n^{th} harmonic frequency is given by the series (2.1) as

$$\sigma(\omega_n) = C_n e^{i\omega_n t} + C_{-n} e^{-i\omega_n t}.$$

But since $C_{-n} = C_n^*$, this may be written as

$$\sigma(\omega_n) = 2(\text{Re } C_n \cos \omega_n t - \text{Im } C_n \sin \omega_n t).$$

It follows from this that the RMS value of $\sigma(\omega_n)$ is expressible as

$$\begin{aligned} \left\langle \sigma^2(\omega_n) \right\rangle_t^{1/2} &= \left[4 \left\langle [\text{Re } C_n \cos \omega_n t]^2 + [\text{Im } C_n \sin \omega_n t]^2 - 2[\text{Re } C_n \cos \omega_n t][\text{Im } C_n \sin \omega_n t] \right\rangle_t \right]^{1/2} \\ &= \left[2(\text{Re}^2 C_n + \text{Im}^2 C_n) \right]^{1/2} = \sqrt{2} |C_n|. \end{aligned}$$

Here the symbol $\langle F(t) \rangle_t$ denotes the time average of $F(t)$ over the period $\frac{2\pi}{\omega_n}$.

For $n = 0$, $\sigma_{\text{D.C.}} = C_0 = |C_0|$. The ratio of the RMS power in the n^{th} harmonic to the D.C. power level, a useful measure of the effect of frequency variation on σ , may therefore be written

$$\frac{\text{RMS } \sigma(\omega_n)}{\sigma_{\text{D.C.}}} = \sqrt{2} \left| \frac{C_n}{C_0} \right|.$$

This set of quantities is referred to as the relative power spectrum.

The C_n are given by

$$C_n = \frac{1}{T} \int_0^T \sigma(t) \exp(-i 10n \pi t) dt \quad (2.2)$$

where $T = 0.2$ sec. In order to evaluate this integral several approximations are introduced. It is assumed that the echo pulse is of the same form and duration as the transmitted one and that the range variation is not sufficient to effect a variation in time delay. The return may then be taken as consisting of 6μ sec. pulses at 300 pulses/sec., and subject to the 5 cycle frequency sweep. Further, it is assumed that this 6μ sec. pulse width is small enough so that both the operating frequency and the exponential appearing in the integral for C_n are essentially constant over a single pulse. (See App. C).

The integral over t for C_n may now be replaced by a sum of the contributions from the 60 pulses which occur during the 0.2 sec. frequency sweep. The continuous variable t is replaced by $t_r = (r/300)$ sec., $r = 0, 1, \dots, 59$. Each contribution endures for $\Delta t_r = 6\mu$ sec. rather than the infinitesimal dt . Also, $\sigma(t)$ is replaced by $\sigma(\lambda_r)$ where λ_r is given as a function of t_r by the sawtooth waveform of the frequency modulation. Two modes of operation are specified, corresponding to frequency excursions of $\pm 1\%$ and $\pm 2\frac{1}{2}\%$ respectively about the 425 Mc nominal operating frequency. Assuming the sawtooth to start at the low end of the frequency range, the relations between λ_r and t_r are given approximately as follows* (with λ given in cm):

*The smallness of the frequency sweep permits conversion of frequency linear in time to wavelength linear in time.

$$\lambda_r = -7.21 t_r \text{ cm} + 71.3 \text{ cm} = -\frac{7.21}{300} r \text{ cm} + 71.3 \text{ cm} \quad (\text{Mode 1}) \quad (2.3)$$

$$\lambda_r = -17.8 t_r \text{ cm} + 72.4 \text{ cm} = -\frac{17.8}{300} r \text{ cm} + 72.4 \text{ cm} \quad (\text{Mode 2}) .$$

Thus for a given aspect the dependence of σ on λ , determined theoretically, is converted into the form $\sigma(r)$ through the application of the relations of equation (1.3). From this expression for $\sigma(r)$ we obtain

$$C_n = \frac{1}{T} \Delta t_r \sum_{r=0}^{59} \sigma(r) \exp(-i 10n \frac{\pi r}{300})$$

where $T = 0.2$ sec. and $\Delta t_r = 6\mu$ seconds. Upon the substitution of the numerical values of T and Δt_r , this equation reduces to

$$C_n = (3 \times 10^{-5}) \sum_{r=0}^{59} \sigma(r) \exp(-i n \pi r / 30). \quad (2.4)$$

The theoretical cross sections of an aircraft or a missile can usually be expressed in the form

$$\sigma = \sum_{i=-1}^2 A_i \lambda^i .^*$$

Equation (2.3) indicates that the wavelength can be expressed in the form

$$\lambda = Y - X t = Y(1 - \frac{X}{Y}t)$$

and that $Xt \ll Y$. Thus we may write

* This is, of course, the "average" or "random phase" result. The "relative phase" result for the theoretical calculation of cross section, which will usually prove to be of more value in a power spectrum study, is used in Section 3.

$$\lambda^{-1} \approx \frac{1}{Y} \left(1 + \frac{X}{Y} t\right)$$

and

$$\lambda^2 \approx Y^2 - 2XY t.$$

From the above we obtain

$$\sigma \approx \left(\frac{A_{-1}}{Y} + A_0 + A_1 Y + A_2 Y^2 \right) + \left(\frac{A_{-1} X}{Y^2} - A_1 X - 2A_2 XY \right) t,$$

which we shall write in the abbreviated form $\sigma = S + Rt$. In this analysis

$t = r/300$ ($r = 0, 1, \dots, 59$) and thus upon substitution into equation (2.4)

we obtain

$$C_n = (3 \times 10^{-5}) \left\{ S \sum_{r=0}^{59} \exp(-in\pi r/30) + \frac{R}{300} \sum_{r=0}^{59} r \exp(-in\pi r/30) \right\}. \quad (2.5)$$

For $n = 0$, it is readily seen that

$$C_0 = (3 \times 10^{-5})(5.9R + 60S).$$

From page 82 of the "Smithsonian Mathematical Formulae and Tables of Elliptic Functions" (1947) we have

$$\sum_{r=1}^{N-1} r \cos(rx) = \frac{N \sin(N-1/2)x}{2 \sin(1/2)x} - \frac{1 - \cos(Nx)}{4 \sin^2(1/2)x} \quad (2.6a)$$

and

$$\sum_{r=1}^{N-1} r \sin(rx) = \frac{\sin(Nx)}{4 \sin^2(1/2)x} - \frac{N \cos(N-1/2)x}{2 \sin(1/2)x} \quad (2.6b)$$

The application of these relations together with the relation

$$\sum_{r=0}^{59} \exp(-in \pi r/30) = 60 \delta_{n,0}, \quad n < 60$$

to equation 2.5 yields

$$C_n = (3 \times 10^{-5}) \frac{R}{300} \left\{ \frac{60 \sin(119n\pi/60)}{2 \sin(n\pi/60)} + i \frac{60 \cos(119n\pi/60)}{2 \sin(n\pi/60)} \right\}, \quad n \neq 60j; \quad j = 0, 1, \dots \quad (2.7)$$

Combining equation 2.7 with the above expression for C_0 we finally have

$$\left| \frac{C_n}{C_0} \right| = \frac{|R| \csc(n\pi/60)}{|59R + 600S|}$$

where

$$S = \frac{A_{-1}}{Y} + A_0 + A_1 Y + A_2 Y^2$$

and

$$R = \frac{A_{-1} X}{Y^2} - A_1 X - 2XYA_2.$$

The applicability of this analysis to the higher harmonics is limited by the approximation of the integral for C_n by the summation. However, for $n \leq 30$, the range treated here, the effect is not significant.

It is of interest to note that the relative power spectra can be bounded and that the bound is quite small. To obtain this bound we note that

$$|S| \geq \frac{A_{-1}}{Y} + A_1 Y + A_2 Y^2 \geq Y \left(\frac{A_{-1}}{Y^2} + A_1 X + 2XA_2 Y \right) = Yf$$

since $0 < X < 0.5m$. Also, we observe that

$$|R| \leq \frac{A_{-1}}{Y^2} + A_1 X + 2A_2 XY = f,$$

from which we obtain

$$|59R + 600S| \geq |600|S| - 59|R|| \geq |600Y - 59|f|,$$

and

$$\frac{\sqrt{2} |C_n|}{|C_0|} \leq \frac{\sqrt{2} f \csc(n\pi/60)}{|600Y - 59|f|} \leq \frac{\sqrt{2} \csc(n\pi/60)}{366}$$

since $Y \gg 0.71 m$.

Thus since $\csc(n\pi/60)$ decreases monotonically as n goes from 1 to 30, we obtain

$$\begin{aligned} \frac{\sqrt{2} |C_n|}{|C_0|} &\leq .00387 \csc(n\pi/60) \\ &\leq .00387 \csc(3^\circ) = .074. \end{aligned}$$

SPECTRUM OF THE SQUARE ROOT OF THE CROSS SECTION

If one is interested in determining the spectrum of the square root of the cross section, then the values of $\sqrt{2} |C_n|/|C_0|$ given in the preceding section should be determined using the expressions

$$T C_n = \int_0^T \sqrt{\sigma} \exp(-10 \ln \pi t) dt, \quad T = 0.2 \text{ sec.}$$

or, equivalently

$$C_n = \int_0^1 \sqrt{\sigma(s)} \exp(-2 \ln \pi s) ds. \quad (3.1)$$

In this case, since it will often prove to be more informative, we shall employ the "relative phase" cross section values of cross section. That is, the cross section will be written in the form

$$\sigma = \left| \sum_{\ell=1}^N \sqrt{\sigma_{\ell}} e^{i\phi_{\ell}} \right|^2 \quad (3.2)$$

where

σ_{ℓ} = the cross section of the ℓ th scatterer,

ϕ_{ℓ} = the relative phase angle for the ℓ th scatterer, and

N = the number of scattering surfaces considered in the calculation

3.1 Maximum Value of $\sqrt{2} |C_n|/|C_0|$ as a Function of the Maximum Change in σ

The cross section is always such that $\sqrt{\sigma}$ can be expressed in the form

$$\sqrt{\sigma} = A (1 + f(s)), \quad \text{where } |f(s)| \leq K < 1. \quad (3.1.1)$$

This would mean that

$$A(1 - K) \leq \sqrt{\sigma} \leq A(1 + K)$$

and that

$$\frac{\sigma_{\max}}{\sigma_{\min}} \leq \left\{ \frac{1 + K}{1 - K} \right\}^2 \quad (3.1.2)$$

In determining the power spectra we have

$$C_n = \int_0^1 \sqrt{\sigma} \exp(-i 2n \pi s) ds. \quad (3.1.3)$$

For $n = 0$ we thus have

$$C_0 = \int_0^1 A(1 + f(s)) ds \geq A(1 - K), \quad (3.1.4)$$

and for $n \gg 1$

$$|C_n| = \left| \int_0^1 A f(s) e^{-i2n\pi s} ds \right| \leq AK \quad (3.1.5)$$

Equations (3.1.4) and (3.1.5) thus lead to an upper bound

$$\sqrt{2} |C_n| / |C_0| \leq \sqrt{2} K / (1 - K) \quad (3.1.6)$$

Using equations (3.1.2) and (3.1.6) it is possible to determine the magnitude of this bound as a function of $(\sigma_{\max})/(\sigma_{\min})$; this relation is displayed graphically in Figure G-1. It can readily be noted from Figure G-1 that if $(\sigma_{\max})/(\sigma_{\min})$ is less than 1.30, then $\sqrt{2} |C_n| / |C_0|$ will be less than 0.1.

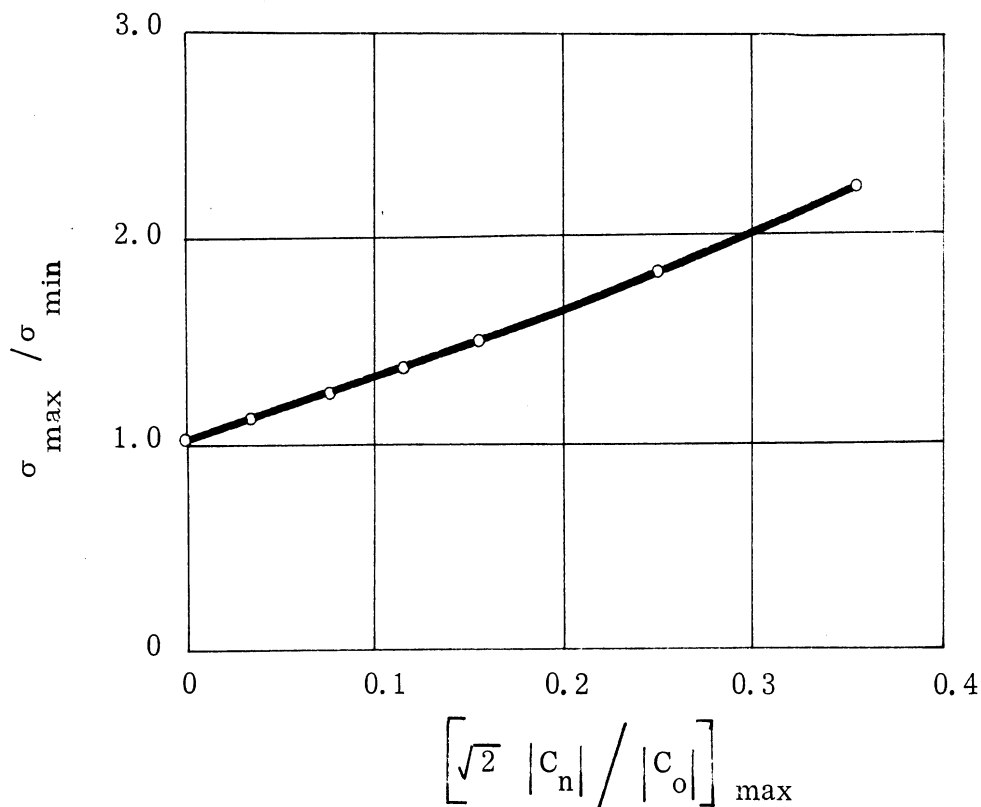


FIG. G-1: $\sigma_{\max} / \sigma_{\min}$ vs. $\left[\sqrt{2} \frac{|C_n|}{|C_o|} \right]_{\max}$

3.2 Maximum Value of $\sqrt{2} \frac{|C_n|}{|C_o|}$ As a Function of the Change in Phase Angle

Let $f(s)$ in equation (3.1.1) have the form $K \cos(\alpha + B\pi s)$. That is

$$\sqrt{\sigma} = A \left\{ 1 + K \cos(\alpha + B\pi s) \right\}, \quad K < 1 \text{ and } B \gg 0. \quad (3.2.1)$$

Thus, $(\sigma_{\max}) / (\sigma_{\min}) \leq (1 + K)^2 / (1 - K)^2$. This form for $\sqrt{\sigma}$ is chosen since it approximates the type of variation expected in the aircraft cross sections.

In addition, due to the fact that in most cases in the consideration of aircraft cross sections the phase angle will change by less than 2π for a 5% change in the frequency (about 425 Mc), we shall restrict our attention to the case of $B \leq 2$.

Direct substitution of this expression into equation (3.1.3) yields

upon integration

$$C_0 = A \left\{ 1 + \frac{2K}{B\pi} \sin(B\pi/2) \cos\left(\alpha + \frac{B\pi}{2}\right) \right\}, \quad (3.2.2)$$

$$C_1 = AK e^{i\alpha} / 2, \text{ for } B = 2^* \quad (3.2.3)$$

and

$$C_n = \frac{AK}{2i} \left\{ e^{i\alpha} \left[\frac{e^{i(B\pi - 2n\pi)} - 1}{B\pi - 2n\pi} \right] - e^{-i\alpha} \left[\frac{e^{-i(B\pi + 2n\pi)} - 1}{B\pi + 2n\pi} \right] \right\} \quad (3.2.4)$$

for $B < 2$.

* $C_n = 0$ for $n \gg 2$ and $B = 2$.

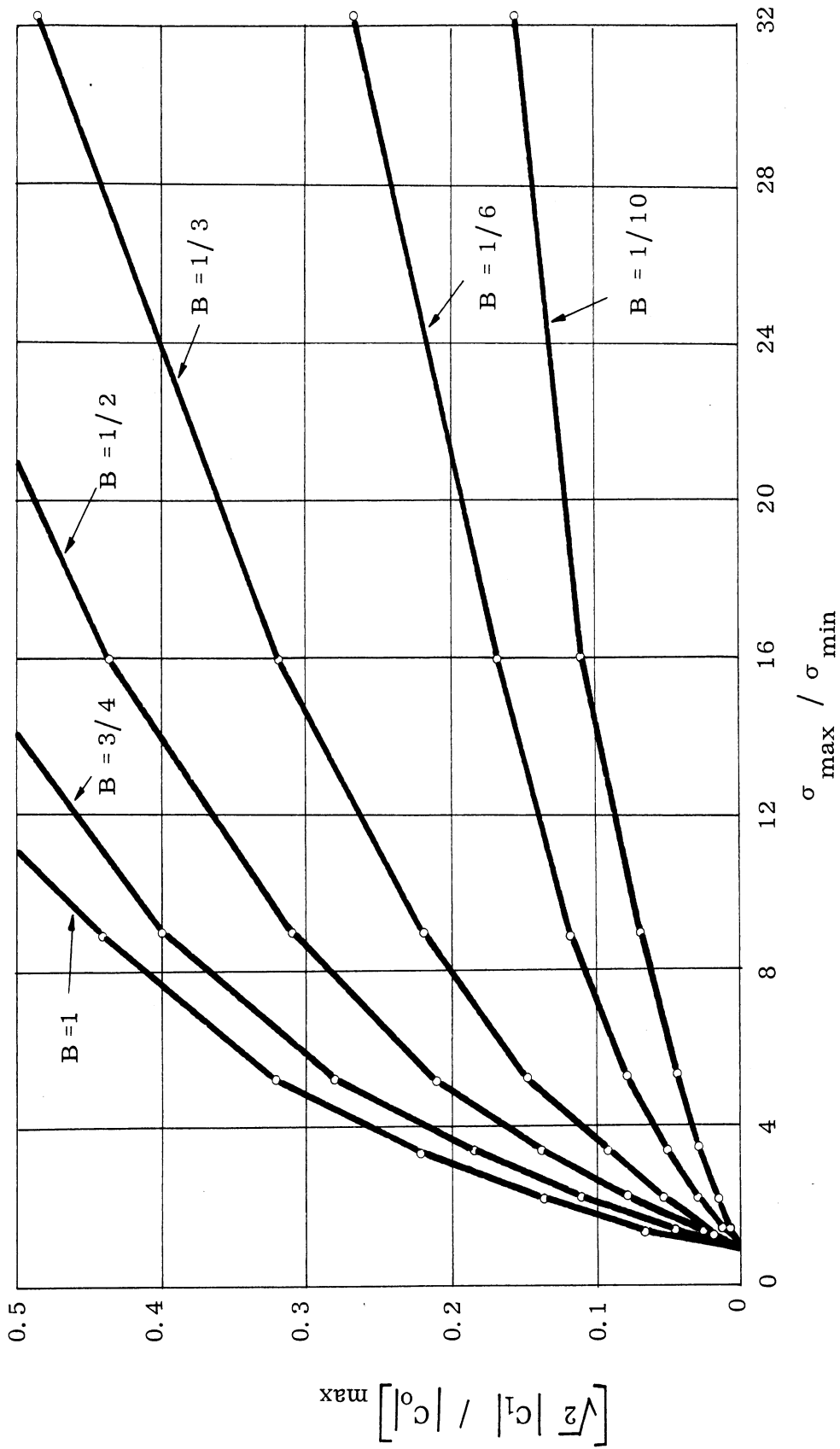


FIG. G-2: $\left[\frac{\sqrt{2}|c_1|}{|c_0|} \right]_{\max}$ AS A FUNCTION OF $(\sigma_{\max} / \sigma_{\min})$ AND B

APPENDIX H

RADIATION LABORATORY REPORTS

1

STUDIES IN RADAR CROSS SECTIONS

- I "Scattering by a Prolate Spheroid", F.V. Schultz (UMM-42, March 1950), W-33(038)-ac-14222. UNCLASSIFIED. 65 pgs.
- II "The Zeros of the Associated Legendre Functions $P_n^m(\mu')$ of Non-Integral Degree", K.M. Siegel, D.M. Brown, H.E. Hunter, H.A. Alperin and C.W. Quillen (UMM-82, April 1951), W-33(038)-ac-14222. UNCLASSIFIED. 20 pgs.
- III "Scattering by a Cone", K.M. Siegel and H.A. Alperin (UMM-87, January 1952), AF-30(602)-9. UNCLASSIFIED. 56 pgs.
- IV "Comparison between Theory and Experiment of the Cross Section of a Cone", K.M. Siegel, H.A. Alperin, J.W. Crispin, Jr., H.E. Hunter, R.E. Kleinman, W.C. Orthwein and C.E. Schensted (UMM-92, February 1953), AF-30(602)-9. UNCLASSIFIED. 70 pgs.
- V "An Examination of Bistatic Early Warning Radars", K.M. Siegel (UMM-98, August 1952), W-33(038)-ac-14222. SECRET. 25 pgs.
- VI "Cross Sections of Corner Reflectors and Other Multiple Scatterers at Microwave Frequencies", R.R. Bonkowski, C.R. Lubitz and C.E. Schensted (UMM-106, October 1953), AF-30(602)-9. SECRET - Unclassified when appendix is removed. 63 pgs.
- VII "Summary of Radar Cross Section Studies under Project Wizard", K.M. Siegel, J.W. Crispin, Jr. and R.E. Kleinman (UMM-108, November 1952), W-33(038)-ac-14222. SECRET. 75 pgs.
- VIII "Theoretical Cross Section as a Function of Separation Angle between Transmitter and Receiver at Small Wavelengths", K.M. Siegel, H.A. Alperin, R.R. Bonkowski, J.W. Crispin, Jr., A.L. Maffett, C.E. Schensted and I.V. Schensted (UMM-115, October 1953), W-33(038)-ac-14222. UNCLASSIFIED. 84 pgs.
- IX "Electromagnetic Scattering by an Oblate Spheroid", L.M. Rauch (UMM-116, October 1953), AF-30(602)-9. UNCLASSIFIED. 38 pgs.

- X "Scattering of Electromagnetic Waves by Spheres", H. Weil, M.L. Barasch and T. A. Kaplan (2255-20-T, July 1956), AF-30(602)-1070. UNCLASSIFIED. 104 pgs.
- XI "The Numerical Determination of the Radar Cross Section of a Prolate Spheroid", K.M. Siegel, B.H. Gere, I. Marx and F.B. Sleator (UMM-126, December 1953), AF-30(602)-9. UNCLASSIFIED. 75 pgs.
- XII "Summary of Radar Cross Section Studies under Project MIRO", K.M. Siegel, M.E. Anderson, R.R. Bonkowski and W.C. Orthwein (UMM-127, December 1953), AF-30(602)-9. SECRET. 90 pgs.
- XIII "Description of a Dynamic Measurement Program", K.M. Siegel and J.M. Wolf (UMM-128, May 1954), W-33(038)-ac-14222. CONFIDENTIAL. 152 pgs.
- XIV "Radar Cross Section of a Ballistic Missile", K.M. Siegel, M.L. Barasch, J.W. Crispin, Jr., W.C. Orthwein, I.V. Schensted and H. Weil (UMM-134, September 1954), W-33(038)-ac-14222. SECRET. 270 pgs.
- XV "Radar Cross Sections of B-47 and B-52 Aircraft", C.E. Schensted, J.W. Crispin, Jr. and K.M. Siegel (2260-1-T, August 1954), AF-33(616)-2531. CONFIDENTIAL. 155 pgs.
- XVI "Microwave Reflection Characteristics of Buildings", H. Weil, R.R. Bonkowski, T.A. Kaplan and M. Leichter (2255-12-T, May 1955), AF-30(602)-1070. SECRET. 148 pgs.
- XVII "Complete Scattering Matrices and Circular Polarization Cross Sections for the B-47 Aircraft at S-band", A.L. Maffett, M.L. Barasch, W.E. Burdick, R.F. Goodrich, W.C. Orthwein, C.E. Schensted and K.M. Siegel (2260-6-T, June 1955), AF-33(616)-2531. CONFIDENTIAL. 157 pgs.
- XVIII "Airborne Passive Measures and Countermeasures", K.M. Siegel, M.L. Barasch, J.W. Crispin, Jr., R.F. Goodrich, A.H. Halpin, A.L. Maffett, W.C. Orthwein, C.E. Schensted and C.J. Titus (2260-29-F, January 1956), AF-33(616)-2531. SECRET. 177 pgs.
- XIX "Radar Cross Section of a Ballistic Missile II", K.M. Siegel, M.L. Barasch, H. Brysk, J.W. Crispin, Jr., T.B. Curtz and T.A. Kaplan (2428-3-T, January 1956), AF-04(645)-33. SECRET. 189 pgs.

- XX "Radar Cross Section of Aircraft and Missiles", K.M. Siegel, W.E. Burdick, J.W. Crispin, Jr. and S. Chapman (WR-31-J, March 1956), SECRET. 151 pgs.
- XXI "Radar Cross Section of a Ballistic Missile III", K.M. Siegel, H. Brysk, J.W. Crispin, Jr. and R.E. Kleinman (2428-19-T, October 1956), AF-04(645)-33. SECRET. 125 pgs.
- XXII "Elementary Slot Radiators", R.F. Goodrich, A.L. Maffett, N.E. Reitlinger, C.E. Schensted and K.M. Siegel (2472-13-T, November 1956), AF-33(038)-28634, HAC-PO L-265165-F31. UNCLASSIFIED. 100 pgs.
- XXIII "A Variational Solution to the Problem of Scalar Scattering by a Prolate Spheroid", F.B. Sleator (2591-1-T, March 1957), AF-19(604)-1949, AFCRC-TN-57-586, AD 133631. UNCLASSIFIED. 67 pgs.
- XXIV "Radar Cross Section of a Ballistic Missile - IV The Problem of Defense", M.L. Barasch, H. Brysk, J.W. Crispin, Jr., B.A. Harrison, T.B.A. Senior, K.M. Siegel, H. Weil and V.H. Weston (2778-1-F, April 1959), AF-30(602)-1853. SECRET. 362 pgs.
- XXV "Diffraction by an Imperfectly Conducting Wedge", T.B.A. Senior (2591-2-T, October 1957), AF-19(604)-1949, AFCRC-TN-57-591, AD 133746. UNCLASSIFIED. 71 pgs.
- XXVI "Fock Theory", R.F. Goodrich (2591-3-T, July 1958), AF-19(604)-1949, AFCRC-TN-58-350, AD 160790. UNCLASSIFIED. 73 pgs.
- XXVII "Calculated Far Field Patterns from Slot Arrays on Conical Shapes", R.E. Doll, R.F. Goodrich, R.E. Kleinman, A.L. Maffett, C.E. Schensted and K.M. Siegel (2713-1-F, February 1958), AF-33(038)-28634 and 33(600)-36192; HAC-POs L-265165-F47, 4-500469-FC-47-D and 4-526406-FC-89-3. UNCLASSIFIED. 115 pgs.
- XXVIII "The Physics of Radio Communication via the Moon", M.L. Barasch, H. Brysk, B.A. Harrison, T.B.A. Senior, K.M. Siegel and H. Weil (2673-1-F, March 1958), AF-30(602)-1725. UNCLASSIFIED. 86 pgs.
- XXIX "The Determination of Spin, Tumbling Rates and Sizes of Satellites and Missiles", M.L. Barasch, W.E. Burdick, J.W. Crispin, Jr., B.A. Harrison, R.E. Kleinman, R.J. Leite, D.M. Raybin, T.B.A. Senior, K.M. Siegel and H. Weil (2758-1-T, April 1959), AF-33(600)-36793. SECRET. 180 pgs.

- XXX "The Theory of Scalar Diffraction with Application to the Prolate Spheroid", R.K. Ritt (with Appendix by N.D. Kazarinoff), (2591-4-T, August 1958), AF-19(604)-1949, AFCRC-TN-58-531, AD 160791. UNCLASSIFIED. 66 pgs.
- XXXI "Diffraction by an Imperfectly Conducting Half-Plane at Oblique Incidence", T.B.A. Senior (2778-2-T, February 1959), AF-30(602)-1853. UNCLASSIFIED. 35 pgs.
- XXXII "On the Theory of the Diffraction of a Plane Wave by a Large Perfectly Conducting Circular Cylinder", P.C. Clemmow (2778-3-T, February 1959), AF-30(602)-1853. UNCLASSIFIED. 29 pgs.
- XXXIII "Exact Near-Field and Far-Field Solution for the Back Scattering of a Pulse from a Perfectly Conducting Sphere", V.H. Weston (2778-4-T, April 1959), AF-30(602)-1853. UNCLASSIFIED. 61 pgs.
- XXXIV "An Infinite Legendre Integral Transform and Its Inverse", P.C. Clemmow (2778-5-T, March 1959), AF-30(602)-1853. UNCLASSIFIED. 35 pgs.
- XXXV "On the Scalar Theory of the Diffraction of a Plane Wave by a Large Sphere", P.C. Clemmow (2778-6-T, April 1959), AF-30(602)-1853. UNCLASSIFIED. 39 pgs.

MISCELLANEOUS REPORTS

1. "Analysis of PADAR and Its Modifications", T. B. Curtz, M. L. Barasch, H. Brysk, T. A. Kaplan, R. E. Kleinman, W. C. Orthwein and H. Weil (2476-1-F, 18 April 1956), AF-33(616)-3186. SECRET. 66 pgs.
2. "The Radar Cross Section of the B-57 Aircraft at X- and S-bands", J. W. Crispin, Jr., T. B. Curtz (2541-1-F, 27 June 1956), AF-18(600)-1550. CONFIDENTIAL. 57 pgs.
3. "Radar Cross Sections of the Regulus I and Regulus II Missiles", J. W. Crispin, Jr., T. B. Curtz, M. L. Barasch (2550-1-F, 1 October 1956), N 123(61756)-4183. SECRET. 76 pgs.
4. "Summary Report on the Radar Reflection Characteristics of Buildings", H. Weil, T. A. Kaplan and W. C. Orthwein (2255-30-P, 31 July 1956) AF-30(602)-1070. SECRET. 63 pgs.
5. "Radar Cross Sections of Conical Bodies of Revolution", K. M. Siegel, H. Brysk, J. W. Crispin, Jr., R. E. Kleinman, and R. F. Goodrich (2488-1-T, 31 October 1956). Cornell Aeronautical Laboratory, Inc., Purchase Order CA-47049. SECRET. 77 pgs.
6. "Radar Cross Sections of the F8U-1 and B-47 Aircraft", K. M. Siegel, (2200(01)-1-T, December 1956) Office of Naval Research Contract Nonr 2200(01). Down-graded to CONFIDENTIAL per letter from U. S. Naval Research Laboratory dated 31 January 1957 (ser 995). 53 pgs.
7. "Supplement to the Report 2200(01)-1-T Radar Cross Sections of the F8U-1 and B-47 Aircraft", J. W. Crispin, Jr. (2500-1-T, 4 March 1957). Nonr 2200(01). CONFIDENTIAL. 35 pgs.
8. "An Investigation of the Vulnerability of the ICBM System to Sand", K. M. Siegel (2361-1-F, 25 March 1957), Ramo-Wooldridge Purchase Order 5009. SECRET. 30 pgs.
9. "Bistatic Augmentation of a Luneberg Lens Reflector", A. L. Maffett, C. E. Schensted, and J. W. Crispin, Jr. (2636-1-F, April 1957) Bendix Systems Division Purchase Order A-1. CONFIDENTIAL. 28 pgs.
10. "The Lockheed-Raytheon AICBM System", M. L. Barasch, H. Brysk, B. A. Harrison, T. B. A. Senior, and K. M. Siegel (2671-1-T, 11 July 1957) Raytheon Mfg. Co. P. O. 71 127 BC 003. SECRET RESTRICTED DATA. 39 pgs.

11. "Theoretical Studies of the Radar Cross Sections of ICBM Tanks", J.W. Crispin, Jr. (2660-1-F, 2 August 1957), AF-30(602)-1694. SECRET. 85 pgs.
12. "Analysis of AN/FPS-17 Radar Data", K.M. Siegel, W.E. Burdick, M.L. Barasch, J.W. Crispin, Jr., L. Jehn, and H. Weil. (2615-1-F, August 1957), AF-33(600)-34359. SECRET. 162 pgs.
13. "Final Report on Radar Reflection Characteristics of Buildings", T.B. Curtz, B.B. Lubitz and K. Najita (2255-1-F, September 1957), AF-30(602)-1070. SECRET. 75 pgs.
14. "Terrain Classification in Terms of Radar Reflection Properties", R. F. Goodrich, (2802-1-F, October 1958). Final Report under Contract with Fairchild Guided Missiles Division. CONFIDENTIAL. 18 pgs.
15. "Interim Technical Note on Structural Camouflage Techniques", T.B. Curtz, C.K. Goberdhan, R.E. Hiatt, B.B. Lubitz, O. Sandus, C.E. Schensted, K.M. Siegel and H. Weil (2744-1-T, February 1959). Report on Contract No. AF-30(602)-1808, RADC-TN-59-87, ASTIA Document No. AD-305653. CONFIDENTIAL. 96 pgs.
16. "Radar Reflectivity of Mortar Shells", R.E. Hiatt, (2862-1-F, February 1959). Final Report on Contract Nonr 2200(03)X with Office of Naval Research. CONFIDENTIAL. 15 pgs.
17. "Summary Progress Report on Detection of Missile Exhausts and Ionization", M.L. Barasch, H. Brysk, W.E. Burdick, S.T. Harmon, R.J. Leite, K.M. Siegel, W.E. Vivian and P.F. Zweifel. (DA-36(039)-sc-75041, 2764-1-P, March 1959). SECRET. 133 pgs.
18. "On Near Zone Antennas", R. F. Goodrich and R. E. Hiatt (2861-1-F, June 1959). Final Report on General Electric Purchase Order 211-500-8668. UNCLASSIFIED. 49 pgs.
19. "Transverse Whistler Propagation", C.O. Hines, W.C. Hoffman and H. Weil. Final Report on AF-19(604)-5553. 2894-1-F (June 1959). UNCLASSIFIED. 34 pgs.
20. "Electromagnetic Scattering by High Density Meteor Trails", H. Brysk, (2871-1-T, June 1959). Report on Contract No. AF-19(604)-4993, AFCRC-TN-59-393. UNCLASSIFIED. 24 pgs.
21. "Scalar Diffraction by an Elliptic Cylinder", N.D. Kazarinoff and R. K. Ritt. (2871-2-T, June 1959). Report on Contract No. AF-19(604)-4993, AFCRC-TN-59-394. UNCLASSIFIED. 23 pgs.